

INFORMATION TO USERS

This manuscript has been reproduced from the microfilm master. UMI films the text directly from the original or copy submitted. Thus, some thesis and dissertation copies are in typewriter face, while others may be from any type of computer printer.

The quality of this reproduction is dependent upon the quality of the copy submitted. Broken or indistinct print, colored or poor quality illustrations and photographs, print bleedthrough, substandard margins, and improper alignment can adversely affect reproduction.

In the unlikely event that the author did not send UMI a complete manuscript and there are missing pages, these will be noted. Also, if unauthorized copyright material had to be removed, a note will indicate the deletion.

Oversize materials (e.g., maps, drawings, charts) are reproduced by sectioning the original, beginning at the upper left-hand corner and continuing from left to right in equal sections with small overlaps. Each original is also photographed in one exposure and is included in reduced form at the back of the book.

Photographs included in the original manuscript have been reproduced xerographically in this copy. Higher quality 6" x 9" black and white photographic prints are available for any photographs or illustrations appearing in this copy for an additional charge. Contact UMI directly to order.

UMI

A Bell & Howell Information Company
300 North Zeeb Road, Ann Arbor MI 48106-1346 USA
313/761-4700 800/521-0600

**A Simplified Structural Assessment Method
for Jacket-Type Platforms in Seismically-Active Regions**

by

James David Stear

B.S. (University of California at Berkeley) 1990
M.S. (University of California at Berkeley) 1992

A dissertation submitted in partial satisfaction of the
requirements for the degree of

DOCTOR OF PHILOSOPHY

in

**ENGINEERING
CIVIL AND ENVIRONMENTAL ENGINEERING**

in the

GRADUATE DIVISION

of the

UNIVERSITY OF CALIFORNIA at BERKELEY

Committee in charge:

Professor Robert G. Bea, Chair
Professor Abolhassan Astaneh-Asl
Professor Alaa E. Mansour

Spring 1999

UMI Number: 9931407

UMI Microform 9931407

Copyright 1999, by UMI Company. All rights reserved.

**This microform edition is protected against unauthorized
copying under Title 17, United States Code.**

UMI
300 North Zeeb Road
Ann Arbor, MI 48103

**A Simplified Structural Assessment Method
for Jacket-Type Platforms in Seismically-Active Regions**

©1999

by

James David Stear

The dissertation of James D. Stear is approved:

J. D. Stear 5/16/99
Chair Date

A. Astaneh-Asllan 5/5/99
Date

A. Mansoori 5/9/99
Date

University of California at Berkeley

Spring 1999

DEDICATION

To my mother, and to the memory of my father

TABLE OF CONTENTS

	<u>PAGE</u>
LIST OF FIGURES	vii
LIST OF TABLES	xiii
1 OVERVIEW	1
1.0 BACKGROUND	1
1.1 OBJECTIVES AND SCOPE	3
1.2 INVESTIGATION APPROACH	6
1.3 OVERVIEW OF ASSESSMENT APPROACH	13
1.4 ORGANIZATION OF DISSERTATION	16
2 BACKGROUND TO EARTHQUAKE ASSESSMENT	18
2.0 INTRODUCTION	18
2.1 MULTI-LEVEL SCREENING AND SIMPLIFIED ANALYSIS METHODS	22
2.2 OFFSHORE DESIGN FOR EARTHQUAKES	28
2.3 ASSESSMENT FOCUS	33
2.4 EARTHQUAKE GROUND MOTIONS IN THE OFFSHORE ENVIRONMENT	34
2.5 EVALUATING STRUCTURAL INTEGRITY	42
2.5.1 Beam-Columns	46
2.5.2 Braces	48
2.5.3 Piles	51
2.5.4 Platform Frames	53
2.5.5 Response Factors for Degrading Systems	61
2.6 RISK ASSESSMENT AND EVALUATION	63
3 PREDICTION OF STRENGTH AND DUCTILITY DEMANDS FROM EARTHQUAKES	66
3.0 INTRODUCTION	66
3.1 SIMPLE LINEAR RESPONSE OF PLATFORMS	72
3.1.1 Horizontal Response	72
3.1.2 Steel Structure Load-Displacement Relationships	73
3.1.3 Foundation Load-Displacement Relationships	75
3.1.4 Mass	77
3.1.5 Modal Analysis	78
3.1.6 Modal Damping Ratios	82
3.1.7 Vertical, Torsional Response	83
3.1.8 Modal Response Spectrum Analysis	84
3.2 SIMPLE LINEAR RESPONSE OF PLATFORMS: EXAMPLE	86

3.2.1	Description of Platform	86
3.2.2	3-D Model Description	87
3.2.3	Vibration Analysis	88
3.2.4	Earthquake Analysis	89
3.2.5	A Design Code Approach to Earthquake Forces	91
3.2.6	Effect of Foundation Flexibility and Added Mass on Earthquake Loads	95
3.3	SIMPLE NONLINEAR RESPONSE OF PLATFORMS	100
3.4	SIMPLE NONLINEAR RESPONSE OF PLATFORMS: EXAMPLE	104
3.4.1	2-D Frame Model	104
3.4.2	Static Pushover Analysis	104
3.4.3	Time History Analysis	108
3.5	SUMMARY	110
4	EVALUATING PLATFORM STRENGTH AND DUCTILITY CAPACITIES	112
4.0	INTRODUCTION	112
4.1	STRUCTURAL ELEMENTS	116
4.1.1	Deck and Jacket Legs	117
4.1.2	Tubular Braces	121
4.1.3	Pile Capacity: Lateral	134
4.1.4	Pile Capacity: Axial	139
4.1.5	Conductors, Mats and Mudlines Braces	141
4.2	COMPONENT STRENGTHS AND GLOBAL STRENGTH	145
4.2.1	Unbraced Deck Bay Strength	146
4.2.2	Braced Bay Strength	148
4.2.3	Foundation Lateral and Overturning Capacity	151
4.2.4	Global Strength	152
4.3	GLOBAL DISPLACEMENT DUCTILITY	154
4.3.1	Simplified Limit Ductility Analysis	154
4.3.2	Inelastic Behavior of Jacket Structures	157
4.3.3	Foundation Rotation Limit	162
4.3.4	Residual Strength Requirement	164
4.4	EXAMPLE APPLICATIONS	164
4.4.1	Case A: South Pass 62 A	165
4.4.2	Case B: Ship Shoal 274 A	172
4.4.3	U. C. Berkeley Frame Tests	180
4.5	SUMMARY	183
5	EARTHQUAKE RESPONSE OF STRENGTH AND STIFFNESS DEGRADING HYSTERETIC SYSTEMS	184
5.0	INTRODUCTION	184

5.1	STATISTICAL STUDY ON R AND F_A	188
5.1.1	Hysteretic Behaviors Considered	189
5.1.2	Earthquake Ground Motions Used	193
5.1.3	Software Used in Study	197
5.2	RESULTS OF STATISTICAL STUDIES	199
5.2.1	Bilinear Degrading/Non-degrading SDOF Systems	199
5.2.2	Jacket-Type SDOF Systems	204
5.2.3	Foundation-Type SDOF Systems	221
5.3	ADDITIONAL PARAMETER STUDIES	230
5.3.1	Effects of Damping on Load Reduction Factors	230
5.3.2	Effects of Medium Stiff and Soft Soils on Load Reduction Factors	233
5.3.3	Results Compared to Current Code Load Reduction Methods	237
5.4	MDOF COMPARISONS	242
5.4.1	MDOF with Strength-Degrading Foundation	243
5.4.2	MDOF with Strength- and Stiffness-Degrading Stories	245
5.5	CONCLUSIONS	247
6	CASE STUDIES INVOLVING APPLICATION OF SIMPLIFIED METHODS	249
6.0	INTRODUCTION	249
6.1	CASE STUDY #1: PLATFORM A	252
6.1.1	Modal Analysis	253
6.1.2	Strength-Level Demand-Capacity Analysis	255
6.1.3	Global Ductility Analysis	261
6.1.4	Ductility-Level Demand-Capacity Analysis	265
6.1.5	Platform A: Summary of Results	269
6.2	CASE STUDY #2: PLATFORM B	270
6.2.1	Modal Analysis	271
6.2.2	Strength-Level Demand-Capacity Analysis	275
6.2.3	Global Ductility Analysis	283
6.2.4	Ductility-Level Demand-Capacity Analysis	288
6.2.5	Platform B: Summary of Results	291
6.3	CASE STUDY #3: PLATFORM C	292
6.3.1	Modal Analysis	293
6.3.2	Strength-Level Demand-Capacity Analysis	297
6.3.3	Global Ductility Analysis	301
6.3.4	Ductility-Level Demand-Capacity Analysis	305
6.3.5	Platform C: Summary of Results	308
6.4	CASE STUDY #4: PLATFORM D	309
6.4.1	Modal Analysis	311
6.4.2	Strength-Level Demand-Capacity Analysis	314
6.4.3	Global Ductility Analysis	318

6.4.4	Ductility-Level Demand-Capacity Analysis	322
6.4.5	Platform D: Summary of Results	325
6.5	CASE STUDY #5: PLATFORM E	327
6.5.1	Modal Analysis	328
6.5.2	Strength-Level Demand-Capacity Analysis	329
6.5.3	Global Ductility Analysis	335
6.5.4	Ductility-Level Demand-Capacity Analysis	337
6.5.5	Platform E: Summary of Results	340
6.6	LARGE-SCALE APPLICATION OF SIMPLIFIED METHODS: BAY OF CAMPECHE PLATFORMS	341
6.7	OBSERVATIONS AND CONCLUSIONS	344
7	A SIMPLIFIED SEISMIC RELIABILITY ANALYSIS	349
7.0	INTRODUCTION	349
7.1	MVFOSM RELIABILITY ANALYSIS	352
7.2	PROBABILISTIC FORMULATION OF DEMAND	355
7.2.1	Variability in Response Spectrum Ordinates	356
7.2.2	Variability Due to Structural Parameters	361
7.2.3	Variability Due to Modal Combination	363
7.3	PROBABILISTIC FORMULATIONS OF CAPACITIES	364
7.3.1	Unbraced Bays	365
7.3.2	Braced Bays	366
7.3.3	Foundation Lateral and Overturning	368
7.3.4	Effective Component Ductility Capacities	368
7.4	PLATFORM YIELD AND COLLAPSE PROBABILITIES	373
7.5	SIMPLIFIED SEISMIC RELIABILITY ANALYSIS: EXAMPLE	374
7.5.1	Simplified Reliability Method	376
7.5.2	Monte Carlo Simulation with Time History Analysis	379
7.5.3	Comparison of Results	380
7.6	CONCLUSIONS	381
8	CONCLUSIONS AND RECOMMENDATIONS	382
8.0	SUMMARY	382
8.1	CONCLUSIONS	384
8.2	RECOMMENDATIONS	386
	REFERENCES	389

LIST OF FIGURES

<u>FIGURE</u>	<u>PAGE</u>
1-1 Investigation Approach Used to Develop Simplified Method	7
1-2 Platform Idealization	10
1-3 Simplified Earthquake Assessment of Platforms	14
2-1 Conventional Jacket-Type Platform	19
2-2 Global Seismicity	20
2-3 Areas of Major Offshore Activity	21
2-4A Platform Assessment Process – Metocean Loading	25
2-4B Platform Assessment Process – Metocean Loading	26
2-5 Work/Energy Balance Between Elastic and Inelastic System	30
2-6 Recommend Framing for Earthquake Areas	31
2-7 Normalized Response Spectra	39
2-8 Elastic Design Response Spectrum	41
2-9 Cyclic Inelastic Behavior of Tubular Beam-Column Cantilever	47
2-10 Cyclic Inelastic Behavior of a Tubular Strut, $D/t=48$, $kL/r=54$	49
2-11 Cyclic Inelastic Behavior of a Tubular Strut, $D/t=33$, $kL/r=24$	50
2-12 Cyclic Axial Loading of a Pile in Soft Clay	51
2-13 Cyclic Effects on a Pile in Stiff Clay	52
2-14 Cyclic Effects on a Pile in Sand	52
2-15 X-braced Frames Tested by Zayas, et al.	57
2-16 Hysteresis of Frames I and II	58
2-17 K-braced Frames with Moderate Slenderness	59
2-18 K-braced Frames with Low Slenderness	60
3-1 Complete MDOF Model of Platform	69
3-2 Horizontal Loading Components	73
3-3 Vertical Load Transfer Mechanisms for Imbedded Piles	76
3-4 Platform A	86
3-5 Platform Vibration Properties (2-D Frame Model)	88
3-6 Platform Vibration Properties (Simple Model)	89
3-7 Platform Loads, $ZPA=0.25g$	90
3-8 Comparison of UBC Forces and 3-D Modal Analysis Forces	95
3-9 Example Platform, Variation in Fundamental Period for Foundation Flexibility	99
3-10 Example Platform, Variation in Fundamental Period with Brace Added Mass	100
3-11 Simplified Inelastic Earthquake Analysis	102
3-12 Global-Load Displacement Behavior of Platform	105
3-13 Scaled Horizontal Displacements in Platform for Different Levels of Deck Displacement	106
3-14 Shape of Assumed Collapse Mechanism for Example Platform	107

4-1	Critical Components in a Jacket-Type Platform	112
4-2	Platform Deck or Jacket Leg Element	118
4-3	M- ϕ Relationship Approximation	119
4-4	Brace-Joint System	122
4-5	Three-Hinge Failure Mode for Braces	123
4-6	Equipment/Structure Amplification Ratios	127
4-7	Tubular Joint Classification	130
4-8	Simple Hysteretic Envelope for Brace Elements	132
4-9	Pile Lateral Collapse Mechanism	135
4-10	Collapse Mechanism for an Unbraced Bay	146
4-11	Deflection of Unbraced Bay	148
4-12	Braced Bay Collapse Mechanism	149
4-13	Reduction in Bay Shear Capacity Due to Leg Moments	150
4-14	Lateral Collapse Mechanism in Foundation	151
4-15	Global Strength Determination	153
4-16	Damage Concentrating in a Deck Bay (Post-Yield Reserve Strength)	156
4-17	Damage Concentrating in a Foundation (Overturning, Plastic)	156
4-18	Damage Concentrating in a Jacket Bay (Softening)	157
4-19	Unzipping Frame	158
4-20	K-Type Frames	159
4-21	South Pass 62A Elevation	165
4-22	End-On Loading Performance, SP 62A	167
4-23	Broadside Loading Performance, SP 62A	168
4-24	Demand-Capacity Analysis of Platform, End-On Loading	170
4-25	Demand-Capacity Analysis of Platform, Broadside Loading	171
4-26	Load-Displacement Behavior for SP 62A	172
4-27	Ship Shoal 274A Elevations	173
4-28	End-On Loading Performance, SS 274A	174
4-29	Broadside Loading Performance, SS 274A	175
4-30	Demand-Capacity Analysis of Platform, End-On Loading	177
4-31	Demand-Capacity Analysis of Platform, Broadside Loading	178
4-32	Load-Displacement Behavior for SS 274A	179
4-33	Global Load-Displacement Envelopes for Frames I and II	182
5-1	JT System Hysteresis	190
5-2	FT System Hysteresis	191
5-3	R Factor for BN	200
5-4	F_4 Factor for BN	201
5-5	COV in R for BN	201
5-6	COV in F_4 for BN	202
5-7	R Factor for BD	202
5-8	F_4 Factor for BD	203
5-9	COV in R for BD	203

5-10	COV in F_a for BD	204
5-11	R Factor for JT40080	205
5-12	F_a Factor for JT40080	205
5-13	COV in R for JT40080	206
5-14	COV in F_a for JT40080	206
5-15	R Factor for JT30080	207
5-16	F_a Factor for JT30080	207
5-17	COV in R for JT30080	208
5-18	COV in F_a for JT30080	208
5-19	R Factor for JT20080	209
5-20	F_a Factor for JT20080	209
5-21	COV in R for JT20080	210
5-22	COV in F_a for JT20080	210
5-23	R Factor for JT11080	211
5-24	F_a Factor for JT11080	211
5-25	COV in R for JT11080	212
5-26	COV in F_a for JT11080	212
5-27	R Factor for JT40060	213
5-28	F_a Factor for JT40060	213
5-29	COV in R for JT40060	214
5-30	COV in F_a for JT40060	214
5-31	R Factor for JT30060	215
5-32	F_a Factor for JT30060	215
5-33	COV in R for JT30060	216
5-34	COV in F_a for JT30060	216
5-35	R Factor for JT20060	217
5-36	F_a Factor for JT20060	217
5-37	COV in R for JT20060	218
5-38	COV in F_a for JT20060	218
5-39	R Factor for JT11060	219
5-40	F_a Factor for JT11060	219
5-41	COV in R for JT11060	220
5-42	COV in F_a for JT11060	220
5-43	R Factor for FT4080	222
5-44	F_a Factor for FT4080	222
5-45	COV in R for FT4080	223
5-46	COV in F_a for FT4080	223
5-47	R Factor for FT2080	224
5-48	F_a Factor for FT2080	224
5-49	COV in R for FT2080	225
5-50	COV in F_a for FT2080	225
5-51	R Factor for FT4060	226
5-52	F_a Factor for FT4060	226

5-53	COV in R for FT4060	227
5-54	COV in F_A for FT4060	227
5-55	R Factor for FT2060	228
5-56	F_A Factor for FT2060	228
5-57	COV in R for FT2060	229
5-58	COV in F_A for FT2060	229
5-59	BN, 10% Damping	231
5-60	JT11060, 10% Damping	232
5-61	FT4060, 10% Damping	232
5-62	R for BN, Alluvium Records	234
5-63	R for JT11060, Alluvium Records	234
5-64	R for FT4060, Alluvium Records	235
5-65	R for BN, Soft Soil Records	235
5-66	R for JT11060, Soft Soil Records	236
5-67	R for FT4060, Soft Soil Records	236
5-68	Effective Load Reduction (Non-degrading)	239
5-69	Effective Load Reduction (Stiffness Degrading)	239
5-70	Effective Load Reduction (Strength and Stiffness Degrading)	240
5-71	Effective Load Reduction (Strength Degrading)	240
5-72	Two-Bay Frame	244
5-73	Braced Frame Model	245
6-1	Platform A	252
6-2	Platform Vibration Properties (Simplified Modal Approach)	254
6-3	Platform Vibration Properties (3-D Model)	255
6-4	Platform Loads, ZPA=0.25 g	256
6-5	Gross Shear Demand-Capacity Profile from Simplified Method	259
6-6	Global Load-Displacement Behavior of Platform A with Unzipping	264
6-7	Global Load-Displacement Behavior of Platform A without Unzipping	265
6-8	Platform B	271
6-9	Platform B End-On Vibration Properties (Simplified Model)	273
6-10	Platform B End-On Vibration Properties (3-D Model)	274
6-11	Platform B Broadside Vibration Properties (Simplified Model)	274
6-12	Platform B Broadside Vibration Properties (3-D Model)	275
6-13	Comparison of Gross End-On Shears, ZPA=0.25 g	276
6-14	Comparison of Gross Broadside Shears, ZPA=0.25 g	277
6-15	Platform B Gross Shear Demand-Capacity Profile from Simplified Method, ZPA=0.34 g, End-On Frames	279
6-16	Platform B Gross Shear Demand-Capacity Profile from Simplified Method, ZPA=0.34 g, Broadside Frames	279
6-17	Global Load-Displacement Behavior of Platform B End-On Components	287
6-18	Global Load-Displacement Behavior of Platform B	

	Broadside Components	287
6-19	Platform C	294
6-20	Platform C End-On Vibration Properties (Simplified Model)	295
6-21	Platform C End-On Vibration Properties (3-D Model)	295
6-22	Platform C Broadside Vibration Properties (Simplified Model)	296
6-23	Platform C Broadside Vibration Properties (3-D Model)	296
6-24	Comparison of Gross End-On Shears, ZPA=0.25 g	298
6-25	Comparison of Gross Broadside Shears, ZPA=0.25 g	298
6-26	Platform C Gross Shear Demand-Capacity Profile from Simplified Method, ZPA=0.34 g, End-On Frames	300
6-27	Platform C Gross Shear Demand-Capacity Profile from Simplified Method, ZPA=0.34 g, Broadside Frames	301
6-28	Global Load-Displacement Behavior of Platform C End-On Components	304
6-29	Global Load-Displacement Behavior of Platform C Broadside Components	304
6-30	Platform D	310
6-31	Platform D End-On Vibration Properties (Simplified Model)	312
6-32	Platform D End-On Vibration Properties (3-D Model)	312
6-33	Platform D Broadside Vibration Properties (Simplified Model)	313
6-34	Platform D Broadside Vibration Properties (3-D Model)	313
6-35	Comparison of Gross End-On Shears	314
6-36	Comparison of Gross Broadside Shears	315
6-37	Platform D Gross Shear Demand-Capacity Profile from Simplified Method, ZPA=0.38 g, End-On Frames	316
6-38	Platform D Gross Shear Demand-Capacity Profile from Simplified Method, ZPA=0.38 g, Broadside Frames	317
6-39	Global Load-Displacement Behavior of Platform D End-On Direction (6 in Compression)	319
6-40	Global Load-Displacement Behavior of Platform D Broadside Direction	320
6-41	Global Load-Displacement Behavior of Platform C End-On Direction (3 in Compression)	320
6-42	Platform E	327
6-43	Platform E End-On Vibration Properties (Simplified Model)	330
6-44	Platform E End-On Vibration Properties (3-D Model)	331
6-45	Platform E Broadside Vibration Properties (Simplified Model)	332
6-46	Platform E Broadside Vibration Properties (3-D Model)	332
6-47	Comparison of Gross End-On Shears, ZPA=0.30 g	333
6-48	Comparison of Gross Broadside Shears, ZPA=0.30 g	333
6-49	Platform E Gross Shear Demand-Capacity Profile from Simplified Method, ZPA=0.31 g, End-On Frames	334
6-50	Platform E Gross Shear Demand-Capacity Profile from Simplified Method, ZPA=0.31 g, Broadside Frames	334
6-51	Global Load-Displacement Behavior of Platform E, Resultants	336

6-52	Trends in TOPCAT/DAMS-SACS Ratios	343
7-1	Response Spectrum, PGV Scaling	358
7-2	Response Spectrum, PGA Scaling	358
7-3	Uncertainty in Response Spectrum Ordinates	359
7-4	Spectral Ordinate Cumulative Probability, T=0.5 sec	359
7-5	Spectral Ordinate Cumulative Probability, T=1.0 sec	360
7-6	Spectral Ordinate Cumulative Probability, T=2.0 sec	360
7-7	Statistics of <i>R</i> Factor: T=0.5 sec, BD, $\mu=2$	370
7-8	Statistics of <i>R</i> Factor: T=1.0 sec, BD, $\mu=2$	370
7-9	Statistics of <i>R</i> Factor: T=2.0 sec, BD, $\mu=2$	371
7-10	Statistics of <i>R</i> Factor: T=0.5 sec, BD, $\mu=4$	371
7-11	Statistics of <i>R</i> Factor: T=1.0 sec, BD, $\mu=4$	372
7-12	Statistics of <i>R</i> Factor: T=2.0 sec, BD, $\mu=4$	372
7-13	Determination of Governing Collapse β	374
7-14	Site Response Spectrum	376

LIST OF TABLES

<u>TABLE</u>	<u>PAGE</u>
2-1 Ductility-Level Earthquakes	32
2-2 Possible Deficiencies in Platforms	33
2-3 Seismic Zones and Scale Factors	40
2-4 Spectrum Soil Amplification Factors	42
2-5 Spectrum Amplification for Seismotectonic Condition	42
3-1 Bearing Stiffness as Related to Bearing Strength	77
3-2 Pile Stiffnesses	87
3-3 Pile Loads, ZPA=0.25 g	91
3-4 Horizontal Pile-Head Stiffnesses (kips/in)	98
3-5 Vertical Pile-Head Stiffnesses (kips/in)	98
3-6 Local Ductility Demands for a Global Ductility of 2.25	106
3-7 Scale Factors Applied to Time History Analyses	108
3-8 Peak Deck Displacements (Time History Analysis)	108
3-9 Global and Local Ductility Demands	108
4-1 Tension and Compression Capacities for Tubular Joints	128
4-2 Side Resistance Factor for Cohesive Soils	140
4-3 Limiting Values of N_q , q and f	141
4-4 Static Pushover Analysis of Jackets	160
4-5 Platform Deck Drifts Due to Foundation Rotation	163
5-1 JT SDOF System Parameters	192
5-2 FT SDOF System Parameters	192
5-3 37 Ground Motions Recorded on Rock	194
5-4A 31 Ground Motions Recorded on Alluvium	195
5-4B 31 Ground Motions Recorded on Alluvium	196
5-5 Ground Motions Recorded on Soft Soil	196
5-6 Comparison of Response Factors, Rock	238
5-7 Earthquake Time Histories Used	243
5-8 SDOF and MDOF Comparisons	245
5-9 SDOF and MDOF Comparisons, Uniform Strength and Stiffness	247
5-10 SDOF and MDOF Comparisons, Soft Story at Base	247
6-1 Pile-Head Axial and Lateral Stiffnesses	253
6-2 Pile Loads, ZPA=0.25 g	256
6-3 Tubular Brace Buckling Capacities	257
6-4 Pile Capacities	257
6-5 Tubular Brace Capacities	260
6-6 Modal Acceleration Components for Platform A	260
6-7 Brace Axial Capacities	261

6-8	Earthquake Time Histories Used	268
6-9	$S_{a\text{-yield}}$, F_μ and Deck Displacement Ratio	268
6-10	Pile-Head Axial and Lateral Stiffnesses	272
6-11	Pile Loads on 66" ϕ	276
6-12	Tubular Brace Characteristics, End-On Frames	281
6-13	Tubular Brace Characteristics, Broadside Frames	281
6-14	Modal Acceleration Components for Platform B	282
6-15	Brace Axial Capacities, End-On Frames	283
6-16	Brace Axial Capacities, Broadside Frames	283
6-17	$S_{a\text{-yield}}$, F_μ and Deck Displacement Ratio for Platform B	289
6-18	Pile Loads on 48" ϕ	297
6-19	$S_{a\text{-yield}}$, F_μ and Deck Displacement Ratio for Platform C	306
6-20	Pile-Head Axial and Lateral Stiffnesses	311
6-21	Peak Pile Loads	314
6-22	$S_{a\text{-yield}}$, F_μ and Deck Displacement Ratio (X major)	324
6-23	$S_{a\text{-yield}}$, F_μ and Deck Displacement Ratio (Y major)	324
6-24	Pile-Head Axial and Lateral Stiffnesses	329
6-25	Peak Pile Loads	330
6-26	$S_{a\text{-yield}}$, F_μ and Deck Displacement Ratio (X major)	338
6-27	$S_{a\text{-yield}}$, F_μ and Deck Displacement Ratio (Y major)	339
6-28	Results from Application of Simplified Screening to PEMEX/IMP Platforms	342
6-29	Mean Ratios of Period, Base Shear and RSR (TOPCAT/DAMS-SACS)	343
6-30	Ranking of Platforms by RSR	344
7-1	Time Histories Used for Spectra	357
7-2	Platform A Sensitivity of Response to Structural Properties	362
7-3	Platform Structural Variables	375
7-4	Yield Reliability	379
7-5	Collapse Reliability	379
7-6	Probabilities of Yield and Collapse	379

ACKNOWLEDGEMENTS

I am indebted to Professor Robert G. Bea for giving me the opportunity to study with him at Berkeley. The support, guidance and encouragement he provided while serving as chair of my dissertation committee are gratefully acknowledged. I am privileged to know him as both a colleague and friend.

I am grateful to Professors Abolhassan Astaneh-Asl and Alaa E. Mansour for taking an interest in my research and serving on my exam and dissertation committees. I thank Professor David B. Ashley for serving as chair my exam committee.

My research could not have been completed without the generous support of the offshore oil community. I am thankful for the support and input provided by the following individuals and organizations: Steve Guynes (ARCO Exploration and Production Technology), Al Mason, Dave Cayle and Tom Stallings (Chevron Petroleum Technology Company), J. Ward Turner (Exxon Production Research Company), Ken Conner (Mobil Technology Company), Faustino Perez, Gregorio Inda, Rafael Ramos and Oscar Valle (PEMEX/IMP), Kris Digre and Al Brooks (Shell Deepwater Development Systems, Incorporated), Tom Miller (Uncal Corporation), Charles Smith and Tommy Laurendine (Minerals Management Service), and Martin Eskijian (California State Lands Commission).

I also thank John Fair and the Structural and Geotechnical Engineering Team at Chevron for giving me the opportunity to transition to the professional world while still completing the final chapters of my dissertation.

Thanks are also due Suzanne Kempton (EERC), Gretchen von Duering (EERC), Mary Cook (CE), Sally Olsen (CE) and Cindy Staffa (CE) for helping me through the administrative aspects of my research and graduate education.

I am indebted to the family and friends who have patiently stood by me through the past five years. My mother Barbara has provided unconditional support and encouragement throughout my academic endeavors; for that I am eternally grateful. I am also thankful for the encouragement provided by my sisters Carol and Suzanne and my brother Robert. Great appreciation is expressed to Mary MacLaughlin, Felix Hack, and Greg Walsh for much good comradeship during my stay at Berkeley. I also extend my thanks to Mehrdad Mortazavi, Kenn Loch, Tao Xu, Derrick Hee, Jun Ying and Zhaohui Jin for their friendship, assistance and council. To all the rest I cannot possibly name here: you have my gratitude.

Last but certainly not least, I express my deepest appreciation to my wife Kathleen. She endured with kindness, patience and understanding a courtship, engagement and marriage which were at times shadowed by the demands of my graduate education. I am forever indebted to her for the love and support she unselfishly provided as I struggled along the uneven path of my academic journey.

CHAPTER ONE:

OVERVIEW

1.0 BACKGROUND

Today there are nearly 8,000 offshore platforms around the globe involved in the exploration, production and storage of oil and natural gas; nearly 4,000 of these are located in the Gulf of Mexico. With such a large concentration of structures in an area prone to severe storm conditions, it is not surprising that the vast majority of design and assessment efforts associated with these platforms focus on survivability when subjected to forces from wind, wave and current.

However, the offshore oil industry also possesses a lengthy, if not as well known, history of operations in regions where earthquakes, and not severe storms, control the design of structures. The first recorded hydrocarbon recovery operations over water took place in 1897 near the town of Summerland, California. What is believed to be the first offshore well was drilled from a wooden pier extending 300 ft from the shoreline. Compared to the frenzy of offshore oil development witnessed in the Gulf of Mexico in the 1950's and 1960's, development of oil resources in major seismic zones continued at a relatively slow but steady pace. The first steel jacket platforms were installed off California in the late 1950's in fairly shallow waters (50 ft or less). The Uniform Building Code or other conventional engineering standards were usually applied to the design of these early platforms, although in some instances earthquake design was neglected entirely. Earthquake design provisions in the early versions of the offshore industry's design standard, API RP 2A (American Petroleum

Institute Recommended Practice for Planning, Designing and Constructing Fixed Offshore Platforms, first edition 1969), continued to reflect the conventional engineering standards of the time.

With the desire to place platforms in deeper waters off California, the oil industry began to recognize that design for platform survivability during large earthquakes was a major consideration. This posed unprecedented challenges for the offshore engineering community, as structural design for most platforms subject to wind, wave and current was typically accomplished using static analysis. Hence, in the 1960's the offshore industry began to sponsor the development of computational programs capable of performing nonlinear dynamic analysis of large frame structures. In addition, testing programs were undertaken in the 1970's to physically evaluate the post-yield performance of tubular steel frames. Efforts were also made to study the cyclic behavior of soils (also of great interest to the nuclear power industry), and to extrapolate the cyclic behavior of steel pipe piles from field test data performed under slow cycling conditions. As a result of these efforts, the industry was able to make rapid progress on enhancing the earthquake design guidelines contained within API RP 2A in the middle 1970's. The platforms which were placed offshore southern California in the 1970's and 1980's were able to benefit greatly from this work.

The number of jacket-type platforms in seismically-active regions of the world's oceans remains small today, numbering perhaps 100 structures; the majority of these are offshore southern California. With new technology extending the life of old oil fields, these platforms, like their brethren in other parts of the world's oceans, are being called upon for

extended service beyond their original design lives. It is clear that some form of structural integrity assessment must be performed for these platforms, taking into account the current conditions of the platforms and revised estimates of the earthquake potential of the surrounding region. While there exist today many nonlinear dynamic software packages such as CAP/SEASTAR, KARMA and USFOS capable of analyzing large jacket-type platforms in the time domain for earthquake ground motions, it must be recognized that these programs require a high degree of expertise to operate. To apply these tools as part of a comprehensive risk assessment involving a large number of structures would be prohibitive in terms of time and money. What is needed is a staged process of assessment, by which the bulk of the structure population can be assessed quickly using cheap, conservative methods, leaving the more problematic cases for further rigorous analysis.

1.1 OBJECTIVES AND SCOPE

The fundamental question addressed by this research is whether it is possible to develop a rational and simplified analysis method to evaluate the structural integrity of jacket-type offshore platforms subjected to severe earthquakes. Therefore, the objective of this research is to answer this question by developing and verifying such a method. The following issues are thus addressed in this research:

- Platform vibration properties.
- Forces on platform components from earthquake excitation.
- Platform displacements and accelerations at different framing levels.
- Strength and displacement ductility of platform structural components.

- Effective increases in static lateral load capacity of platform systems through recognition of the nonlinear hysteretic action of the platform structural system.
- Structural reliability of the global platform system.
- Verification of the simplified method with results from detailed nonlinear dynamic analyses.
- Development of software which performs the simplified analyses.

A pseudo-static approach based on response spectrum analysis offers an excellent means of predicting the forces on platform components, and displacements and accelerations in the platform structure (important for equipment assessment) assuming elastic behavior in the structural system. This requires some knowledge of the vibration properties of the platform. To avoid developing a full-frame model of the platform, however, simple means of estimating the vibration mode shapes and periods of the structure for the primary directions of response must be found.

If forces from the response spectrum analysis exceed the strength capacities of platform components, it does not mean that the platform has collapsed. The platform will have some tolerance for displacements beyond those reached at the strength limit state due to the displacement ductility (i.e., tolerance for post-yield deformation) of the components of the platform. Means must be found to relate this tolerance for displacement, and the associated load-displacement behavior of the platform past the strength limit state, to an “effective” increase in static load capacity.

To determine the global strength and displacement ductility of the platform system, the strength and ductility of platform components (deck bay, jacket bays, foundation) and elements (deck and jacket legs, tubular braces and joints, pile piles and soils) must be determined. Relationships between local displacement ductility and global displacement ductility must be established. To implicitly account for the cyclic content of the earthquake ground motion pulses, cyclic limits on element strength and displacement ductility must be used.

With the above questions answered, it becomes possible to perform deterministic structural integrity assessments of platforms subjected to earthquakes, providing the basics of the platform structure and mass are known, and a response spectrum appropriate to the location of the platform is available. However, earthquake assessment is a practice with many uncertainties. The ground motions occurring at a given location due to an earthquake are essentially a random process, leading to great uncertainty in the response spectrum ordinates. Variability in platform vibration properties and damping will further influence the loads estimated from a response spectrum. Imperfections and inconsistent construction will add uncertainty to structural strength and ductility estimates. Furthermore, the process by which an “effective” dynamic capacity is determined for a platform also contains substantial uncertainties. A probabilistic process must be invoked, so as to obtain answers from the assessment process which are weighted based on the confidence with which each variable is known.

To evaluate the simplified assessment process, comparisons must be made between results obtained from application of the process, and results obtained from application of more detailed nonlinear dynamic analysis methods. In this fashion, the simplified method can be qualitatively (comparing predicted failure modes) and quantitatively (comparing vibration properties, loads, and earthquake spectral or scale factors causing failure) checked for consistency and conservatism relative to more rigorous analysis.

As a final task, once verified, the simplified procedures should be implemented into a program which is capable of performing the necessary calculations.

1.2 INVESTIGATION APPROACH

The investigation approach adopted for this research is diagrammed in Figure 1-1. A review of platform vibration properties was conducted by literature search. Using information in a variety of published sources together with reports provided by the project sponsors, it was established that for typical jacket-type platforms (four to twelve legs, topsides mass greater than 30% of total mass including added mass, sited in 400 ft of water or less), the first and second horizontal modes in each principal direction dominate horizontal response, while the first vertical mode dominates vertical response. A simplified procedure to estimate mode shapes and periods was developed; by separating out the primary steel structure shearing and bending displacement components and the foundation drift and rotation displacement components, flexibility matrices for lateral and vertical displacement could easily be constructed for the platform. These matrices could then be used in a proper modal analysis, or used in hand calculations to estimate vibration properties.

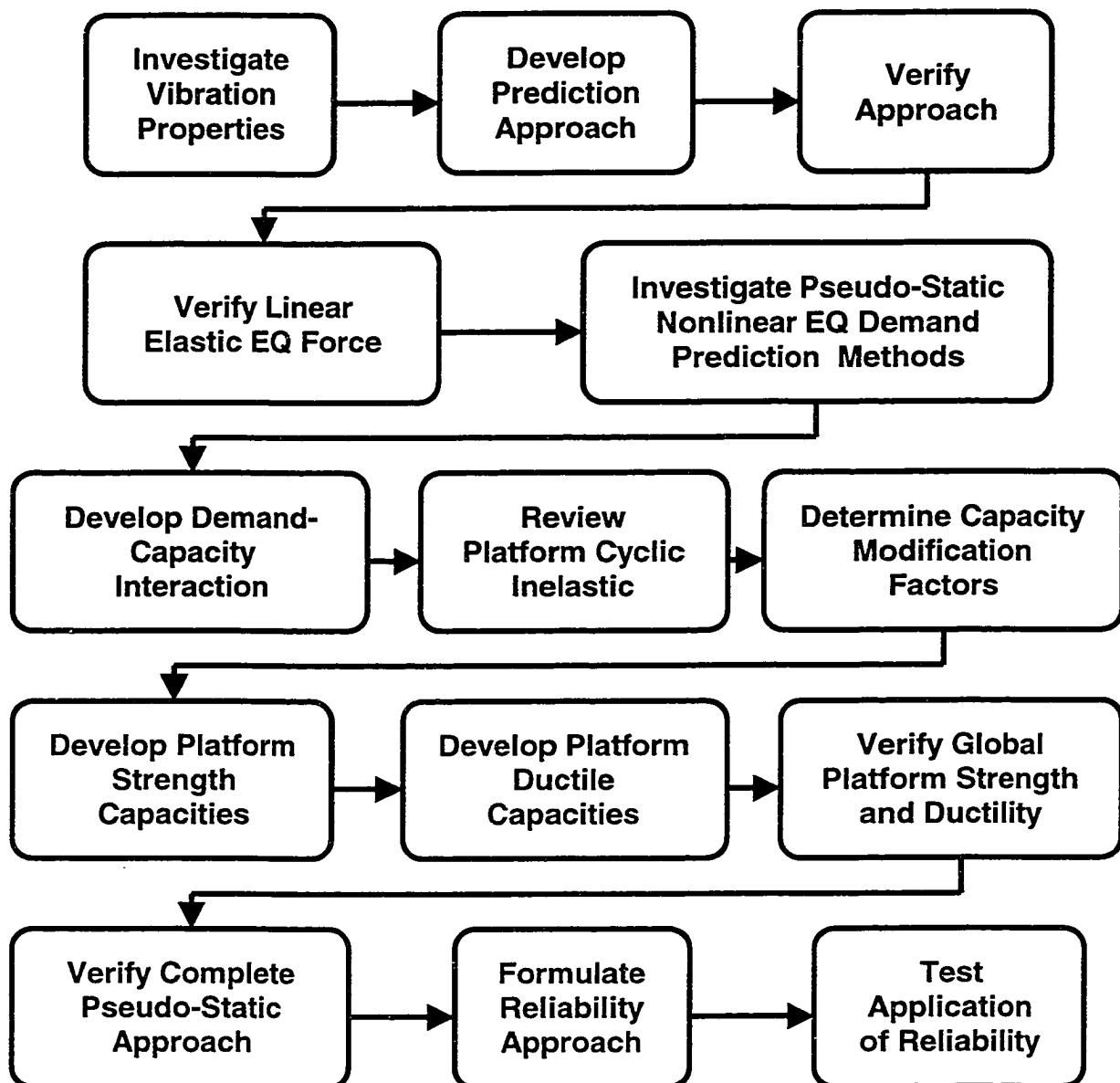


Figure 1-1: Investigation Approach Used to Develop Simplified Method

Together with a response spectrum, these modal properties could be used to estimate earthquake forces on the platform. A simple modified Uniform Building Code (1994) approach was also studied; while it was found to provide suitable estimates of modal forces,

it lacked the ability to provide information on platform displacements and accelerations. The simplified approach was then verified by application to five case study platforms, and comparison to 3-D frame analyses. A sensitivity study evaluating the effects of foundation flexibility (a variable with high uncertainty in offshore engineering) on earthquake loads was also conducted using two of the case study platforms.

A review of nonlinear pseudo-static methods of earthquake analysis was conducted by literature search. Given the tendency for most typical platform systems to be first horizontal mode dominated, it was decided that the response factor approach would provide the necessary bridge between presumed linear but actual nonlinear behavior of yielding platform systems. The literature search revealed a lack of data concerning the behavior of strength and stiffness degrading structural systems; hence a plan was developed to calculate response factors for systems which exhibit this type of behavior. Another literature search was conducted, to identify in a phenomenological sense what types of degrading behavior should be studied. The search revealed that the primary sources of degradation in platform systems subject to cyclic loading are:

- Strength degradation of piles forced to undergo large axial displacements.
- Strength and stiffness degradation of piles forced to undergo large lateral deformations.
- Strength and stiffness degradation of braced frame systems with braces which do not buckle locally.
- Strength and stiffness degradation of braced frame systems with braces which do buckle locally.

- Strength and stiffness degradation of braced frame systems with joints which fail by punching or tearing.
- Strength and stiffness degradation of braced frame systems which unzip due to weak horizontal framing systems or a lack of redundancy.

Using these types of structural degradation as a guide, the responses of a series of single degree-of-freedom (SDOF) systems which exhibited these types of hysteretic behaviors to a family of earthquake time histories recorded on rock were studied. The data from these numerical experiments were used to develop a set of capacity increase (or load reduction) factors suitable for modifying the static load capacity of platform systems which exhibit these types of degradation. These factors are intended to be selected for use with a given structural system based on a match between these systems and certain qualities which the structural system in question possesses. A limited study was also conducted to see how sensitive these factors were to damping and to time histories recorded on other soil types (alluvium, soft soil with a predominant site period). A series of comparisons was then conducted between the SDOF system responses and a number of two, three and four degree-of-freedom systems which possessed elements which would exhibit the types of degradation listed above. Providing the response of the structure was dominated by the first horizontal modes in the principal directions (modal participation of at least 70% to 80%), it was found that the degrading SDOF systems could represent the displacement behavior of the degrading multi degree-of-freedom (MDOF) systems in a reasonable manner.

Returning to the capacity aspects of assessment, the platform system was first characterized as a series system of different components (see Figure 1-2): structural bays and a foundation. Each component, in turn, was recognized as consisting of a parallel set of elements: legs, braces and joints, and piles. The yield strength of the platform is governed by the yielding of the first element in the weakest component. The ultimate strength of the platform is governed by the lowest ultimate strength of all the platform components. Beyond the displacement associated with the point of ultimate strength of the platform, the platform can tolerate additional displacement up to the point at which the platform system becomes unstable.

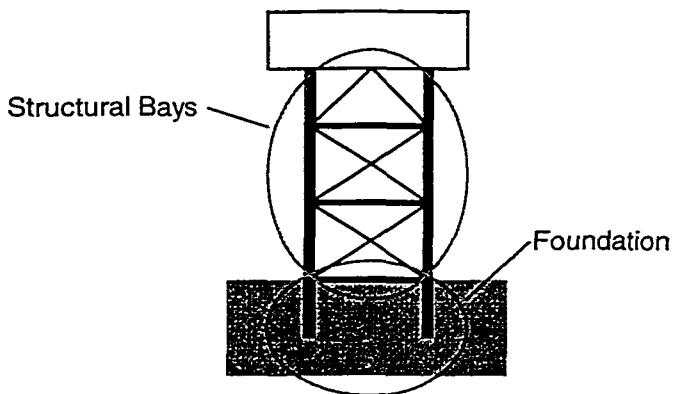


Figure 1-2: Platform Idealization

Using plastic analysis concepts together with virtual work, strength capacities of the different components were formulated. Using test data found during a literature search, cyclic displacement ductility limits were established for structural elements. These limits, set for beam-columns, are intended to capture the amount of repeatable inelastic deformation a tubular member can support without suffering local buckling. If an element's cyclic

displacement ductility limit is exceeded, it is considered incapable of supporting load. Joints were considered to have no strength past yield, unless grouted; in that case, they were assumed to behave as elastic-plastic elements. Damaged members were assumed to possess no displacement ductility. In lieu of developing a static pushover analysis procedure, approximate procedures were developed to relate global and local displacements in a yielding platform, taking into account the initial load pattern forcing the displacements, structural redundancy, stiffness and strength discontinuities, and element changes in stiffness and strength. Platform limits on global displacement ductility were established by relating back to the local cyclic displacement ductility capacities of gravity load-supporting members. The simplified global strength and global displacement ductility analysis procedures were verified through application to five case study platforms, and comparison to static pushover analysis results.

With the simplified modal properties determination procedure, simplified global strength and displacement ductility capacity calculation procedures and the nonlinear response factors developed, the deterministic portion of the assessment process was complete. To evaluate the process, the approach was applied to the analysis of the five case study platforms, which were also subjected to nonlinear dynamic analysis for a limited number of earthquake time histories. By comparing the scale factors applied to the time histories (previously scaled to the point at which yielding began in the platforms) needed to cause a certain amount of damage in the platforms during the time history analyses to the capacity modification factor associated with each platform, the accuracy and conservatism of the simplified methods could be assessed.

A mean-value first-order second moment (MVFOSM) reliability approach was adopted for use in performing reliability analysis as part of the simplified assessment approach. Safety indices are estimated for each platform component. The platform is idealized as a series system; failure of one component (structural bays or foundation) will result in failure of the complete system. Based on the results of a literature search, it was suspected that the primary source of uncertainty was to be found on the demand side (spectral ordinates); however, the uncertainty associated with the demand-capacity interaction (response factors) was also found to be significant for high levels of displacement ductility capacity. The simplified reliability approach was used to estimate the probability of failure of a small platform for a single earthquake source; the probability of failure of this platform was also estimated using a Monte Carlo approach, and the results were compared.

The simplified vibration procedure, simplified global strength and displacement ductility capacity calculation procedures and the MVFOSM reliability procedures have been incorporated into a program called TOPCAT: Template Offshore Platform Capacity Asessment Tools. The program consists of a MS Excel v7.0 workbook with 15 modules containing calculation algorithms and input/output control features written in MS Visual Basic. Information on the program and its use is available in the TOPCAT User Manual developed by Stear and Bea (1999).

1.3 OVERVIEW OF ASSESSMENT APPROACH

The assessment approach developed for this research is diagrammed in Figure 1-3. Information of the global dimensions and layout of the platform must be specified, along with joint, brace, leg and pile dimensions. A soil profile must be defined, with the user supplying soil adhesion data. A response spectrum must also be defined.

Modal properties are calculated first. The mass of the platform structure and supported equipment is calculated and lumped at the decks and horizontal framing levels of the platform. A flexibility matrix associated with four separate modes of lateral response (structure shear, structure bending, foundation drift, foundation rotation) is constructed. Only the deck legs and diagonal braces are considered for structure shear; only the legs are considered for structure bending; only the piles are considered for foundation drift and rotation. A flexibility matrix for one mode of vertical response is also constructed; only the legs and piles are considered. Using the mass and flexibility matrices, an iterative approach is used to solve the standard eigenvalue problem and determine mode shapes and periods.

Using the platform mode shapes and periods, modal responses are determined and combined. Shear demands for each bay in the structure are determined for each principal direction and left separate (braces parallel to one principal axis will not resist shears parallel to the other); shear components for both principal directions at the foundation level are combined. Axial forces from overturning are combined with axial forces from vertical response.

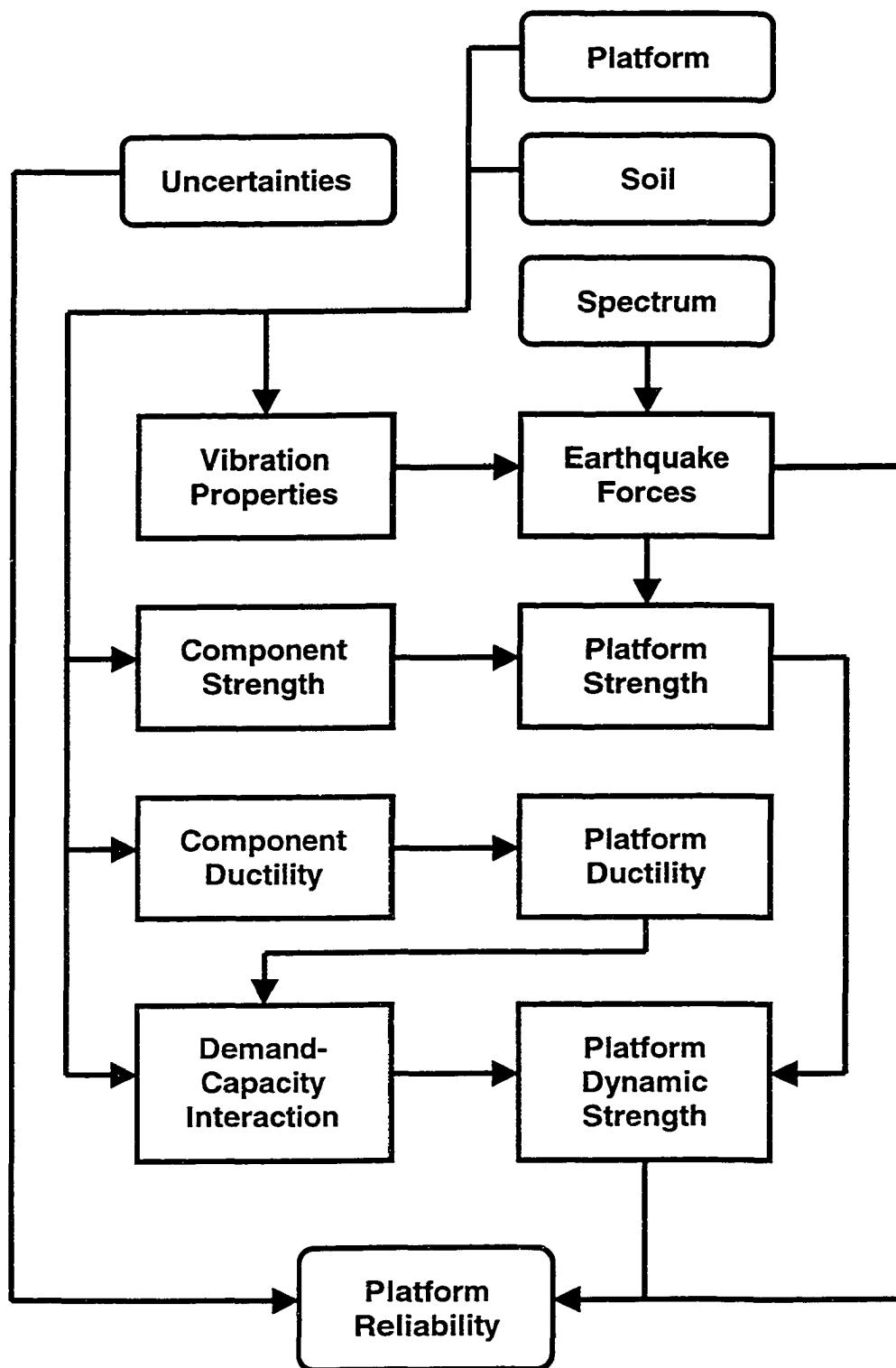


Figure 1-3: Simplified Earthquake Assessment of Platforms

Platform component strength capacities are calculated using plastic analysis and virtual work. Unbraced deck bays are assumed to reach ultimate strength when all legs have formed double hinges; the capacity of the associated portal mechanism is reduced to account for P - Δ effects. Braced bays are assumed to reach capacity when the weakest brace in the bay reaches its buckling load. The foundation will reach its lateral capacity when double hinges form in the piles; it will reach its overturning capacity when the first pile yields.

The platform global strength capacity is found by comparing the response demands with the requisite component capacities. If none of the platform components have their strength capacities exceeded, the platform is assumed to remain linear. If performing a deterministic assessment, this would be an indication of satisfactory performance. If platform components, however, have had their strengths exceeded, it is necessary to evaluate the global displacement ductility of the platform, and to determine an appropriate response factor.

The global load capacity of the platform is defined as the base shear the platform is subject to when the first component yields. Platform global displacement ductility capacity is determined by two approximate methods. With the first method, displacement is assumed to concentrate in the first component to yield. In the second method, displacement is assumed to reflect the elastic pattern of displacements associated with the lateral load pattern calculated from the response spectrum analysis. Using each approximation, the structure is allowed to displace until the displacement ductility of one of the gravity load-carrying supports is exceeded. Based on the characteristics of the component to yield, i.e. piles or structure, type of framing, member sizes, a response factor is selected and used to modify the

global base shear capacity of the platform. This modified base shear is the effective dynamic capacity of the platform, and can be compared directly to the elastically-calculated base shear found from the response spectrum analysis. If yielding is indicated in more than one component, the effective dynamic capacity is determined for each instance of yielding. Thus, a range in effective dynamic capacity is determined, depending on the displacement ductility tolerance of the elements in the different collapse mechanisms and the associated hysteretic behavior of the mechanism.

Taking into account uncertainties and biases, a MVFOSM reliability analysis is performed. Safety indices are determined for each platform component. Reliability of the platform system is taken as the lowest calculated reliability from the individual components.

1.4 ORGANIZATION OF DISSERTATION

This dissertation is organized into eight chapters:

- Chapter Two contains a summary of issues related to the seismic assessment of jacket-type platforms.
- Chapter Three describes simplified procedures by which the vibration properties of platforms are estimated, and reviews pseudo-static approaches for determining earthquake force and displacement demands.
- Chapter Four develops strength and ductility capacities of the major platform elements, formulates platform component strength capacities, and presents two approximate approaches for estimating platform global displacement ductility.

- Chapter Five examines a major aspect of demand-capacity interaction affecting jacket-type platforms: nonlinear dynamic behavior of the jacket and foundation. Response factors relating linear and nonlinear system response to earthquake excitation are developed for use with the pseudo-static assessment process.
- Chapter Six compares application of the simplified assessment approach with results from more rigorous state-of-the-art analyses for five platforms. An application of the simplified approach to a fleet twenty of platforms is also summarized.
- Chapter Seven introduces a reliability framework, using MVFOSM methods, which encompasses the simplified approach and allows for the incorporation of uncertainties into the assessment process. In addition, an example application is conducted, in order to compare the simplified reliability approach to results from a Monte Carlo simulation.
- Chapter Eight summarizes the conclusions reached by this research, and lists recommendations for future research work

CHAPTER TWO:

BACKGROUND TO EARTHQUAKE ASSESSMENT

2.0 INTRODUCTION

A typical jacket-type platform is shown in Figure 2-1. This platform consists of three major components: (1) a steel frame assemblage (referred to as the jacket or template) made up of tubular bracing members, (2) steel pipe piles which either pass through the legs of the frame assemblage or are attached at the base of the frame, and penetrate into the soil beneath the platform, and (3) a deck structure supported by tubular steel legs which are attached to the top of the frame. The deck supports drilling, production and/or support equipment. Drilling and production platforms will also support well-conductors, which are steel pipes that penetrate into the soil beneath the platform and serve as guides and conduits for drilling equipment. Conductors typically have strong lateral support at the deck and at points in the jacket, but weak vertical support. There might also be additional structural at the mudline in the way of mud mats, which are intended to keep the jacket from sinking into the foundation soil prior to the placement of the piles. The section supporting the deck will in some cases have tubular bracing like those in the jacket; however, many older platforms do not have bracing in this portion of the structure due to both constructability concerns and a desire to keep this section free of members which would increase hydrodynamic drag on the platform. Piles which penetrate through the legs of the platform (main piles) are connected to the jacket by welds at the top of the jacket; some platforms also have cement grout in the pile-jacket leg annulus. Piles attached at the bottom of the jacket (skirt piles) are either welded or grouted into guides which are connected to the jacket structure.

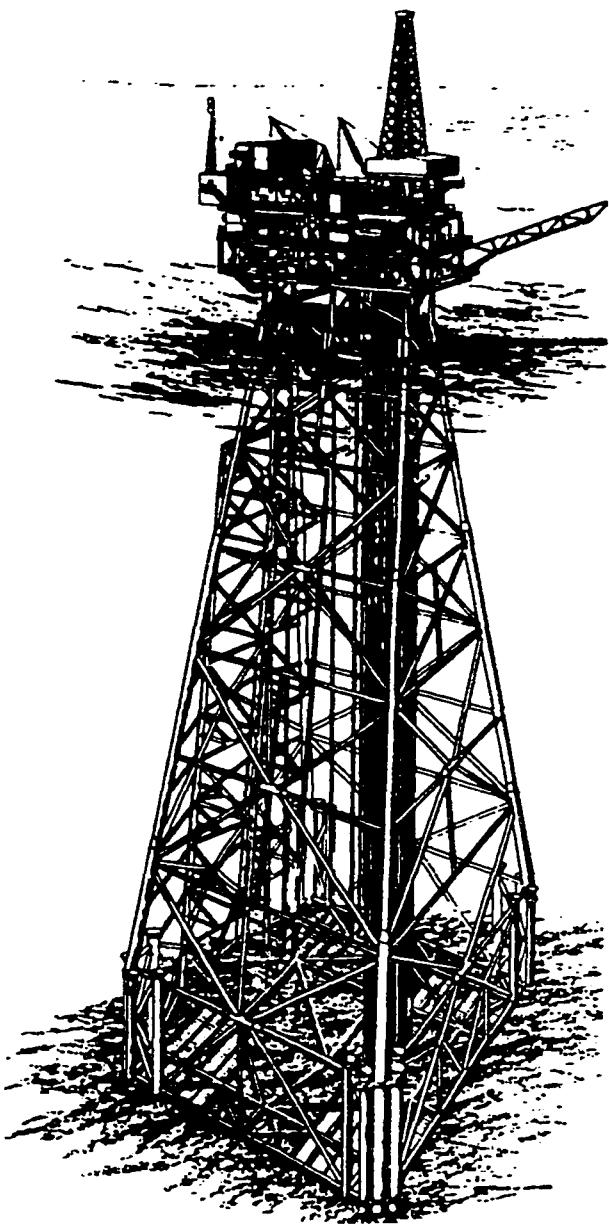


Figure 2-1: Conventional Jacket-Type Platform

There are approximately one hundred platforms similar to the one shown in Figure 2-1 in service in regions of significant historical seismicity. The majority of these platforms are located offshore southern California, with others deployed in locations such as Alaska, Japan, China, Indonesia, Venezuela and Chile. Figures 2-2 and 2-3 allow for a comparison between

areas of seismic activity and offshore oil infrastructure. Most of these one hundred platforms are in shallow to moderate water depths (a few fathoms to 400 ft), although a few are in depths close to 1,000 ft. Many of the shallow water platforms were installed in the 1960's and early 1970's, with the deeper structures being placed in the late 1970's and early 1980's.

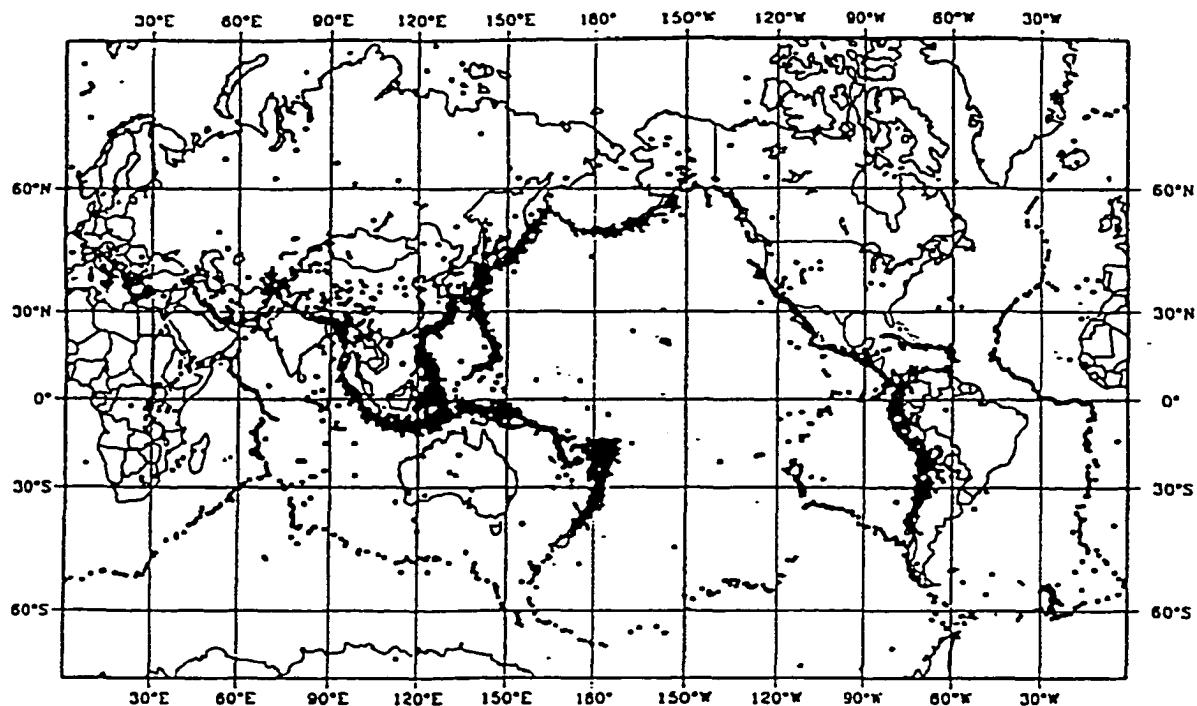


Figure 2-2: Global Seismicity (Bolt, 1993)

With the development of new exploration, drilling and recovery technologies, the oil industry has been able to increase or maintain the productivity of many fields which were originally anticipated to yield useful service lives of perhaps twenty five years. This benefit of extending field life has in turn resulted in a dilemma for the offshore oil industry; many of the platforms currently in service were designed and installed in the 1960's and 1970's, and are nearing the end of their intended service periods from a structural integrity standpoint. Many

of these older structures were designed to much lower environmental loads than are currently required by today's design standards, have damage from corrosion and accidents, and have been subject to field modifications such as the addition of equipment.

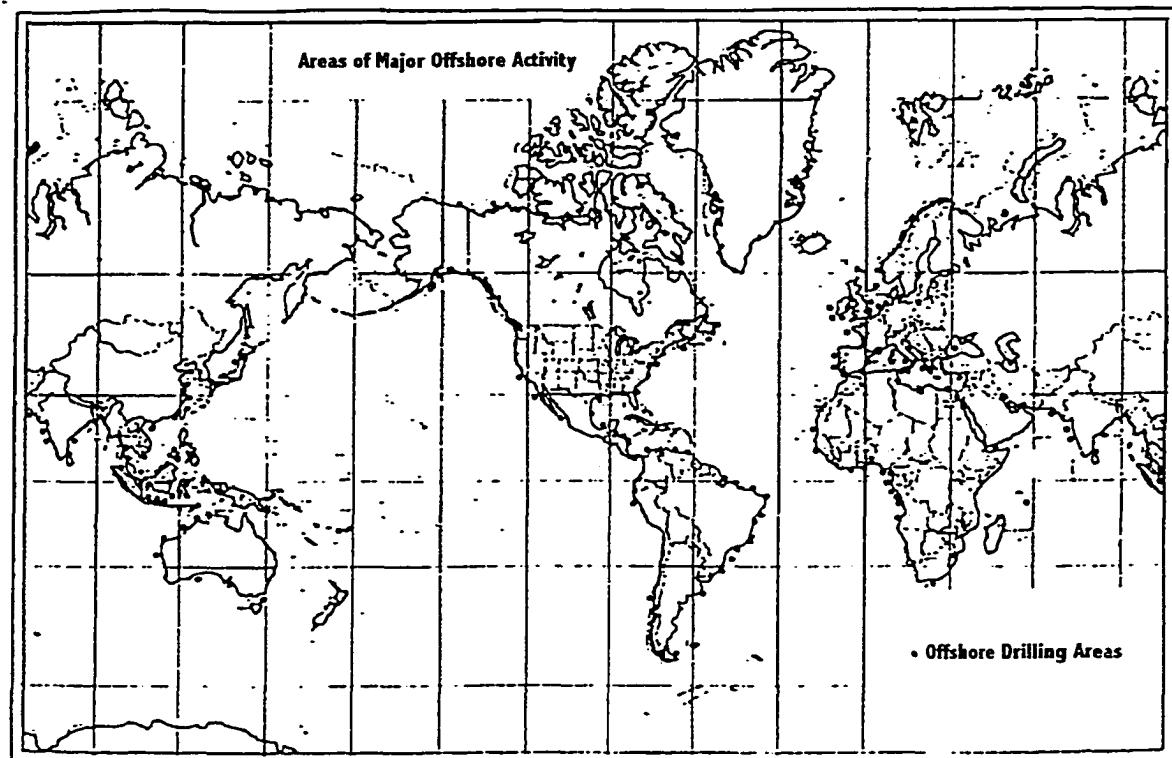


Figure 2-3: Areas of Major Offshore Activity (Smith, 1994)

While nonlinear structural analysis software packages suitable for the performance of structural integrity assessments are available, to apply this software is both expensive and requires a great deal of expertise. Application of this software to a large number of structures is impractical on grounds of cost. Hence, the concept of multi-level screening, that is, the use of successive levels of analysis of increasing complexity (and cost) to perform platform

assessments, has become very attractive. Substantial effort has been devoted in recent years to develop cheap, conservative methods of analysis, by which the bulk of the platform population can be assessed quickly, leaving the more problematic cases for further rigorous analysis. To date, simplified methods have been successfully developed and verified for the assessment of platforms for wind, wave and current forces; however, little work has been performed on methods suitable for assessing platforms for severe earthquakes.

This chapter presents background material associated with the assessment of jacket-type platforms in seismically-active regions. The concept of multi-level screening as it pertains to the offshore industry is summarized, with a short discussion of previous work performed on the development of simplified methods. A brief history of the design of offshore structures in earthquake regions is presented. Issues prompting an assessment are stated, and a review of earthquake ground motions with emphasis on the offshore environment is made. Issues concerning the evaluation of structural integrity of offshore platforms are highlighted, with an emphasis on those aspects which must be approximated by a simplified pseudo-static analysis. The chapter concludes with a brief discussion of risk policy in the offshore community and risk mitigation options.

2.1 MULTI-LEVEL SCREENING AND SIMPLIFIED ANALYSIS METHODS

In 1996, the American Petroleum Institute issued a supplement Section 17 to API RP 2A-WSD twentieth edition containing a standard methodology for the assessment of existing platforms. This supplement represents the culmination of nearly eight years of industry, government and academic endeavors to develop and evaluate methods for assessing aging

platforms. The methodology contained in the supplement is a multi-level approach to the problem of screening large fleets of platforms; the basic process is diagrammed in Figure 2-4. This process allows platform owners to arrive at assessment decisions based on qualitative analysis of such factors as life safety, failure consequence and original design basis prior to application of structural analysis. Furthermore, if the platform is unable to pass a design level analysis, the use of ultimate strength analysis methods is permitted. This process represents a departure from the previous pass-fail approach used by the industry (Miller, et al., 1990), in which platforms were assessed by linear-elastic structural analysis, with the intent of satisfying the design basis requirements contained within the current edition of API RP 2A-WSD.

An important provision contained within Section 17 allows for the use of simplified procedures for evaluation of the adequacy of existing platforms, providing they are subject to rigorous verification. Simplified methods of structural integrity assessment for platforms has been a subject of some interest to the offshore oil industry since 1990; several approaches have been developed and verified and are now being applied in practice by platform owners. Two such approaches are those developed by Bea and DesRoches (1993) and Bea and Mortazavi (1995) suitable for assessing platforms for wind, wave and current loads. These two related approaches are simple static demand-capacity analyses. Lateral load capacities for the deck bay, jacket bay and foundation (lateral and overturning) of a platform are developed using plastic analysis. Loads and capacities are confined to the principal axes of the platform, so as to maximize the demand on the jacket bays. Loads from wind, wave and current are estimated assuming the structure is lumped in line with the wave crest. A

comparison is then made between the lateral load capacity of each of the above components, and the imposed lateral load. Mortazavi and Bea (1996) have also incorporated a simplified reliability analysis into their approach, to allow for the inclusion of load and capacity uncertainties. The platform is considered to be a series system (deck bay, jacket bays, foundation), with probability of failure of the entire system governed by the lowest component probability of failure in the system.

The approaches developed by Bea and DesRoches (1993) and Bea and Mortazavi (1995) have been compared against results from static pushover analyses of several older platforms (Bea, et al., 1995; Stear, Bea, 1997A), a modified linear elastic structural analysis method (Stear, Bea, 1997B) as well as against results from displacement tests of low-redundancy frames (Mortazavi, Bea, 1997). Using base shear at ultimate strength as an index of platform capacity, the respective effective biases between the simplified analyses and the three comparisons were 1.03, 0.95 and 1.05 for the frame tests. The amount of effort which went into performing the simplified analyses was on the order of 1/30 of that required for performing and interpreting the static pushover analyses.

A surprising benefit of the simplified analyses was their utility in checking the results of the static pushover analyses; in several instances modeling errors were identified in the static pushover analyses when initial comparisons were made between the two (Bea, et al., 1995). Given the complexity of current nonlinear finite-element software, it appears inevitable that even with experienced users, modeling errors, and in some cases program errors, are an important consideration.

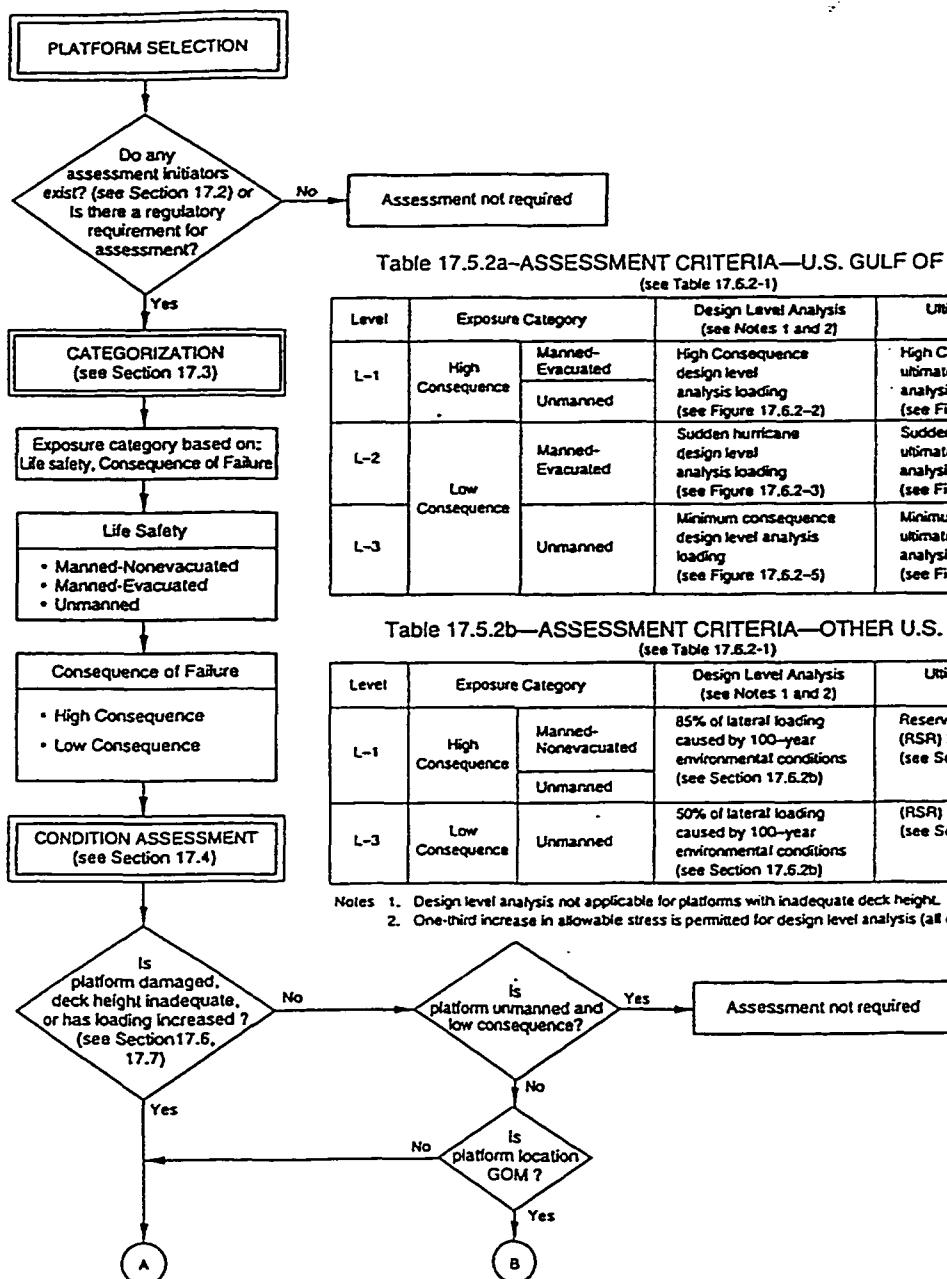


Figure 2-4A: Platform Assessment Process – Metocean Loading (API, 1996)

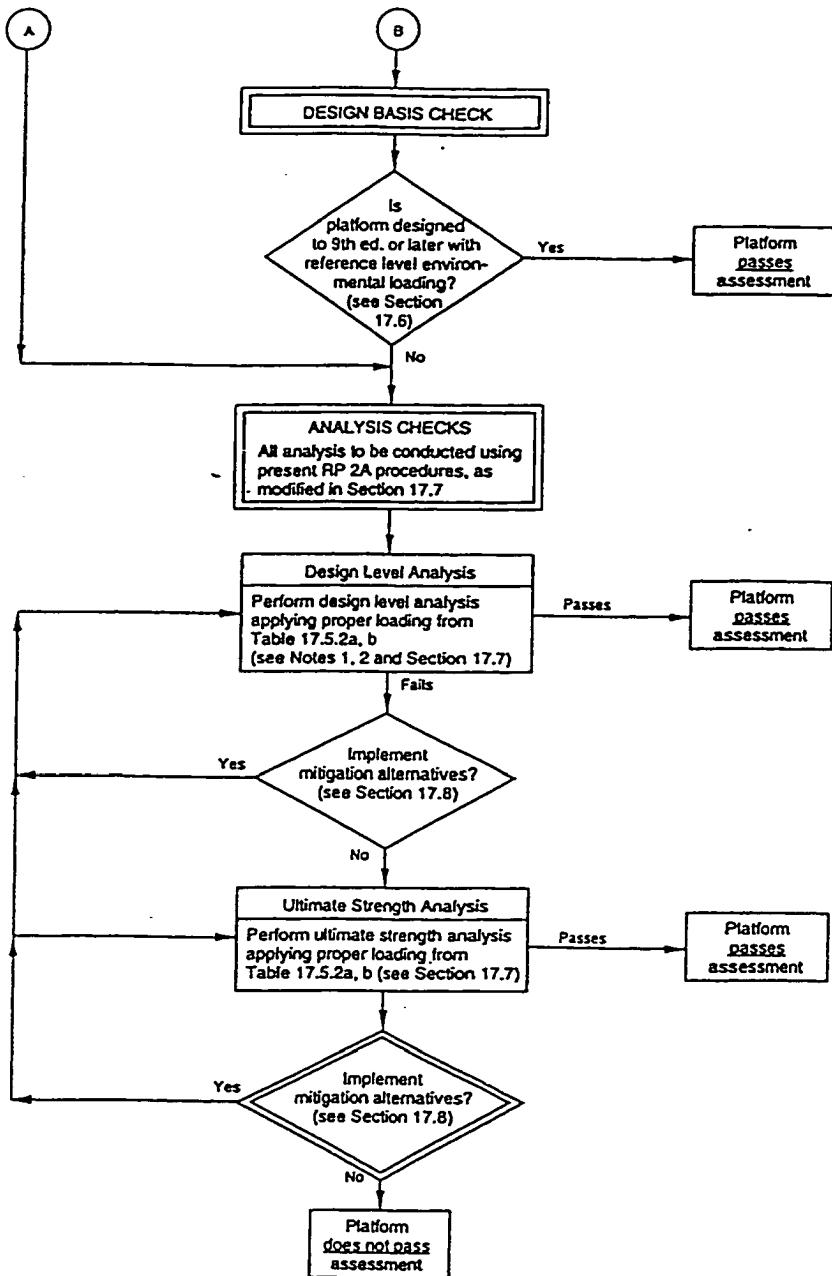


Figure 2-4B: Platform Assessment Process – Metocean Loading (API, 1996)

Recent industry efforts to assess existing platforms for earthquakes have concentrated on the application of time history analysis software to perform detailed assessments (Miller, et al.,

1990; Kallaby, et al., 1993); Section 17 recommends dynamic analysis for platforms which do not pass the initial levels of screening. “Dynamic analysis” as used within Section 17 does not preclude the use of simplified pseudo-static methods such as static pushover analysis, if sufficient justification can be shown that the equivalent static method provides results similar to those of time history analysis (Craig, Digre, 1994).

Work on simplified methods for earthquake assessment of offshore platforms has been increasing in recent years, as assessments of platforms offshore southern California continue, and as new international standards are being developed for the design of platforms subject to earthquakes. The draft of the new International Standards Organization (ISO) standard for the design of platforms for earthquakes suggests estimating earthquake loads for use with static analysis from a ductility-modified elastic response spectrum (Bea, 1996); the response spectrum ordinates are reduced by factors which relate the behavior of linear and nonlinear SDOF systems. These factors, based on a qualitative review of existing response factor approaches, are intended to represent the effective reduction in elastically-calculated load which can be gained by a yielding system with a specific type of load-displacement behavior (hysteresis) and tolerance for displacement beyond yield (ductility). This approach is identical in concept to the response or “R” factor approach contained in current editions of the Uniform Building Code. Selection of the appropriate factor to use is made based on qualitative assessment of the proposed platform’s framing system ductility and reserve or residual strength. Bea (1996) recommends that as an alternative static pushover analysis be used to establish a global load-displacement hysteresis envelope (“backbone curve”), which, together with the fundamental period and damping of the platform, can be used to define an

equivalent nonlinear SDOF system, and an appropriate factor can be chosen from other published sources. Further work is needed, however, to develop factors which are associated with a wider range of hysteretic behaviors of the type exhibited by platform structural systems, and to develop better methods to link these factors back to platform structural configuration. This topic is a major subject of this research.

2.2 OFFSHORE DESIGN FOR EARTHQUAKES

Early California platforms dating from the 1950's and 1960's were commonly designed using procedures from the Uniform Building Code, which at that time entailed static analysis of the structure subject to a lateral load associated with a 0.1 g acceleration. Vertical loads were typically not included (Miller, et al., 1990; Kallaby, et al., 1993); in some cases, earthquake loads were neglected entirely. When the first edition of API RP 2A-WSD was published in 1969, the recommendations it had for estimating earthquake forces were taken from then-current versions of the Uniform Building Code (API, 1969).

It was not until the mid 1970's that the offshore engineering community began to develop its own set of design guidelines. The seventh and eighth editions of RP 2A-WSD first proposed the use of two-level design criteria, by which platforms should be designed for:

- A strength-level earthquake, associated with a 5% to 20% probability of being exceeded during the design life of the structure (return period of approximately 100 to 200 years); the structure should essentially remain elastic for this event.
- A ductility-level earthquake, associated with a 2% to 10% probability of being exceeded during the design life of the structure (return period of approximately 1,000 to 2,000

years); the structure need not remain elastic but should be detailed to safeguard against collapse or loss of the platform from failure of equipment.

These editions of RP 2A-WSD included explicit guidelines on how the strength-level and ductility-level structural integrity performance of the platform was to be established; while strength-level performance was met by satisfaction of allowable stresses in members, ductility-level performance was satisfied by use of static pushover analysis following an approach described by Kallaby and Millman (1975). Using a load pattern associated with modal forces, and recognizing that the current recommended ratio between strength-level earthquake intensity and ductility-level earthquake intensity was two, the structure would be forced to displace until four times the strain energy absorbed by the strength-level event had been absorbed by the structure as measured through global load-deflection without loss of stability. The rational for the approach stems from observations made by Veletsos and Newmark (1960) on the relationship between the peak responses of linear and elastic-plastic systems subjected to earthquakes; in the constant-velocity range of a response spectrum (period range 0.1 to 0.5 sec) the effective reduction in elastic load for an elastic-plastic system will be given approximately by:

$$R = \sqrt{2\mu - 1}$$

The rational for the procedure stems from the concept of balancing strain energy between the true inelastic system and an equivalent elastic system subject to an elastically-calculated response spectrum load; the factor of four represents the energy which must be absorbed if the ground motion scale factor were doubled. This concept is diagrammed in Figure 2-5; the strain energies $E1$ and $E2$ must be equal.

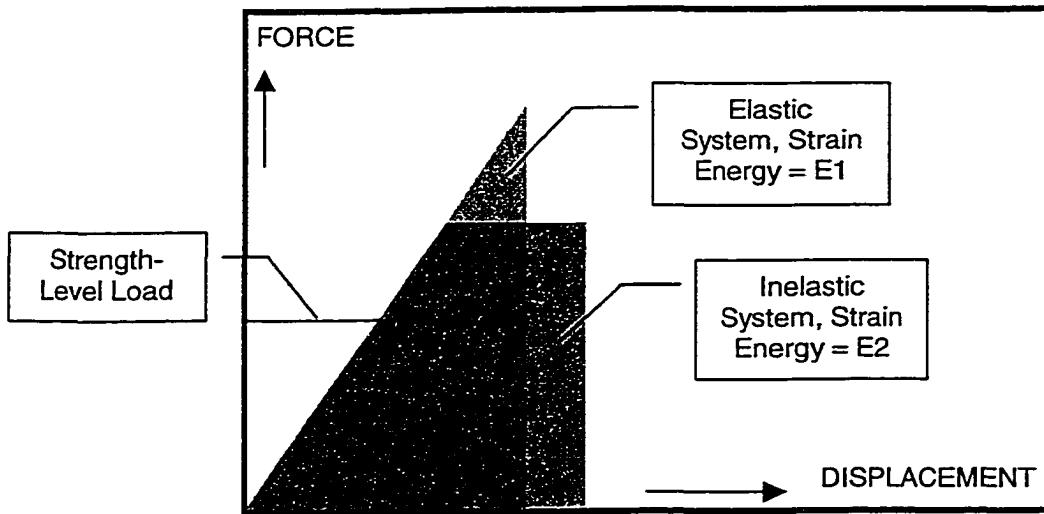


Figure 2-5: Work/Energy Balance Between Elastic and Inelastic System

Starting with the fifteenth edition of RP 2A-WSD, the explicit ductility requirements were removed, and a set of standards of good seismic design practice were substituted. These changes were based on a number of research projects which had studied the ductile performance of large, redundant platforms subjected to nonlinear time history analysis using state-of-the-art software and material modeling (API, 1984). After a review of these projects the API committee concluded that platforms would remain stable under earthquake loading in excess of strength-level providing:

- The platform being designed was detailed such that redundant, symmetric framing was used (Figure 2-6), bracing members were sized to keep slenderness ratios (kL/r) below 80 and diameter-to-thickness ratios (D/t) below $1,300/F_y$, joints were detailed to withstand the tension capacity of attached members, and cyclic soil properties were used to estimate foundation strengths and stiffnesses.

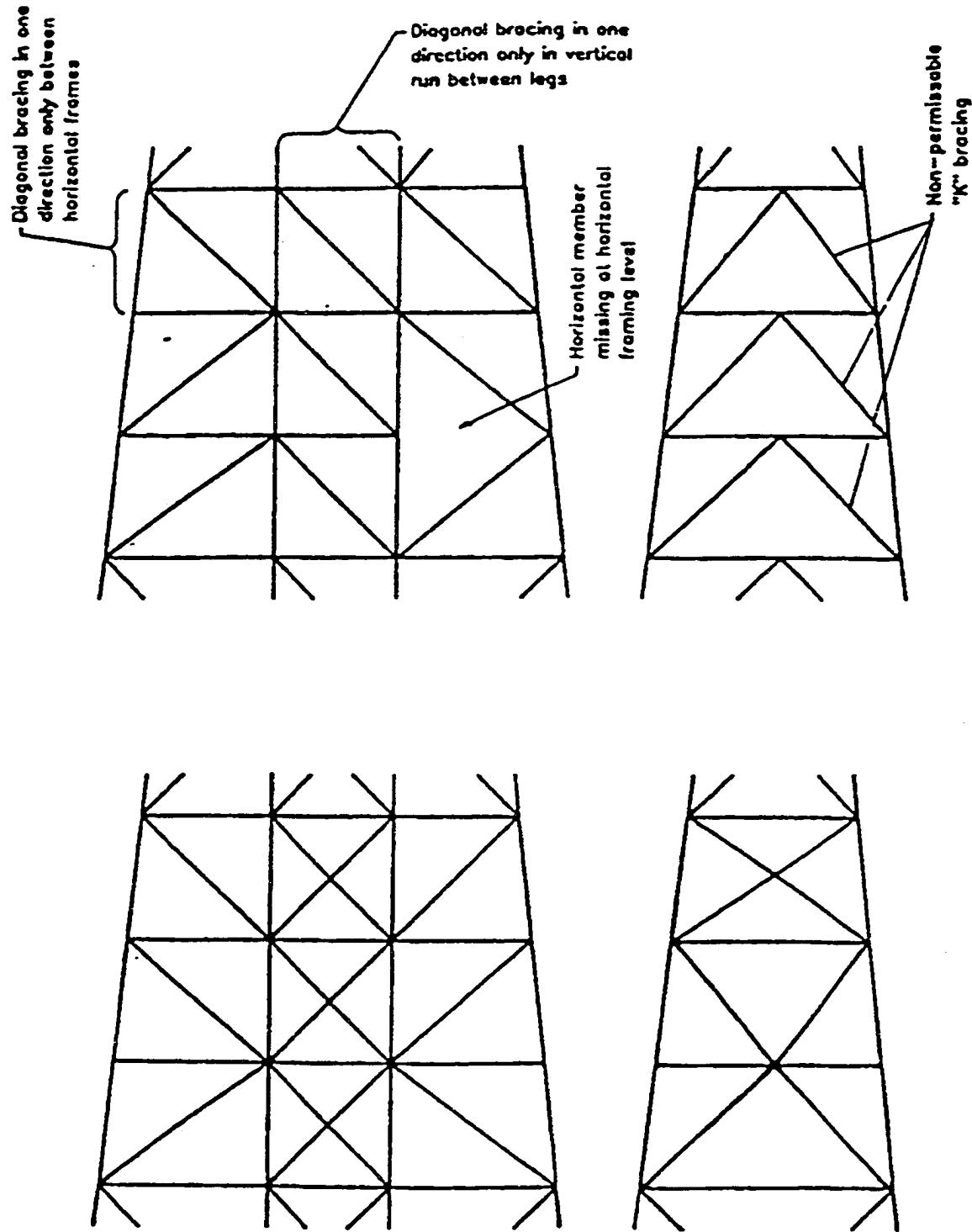


Figure 2-6: Recommended Framing for Earthquake Areas (API, 1993)

- The scale in intensity between the strength-level and ductility-level earthquake time histories was two or less (as measured by earthquake spectrum zero-period acceleration or ZPA or earthquake time history peak ground acceleration or PGA) these standards would ensure satisfactory performance.

Ductility-level analysis would be required only if these conditions were not met.

The ISO, in an effort to standardize design practices worldwide, recently began to review the earthquake provisions contained within RP 2A-WSD, with the intent of adapting them as part of a global standard. It was recognized that the provisions within RP 2A-WSD were originally developed with a focus on California and Alaska, and therefore can be too conservative for many other parts of the world (Craig, 1996). In addition, the ISO has desired to incorporate limited consequence factors into the design process, so that platforms involving life safety and environmental catastrophe will be better protected than platforms with no life safety issues and little consequence of failure (Table 2-1).

Table 2-1: Ductility-Level Earthquakes (Bea, 1996)

SSL	Category	DLE
1	Unmanned, minimum processing, little oil storage, with shut-in valves down-hole	none required
2	Intermittently manned, minimum production, little oil storage, with shut-in valves down-hole	1,000 year
3	Manned, minimum production, little oil storage, with shut-in valves down-hole	10,000 year
4	Manned, drilling or production, significant oil storage	set by owner and regulator, case by case

While a 200-year event is still recommended for the strength-level earthquake, the ductility-level earthquake is based on platform structural safety levels (SSLs) as shown in Table 2-1. The structural safety levels represent in an abstract sense the consequences which must be considered if the platform should fail in service.

2.3 ASSESSMENT FOCUS

Platform earthquake assessments generally focus on ductility-level performance, primarily for economic reasons. Older platforms have, in general, three areas of deficiency (Smith, 1994): inadequate design ground motion levels, inadequately arranged or detailed structural framing, or reduced capacity resulting from damage, corrosion or fatigue cracking. This latter item can also be an issue for new platforms, when damage occurs after installation. These deficiencies fall into four categories: design, construction, operation and accidental. These are listed below in Table 2-2.

Table 2-2: Possible Deficiencies in Platforms (Smith, 1994)

Design	Earthquake forces underestimated, inadequate jacket/deck bay framing, inadequate joint design, poor corrosion protection, unanticipated scour, gravity loads not accurate
Construction	Misalignment legs/braces/joints, undercut welds, insufficient penetration welds, tank welds, lamellar tearing, insufficient pile penetration, load-out, transportation or launch damage to primary structural elements
Operation	Corrosion protection not maintained, boat bumpers and landings not maintained, trash dumping resulting in strikes on legs and braces, field modifications to structure including addition of well conductors, production risers and deck equipment above design, poorly engineered and implemented repairs to primary structural elements
Accidental	Boat/barge collisions, dropped objects, fires, explosions and blowouts

An important step in an assessment is therefore the preparation of a platform condition report. After a full service life, it is very likely that the platform which is in place will be somewhat different from the platform design drawings.

2.4 EARTHQUAKE GROUND MOTIONS IN THE OFFSHORE ENVIRONMENT

Up-to-date estimates of the loading environment are established by a review of the current design guidelines existing for the region in which the platform is located. In the case of an earthquake assessment, this could entail the development of a site-specific set of earthquake ground motions (either as a family of time histories, or by developing a response spectrum). Prediction of earthquake ground motions at offshore locations is not the focus of this research. However, for the purpose of completeness the procedure used to determine the ground motions a platform might be subject to at a given location will be summarized. Special attention is given to differences between onshore and offshore motions.

Earthquake ground motions are primarily caused by the sudden release of energy resulting from the slippage or rupture of rock along fractures in the earth's crust known as faults. The energy released propagates outward from the location of the rupture in the form of waves; these waves are felt as ground motion as they propagate through locations near the rupture zone.

Of prime importance to the engineer are recordings of the time-dependent variation in ground acceleration, velocity and displacement resulting from past earthquakes. With this information, it is possible to construct site response spectra and to perform more complex

time history analysis. The problem becomes one of selecting which time history traces of ground motion to use in order to characterize the likely motions at the site.

Selection of ground motions will depend upon the following:

- The earthquake sources likely to affect the site (i.e., faults).
- The intervening geology between the site and the source faults.
- The geology local to the site.

By matching source, intervening geology and local geology characteristics for the site in question to those of the recording sites, the engineer can obtain a picture of the types of earthquake ground motions which might affect the site due to different source faults. However, this process is very empirical, and quite often it is necessary to scale or modify existing ground motion records in some way to make up for the lack of a perfect match between recording sites and the site under investigation.

Earthquake fault sources will be characterized by type, distance to site, depth below ground surface, potential rupture length, slip or displacement rate, and historical activity (Idriss, 1985). Fault type and potential rupture length have been correlated to likely earthquake magnitude, which, together with distance, can be used to scale ground motions via common attenuation relationships relating peak ground acceleration and peak ground velocity to magnitude and distance. Depth below ground will help characterize the frequency content of the motions; shallow earthquakes tend to have very high accelerations near the fault source indicating energy in the high frequency range, while for deep sources, much of the high frequency range will be damped out. Fault type and distance have also been correlated with

shaking duration; reverse-type faults in subduction zones have been responsible for some of the longer duration earthquakes recorded (Prince William Sound, Alaska, 1964; Valparaíso, Chile, 1985; Michoacán, Mexico, 1985), while the “spreading” in time phenomenon associated with the propagation of seismic waves is well-established (Bolt, 1993). Slip rate and historical activity are used to estimate the likelihood of an earthquake actually occurring on the fault during a given period of time; this is crucial in establishing a probability of occurrence for a given earthquake magnitude at a source fault for an exposure time interval.

The effects of intervening geology on ground motion are still a subject of much research. The geology of the material through which the waves pass may change the general attenuation patterns somewhat; the size of seismic waves may be either increased or decreased as they pass from rigid rock to softer materials. Also, waves may be reflected off layers of stiff soil, hence changing the general pattern of propagation (Bolt, 1993).

Local soil conditions can have a great impact on the ground motions induced by passing seismic waves. Pockets of soft soil surrounded by firm soils and transition areas between firm and soft soils can be excited into motion if the passing waves possess frequencies close to the frequencies of the soil column at the site; these can result in great amplification of ground motion, as seen in western region of the old lake zone of Mexico City in the 1985 Michoacán earthquake, and to a lesser degree in the Marina District of San Francisco in the 1989 Loma Prieta earthquake (Bolt, 1993). In many cases, finite-element models of the soil column at a known soft-soil site will be developed and subject to base ground motions

recorded at rock or firm sites, in order to evaluate the resulting motions at the surface of the soil column which can occur from resonant action.

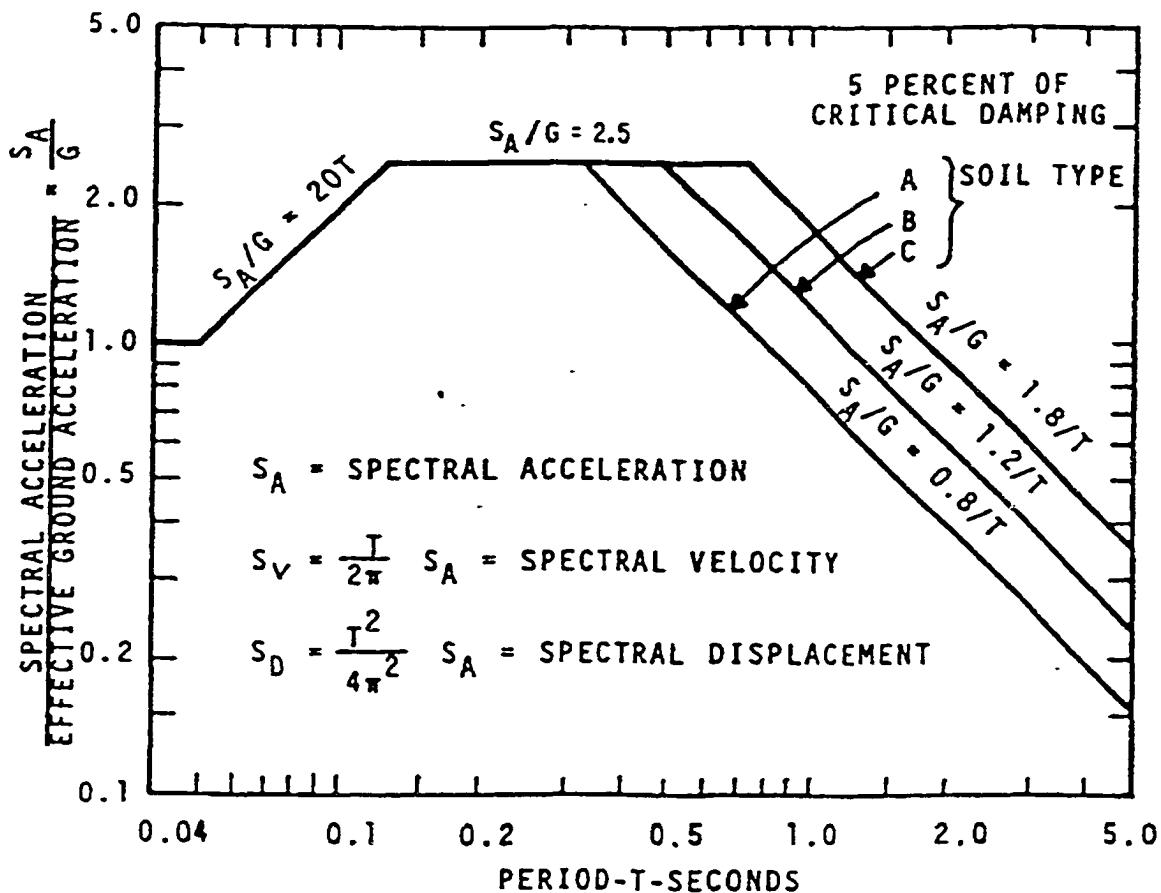
The number and variety of recorded ground motions existing today is growing, but the majority of records are from earthquakes which have occurred in the past twenty years (Naeim, Anderson, 1993). While synthetic ground motion time histories are available, from the author's perspective there is still a general preference within the engineering community to use historically-recorded motions.

Determining the earthquake sources which can affect an offshore site poses a special challenge, as the seismic history of offshore regions is not well known (Smith, 1994). In addition, the number of recorded records at offshore sites is very small. Those records which have been made exhibit characteristics which are different in some ways from their onshore counterparts. As mentioned previously, it is recognized that local pockets of very soft soils and transition zones from firm to soft soils can exhibit severe resonance for certain ground motions, resulting in amplification of ground excitation as compared to nearby sites on firm soil or rock. This has been demonstrated in recent years in both the 1985 Michoacán and the 1989 Loma Prieta earthquakes (Bolt, 1993). However, while many offshore regions consist of layers of soft soils overlaying firm soils, this type of destructive resonance has not yet been observed. This could be due to a number of factors. Reece, et al. (1981) suggested that ground excitation might rapidly attenuate in extended regions of saturated seafloor soils, and that severe resonance might occur only in pockets of soft soil surrounded by firm or near the transition areas between firm soil and soft soil.

Reece, et al. (1981) noted in a limited study of earthquake ground motions that horizontal accelerations for offshore sites were perhaps 10% to 20% lower than for corresponding onshore sites for recordings taken at similar distances during the same event. A comparison made by Smith (1994) of several onshore and offshore records taken during the same earthquake indicated that for equal epicentral distances, there was no significant difference between the horizontal accelerations recorded at the two sites, but the vertical accelerations at the offshore site were perhaps 50% as strong as those at the onshore site. This difference in vertical accelerations between onshore and offshore sites was also documented by Sleefe (1990), who noticed differences of up to a full order of magnitude between onshore and offshore vertical accelerations. Crouse (1992) has suggested that this difference may be due to the presence of deep water above the offshore sites. Vertical components of earthquake acceleration are typically composed of propagating P-waves (primary, or compression waves), while horizontal accelerations are mainly due to S-waves (secondary or shear waves). Water cannot transmit shear, but can transmit compression; therefore this may serve to substantially change onshore and offshore vertical accelerations. API (1993), however, suggests to conservatively assume that peak vertical acceleration should be taken as 50% of the peak horizontal acceleration, which is the current practice used by the onshore structural engineering community.

API (1993) includes elastic design response spectra for use in preliminary design (Figure 2-7). The spectra were developed for $\xi = 5\%$ critical damping; if the system has different damping the spectral ordinates can be adjusted by:

$$D = \frac{\ln(100/\xi)}{\ln(100/5)}$$



SOIL TYPE

- ROCK — CRYSTALLINE, CONGLOMERATE, OR SHALE-LIKE MATERIAL GENERALLY HAVING SHEAR WAVE VELOCITIES IN EXCESS OF 914 M/SEC (3000 FT/SEC).
- SHALLOW STRONG ALLUVIUM — COMPETENT SANDS, SILTS AND STIFF CLAYS WITH SHEAR STRENGTHS IN EXCESS OF ABOUT 72 kPa (1500 PSF), LIMITED TO DEPTHS OF LESS THAN ABOUT 61 M (200 FT), AND OVERLYING ROCK-LIKE MATERIALS.
- DEEP STRONG ALLUVIUM — COMPETENT SANDS, SILTS AND STIFF CLAYS WITH THICKNESSES IN EXCESS OF ABOUT 61 M (200 FT) AND OVERLYING ROCK-LIKE MATERIALS.

Figure 2-7: Normalized Response Spectra (API, 1993)

For strength-level analysis, the spectra are scaled according to five different zones, much in the same way the UBC response spectrum is categorized. The zones, and their corresponding effective horizontal ground accelerations, are shown in Table 2-3:

Table 2-3: Seismic Zones and Scale Factors (API, 1993)

Z	1	2	3	4	5
G	0.05	0.10	0.20	0.25	0.4

These spectra are intended for use off the coasts of the United States, including Alaska and Hawaii. The accelerations are associated with a return period of 200 years.

An elastic design response spectrum have also been developed as part of the ISO process to develop standard earthquake design guidelines for offshore platforms (Crouse, 1996; Bea, et al., 1999). Effort has been made to take advantage of seismic hazard data which has been collected over the past twenty years, including geological, tectonic, and seismicity data, ground-motion data recorded in different tectonic regimes and on different local geologies, and probabilistic seismic hazard studies performed at many sites and regions around the world. The ISO spectrum is shown in Figure 2-8. The spectrum is scaled much like the API (1993) spectrum for five different zones around the world; the ground accelerations associated with the zones are obtained by dividing the zone number by ten. These values of ground acceleration correspond to the 200-year return period event associated with each region.

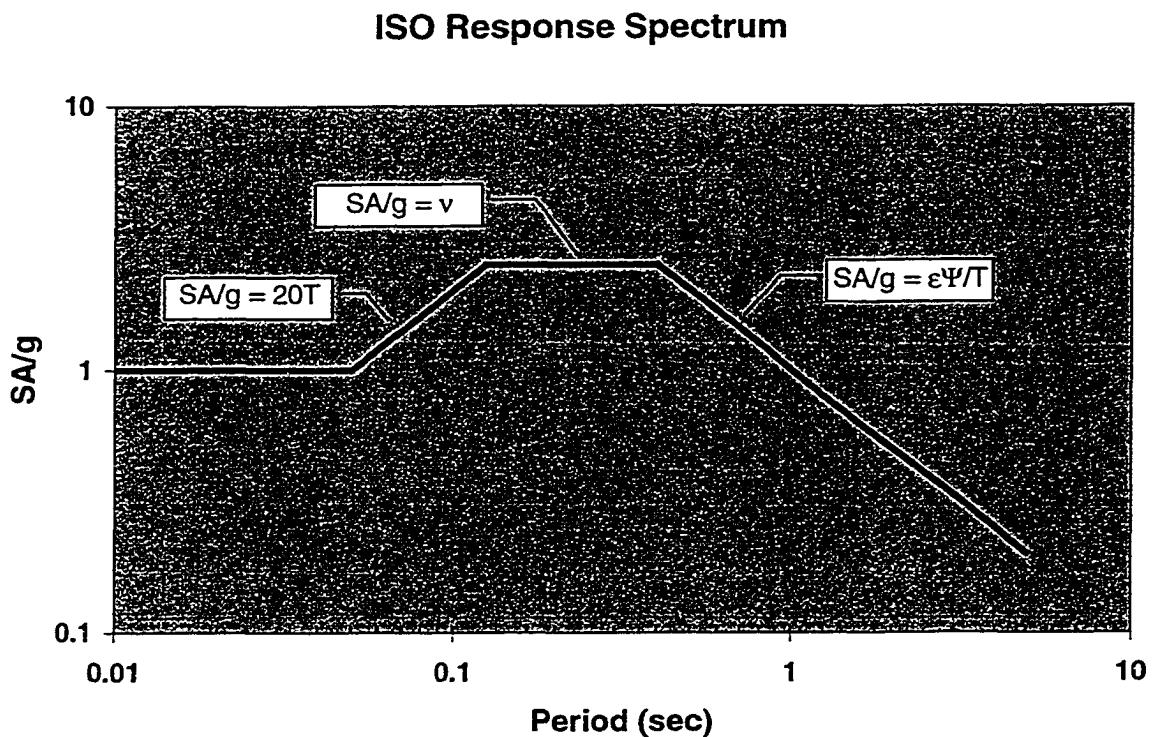


Figure 2-8: Elastic Design Response Spectrum (Bea, et al., 1999)

This spectrum has also been developed for $\xi = 5\%$ critical damping; the same scale factor D suggested by API (1993) can be applied to adjust the spectral ordinates in a different value of damping is needed. The spectrum is identical to the API (1993) response spectra for periods less than 0.125 sec. For periods higher than 0.125 sec, the spectra shape are controlled by three parameters: v , a site classification factor for the short period range controlled by local soil conditions; Ψ , a site classification factor for the long period range controlled by local soil conditions; and ε , a site classification factor for the long period range controlled by seismotectonic conditions. These factors are shown in Tables 2-4 and 2-5 for a range of soil and seismotectonic conditions.

Table 2-4: Spectrum Soil Amplification Factors (Bea, et al., 1999)

Class	Site	Shear Wave Velocity (fps)	ψ	ν
A	Rock	$V_s \geq 2,500$	1.0	2.5
B	Stiff to Very Stiff Soils	$2,500 > V_s \geq 1,200$	1.25	3.3
C	Moderately Stiff Soils	$1,200 > V_s \geq 600$	1.5	3.5
D	Soft to Medium Stiff Clays ¹	$V_s \leq 600$	2.0	4.5
E	Unusual	?		do site-specific study

¹ Layer should be greater than 10 ft thick

Table 2-5: Spectrum Amplification for Seismotectonic Condition (Bea, et al., 1999)

Seismotectonic Condition	ϵ
Shallow Crustal Faulting Zones	1.0
Deep Subduction Zones	0.8
Mixed Shallow Crustal Faulting and Deep Subduction Zones	0.9
Intraplate Zones	0.8
default	1.0

It is emphasized that both the API and ISO spectra are very approximate, and are intended for preliminary design or assessment purposes. Both carry the caution that in moderate to high zones of seismicity where high consequence of failure is a concern or where unstable soils exist, a site-specific study should be performed.

2.5 EVALUATING STRUCTURAL INTEGRITY

The fundamental goal of a structural integrity assessment is to ensure that the load capacity of the platform is not exceeded by the demand placed upon it by environmental or operational conditions. In assessing a platform for earthquakes, the analysts desires to demonstrate that the platform members will not suffer damage during a strength-level event, and that the composite platform system will not collapse during a ductility-level event. To accomplish this task requires knowledge of the strength and ductility of platform elements (braces, legs,

joints, mats, piles), and a method for translating earthquake excitation into forces and displacements on these elements and the platform system as a whole.

A vibrating platform is a complicated dynamic system. There will be significant fluid-structure interaction, in the way of added hydrodynamic mass and hydrodynamic radiation and drag damping; these interactions will depend on the shape, surface, rigidity, and orientation of members as well as on the effective flow conditions of the fluid (Clough, 1960). There will also be significant soil-structure interaction; soil surrounding the foundation piles beneath the platform will be deformed plastically even at low levels of dynamic excitation, energy can be radiated away from the structure into the soil medium, soil mass can be excited into motion and soil properties will change in relation to the loading rate, amount of deformation, and number of loading cycles (Bea, 1980). Load-displacement behaviors of piles forced to displace beyond their effective yield point are shown in Figures 2-9 and 2-10. There might also be a danger of liquefaction of the foundation soils when subjected to vibration, which results in a loss of shear strength. Finally, depending on the amplitude and duration of motion, members in the steel portion of the structure might yield, buckle, or fracture. Load-displacement behavior of tubular beam-columns and axial struts are shown in Figures 2-11 and 2-12; global frame behaviors for an X-braced frame and K-braced frame are shown in Figures 2-13 and 2-14.

Explicit consideration of these effects requires nonlinear time history analysis. There exist today many excellent commercial analysis tools such as CAP/SEASTAR, KARMA and USFOS which enable an engineer to perform analyses of this type, but operation of these

tools requires considerable time, data storage space, and above all else, good engineering judgment. Simply possessing the capability to perform very detailed analyses provides no assurance that models which represent the likely behavior of a structure will be developed (Bea, 1986). Analysis resources may be better spent on several simpler analyses rather than one or two very complex ones. The very complex nature of the problem together with the uncertainties in the fluid-structure, soil-structure and structural member behavior emphasizes the point that models which consider a range of behavior should be used (API, 1993).

Even with powerful dynamic analysis tools, there is still an element of approximation involved in the actual analysis. Material properties for some elements such as soil will be known only with great uncertainty. The actual properties of the soil beneath the platform can only be obtained by sampling, and it has been well-established from experience that sampling techniques cannot currently eliminate much of the uncertainty associated with soil properties, and that the techniques themselves may introduce bias and additional uncertainty into the soil property estimates (Bea, 1986). While physical theory models of braces have advanced to great levels of sophistication, some aspects of cyclic post-buckling behavior can still only be accounted for through phenomenological means. The phenomenological relationships developed to represent the effects of local buckling and fracture in cycling braces are based on limited sets of test data accumulated from sources such as Sherman (1980) and Zayas, et al. (1980B).

Application of nonlinear time history techniques requires considerable judgment to determine what exactly constitutes “failure” of a platform system or any other structure system (Craig, et al., 1993). Measures to determine failure might be:

- Global (deck) displacement
- Local deformation (story drift, joint distortion, brace strain, plastic hinge rotations)
- Energy absorption (accumulated strain energy in elements)
- Residual static capacity (pushover capacity after the extreme seismic event)
- The point of instability in the numerical solution of the problem.

A combination of several of the above is likely the best approach.

Means exist to approximate many of the special dynamic effects within the framework of modal analysis and static analysis. Added mass is calculated based on the projected area of members in the direction of expected motion, and added to the mass of the structure as a constant (Clough, 1960); fluid damping is usually represented by a small contribution to modal damping or neglected entirely (Newmark, Rosenblueth, 1971). The effects of nonlinear load-displacement behavior in structural elements on the global response of a platform can be approximated by considering the platform to effectively behave as a nonlinear SDOF system, and then either:

- Use a SDOF system with hysteretic behavior matching that of the platform to estimate a normalized peak displacement of the platform system, and relate this normalized displacement back to local element displacements by the static pushover analysis displacement pattern.

- Use a response factor based on statistical comparisons between elastic SDOF systems and nonlinear SDOF systems with load-displacement behaviors similar to that of the global platform system to factor down the elastically-calculated loads on the platform, implicitly accounting for nonlinear behavior of the platform system.

The two major issues facing application of pseudo-static approaches to the analysis of offshore platforms are the need for (1) meaningful displacement limits for platform structural elements which will implicitly account for the effects of cyclic loading, and (2) response factors which relate the types of nonlinear load-displacement behaviors exhibited by platform structural elements, and in turn the global platform system, to elastic platform response. To address these issues, the behaviors of platform structural elements and complete platform structural systems and previous work on the subject of response factors for platforms should be reviewed.

2.5.1 Beam-Columns

Beam-columns make up the legs and piles of offshore platforms. Typical performance of a semi-compact steel tubular cantilever beam-column under lateral load as part of a portal mechanism is shown in Figure 2-9. The stiffness of the cantilever softens after the initiation of yielding at its base from combined bending and axial stresses. Lateral load can increase until either a plastic hinge forms at the base of the cantilever and/or local buckling of the tube wall begins. Following local buckling, effective lateral load capacity will decrease. Inelastic cycling of the cantilever will lead to fracture in the locally-buckled region.

Sherman (1979) studied the monotonic and cyclic post-local buckling behavior of tubular beam-columns in a project funded by Shell Oil Company. The tests used sets of tubulars with D/t ratios of 36 (PA series, L/D ratio of 4.5), 48 (PB series, L/D ratio of 4.4 and PC series, L/D ratio 11.1) and 80 (PD series, L/D ratio 4.3), and axial loads P/P_y of approximately 0.0, 0.2, 0.4, 0.6 and 0.8. For the cyclic tests, these members were cycled in a cantilever fashion to peak unidirectional displacement ductilities (measured from a reference point established by assuming the load-displacement behavior up to the point of maximum supportable load was nearly linear, instead of using the true yield point) ranging from 2.0 to 10.2 until failure occurred (defined by tearing and/or less than 10% of maximum measured lateral load capacity remaining).

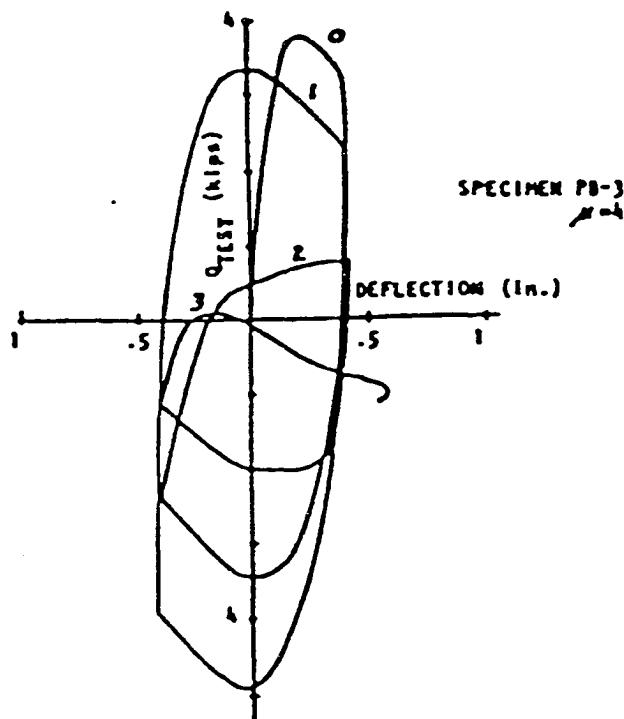


Figure 2-9: Cyclic Inelastic Behavior of Tubular Beam-Column Cantilever
(Sherman, 1979)

These tests indicated that even for small ($0.2 P/P_y$) values of axial load and low ($\mu = 2$) ductility demands, test specimens of series PB, PC and PD exhibited severe strength degradation (as much as 70%) after the first two or three complete cycles from local buckling; many specimens failed after less than six cycles. The PA series specimens, which were not tested for $\mu = 2$, performed similarly at $\mu = 4$, but for only two of three cycles before failure. While these results represent a limited data set, cursory examination indicates tubular beam-columns of this type, which encompass most platform legs and pipe piles, should not be expected to perform well inelastically when forced to displace laterally as part of a portal mechanism in the presence of vertical load.

2.5.2 Braces

Struts, or braces, make up the lateral load-resisting elements of the steel portion of a jacket-type platform. Typical performance of steel tubular struts is shown in Figures 2-10 and 2-11. Following buckling, the strut becomes unstable, and must shed axial load. The range over which this occurs is variable, and depends upon the section properties and effective length. Reloading straightens the strut out, placing it in tension. Subsequent cycles of compression and tension will exhibit a reduction in effective buckling load, and continued cycling at high strain will result in local buckling and fracture.

Sherman (1980) also studied the monotonic and cyclic post-local buckling behavior of tubular struts. The tests used sets of tubulars with D/t ratios of 36 (SA series, L/D ratio of 20), 48 (SB series, L/D ratio of 20, and SC series, L/D ratio of 50) and 80 (SD series, L/D ratio of 20), and two-point lateral loads Q/Q_y of approximately 0.0, 0.1, 0.2, 0.4 and 0.8. All

members had fixed end conditions, so the effective lengths of all test specimens can be considered near 0.5. These members were cycled axially to peak unidirectional displacement ductilities ranging from 2.0 to 9.2 until failure occurred (defined by tearing and/or less than 10% of maximum measured axial load capacity remaining). The SA series struts tended to degrade to 50% of original axial capacity over 10 cycles of $\mu = 4$, even in the presence of a lateral load of $Q/Q_y = 0.8$. The SB series performed similarly, but began to deteriorate and fail for lateral loads of $Q/Q_y = 0.4$. The SC series performed similarly to SB for a lower level of cyclic displacement ($\mu = 2$), while the SD series exhibited very limited post-buckling displacement ductility.

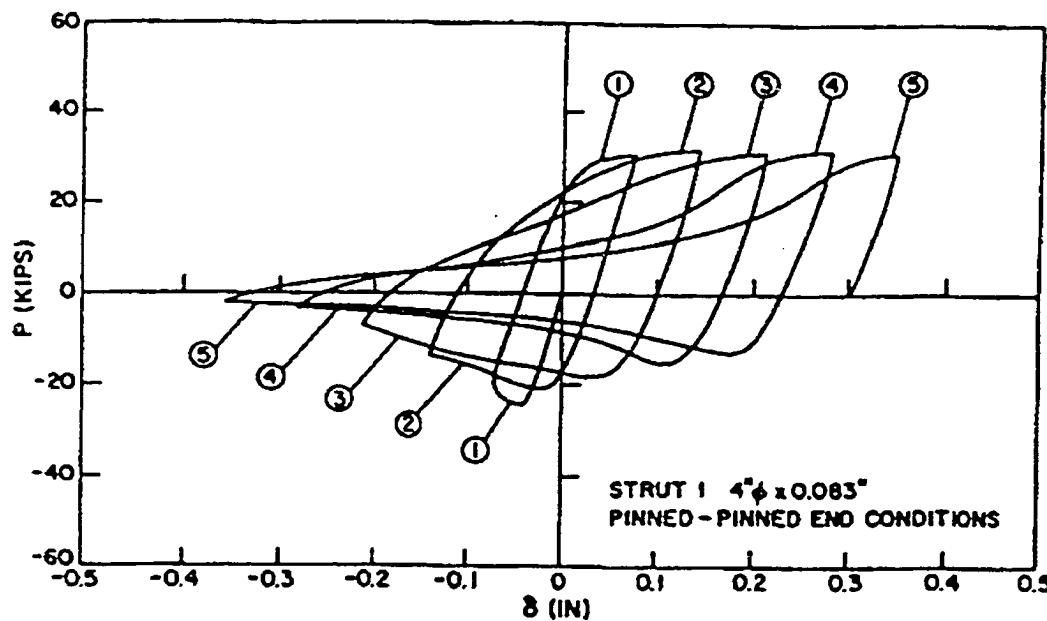


Figure 2-10: Cyclic Inelastic Behavior of a Tubular Strut, $D/t = 48$, $kL/r = 54$
(Zayas, et al., 1980B)

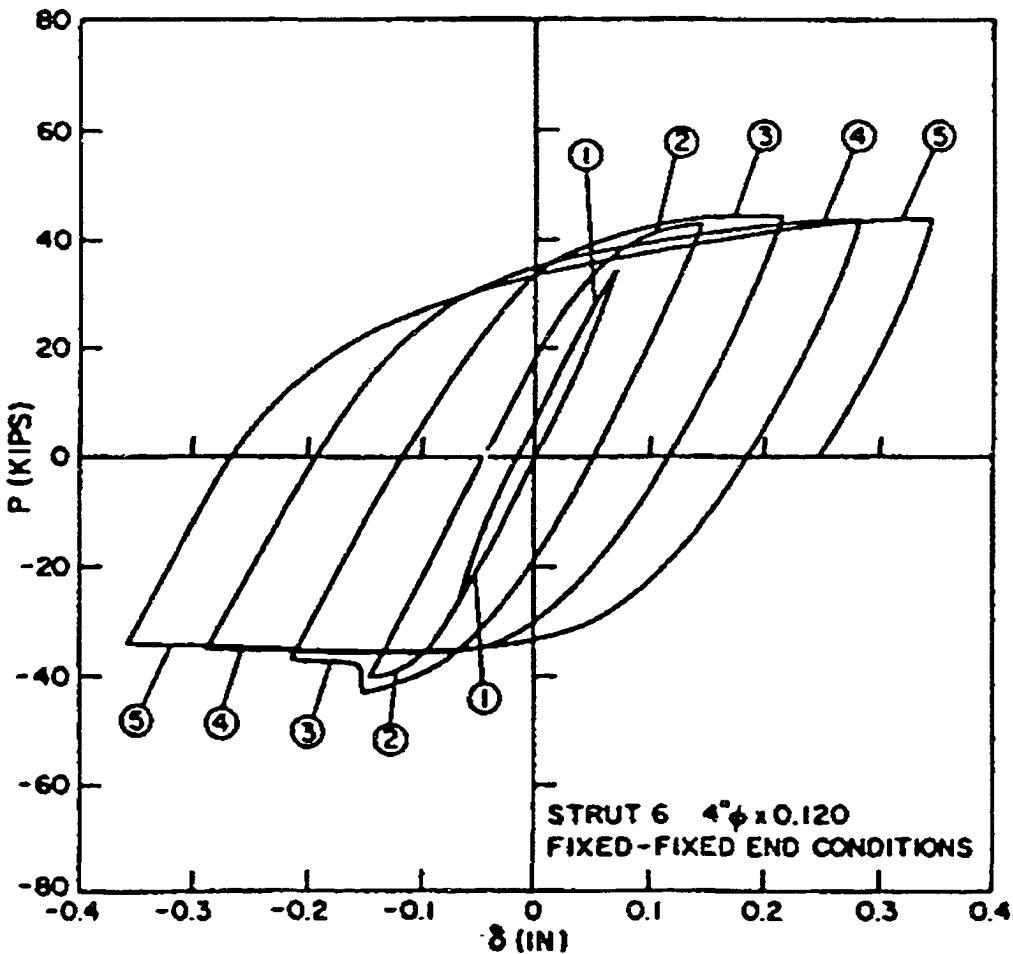


Figure 2-11: Cyclic Inelastic Behavior of a Tubular Strut, $D/t = 33$, $kL/r = 24$
 (Zayas, et al., 1980B)

Zayas, et al. (1980B) studied the cyclic post-buckling behavior of tubular struts as part of a project at U. C. Berkeley focussed on the earthquake performance of tubular offshore platforms. The tubular tests used sets of tubulars, both annealed and un-annealed steel, with D/t ratios of 33 and 48 and kL/r ratios of 25 (fixed) and 54 (pinned). The members were cycled axially, with progressively increasing levels of ductility demand over the course of 15 cycles. The annealed struts clearly outperformed those which were not heat-treated. The

strut with D/t of 33 and kL/r of 24 developed displacement ductilities of 6 or more without a reduction of more than 50% in axial capacity, over the course of 15 cycles. The strut with D/t of 48 and kL/r of 54 developed displacement ductilities of less than 3 before suffering a reduction of more than 50% in axial capacity from local buckling, over the course of 3 cycles.

2.5.3 Piles

Tubular steel pile piles make up the foundations of jacket-type platforms. For certain types of soils, load-displacement behavior at the pile head will exhibit substantial strength degradation, and moderate stiffness degradation, when the pile is subject to cyclic inelastic loading.

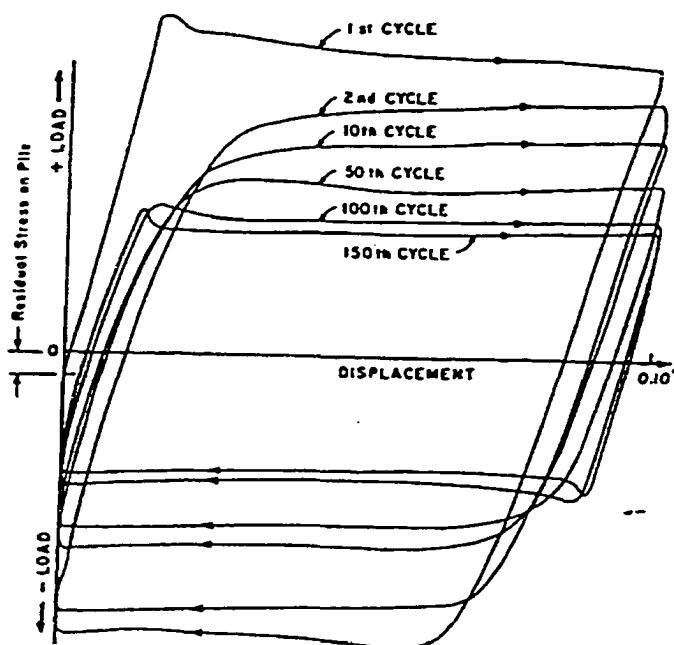


Figure 2-12: Cyclic Axial Loading of a Pile in Soft Clay (Holmquist, Matlock, 1976)

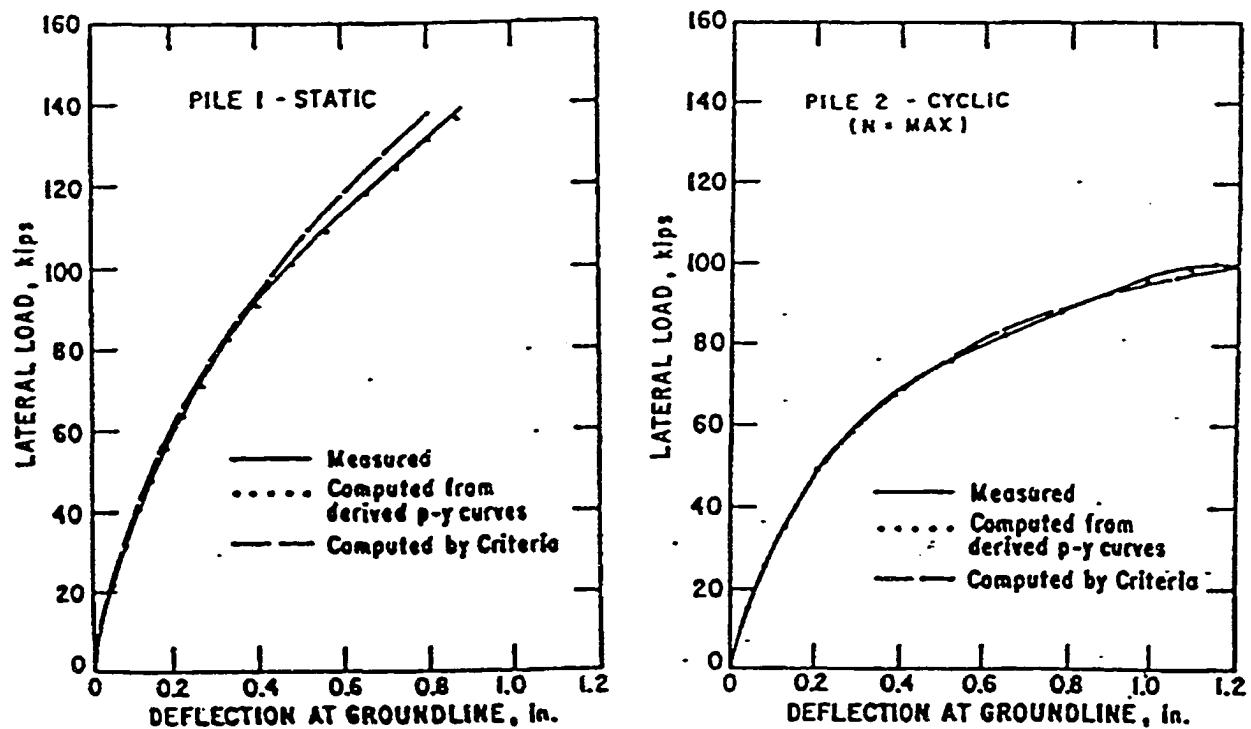


Figure 2-13: Cyclic Effects on a Pile in Stiff Clay (Reese, et al., 1975)

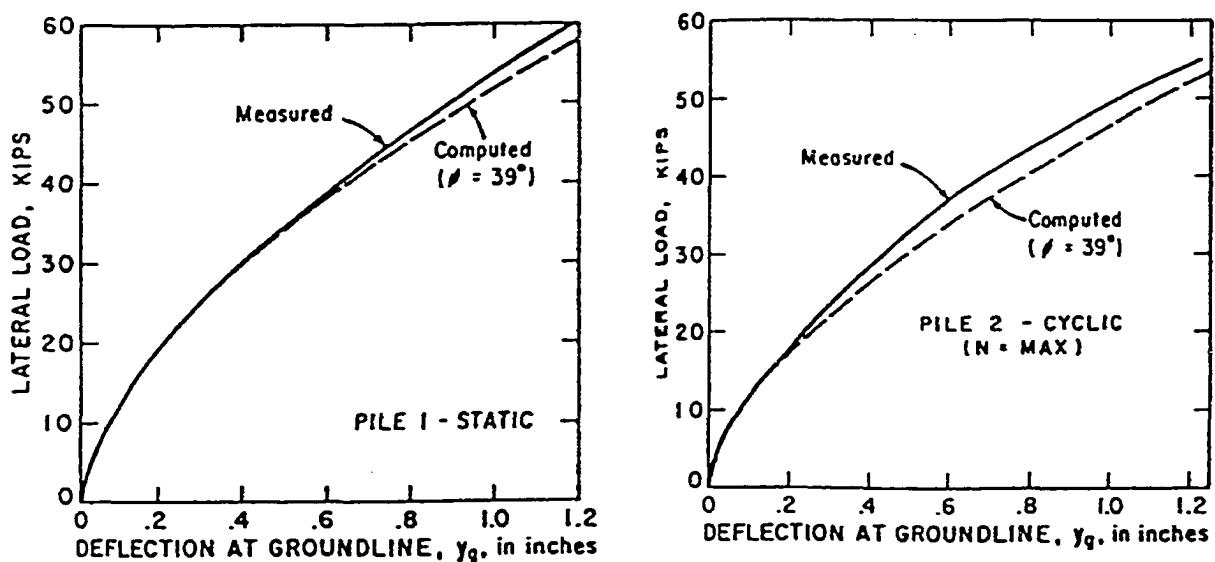


Figure 2-14: Cyclic Effects on a Pile in Sand (Reese, et al., 1974)

High rates of loading, however, will increase the effective strength capacity of a pile. Axial load-displacement behavior as measured at the pile head is shown in Figure 2-12 for a pile in soft clay subject to cyclic loading. Figure 2-13 depicts lateral load-displacement behavior as measured at the pile head for a pile in stiff clay in a pre- and post-cycled state. Figure 2-14 depicts lateral load-displacement behavior as measured at the pile head for a pile in dense sand in a pre- and post-cycled state.

Piles forced to displace laterally will eventually yield, form plastic hinges, and generally be subject to the same behavioral constants as tubular steel beam-columns. A pile displacing axially, however, has no physical restriction on displacement; ultimately the axial displacement capacity will be governed by stability of the supported platform.

2.5.4 Platform Frames

Of equal importance to the behavior of structural elements is the behavior of platform structures. This is an important consideration when a decision must be made regarding the selection of an appropriate response factor as part of a simplified pseudo-static analysis. The load-displacement behavior of platforms which yield in their foundations or unbraced bays will reflect the load-displacement behavior of elements in these components. Platforms which yield in the braced portions of their jackets, however, will tend to exhibit more complicated behavior; braces will buckle, and load will be redistributed to other portions of the jacket. This is a complicated process, but can be determined from static pushover analysis.

The load-displacement behavior exhibited by a yielding braced frame will depend upon several factors:

- The sizes and slenderness of diagonal members. Members with poor post-buckling performance will lead to rapid weakening of frame sections after buckling, leading to the formation of soft stories in the frame.
- The presence of horizontal members. These members will redistribute the load from buckling diagonal members to other braces in the frame. A frame without horizontals or with weak horizontals will tend to “unzip” after diagonal members buckle, as load cannot be transferred to tension members. The effective load the platform system is able to support will drop.
- The orientation of bracing members in a section. If members in a section are oriented such that they will all be placed in compression at the same time, it is possible that they will all buckle when the first member buckles, as load will be redistributed to compression members as opposed to tension members. The result will be the formation of a soft story, and a drop in supportable lateral load.
- The presence of K-type bracing. K-type bracing configurations tend to exhibit poor load-displacement behavior unless the horizontal member is very strong. If the horizontal member is weak, it will likely form a plastic hinge following the buckling of the compression brace in the K, due to action of the unbalanced load in the tension brace. This will usually result in the formation of a soft story, and a drop in supportable lateral load. If the horizontal member is strong, forces in the legs will be higher than in other bracing systems.

- X-bracing. X-bracing configurations in a bay will be more effective than single braces. However, it should be noted than a brace which is part of an X will tend to buckle between the center of the X and the corner; inelastic deformation will be concentrated in the buckled section, leading to a more rapid exhaustion of displacement ductility capacity than a single brace which spans an equal section. It should be noted that K-braces which share common vertices will behave as an X-brace across multiple bays; this is a very effective combination.
- The presence of large grouted jacket legs. Grouted jacket legs have substantial stiffness, and will contribute to the overall resistance of the jacket bays.
- The durability of tubular joints. Joints which fail by collapse, tearing or punching will result in the removal from the load path of attached braces. This can result in drops in section strength, followed by the formation of a soft story.
- The presence of any structural sections with radically different stiffness and/or strength. Sections of this type will likely become soft stories, by yielding well in advance of other sections, or by being subject to large localized displacements.

The good practice recommendations of RP 2A-WSD reflect these facts. A platform which has stocky members with low slenderness, strong horizontal frames, symmetric member orientations and no weak-beam K-braces will perform globally very much like an elastic-plastic system, and will possess some reserve strength; a platform which has any of the negative qualities listed will tend to lose strength after the first member buckles, and will quickly concentrate damage in the weakened section.

Zayas, et al. (1980A) have studied the cyclic inelastic behavior of two braced frames made of tubular members approximating offshore platform structures. Frame parameters are shown in Figure 2-15; while their cyclic load-displacement behaviors are shown in Figure 2-16. Both platforms have strong joints and strong horizontal framing; however, the diagonal braces in Frame I are sized to $D/t = 42$, while those in Frame II are $D/t = 33$. Frame II exhibits more robust hysteretic behavior than its companion. Frame I was able to develop a global displacement ductility of three prior to loss of strength through member failures; Frame II was able to develop a global displacement ductility of five prior to a similar loss. Both platforms exhibit a gradual loss in effective strength with each cycle; this is associated with the drop in buckling capacity of members after the first instance of buckling. The loss becomes more pronounced as local buckling occurs within braces, which occurs earlier for Frame II. Both frames sustained damage to diagonals in both bays; both eventually suffered tearing of the braces in the top bay, followed by the formation of a portal mechanism in this bay.

Other researchers have studied the cyclic behavior of K-brace frames; however, to the knowledge of the author no cyclic testing has been performed on K-braced frames constructed from circular tubular members similar to those commonly used in the construction of offshore platforms. Shibata and Wakabayashi (1984) tested a variety of K-braced frames with strong beams, weak beams, and stocky and slender braces; results from several of these tests are shown in Figures 2-17 and 2-18.

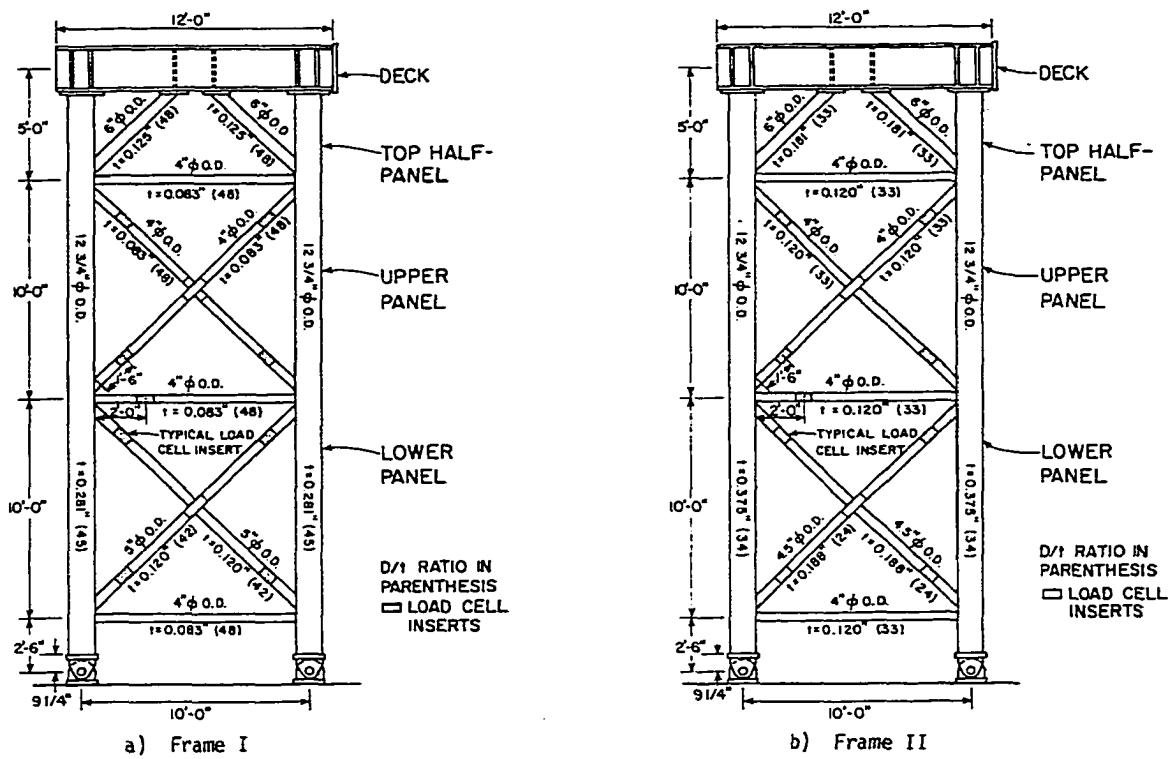


Figure 2-15: X-braced Frames Tested by Zayas, et al. (1980A)

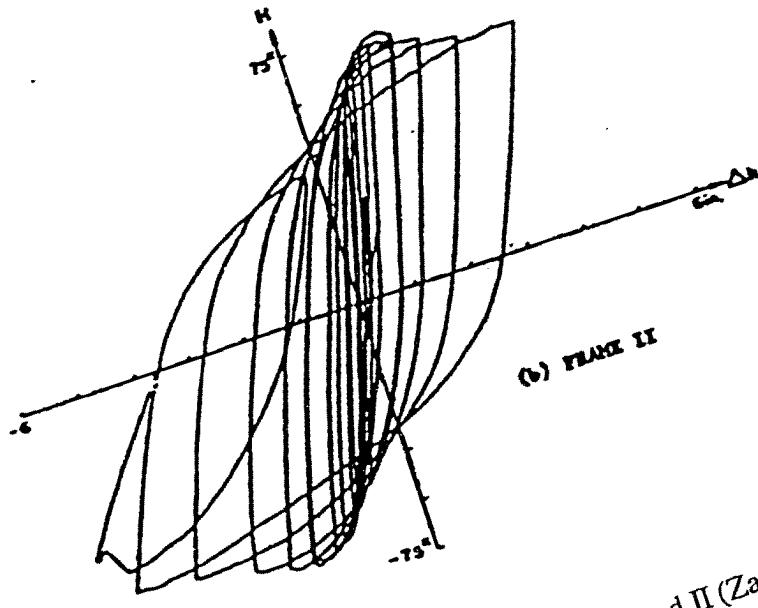
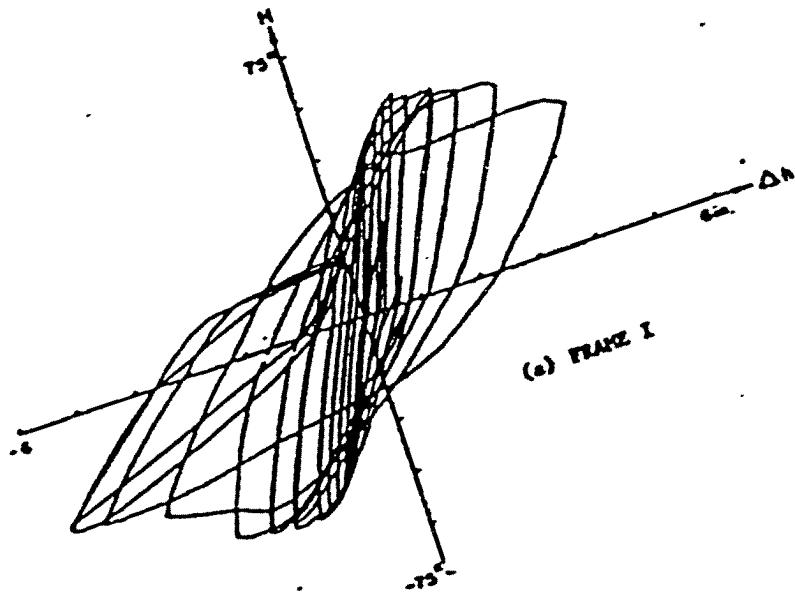


Figure 2-16: Hysteretic Behavior of Frames I and II (Zayas, et al., 1980A)

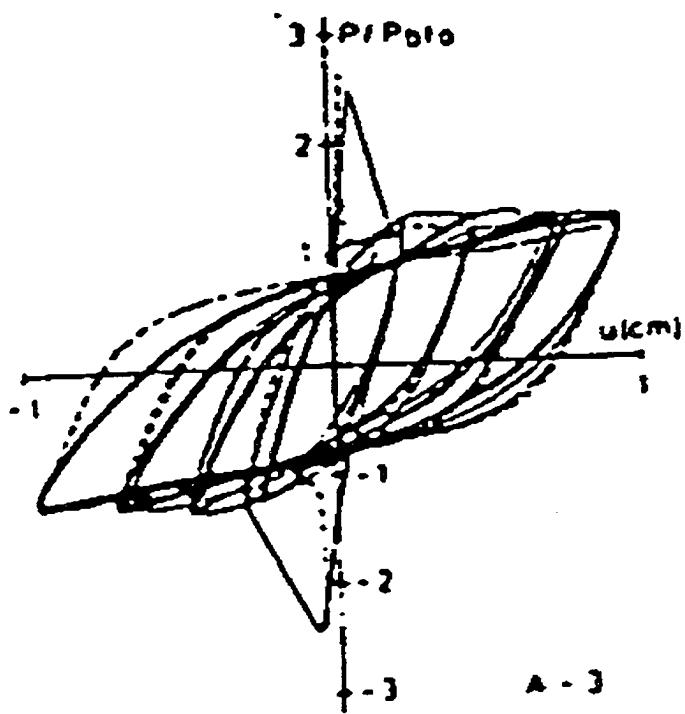
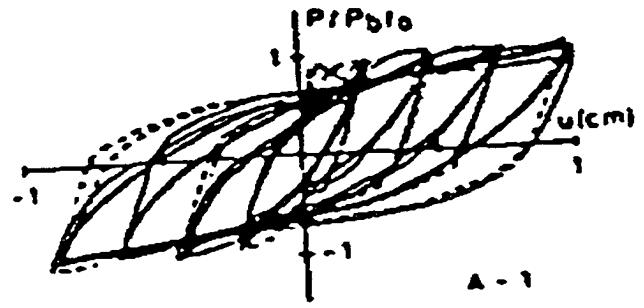


Figure 2-17: K-braced Frames with Moderate Slenderness (Shibata, Wakabayashi, 1984)

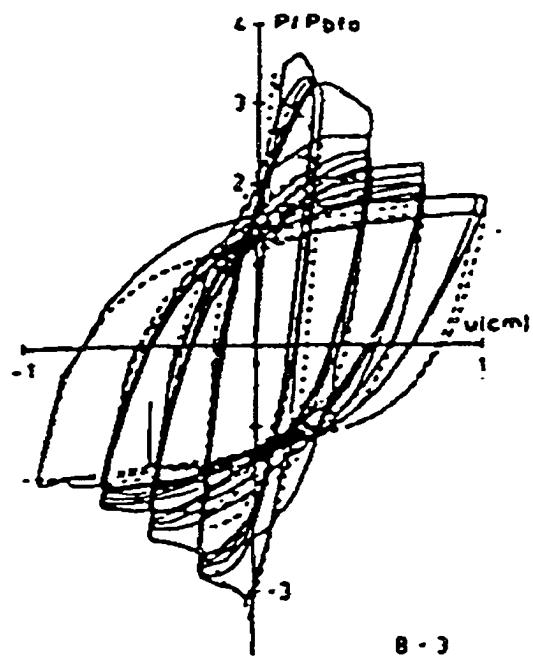
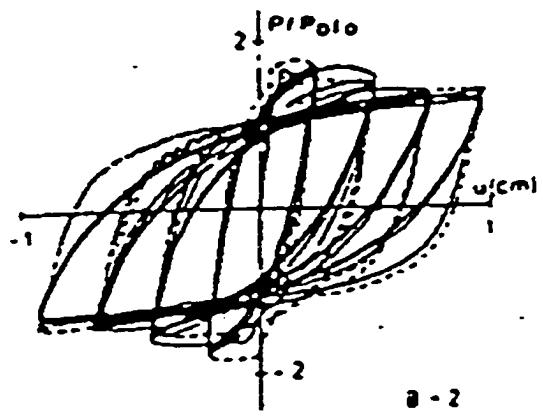


Figure 2-18: K-braced Frames with Low Slenderness (Shibata, Wakabayashi, 1984)

The members in these K-type frames were steel plate sections. Tests A-1 and A-3 used members with intermediate slenderness, while tests B-2 and B-3 used stockier members. A-1 and B-2 were strong beam tests, while A-3 and B-3 were weak beam tests. The strong beam K-brace frames exhibited hysteresis which was large controlled by the buckling and yielding of braces, while the weak beam tests exhibited sudden losses in strength following member buckling, and hysteresis controlled by the formation of a plastic hinge in the beam.

2.5.5 Response Factors for Degrading Systems

The use of response factors to modify the elastically-calculated loads from a response spectrum on a nonlinear structural system was in the author's recollection believed to have originally been suggested by Veletsos and Newmark (1960). By assuming the structure to behave as a nonlinear SDOF system, and using statistical studies relating the response of a nonlinear SDOF system with hysteretic behavior mimicking that of the complete structure to an equivalent elastic SDOF system (i.e. with the same period and damping), an estimate as to the effective reduction in elastically-calculated load from a response spectrum due to acceptable inelastic behavior could be made. This reduction implicitly recognizes that the structure has some tolerance for inelastic deformation, and allows for convenient linear approximation of the effects of this deformation tolerance on earthquake response.

The response or R factor approach to design of structures is a feature of many building codes (Miranda, Bertero, 1994). R factors such as those in the Uniform Building Code are intended to be applied in the design of structures which are first lateral mode dominated. While structures with five or six lateral DOF can in some cases be largely controlled by first mode

response, structures with many DOF and evenly distributed mass will likely have very significant higher mode effects, thus making such an approximation unrealistic (Clough, Benuska, 1967). Most jacket-type offshore platforms can be idealized as structures with perhaps three to six lateral DOF (associated with platforms in water depths of 40 ft to 400 ft), and with the presence of a large mass at the top level most lateral response tends to be concentrated in the first mode (Smith, 1994). Deep water structures would likely have more noticeable higher mode responses.

Numerous studies have been conducted in recent years to determine or revise *R* factors for common structural systems. Much work has been devoted to the study of bilinear elastic-plastic or strain hardening systems, with and without stiffness degradation; Miranda (1991) and Nassar and Krawinkler (1990) are two recent examples. These studies have confirmed that the allowable load reduction due to nonlinear behavior is strongly dependent upon:

- The period of the SDOF system.
- The soil conditions at the site.

A limited number of studies have been performed using nonlinear systems with different types of strength degradation; a study performed by Al-Sulaimani and Roessel (1985) is perhaps the best example. This study confirmed that the response factor was also sensitive to the hysteretic behavior of the system when strength degradation was possible; systems with strength degradation should have lower allowable load reduction than systems without.

Clearly, two of the likely mechanisms which will form in an offshore platform will exhibit both stiffness and strength degradation. Hence, to apply response factors determined from

the analysis of elastic-plastic and bilinear strain-hardening systems is possibly unconservative, depending on the severity of the strength degradation in the mechanism. To apply the response factor concept to offshore platform assessment and design, response factors which simulate the hysteretic behavior of platform systems must be developed.

2.6 RISK ASSESSMENT AND EVALUATION

The emphasis thus far has been on the demand-capacity interaction portion of a structural integrity assessment for platforms subjected to earthquakes. It must be recognized that the variables which enter into this demand-capacity analysis are not deterministic. Incorporation of information regarding the uncertainty in demand, capacity and demand-capacity interaction can allow probabilities of failure (judged with respect to the limit states applied to the problem) to be determined. These probabilities can be used to judge the relative confidence in the results of different failure mode demand-capacity assessments.

However, estimating the probability of failure of the platform system is only part of the overall risk management equation. The probability of failure must be combined with the potential consequences of failure, in order to make a weighted judgment regarding the suitability of continued service for an offshore platform. An attempt has been made with RP 2A-WSD Section 17 to standardize this process for the offshore oil industry, by introducing consequence-based criteria for design and assessment. Section 17 contains provisions to rank platforms according to life safety and failure consequence, and allow for less severe design and assessment criteria for platforms with no life safety concerns and low failure

consequence. Similar guidelines have been included in the proposed ISO guidelines for earthquake design of platforms (Craig, 1996).

If a platform cannot pass the requisite screening levels, it is unfit for service. In this case, the owner has the option of mitigating the risk or decommissioning the platform. There are two effective options for mitigating the risk:

- Reducing the probability of failure, by reducing loads and/or increasing capacities.
- Reducing the consequences of failure.
- Reduce the uncertainties associated with loads and capacities.

Common strategies for reducing loads and increasing capacities are:

- Removal of deck equipment, conductors and piping.
- Removal of marine growth.
- Grouting braces, joints, legs and piles.
- Installing support jackets adjacent to the existing structure, or adding skirt piles.

For platforms in seismic regions, care must be taken when evaluating changes in capacity due to the connection between demand and capacity. Changes in mass (decks, marine growth reduction) can be used to reduce loads but will also change the vibration properties of the platform. Changes in strength can change stiffness, changing the vibration characteristics of the platform and hence increase the effective earthquake load attracted to the platform.

Consequences of failure can be grouped into three categories: loss of life, environmental pollution, and loss of resources, property and production. The following are measures suggested by Billington, et al. (1993) for reducing risk through adjustment of failure consequence:

- Increasing life safety by evacuation. This does not work for earthquakes, where there is no effective warning time. However, an alternative would be to reduce manned operations on the platform, in order to reduce the time during which crew are exposed to the possibility of failure.
- Remove oil storage, install safety shutdown valves.
- Move key facilities away, and consider re-drilling at other locations.

For probabilistic risk assessment, effort can be made to collect more data, and to remove biases from existing data. This is a challenging task for the problem of earthquake assessment. Earthquake ground motions contain much inherent uncertainty which cannot be eliminated due to their random nature. Better estimates of component post-yield and post-buckling performance must currently be derived from testing, given the limitations of today's theory regarding such phenomenon.

CHAPTER THREE:
PREDICTION OF STRENGTH AND DUCTILITY DEMANDS
FROM EARTHQUAKES

3.0 INTRODUCTION

The fundamental goal of an earthquake analysis is to estimate the loads, displacements and number of number of load or displacement cycles a structure will be subject to when excited by ground motion. An engineer can then compare these earthquake demands against the capacity of the structure, as controlled by the strength, ductility and robustness of its structural components and by the tolerable loads and displacements critical equipment can withstand, to ensure the structure is capable of withstanding these demands.

Earthquake analysis of offshore platforms poses special challenges to an engineer. A platform differs from the average onshore building by (1) being surrounded by water and (2) possessing in many cases a noticeably flexible foundation. Hence, the analysis of a platform will entail accounting for fluid-structure interaction and soil-structure interaction in addition to accounting for non-linear behavior in the platform structure itself.

The presence of water around the platform has two principal effects:

- The effective inertia of the platform is increased by the added mass effect (Clough, 1960).
- There will be an effective resisting force to motion proportional to the square of the velocity of the platform (drag force on the platform as it moves relative to the water, Clough, 1960).

There is also an additional velocity-proportional force which acts to resist motion due to the generation of waves (radiation damping, Clough, 1960); however, for structures consisting of small-diameter tubular members this force is small relative to drag and is often neglected (Brebbia, Walker, 1979). These hydrodynamic effects exhibit some dependence on:

- Fluid flow uniformity, expressed by the Keulegan-Carpenter (KC) number:

$$KC = \frac{UT}{D}$$

where U and T are the velocity amplitude and period of the oscillation and D is the diameter of the member moving through the fluid.

- Fluid flow regime (measure of turbulence), expressed by Reynolds number (Re):

$$Re = \frac{UD}{\nu}$$

where ν is the fluid viscosity.

- Member shape and roughness.
- Proximity to sea floor and to free surface.

Obviously, rigorously accounting for the hydrodynamic action can be a challenging task analytically.

The foundation poses additional complications. The load-displacement behavior exhibited by piles and mats is non-linear, even at small levels of displacement. This is due in part to small amounts of plastic deformation in soils adjacent to piles and foundation mats, and also due to the fact that soils adjacent to such elements rarely possess uniform properties (Bea, 1986).

Many soils exhibit strong loading rate dependence; hence, piles and mats will appear to gain strength and stiffness relative to their static values due to the load rate-proportional resistance of the soils (Bea, 1986). “Free-field” soils, those not adjacent to the platform but adjacent to the “near-field” soils, which are adjacent to the platform, can be excited into motion by the platform, providing additional inertial resistance at foundation level. Movement of free-field soils during an earthquake can result in additional stresses being induced in piles (Bea, et al., 1979). In addition, compression waves transmitted from the near-field soils to the free-field soils serve as another source of damping force (Richart, et al., 1970); while this is a significant source of damping for structures such as nuclear power containment buildings and gravity base platforms, it is often neglected for pile-supported jacket-type platforms as being small relative to the energy dissipated through hystereris of foundation soils (Penzien, 1975). Pile and mat foundations can also exhibit strength and stiffness reduction when subjected to large displacement cycling (Bea, 1986).

The steel structure of a jacket-type platform is made up of tubular steel members. Most platforms are essentially braced frames, although some may have unbraced sections immediately beneath the deck. Analysis of structures such as these poses little difficulty so long as the members do not yield or buckle; however, if the platform is subjected to severe motions yielding, and, more importantly buckling will take place, resulting in non-linear behavior of these elements and the platform as a whole. This non-linear behavior can be exacerbated if the platform does not possess sufficient redundancy or has undesirable framing configurations, and the platform will degrade globally in stiffness and strength (Gates, et al.,

1977). In addition, the tubular joint connections between members can fracture under repeated cycling due to low cycle fatigue, leading to similar global degradation.

The most accurate means of accounting for all of these effects is to construct a MDOF model of the platform as shown in Figure 3-1, and perform dynamic (time history) analysis using this model. An engineer can track the time-dependent response of all elements within the platform, in addition to evaluating the complex fluid-structure and soil-structure interaction. With each analyses, the engineer can assess the earthquake demand and earthquake demand-platform capacity interaction explicitly, and thus obtain an extremely detailed analytical picture of the stresses, strains, and stress or strain cycles each element is subject to. However, to build, analyze and especially to process the results of such a model represents a great commitment of time and effort, and requires experience with the analysis tools.

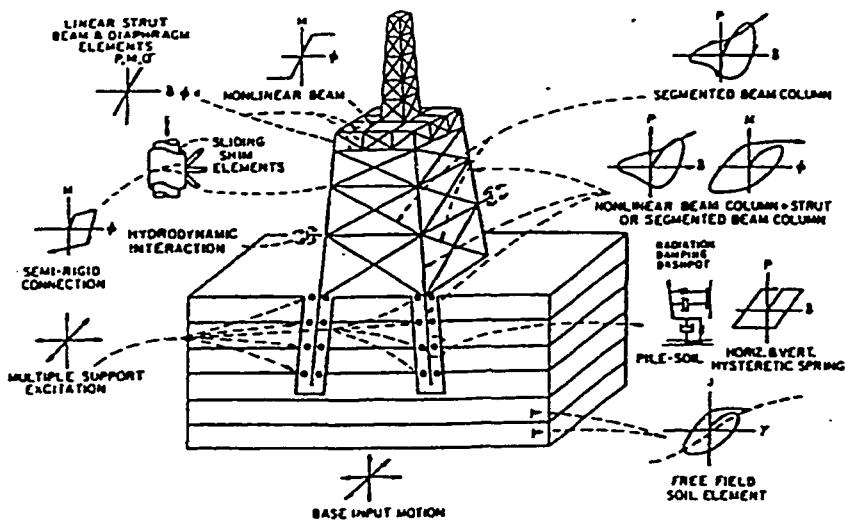


Figure 3-1: Complete MDOF Model of Platform

As an alternative to dynamic analysis, an engineer might choose instead to first apply a static analysis method which approximates the true dynamic response of the platform. Static analysis approaches to earthquake analysis have long been used as an alternative to dynamic analysis (Chopra, 1995), and in many cases will suffice to quickly show loads and demands on structural components, so that weak links and configurations with poor ductility and robustness can quickly be identified.

Perhaps the most common approach to estimating forces and displacements for use in a static analysis is modal response spectrum analysis (Chopra, 1995). This approach allows an engineer to establish the peak response (base shear, overturning moment, etc.) associated with each vibration mode of the structure; these peak responses are then combined to obtain the total response. The true phase between these responses is unknown, however; furthermore the number of load cycles is invisible to the engineer. Also, modal response spectrum analysis is strictly valid for linear systems.

However, based on observed trends between the responses of elastic and inelastic systems, various approximate methods of using response spectrum results to estimate inelastic displacement demands have been proposed. These approaches usually entail either assuming the elastic and inelastic displacements throughout the structure will be the same (Veletsos, 1969; Newmark, Hall, 1982) or by assuming that inelastic response will be concentrated in the first lateral modes, and hence the structure may be analyzed using static pushover analysis together with forces from a response spectrum analysis modified by a factor to account for demand-capacity interaction (Saiidi, Sozen, 1979; Lin, Mahin, 1983; Miranda, 1991;

Lawson, et al., 1994). While the first type of approach is usually good at capturing higher mode contributions to displacements, it suffers from not being able to account for the damage concentration which is typically found in yielding structures (Luyties, et al., 1976; Haviland, et al., 1976). Likewise, the second type of approach has achieve excellent results at predicting the response of structures with moderate numbers of degrees of freedom (Miranda, 1991), but is (1) sensitive to the load pattern used to perform the pushover analysis, and (2) unable to represent higher mode effects. Furthermore, both approaches suffer when the number of DOF is large as in a very tall building (Clough, Benuska, 1967). However, these static methods can be applied quickly and cheaply over a wide range of parameters to develop a good response picture.

This chapter outlines a simple pseudo-static approach by which earthquake-induced forces and displacements on platforms can be estimated. Using the basic global mass and load-displacement properties of a platform, the vibration properties of the platform are estimated from modal analysis. These properties are used together with response spectrum analysis to estimate forces on the platform. A simple design code-based approach for estimating earthquake forces is also evaluated, and a brief parameter study focussed on the effects of foundation flexibility and added mass on vibration properties, and hence earthquake forces, is also conducted. For estimating inelastic displacements, it is assumed damage will concentrate in the first mode, and hence static pushover analysis together with response spectrum forces and a demand-capacity modification factor can be used to estimate the inelastic response of the platform.

The simplified modal method is used to determine the vibration properties of a simple platform; these results are compared to those obtained from response spectrum analysis of a traditional full frame 2-D model. In addition, earthquake demands estimated using both the simplified modal response spectrum method and time history analysis of the full frame 2-D model are estimated for comparison purposes for a series of three earthquakes. The simplified inelastic method is used to estimate the inelastic response of the simple platform; this result is compared to results from non-linear time history analyses of the full frame 2-D model for a series of three earthquakes.

3.1 SIMPLE LINEAR RESPONSE OF PLATFORMS

The process by which earthquake demands on a platform are estimated begins with modal analysis. By considering the primary bending, shear and foundation force-displacement mechanisms in the platform, simple estimates of platform lateral and vertical vibration properties are made. These properties are developed on both principal horizontal axes and the vertical axis; it is assumed there is no significant torsion. The vibration properties are then used in a response spectrum analysis to estimate earthquake loads the platform will be subject to assuming elastic behavior.

3.1.1 Horizontal Response

The horizontal response of a platform may be thought of as consisting of three components, as shown in Figure 3-2. There is a bending component, from the cantilever deflection of the platform due to the axial loads on the piles from overturning; a shear component, from the shear deformations of each braced jacket bay and the foundation immediately beneath the

jacket; and a rotation component, due to the rotation of the jacket at the mudline due to tension and compression in the piles.

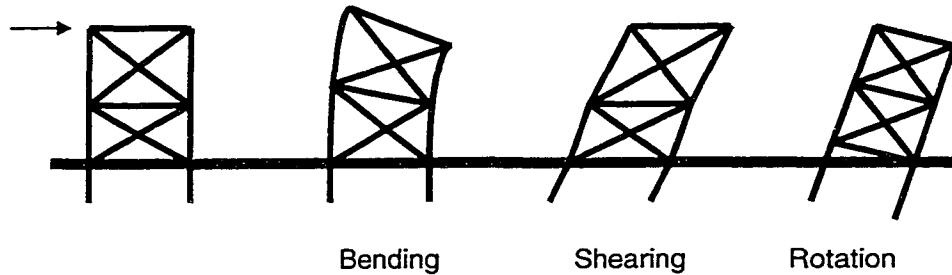


Figure 3-2: Horizontal Response Components

3.1.2 Steel Structure Load-Displacement Relationships

Using very simple structural relationships, it is possible to establish the load-deflection properties of each individual response component without much effort. Deflections due to bending may be found from:

$$\Delta = \frac{PL^3}{3EI}$$

where I refers to the moment of inertia of the platform tower structure based on the platform pile cross sections, and L is the height at which load is applied.

Shear deflections may be found by considering the deformation of the individual shear force-displacement mechanisms at each level in the platform. For a braced jacket bay, the shear stiffness can be estimated as:

$$k_{bay} = \sum_{i=1}^{n_{brace}} k_i \cos^2 \theta_i$$

where:

k_i = axial stiffness of each individual brace, EA/L

θ_i = angle between each brace and the horizontal

The flexibility of tubular joint connections is not included, and the stiffness contribution of jacket-legs can be ignored in most cases. However, some platforms possess large diameter legs, with a grouted pile-jacket leg annulus; this will result in substantial stiffness contribution from the legs, depending on the size of the braces.

For bays which do not have braces (the deck bay on many platforms do not) the shear deformation will be controlled by the bending of the platform legs. In this case, the shear stiffness may be estimated from:

$$k_{bay} = \sum_{i=1}^{n_{leg}} k_i$$

where:

k_i = effective horizontal stiffness of each individual leg, assumed $12EI/L^3$

The end conditions at the top and bottom of each leg could contribute to reducing this stiffness, if there is much rotational flexibility. Unbraced leg sections in the jacket will likely have stiffnesses closer to $6EI/L^3$. Some platforms will have very large leg sections relative to the size of the diagonal braces; when the leg-pile annulus is grouted on these structures, the effective bay stiffness associated with the legs will be large. In these cases, the bay stiffness associated with the legs should be calculated as above and added to the bay stiffness associated with the braces.

The effective increase in bay stiffnesses due to battered legs is not included in the simplified vibration properties formulation.

3.1.3 Foundation Load-Displacement Relationships

For most jacket-type platforms, the shear stiffness at the foundation level is usually based only on the lateral stiffnesses of both the piles and any well conductors. However, the effective stiffness due to contact between mud mats and mudline braces and the seabed can be significant. Therefore, a bounding approach should be used to evaluate the effect of foundation stiffness. For lower-bound purposes, the stiffness is based upon the stiffnesses of only the piles and conductors. For the upper-bound, the stiffness includes the effects of mud mats and mudline braces.

As the lateral load-displacement behavior exhibited by piles even at low levels of displacement is non-linear (Reese, et al., 1975), it is necessary to approximate an equivalent linear stiffness. The lateral stiffness contribution of a pile or conductor will also depend not only on the soil properties, but also upon the fixity of the connections between the pile or conductor and the platform structure. For the simplified analysis process, the following relationship is used to estimate the lateral stiffness of piles and conductors:

$$k_{pile-x} = \frac{3EI_p}{d_{hinge}^3}$$

where:

I_p = moment of inertia of the piles

d_{hinge} = estimated depth of hinge formation in pile when it forms a mechanism

This relationship assumes the pile first forms one hinge, and is able to drift before forming the second; it is similar to an approximate one commonly used in preliminary design of pile-supported platforms (Dawson, 1982). In the approximate formula, a stiffness coefficient of 12 instead of three is used, and the presumed depth of plastic hinge formation is varied between five and ten pile diameters.

Deflections from foundation rotation are calculated considering the platform to be a rigid structure mounted on a rotational spring. This spring stiffness is given by (assuming no mat or mudline brace contributions):

$$k_\theta = \sum_{i=1}^{n_{pile}} k_{pile-z} L_i^2$$

where L_i is the distance to the pile from the axis of rotation. Pile axial stiffness k_{pile-z} can be approximated based on the mechanism by which load is transferred from the pile to the foundation soil (Bea, 1980). The vertical stiffness is derived by considering the basic stiffness EA/L of the pile column and then modifying this stiffness for the mechanism by which vertical loads are transferred to the surrounding soil. Various transfer mechanisms are shown below in Figure 3-3.

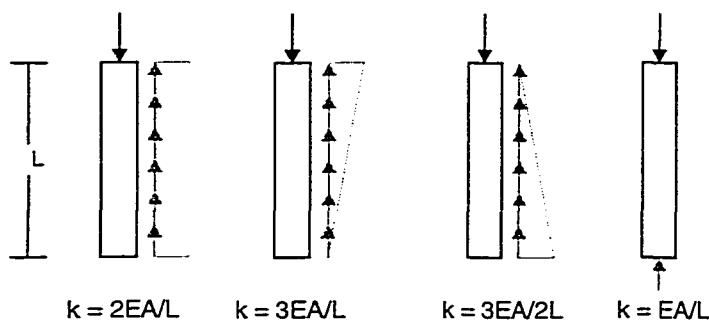


Figure 3-3: Vertical Load Transfer Mechanisms for Imbedded Piles

Sliding and bearing stiffness due to the contact between mud mats, mudline braces and the sea floor can be estimated based on the contact area. Bearing and sliding stiffnesses are assumed to be controlled by the bearing strength of the supporting soil. The values of soil stiffness per unit area shown in Table 3-1 are used for this purpose. The unit sliding stiffness is estimated as 50 % of the unit bearing stiffness (Barkan, 1962).

Table 3-1: Bearing Stiffness as Related to Bearing Strength (Barkan, 1962)

Soil Group	Bearing Stress (kips/ft ²)	Vertical Stiffness (kips/ft ³)
Weak	3 or less	190
Medium	3 to 7	190 to 310
Strong	7 to 10	310 to 620
Rock	10 or more	620

3.1.4 Mass

Masses are lumped at each horizontal framing level and at the deck. These masses include the mass of any hydrodynamic added mass or contained mass, marine growth, mounted equipment, and conductors. For cylindrical members, the approximate hydrodynamic added mass per unit length is defined by (Clough, 1960):

$$m_{added} = K\rho_w \pi r^2 \sin\theta$$

where:

K = flexibility factor for members; ranges from 0.6 for pinned-end members to 1.0 for fixed-end members

ρ_w = density of the surrounding fluid

r = radius of the member

θ = the angle between the cylindrical length axis and the direction of translation

To account for proximity to the free surface, the added mass is further scaled according to (Goyal, Chopra, 1989):

$$m_{added}(z) = m_{added} \text{ when } z > 0.1 H_o$$

$$m_{added}(z) = m_{added}(z / 0.1 H_o) \text{ when } z \leq 0.1 H_o$$

where:

z = depth below the surface at mass point

H_o = water depth

Soil mass consisting of the soil contained within the piles to a depth of $d_{hinge}/2$ is included in the mass lumped at the mudline.

3.1.5 Modal Analysis

Considering the platform to be a system of lumped masses (one at each horizontal framing level, the decks, and the mudline), the flexibility matrix for this simple system can easily be constructed by summing the component responses to unit loads at each level. The increase in flexibility due to $P-\Delta$ effects is presumed to be small and hence is not included. The vibration properties of the system can then be found through solution of the standard eigenvalue problem of the form:

$$\mathbf{f}\mathbf{m}\phi_n = \frac{1}{\omega_n^2} \phi_n$$

where:

\mathbf{f} = matrix of flexibility coefficients

\mathbf{m} = matrix of lumped masses

ϕ = mode shape

ω = natural frequency

This form has the advantage of converging to the largest values of $1/\omega^2$ with each iteration, which correspond to the largest periods. In this fashion, the first mode will be found first, then the second, and so on. Solution of this problem is a popular subject in engineering; readers desiring further information should consult Timoshenko, et al. (1974) and Parlett (1980). The iteration process used in the solution of the standard eigenvalue problem is summarized below for the sake of completeness.

1. Start with an arbitrary trial vector, ϕ_n , and solve $\mathbf{f}\mathbf{m}\phi_n = \mathbf{y}$.
2. Obtain an estimate of the associated eigenvalue, λ_n , by taking the ratio between components of ϕ_n and \mathbf{y} having the same index; hence $\lambda_n \approx y_i / \phi_{ni}$.
3. Normalize \mathbf{y} by y_i to get $\bar{\mathbf{y}}$. Check to see if all $\bar{y}_i = \phi_{ni}$; if this condition is met, ϕ_n is a valid eigenvector and λ_n the correct associated eigenvalue. If not, set $\phi_n = \bar{\mathbf{y}}$ and return to step 1.

In order to obtain eigenvectors and eigenvalues associated with higher modes, it is necessary to ensure that successive eigenvectors are orthogonal to one another (the orthogonality condition, $\phi_i \mathbf{m} \phi_j = 0$, ensures that the work done by i^{th} mode inertia forces going through j^{th} mode displacements is zero). This may be accomplished by enforcing the orthogonality condition when determining successive eigenvectors:

1. With the eigenvector ϕ_1 determined, and with a trial vector ϕ_2 estimated, applying the orthogonality condition $\phi_1 \mathbf{m} \phi_2 = 0$ gives (assuming a diagonal mass matrix):

$$m_{11}\phi_{11}\phi_{21} + m_{22}\phi_{12}\phi_{22} + m_{33}\phi_{13}\phi_{23} + \dots + m_{jj}\phi_{1j}\phi_{2j} = 0$$

2. Solving for ϕ_{21} (this is an arbitrary choice) gives:

$$\phi_{21} = -\frac{m_{22}\phi_{12}\phi_{22}}{m_{11}\phi_{11}} - \frac{m_{33}\phi_{13}\phi_{23}}{m_{11}\phi_{11}} - \dots - \frac{m_{jj}\phi_{1j}\phi_{2j}}{m_{11}\phi_{11}}$$

3. Calculating ϕ_{21} using the above expression prior to using ϕ_2 as a trial vector ensures orthogonality between ϕ_2 and ϕ_1 . This may be accomplished using the following matrix multiplication:

$$\phi_{2 \text{ trial}} = \mathbf{T}_{S1} \phi_2$$

where: $\mathbf{T}_{S1} = \begin{bmatrix} 0 & -\frac{m_{22}\phi_{12}}{m_{11}\phi_{11}} & -\frac{m_{33}\phi_{13}}{m_{11}\phi_{11}} & \dots & -\frac{m_{jj}\phi_{1j}}{m_{11}\phi_{11}} \\ 0 & 1 & 0 & \dots & 0 \\ 0 & 0 & 1 & \dots & 0 \\ \dots & \dots & \dots & \dots & \dots \\ 0 & 0 & 0 & \dots & 1 \end{bmatrix}$

\mathbf{T}_{S1} is referred to as a “sweeping” matrix, as it acts to sweep out or suppress the first mode characteristics and allow the second mode to be come dominant. As \mathbf{T}_{S1} is used with each iteration of ϕ_2 , it may be used to reformulate $\mathbf{f}\mathbf{m}$ according to $\mathbf{f}\mathbf{m}_{S1} = \mathbf{f}\mathbf{m}\mathbf{T}_{S1}$, and then operate directly on the reformulated matrix.

Higher modes may be determined by successive application of sweeping matrices. For example, a sweeping matrix \mathbf{T}_{S2} for removing the dominance of ϕ_2 may be constructed, and then used together with \mathbf{T}_{S1} to allow the third mode ϕ_3 to become dominant. This matrix \mathbf{T}_{S2} would be constructed by using the fact that $\phi_1 \mathbf{m} \phi_3 = 0$ and $\phi_2 \mathbf{m} \phi_3 = 0$. This gives the following:

$$m_{11}\phi_{11}\phi_{31} + m_{22}\phi_{12}\phi_{32} + m_{33}\phi_{13}\phi_{33} + \dots + m_{jj}\phi_{1j}\phi_{3j} = 0$$

$$m_{11}\phi_{21}\phi_{31} + m_{22}\phi_{22}\phi_{32} + m_{33}\phi_{23}\phi_{33} + \dots + m_{jj}\phi_{2j}\phi_{3j} = 0$$

Using the first equation to find a relationship for ϕ_{31} , the following relationship can be developed for ϕ_{32} :

$$\phi_{32} = -\frac{m_{33}(\phi_{11}\phi_{23} - \phi_{21}\phi_{13})}{m_{22}(\phi_{11}\phi_{22} - \phi_{21}\phi_{12})} - \frac{m_{44}(\phi_{11}\phi_{24} - \phi_{21}\phi_{14})}{m_{22}(\phi_{11}\phi_{22} - \phi_{21}\phi_{12})} - \dots - \frac{m_{jj}(\phi_{11}\phi_{2j} - \phi_{21}\phi_{1j})}{m_{22}(\phi_{11}\phi_{22} - \phi_{21}\phi_{12})}$$

The sweeping matrix is thus:

$$\mathbf{T}_{S2} = \begin{bmatrix} 1 & 0 & 0 & \dots & 0 \\ 0 & 0 & -\frac{m_{33}(\phi_{11}\phi_{23} - \phi_{21}\phi_{13})}{m_{22}(\phi_{11}\phi_{22} - \phi_{21}\phi_{12})} & \dots & -\frac{m_{jj}(\phi_{11}\phi_{2j} - \phi_{21}\phi_{1j})}{m_{22}(\phi_{11}\phi_{22} - \phi_{21}\phi_{12})} \\ 0 & 0 & 1 & \dots & 0 \\ \dots & \dots & \dots & \dots & \dots \\ 0 & 0 & 0 & \dots & 1 \end{bmatrix}$$

This is then used together with \mathbf{T}_{S1} to reformulate \mathbf{fm} according to $\mathbf{fm}_{S2} = \mathbf{fm}\mathbf{T}_{S1}\mathbf{T}_{S2}$.

If modal analysis is not possible, the simple approach conveniently provides displacements which may then be used together with Rayleigh's method to obtain approximate vibration periods:

$$T_1 = 2\pi \sqrt{\frac{\sum_{j=1}^N m_j u_j^2}{g \sum_{j=1}^N m_j u_j}}$$

$$\phi_1 = \mathbf{u} / u_{\max}$$

where \mathbf{u} is the vector of nodal displacements associated with nodal forces gm_j . This approach is very amenable to hand calculation.

3.1.6 Modal Damping Ratios

Damping mechanisms in a platform will include structural damping, hydrodynamic radiation and viscous damping, foundation radiation damping and foundation hysteretic behavior represented by equivalent viscous damping. The effect of these different energy-dissipating mechanisms is generalized into equivalent viscous damping, which is then expressed as modal damping ratios (percentage of critical damping).

Newmark and Rosenblueth (1971) recommend a damping ratio of 2% to 3% for welded steel structures subjected to moderate excitation. As hydrodynamic radiation damping is small for tubular steel structures, it is neglected. Hydrodynamic drag damping is taken as 0.5% (Clough, 1960). Previous studies (Penzien, 1975) have shown that the majority of effective modal damping for platforms will come from foundation hysteretic mechanisms (primarily from yielding of top soil under the platform mudline elements, and small amounts of yielding around the piles); radiation damping for pile foundations is small. For hysteretic foundation mechanisms, as the level of excitation increases, the effective damping will also increase. Based on the study of a platform's response to earthquake excitation, Mason, et al. (1985) estimated modal damping ratios on the order of 5% or greater for low levels of excitation. These results are in good agreement with those determined from forced vibration tests documented by Ruhl (1976). Bea (1986) suggests a damping ratio of 10% or higher to represent the hysteretic action in the foundation for strong levels of excitation. However, the relationship between effective foundation damping from hysteresis and earthquake excitation level is difficult to predict without iteration. Therefore, the lower value of damping (5%) should be used first; if formation of a foundation collapse mechanism is indicated, the higher

value (10%) should then be used to represent the energy dissipated prior to the formation of a complete collapse mechanism.

Veletsos and Meek (1974) suggest the following apportionment of damping between structure and foundation for the fundamental mode, to represent the relative energy dissipation of each mechanism:

$$\tilde{\xi}_1 = \xi_{foundation} + \frac{\xi_{structure}}{(\tilde{T}_1 / T_1)^3}$$

where T_1 is the period of the platform assuming a fixed base, and \tilde{T}_1 is the period including foundation flexibility. As foundation damping tends to be predominant in the first mode (Veletsos, 1977), it is neglected for the higher modes. This appears to be in agreement with results obtained by Ruhl (1976) and Mason, et al. (1989), who observed measured damping ratios in the field decreased for higher modes.

3.1.7 Vertical, Torsional Response

Platform vertical response may be determined in a similar fashion as for horizontal response. In this case, only the axial stiffnesses of the jacket legs and piles are used to construct the flexibility matrix; the solution procedure to find vertical modes will be the same as for horizontal modes.

For platforms possessing significant mass and/or stiffness eccentricities, torsion response may also be developed in a simple fashion. Rotational stiffnesses between framing levels can be developed based on the layout of the diagonal braces (or piles, for the foundation level),

while mass moments of inertia can be derived from the spatial distribution of the mass at each level. For the purpose of the simplified assessment process, torsion is not explicitly considered.

3.1.8 Modal Response Spectrum Analysis

Together with an appropriate response spectrum, modal demands such as bay shear V_{in} , bay drift Δ_{in} , overturning moment M_{bn} and foundation vertical force F_{vb} may be estimated as shown below:

$$V_{in} = \sum_{j=1}^N \Gamma_n m_j \phi_{jn} \left(\frac{4\pi}{T_n^2} \right) D_n$$

$$\Delta_{in} = \Gamma_n D_n (\phi_{in} - \phi_{i-1n})$$

$$M_{bn} = \Gamma_n L_n^\theta \left(\frac{4\pi}{T_n^2} \right) D_n$$

$$F_v = \sum_{j=1}^N m_j \left(\frac{4\pi}{T_v^2} \right) D_v$$

where:

D_n = modal displacement from response spectrum

n = mode index

j = DOF index

Total demands are obtained by combining the separate modal demands. As the phasing between the peak modal responses is unknown, the resulting total demand is an approximation to the true demand. There are several common modal combination rules

which are used today in structural engineering practice. One of the most popular in engineering practice is the square-root-sum-of-the-squares (SRSS) rule, developed by Rosenblueth (1951). This rule provides excellent response estimates for structures which have well-separated modal periods, i.e. where the ratio between successive periods is on the order of 1.5 for systems with 5% damping. To account for closely-spaced modal periods, the complete-quadratic-combination (CQC) rule is sometimes used; a correlation coefficient is estimated which accounts for the near in-phase response of closely-spaced modes (Chopra, 1995). A very conservative rule is the absolute-sum (ABS) rule; this rule assumes all responses are in-phase. ABS is very conservative, and is seldom used. Another rule which has been used is the so-called NRL-SRSS, proposed by engineers at the Naval Research Laboratory. This rule assumes the first two modes are always in phase, and hence are combined using ABS; the combined first and second mode response is then combined using SRSS with the remaining modes. As most offshore platforms examined as part of this study have well-separated modes; the SRSS rule is used to combine the modal responses.

An important issue when using a design response spectrum is the scaling and combination of directional responses. Early versions of API RP 2A-WSD recommended using a 1.0/0.66/0.5 ratio for spectral ordinate scaling between principal horizontal, perpendicular horizontal and vertical components, and the SRSS rule to combine responses; the nineteenth and later editions recommends using a 1.0/1.0/0.5 ratio. This can have a significant impact on performance estimates of the foundation and unbraced deck portals, which are more sensitive to off-axis loads than the structural bays.

3.2 SIMPLE LINEAR RESPONSE OF PLATFORMS: EXAMPLE

In this section, the simple linear response analysis procedure is used to determine earthquake loads on a small offshore platform. Results from the simple analysis are compared to results from response spectrum analysis and time history analysis of a full frame 2-D model.

3.2.1 Description of Platform

Platform A is a hypothetical design for a symmetric 4-leg production platform (see Figure 3-4). The structure is designed for 100 ft water depth. The deck is at +50 ft MWL and supports a load of 5,000 kips.

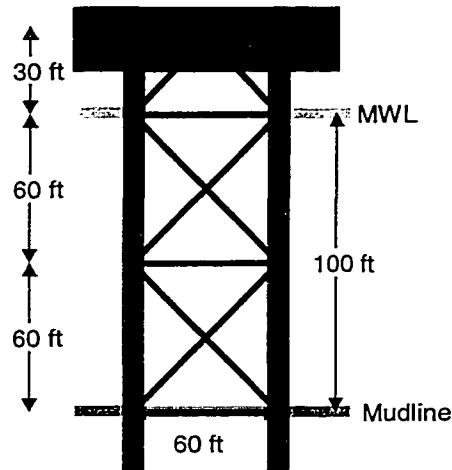


Figure 3-4: Platform A

The main diagonals in the first jacket bay are 24 inch-diameter (w.t. 0.5 inch), while those in the second bay are 30 inch-diameter (w.t. 0.625 inch); the diagonals in the deck bay are 36 inch-diameter (w.t. 0.75 inch). The legs are 78 inch-diameter (w.t. 0.875 to 1.125 inches); they are grouted, and possess heavy joint cans. The piles are 72 inch-diameter (w.t. 1 to 1.5

inches), and are designed for 150 ft penetration in medium to stiff clay. The shear strength of the clay is 2.5 kips/ft² at the surface, and increases by 0.01 kip/ft² per ft of depth. The pile ends are founded on a very stiff soil layer (rock) which has a shear strength of 184 kips/ft². All steel is A36.

3.2.2 3-D Model Description

A full frame 2-D model was developed for DRAIN2DX (Prakash, et. al., 1993). A constant amount of added mass was added to the mass of submerged members. For the model, joints were assumed to be rigid, and the deck was assumed to act as a rigid diaphragm. Braces in the model were represented by struts as opposed to beam-column elements. All structural steel elements in the platform were given stiffness-proportional viscous dampers, which were tuned to give a first mode damping ratio of 1% of critical.

In lieu of rigorously modeling the pile-soil interaction as part of the 2-D model, a model of a single pile was developed in accordance with API (1993) recommendations, and then used to derive pile head load-displacement relationships. Stiffness-proportional viscous dampers were then assigned to each element, which were tuned to increase the first mode damping ratio to 5% critical. Approximate elastic stiffnesses for these pile-head elements were used in the simplified analysis to provide consistency; these stiffnesses are shown in Table 3-2.

Table 3-2: Pile Stiffnesses

Pilehead Springs	Stiffness (Pile Model)
Vertical	3150 kips / in
Horizontal	470 kips / in
Rotational	40×10^6 kip-ft / rad

3.2.3 Vibration Analysis

The major vibration characteristics of the structure estimated using the two approaches are shown below in Figures 3-5 and 3-6. The simple method provides excellent estimates of the first two horizontal mode periods as compared with the 2-D frame analysis, but subsequent period estimates begin to deviate. The vertical mode period found from the simple method is also in good agreement with the period estimated in the 2-D frame analysis.

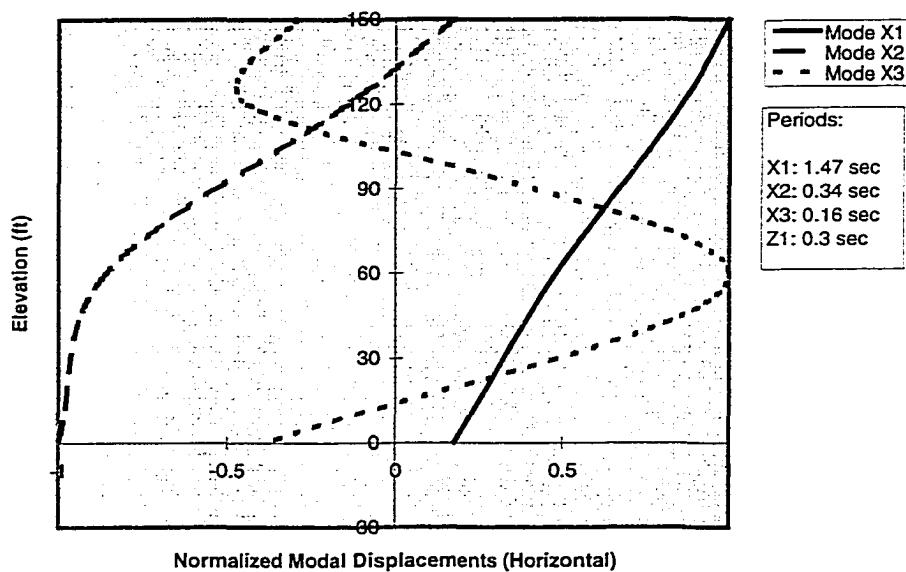


Figure 3-5: Platform Vibration Properties (2-D Frame Model)

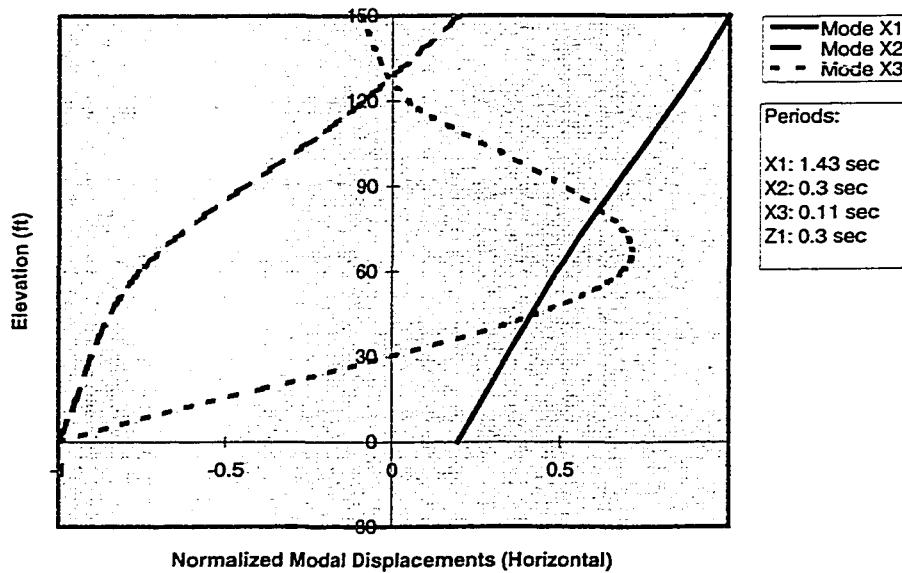


Figure 3-6: Platform Vibration Properties (Simple Model)

3.2.4 Earthquake Analysis

Both the simple and 2-D frame modal analyses utilized the API Soil B response spectrum (API, 1993) to derive earthquake loads once vibration properties were established. Loads were assumed to act simultaneously on the platform vertical and horizontal principal axes; the square-root sum-of-the-squares (SRSS) rule was used to combine the individual modal and directional responses. The load case used in both analyses consisted of the load on one horizontal axis found using the API spectrum for a ZPA of 0.25g combined with load on the vertical axis found using 0.125g. In addition to the response spectrum analyses; the 2-D frame model was analyzed using time history analyses for three earthquake ground motion records: Imperial Valley 1940 (El Centro Pump Plant S00E), Kern County 1952 (Taft Lincoln School Tunnel S69E) and Puget Sound 1949 (Highway 1 Test Lab Olympia N04W), all scaled to a PGA of 0.25g. All of these records were taken from the US National

Geophysical Data Center catalog of digitized strong motion (US NGDC, 1996); all records used have been corrected as described by Naeim and Anderson (1993).

Horizontal shears acting at each level along with peak pile loads are shown in Figure 3-7 and Table 3-3 for both modal analyses and the maximum results from the three time history analyses. Loads calculated from the two response spectrum analyses are, not surprisingly, in excellent agreement, given the agreement between the estimated platform vibration properties and the fact that most of the platform response is in the first few modes. The peak loads from the time history analyses are either enveloped or very close to the peak loads estimated from the simple method. The peak loads from all three methods differ by at most 5%.

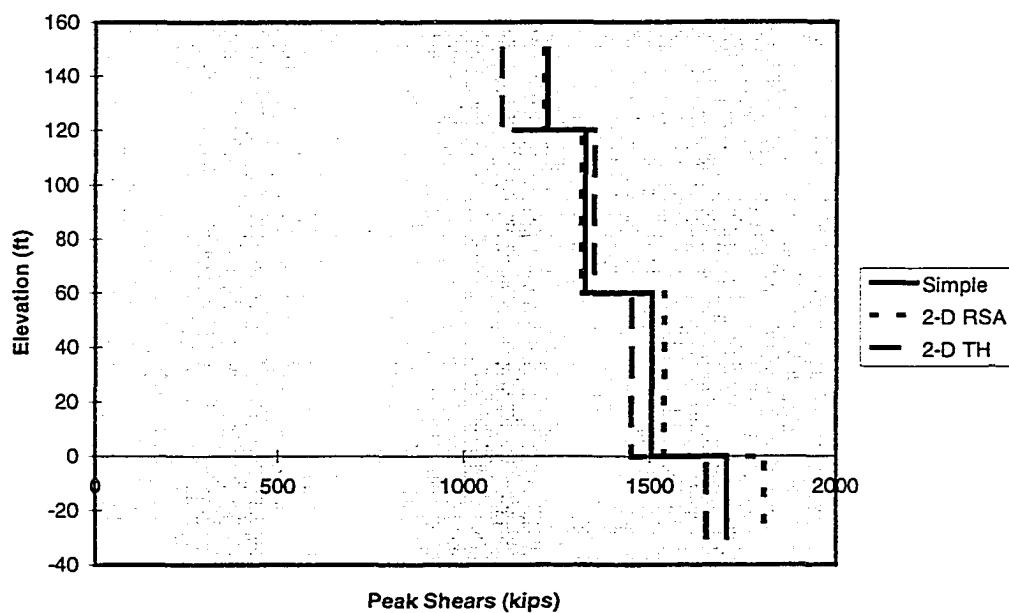


Figure 3-7: Platform Loads, ZPA = 0.25 g

Table 3-3: Pile Loads, ZPA = 0.25g

Pile Load	2-D RSA (kips)	Simple RSA (kips)	2-D TH (kips)
Tension	359	362	301
Compression	3859	3862	3823
Lateral	541	511	460

3.2.5 A Design Code Approach to Earthquake Forces

As an alternative to rigorously evaluating the vibration properties of a platform using modal analysis and then applying the response spectrum approach, there exist several semi-empirical earthquake-demand estimating approaches such as the one contained in Chapter 16 of the Uniform Building Code (UBC, 1994). These approaches are based upon the study of general trends of structural response to earthquakes, and are intended to allow for the development of forces with which a structural design can be started.

The UBC approach for horizontal forces assumes the structure in question has no great stiffness discontinuities, and that higher mode effects will decrease rapidly in significance. A total approximate base shear is estimated, and then distributed over the height of the structure in proportion with the mass at each level. In addition, a concentrated force is applied at the top to ensure that forces from higher modes will not be neglected in the upper portions of the structure.

To evaluate the utility of this approach in estimating earthquake demands for offshore structures, the basic force estimating procedure has been adapted for use with the API response spectrum. Base shear (immediately above the foundation) is estimated from:

$$V = SA_{T_1}W$$

where:

SA_{Tf} = pseudo-acceleration from response spectrum for fundamental period

W = total mass of the structure, not including foundation

The UBC recommends the following formula to estimate fundamental horizontal periods for braced frame structures:

$$T_1 = 0.02(h)^{0.75}$$

where:

h = height of structure above ground line (ft)

This period assumes no foundation flexibility, and hence will be too rigid for most offshore platforms. However, if estimates of foundation stiffnesses can be made, the fundamental period may be modified according to a period-lengthening procedure suggested by Veletsos and Boaz (1979):

$$\tilde{T}_1 = T_1 \sqrt{1 + \frac{k_1^*}{K_x} \left[\frac{1}{1 - (T_o / \tilde{T}_1)^2} + \frac{K_x h_1^{*2}}{K_\theta} \right]}$$

where:

T_1 = fixed-base fundamental period

T_o = natural period of foundation mass

k_1 = effective horizontal stiffness of fixed-base fundamental

K_x = horizontal stiffness of foundation

K_θ = rotational stiffness of foundation

h_1^* = effective mass center above base, not including foundation mass

The effective horizontal stiffness may be approximated by:

$$k_1 = \frac{4\pi^2(0.9M_1)}{T_1^2}$$

where:

M_1 = inertial mass of platform (it is assumed the first lateral mode has 90% mass participation)

The natural period of the foundation mass may be estimated from:

$$T_o = 2\pi \sqrt{\frac{W_o}{gK_x}}$$

where:

W_o = weight of foundation mass included in model

g = acceleration due to gravity

The forces distributed at the various levels in the structure are then determined in accordance with:

$$F_x = \frac{(V - F_t)w_x h_x}{\sum_{i=1}^n w_i h_i}$$

where:

F_t = $0.07VT_I$

w = mass at level

h = height of level

F_t is applied at the top of the structure, in addition to F_x at the top level. To obtain an estimate of the shear imposed on the foundation, the maximum base shear V found above is combined with an approximate value of the inertia force of the foundation mass (Veletsos, Boaz, 1979):

$$V_o = \left(\left(\frac{W_o A_o}{g} \right)^2 + V^2 \right)^{0.5}$$

where:

A_o = pseudo-acceleration of the foundation mass calculated from the response spectrum

To evaluate the utility of this modified UBC approach, it has been applied to the analysis of the example platform. Earthquake shears determined from 2-D response spectrum analysis (the SRSS rule was used to combine modes) are shown together with shears estimated by the modified UBC approach in Figure 3-8. The same pile and conductor stiffnesses used in the previous section were used to develop foundation translation and rotation stiffnesses.

The shears found using the UBC approach agree quite well with those found through application of 3-D RSA, being within 6% of the RSA values. The fundamental period estimate is quite good, 1.44 sec compared to 1.47 sec from 2-D modal analysis.

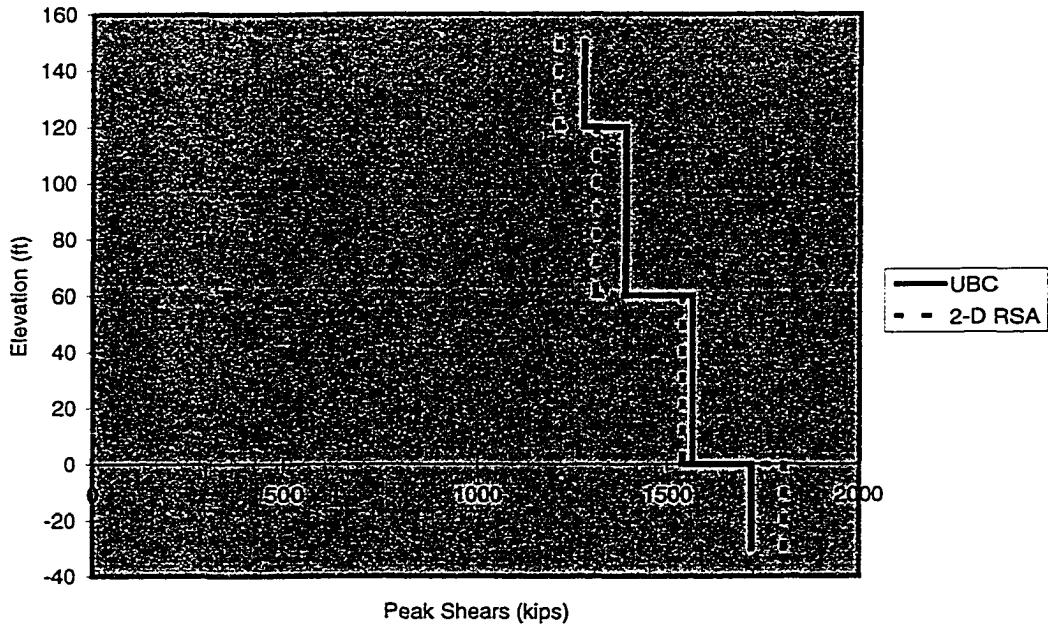


Figure 3-8: Comparison of UBC Forces and 3-D Modal Analysis Forces

3.2.6 Effect of Foundation Flexibility and Added Mass on Earthquake Loads

As the foundation is a significant source of platform flexibility, it is important that the associated stiffness properties of the foundation be well represented. Typically, stiffnesses for piles and conductors are developed by modeling the pile as a segmented beam supported by springs, and then developing pile-head load-deflection behavior from these models. In lieu of using the above procedure, a number of approximate approaches are available to estimate pile-head stiffnesses. Perhaps the most common approaches to estimating lateral and axial pile-head stiffnesses are those described in Section 3.1.3. There are, however, several other methods of approximation.

One alternative for pile-head horizontal stiffness is that used by Penzien (1975) in a series of studies of offshore platforms subjected to earthquakes:

$$k_x = 18.2Gr \frac{(1 - v^2)}{(2 - v)^2}$$

where:

G = shear modulus of the foundation soil

v = Poisson's ratio for the foundation soil

r = pile radius

This horizontal stiffness k_x is derived using elastic half-space theory and assuming the pile is deeply imbedded. Unless the foundation is extremely soft, the horizontal loads will be transferred quite rapidly to the surrounding soil with depth. Hence, the horizontal stiffness of each pile may be derived by considering the pile-head to be a rigid circular footing supported on an elastic medium. It is assumed to connection between the pile and jacket is rigid and allows for no pile-head rotation.

Another approach to estimating pile head stiffnesses is that suggested by Dobrey, et al. (1980). These approximations are based on previous work by Novak (1974) and Blaney, et al. (1976). Assuming foundation strength to rely upon soil elastic modulus and assuming as a basis a beam on an uniform elastic foundation, pile-head stiffnesses take the form:

$$k_z = 0.8 \frac{E_p A}{r} \left(\frac{E_s}{E_p} \right)^{0.5}$$

$$k_x = 2 \frac{E_p I}{r^3} \left(\frac{E_s}{E_p} \right)^{0.75}$$

$$k_\theta = 1.6 \frac{E_p I}{r} \left(\frac{E_s}{E_p} \right)^{0.25}$$

$$k_{\alpha x} = -1.2 \frac{E_p I}{r^2} \left(\frac{E_s}{E_p} \right)^{0.5}$$

where:

E_p = Elastic modulus of pile material

E_s = Elastic modulus of soil material

I = Moment of inertia of pile steel cross-section

Assuming there is no applied moment at the pile head, the effective horizontal stiffness may be represented by:

$$k_{x\text{effective}} = k_x - \frac{k_{\alpha x}^2}{k_\theta + k_{\theta\text{structure}}}$$

This effective stiffness will vary depending on the amount of rotational stiffness supplied by the structure attached to the pile head, $k_{\theta\text{structure}}$. These formulas are intended for intermediate values of E_s/E_p , and r/L ratios in the range of 10 to 50.

A comparison has been made between the various approximate pile-head stiffness and those derived during the course of the example platform analysis described earlier. Pile-head stiffnesses from the different approximations along with those used in the examples are shown below in Tables 3-4 and 3-5:

Table 3-4: Horizontal Pile-Head Stiffnesses (kips/in)

D	$12EI/L^3$ $L=5D$	$12EI/L^3$ $L=10D$	Penzien	Dobry	FE
72"	1093	136	870	515	469

Table 3-5: Vertical Pile-Head Stiffnesses (kips/in)

D	$3EA/L$	EA/L	Dobry	FE
72"	10933	3644	2915	3150

There is much variation between the approximate methods and the springs derived from the finite-element analysis. However, it must be remembered that these estimates may be obtained with much less effort than constructing and analyzing a segmented pile model. Furthermore, given the fact that soil properties may possess significant biases due to sampling and testing methods, there will be an element of variation to the springs derived from detailed analyses; this must be recognized by the analyst. The best of action when making use of these approximations is to select sets which will provide upper and lower bounds on the stiffnesses.

The stiffness contributions of landing mud mats and mudline braces were often ignored in the design of early platforms. The contact between the foundation soil and these elements can, however, provide great resistance if the supporting soil is strong enough. To study the effect of foundation flexibility on the horizontal response of a platform, the axial and horizontal pile-head stiffnesses used with the example platform were varied with respect to the values calculated from the detailed analysis (see Tables 3-4 and 3-5). The variation in fundamental horizontal period for the platform is shown in Figure 3-9. The period is seen to change from

1.25 sec to 2.0 sec; this could have a significant effect on calculated loads, depending upon the response spectrum being used.

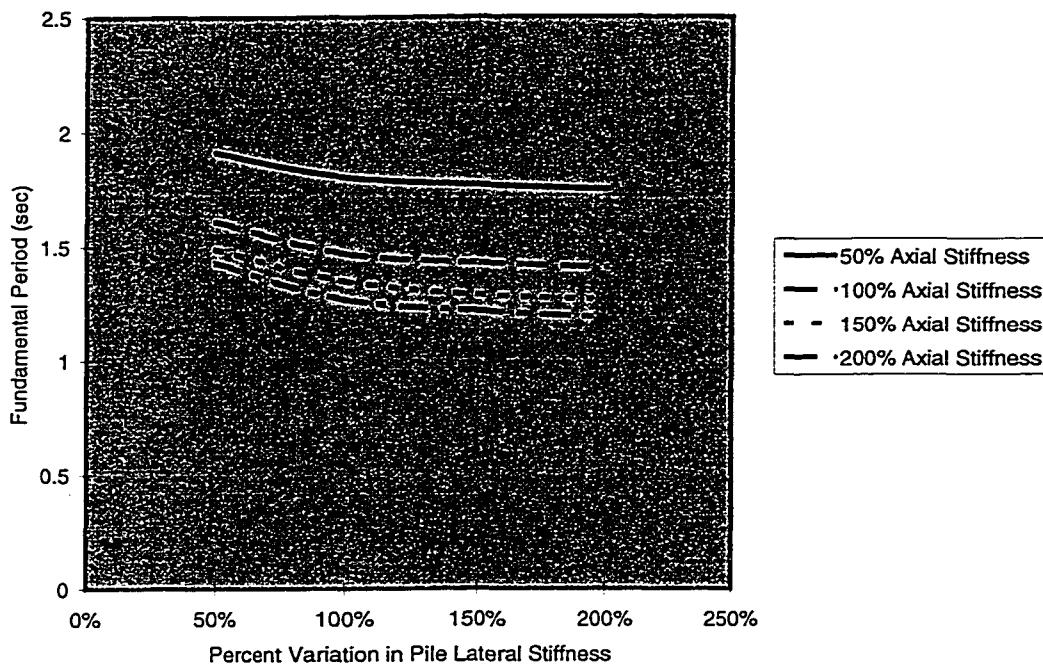


Figure 3-9: Example Platform, Variation in Fundamental Period for Foundation Flexibility

The variation in fundamental lateral period with added mass was also studied for the example platform. The added mass coefficient for tubular braces was varied from 1.0 to 0.0; it was not varied for legs, as they are considered not to be flexible in the sense defined by Clough (1960). Figure 3-10 shows the variation in fundamental period with the range of added mass coefficients considered. The variation is seen to be small; the tendency for brace added mass to be of lower important for structures less than 400 ft was also noted by Ruhl (1976) in a study of platforms in more moderate depths. Structures in deeper depths (1000 ft) will have more pronounced sensitivity to brace added mass.

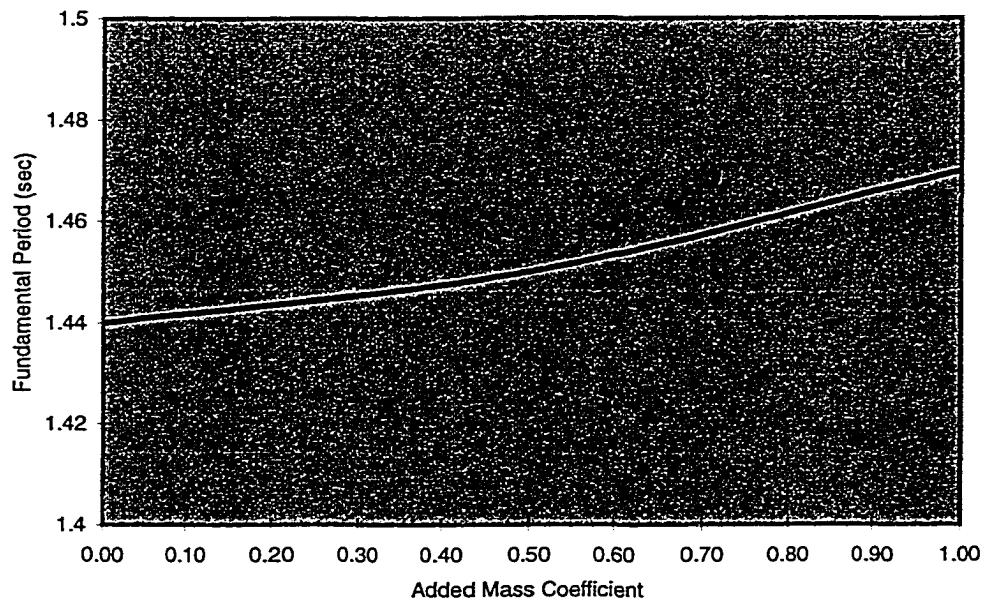


Figure 3-10: Example Platform, Variation in Fundamental Period with Brace Added Mass

3.3 SIMPLE NON-LINEAR RESPONSE OF PLATFORMS

If the loads determined by the simplified response spectrum analysis exceed the yield capacities of platform structural components, the platform is assumed to suffer inelastic damage. The location and amount of damage is estimated by assuming the platform behaves as a non-linear SDOF system (response is assumed dominated by the first mode). The damage is assumed to concentrate in the collapse mechanism which begins to form under application of first mode forces to the platform.

Two approximate approaches can be taken to determine the effective inelastic demand on the platform: (1) effective dynamic load or (2) peak displacement demand. These approaches are diagrammed in Figure 3-11. Both approaches begin by application of static pushover analysis to determine the lateral load at which the platform yields, and the limiting lateral

global displacement the platform can be forced to prior to sustaining unacceptable damage. For the first approach, the displacement limit and the cyclic hysteresis behavior the platform will exhibit globally as well as the fundamental period of the platform will enable selection of a load reduction factor R . This factor represents the effective reduction in elastically-calculated load which is allowed by nonlinear behavior. The effective dynamic load on the platform is then expressed by the elastic force estimated from response spectrum analysis reduced by the load reduction factor. The capacity of the platform is then assessed for this reduced load:

$$F_{yield} > \frac{F_{elastic}}{R}$$

where $F_{elastic}$ is the base shear corresponding to the first mode forces determined from the elastic response spectrum for the level of earthquake excitation specified. F_{yield} is the base shear from first mode forces which results in yielding in the platform determined from the static pushover analysis. It must be noted that this base shear is not the true base shear from the earthquake; it is used as a convenient reference to quantify the total lateral load needed to induced yielding.

For the second approach, the yield force, the associated hysteretic behavior and the fundamental period enable the selection of a displacement modification factor, F_d . The factor represents the ratio between equivalent linear and nonlinear SDOF system displacements. The effective global displacement demand is thus the elastically-calculated deck displacement increased or decreased by the displacement modification factor. The capacity of the platform is assessed for this modified displacement as:

$$\Delta_{collapse} > \Delta_{elastic} F_\Delta$$

where $\Delta_{elastic}$ is the elastically-calculated deck or global displacement, and $\Delta_{collapse}$ is the maximum tolerable global displacement of the platform. The two approaches are similar, but not exactly equivalent; load reduction factors are generally developed to restrain a system to a maximum fixed displacement ductility, while displacement modification factors simply relate mean elastic and inelastic displacements. Yield force is random and displacement ductility is fixed for load reduction factor determination, while yield force is fixed and displacement ductility is random for determining displacement modification factors.

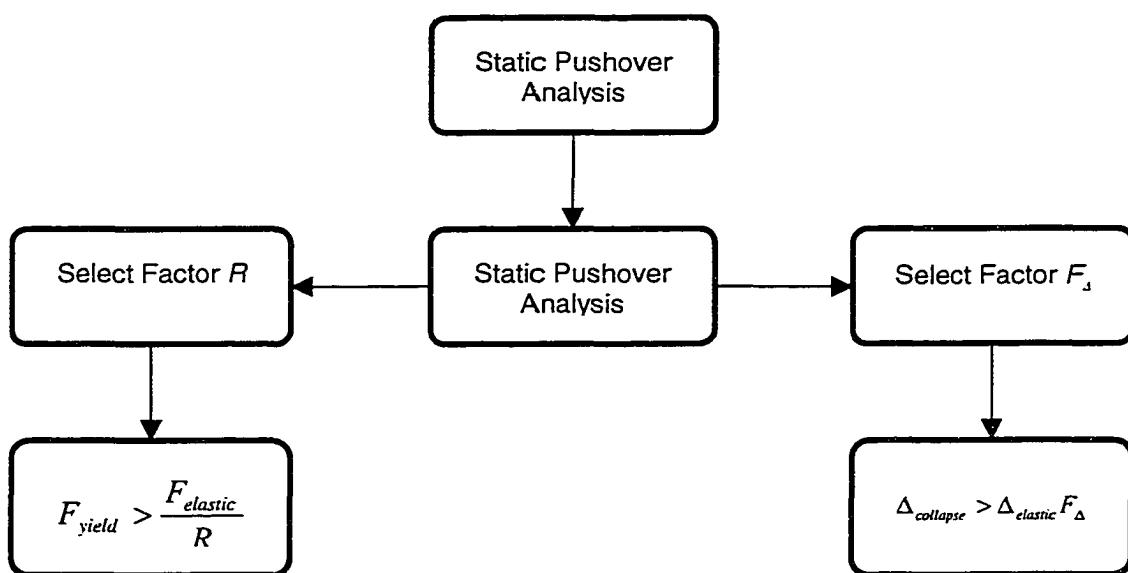


Figure 3-11: Simplified Inelastic Earthquake Analysis

R factors have been used for many years in the evaluation of design forces for onshore structures. The basic definition is given by Miranda and Bertero (1994):

$$R = \frac{F_{yield-elastic}(\mu = 1)}{F_{yield}(\mu = \mu_{design})}$$

This factor represents the maximum effective reduction in strength which may be taken to ensure a ductility of μ_{design} is not exceeded as a non-linear SDOF system responds to earthquake excitation. In a similar sense, it represents the maximum value of the overload ratio (elastic response spectrum forces to yield force) which may be tolerated by an SDOF system without exceeding the specified ductility of the system.

F_A factors are expressed by:

$$F_A = \frac{\Delta(F_{elastic})}{\Delta(F_{yield} < F_{elastic})}$$

Miranda (1991), while not specifically referring to this ratio as a factor, suggested use of this ratio in checking the displacements of inelastic systems from an elastic response spectrum for clearance and stability purposes.

A major goal of this study is the determination of R and F_A factors which account for the interaction between the hysteretic behavior exhibited by platform systems, overload ratio, and associated ductility demand. This topic is the subject of Chapter Five.

It must be emphasized that an approximate analysis of the type shown in Figure 3-11 will be sensitive to the load pattern used to estimate the formation of a collapse mechanism in the

platform. Miranda (1991) suggests the use of two load patterns when performing the static pushover analysis used to correlate global ductility with local ductility capacity: one based on a triangular load pattern, and one based on a uniform load pattern.

3.4 SIMPLE NON-LINEAR RESPONSE OF PLATFORMS: EXAMPLE

In this section, the simple non-linear response procedure is used to estimate the global ductility demand on the same offshore platform considered in Section 3.2 when subjected to very severe earthquakes. The results from the simplified analyses are compared to results from 2-D time history analysis. As the focus of the analysis is on lateral response, vertical excitation is ignored.

3.4.1 2-D Frame Model

The 2-D DRAIN2DX frame model used in Section 3.2 was utilized again for the time history analyses. Strut behavior was assumed to be elastic-plastic, thus the platform was not of a type which would suffer strength loss at large displacements or suffer from unzipping of the braced frame. Strut compression strengths were taken as approximately 80% of the fully-plastic strength in tension. The goal of this analysis is not to predict the actual capacity of the platform, but to demonstrate application of the simplified procedure used to estimate demands.

3.4.2 Static Pushover Analysis

A static pushover analysis was performed to establish the global load-displacement behavior exhibited by the platform. Using a load pattern based on first mode forces, the platform was

forced to displace until a gross global ductility of 2.25 was reached, as shown in Figure 3-12. This ductility was established by using a deck yield displacement of 17 inches, which is the onset of severe non-linear behavior. If the point of initial yield was used (13 inches), the ductility demand on the platform is 2.94.

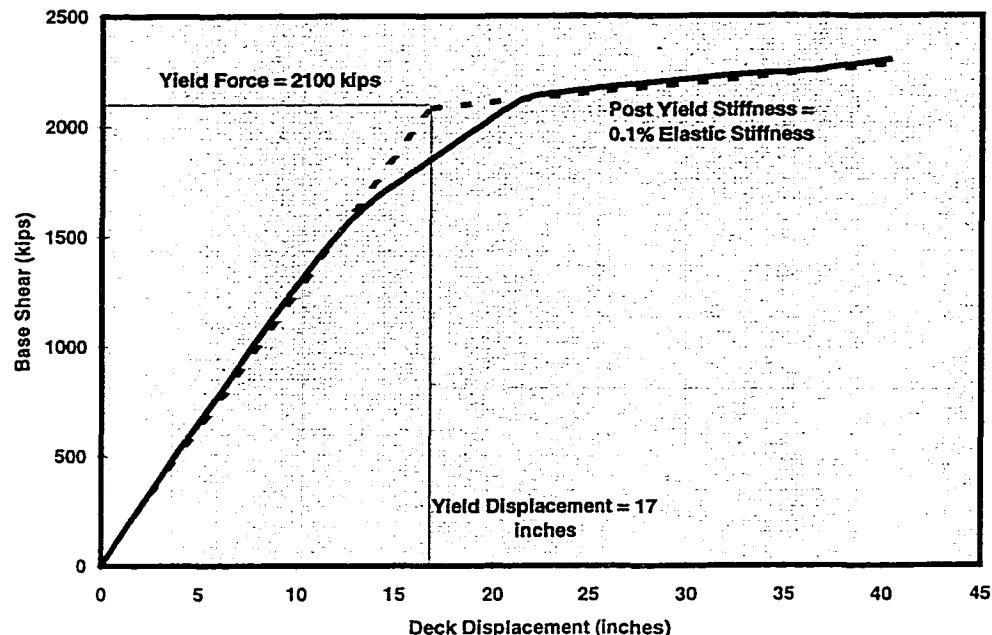


Figure 3-12: Global Load-Displacement Behavior of Platform

The load-displacement behavior exhibited by the platform in this mode is roughly bilinear, with strain-hardening ratio of approximately 0.001. The yield strength (base shear) of the platform is 2100 kips. This corresponds to a spectral acceleration of 0.71g. This would correspond to the API (1993) Soil B response spectrum scaled to a PGA of 0.86g. The relationship between global and local displacement established by the static pushover analysis is shown below in Figure 3-13 for several levels of deck displacement. In addition, the local ductility demands associated with the global displacement ductility of 2.25 are

shown in Table 3-6. Local ductility is expressed for the elements in a structural section which yield; in this case, yielding was confined to the diagonal braces in the first and second jacket bays, hence the value displayed is the axial displacement ductility of the most severely loaded brace in each bay. If no yielding took place in a section, the associated ductility demand was specified as zero. The shape of the collapse mechanism indicated by the analysis is shown in Figure 3-14.

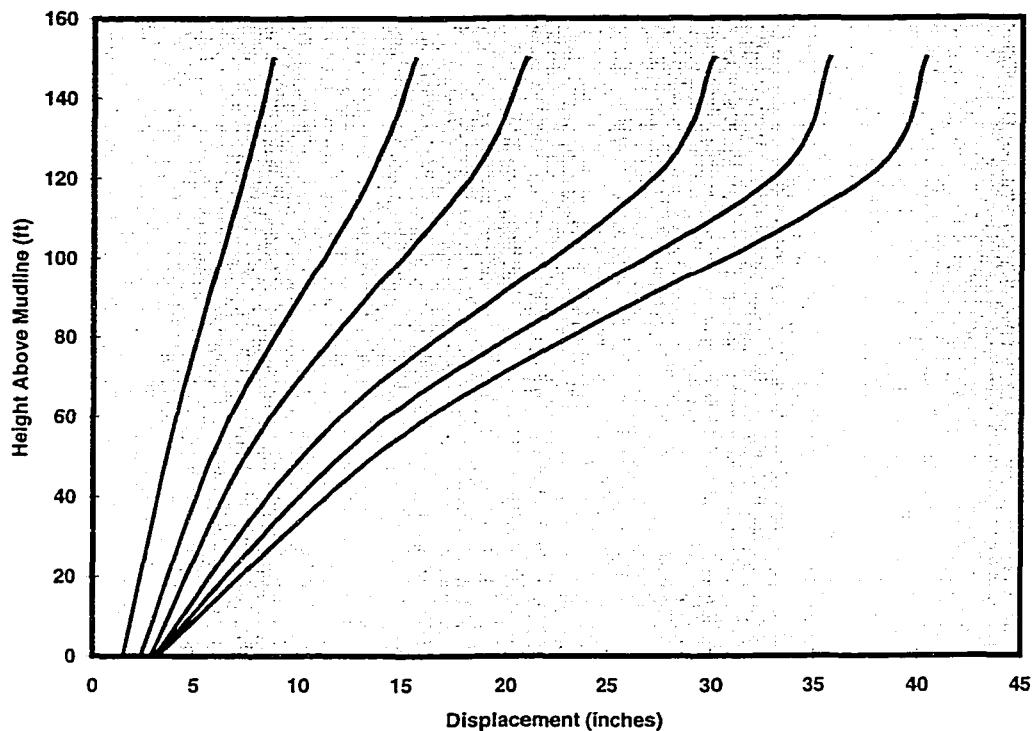


Figure 3-13: Scaled Horizontal Displacements in Platform for Different Levels of Deck Displacement

Table 3-6: Local Ductility Demands for a Global Ductility of 2.25

Structural Section	Ductility Demand
Deck Bay	0
First Jacket Bay (Braces)	15.9
Second Jacket Bay (Braces)	7.23
Foundation	0

Assuming ductility is to be limited to 2.25, using data from Miranda (1991) a reduction factor R of approximately 2.25 is selected. Therefore, so long as the elastically-calculated base shear remains below $2100 \text{ kips} \times 2.25 = 4725 \text{ kips}$, the global ductility demand on the platform should not exceed 2.25. This corresponds to a spectral acceleration of 1.59g, which is very unlikely in this period range. To achieve this acceleration, the API (1993) response spectrum would need to be scaled to a PGA of 1.92g.

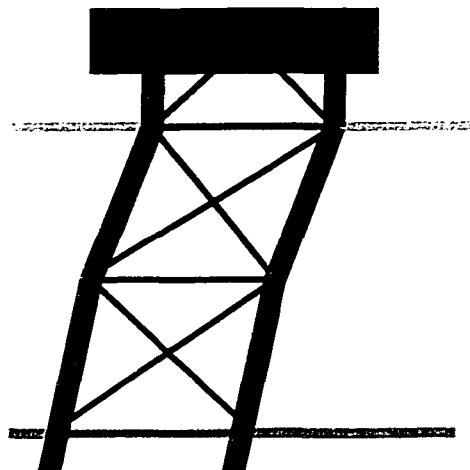


Figure 3-14: Shape of Assumed Collapse Mechanism for Example Platform

Similarly, again using data from Miranda (1991) a displacement modification factor F_d of approximately 0.95 is determined. Hence, so long as the elastically-calculated deck displacement of the platform does not exceed 36 inches, the displacement ductility should not exceed 2.25. This corresponds to a slightly higher spectral acceleration of 1.69g, with a corresponding API (1993) spectrum PGA of 2.05g.

3.4.3 Time History Analyses

To evaluate the accuracy of the ductility demand prediction process, the platform was analyzed for the three time histories used in Section 3.2. The time histories were all scaled to provide a spectral acceleration of 1.59g at a period of 1.45 sec with 5% critical damping. The scale factors which had to be applied to the time histories are shown in Table 3-7, along with their unscaled PGA. These scale factors correspond to very unrealistic conditions; however, the goal of this exercise to demonstrate the simplified assessment process, and not perform an actual assessment. For reference purposes, the peak deck displacements from each of the time history analyses are shown in Table 3-8. The peak ductility demands are shown in Table 3-9.

Table 3-7: Scale Factors Applied to Time History Analyses

Earthquake Record	PGA (g)	Scale Factor
Imperial Valley (El Centro)	0.28	14.05
Kern County (Taft)	0.18	12.71
Puget Sound (Olympia)	0.16	11.58

Table 3-8: Peak Deck Displacements (Time History Analysis)

Earthquake Record	Deck Displacement (inches) – Elastic	Deck Displacement (inches) - Inelastic
Imperial Valley (El Centro)	34	36
Kern County (Taft)	34	31
Puget Sound (Olympia)	34	24

Table 3-9: Global and Local Ductility Demands

Ductility	El Centro	Taft	Olympia
Global (first yield)	2.76	2.38	1.85
Global (gross yield)	2.12	1.82	1.41
Deck Bay (Braces)	1.44	1.39	1.01
First Jacket Bay (Braces)	11.87	9.96	6.33
Second Jacket Bay (Braces)	5.61	3.97	2.14
Foundation (Lateral)	1.09	1.29	0

Using the scale factors in Table 3-7, the analyses indicate that the platform gross global displacement ductility will not exceed 2.25 for the time histories considered. Judging from the values in Table 3-8, it is likely that if the time histories were scaled to the spectral acceleration value corresponding to application of the F_4 factor, the actual deck displacement would have been slightly higher than 2.25, but still very close. It is important to recognize that these response factors are random variables, and there will be substantial variability when they are applied to jagged spectra.

Equally important, however, is the similarity between the local ductility demands estimated in Section 3.4.2 and those shown here. The statically-estimated ductility demands are very close to those estimated from time history analyses in the areas of most severe damage concentration (the first and second jacket bays), deviating in proportion to the differences in the estimated deck displacements between the two analyses. For the Kern County Taft record, the difference in estimated global ductility demand is at most 6%, while local demands in the area of damage concentration are less close (approximately 25% difference). The Imperial Valley El Centro record and Puget Sound Olympia record are less in agreement, with differences of 23% and 40% respectively in gross global displacement ductility, and differences as high as 50% and 72% in local ductility; however, this difference can be traced in part to the deck displacement used in the static analysis and the deck displacements estimated by time history analyses. As a structure yields, it may shift off the peak areas of the spectrum, while an elastic system is trapped at the peak. This could likely be improved if a simple non-linear SDOF was used to estimate the target deck displacement for the pushover analyses, as proposed by Miranda (1991). Response factors are statistically averaged over

many results and are intended for use with smooth design spectra; hence they will not capture effects such as period shifting on a jagged spectrum.

Overall, the SDOF approximation to response for this platform provides a good approximation to the non-linear behavior estimated through application of time history analyses; the time history ductility demands are estimated very closely or enveloped by the results of the static analysis. The static analysis is also able to capture the most likely collapse mechanism to form, as well (first and second jacket bays). However, these results should be viewed with some caution. This platform has roughly four horizontal DOF (one at the deck and each horizontal framing level), and the majority of mass (86%) participates in the first mode. The amount of inelastic behavior observed in the time history analyses is small, with global ductility demands close to unity. Furthermore, by use of stiffness-proportional damping, the response of higher modes will be highly damped as compared to the first mode. However, while this can possibly have a significant effect on response prior to yielding, damping effects on a yielding structure are expected to be of secondary importance. Application of the simple non-linear analysis process, with the goal of assessing its accuracy and limitations, is explored further in Chapter Six.

3.5 SUMMARY

Simple procedures for estimating the linear and non-linear earthquake demands on offshore platforms have been presented. Linear demands on platforms are estimated first by approximating the vibration properties of the platform through a simple modal analysis, and then performing response spectrum analysis. Non-linear demands are determined by

assuming the platform behaves as a non-linear SDOF system, and that the pattern of damage concentration can be established by static pushover analysis.

An example simple linear analysis has been performed on a small platform. The simple modal procedure is found to accurately predict the principal vibration properties of the platform when compared to modal analysis using a 2-D full frame model. Forces estimated using response spectrum analysis together with the simple modal results compare well with the results of response spectrum analysis and three time history analyses using the full frame 2-D model of the platform. In addition, a design code approach to earthquake force calculation is evaluated; this approach, based on procedures of the UBC (1994) combined with period-lengthening approximations for foundation flexibility, is found to compare favorably with results from the simplified analysis and the 2-D frame model. Parameter studies are conducted to evaluate the effects of foundation flexibility and brace added mass; for the platform studied foundation flexibility was found to be an important consideration for vibration properties, while brace added mass was of lesser importance.

An example simple non-linear analysis has also been performed on the same platform. The simple non-linear analysis approach is able to predict the satisfactory behavior of the platform; in addition, the pattern of damage concentration developed by assuming the platform behaves as a SDOF system compares well with the damage estimated from time history analysis.

Additional case studies which utilize these simple methods are documented in Chapter Six.

CHAPTER FOUR:

EVALUATING PLATFORM STRENGTH AND DUCTILITY CAPACITIES

4.0 INTRODUCTION

The structure of a typical jacket-type offshore platform consists of two types of critical components (see Figure 4-1): bays in the structure (both deck leg and jacket sections) and the foundation.

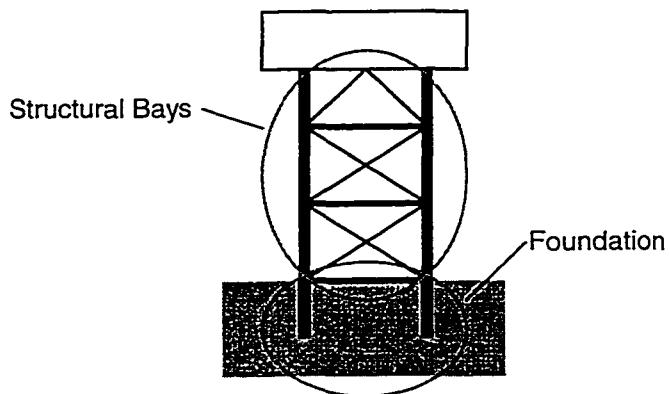


Figure 4-1: Critical Components in a Jacket-Type Platform

A bay in the structure consists of a series of parallel elements (either diagonal braces or unbraced leg sections) which act primarily to resist horizontal loads. The foundation also consists of a series of parallel elements: the piles (both main and skirt), conductors and mudline structure. The foundation elements act to resist both horizontal and overturning loads.

It is convenient for assessment purposes to define a "global" capacity for structures with respect to environmental loads. The global capacity represents the maximum supportable

load, acceptable displacement or energy absorption (as related to the demand measure) the structure can tolerate before undesirable behavior results, such as yielding, equipment failure or total collapse. For storm loads, the maximum supportable lateral load (i.e. base shear) is commonly used as a measure of global capacity. For a given pattern of lateral forces associated with an extreme storm wind, wave and current, the capacity of the platform is reached when the loads on one of the platform structural components (bays or foundation) exceed the load capacity of that component, i.e. a collapse mechanism is initiated. The occurrence of first member failure in a component is commonly taken to represent formation of a collapse mechanism for storm conditions, due to the sustained nature of the load and the low reserve strength typically exhibited by these structures. The storm load capacity of the platform is thus dependent upon both the strengths of its components (which are in turn dependent upon the strengths of the elements which make up the components) and the pattern of forces which results in component failure. The dependence of storm load capacity on the pattern of applied forces cannot be neglected; simply scaling up a fixed load pattern as opposed to changing the load pattern to represent increasing wave heights will concentrate load low in the structure, which can lead to misidentification of the correct collapse mechanism which will form. Cyclic loading is generally ignored for storm capacity determination, unless the engineer wishes to make use of capacity beyond first member failure (Hellan, et al., 1993).

Determining a global platform capacity for resistance against earthquake ground motions poses a greater challenge to an engineer than determining storm load capacity. The response of a platform is dependent upon the strength and stiffness of its components (both pre- and

post-yield), and the amplitude and sequence of ground motion “pulses.” Damage and failure in a platform subject to earthquakes can involve the following:

- The combined action of many modal responses
- Repeated cycling leading to fracture
- Changes in platform strength and stiffness which result in more severe demands

To explicitly evaluate the capacity of the platform to withstand a severe ground motion while accounting for these dynamic concerns requires time history analysis. In this case, the capacity of the platform will be expressed in terms of ground motion parameters representative of the earthquake severity, as opposed to more traditional measures such as base shear.

However, it is possible to implicitly account for these dynamic concerns while using equivalent static capacity measures if the system under evaluation is a relatively simple one. If the initiation of failure in the platform is due to response quantities dominated by the first lateral mode, the platform can be idealized as a nonlinear SDOF system, with yield strength equal to the first lateral mode base shear which results in first member failure in the platform, and a displacement ductility capacity equal to the global displacement ductility the platform can develop (using deck displacement as a measure) under the action of first lateral mode forces. The hysteretic behavior of the equivalent SDOF will be identical to the hysteretic behavior exhibited by the platform subject to first lateral mode forces. The yield strength of the SDOF is thus the equivalent earthquake load capacity of the platform, and the displacement ductility the SDOF can develop is the earthquake displacement ductility capacity of the platform. The use of this SDOF approximation has been discussed previously

in Chapter Three; the reader is referred to that chapter for additional references on the topic. It is important to recognize that this approximation is strongly dependent upon the load pattern used to estimate the global load capacity and the formation of a collapse mechanism which controls the platform displacement ductility.

The global load capacity and global displacement ductility can be adjusted to account for the dynamic concerns. It is possible to bias the load capacity based on a ratio of the portion of first mode response which initiates failure in a component to the total response which initiates failure. To safeguard against local buckling and fracture, cyclic displacement ductility limits for elements can be used (derived from test data and/or theory) when deriving the global ductility capacity of the platform. Changes in demand from the elastic state to the inelastic state can be accounted for by analyzing the equivalent non-linear SDOF using time history analysis, or by using a response factor R or F_d which relates the response of linear and non-linear SDOF systems to modify results from an elastic response spectrum.

This chapter documents procedures to determine the global load and displacement ductility capacities of offshore platforms. These procedures, while approximate, are intended to satisfy the following:

- Allow for identification of weak links in a platform structural system
- Evaluate the effective global strength of a platform, as expressed by base shear
- Evaluate the effective global displacement ductility of a platform, as expressed by deck displacement

Procedures to characterize the strengths and displacement ductilities of structural elements such as legs, braces, piles and mudline members are developed first. Building on the element strength capacities, expressions for the strength of the critical structural components are then formulated. From the interaction of these component capacities and an applied load pattern, the global strength of the platform can be determined. By assuming damage concentrates in platform components which yield, the displacement ductility of the platform as controlled by the displacement ductilities of the platform elements can be approximated.

These capacity determination procedures are applied to the evaluation of four structures: two tubular X-braced frames studied by Zayas, et al. (1980A), and two Gulf of Mexico platforms studied by Stear and Bea (1997A). Using information on the elements and geometry of the structures and the applied load pattern, the global strength of the structures, global cyclic displacement ductility capacity, and cyclic hysteretic envelope are estimated.

4.1 STRUCTURAL ELEMENTS

The main structural components in jacket-type platforms, i.e. the deck and jacket bays and the foundation, consist of parallel structural elements. Deck and jacket bays are made up of tubular braces and tubular legs or columns; these elements provide lateral resistance by axial loading of the braces and bending of the legs. The foundation consists of piles, conductors and mudline structure such as mats and horizontal braces; these elements provide lateral resistance by bending of the legs and conductors and contact between the mudline structure and top soil layer, and provide overturning resistance by axial loading of the piles and bearing

of the mudline structure on the top soil layer. In the following subsections, strength and ductility capacities for each of these different elements are formulated using a combination of simple plastic analysis and empirical results from structural testing. These element capacities are used in Section 4.2 to develop estimates for component capacities, which are then related to the platform global capacities.

4.1.1 Deck and Jacket Legs

A platform deck or jacket leg is a beam-column as shown in Figure 4-2. Assuming hinges form at the top and bottom of the leg, the maximum lateral load P the leg can support is:

$$P = \frac{2M_u}{H} - V_{p\Delta}$$

M_u is the ultimate moment which can be resisted by the legs in the presence of axial load, and can be estimated from the following M - P interaction equation for tubular cross sections:

$$M_u = M_{cr} \cos\left(\frac{\pi}{2} \frac{Q}{P_{crl}}\right)$$

where, using relationships from API (1993) for tubular members:

$$M_{cr} = M_p \quad \text{for } F_y D/t < 1500$$

$$M_{cr} = M_p \left(1.13 - 2.58 \left(\frac{F_y D}{tE} \right) \right) \quad \text{for } 1500 \leq F_y D/t < 3000$$

$$M_{cr} = M_p \left(0.94 - 0.76 \left(\frac{F_y D}{tE} \right) \right) \quad \text{for } 3000 \leq F_y D/t$$

$$P_{crl} = F_y A \quad \text{for } D/t \leq 60$$

$$P_{crl} = F_y A \left(1.64 - 0.23 \left(\frac{D}{t} \right)^{0.25} \right) \quad \text{for } D/t > 60$$

M_{cr} and P_{crl} represent, respectively, the maximum moment and maximum axial force the member cross-section can support without the initiation of local buckling of the tubular wall.

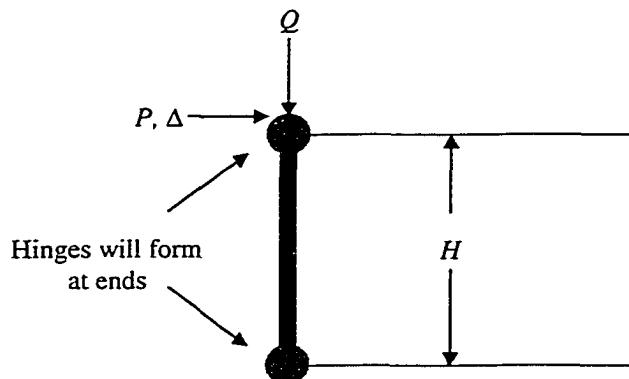


Figure 4-2: Platform Deck or Jacket Leg Element

V_{P_Δ} is an additional lateral force due to 1st-order P - Δ effects which reduces the effective lateral load capacity of the two-hinge mechanism:

$$V_{P_\Delta} = \frac{Q\Delta}{H}$$

To estimate Δ_{max} , the maximum lateral displacement the mechanism can tolerate, it is first necessary to establish the cross-section behavior. The nonlinear load-displacement behavior of bending cross-sections is approximated as shown in Figure 4-3:

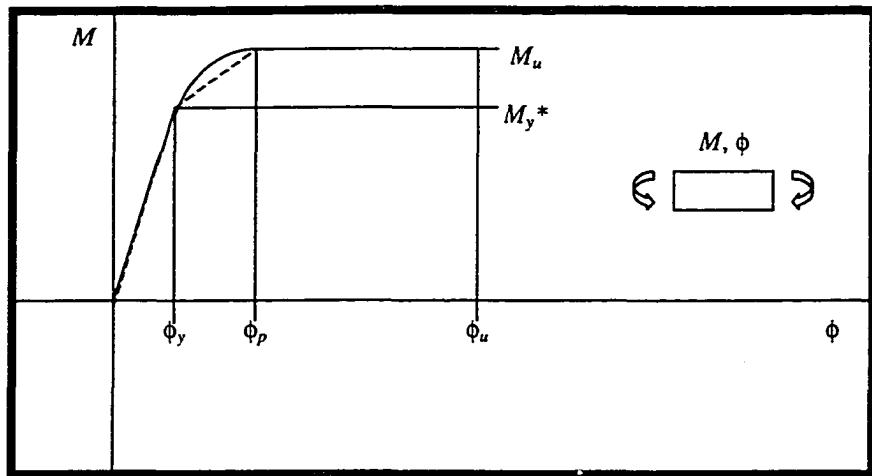


Figure 4-3: M - ϕ Relationship Approximation

M_u represents the maximum moment the cross-section can develop in the presence of axial load, as determined from the interaction equation. M_y^* is the yield moment, also determined accounting for interaction:

$$M_y^* = M_y \cos\left(\frac{\pi}{2} \frac{Q}{P_{crl}}\right)$$

ϕ_y is the cross-section rotation corresponding to M_y^* . ϕ_p is the cross-section rotation corresponding to the development of the plastic moment capacity of the section, and is twice ϕ_y . The effective rotation ductility of the cross-section μ_e will be given by the ratio of ϕ_u to ϕ_y .

The maximum tolerable hinge rotation for the cross-section will be controlled by either local buckling or fracture of the extreme fibers. For typical offshore tubular members with D/t greater than 25 (semi-compact), rotation will typically be limited by local buckling (Marshall, 1982). Local buckling in bending of tubular sections is sensitive to the following parameters:

- D/t ratio
- Axial load in the member
- Number and sequence of load cycles
- Imperfections in the member

To remain within the confines of a simplified analysis, it is desirable to use a performance limit on hinge rotations which will provide protection against local buckling for a large number of load cycles, so that information on applied load cycles need not be obtained when performing an assessment. As documented in Chapter Two, Sherman (1979) demonstrated that tubular beam-columns subjected to both axial load and bending would typically not exhibit sustainable ductility in excess of two under cyclic conditions. Sections which did not meet the compact section criteria suffered degradation prior to reaching this limit. Hence, recognizing the importance of protecting vertical supports, and recognizing their limited ductility based on test results, the following limits will be used for assessment purposes:

- For non-compact sections ($D/t > \lambda_r$):

$$\mu_s = 1.0$$

- For semi-compact sections ($\lambda_r \geq D/t > \lambda_p$):

$$\mu_s = \left(1 + \left(\frac{\lambda_r - D/t}{\lambda_r - \lambda_p} \right) \right) \text{ but not less than } 1.0$$

- For compact sections ($D/t \leq \lambda_p$):

$$\mu_\phi = 2.0$$

where:

$$\lambda_p = \frac{1,500}{F_y} \quad \text{Compact section requirement}$$

$$\lambda_r = \frac{3,000}{F_y} \quad \text{Semi-compact section requirement}$$

With the cross-section behavior established, it is then possible to relate the yield and plastic behavior of the cross-section to the P,Δ behavior of the member. The approximate yield displacement Δ_y of the beam will be:

$$\Delta_y = \frac{6M_y * H^2}{EI}$$

and thus the approximate displacement limit of the two-hinge mechanism will be:

$$\Delta_{max} = \mu_\phi \Delta_y$$

As these limits are based on M_y^* , the effective reduction in displacement capacity due to axial load is implicitly accounted for.

4.1.2 Tubular Braces

Tubular braces in offshore platforms are often treated as simple strut elements which only resist axial load. The axial strength of a tubular brace can be considered as the lesser of the axial strength of the brace and the strength of the joints by which it is connected to other structural members, as shown in Figure 4-4:

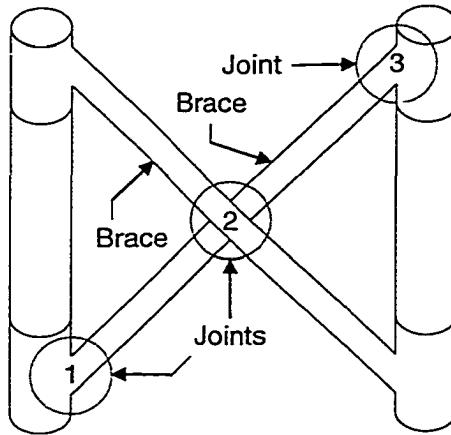


Figure 4-4: Brace-Joint System

Simple brace axial strength estimates can be derived from plastic analyses and beam theory. Tubular braces are assumed to be capable of developing full plastic strength in tension. The axial compression capacities of tubular braces can be calculated assuming a three-hinge failure mode at collapse (Figure 4-5), as described by Bea and Mortazavi (1995). Based on this three-hinge failure mode, the exact solution for the ultimate bending moment in a beam-column at collapse is given by:

$$M_u = \left(\frac{1}{1 + 2 \frac{\sin 0.5\epsilon}{\sin \epsilon}} \right) \frac{1}{\epsilon^2} \left(\frac{1}{\cos 0.5\epsilon} - 1 \right) (wl^2 + 8P_u \Delta_0)$$

where:

$$\epsilon = l \sqrt{\frac{P_u}{EI}}$$

and:

P_u = ultimate axial capacity of tubular brace

w = distributed local load

l = length of brace

Δ_0 = initial out-of-straightness

E = elastic modulus

I = cross-section moment of inertia of brace

Using P - M interaction in the brace as a second equation relating M_u and P_u :

$$\frac{M_u}{M_p} - \cos\left(\frac{\pi}{2} \frac{P_u}{P_p}\right) = 0$$

where:

M_p = plastic moment capacity of brace cross section

P_p = tension capacity of brace cross section, $F_y A$

and solving for Δ_0 assuming $P_u = P_{crl}$ from API RP 2A (1993), it is possible to solve for P_u using iteration.

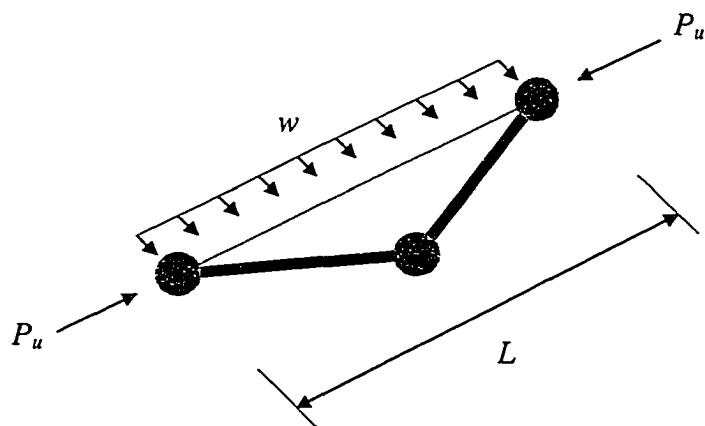


Figure 4-5: Three-Hinge Failure Mode for Braces

The distributed local load on the brace results from local response of the brace to earthquake excitation. The local acceleration, and hence the local force, can be determined by treating each brace as equipment mounted on the platform, and applying one of several common modal analysis techniques to estimate the appropriate local response. This subject has been a topic of research for many years, and much literature exists on the subject. An excellent summary of approaches used to estimate mounted equipment response in structures is presented by Bowen and Bea (1995).

The approach selected for estimating the local accelerations for the purposes of this study is one proposed by Biggs and Roessel (1970). It was originally developed to predict the response of mounted equipment in nuclear power plants. The procedure is organized into five steps:

1. Obtain the acceleration at the DOF x corresponding to the point of equipment support for each structure vibration mode i :

$$\ddot{u}_{xi} = \Gamma_i \phi_{xi} S A_i$$

2. Obtain the spectral accelerations for the equipment modes j :

$$\ddot{u}_j = S A_j$$

3. If the ratio of equipment mode period to structure mode period, T_{ej} / T_{si} , is less than 1.25, modify the structure's acceleration \ddot{u}_{xi} at the DOF of attachment by the amplification ratio A_{ej} / A_{si} which relates the interaction between the equipment and structure, and assign to \ddot{u}_{ij} :

$$\ddot{u}_{ij}' = \left(\frac{A_{ej}}{A_{si}} \right) \ddot{u}_{xi}$$

4. Otherwise, modify the equipment mode's spectral acceleration by A_{ej} / A_{si} , and assign to

$$\ddot{u}_{ij}'' :$$

$$\ddot{u}_{ij}'' = \left(\frac{A_{ej}}{A_{si}} \right) S A_j$$

5. Perform the above tasks for each mode of the structure. When done, combine the resulting accelerations according to the SRSS rule to get the equipment modal acceleration:

$$\ddot{u}_j = \sqrt{ \sum_{i \text{ over all } \ddot{u}'} (\ddot{u}_{ij}')^2 + \frac{\sum_{i \text{ over all } \ddot{u}''} (\Gamma_i \phi_{xi} \ddot{u}_{ij}'')^2}{\sum_{i \text{ overall all structure modes}} (\Gamma_i \phi_{xi})^2} }$$

Repeat the above tasks for each equipment mode. This will provide spectral accelerations for all equipment modes, after which forces can be determined using modal analysis procedures.

There are two limiting cases of equipment response that are important to understand. The first is the case in which the equipment is very stiff compared with the supporting structure. The equipment must move in the same manner as its support. The motion and the maximum acceleration of the equipment mass, A_e , must be the same as that of the supporting point on the structure, A_s . Thus $A_e = A_s$.

The second limiting case is that of very flexible equipment, where the period of the equipment, T_e , is much greater than that of the supporting structure, T_s . The internal distortion of the structure is relatively unimportant and the equipment will behave as though it is supported directly on the ground. In this case, the maximum acceleration of the equipment is equal to the maximum acceleration of the ground.

Between these two limiting cases, there is interaction between the equipment and the structure. The structure behaves as a frequency filter, developing harmonic components with frequencies equal to the modal frequencies of the structure. If the equipment has a natural frequency close to one of these harmonic components, the motion can be amplified. Near the point of resonance ($T_e \approx T_s$), the maximum acceleration of the equipment can be several times that of the supporting structure. The amplification (A_e / A_s) will be proportional to the number of cycles of motion, N (for low damping $A_e / A_s \approx N\pi$). Given a sufficient number of cycles (e.g. $N \geq 3$), the amplification is limited by damping ($A_e / A_s \approx 0.5\xi$).

Based on the results of time history analyses of jacket-type platform structures with deck-mounted substructures, Bowen and Bea (1995) developed an equipment acceleration magnification ratio relationship for use in determining accelerations on deck-mounted equipment (Figure 4-6). This relationship will be used to calculate the amplification ratios necessary for determining brace local accelerations. The relationship is based on a structure damping ratio of 5% and an equipment damping ratio of 2%. The acceleration magnification ratio shown in Figure 5-1 represents a mean result; at a given period ratio (ratio of equipment

period, T_e , to structure period, T_s) the coefficient of variation of the acceleration magnification ratio is estimated to range from 10% to 15%.

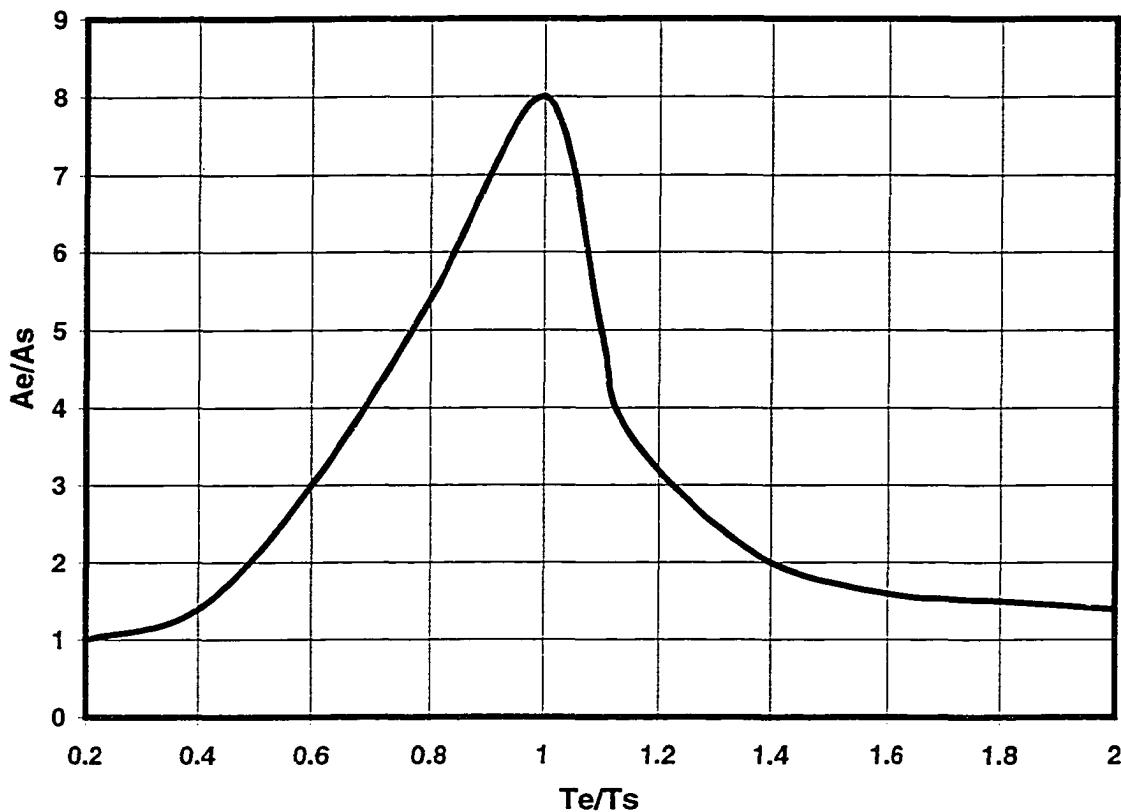


Figure 4-6: Equipment/Structure Amplification Ratios (Bowen, Bea, 1995)

Braces are assumed to respond in their fundamental lateral mode. The period associated with this mode may be calculated from (Schiff, 1990):

$$T_e = \frac{1}{(\lambda / 2\pi d^2)(EIg / w_d)^{0.5}}$$

where the distributed load w_d is the weight per unit length of brace, including any added hydrodynamic mass. λ is a dimensionless factor related to the support end conditions and to

the vibration mode. For the fundamental lateral mode, λ ranges from π^2 for a simply-supported beam to 22.373 for a fixed-fixed beam. The resulting acceleration is used to calculate the effective local lateral load induced on the brace; the local load w is simply $(w_d/g)\ddot{u}_l$. A parameter study is conducted on two of the case study platforms in Chapter Six, in order to assess the significance of this local load.

In addition to the axial capacity of the brace, it is necessary to evaluate the ability of the end connections to support the development of the brace's full capacity. Tubular joint tension and compression capacities can be established through application of empirical formulas documented in API (1993). These formulas are shown below in Table 4.1, they apply to the different joint configurations shown in Figure 4-7.

Table 4.1: Tension and Compression Capacities for Tubular Joints

Joint Type	Tension	Compression
T, Y	$f_y T^2 (3.4 + 19\beta)$ $\sin \theta$	$f_y T^2 (3.4 + 19\beta)$ $\sin \theta$
DT, X	$f_y T^2 (3.4 + 19\beta)$ $\sin \theta$	$f_y T^2 (3.4 + 13\beta)$ $\sin \theta Q_\beta$
K	$f_y T^2 (3.4 + 19\beta)$ $\sin \theta Q_g$	$f_y T^2 (3.4 + 19\beta)$ $\sin \theta Q_g$

where:

$$Q_g = 1.8 - 0.1 \frac{g}{T} \text{ for } \gamma \leq 20$$

$$Q_g = 1.8 - 4 \frac{g}{D} \text{ for } \gamma > 20$$

$$Q_\beta = \frac{0.3}{\beta(1 - 0.833\beta)} \text{ for } \beta > 0.6$$

$$Q_\beta = 1.0 \text{ for } \beta \leq 0.6$$

and:

$$\beta = d / D$$

$$\gamma = d / 2T$$

g = gap in branches of K-type joints

D = chord diameter

t = chord thickness

d = branch (brace) diameter

These relationships are known to provide conservative estimates of joint capacity, especially for X-joints (Bea, Mortazavi, 1995).

The post-yield behavior of the joint-brace-joint system is very complex. For the purposes of assessment, this section will concentrate on the post-yield behavior of the brace-portion of the system only. It is generally accepted that joints are not desirable locations to concentrate damage in a structure, as their configurations give rise to stress concentrations which can lead to cracking and fracture at low levels of plastic strain even for low numbers of cycles. Hence, if the joints are the weak link in a joint-brace-joint system, the system will be assumed to possess no displacement tolerance beyond yield.

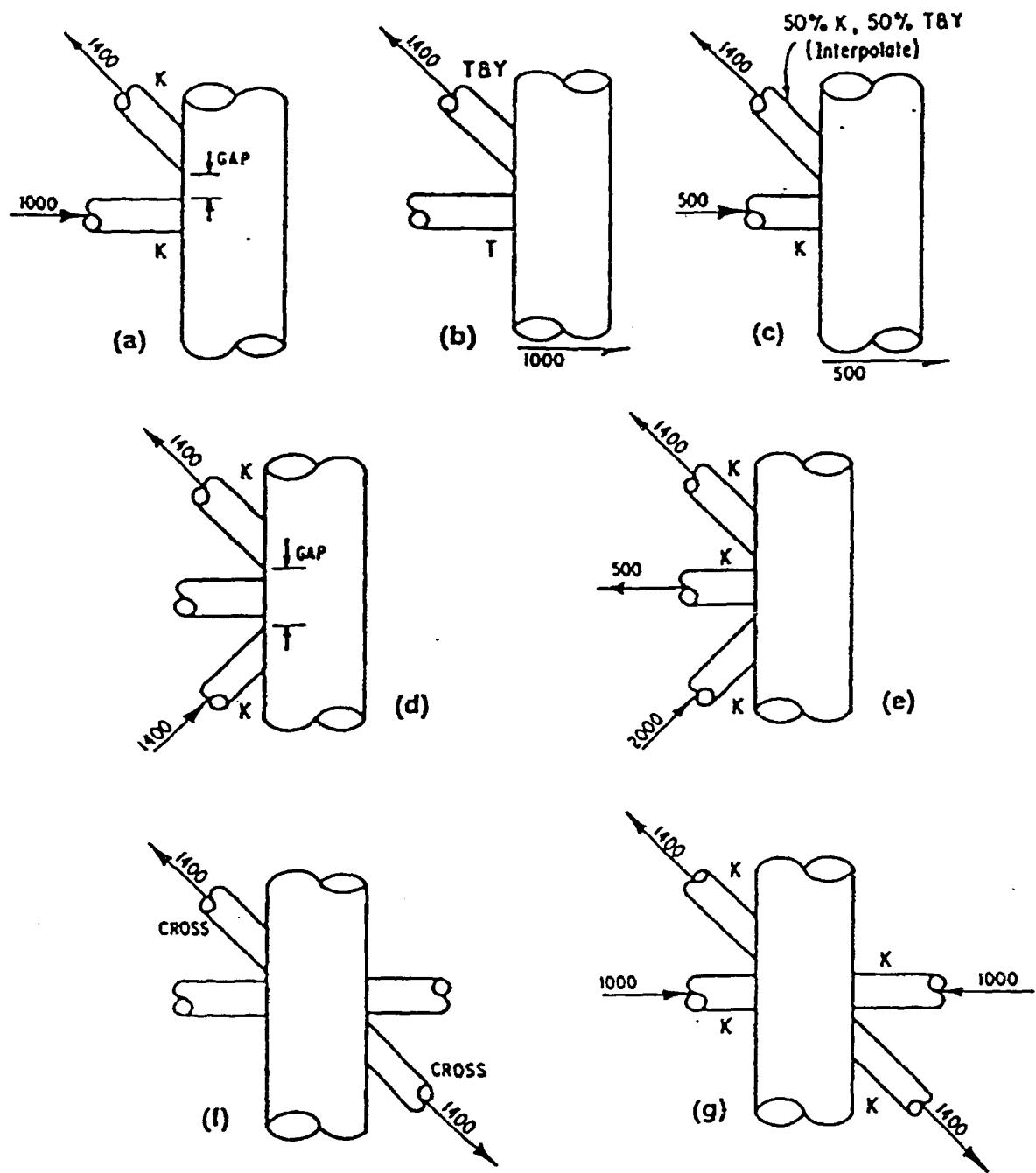


Figure 4-7: Tubular Joint Classification (API, 1993)

The behavior of braces which are alternately loaded beyond their yield and buckling capacities is very difficult to predict analytically. Traditionally, three approaches to modeling braces have been used: phenomenological models, physical models and finite-element models (Zayas, et al, 1981). Phenomenological models seek to replicate or mimic the behavior of braces as determined from experiments, while physical models and finite-element models seek to duplicate brace behavior based on rigorous evaluation of the stress and strain states in the brace. To date, phenomenological models are still the elements of choice when it comes to modeling the cyclic behavior of buckling/yielding braces, as this behavior has proved difficult to develop practical physical elements for. In particular, the following phenomenon provide complications:

- The Bauschinger effect, by which the stress-strain behavior of materials becomes more rounded after inelastic strain reversals. This leads to a reduction in a brace's buckling strength after the first cycle of buckling and then yielding in tension.
- Local buckling of the member wall when the member is placed in compression. This leads to localized areas of concentrated inelastic strain; repeated cycling of the member will cause cracking and eventual failure in the regions of local buckling.

For the purpose of performing a simplified static assessment, emphasis is placed on determining (1) a brace's maximum displacement capacity prior to the occurrence of local buckling, and (2) the effective reduction in load capacity with cyclic inelastic straining. Brace load-displacement behavior will thus be represented by the envelope curve shown below in Figure 4-8:

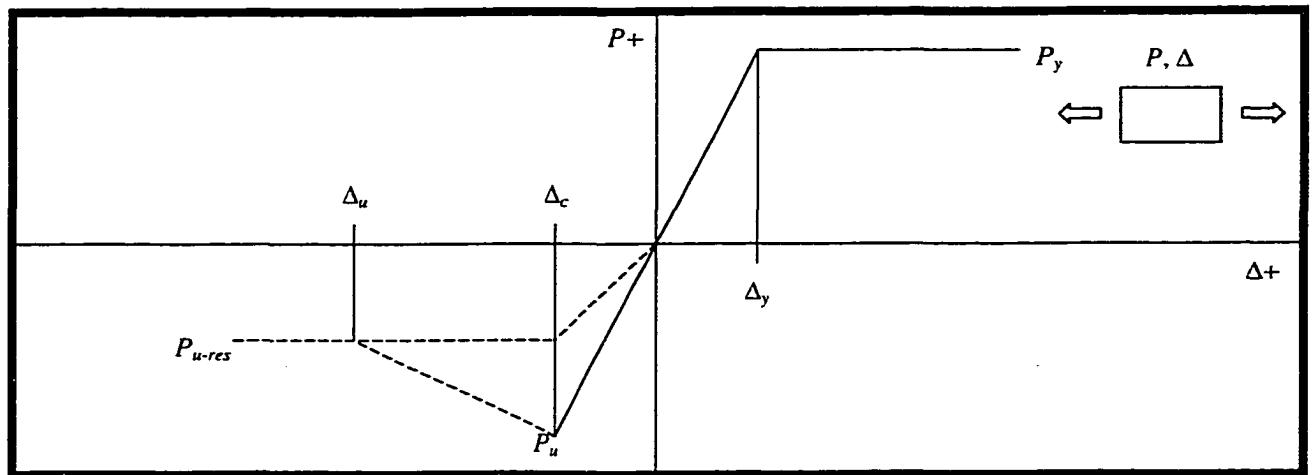


Figure 4-8: Simple Hysteretic Envelope for Brace Elements

If it is determined from the static demand-capacity analysis that a brace's compression capacity is exceeded by cyclic-type loads, the brace buckling strength is changed to P_{u-res} , an effective reduced strength which represents the strength on subsequent cycles. The compression stiffness is also modified, so that the buckling displacement remains the same. The element has a displacement tolerance Δ_u in compression, which represents the point at which local buckling will occur, leading to severe deterioration of the member.

It is assumed for non-cyclic loading, envelope curves estimated in this manner can still be taken as an effective measure of the post-buckling axial load-displacement behavior of braces. While this approximation will be conservative for short, stocky braces (low kL/r , D/t), which can exhibit a short plateau on the load-displacement curve in compression following buckling, it provides a very reasonable estimate of the behavior of behavior of

braces with more moderate length and aspect, which tend to exhibit an immediate drop in supportable load following buckling.

The reduction in buckling capacity of braces after one inelastic strain cycle has been studied by many researchers. A reduction of 20% is commonly taken, although this is very approximate (Astaneh, 1996). Jain, et al. (1978) proposed a reduction in strength based loosely on the buckling mode of the member, as represented by kL/r :

$$P_{u-res} = P_u \left(\frac{18}{kL/r} \right)$$

The compression displacement limit for braces is estimated based on cyclic compression displacement ductility limits proposed by Astaneh (1996). These relate the buckling mode, as represented by kL/r , and local buckling potential, as represented by D/t , to the maximum amount of displacement ductility μ_c which can be obtained in compression from the member without sever deterioration of the cross-section when subject to cyclic inelastic straining.

Based on column buckling:

$$\mu_c = 6 \text{ for } \lambda_c \leq 1$$

$$\mu_c = 6 - 10(\lambda_c - 1) \text{ for } 1.5 \geq \lambda_c > 1$$

$$\mu_c = 1 \text{ for } \lambda_c > 1.5$$

where:

$$\lambda_c = \frac{kl}{\pi r} \sqrt{\frac{F_y}{E}}$$

Based on cross-section properties:

$$\mu_c = 6 \text{ for } D/t \leq \lambda_p$$

$$\mu_c = 6 - 5 \left(\frac{D/t - \lambda_p}{\lambda_r - \lambda_p} \right) \text{ for } \lambda_r \geq D/t > \lambda_p$$

$$\mu_c = 1 \text{ for } D/t > \lambda_r$$

where λ_p and λ_r are the compact and semi-compact section limits.

Beyond the cyclic ductility limit for braces in compression, the member is considered to lose capacity for load due to local buckling. The effective strength of the brace is assumed to vary linearly from the residual value at μ_c to zero at $2\mu_c$ in this range.

Braces which are loaded in tension are assumed to behave as elastic-plastic elements. Barring the presence of flaws or defects, these braces can develop very large strains prior to fracture. Braces in tension are assumed to have a displacement ductility of 20 for the purpose of assessment.

4.1.3 Pile Capacity: Lateral

The horizontal strength capacity of an imbedded pile is estimated based on the assumption that the supporting piles will yield by either (1) forming plastic hinges at the base of the jacket and at some depth below the mudline, or (2) by complete shear failure in the soil (Figure 4-9).

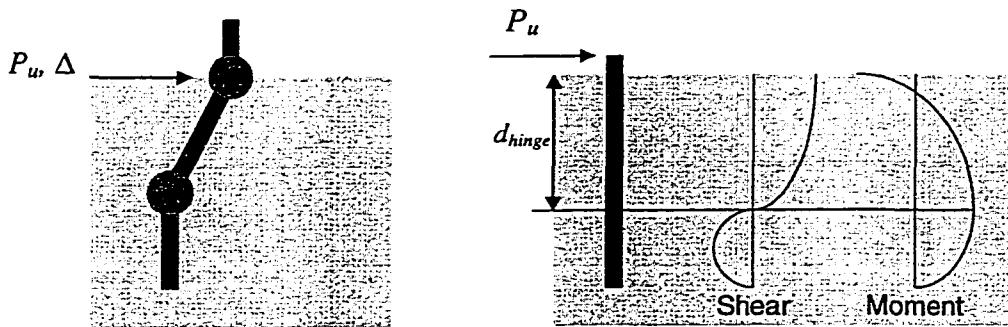


Figure 4-9: Pile Lateral Collapse Mechanism

The lateral load applied at the pile head which results in the formation of the two-hinge mechanism can be determined by successively checking for the location of the second plastic hinge which will form when the pile fails (the first is assumed to be at the base of the jacket). A hinge depth d_{hinge} is initially selected, and then the lateral capacity is approximated using two physical relationships. The first relationship is formulated assuming the selected point is the point of zero shear, and hence the pile lateral capacity $P_{u,l}$ can be obtained by summing up the incremental lateral capacity of the soil to this depth:

$$P_{u,l} = \int_0^{d_{hinge}} p_s(z) dz$$

where:

$$p_s(z) = \text{unit soil strength at depth } z$$

The second relationship is formulated using virtual work; the virtual displacement is the rotation of the second hinge:

$$P_{u,l} = \left[2M_u + \int_0^{d_{hinge}} z \cdot p_s(z) dz \right] \cdot \left(\frac{1}{d_{hinge}} \right)$$

where:

M_u = plastic moment capacity of pile section computed using P - M interaction

When the values of lateral capacity calculated using the two methods are in agreement, the true location of the hinge has been found, and hence the two values represent the correct lateral capacity. If the values do no converge, the pile will fail by shearing through the soil; in this case, the capacity will be given by the first relationship.

Unit pile soil resistance for cohesive soils with undrained shear strength S_u is taken to be:

$$p_s = 9S_u D$$

where D is the pile diameter. This formulation is supported by studies documented by Matlock (1970) and Randolph and Houlsby (1984) based on results for smooth piles. Unit soil resistance for cohesionless soils is estimated using a relationship from Broms (1964):

$$p_s = 3\gamma \cdot z \cdot D \cdot K_p$$

where:

$$K_p = \tan^2 \left(45 + \frac{\phi}{2} \right)$$

and:

γ = submerged unit weight of the soil

ϕ = effective angle of internal friction of the soil

The inelastic lateral displacement capacity Δ_u of the pile-head is estimated from the amount of cyclic plastic hinge rotation the piles can withstand, as calculated from the hinge ductility

relationships for beam-columns proposed by Astaneh (1996) documented in Section 4.1.1.

Δ_u can be expressed by:

$$\Delta_u = \mu_\phi \Delta_y$$

where Δ_y is the estimated pile head lateral displacement at which plastic hinges form in the pile.

It is well-established that the effective lateral load-displacement behavior exhibited at the pile head is very sensitive to the loading rate and the amplitude and number of loading cycles (API, 1993). High rates of load will result in effective increases in strength and stiffness; repeated loadings of the pile into the inelastic regime will result in strength and stiffness degradation. In a static analysis of a dynamic problem, these effects must be accounted for implicitly. While the subject of dynamic pile response is still a subject of much active research, a number of empirical relationships have been developed to allow engineers to assess the effects of loading rate and loading cycles on pile capacity in a simplified manner. It is important, however, that a range of parameters be considered when making such approximations, given the uncertainties involved in the problem.

Bea (1986) suggests the following effective increase in pile lateral (and axial) strength due to high rates of loading:

$$\beta_R = 1 + F \log\left(\frac{t_r}{t_s}\right)$$

t_r and t_s are respectively the dynamic loading rate and static or reference loading rate at which the pile capacity was first estimated (this is the loading rate associated with the evaluation of soil properties); both expressed in terms of percent of baseline pile capacity loaded per unit time. F is an empirical factor representing the rate at which stiffness and strength increase or decrease per log cycle change in the loading rate; it is in the range of 0.01 to 0.03 for sands, 0.02 to 0.07 for silts, and 0.02 to 0.12 for clays. For loading rates associated with earthquakes, effective increases in pile lateral capacity of 50% to 100% could be obtained, depending on the soil surrounding the pile.

Piles which are cycled below their ultimate capacity tend to exhibit little degradation in strength and stiffness (Bea, 1986). However, piles loaded beyond their ultimate capacity, i.e. into the gross inelastic regime, will progressively deteriorate with each load cycle, due to changes in soil properties and the formation of gaps between the pile and soil. This loss in strength can be expressed by:

$$\beta = 1 - \psi(1 - \delta)$$

ψ is referred to as the strength degradation factor, and represents the ratio of the measured percentage change in soil strength to the measured percentage change in soil stiffness; ψ is determined from tests for a range of cycles and strains. δ is referred to as the degradation index, and is a ratio of the secant shear modulus for a given cycle to the secant shear modulus for the first cycle. δ is also determined from tests for a range of strain levels. In lieu of estimating the number and magnitude of inelastic loading cycles, the effects of degradation can be bounded by using fully-cycled soil properties to estimate the pile strength and

stiffness; pile stiffness is assumed to decrease in direct proportion with pile strength. It is important to note that the ductility capacity of the pile will not change in this case, as the pile hinge rotation yield displacement remains the same.

4.1.4 Pile Capacity: Axial

The procedure by which the axial capacities P_z of piles are determined is straightforward: the individual soil layer friction contributions and, for the case of compression loading, the bottom layer end-bearing capacities, are determined and then summed; P_z is taken as the minimum of either this sum or the pile yield strength $F_y A$:

$$P_z = qA_p - wL_p + \int_0^{L_p} f(z)A_s dz$$

where:

q = normal end yield force per unit of pile-end area

f = shear yield force per unit of embedded shaft surface area

A_p = area of pile tip

A_s = embedded shaft surface area per unit length of pile

A = steel cross-section area of pile

L_p = pile length

w = weight of pile and soil plug per unit length

The end-bearing capacity can only be mobilized when the friction capacity of the internal soil plug exceeds the end-bearing capacity.

The bearing strength q of cohesive soil with undrained shear strength S_u is:

$$q = 9S_u$$

The ultimate shaft friction is estimated from the following relationship:

$$f = \kappa S_u$$

where κ is the side resistance factor. Focht and Kraft (1986) provide values for κ as a function of S_u :

Table 4-2: Side Resistance Factor for Cohesive Soils, from Focht and Kraft (1986)

S_u , ksf	κ
< 0.5	1.0
0.5 to 1.5	1.0 to 0.5
> 1.5	0.5

For cohesionless soils, the ultimate bearing capacity is estimated from:

$$q = N_q \sigma_v$$

N_q is a bearing capacity factor dependent on the friction angle ϕ of the soil. σ_v is the effective pressure at the pile tip. The unit shaft resistance per unit length of pile is taken to be:

$$f = k \sigma_{vi} \tan \theta$$

where:

k = lateral earth pressure coefficient, assumed to be 0.8 (API, 1993)

σ_{vi} = effective overburden pressure at depth

θ = friction angle between soil and pile, taken as $\phi - 5^\circ$

The unit shaft resistance and unit end-bearing capacity cannot increase indefinitely with pile penetration; the following limiting values for N_q , q and f are used from Focht and Kraft (1986):

Table 4-3: Limiting Values of N_q , q and f , from Focht and Kraft (1986)

ϕ , degrees	N_q	q , ksf	f , ksf
20	8	40	1.0
25	12	60	1.4
30	20	100	1.7
35	40	200	2.0

Providing the mechanism by which the pile yields involves yielding of the soil and not the yielding of the pile steel, there is no effective limit to the axial displacement ductility. Hence, limits on the axial yielding of piles will be established from consideration of the overall stability of the platform system.

As with lateral loading of piles, the axial strength and stiffness measured at the pile head are dependent upon both loading rate and magnitude and number of loading cycles. The same approximations used to account for dynamic effects on pile lateral capacity can be used to adjust the static axial capacity of piles (Bea, 1986).

4.1.5 Conductors, Mats and Mudline Braces

In addition to the support provided by piles, a fixed offshore platform can also benefit from the resistance provided by well conductors, mud mats and mudline braces. While it is common for engineers to consider the strength and stiffness of conductors and mud mats in

the design of modern platforms for all conditions, these elements were typically neglected in earlier designs when considering environmental load cases such as storms and earthquakes. The neglect of these elements, together with conservative modeling of pile-soil interaction, has lead to the belief in the offshore engineering community that many early jacket-type platform foundations are weak and very flexible.

Historical performance of platforms continues to demonstrate the robustness of marine foundations for older platforms; investigations performed by Bea, et al. (1997) and Stear and Bea (1997A) on platforms subjected to intense storms, for example, have demonstrated that use of current API pile-soil interaction design guidelines and the neglect of mudline element action in reassessment will lead to substantial under-prediction of platform foundation capacities. In addition, vibration field data recorded by Ruhl (1976) and Mason, et al. (1989) confirm that mudline elements greatly increase the effective lateral and rotational (rocking) stiffness of platform foundations; differences in design fundamental lateral periods and field measured fundamental lateral periods of 100% or more have been noted by these two sources.

Due to the significant effects these elements can have on global platform strength, simple approximations are included in this chapter for accounting for their effects. Expressions for the effective stiffness of these elements have been included in Chapter Three.

Conductors are treated as piles which offer lateral support only. This is due to the fact that conductors do not generally have strong or stiff vertical connections to the platform structure.

Mud mat and mudline brace foundation capacity contributions are determined using approaches suggested by Section 6.13 of API RP 2A-WSD (1993) for mat foundations. It is assumed that these elements are very strong and stiff compared to the underlying soil; hence strengths will be dictated by the soil properties. Bearing and sliding capacities for these elements are determined using the following:

For elements founded on cohesive soils (clays):

$$Q = 5.14cA \quad \text{maximum bearing strength}$$

$$H = cA \quad \text{maximum sliding strength}$$

where:

c = undrained shear strength of soil

A = foundation contact area

For elements founded on cohesionless soils (sands):

$$Q = 0.3\gamma'BN_y A \quad \text{maximum bearing strength}$$

$$H = c'A + Q \tan \phi' \quad \text{maximum sliding strength}$$

where:

γ' = effective unit weight of soil

B = minimum lateral foundation dimension, assumed to be unity

$$N_r = 2(N_q + 1) \tan \phi'$$

$$N_q = (\exp[\pi \tan \phi']) (\tan^2(45^\circ + \phi'/2))$$

ϕ' = effective friction angle of Mohr envelope

c' = effective cohesion intercept of Mohr envelope, assumed 0 for sand

A = foundation area

The lateral capacity provided by mudline elements is taken as the product of the contact areas of all mats and mudline braces (the contact areas for braces are assumed to be DL) with the soil sliding and bearing strength. It is assumed that mats and mudline braces actively contribute to bearing strength only when placed in compression; i.e. they do not provide support against uplift.

Conductors are assumed to exhibit the same inelastic performance as piles, and have similar ductility limits derived on the basis of critical hinge rotations. The inelastic sliding and bearing behavior of mats and mudline braces is complex, but similar to the behavior of piles and conductors; these elements will exhibit effective increases in strength and stiffness for high rates of load, and decreases in strength and stiffness for cyclic inelastic loading, primarily due to the sensitivity of soil material properties to these load characteristics. Limits on the maximum tolerable inelastic displacements associated with these elements will be derived from considerations of the overall stability of the platform system.

It is emphasized that these approximate element strengths are intended to allow an engineer to assess the possible significance of additional foundation capacity from elements other than piles. The true contributions to foundation strength of conductors, mudline braces, and mud mats will also depend upon the strength and stiffness of the connections and other elements which may be in the load path between the element and the platform structure; no provisions for checking the capacities of these connections and additional elements are provided in this document.

4.2 COMPONENT STRENGTHS AND GLOBAL STRENGTH

The process of determining platform global strength and displacement ductility begins with the determination of the strength capacities of platform components: lateral load capacities for the deck bay, the jacket bays, and the foundation lateral mechanism and moment capacity for the foundation overturning mechanism. Based on a comparison of the resulting component strength capacity profile with a specified pattern of loads, likely platform collapse mechanisms and the lateral load level which initiates these mechanisms can be identified.

In this section, load capacities for the different platform components are formulated using the element strength capacities described in Section 4.1. These capacities are formulated including the effects of $P\Delta$ strength reduction and batter force strength increase. The component capacities are then related to the global strength of the platform.

4.2.1 Unbraced Deck Bay Strength

Unbraced bays are assumed to behave like portal frames which form hinges in the supporting columns. The strength capacity of an unbraced bay will be reached when plastic hinges have formed in all of the supporting legs, as shown in Figure 4-10:

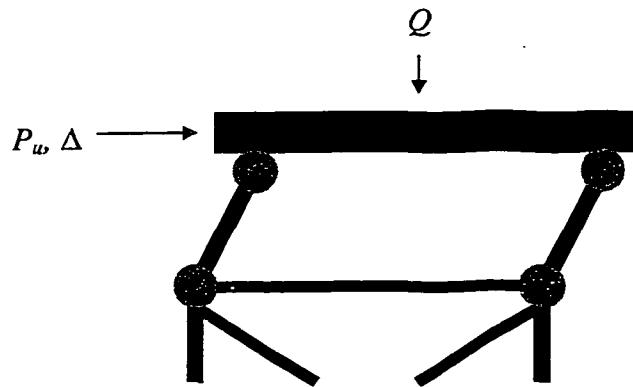


Figure 4-10: Collapse Mechanism for an Unbraced Bay

Accounting for P-Δ effects, and assuming uniform leg sizes, the effective shear force capacity P_u of the bay is:

$$P_u = \frac{2nM_u}{H_d} - V_{P\Delta}$$

where:

H_d = height of bay

n = number of legs in the bay

M_u = ultimate moment which can be resisted by the legs in the presence of axial load

$V_{P\Delta}$ is the additional shear force due to first-order P - Δ effects:

$$V_{P\Delta} = \frac{Q\Delta}{H_d}$$

where Δ is the lateral displacement of the bay needed to form a fully-plastic mechanism. This displacement will consist of two parts: the bending deflection of the legs in the unbraced bay, and an associated rigid body component due to the rotation of the leg cross-sections at the bottom of the bay, as shown in Figure 4-11.

An equivalent rotational stiffness $k_{\phi-leg}$ at the bottom of each unbraced leg which accounts for rotation of the cross-section due to bending and from deflection of the braced section beneath the bay can be estimated by (Bea, Mortazavi, 1995):

$$\frac{1}{k_{\phi-leg}} = \frac{H_b}{EI_b \cos \beta} \left(1 - \frac{3k_{bay}H_b^3}{4k_{bay}H_b^3 + 12EI_b \cos \beta} \right)$$

where:

H_b = height of braced bay beneath unbraced section

I_b = moment of inertia of leg section in braced bay beneath unbraced section

β = angle of batter on jacket

k_{bay} is the lateral stiffness associated with the braced section:

$$k_{bay} = \frac{1}{2} \sum_{i=1}^{n-brace} \frac{EA_i \cos^2 \theta_i}{L_i}$$

where A and L are the cross-section and length of diagonal braces. The total displacement will thus be given by:

$$\Delta = M_u H_d \left(\frac{H_d}{6EI_d} + \frac{1}{k_{\phi-leg}} \right)$$

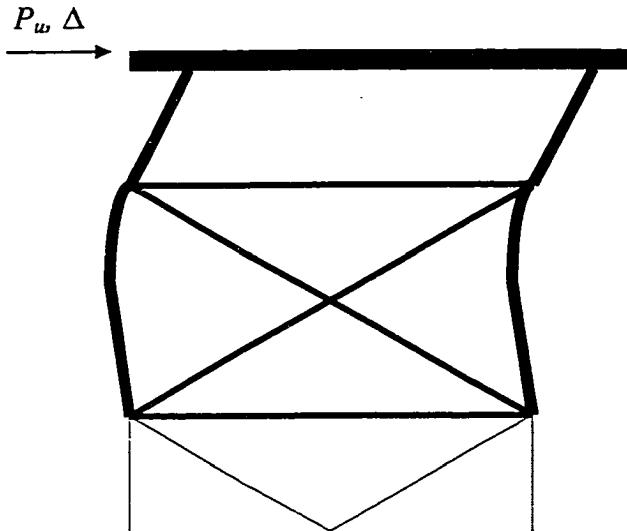


Figure 4-11: Deflection of Unbraced Bay

4.2.2 Braced Bay Strength

The shear force which can be resisted by a braced bay is dependent on the axial tension and compression capacities of the bracing members and their connections to the jacket legs. A mechanism is assumed to form in the bay when the first member in the load path fails (Figure 4-12). The shear force capacity P_{ubay} of a braced jacket bay will be given by:

$$P_{ubay} = \sum_{i=1}^N \Delta_{tsr} K_i + F_{tL}$$

where:

- Δ_{1st} = displacement of bay top needed to cause yielding of most likely member to fail, found from the smallest ratio of $(P_{ui}/K_i)\cos\theta$
- K_i = effective horizontal stiffness of individual braces, $(EA/L)\cos^2\theta$
- P_{ui} = minimum of either brace axial strength or strength of tubular joints by which brace is attached to jacket legs
- F_{1L} = batter forces from legs associated with first mode response
- θ = angle between brace and horizontal

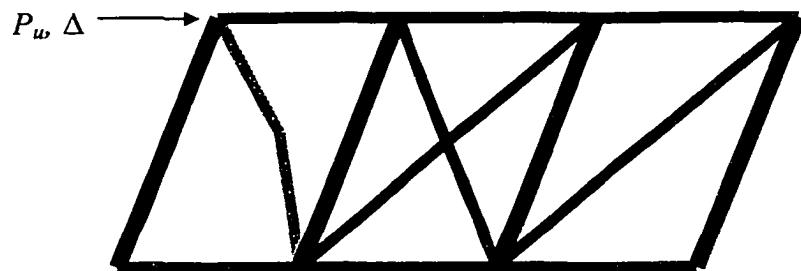


Figure 4-12: Braced Bay Collapse Mechanism

If there is an unbraced portal above a braced section, such as an unbraced deck bay or a bay in which the braces have collapsed due to large displacements, there can be significant reduction in the capacity of the braced section due to the need to balance the large bending moments in the legs of the unbraced section, as shown in Figure 4-13. This can be accounted for by further reducing the shear capacity of the braced section by the effective shear needed to balance the leg moments induced by the deflection of the portal frame. This reduction V_{bend} can be approximately expressed by:

$$V_{bend} = \frac{nM_{leg}}{H_b}$$

The moment at the tops of the legs in the bay M_{leg} due to load P on the unbraced bay is given by (Bea, Mortazavi, 1995):

$$M_{leg} = \frac{\frac{PH_d^2}{2EI_d} + \frac{PH_d}{k_{\phi-rot}}}{\frac{H_d}{EI_d} + \frac{1}{k_{\phi-rot}}} - PH_d$$

This effective reduction in capacity is not considered between braced bays; however, if a braced bay is subject to large displacements (large enough to damage the braces in the bay), depending on the size of the legs the leg moments at the base of the damage bay can become large enough to cause significant reduction in the capacity of the next bay down. This can lead to progressive collapse of braces in bays beneath the first bay to be damaged.

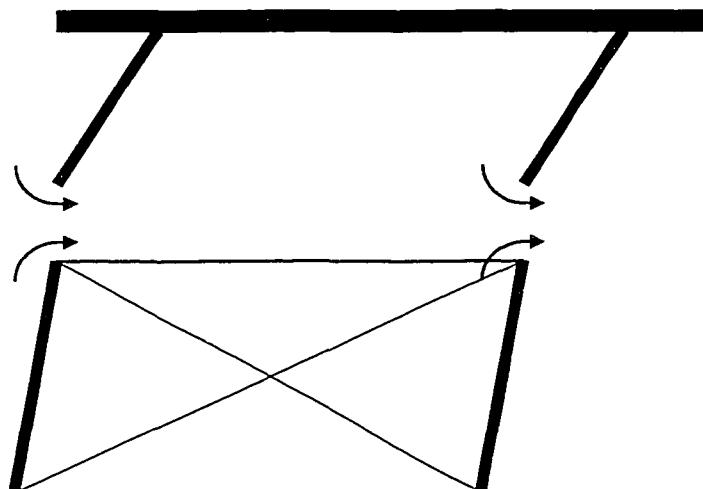


Figure 4-13: Reduction in Bay Shear Capacity Due to Leg Moments

As $P-\Delta$ effects are usually quite small for braced bays, they are neglected in this formulation. The effective lateral strength contribution of the jacket legs in bending is typically neglected; however, some platforms have unusually massive legs which will offer substantial contributions to capacity even at small bay displacements. Based on a limited study of jacket bay sections, the approximate increase in bay capacity due to bending action of the legs can be estimated by:

$$P_{leg} = \frac{n^4 EI_b}{H_b} \Delta_{1st}$$

4.2.3 Foundation Lateral and Overturning Capacity

In addition to lateral collapse mechanisms which may form in the jacket and deck bay, it is also possible for a collapse mechanism to form in the foundation based on the hinging of all piles and conductors, and the sliding of all mudline elements (Figure 4-14):

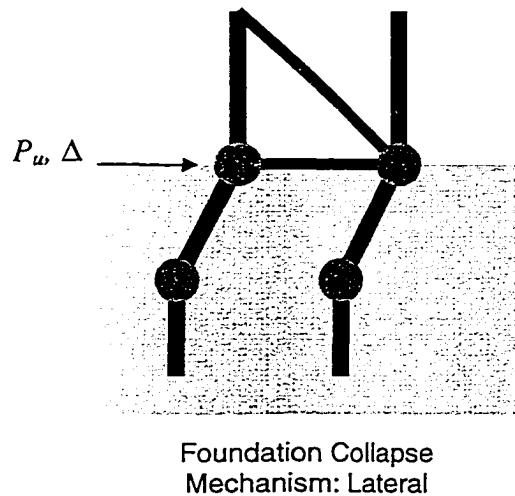


Figure 4-14: Lateral Collapse Mechanism in Foundation

The strength of this mechanism is assumed to be controlled by hinge formation in the piles.

The strength capacity is thus:

$$P_u = \sum_{i=1}^{n-pile} P_i + \sum_{i=1}^{n-conductors} P_i + \sum_{i=1}^{n-mat\ brace} H_i + F_{IL}$$

The last mechanism considered is that of foundation overturning or rotation. The rotation capacity of the foundation is also assumed to be controlled by the piles. Hence, rotation capacity will be given by:

$$M_\theta = \sum_{i=1}^{n-pile} P_i L_{xi} + \sum_{i=1}^{n-mat\ brace} Q_i L_{xi} - M_{P\Delta}$$

where L_x is the distance from the pile or mudline element to the axis of rotation. $M_{P\Delta}$ is the moment induced at the based from P - Δ effects; it is given approximately by:

$$M_{P\Delta} = \sum_{i=1}^{n-masses} Q_i \Delta_i$$

The deflections Δ_i are those associated with platform response to first mode forces.

4.2.4 Global Strength

As noted previous, the global strength of the platform is defined as the total load or base shear the platform is subject to when the first occurrence of component yielding takes place. This is determined by comparing the component strengths with the reference load pattern, and scaling the load pattern up or down to achieve the result of first component yield, as shown in Figure 4-15.

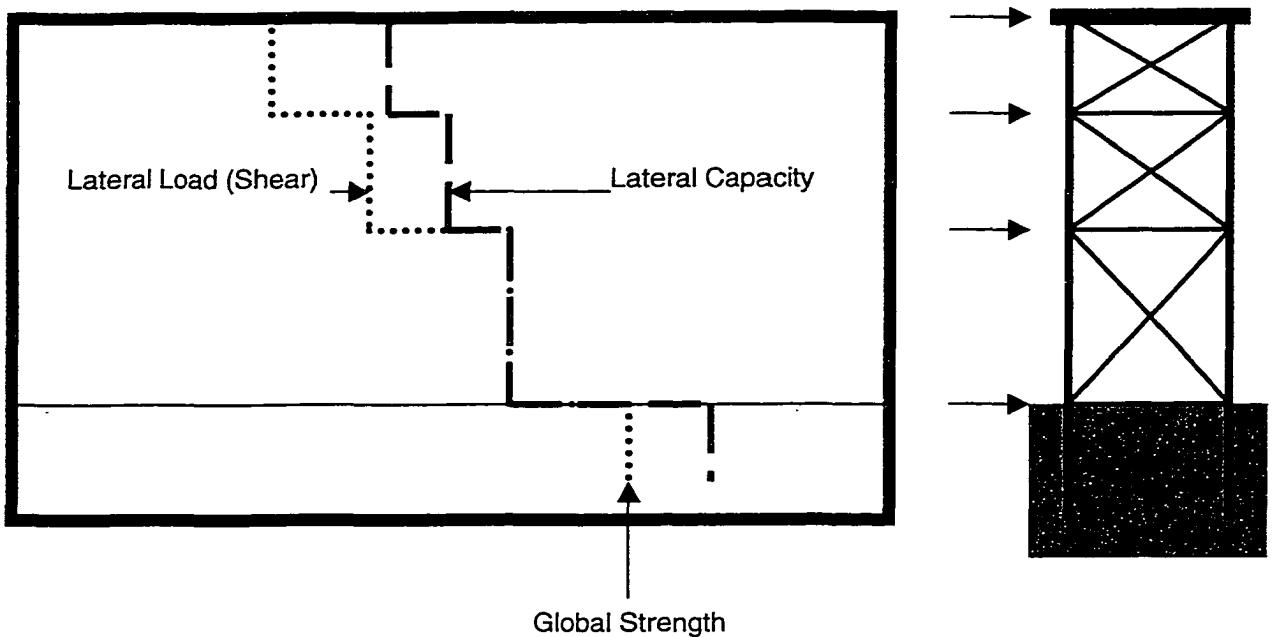


Figure 4-15: Global Strength Determination

The reference load pattern is taken to be those forces associated with first horizontal mode response. It must be emphasized that including higher mode contributions to response can obviously result in component yielding at lower levels of the reference base shear than the reference base shear determined using first mode forces alone, and can result in yielding in components different from the yielding pattern established using first mode forces. This will be a function of the relative modal participation factors for the different component demands, the phasing between modal responses, and the earthquake response spectrum ordinates associated with the higher modes. Hence, upper and lower bounds on the global strength of the platform should be determined. The upper-bound strength is assumed to be that determined from application of first mode forces only, while the lower bound strength is that estimated using responses which include higher mode contributions.

4.3 GLOBAL DISPLACEMENT DUCTILITY

The global displacement ductility of a platform or other structure can be established from static pushover analysis. Using a specific load pattern, the deck or roof is forced to displace until either unacceptable damage has occurred to a gravity support, or another pre-defined displacement limit has been reached. The load-displacement curve developed from this analysis can be taken to represent the envelope on global hysteretic behavior of the structure.

There exist today many capable static pushover analysis programs such as DRAIN, CAP and USFOS. To apply them to the task of determining the global displacement ductility of a platform requires considerable time and effort, and is therefore inappropriate at the early stages of assessment. A simple approach is needed by which an analyst can quickly assess which portions of a platform are likely to yield, and what displacement ductility those components are capable of developing.

In this section, an approximate approach for assessing the global displacement ductility of platforms is described. Damage is assumed to concentrate in components of the platform which undergo yielding. Hence, the post-yield load-displacement behavior of a platform is assumed to be controlled by the load-displacement behavior of the component which yields first: the deck bay, the jacket, or the foundation.

4.3.1 Simplified Limit Ductility Analysis

The process by which the global displacement ductility of a platform is estimated is referred to as Simplified Limit Ductility (SLD) Analysis. The process is outlined as follows:

- From the global load-strength capacity comparison, determine the most heavily loaded component. This component is assumed to control the ductile behavior of the platform.
- Using the simplified flexibility model developed in Chapter Three, determine the deck displacement for the specified load pattern, with the load scaled such that the demand/capacity ratio for the identified critical component is unity.
- If the component is of a type which will exhibit some reserve strength following yield, linearly scale up the displacements associated with all non-yielding components according to the reserve strength which can be developed. Add to this value the inelastic displacement of the yielding component, assuming it develops its full displacement ductility. The resulting total displacement is the displacement ductility of the platform. Increase the effective global load at this point such that the demand/capacity ratio for the identified critical component at its reserve strength value is unity. Refer to Figure 4-16 for an illustration.
- If the component is of a type which will exhibit a loss of strength or plastic behavior following yield, the nonyielding components are assumed to be “frozen;” add to the yield deck displacement the inelastic displacement of the yielding component, assuming it develops its full displacement ductility. Decrease the global load associated with post-yield behavior by the amount of lost load capacity associated with the component. Refer to Figures 4-17 and 4-18 for illustrations.

This procedure allows an analyst to quickly assess the approximate global displacement ductility a platform possesses based on the displacement ductility of its components.

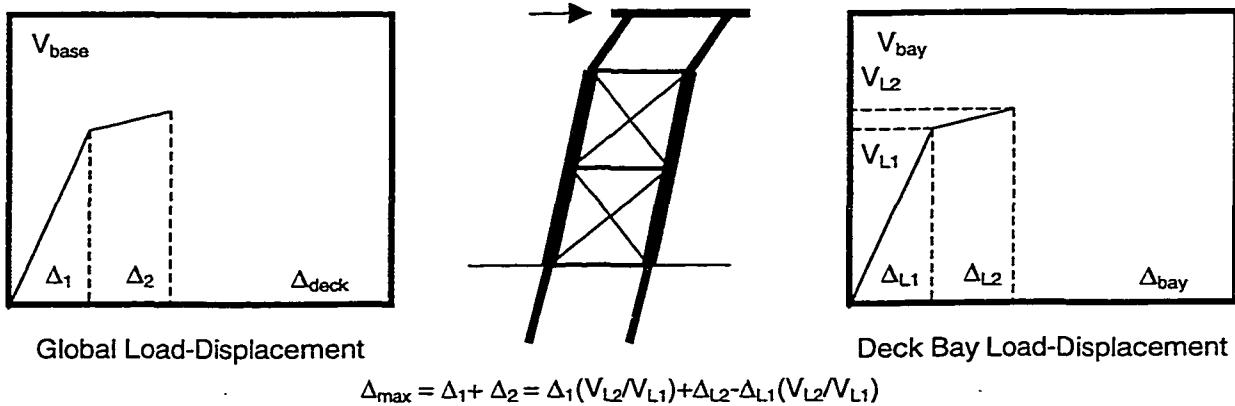


Figure 4-16: Damage Concentrating in a Deck Bay (Post-Yield Reserve Strength)

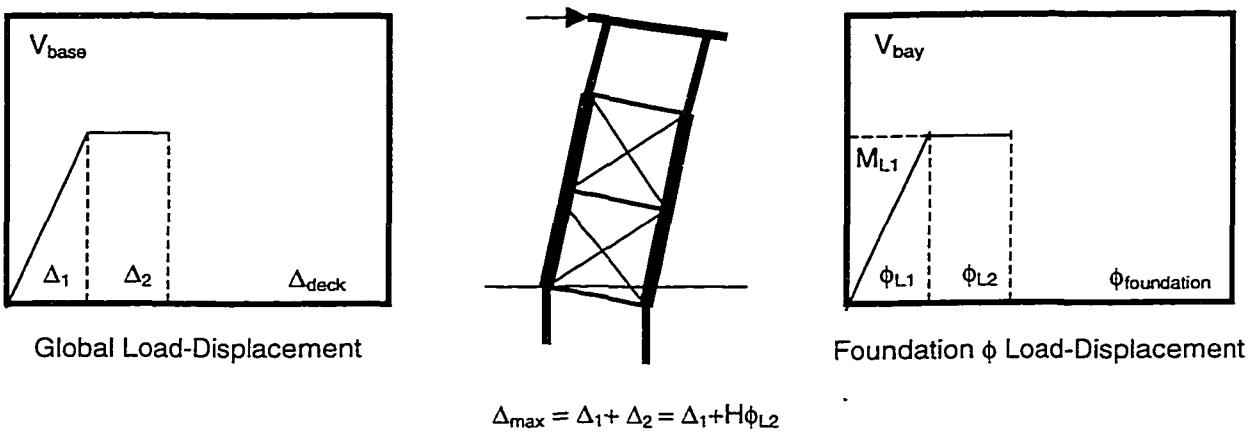


Figure 4-17: Damage Concentrating in a Foundation (Overturning, Plastic)

Yielding which occurs in an unbraced deck bay or the foundation can be treated in a straightforward manner. Yielding in a jacket, however, is generally much more complicated, due to the mechanism by which load is redistributed as members buckle. In lieu of rigorously modeling the load transfer process of a jacket, several additional approximations are utilized to capture the behavior of jackets which have weak members with poor post-buckling performance and/or insufficient horizontal framing for load redistribution.

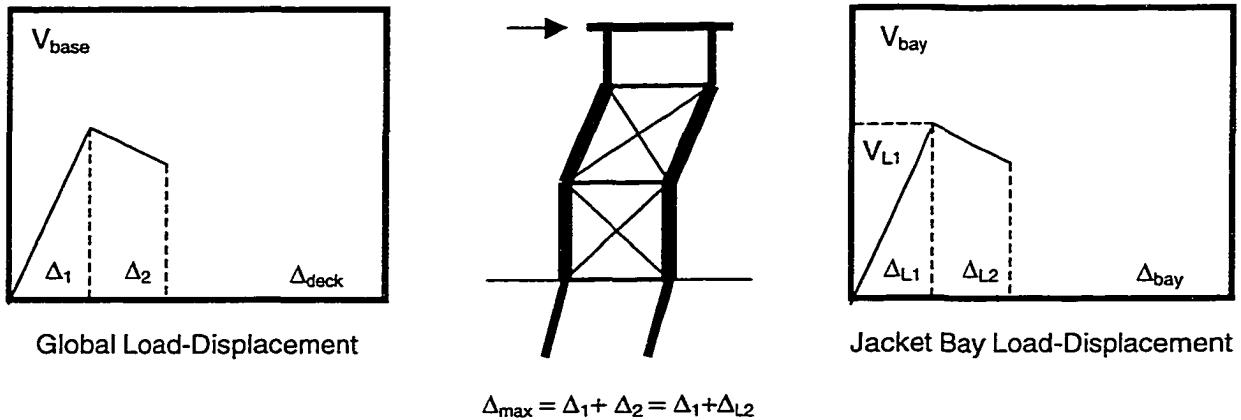


Figure 4-18: Damage Concentrating in a Jacket Bay (Softening)

4.3.2 Inelastic Behavior of Jacket Structures

The jacket-portions of most platforms designed and built in the past twenty years tend to be very robust structures, with the designs benefiting from industry experience established in the years prior to that time. Most of these structures are made up of tubular members with low kL/r and D/t ratios, adequate horizontal framing exists between jacket bays to ensure loads can be redistributed to the foundation without losses in global lateral strength, and the use of weak-beam K-type bracing is largely avoided.

However, many older structures have tubular members with poor post-buckling behavior, do not possess strong horizontal framing between jacket bays, and the use of K-type bracing was common up until the early 1970's. These structures tend to exhibit losses in lateral strength following global yielding.

As discussed in Chapter Two, numerous studies have been performed on the load-displacement behavior of frames of these types. From these studies, the following conclusions can be drawn:

- Low D/t and kL/r ratios generally indicate tubular members with very favorable post-buckling performance, i.e. strength does not degrade and local buckling is avoided. Platforms with braces which exhibit poor post-buckling behavior will often develop weak story-type mechanisms, leading to damage concentrated at a single level.
- Horizontal framing substantially improves the post-yield load-displacement behavior of platforms. Structures with insufficient horizontal framing can exhibit “unzipping” behavior, which occurs when a bracing member loses strength, and there is no continuous load path to members below the failed member. These other members will then go unutilized, leading to an effective drop in load capacity of the next section down. This will result in the formation of weak story mechanisms in the jacket frame, and damage will likely concentrate in these regions, as shown in Figure 4-19.

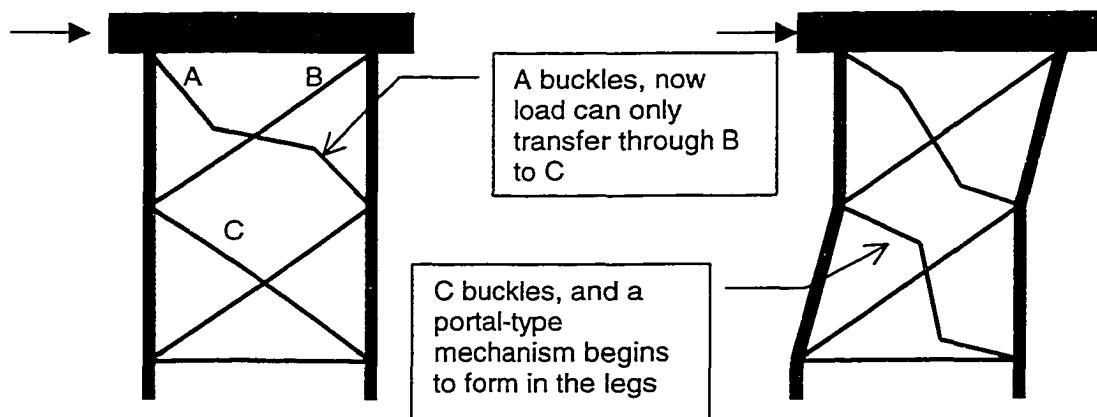


Figure 4-19: Unzipping Frame

- Structures which possess K-type framing of the type shown in Figure 4-20 exhibit sudden reductions in strength following the buckling of braces. This will occur if the horizontal member or K-joint cannot support the imbalance in vertical load which results when one brace buckles and the other is in tension. If a hinge forms in the horizontal, the tension member will be unable to develop its full tension capacity, and the main source of energy dissipation will be the hinge in the horizontal. This will result in a drop in effective strength of the frame, and damage concentration will likely occur in the section.



Figure 4-20: K-Type Frames

In lieu of rigorously tracking the load redistribution associated with buckling of braces in jackets with weak framing through static pushover analysis, it is desirable to first apply a qualitative procedure to quickly evaluate the potential loss in strength following member buckling. To assist in the development of such an approach, the post-yield behavior of ten jacket structures was examined. These jackets had been previously analyzed using static pushover analysis by Gates, et al. (1977), Bea, et al. (1997), Bea, et al. (1995), Stear and Bea (1997A) and Hellan, et al. (1993). All platforms possessed diagonal bracing members with D/t between 30 to 70 and kL/r between 40 and 80. Table 4-4 depicts the global characteristics of these jackets and results from the analyses.

Residual strength for these structures was seen to vary from 60% to 100% of the initial yield load. Most of the jackets in Table 4-4 were able to develop global displacement ductilities of two or more following yielding, prior to formation of hinges in the legs. Where weak K-type bracing was associated with the failure mechanism, the structural system tended to exhibit losses in supportable lateral load of 30% to 40%. For platforms lacking sufficient horizontal framing, drops in supportable load ranged from 30% to 10%.

Table 4-4: Static Pushover Analysis of Jackets

Platform	# Legs	H (ft)	# Bays	Horz.	Bracing	Mechanism	Residual
SoCal ¹	4	100	2	weak	X	unzipping across two bays	0.68
SoCai ¹	4	100	2	strong	X	two bays	0.90
A - BS ²	8	118	4	weak	K	one bay	0.60-0.74
A - EO ²	"	"	"	weak	S	two bays	0.79
B ⁵	4	157	7	weak	K	unzipping across two bays	0.68
C - BS ²	8	137	4	weak	K	one bay	0.73
C - EO ²	"	"	"	strong	S	one bay	0.85-1.00
D - BS ²	8	137	4	weak	K	one bay	0.76
D - EO ²	"	"	"	strong	S	one bay	0.78
A - BS ³	8	340	6	weak	S	one bay	0.82-0.89
A - EO ³	"	"	"	weak	S	unzipping across two bays	0.60-0.80
B - BS ³	8	213	5	weak	S	three bays	0.88
B - EO ³	"	"	"	weak	S	unzipping across two bays	0.78
A0 - BS ⁴	8	NA	4	strong	K	one bay	0.80
A0 - EO ⁴	"	"	"	strong	S	one bay	0.80
A1 - BS ⁴	8	NA	4	weak	K	unzipping across two bays	0.60
A1 - EO ⁴	"	"	"	strong	S, X	one bay	0.80

¹ Gates, et al. (1977)

² Bea, et al. (1995)

³ Stear, Bea (1997A)

⁴ Hellan, et al. (1993)

⁵ Bea, et al. (1997)

To implicitly account for the effects of having minimum horizontal framing or weak-beam K-bracing, a set of approximate guidelines was developed based on the platforms in Table 4-4:

- A weak-story mechanism is assumed to occur at the location of the bracing system in question; displacement will be concentrated in this mechanism.

- For platforms with eight or more legs, the post-yield strength of a K-brace mechanism is estimated assuming tension members can only develop 60% capacity, while the post-yield strength of a mechanism in a structure with otherwise insufficient horizontal framing is estimated assuming tension members can only develop 80% capacity. This is done to qualitatively represent the fact that tension members in sections of these types are unable to develop their full tension capacities due to a lack of load path redundancy.
- For platforms with fewer than eight legs, the post-yield strength of a K-brace mechanism and the post-yield strength of a mechanism in a structure with otherwise insufficient horizontal framing is estimated assuming tension members can only develop 60% capacity. This is done to qualitatively represent the fact that tension members in sections of these types are unable to develop their full tension capacities due to a lack of load path redundancy, and that there is less redundancy in these more minimal structures.

It must be recognized that this approach is quite approximate, and to qualitatively establish the likely post-yield characteristics of a jacket without resorting to static pushover analysis. In all likelihood damage will not exclusively concentrate in the first bay to fail; in several of the jackets listed in Table 4-4, the collapse mechanism was spread over two or more bays. However, by assuming damage is limited to one bay, a conservative estimate of the associated displacement ductility can be made.

Adequacy of horizontal framing can be challenging to judge without a complete model of the horizontal frame. The ability of the horizontal member of a K-brace to transfer load without

hinging can be determined by analyzing the member as a beam column as in Section 4.1.1; the “lateral” load capacity of the horizontal should be greater than the vertical component of the unbalanced tension load in one brace resulting from the complete collapse of the other in buckling. For a conservative screening, horizontal members in single and X-brace configurations should be able to develop the tension capacity of members above and below them in the load path, to provide load path redundancy when compression members fail.

For jackets which have robust horizontal framing, but are not redundant to the point where they exhibit reserve strength, damage is assumed to concentrate in the jacket, but is distributed across bays. The displacements in the jacket are assumed to vary linearly with the displacement in the yielding portion of the jacket, up until the cyclic displacement ductility limits of the braces in the yielding portion are exceeded, representing local buckling and rapid degradation of capacity.

4.3.3 Foundation Rotation Limit

If the mechanism which forms is that of foundation rotation, the governing performance criteria will be that of overall stability, as opposed to that of loss of strength in vertical load-supporting members. This is due to the fact that the piles due not suffer permanent degradation when subject to inelastic straining, so long as the yielding is occurring in the surrounding soil. In theory the platform could survive drifts up to the point at which the $P-\Delta$ moment equals the moment capacity of the foundation; obviously, however, this provides no margin for safety. Prior to approaching this point, it is very likely that severe damage will

have occurred to mudline structural elements such as mats and braces, and to conductors, piping and other mudline equipment from the amount of rotation.

Current design practice generally limits plasticity in foundation overturning to ductility demands which will occur in the piles in forming a fully-plastic foundation mechanism. This is typically indicated by the yielding of one or two piles in compression. It is important, however, to consider $P\Delta$ effects which will occur associated with these displacements.

Platform deck drift levels at foundation rotation yield and at formation of a plastic foundation rotation mechanism (assuming the foundation rotates as a rigid plate, and the steel structure above the mudline behaves as a rigid body) are shown below in Table 4-5 for eight platforms:

Table 4-5: Platform Deck Drifts Due to Foundation Rotation

Name, # Legs	H (ft)	Axis	% Δ_y	% M_{P-y}	% Δ_u	% M_{P-u}
SoCal ¹	100	-	0.53	0.55	1.02	0.45
D ²	137	BS	0.22	0.05	0.93	0.19
"	"	EO	0.38	0.08	0.38	0.08
C ²	137	BS	0.27	0.1	0.83	0.24
"	"	EO	0.5	0.18	0.5	0.18
A ³	340	BS	0.26	0.28	1.15	1.03
"	"	EO	0.43	0.45	0.43	0.45
B ³	213	BS	0.33	0.26	1.28	0.80
"	"	EO	0.64	0.48	0.64	0.48

¹ Gates, et al. (1977)

² Bea, et al. (1997)

³ Stear, Bea (1997A)

The deck drift associated with yielding in the foundation is in the range of 0.22% to 0.64%, with a mean of 0.39%, while the drift associated with formation of a fully-plastic mechanism is in the range of 0.38% to 1.28%, with a mean of 0.79%. The moment induced at the base from $P\Delta$ effects at mechanism formation is at most 1.03% of the base plastic moment capacity for the platforms studied, the mean value of this fraction is 0.43%.

Based on the platforms examined, a limit of 1% deck drift due to foundation rotation will be used in this assessment criteria. For platforms of similar design, this restriction will keep the moment induced by P - Δ effects to approximately 1% of the foundation plastic moment capacity.

4.3.4 Residual Strength Requirement

There exist no definitive guidelines on the minimum amount of residual strength a platform should possess following a severe seismic event. However, it is obvious that some margin must be provided for, to protect against aftershocks and other environmental forces. Zayas, et al. (1980A) suggested a reserve lateral load capacity of 70% of ultimate load for illustrative purposes when discussing an example frame subject to cyclic inelastic loading; this criteria, while recognized as subjective, will be adopted here as a minimum requirement for robustness. Platforms not meeting this criteria should be considered extreme liabilities for severe earthquakes.

4.4 EXAMPLE APPLICATIONS

The simplified strength and displacement ductility assessment approaches described in the previous sections were applied to the analysis of four structures: two 8-leg Gulf of Mexico platforms analyzed by Stear and Bea (1997A), and two three-bay X-braced frames tested at U.C. Berkeley by Zayas, et al. (1980A). The cases selected emphasize failure occurring in the jacket portions of each structure. The two Gulf of Mexico platforms have weak horizontal framing and bracing members with poor post-buckling performance. The two X-braced frames have strong horizontal framing, but differ in bracing member strength and

post-buckling performance. For each case, comparisons were made between the effective global strength, indicated failure mechanism, global displacement ductility, and general shape of the hysteresis curve determined from the simplified approaches and the results from the two listed investigations.

4.4.1 Case A: South Pass 62 A

South Pass 62 A is an 8-leg jacket located in the Gulf of Mexico (Figure 4-21). Braces in the platform have high D/t (50+) and kL/r (80+) ratios, indicative of poor post-buckling performance.

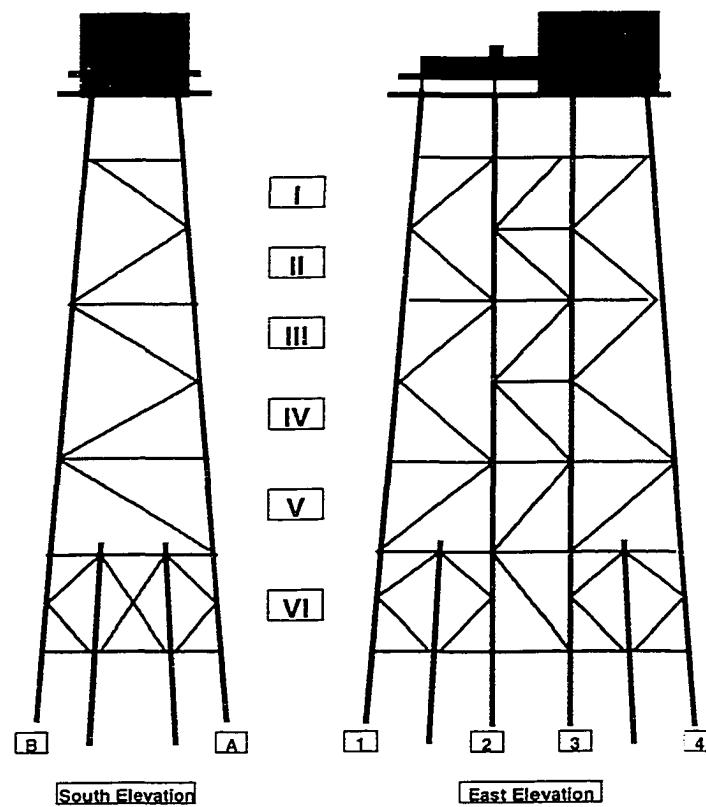


Figure 4-21: South Pass 62A Elevations

This platform has been extensively analyzed by Stear and Bea (1997A) using the program USFOS.

Ultimate strength (static pushover) analyses were performed for two cases of loading for this structure: wave attack on the end-on axis and wave attack on the broadside axis. The resulting global-load displacement curves for each load case, together with the collapse mechanisms which formed, are shown in Figures 4-22 and 4-23.

For the case of end-on loading, collapse was initiated by the buckling of braces in the fourth jacket bay, followed by the buckling of braces in the third jacket bay. The platform exhibited a sudden loss in strength, characteristic of “unzipping” due to lack of load path redundancy; tension braces in these two bays were unable due to develop full capacity. The platform exhibited a global strength of approximately 7,400 kips, and exhibited severely degrading global load-displacement behavior. Residual strength varied from 4,300 kips to 6,200 kips. Hinging of the platform legs in the weakened region at a global displacement ductility of approximately two.

For the case of broadside loading, collapse was initiated by the buckling of a compression brace in the second jacket bay, following which two of the remaining braces in the bay developed their plastic (tension) capacities; the remaining brace was unable to mobilize its full tension capacity. The platform exhibited a moderate loss in strength following the buckling of the compression brace in this bay; damage concentrated in this bay until hinging of the legs and buckling of other members began at a global displacement ductility of

approximately two. Global load capacity was determined to be 9,500 kips; residual strength varied from 8,500 kips to 9,100 kips while inelasticity was confined to this bay.

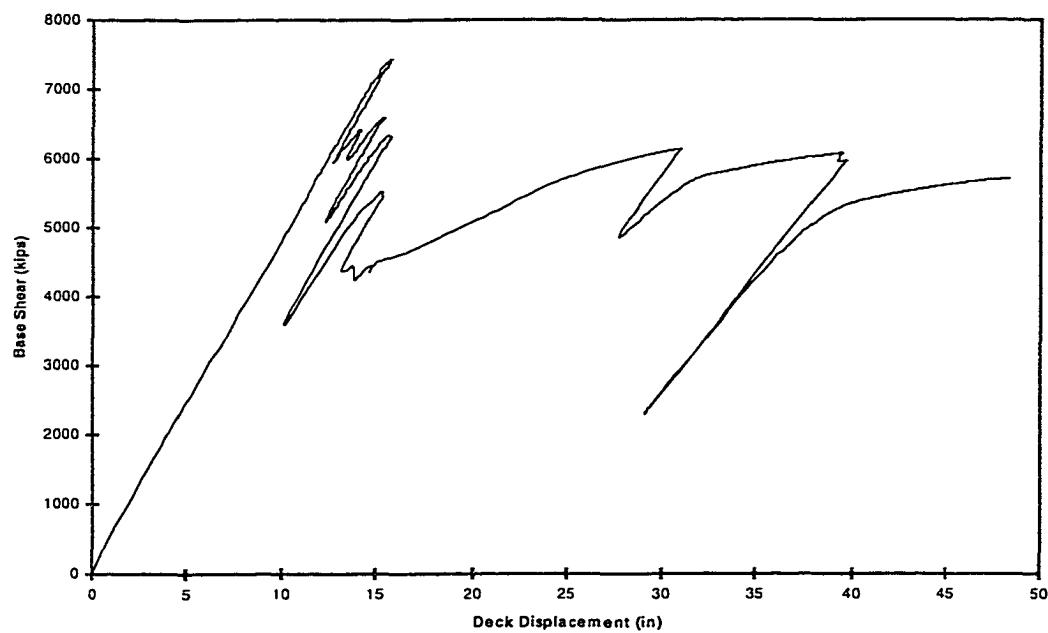
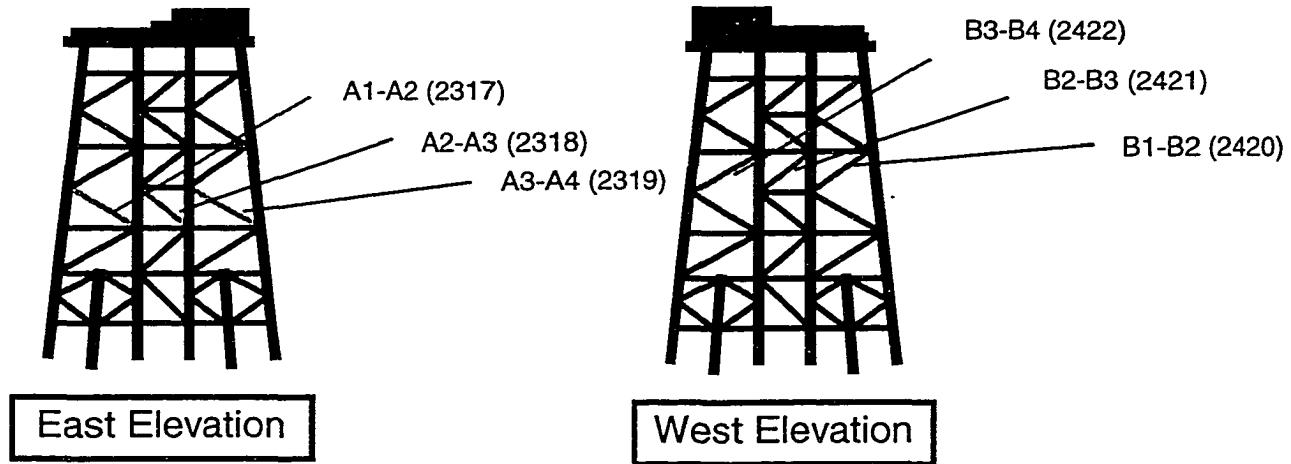


Figure 4-22: End-On Loading Performance, SP 62A

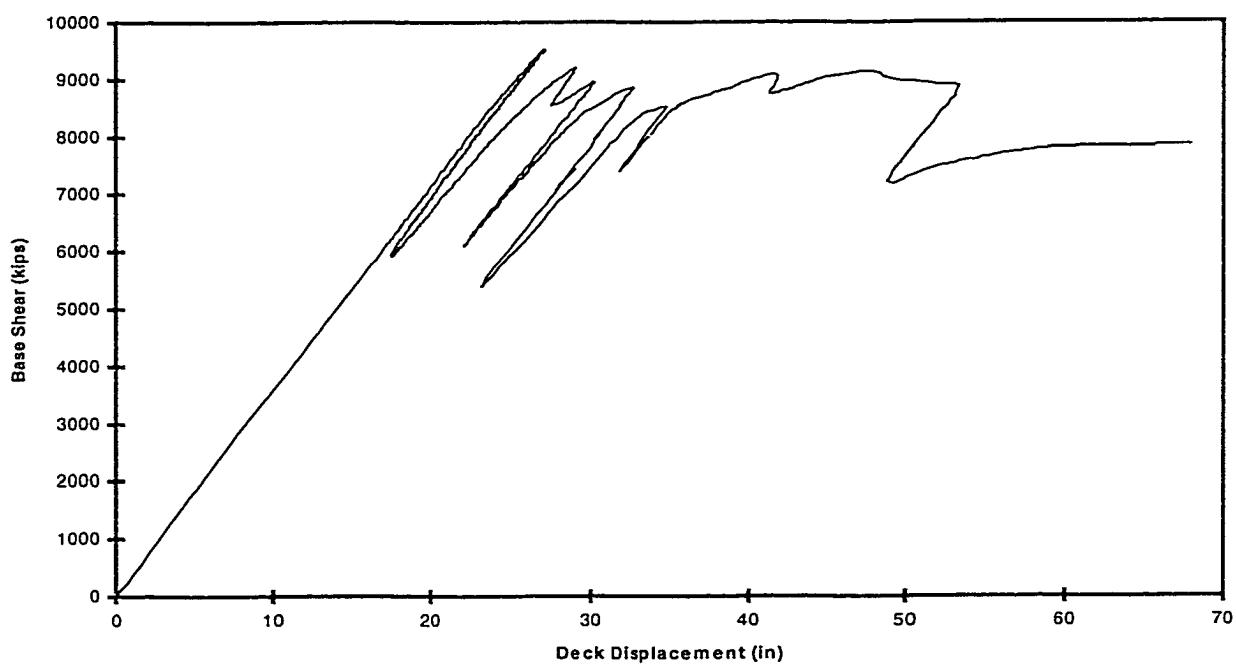
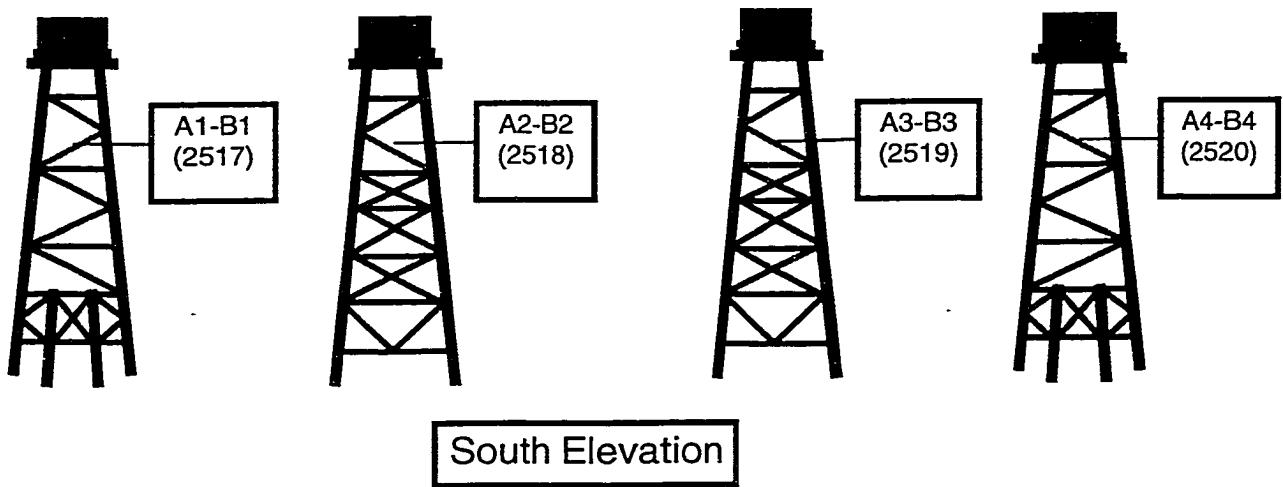


Figure 4-23: Broadside Loading Performance, SP 62A

This platform was also analyzed using the simplified procedures described previously in this chapter and in Chapter Three. Strength capacities were first formulated for components for both the end-on and broadside direction. A demand-capacity assessment was then conducted, using a load pattern matching that used in the static pushover analyses representative of the wind, wave and current forces. Strength demand-capacity curves are shown below in Figures 4-24 and 4-25.

The end-on assessment indicates the platform will collapse by forming a mechanism in the second jacket bay; however, the third and fourth bays are also close to collapse. The collapse load is approximately 7,450 kips. The trend in collapse behavior is comparable to that found from the static pushover analysis; the collapse load estimates between the two methods are in excellent agreement.

The broadside assessment indicates the platform will collapse by forming a mechanism in the second jacket bay; the first bay is also close to collapse while the deck bay legs are close to yielding. The collapse load is approximately 7,800 kips. The trend in collapse behavior compares well with that identified in the static pushover analysis; the predicted collapse load is 18% less than that found from the static pushover analysis.

The procedures of Chapter Three were used to develop flexibility matrices for the structure for both the end-on and broadside directions; using these matrices together with load vectors representative of the end-on and broadside loads, the deck displacements at collapse initiation were estimated. As this structure does not possess horizontal framing at all levels, it was

judged to fall into the category of minimum or weak horizontal framing. Hence, damage was assumed to concentrate in the first jacket bays to yield. Using the post-buckling performance of braces in each of the weakest bays, and assuming the braces in tension also lose capacity due to lack of load path redundancy, envelope curves were constructed for both the end-on and broadside directions of loading (see Figure 4-26).

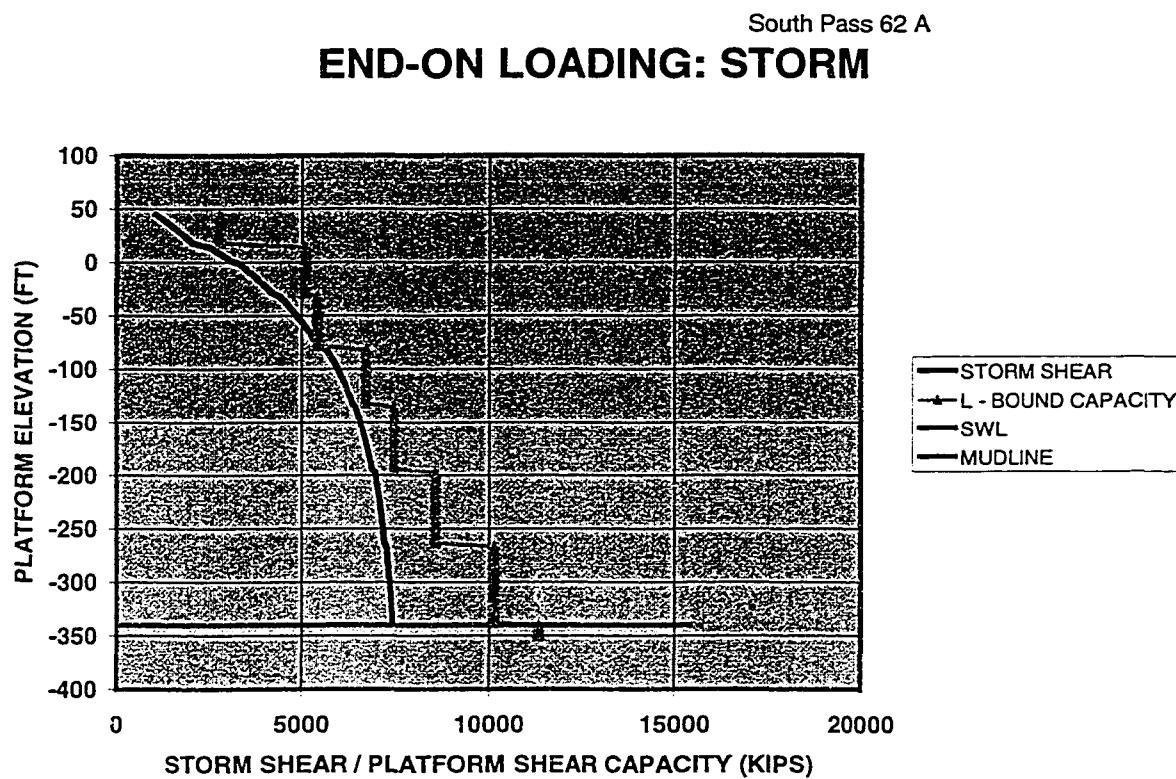


Figure 4-24: Demand-Capacity Analysis of Platform, End-On Loading

Comparison of Figure 4-26 with 4-22 and 4-23 indicates the general trend of strength loss is duplicated by the simplified approach, although the results are not identical, as expected. The fraction of residual predicted by the simplified method is 61% for the end-on load case, and 81% for the broadside case. From the static pushover analyses, the end-on residual varies

from 60% to 80%, while the broadside residual varies from 80% to 90%. The static pushover analyses indicate the platform is capable of developing global displacement ductilities of 2.0 to 2.5 for both cases prior to hinge formation in the legs, while the simplified approach indicates 2.1 and 1.7 for the end-on and broadside cases.

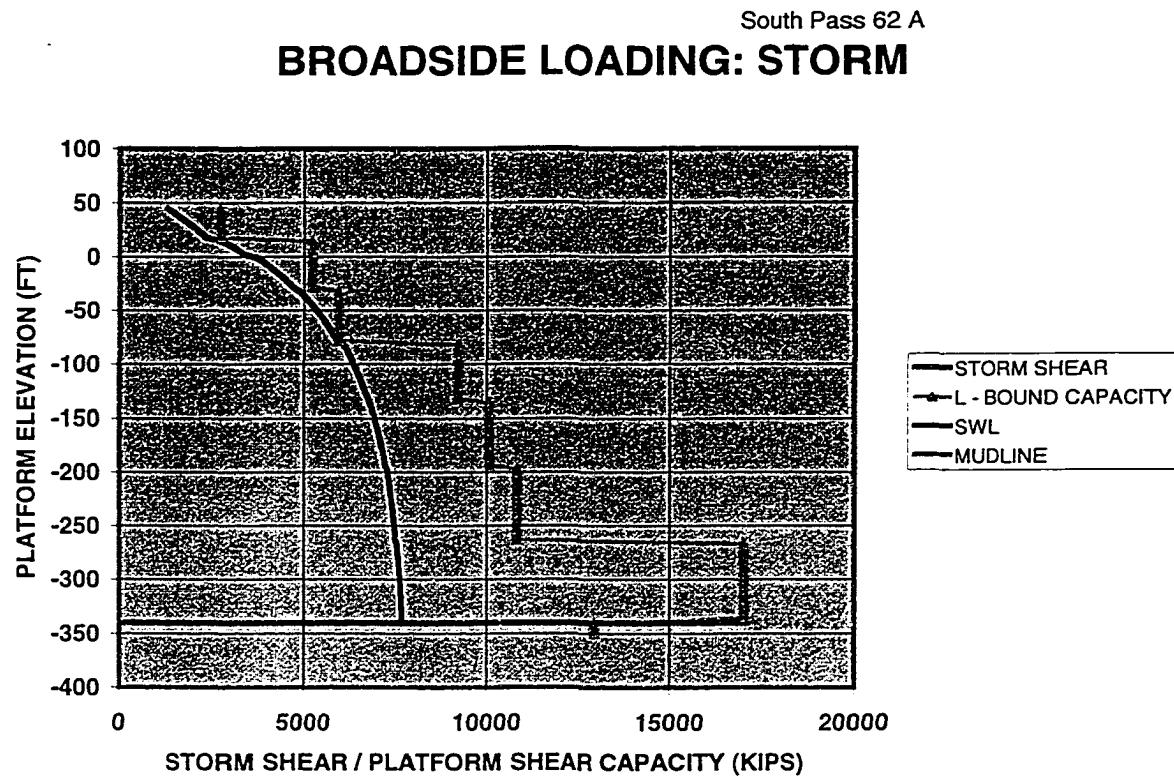


Figure 4-25: Demand-Capacity Analysis of Platform, Broadside Loading

The simplified method succeeds in providing the following:

- Good estimates of lateral strength
- Hysteresis curves reflecting the likely loss in strength due to minimum framing and poor brace post-buckling characteristics
- Good estimates of global displacement ductility capacity as based on leg hinging

Global Load-Displacement Behavior

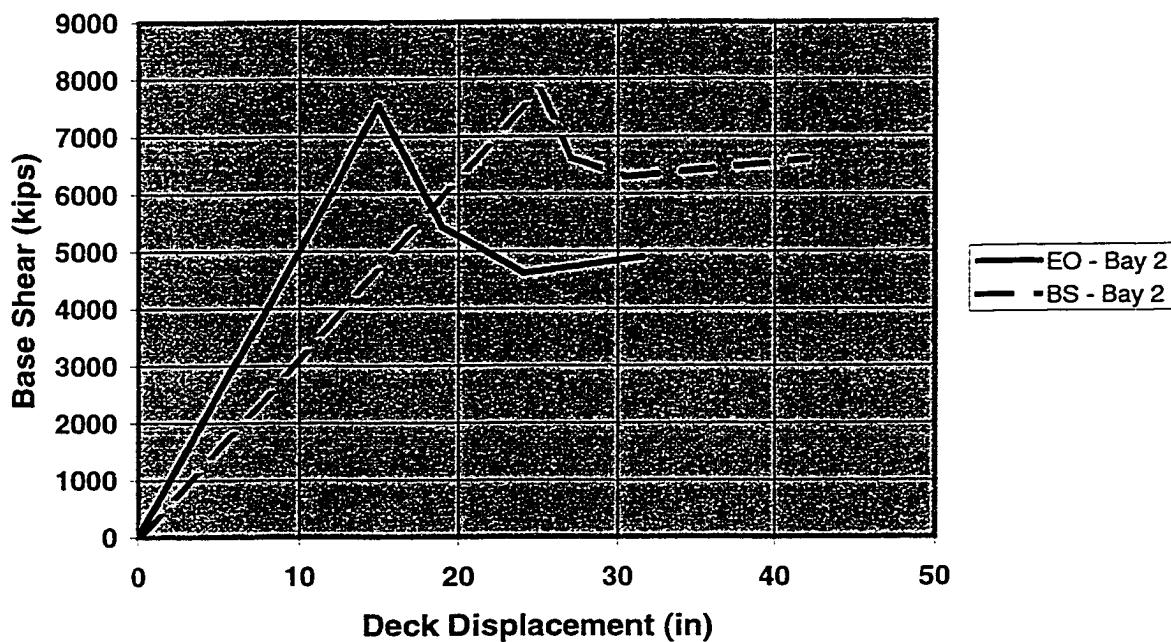


Figure 4-26: Load-Displacement Behavior for SP 62A

4.4.2 Ship Shoal 274A

Ship Shoal 274A is an 8-leg jacket located in the Gulf of Mexico (Figure 4-27). Braces in this platform have moderate D/t (30 to 60) and kL/r ratios (60+), indicating moderate post-buckling performance. This platform has been extensively analyzed by Stear and Bea (1997A) using the program USFOS.

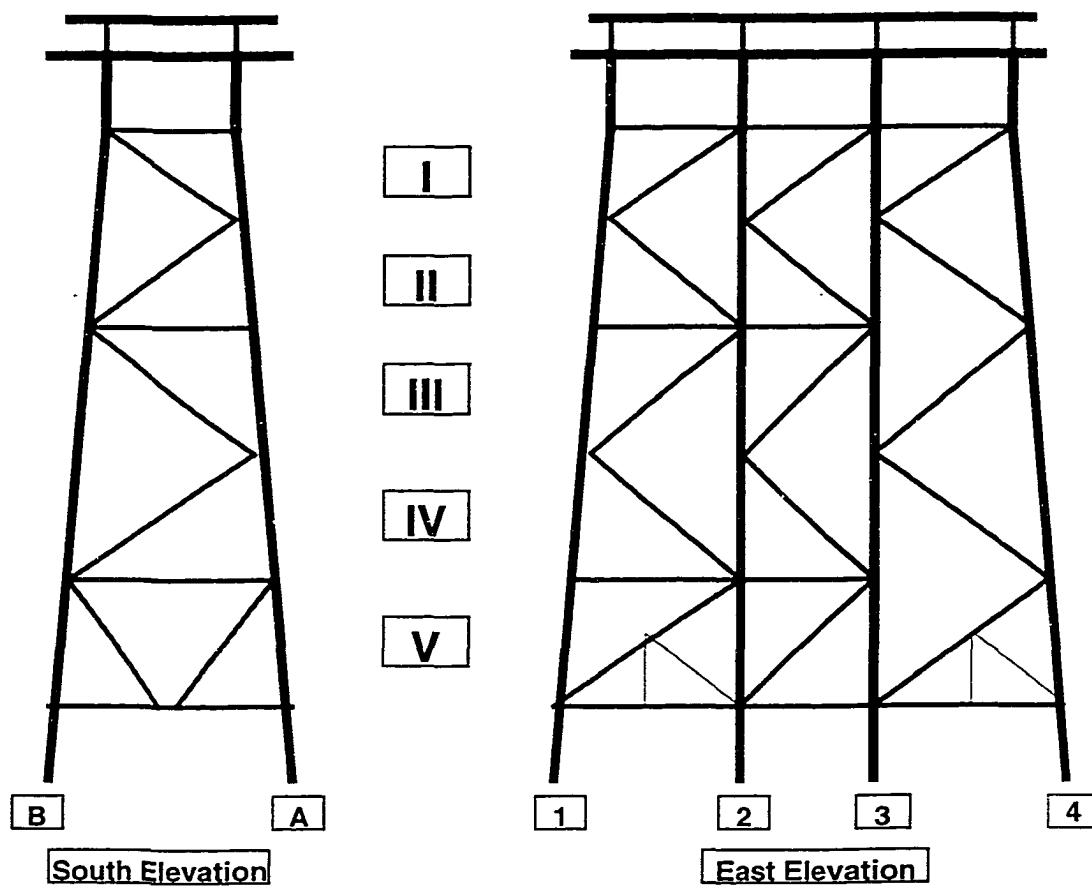


Figure 4-27: Ship Shoal 274A Elevations

Ultimate strength (static pushover) analyses were performed for two cases of loading for this structure: wave attack on the end-on axis, and wave attack on the broadside axis. The resulting global load-displacement curves for each load case, together with the collapse mechanisms which formed, are shown in Figures 4-28 and 4-29.

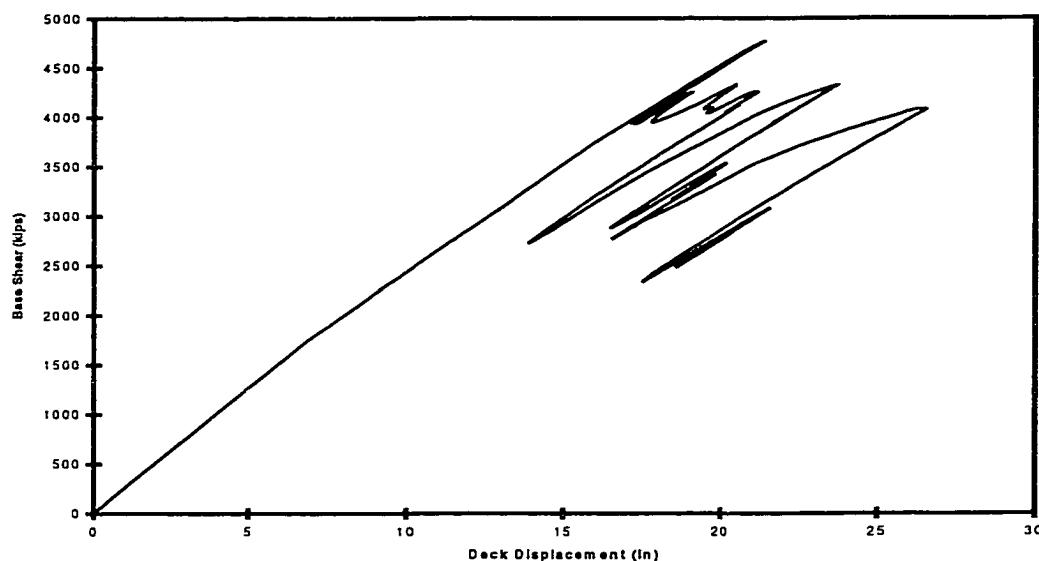
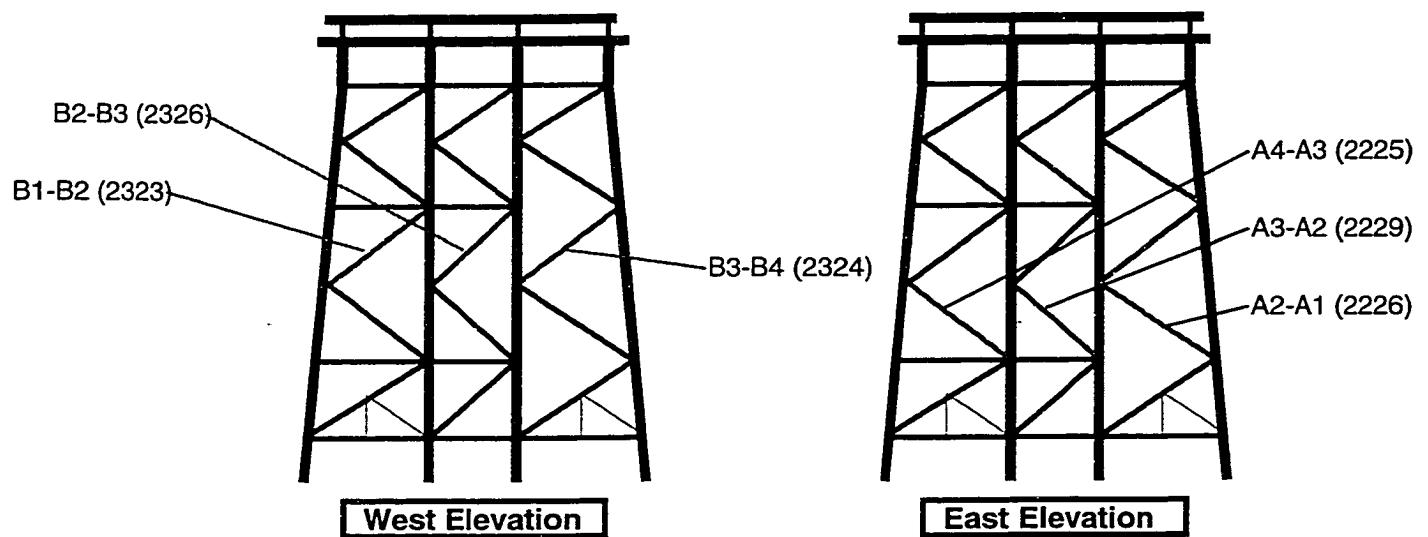


Figure 4-28: End-On Loading Performance, SS 274A

For the case of broadside loading, collapse was initiated by the buckling of a brace in the first jacket bay, followed by buckling of braces in the second and third jacket bays. A mechanism began to form across all three bays; the analysis was terminated prior to the formation of

hinges in the legs. Global load capacity was determined to be 5,250 kips, with a residual capacity of approximately 4,700 kips.

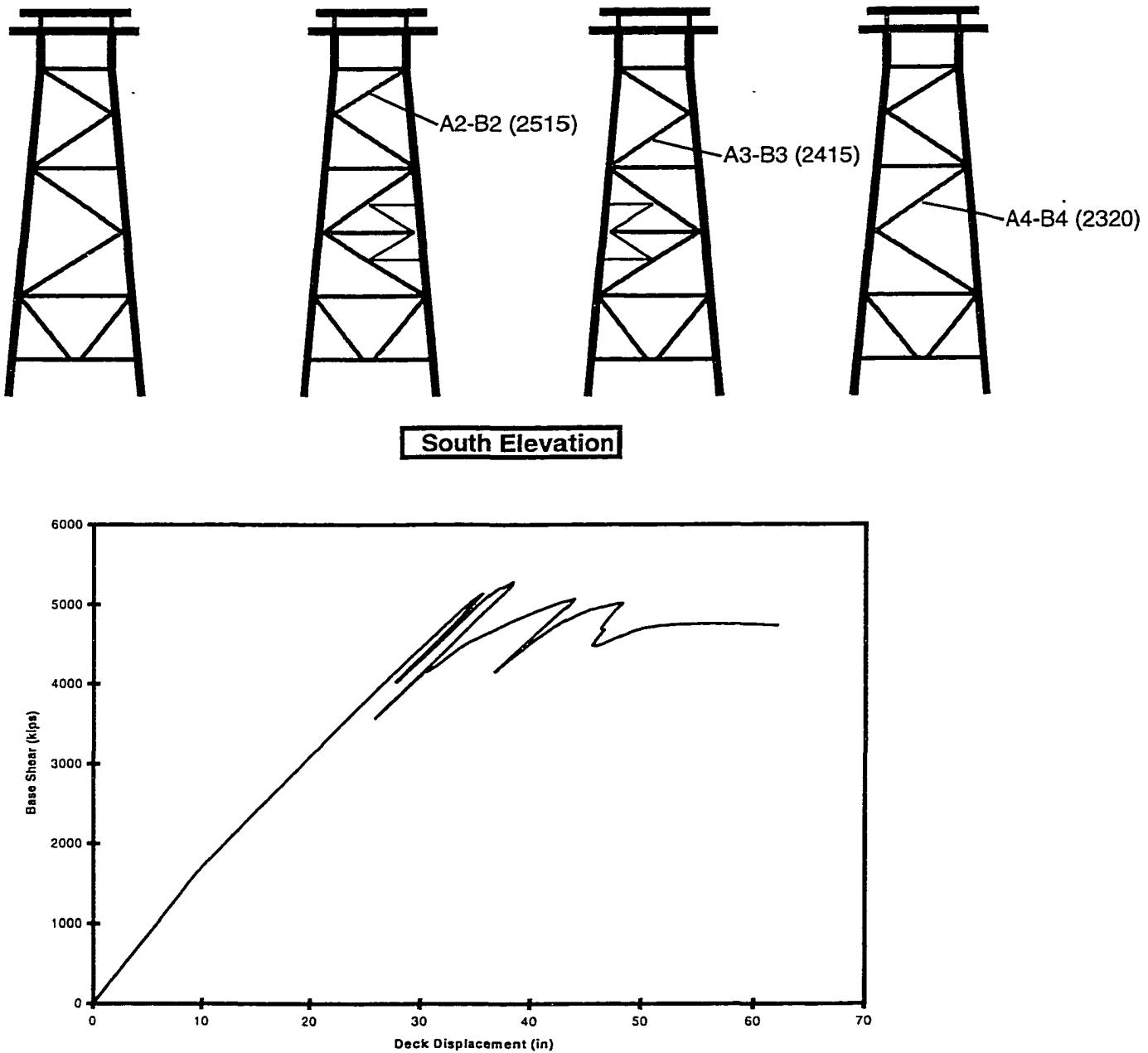


Figure 4-29: Broadside Loading Performance, SS 274A

This platform was also analyzed using the simplified procedures described in this chapter and Chapter Three. Strength demand-capacity curves are shown in Figures 4-30 and 4-31, while load-displacement behavior is shown in 4-32.

For the case of end-on loading, collapse was initiated by the buckling of braces in the third jacket bay, following by the buckling of braces in the fourth jacket bay. The platform exhibited a progressive loss in strength, characteristic of gradual unzipping. The platform exhibited a global strength of approximately 4,570 kips. Residual strength was tracked as low as 3,800 kips; the analysis was terminated prior to the formation of hinges in the legs.

The end-on assessment indicates the platform will collapse by forming a mechanism in the third jacket bay; the fourth jacket bay is also very close to failure. The collapse load is approximately 4,410 kips. The simplified ductility analysis for this direction of load indicates the platform has a residual strength ratio of approximately 66%, and is capable of developing a global displacement ductility of approximately 1.7 prior to hinging of the legs. The strength and identified collapse mechanism are in excellent agreement with those found during the static pushover analysis; the load-displacement behavior compares reasonably well to that found from the static pushover analysis.

The broadside assessment indicates the platform will collapse by forming a mechanism in the third jacket bay; however, the remaining jacket bays and the deck bay are also very close to failure. The collapse load is approximately 5,050 kips. The simplified ductility analysis for this direction of load indicates the platform has a residual strength ratio of approximately

66%, and is capable of developing a global displacement ductility of approximately 1.5 prior to hinging of the legs. The strength and identified collapse mechanism are in excellent agreement with those found during the static pushover analysis; however, the load-displacement behavior is predicted as being much more severely degrading than observed in the static pushover analysis. While it was assumed at the outset that this platform would not be able to transfer load due to insufficient horizontal framing, closer inspection revealed that the platform does possess sufficient redundancy for transferring forces from buckling members in the broadside direction. Furthermore, the fact that the platform does not have any obvious weak sections allows likely damage to be distributed over multiple bays.

Ship Shoal 274A
END-ON LOADING: STORM

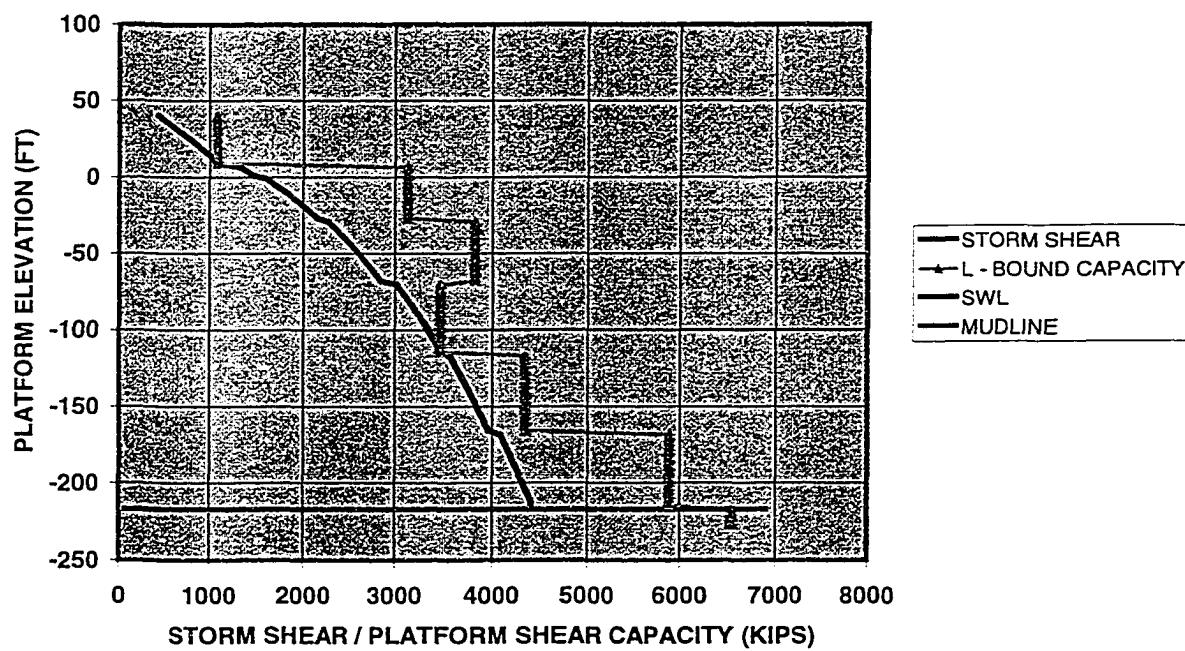


Figure 4-30: Demand-Capacity Analysis of Platform, End-On Loading

For comparison purposes, the global load-displacement behavior of the platform in the broadside direction was also estimated assuming damage was distributed in the jacket prior to the occurrence of local buckling in a member. This plot is also shown in Figure 4-32. This estimate, which can be taken as an upper bound on performance, indicates the platform has a residual strength ratio of approximately 0.80. The global displacement ductility is also slightly higher, at 1.7. Overall, this upper bound result is closer to the behavior observed in the static pushover analysis.

Ship Shoal 274A
BROADSIDE LOADING: STORM

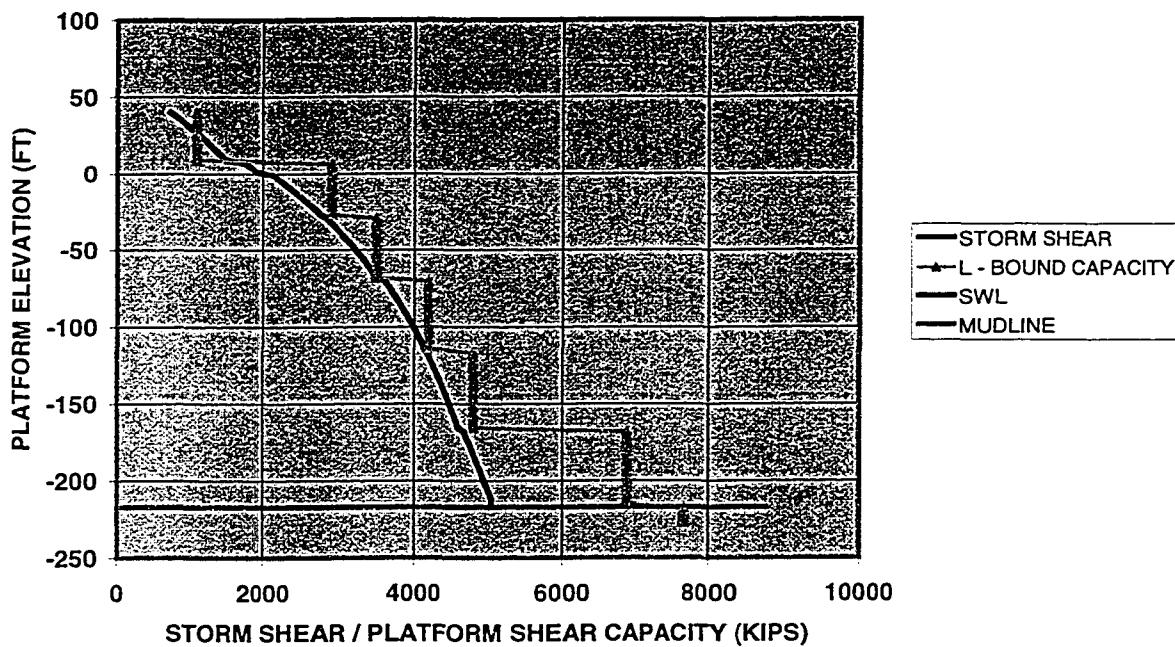


Figure 4-31: Demand-Capacity Analysis, Broadside Loading

Again, the simplified method succeeds in providing the following:

- Excellent estimates of lateral strength

- Hysteresis curves reflecting the likely loss in strength due to minimum framing and poor brace post-buckling characteristics
- Good estimates of global displacement ductility capacity as based on leg hinging

Upper and lower bounds on platform global load-displacement behavior can be determined by invoking different assumptions on how damage concentrates in the jacket structure. The true load-displacement behavior of a structure will lie between the two ranges determined from assuming concentrated damage and distributed damage.

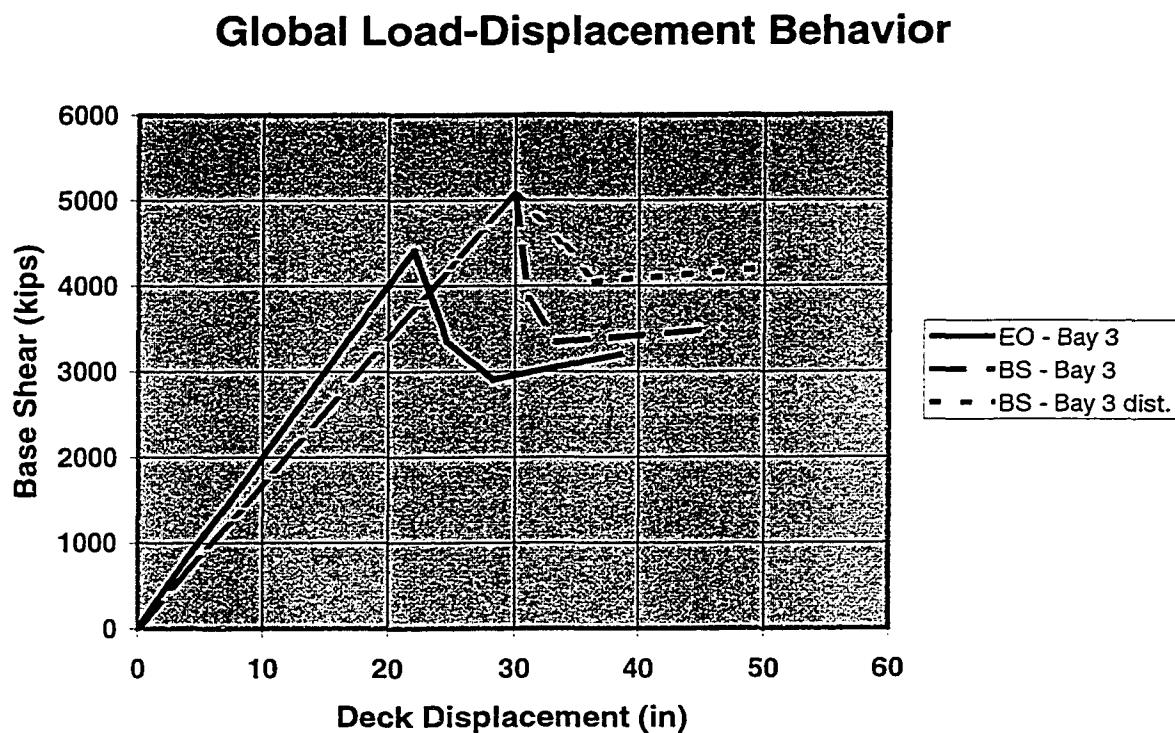


Figure 4-32: Load-Displacement Behavior for SS 274A

4.4.3 U. C. Berkeley Test Frames

The simplified procedures developed in this chapter and Chapter Three were also applied to the analysis of two steel frames tested at U. C. Berkeley by Zayas, et al. (1980A). Particulars of the two frame models are shown in Chapter Two Figure 2-15. The frames are similar in overall dimensions; the difference is in the D/t ratios of the members. Frame I consists of members with D/t ratios of 48, while Frame II members have D/t ratios close to 33. Both frames have horizontal braces capable of transferring load when main diagonal members begin to buckle. The braces in the top K-brace panel were designed to preclude buckling during the test.

Both frames were subjected to a series of loading cycles with progressively increasing displacement magnitudes. A hydraulic ram was used to induce displacement at the deck portion of each frame, and the resulting hysteretic behavior was recorded. Hysteresis loops for both frames are shown in Chapter Two Figure 2-16. In both frames, yielding and buckling began in the top panel, and progressed to the bottom panel. The braces in the top panels were subject to three or four cycles of inelastic displacement prior to moving the frame to the point where bottom panel braces buckled. Frame I exhibited a global strength of approximately 56.6 kips, which occurred at a global ductility of 1.51 as measured from the incipient point of nonlinear behavior. Frame I was able to develop a global displacement ductility of 3.1 while supporting loads up to 70% of maximum. Frame II exhibited a global strength of 73.5 kips, which occurred at a global ductility of 1.62 as measured from the incipient point of nonlinear behavior. Frame II was able to developed a global displacement ductility of 5.0 while supporting loads up to 70% of maximum. Using maximum strength as

a reference point, Frame I can be considered to have developed a gross global ductility of 2.0, while Frame II developed a gross global ductility of 3.0.

The simplified procedures described in this chapter and Chapter Three were used to analyze the two frames. Assuming a single load applied at the top, the capacity of both frames was controlled by buckling of braces in the top X-braced panel bay. The maximum load for Frame I was estimated as 57 kips, while the maximum load for Frame II was 80 kips. These values are in excellent agreement with those observed during the tests.

Global load-displacement envelope curves were developed for the two frames, and are shown in Figure 4-33. Displacement is plotted up to the point at which the braces in the top panel have reached twice the displacement associated with local buckling of the compression brace in that panel. In both cases, damage was assumed to be distributed up until local buckling occurred in a member; following that damage was assumed to concentrate in the frame level. To be consistent with the tests, buckling was assumed to take place between the center of each X and the legs; while this reduces the effective buckling length dramatically, it increases the concentration of damage in a buckling brace, as damage is essentially confined to one-half of the X. Also, the lateral force induced in the bottom panel by bending of the legs in the top panel was artificially suppressed to avoid formation of a two-panel mechanism. This forces damage to concentrate in the top panel.

Global Load-Displacement Behavior

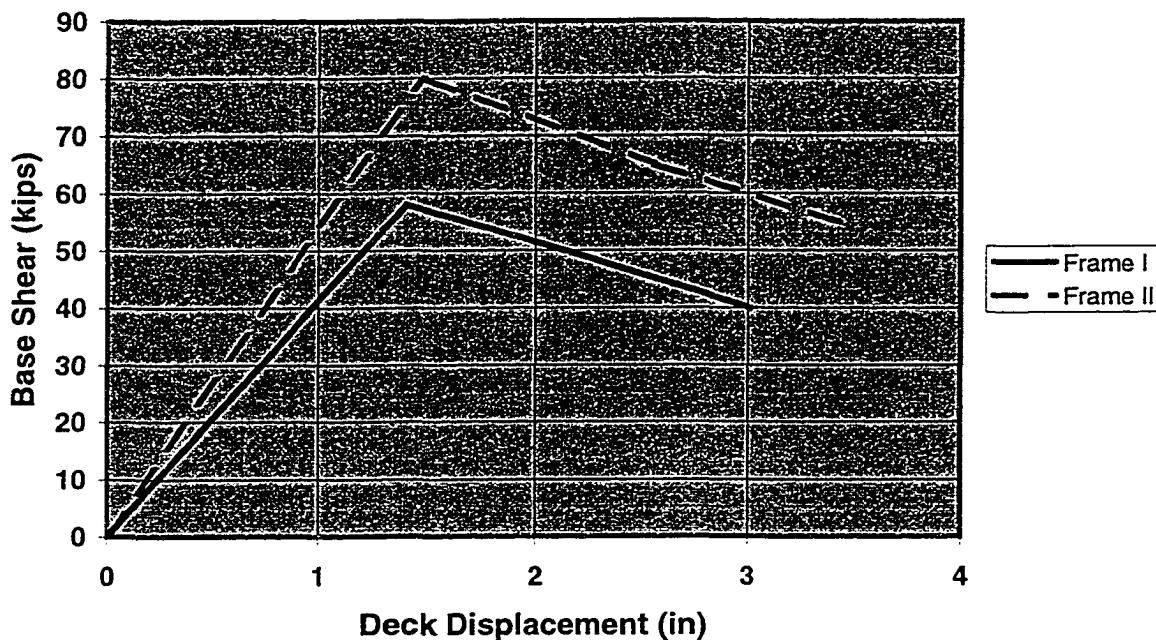


Figure 4-33: Global Load-Displacement Envelopes for Frames I and II

The envelope curves determined compare reasonably well with the hysteresis loops determined from the experiment. Application of the simple approach indicates Frame I is capable of developing a global displacement ductility of 2.1, while Frame II is indicated as developing a global displacement ductility of 2.3. In both cases, residual strength drops to approximately 70% of maximum over the full range of displacement. The results for Frame I are in good agreement with those from the test; the results for Frame II are somewhat conservative so far as displacement ductility and residual strength are concerned. This is due in part to the limits which are placed on the range of cyclic displacement ductility for braces in Section 4.1.2; in reality, the braces in Frame II were able to develop cyclic displacement ductilities of 7.0 and higher during the course of the tests.

4.5 SUMMARY

Simple expressions have been documented by which the basic structural elements of a platform, the braces, legs and piles, can be characterized in terms of stiffness, strength, cyclic displacement ductility and post-yield load-displacement behavior. Based on the performance of these elements, the platform global strength and cyclic displacement ductility can be assessed. The strength of the platform is determined from the first collapse mechanism to form in a structural component. The cyclic displacement ductility capacity of the platform is based on the displacement of the deck which can be reached at the point at which either platform stability is lost, or the point at which major gravity load-carrying members have their cyclic displacement ductility capacities exceeded.

Example applications of the procedures have been made for a series of four structures: two Gulf of Mexico jacket platforms subjected to storm loads, and two X-braced frames tested at U. C. Berkeley by Zayas, et al. (1980A). The procedures provide estimates of structure strength in good agreement with those from static pushover analysis; post-yield behavior is also reasonably represented. It is important, however, to recognize that the procedure by which global displacement ductility is estimated is very approximate; this procedure is based in part on observations of how damage is typically distributed in structures, and makes use of simplifying assumptions regarding the statics of load redistribution.

Additional case studies which demonstrate the application of these methods are contained in Chapter Six.

CHAPTER FIVE:
EARTHQUAKE RESPONSE OF STRENGTH AND STIFFNESS DEGRADING
HYSTERETIC SYSTEMS

5.0 INTRODUCTION

The use of load reduction factors R in the design of structures for earthquakes was first proposed by Veletsos and Newmark (1960). The R factor represents the effective allowable reduction in elastically-determined design load for a SDOF system, given that the system is capable of tolerating deformations in excess of yield:

$$R = \frac{F_y(\mu=1)}{F_y(\mu=\mu_{max})}$$

Load reduction factors have been incorporated into most earthquake design codes, and are intended to allow for the design of simple buildings using elastic analysis.

These factors are established from statistical comparisons made between elastic and inelastic SDOF systems subject to earthquakes. Numerous studies have been performed over the years to determine or revise R factors for common structural systems. Much work has been devoted to the study of bilinear elastic-plastic or strain hardening systems, with and without stiffness degradation. Miranda and Bertero (1994) provide an excellent summary of previous studies on load reduction factors for systems of this type; these studies have indicated the following trends:

- The factors are strongly dependent on the period of the system (Anagnostopoulos, 1972; Miranda, 1991, Newmark, Hall, 1973; Riddell, Newmark, 1979; Nassar, Krawinkler,

1991; Lai, Biggs, 1980; Elghadamsi, Mohraz, 1987; Riddell, et al., 1989; Hidalgo, Arias, 1990; Al-Sulaimani, Roessett, 1985).

- The factors are strongly dependent on the local soil conditions at the site. Factors derived using rock and alluvium ground motions will be quite different from those derived using ground motions recorded on soft soil with low shear wave velocities (Miranda, 1991).
- The factors are not dependent on the distance from the earthquake source, the earthquake magnitude, the strong motion duration, the focal depth of the earthquake, or the earthquake source mechanism (Nassar, Krawinkler, 1990; Miranda, 1991).
- The factors are not strongly dependent on the phenomenon of stiffness degradation for elastic-plastic and bilinear systems (Anagnostopoulos, 1972; Riddell, Newmark, 1979; Nassar, Krawinkler, 1990).
- The factors are not strongly dependent on the viscous damping in the structure for all but the shortest periods (Riddell, Newmark, 1979; Peng, et al., 1988).

As opposed to finding the mean load reduction associated with a fixed value of displacement ductility, it might be desirable to instead find the mean displacement ductility associated with a fixed value of elastic overload ratio. This relationship, referred to in this chapter as a displacement modification factor F_d , can be used in a similar role to that of the load reduction factor; in lieu of making comparisons in force-space for a prescribed displacement ductility capacity, comparisons can be made in displacement-space for a prescribed amount of overload ratio between system strength and elastic force.

It must be recognized that these factors are random variables. Results obtained from many of the above studies have indicated a steady increase in variability for increasing levels of overload ratio or ductility demand. Miranda (1991) conducted a very thorough study of the statistical variability for R ; statistical variability fell in the range of 20% to 50%, was mostly insensitive to structure period, but showed moderate dependence on increasing displacement ductility capacity. These results indicate the factors have consistent properties over a practical range and can therefore be used within bounds of statistical confidence.

Few studies, however, have been performed on the evaluation of such factors for systems which exhibit strength and stiffness degradation of the type associated with platform systems as discussed in Chapter Two. Limited studies have been performed by Anagnostopoulos (1972) and Al-Sulaimani and Roessel (1985); while these studies have established the dependence of load reduction factors on the hysteretic behavior of systems where loss of strength with displacement is a concern, the studies performed were limited in the number of trials, and hence do not provide a sufficient statistical basis for confident development of load reduction factors. Additional limited studies have been performed by Mahin and Boroscheck (1991) and MacCrae and Kawashima (1991); these studies again confirm the sensitivity of allowable strength reductions and associated displacement demands to degrading strength, but do not provide additional insight to the statistics of such systems which may be used in design and assessment.

This chapter documents a study performed to determine R and F_d factors for SDOF systems with hysteretic behaviors similar to those exhibited by offshore structural systems; namely,

those which exhibit strength and stiffness degradation with cycling. These factors are intended to be used in conjunction with the results of ultimate strength (static pushover) analyses and elastically-calculated loads or displacements from a response spectrum. Assuming the platform system is dominated largely by the first lateral modes, the capacity of the platform will be determined from either:

$$F_{yield} > \frac{F_{elastic}}{R}$$

where $F_{elastic}$ is the base shear corresponding to the first mode forces determined from the elastic response spectrum for the level of earthquake excitation specified, and F_{yield} is the base shear from first mode forces which results in yielding in the platform determined from the static pushover analysis, or:

$$\Delta_{collapse} > \Delta_{elastic} F_\Delta$$

where $\Delta_{elastic}$ is the elastically-calculated deck or global displacement, and $\Delta_{collapse}$ is the maximum tolerable global displacement of the platform.

These factors allow for the implicit consideration of the dynamic behavior of the actual yielding system, and modify the results of a static analysis accordingly. It must be recognized that these factors are random variables; hence, a prime objective of the study is to establish the statistical properties of these factors.

In addition to determining these factors for strength and stiffness degrading systems, a number of comparison cases are performed in which MDOF systems with strength and stiffness degrading elements are analyzed using time history analysis, and then global and

local ductility demands are compared to results from use of an equivalent SDOF. These cases are intended to qualitatively explore the limitations of the equivalent SDOF concept.

5.1 STATISTICAL STUDY ON R AND F_d

It is instructive to review several basic behavioral characteristics of strength and stiffness degrading systems. Strength-degrading systems can be subject to displacement demands two to three times higher than those in an elastic-plastic or strain-hardening system with the same yield strength. However, studies conducted by Mahin and Boroscheck (1991) and others have demonstrated that strength degradation coupled with stiffness degradation will result in less significant increases in displacement demand; this behavior trend is consistent with the trend for elastic-plastic and strain-hardening systems with stiffness degradation to exhibit less displacement demand than counterpart systems without stiffness degradation. This is due in part to the fact that stiffness-degrading systems will accumulate permanent offset at a slower rate than a non-stiffness degrading system; the trend for a stiffness-degrading system is to return towards the initial position, thus reducing the potential to accumulate displacements by “ratcheting” in one direction of displacement.

Strength-degrading systems can develop a significant unbalance in directional strength after initially yielding in a given direction,. As observed by Newmark and Rosenblueth (1971) and others, systems with this type of directional strength imbalance will tend to rapidly accumulate displacement on the side which yields first (and hence suffers strength loss); this is due in part to the fact that the “strong” side stores elastic strain energy, and rebounds

toward the weaker side to dissipate this energy. Stiffness degradation can reduce the deleterious effects of this imbalance.

Another important issue for strength-degrading systems is the duration of excitation. As observed by Mahin (1976), systems which do not reach a plateau of strength after degradation are inherently unstable, and will collapse (reach zero strength) if the ground motion duration is sufficiently long. This is of particular importance for systems which are subject to significant P - Δ effects. While the platform systems considered in this dissertation are generally restricted for assessment purposes to a stable residual strength level, duration of shaking is still important from the standpoint that longer motions will inevitably drive the structural system to this residual strength.

A statistical study of nonlinear SDOF systems with strength and stiffness degrading hysteresis subjected to earthquakes was performed in order to determine load reduction and displacement modification factors. The sections below describe the systems analyzed, the ground motions used, and the software used to conduct the study.

5.1.1 Hysteretic Behaviors Considered

Referring back to the Figures of Section 2.5 in Chapter Two, it is clear that many platform systems will lose strength and stiffness with cyclic inelastic loading. As a consequence, these systems must be designed to higher load levels than bilinear elastic-plastic or strain-hardening systems, in order to keep displacement demands to similar levels.

Based on a qualitative review of the hysteretic behaviors associated with platform structural systems, it was decided to focus on two general types of degrading behavior:

- Strength and stiffness degradation, with hysteresis bounded by a trilinear envelope as shown in Figure 5-1. This behavior was chosen to characterize hysteresis associated with yielding in platform jacket structures. These systems are referred to as jacket-type or JT systems.
- Strength degradation alone, with the rate of degradation dependent upon the amount of accumulated inelastic deformation with each cycle, as shown in Figure 5-2. This behavior was chosen to represent the hysteresis associated with yielding in platform foundations. These systems are referred to as foundation-type or FT systems.

In addition, bilinear strain-hardening behavior with and without stiffness degradation was also considered, for the purpose of comparison. These systems are referred to as bilinear degrading (BD) or bilinear non-degrading (BN) systems. The amount of strain hardening was kept small (3% of elastic stiffness).

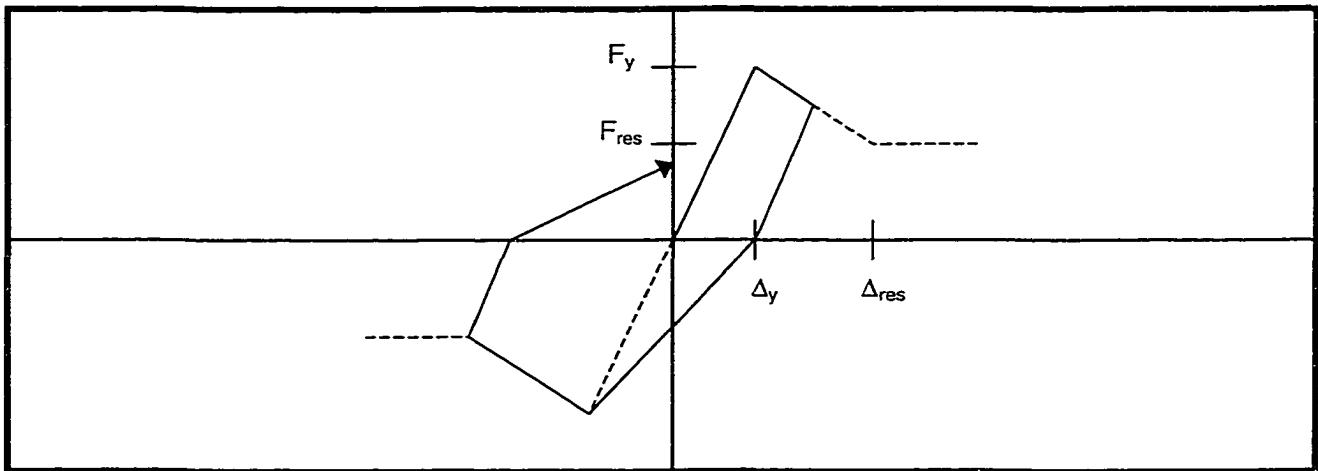


Figure 5-1: JT System Hysterisis

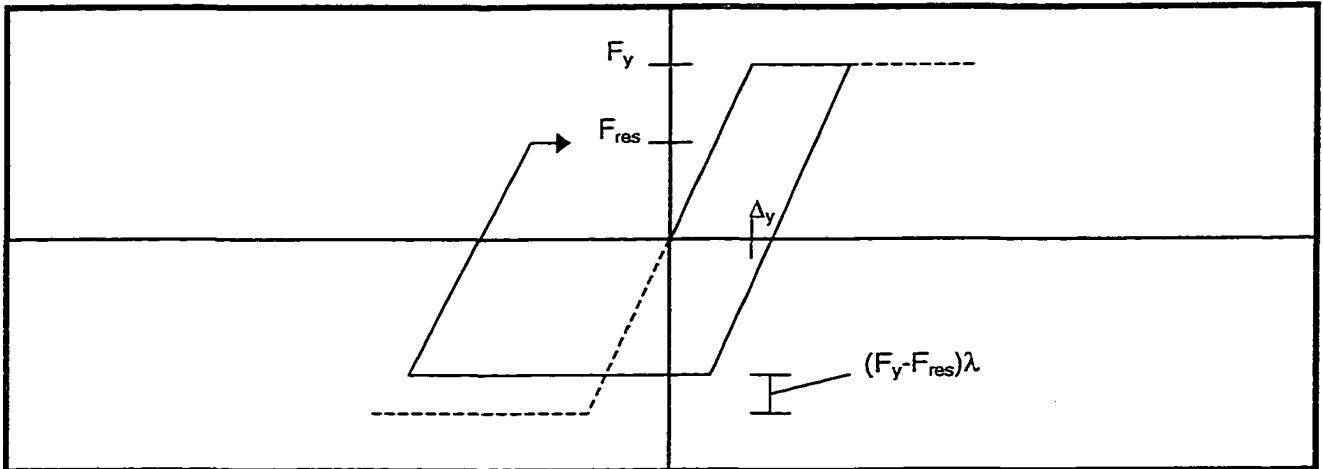


Figure 5-2: FT System Hysteresis

The JT and BD systems utilize a stiffness degradation algorithm developed by Clough and Johnson (1967). This model is simple, and was judged to represent the cyclic behavior of braced frames to a reasonable degree. Other studies have experimented with models which exhibit “pinching” behavior as part of a stiffness degradation scheme, such as those described by Gates (1978); however, for the purpose of developing generic factors, it was felt that fewer initial variables would be best.

JT systems are controlled by two parameters: residual strength, designated F_{res} , and the displacement associated with reaching the residual strength plateau, designated Δ_{res} . F_{res} is specified as a fraction of the yield strength F_y of the system, while Δ_{res} is specified as a multiple of the yield displacement Δ_y of the system. Table 5-1 lists the JT SDOF system parameters which were considered in the course of the investigation. These parameters were selected to cover the range in degrading behavior commonly observed in braced frames, as

well as to represent the period range covered by the fundamental lateral modes of most offshore platforms.

Table 5-1: JT SDOF System Parameters

Variable	Values
Period T (sec)	0.5, 0.6, 0.7, 0.8, 0.9, 1.0, 1.1, 1.2, 1.3, 1.4, 1.5, 1.6, 1.7, 1.8, 1.9, 2.0, 2.2, 2.4, 2.6, 2.8, 3.0, 3.5, 4.0
Damping β (% critical)	5%, 10% ³
F_{res} (% yield strength)	80%, 60%
Δ_{res} (fraction of yield displacement)	1.1, 2, 3, 4
Ductility Capacity μ^1	1 (i.e. elastic), 2, 3, 4
Normalized Yield Strength F_y^2	100% (elastic), 75%, 50%, 25%

1 Target values for determination of load reduction factors

2 Target values for determination of displacement modification factors

3 10% was considered in a limited number of cases, as discussed in Section 5.3

FT systems are also controlled by two parameters: residual strength F_{res} and incremental strength reduction λ . λ is used in the manner suggested by Matlock, et al. (1978) for piles to reduce strength with each successive cycle according to:

$$F_{i+1} = (1 - \lambda)(F_i - F_{res}) + F_{res}$$

Strength reduction does not take place until inelastic strain reversal has occurred. The parameters used in the study of FT systems are shown below in Table 5-2:

Table 5-2: FT SDOF System Parameters

Variable	Values
Period T (sec)	0.5, 0.6, 0.7, 0.8, 0.9, 1.0, 1.1, 1.2, 1.3, 1.4, 1.5, 1.6, 1.7, 1.8, 1.9, 2.0, 2.2, 2.4, 2.6, 2.8, 3.0, 3.5, 4.0
Damping β (% critical)	5%, 10% ³
F_{res} (% yield strength)	80%, 60%
λ	0.2, 0.4
Ductility Capacity μ^1	1 (i.e. elastic), 2, 3, 4
Normalized Yield Strength F_y^2	100% (elastic), 75%, 50%, 25%

1 Target values for determination of load reduction factors

2 Target values for determination of displacement modification factors

3 10% was considered in a limited number of cases, as discussed in Section 5.3

BD and BL systems were analyzed for the same range of periods, ductility capacities and normalized yield strengths as the JT and FT systems; damping was restricted to 5%.

5.1.2 Earthquake Ground Motions Used

In the past few years significant efforts have been devoted to recording and collating earthquake time histories. An excellent source of records is available from the National Geophysical Data Center (1996); this set of records contains over 15,000 time histories recorded during earthquakes occurring around the world between 1933 and 1994. While the vast majority of records have been recorded in the past twenty years, this set still contains enough variability to be adequate for general design standard development purposes. The records on this set are available as uncorrected time histories, corrected time histories, and elastic response spectra.

The development of load reduction factors and displacement modification factors was based on analyses conducted using 37 ground motions recorded on rock. These ground motions are listed in Table 5-3. In selecting these ground motions, effort was made to use many of the same ground motions utilized as part of a previous study conducted by Miranda (1991). This was deemed desirable as it provides a source for qualitative comparison of the results generated by this current study. Initially, use of corrected acceleration records as described by Naeim and Anderson (1993) was planned for the study; however, uncorrected acceleration records were eventually decided upon for three reasons: (1) uncorrected records were used by Miranda (1991), (2) the method of correction is known to change the character, in some cases

substantially, of these records, depending on the correction method, and (3) several of the corrected records were found to contain data errors.

Table 5-3: 37 Ground Motions Recorded on Rock

Station	Geology	Event	Mag.	Ep. Dis. (km)	Dir.	PGA (g)	PGV (cm/sec)
San Francisco Golden Gate Park	Siliceous Sandstone	San Francisco March 22, 1957	5.3 ML	11	N10E S80E	0.08 0.11	4.91 4.61
Parkfield Cholame Shandon No. 2	Rock	Parkfield June 27, 1966	5.6 ML	7	N65E	0.48	78.09
Castaic Old Ridge Road	Sandstone	San Fernando February 9, 1971	6.5 ML	29	N21E N69W	0.32 0.27	17.16 27.82
Ljolleo	Sandstone and Volcanic Rock	Central Chile March 3, 1985	7.8 MS	45	N10E S80E	0.67 0.43	23.70 43.60
Valparaiso	Volcanic Rock	Central Chile March 3, 1985	7.8MS	84	N70E S20E	0.18 0.16	16.30 9.70
La Union	Metavolcanic Rock	Michoacan September 19, 1985	8.1 MS	84	N00E N90E	0.17 0.15	20.34 11.70
La Villita	Gabbro Rock	Michoacan September 19, 1985	8.1 MS	44	N00E N90E	0.13 0.12	16.11 10.51
Zihuatanejo	Tunalite Rock	Michoacan September 19, 1985	8.1 MS	135	N90W S00E	0.10 0.16	15.86 18.34
National Geographic Institute	Balsamo Formation	San Salvador October 10, 1986	5.4 MS	5.7	270 180	0.53 0.39	72.70 56.10
Institute of Urban Construction	Fluviate Pumice Rock	San Salvador October 10, 1986	5.4 MS	5.3	90 180	0.38 0.67	39.20 55.60
Geotechnical Investigation Center	Fluviate Pumice Rock	San Salvador October 10, 1986	5.4 MS	4.3	180 90	0.42 0.68	61.80 80.00
Mt. Wilson Caltech Seismic Station	Quartz Diorite	Whittier-Narrows October 1, 1987	6.1 ML	19	90 360	0.19 0.13	4.09 4.32
Corralitos Eureka Canyon Road	Landslide Deposits	Loma Prieta October 17, 1989	7.1 MS	7	90 360	0.47 0.62	47.50 55.20
Santa Cruz UCSC	Limestone	Loma Prieta October 17, 1989	7.1 MS	16	90 360	0.41 0.43	21.20 21.20
San Francisco Cliff House	Franciscan Sandstone	Loma Prieta October 17, 1989	7.1 MS	99	90 0	0.11 0.07	21.00 11.20
San Francisco Pacific Heights	Franciscan Sandstone	Loma Prieta October 17, 1989	7.1 MS	97	360 270	0.05 0.06	9.88 14.30
San Francisco Presidio	Serpentine	Loma Prieta October 17, 1989	7.1 MS	98	90 0	0.20 0.10	33.50 13.30
San Francisco Rincon Hill	Franciscan Sandstone	Loma Prieta October 17, 1989	7.1 MS	95	90 360	0.09 0.08	11.60 7.34
Yerba Buena Island	Franciscan Sandstone	Loma Prieta October 17, 1989	7.1 MS	95	90 360	0.06 0.03	14.70 4.61

Table 5-4A: 31 Ground Motions Recorded on Alluvium

Station	Geology	Event	Mag.	Ep. Dis. (km)	Dir.	PGA (g)	PGV (cm/sec)
El Centro Irrigation District	Alluvium	Imperial Valley May 18, 1940	6.3 ML	8	S90W	0.21	36.92
Taft Lincoln School Tunnel	Alluvium	Kern County July 21, 1952	7.7 MS	56	S69E	0.17	17.71
Los Angeles 445 Figueroa St.	Alluvium	San Fernando February 9, 1971	6.5 ML	41	N52E	0.15	17.38
Hollywood Free Field	Alluvium	San Fernando February 9, 1971	6.5 ML	35	N90E	0.21	21.14
Hollywood 1901 Avenue of the Stars	Silt and Sand Layers	San Fernando February 9, 1971	6.5 ML	38	S44W	0.15	16.74
Sendai City Kokutetsu Building	Alluvium	Miyagi-Ken-Oki June 12, 1978	7.4 MS	110	N90W	0.44	57.01
Meloland Interstate 8 Overpass	Alluvium	Imperial Valley October 15, 1979	6.6 ML	21	360	0.31	71.65
Bonds Corner Highways 98 and 115	Alluvium	Imperial Valley October 15, 1979	6.6 ML	3	S50W	0.77	44.07
James Road El Centro Array #5	Alluvium	Imperial Valley October 15, 1979	6.6 ML	22	S50W	0.37	86.56
Imperial Valley College El Centro Array #7	Alluvium	Imperial Valley October 15, 1979	6.6 ML	21	S50W	0.45	107.80
El Almendral	Compacted Fill	Central Chile March 3, 1985	7.8 MS	84	N50E	0.29	26.90
Vina Del Mar	Alluvial Sand	Central Chile March 3, 1985	7.8 MS	88	S20W	0.36	33.20
Zaculta	Alluvium	Michoacan September 19, 1985	8.1 MS	49	S00E	0.26	30.39
Alhambra Freemont School	Alluvium	Whittier-Narrows October 1, 1987	6.1 ML	7	180	0.30	21.63
Altadena Eaton Canyon Park	Alluvium	Whittier-Narrows October 1, 1987	6.1 ML	13	360	0.31	10.43
Burbank California Fed. Savings	Alluvium	Whittier-Narrows October 1, 1987	6.1 ML	26	130	0.22	12.61
Downey County Maintenance Bldg.	Deep Alluvium	Whittier-Narrows October 1, 1987	6.1 ML	17	180	0.20	29.27
Inglewood Union Oil Yard	Terrace Deposits	Whittier-Narrows October 1, 1987	6.1 ML	25	90	0.23	16.28
Los Angeles 116 th St. School	Terrace Deposits	Whittier-Narrows October 1, 1987	6.1 ML	22	360	0.40	18.65
Los Angeles Baldwin Hills	Alluvium over Shale	Whittier-Narrows October 1, 1987	6.1 ML	27	360	0.15	7.51
Los Angeles Hollywood Storage Fac.	Alluvium	Whittier-Narrows October 1, 1987	6.1 ML	25	360	0.21	8.99
Los Angeles Obregon Park	Alluvium	Whittier-Narrows October 1, 1987	6.1 ML	10	360	0.44	22.07
Long Beach Rancho Los Cerritos	Alluvium	Whittier-Narrows October 1, 1987	6.1 ML	27	90	0.25	18.48
San Marino Southwestern Academy	Alluvium	Whittier-Narrows October 1, 1987	6.1 ML	8	360	0.20	12.87
Tarzana Cedar Hill Nursery	Alluvium	Whittier-Narrows October 1, 1987	6.1 ML	44	90	0.63	24.20
Whittier 7215 Bright Tower	Alluvium	Whittier-Narrows October 1, 1987	6.1 ML	10	90	0.63	27.10

Table 5-4B: 31 Ground Motions Recorded on Alluvium (continued)

Capitola Fire Station	Alluvium	Loma Prieta October 17, 1989	7.1 MS	9	360	0.46	36.10
Hollister South and Pine	Alluvium	Loma Prieta October 17, 1989	7.1 MS	48	360	0.36	62.80
Oakland 2-Story Office Building	Alluvium	Loma Prieta October 17, 1989	7.1 MS	92	290	0.24	37.90
Alba 900 S. Fremont	Alluvium	Whittier-Narrows October 1, 1987	6.1 ML	8	90	0.29	10.84
Stanford Parking Garage	Alluvium	Loma Prieta October 17, 1989	7.1 MS	51	360	0.26	33.18

Table 5-5: 24 Ground Motions Recorded on Soft Soil

Station	Geology	Event	Mag.	Ep. Dis. (km)	Dir.	PGA (g)	PGV (cm/sec)
Bucharest Building Research Institute	Soft	Romania March 4, 1977	7.1 MS	174	EW SN	0.17 0.20	32.62 75.11
SCT	Soft Clay	Michoacan September 19, 1985	8.1 MS	385	N90W S00E	0.17 0.10	60.50 38.74
Central de Abastos Refrigeration	Soft Clay	Michoacan September 19, 1985	8.1 MS	389	99.53 77.52	0.10 0.08	34.57 24.85
Central de Abastos Office	Soft Clay	Michoacan September 19, 1985	8.1 MS	389	76.56 67.95	0.08 0.07	41.86 34.98
Colonia Roma	Soft Clay	Acapulco April 25, 1989	6.9 MS	0	N90W S00E	0.06 0.05	11.90 10.92
Emeryville Free Field South	Bay Mud	Loma Prieta October 17, 1989	7.1 MS	97	350 260	0.21 0.26	21.50 41.06
Oakland Outer Warf Harbor	Bay Mud	Loma Prieta October 17, 1989	7.1 MS	95	305 125	0.27 0.29	42.30 40.80
Treasure Island Naval Base	Fill	Loma Prieta October 17, 1989	7.1 MS	98	90 360	0.16 0.10	33.40 15.60
San Francisco International Airport	Bay Mud	Loma Prieta October 17, 1989	7.1 MS	79	90 360	0.33 0.23	29.26 26.45
San Francisco 18-Story Commercial Bldg.	Fill over Bay Mud	Loma Prieta October 17, 1989	7.1 MS	95	80 350	0.13 0.16	17.11 15.76
Foster City Redwood Shores	Bay Mud	Loma Prieta October 17, 1989	7.1 MS	63	90 0	0.28 0.26	45.40 31.80
Emeryville Free Field North	Bay Mud	Loma Prieta October 17, 1989	7.1 MS	97	350 260	0.20 0.22	15.74 37.94

As an important issue for strength-degrading systems is the duration of excitation, effort was made to select motions which were recorded during long-duration events. As observed by Mahin (1976), systems which do not reach a plateau of strength after degradation are inherently unstable, and will collapse (i.e. reach zero strength) if the ground motion duration

is sufficiently long. While the platform systems considered in this dissertation are generally restricted for assessment purposes to a stable residual strength level, duration of shaking is still important from the standpoint that longer motions will inevitably drive the structural system to this residual strength.

In addition, two additional sets of ground motions, 31 recorded on alluvium and 24 recorded on soft soil were also used for limited studies of the effects of local soil conditions on these factors. These ground motions are listed in Tables 5-4 and 5-5; these studies are discussed in Section 5.4.

5.1.3 Software Used in Study

Performance of this study involves use of software which is capable of solving the differential equation governing the motion of an inelastic viscously-damped SDOF system subjected to time-varying ground acceleration:

$$m\ddot{u}(t) + c\dot{u}(t) + k(u(t))u(t) = -m\ddot{u}_g(t)$$

where:

m = mass

c = damping coefficient, $4\pi m \xi / T$

and k is the displacement-varying restoring force coefficient. In an elastic system, k is constant.

Many programs have been developed over the years to solve this relationship using numerical step-by-step integration. These programs can be divided up into two categories: academic programs and commercial programs.

The academic programs are freely available; however, they are usually written in older code (Fortran) and have not been maintained over time. As such, they will not always function predictably with today's PC operating systems (Win95 and Windows NT). One of the better known academic programs is NONSPEC, developed by Lin and Mahin (1983). This program has spawned a number of others such as NLSPECTRA (Miranda, 1991), NOSPEC (Khatib, et al., 1988) and PCNSPEC (Boroscheck, 1991). All of these programs perform the required integration using the linear acceleration method (Newmark, 1959). Equilibrium violations due to changes in the displacement-varying restoring force within a time step are minimized by varying the integration time step and by enforcing equilibrium by modifying the acceleration at the end of the step.

It is also possible to make use of a variety of commercial nonlinear dynamic structural analysis programs such as DRAIN (Powell, 1993), PC-ANSR (Maison, 1990), and IDARC (Reinhorn, 1995) to perform studies of this type. This approach offers the advantage of using software which usually has more rigorous quality standards. However, these programs must be controlled in a batch execution mode in order to perform the number of calculations required; this can become quite cumbersome, as the input file for the program must be rewritten each time another iteration is desired.

To perform this study, it was decided to upgrade the old NONSPEC code to a more modern environment. PCNSPEC was translated from Fortran to MS Visual Basic, and modified to allow for the analysis of SDOF systems with hysteretic behavior appropriate to JT and FT systems. This new program, JINSPEC, was then used to carry out the statistical studies documented in Section 5.2.

5.2 RESULTS OF STATISTICAL STUDIES

The main goals of the statistical studies were to develop load reduction factors and displacement modification factors for SDOF systems which exhibit hysteretic behavior similar to that of jacket-type platforms. Overall, 68,816 SDOF system – ground motion combinations were analyzed. Results from the studies are broken up into three sections, each associated with the different systems (BD/BN, JT, FT) studied. Each section contains mean load reduction factors, mean displacement response factors, and coefficients of variation for the different factors appropriate to the individual systems. The results for BD, JT and FT systems are compared to results from BN systems, in order to assess the differences between these degrading systems and convention bilinear systems.

5.2.1 BD/BN SDOF Systems

Results for BN systems are shown in Figures 5-3 to 5-6, and results for BD systems are shown in Figures 5-7 to 5-10. The BN system analysis confirms trends for bilinear non-degrading systems which have been identified in previous analysis, namely:

- The mean load reduction in design force permitted by nonlinear behavior is bounded over most of the period range by $1/\mu$.

- The mean ratio between elastic and inelastic displacements is approximately one over most of the period range.

These trends begin to change for periods in the range of 0.5 sec to 1.0 sec, most noticeably for systems forced to develop higher ductility.

Comparison of the BN and BD load reduction and displacement modification factors reveals that stiffness degradation does noticeably change the character of these factors. Load reduction factors are approximately 10% to 20% greater for the BD system, whereas displacement modification factors are smaller by a similar proportion. Trends in variability between the different factors, however, are similar; coefficients of variation range from 10% to as high as 45%.

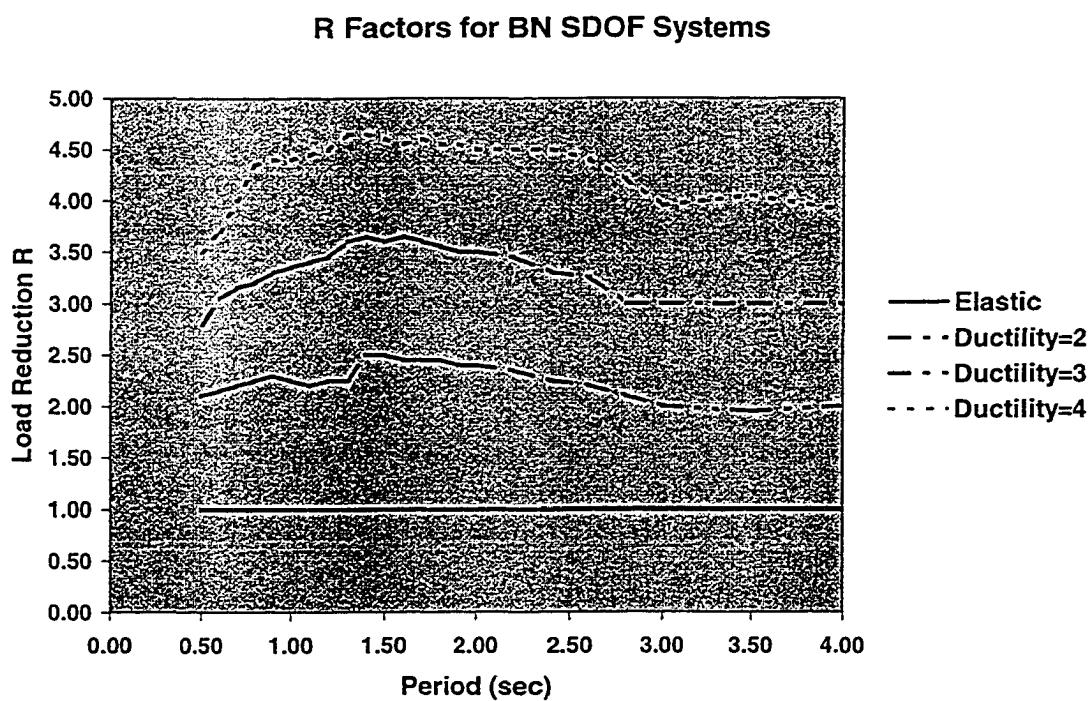


Figure 5-3: R Factor for BN

F-D Factors for BN SDOF Systems

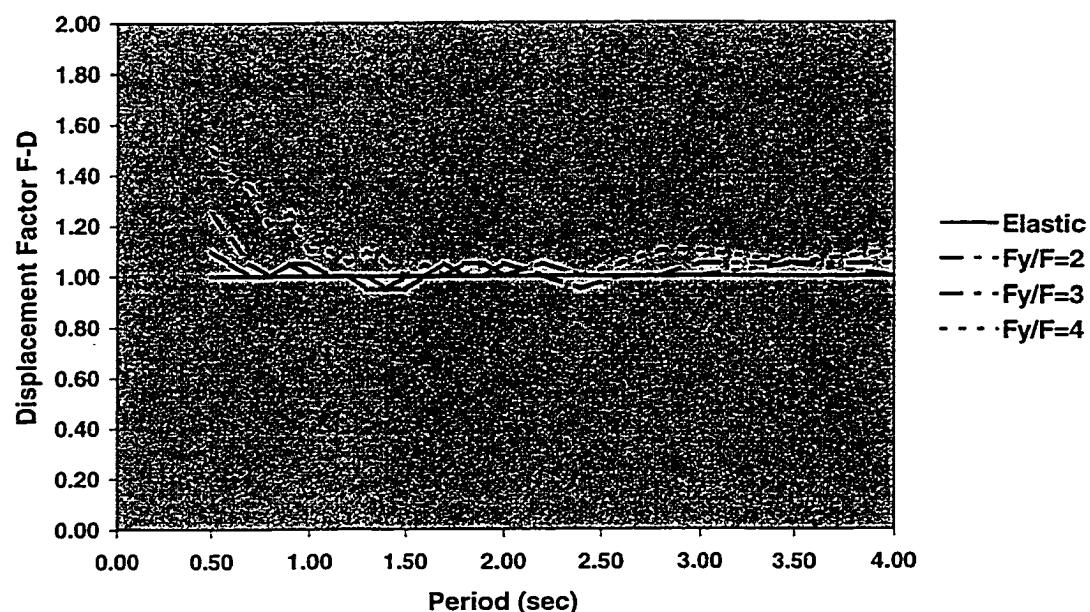


Figure 5-4: F_d Factor for BN

R Factor COV for BN SDOF Systems

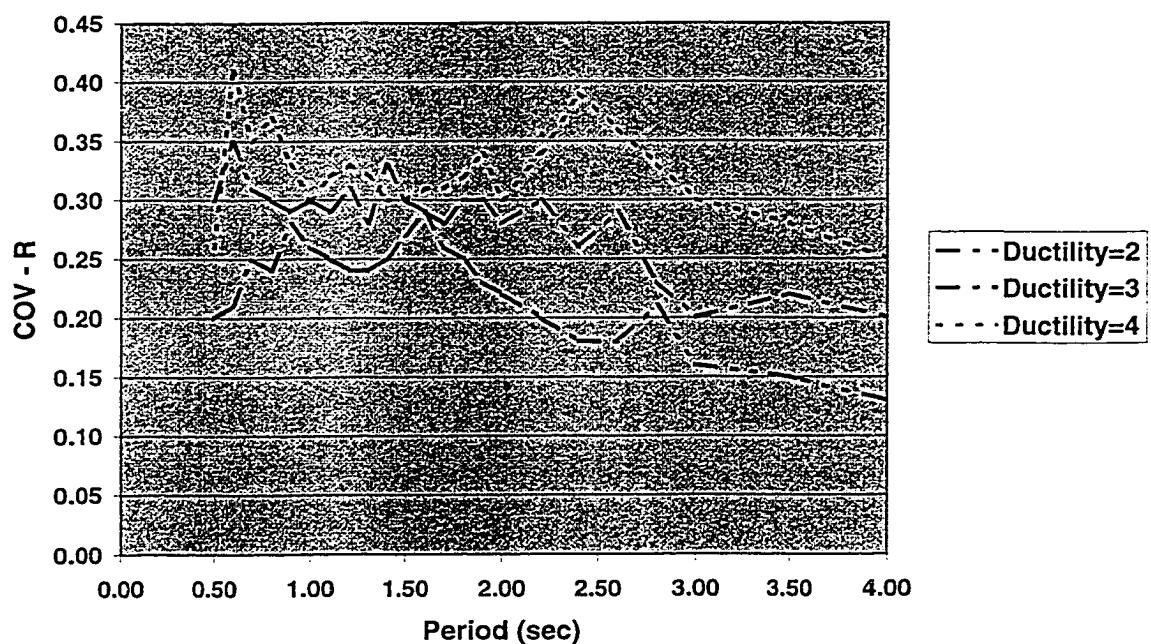


Figure 5-5: COV in R Factor for BN

F-D Factor COV for BN SDOF Systems

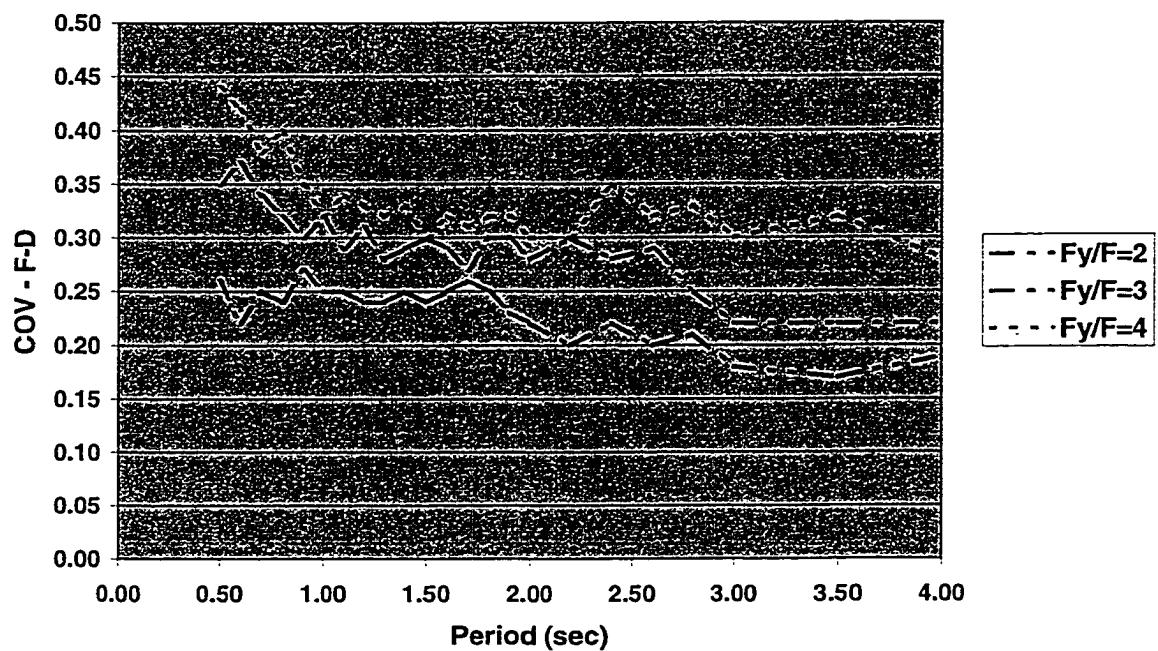


Figure 5-6: COV in F_D Factor for BN

R Factors for BD SDOF Systems

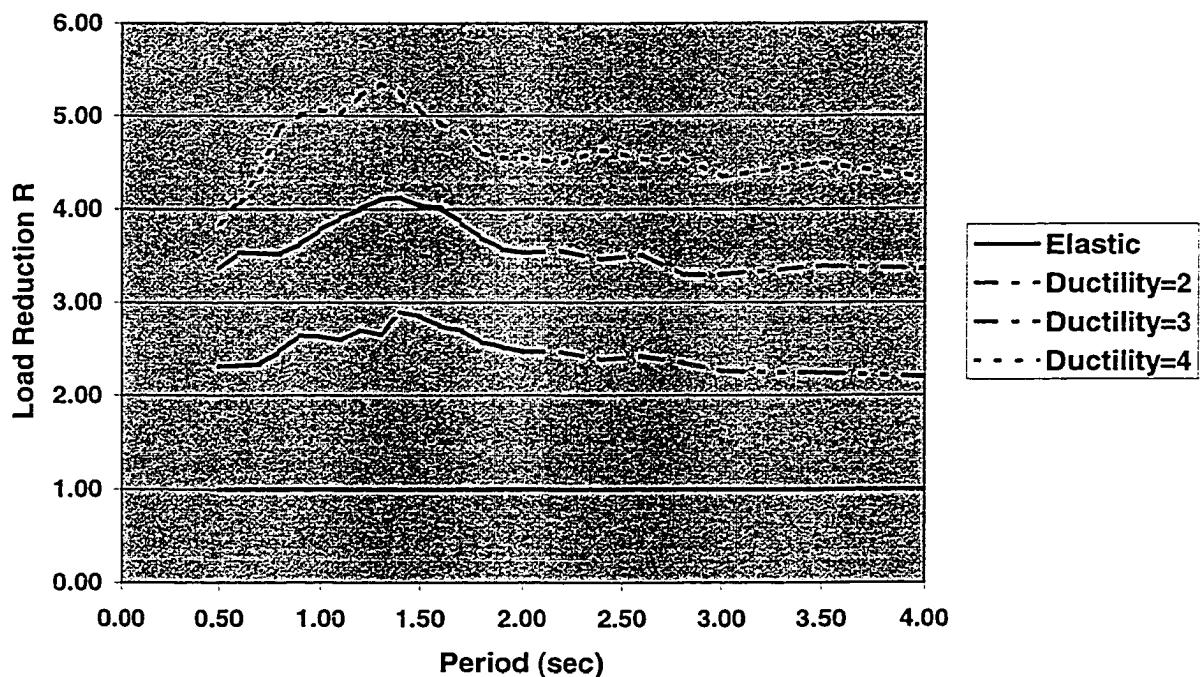


Figure 5-7: R Factor for BD

F-D Factors for BD SDOF Systems

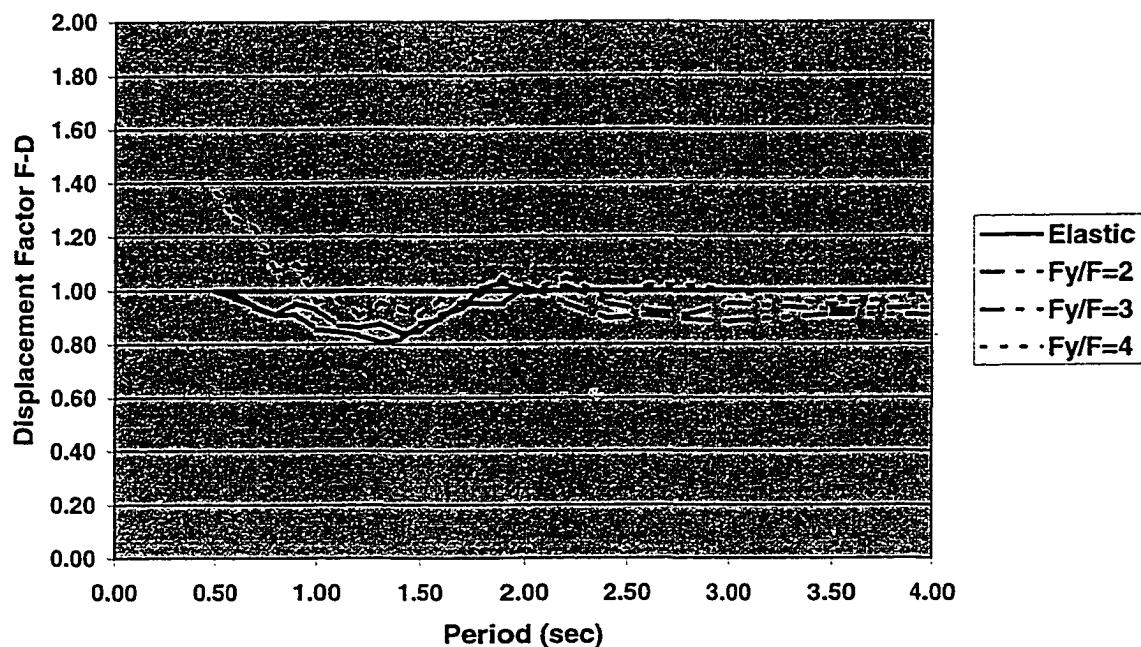


Figure 5-8: F_d Factor for BD

R Factor COV for BD SDOF Systems

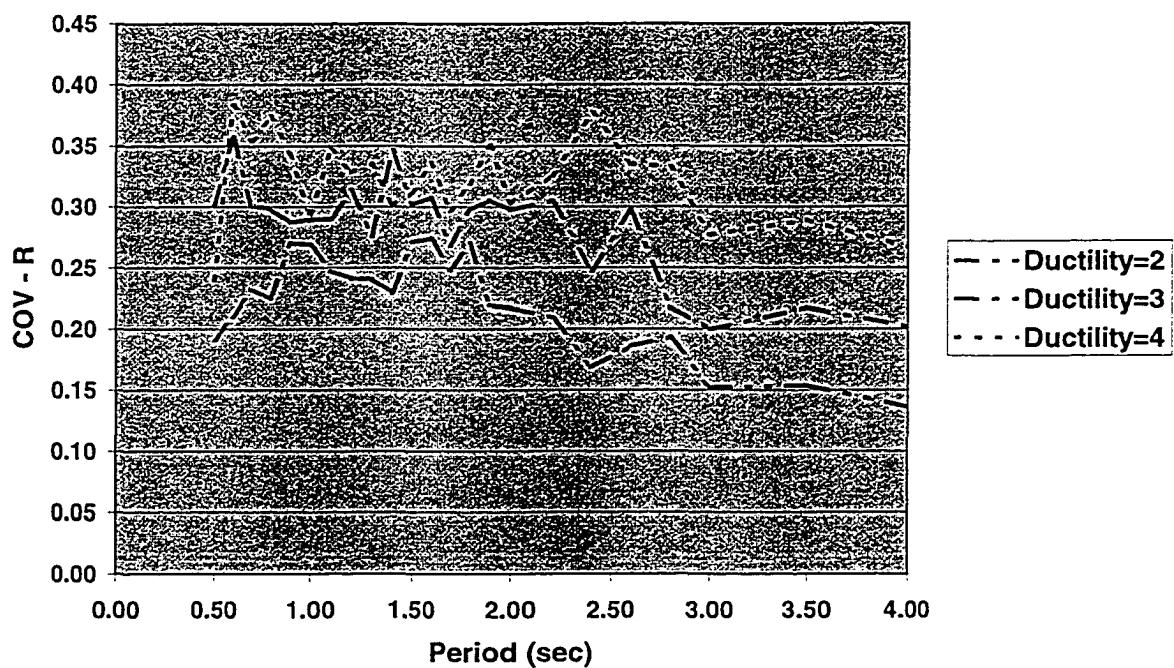


Figure 5-9: COV in R Factor for BD

F-D Factor COV for BD SDOF Systems

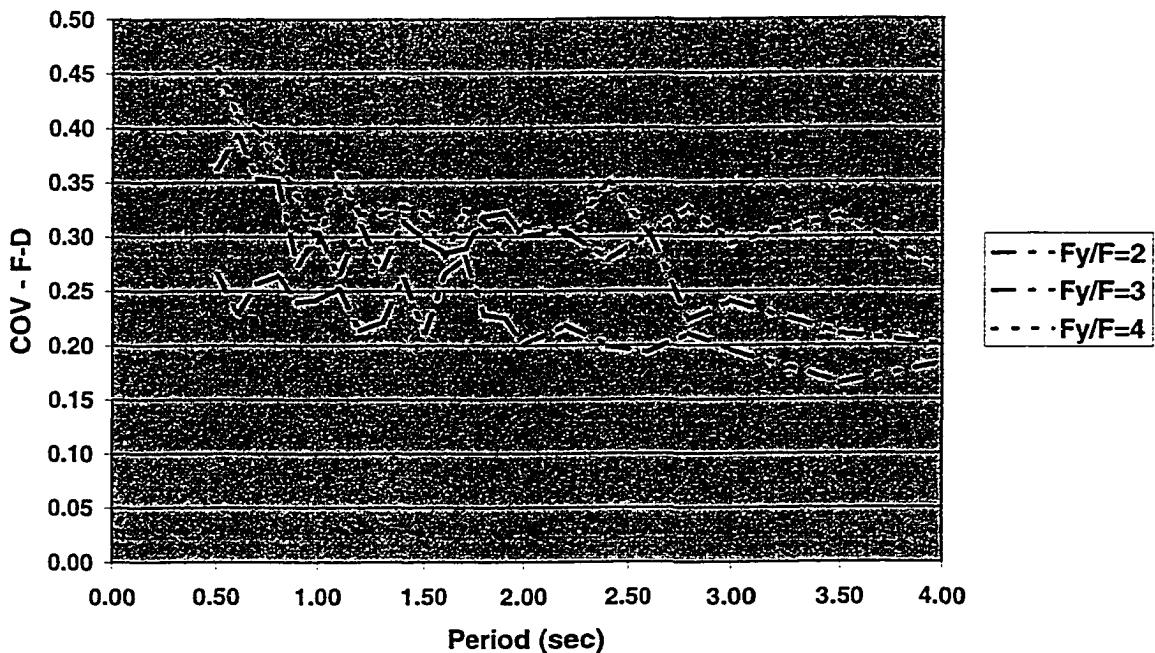


Figure 5-10: COV in F_d Factor for BD

5.2.2 JT SDOF Systems

Results for JT systems are shown in Figures 5-11 to 5-42. The results are matched to each type of JT system using a five-digit code. The first three digits describe the point at which the negative slope on the envelop intersects the residual strength. The last two digits describe the residual strength as a percentage of initial yield strength.

JT systems show marked reductions in load reduction factors, and corresponding increases in displacement modification factors, as compared to BN systems. The most severely degrading system, JT11060 (5-39 to 5-42), exhibits strength reduction factors which are 20% to 30% less than those of BN systems, while displacement modification factors are inmost cases 40%

to 50% greater than those for BN systems. Variability in the response of the JT degrading systems is moderately higher than that for the BN systems.

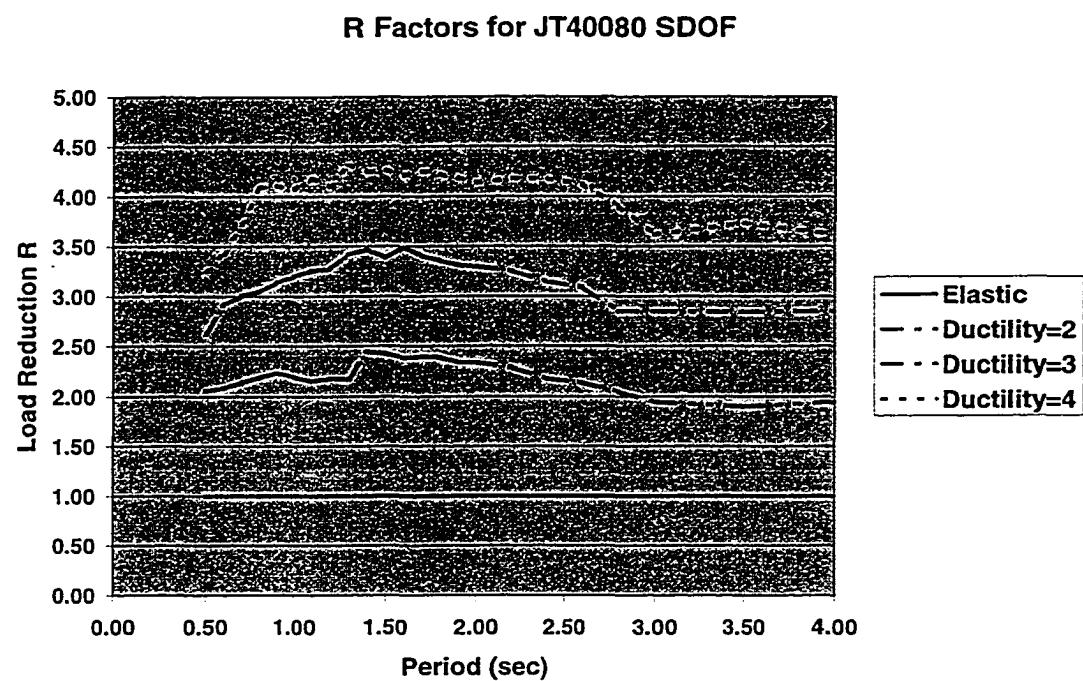


Figure 5-11: R Factor for JT

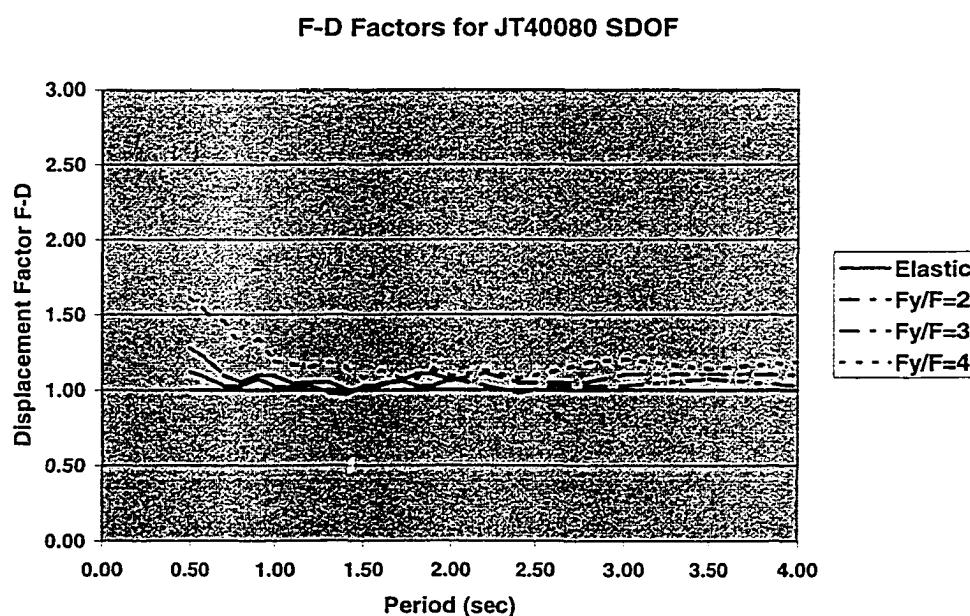


Figure 5-12: F_d Factor for JT

R Factor COV for JT40080 SDOF

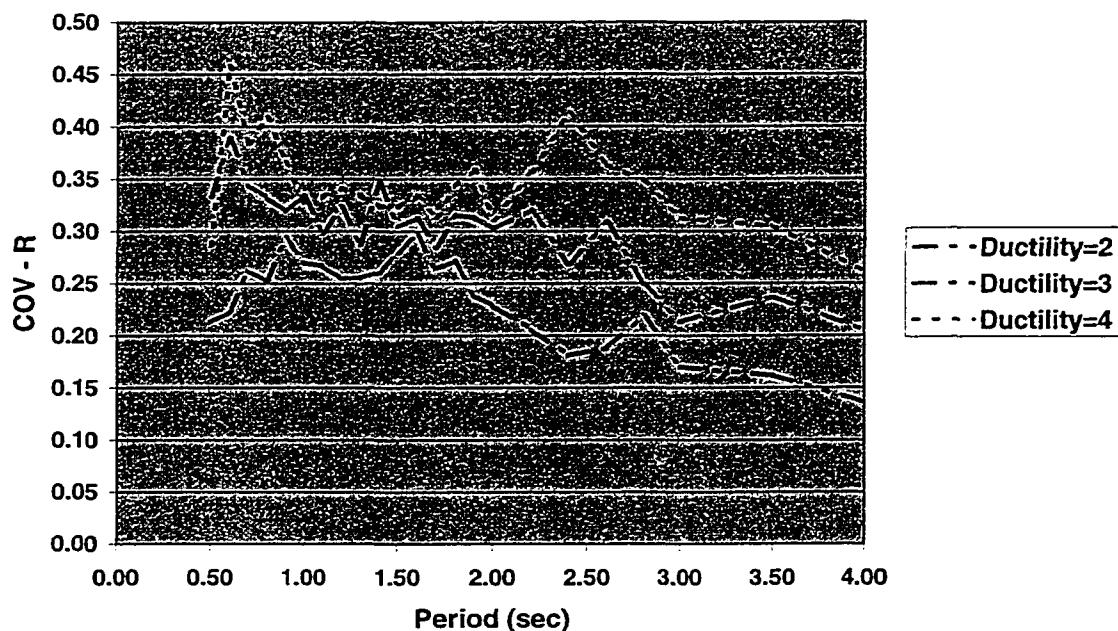


Figure 5-13: COV in R Factor for JT

F-D Factor COV for JT40080 SDOF

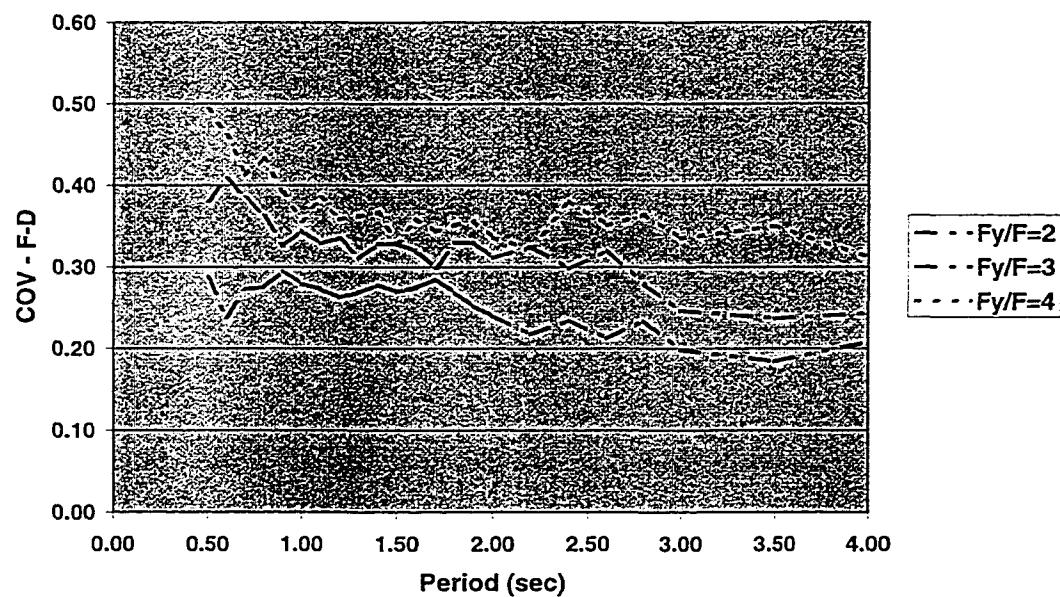


Figure 5-14: COV in F_d Factor JT

R Factors for JT30080 SDOF

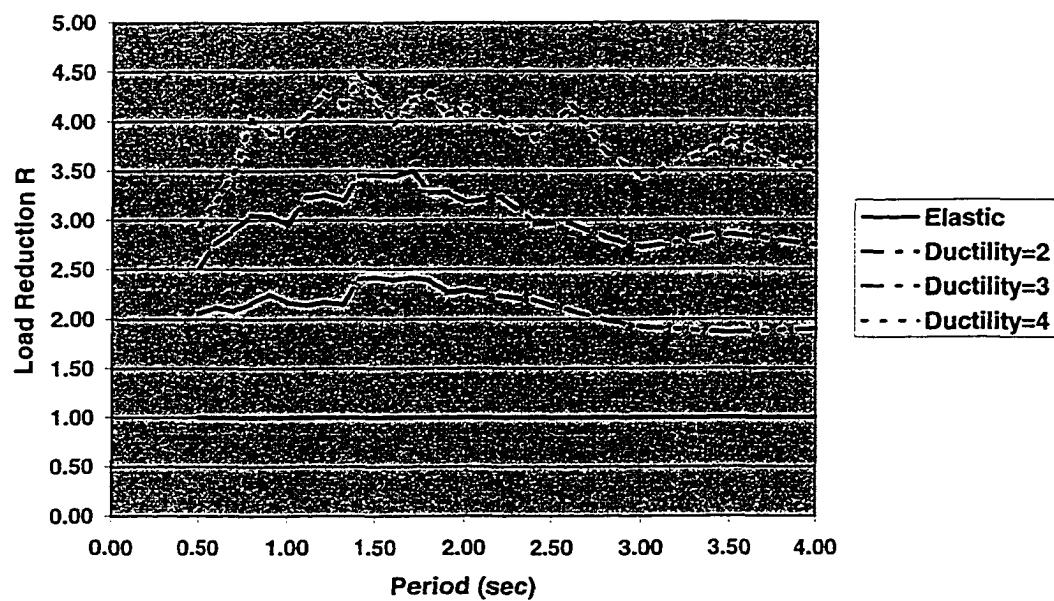


Figure 5-15: R Factor for JT

F-D Factors for JT30080 SDOF

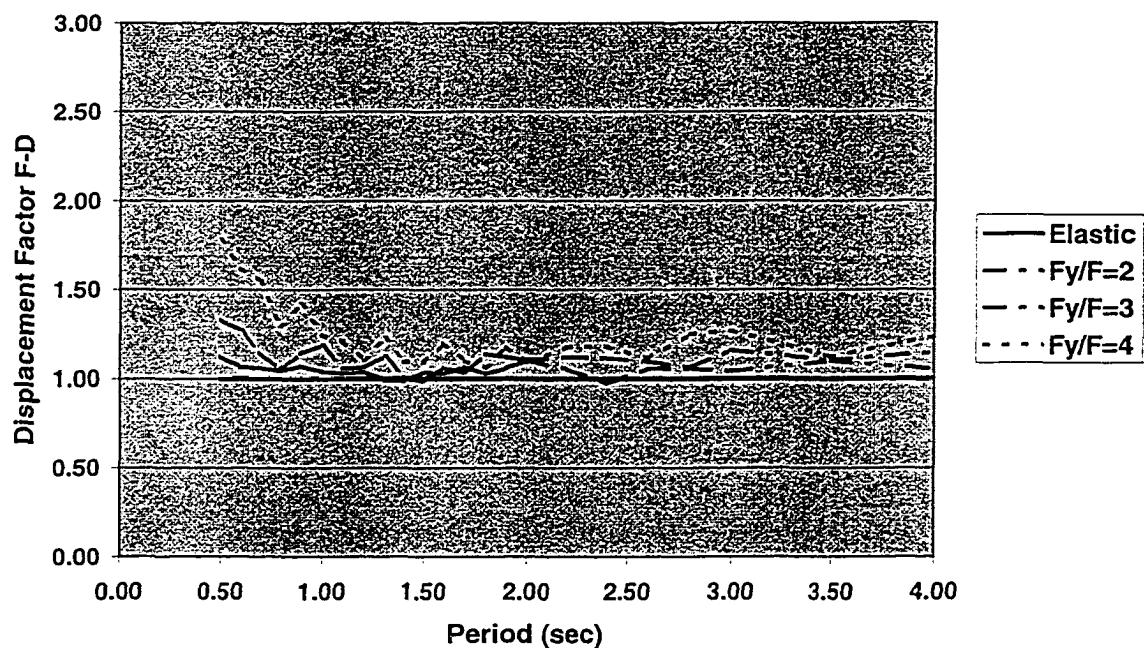


Figure 5-16: F_d Factor for JT

R Factor COV for JT30080 SDOF

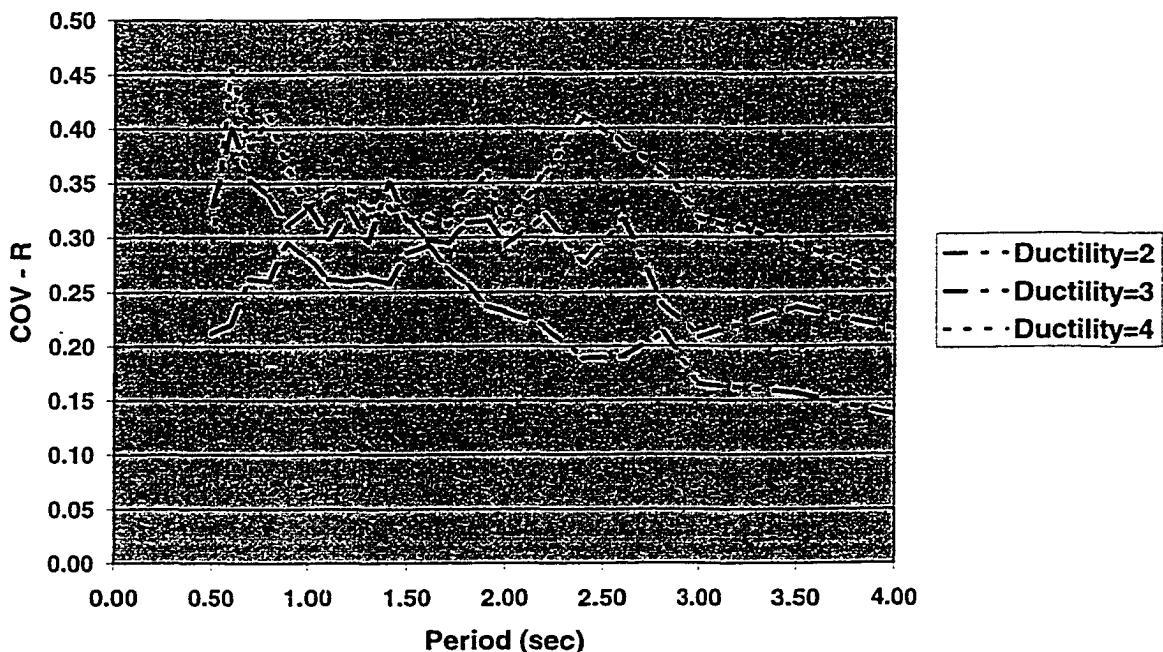


Figure 5-17: COV in R Factor for JT

F-D Factor COV for JT30080 SDOF

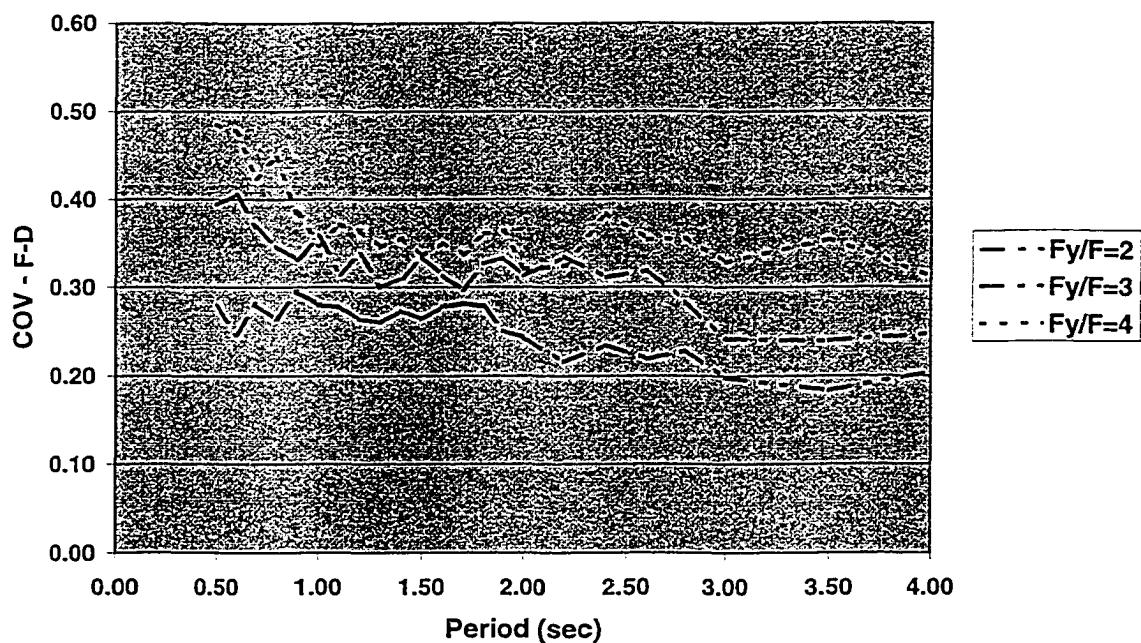


Figure 5-18: COV in F_d Factor for JT

R Factors for JT20080 SDOF

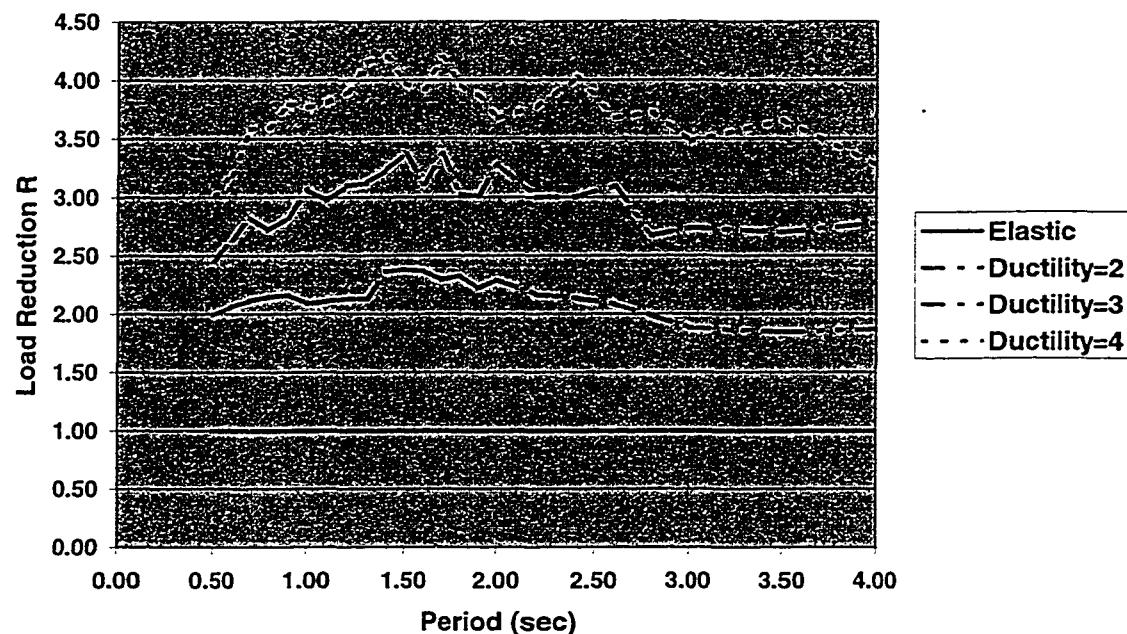


Figure 5-19: R Factor for JT

F-D Factors for JT20080 SDOF

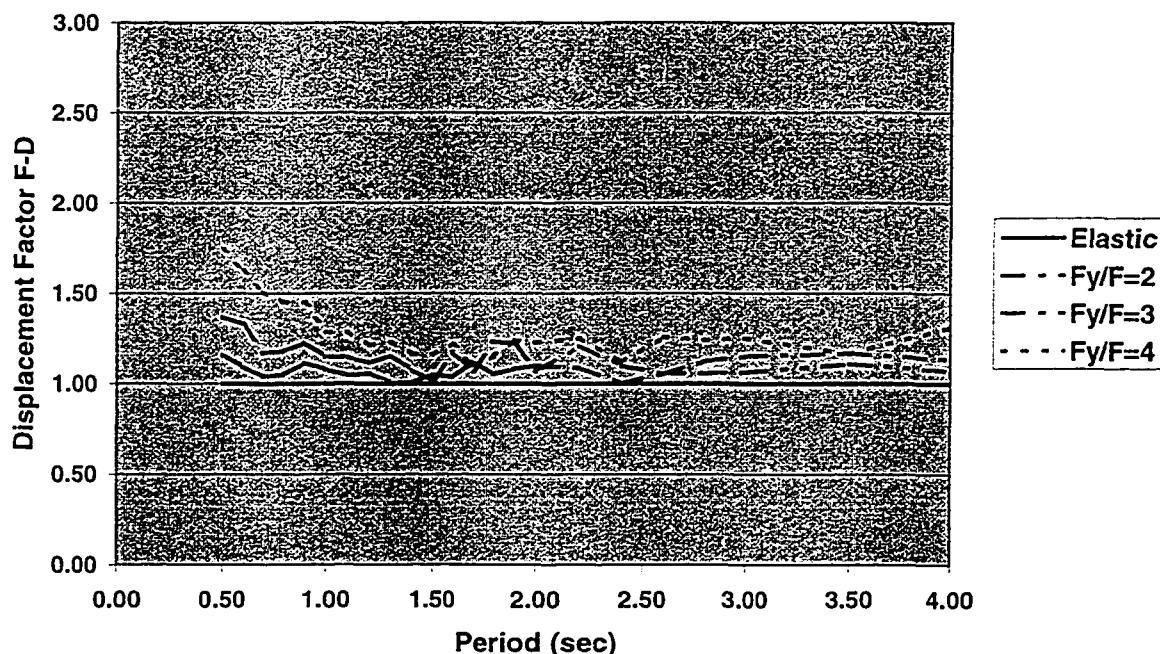


Figure 5-20: F_d Factor for JT

R Factor COV for JT20080 SDOF

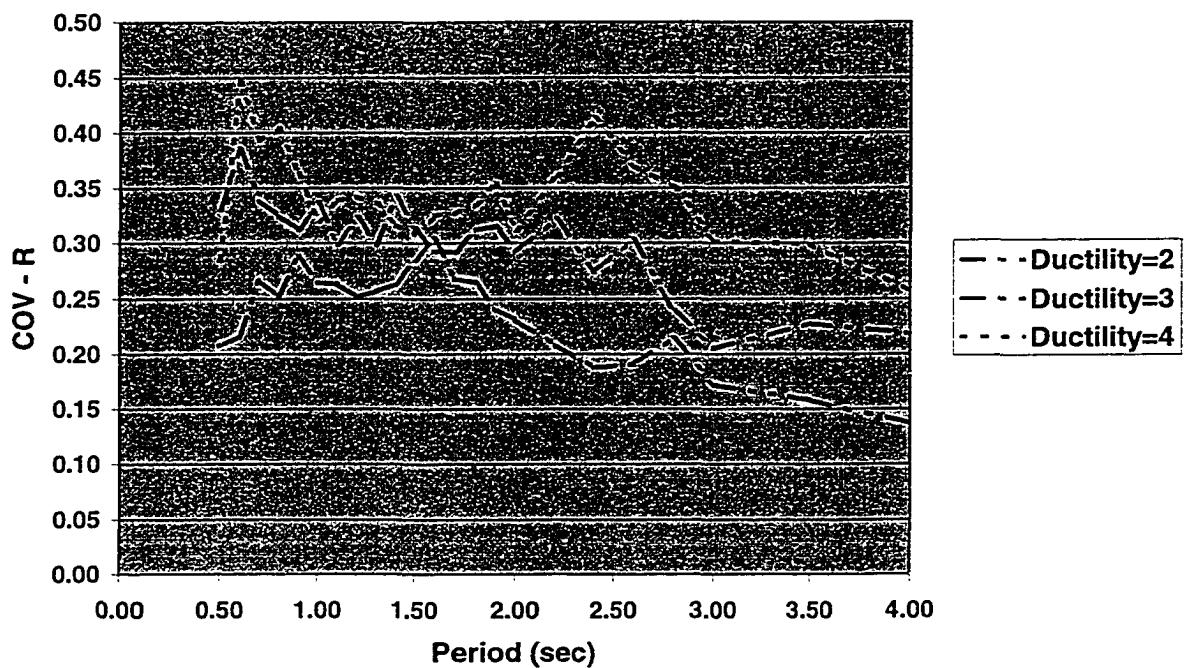


Figure 5-21: COV in R Factor for JT

F-D Factor COV for JT20080 SDOF

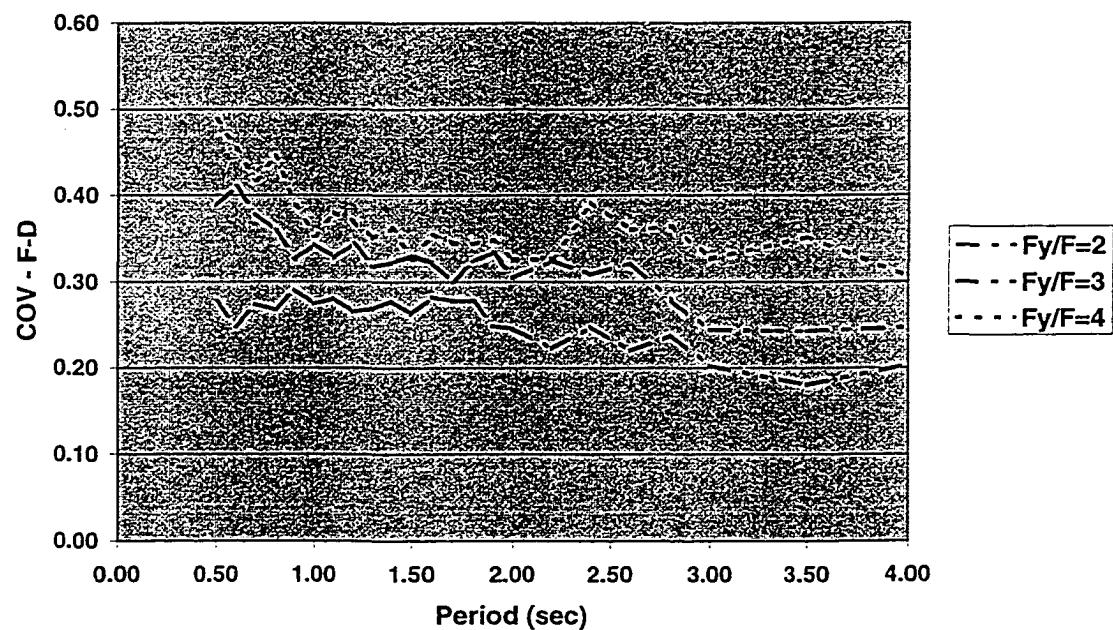


Figure 5-22: COV in F_d Factor for JT

R Factors for JT11080 SDOF

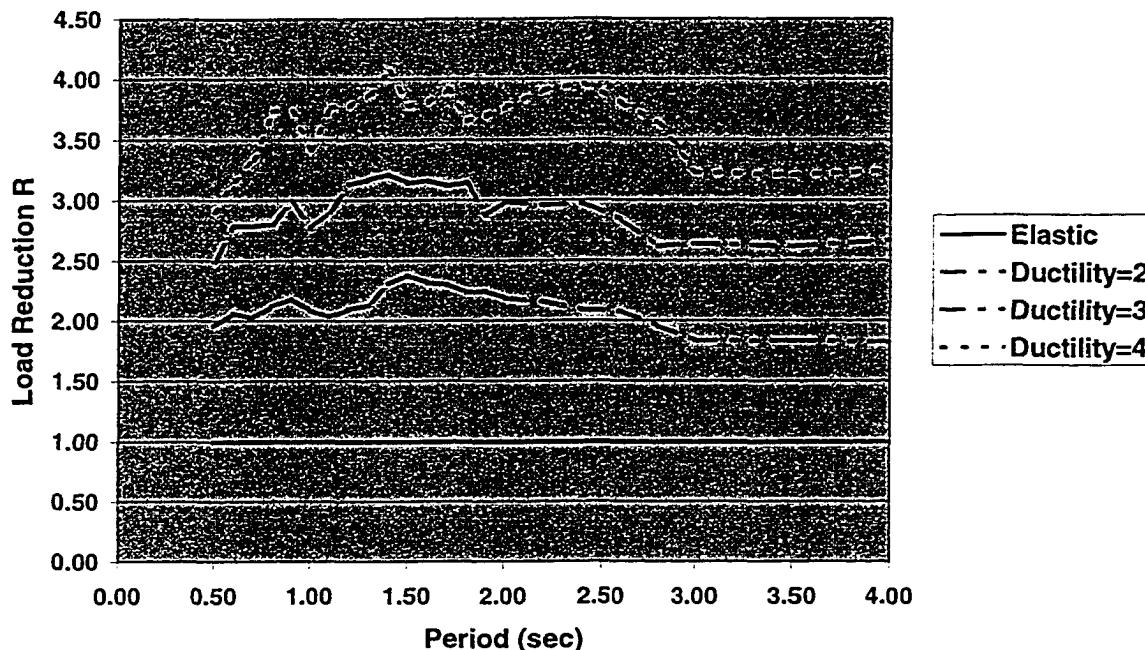


Figure 5-23: R Factor for JT

F-D Factors for JT11080 SDOF

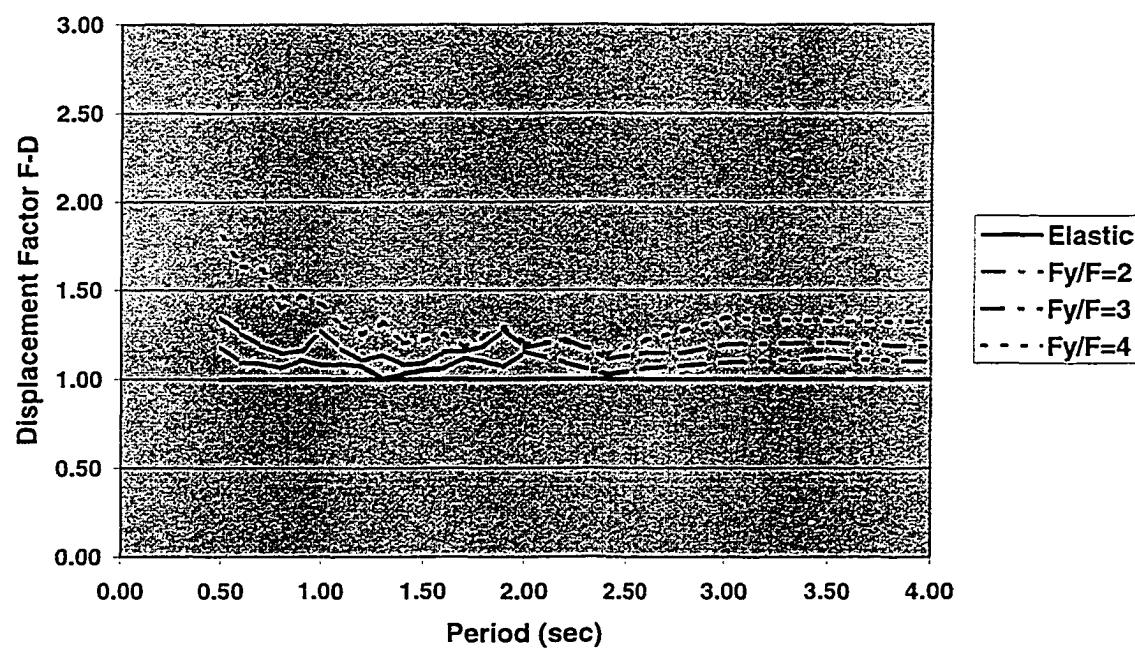


Figure 5-24: F_d Factor for JT

R Factor COV for JT11080 SDOF

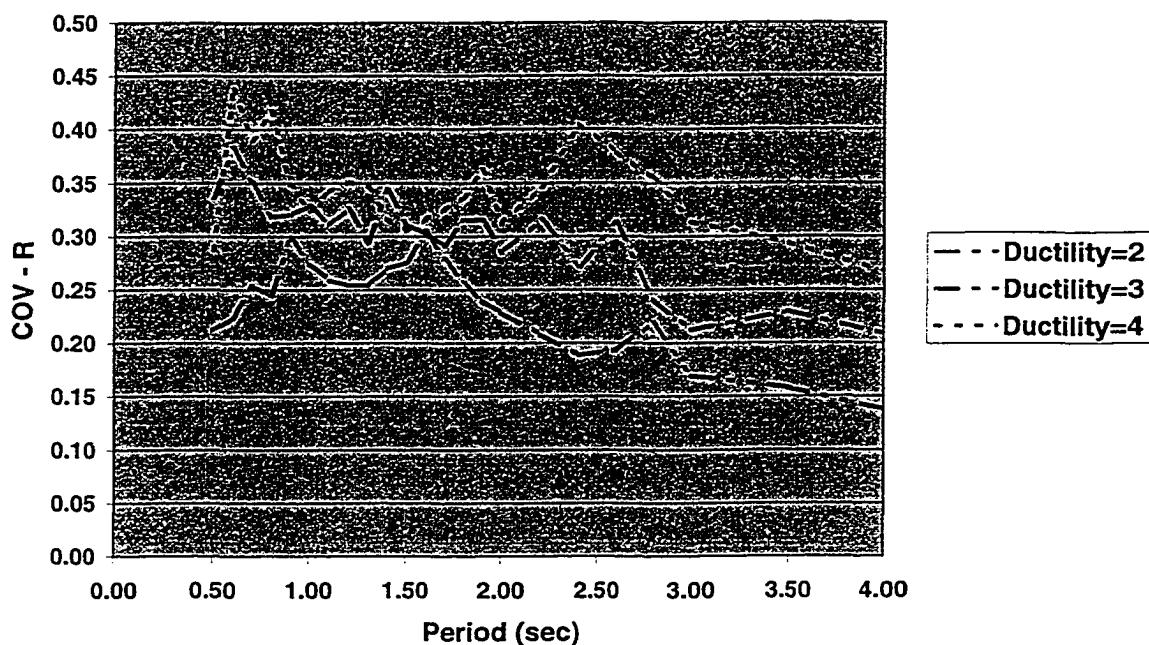


Figure 5-25: COV in R Factor for JT

F-D Factor COV for JT11080 SDOF

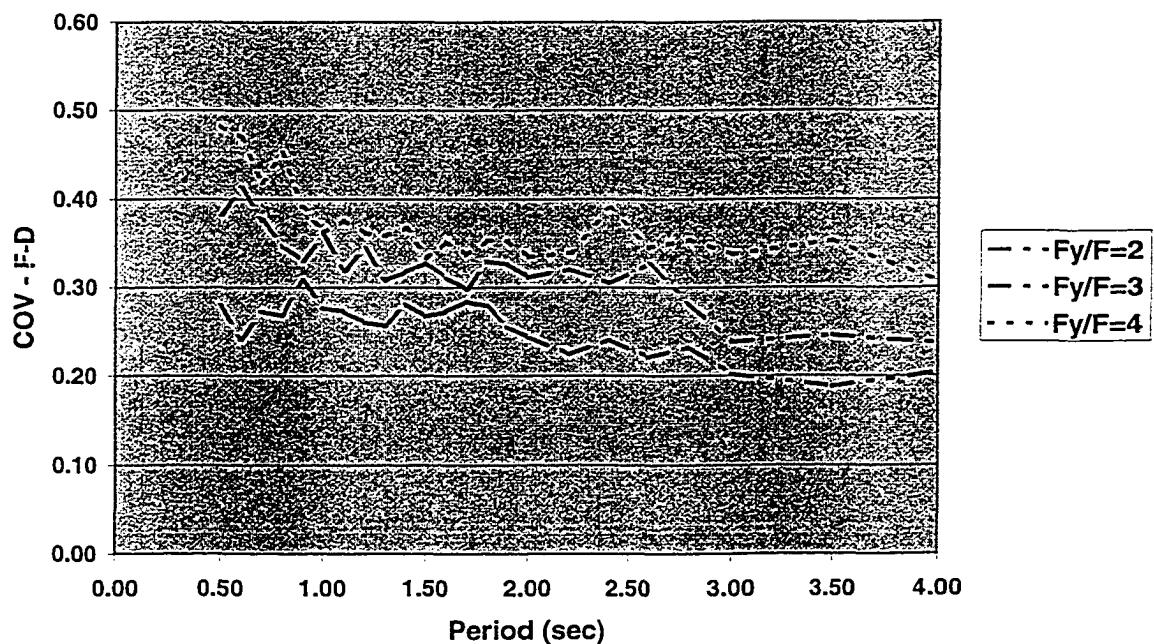


Figure 5-26: COV in F_d Factor for JT

R Factors for JT40060 SDOF

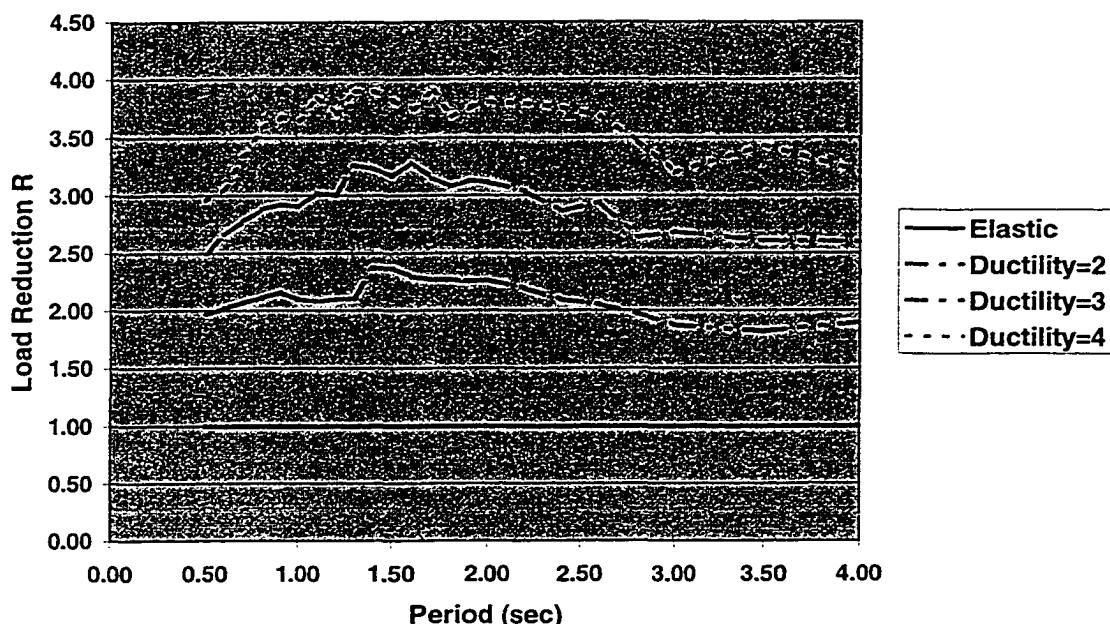


Figure 5-27: R Factor for JT

F-D Factors for JT40060 SDOF

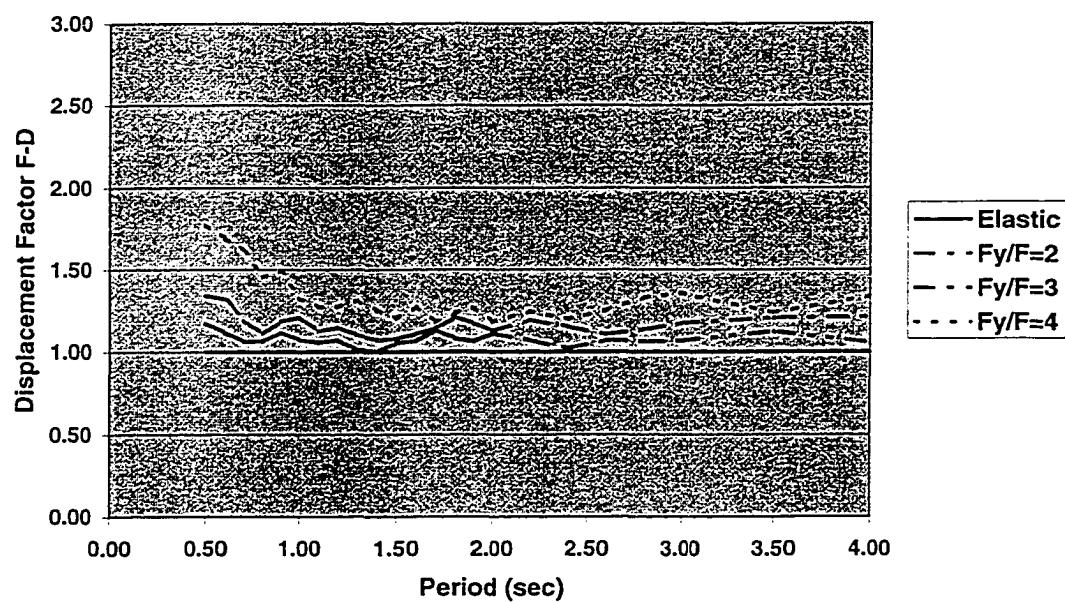


Figure 5-28: F_d Factor for JT

R Factor COV for JT40060 SDOF

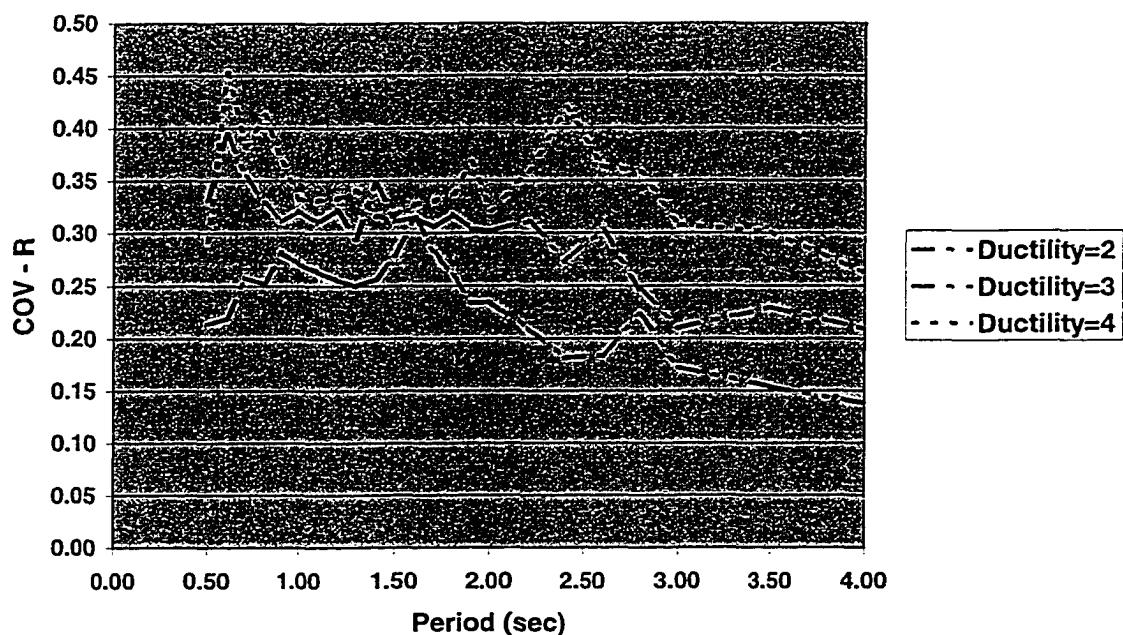


Figure 5-29: COV in R Factor for JT

F-D Factor COV for JT40060 SDOF

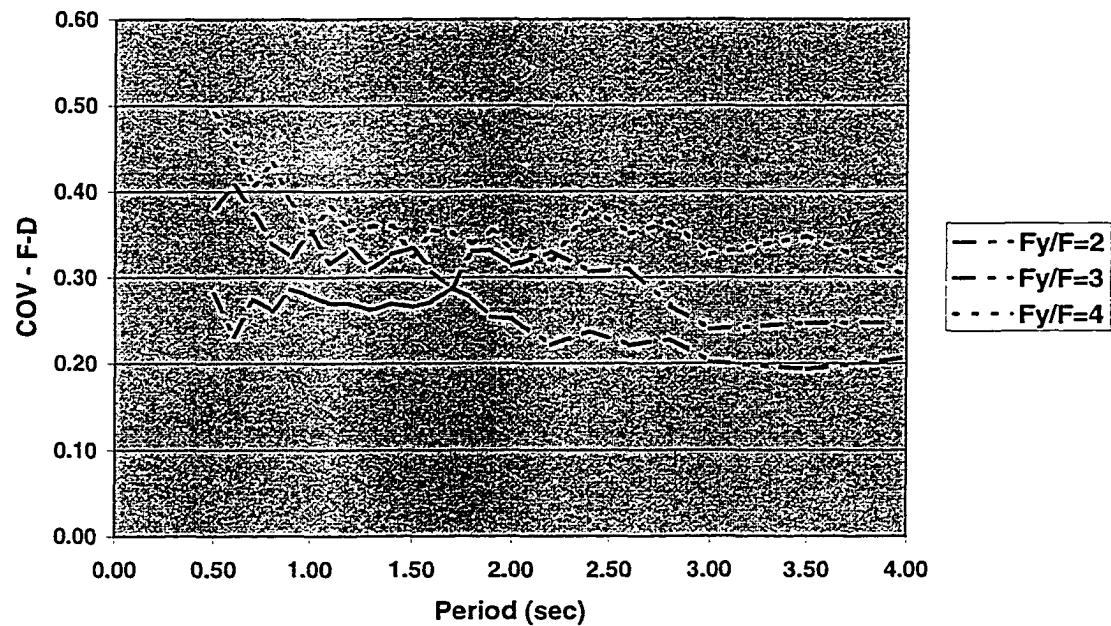


Figure 5-30: COV in F_d Factor for JT

R Factors for JT30060 SDOF

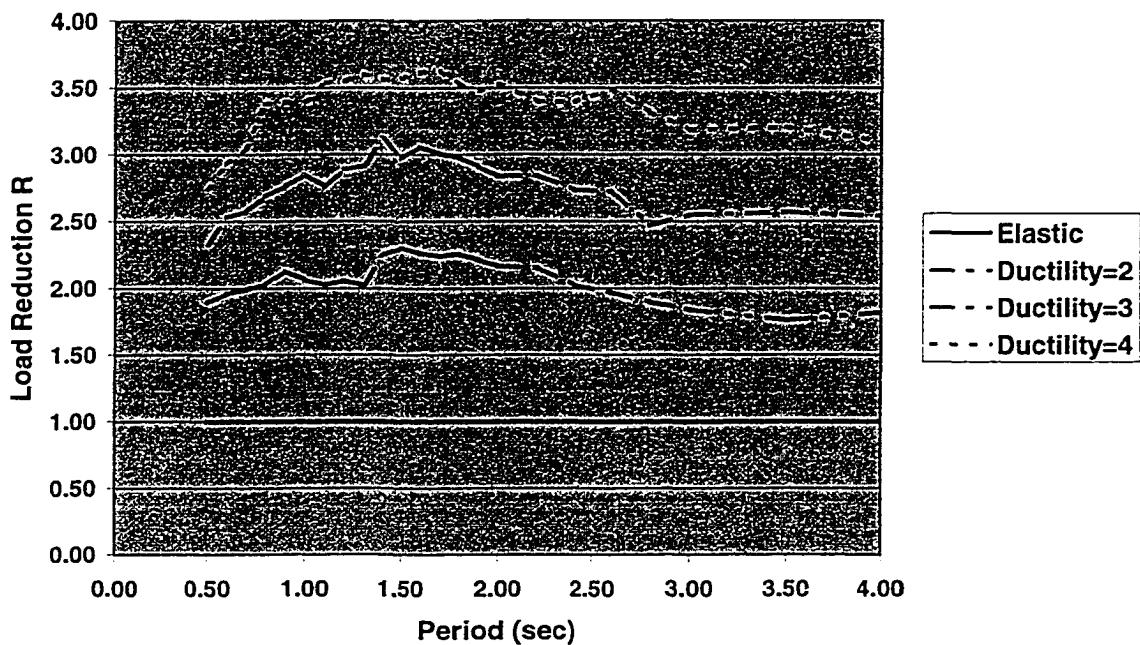


Figure 5-31: R Factor for JT

F-D Factors for JT30060 SDOF

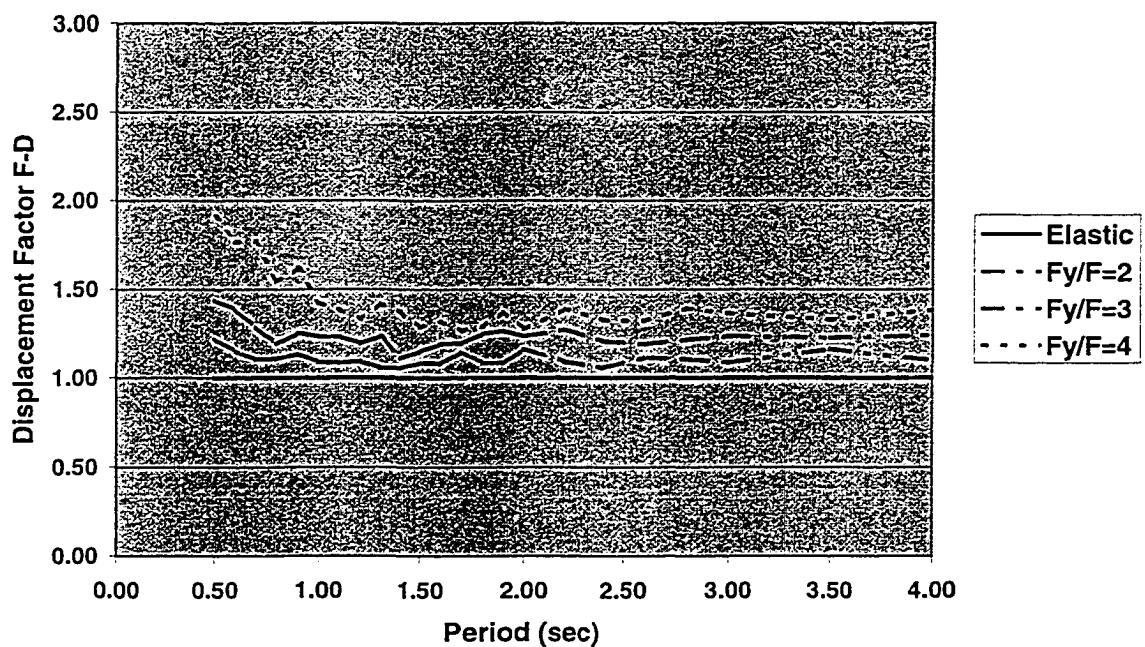


Figure 5-32: F_d Factor for JT

R Factor COV for JT30060 SDOF

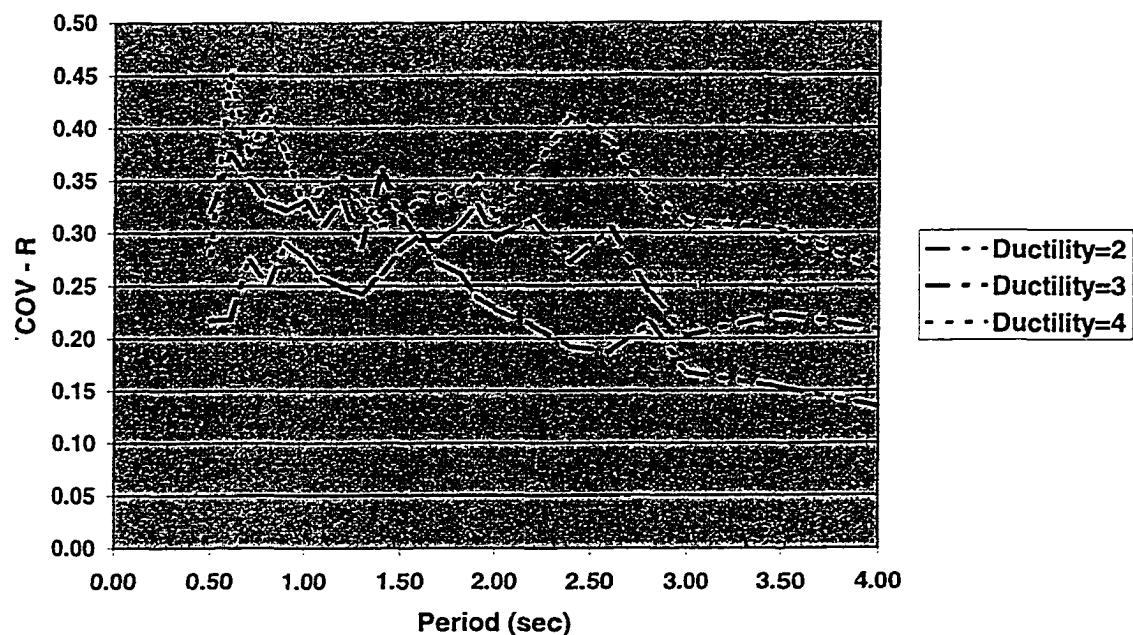


Figure 5-33: COV in R Factor for JT

F-D Factor COV for JT30060 SDOF

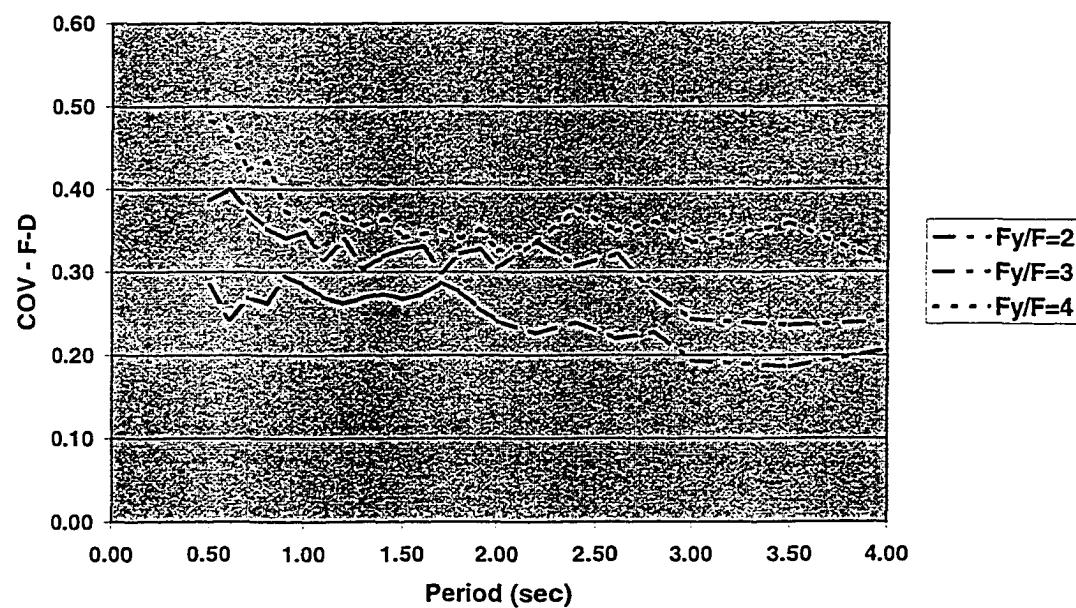


Figure 5-34: COV in F_d Factor for JT

R Factors for JT20060 SDOF

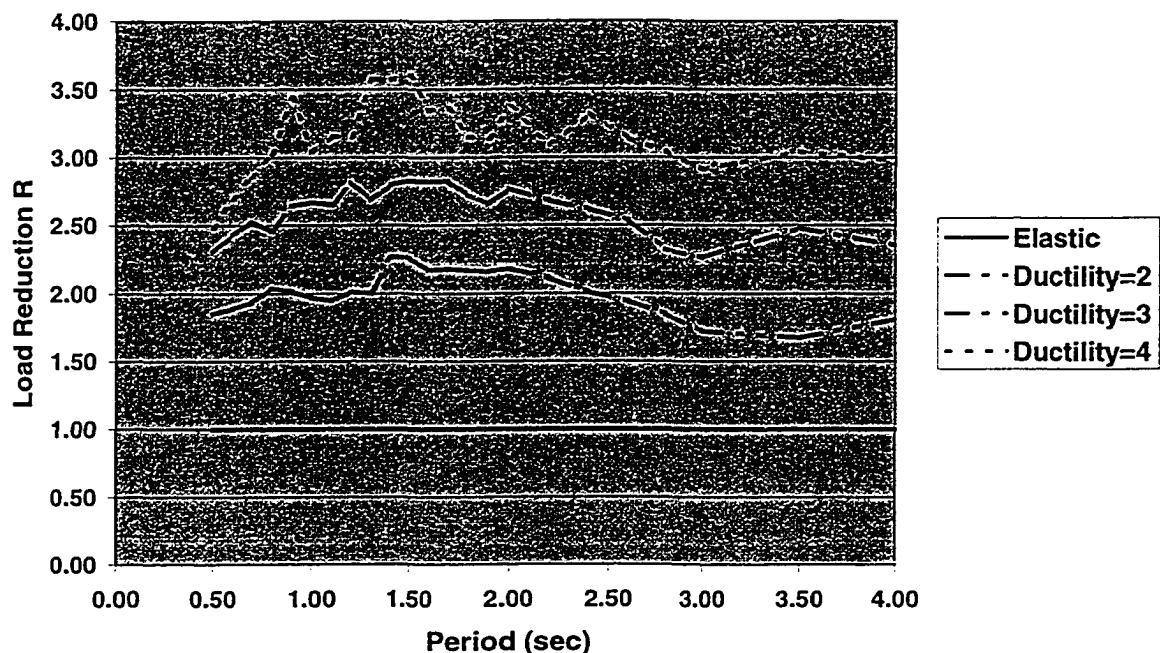


Figure 5-35: R Factor for JT

F-D Factors for JT20060 SDOF

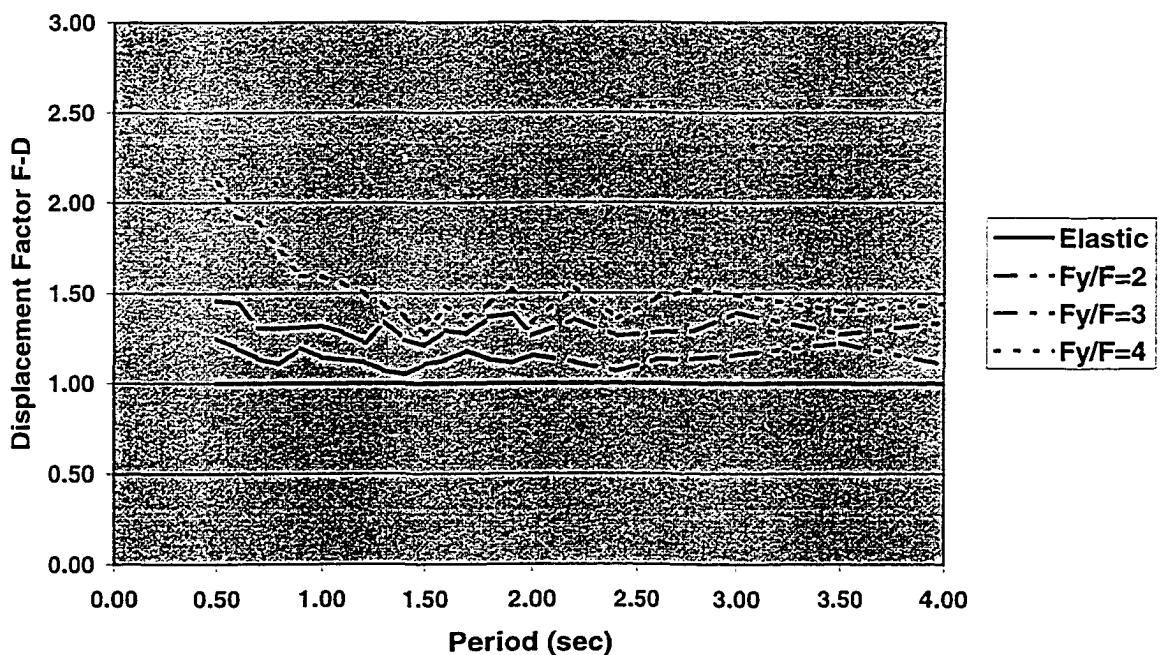


Figure 5-36: F_d Factor for JT

R Factor COV for JT20060 SDOF

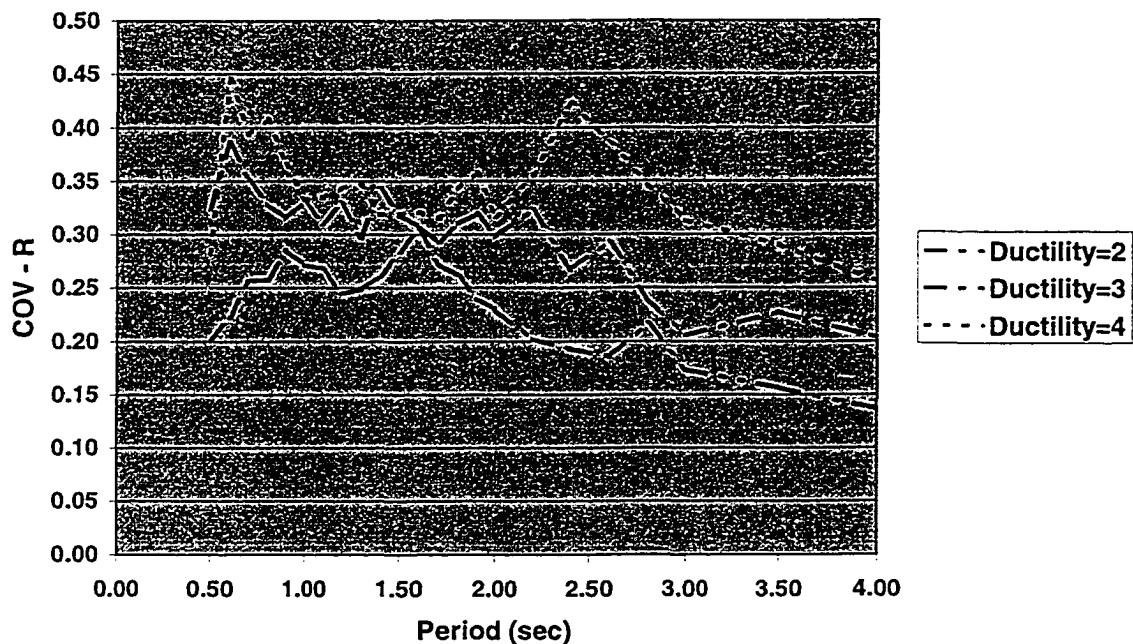


Figure 5-37: COV in R Factor for JT

F-D Factor COV for JT20060 SDOF

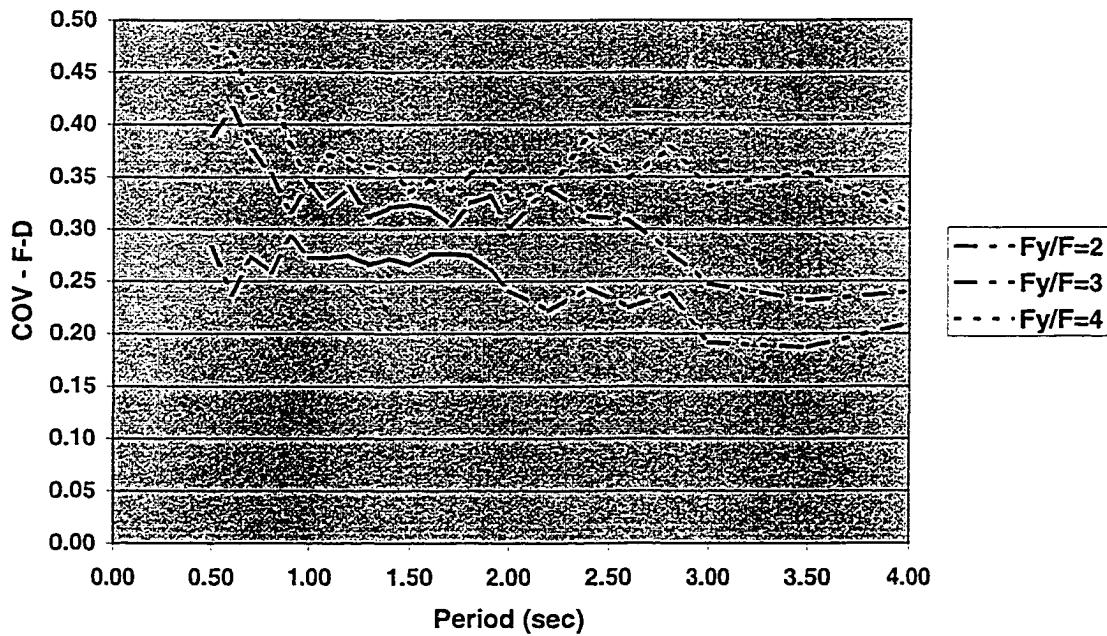


Figure 5-38: COV in F_d Factor for JT

R Factors for JT11060 SDOF

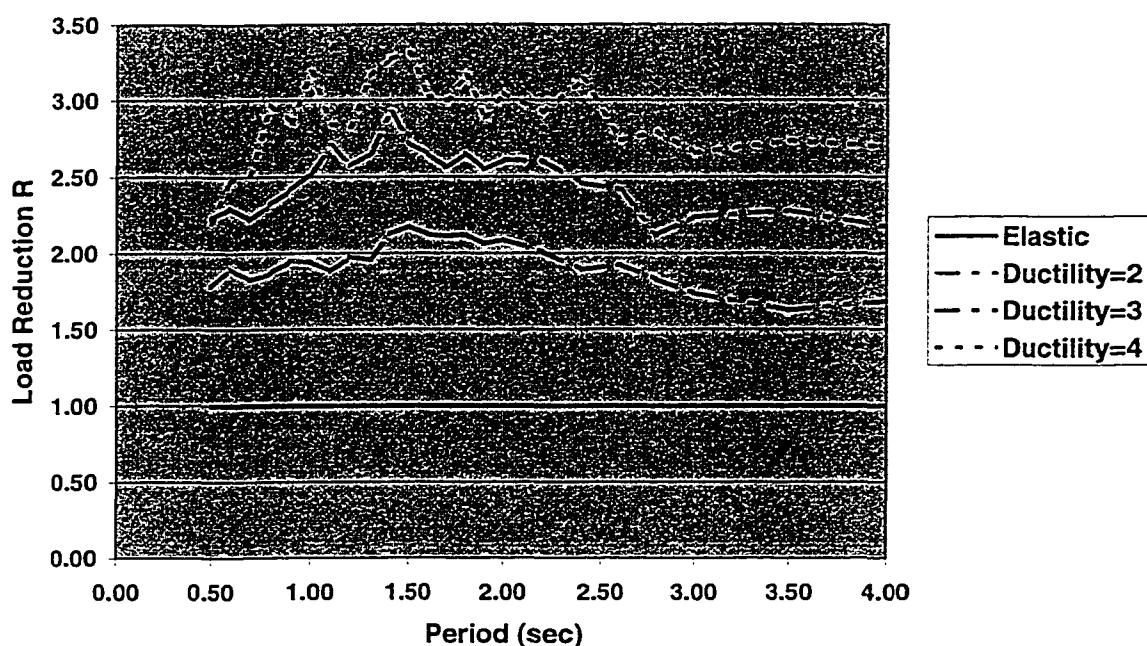


Figure 5-39: R Factor for JT

F-D Factors for JT11060 SDOF

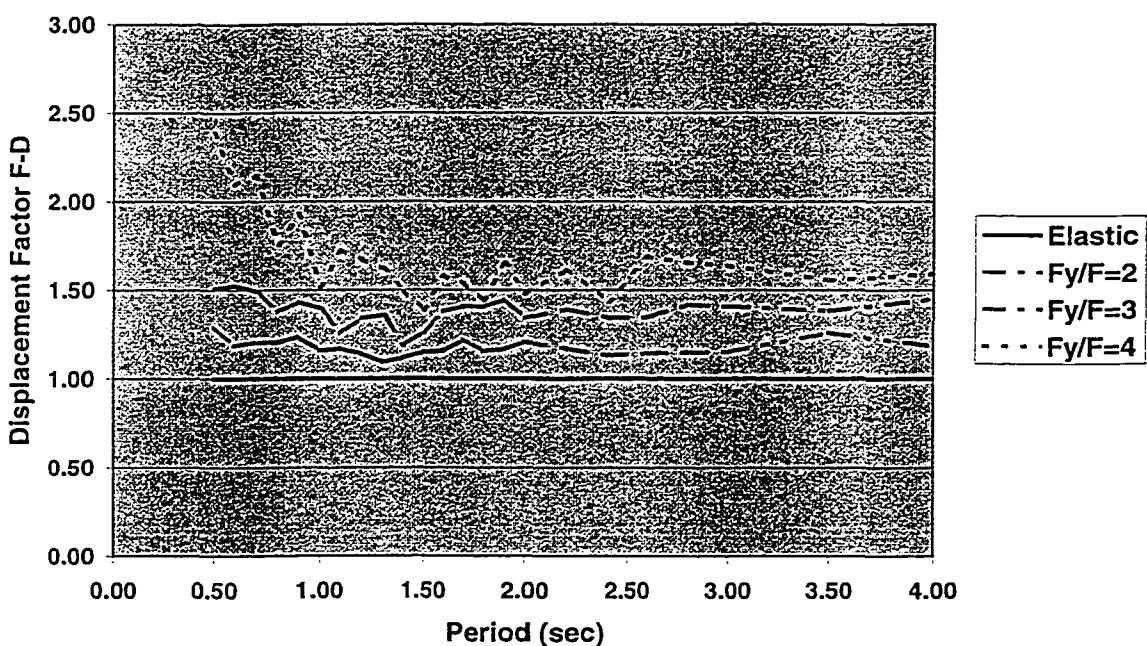


Figure 5-40: F_d Factor for JT

R Factor COV for JT11060 SDOF

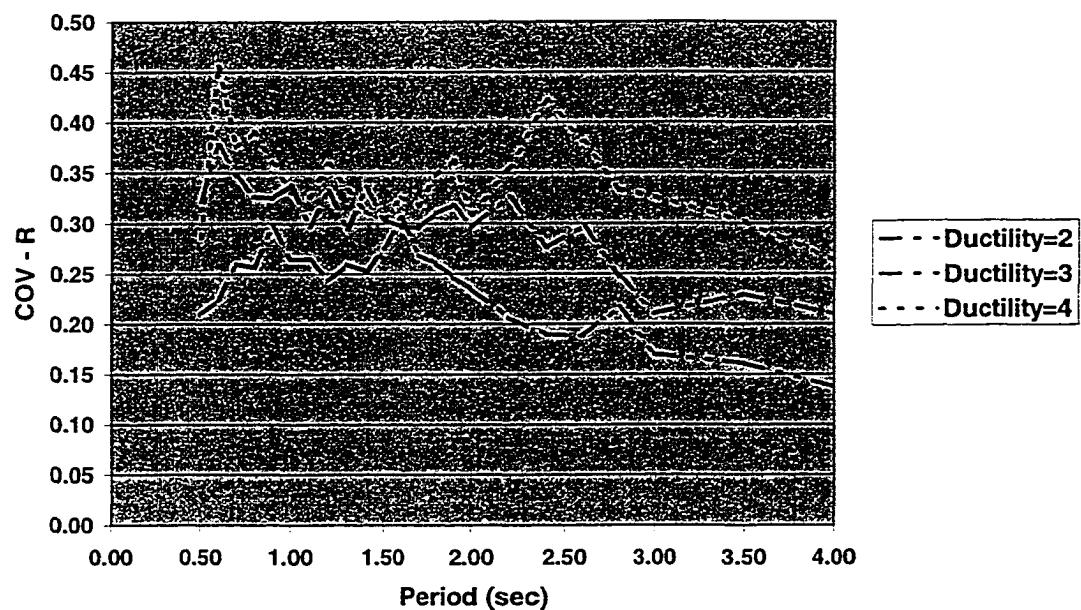


Figure 5-41: COV in R Factor for JT

F-D Factor COV for JT11060 SDOF

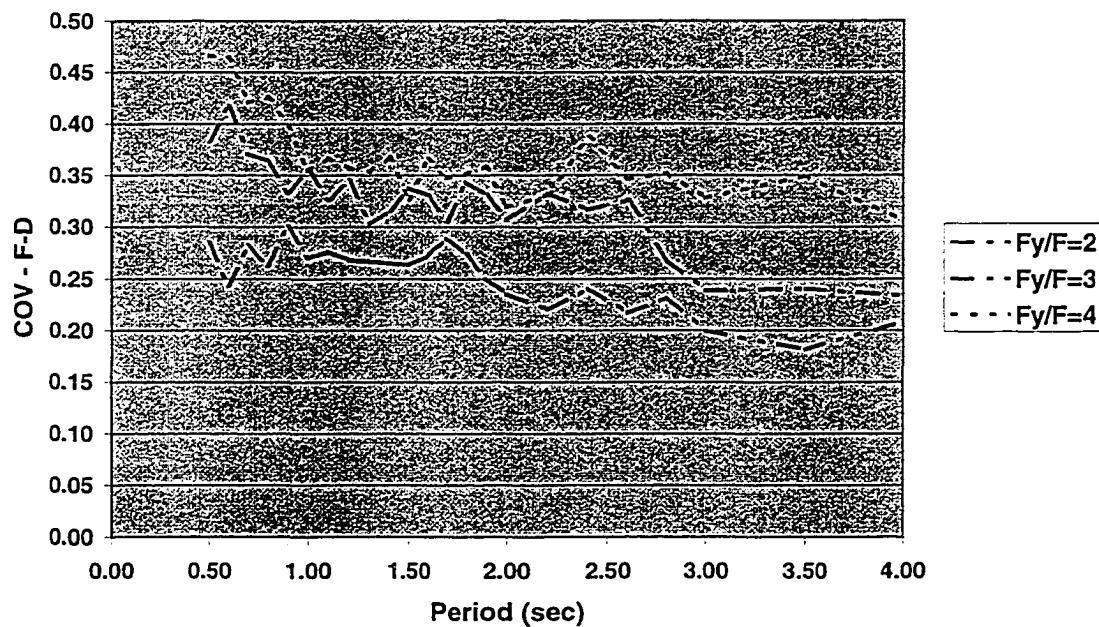


Figure 5-42: COV in F_d Factor for JT

5.2.3 FT SDOF Systems

Results for FT systems are shown in Figures 5-43 to 5-50. The results are matched to each type of FT system using a four-digit code. The first two digits describe the strength reduction factor λ . The last two digits describe the residual strength as a percentage of initial yield strength.

The FT systems tend to exhibit severe changes in load reduction and displacement modification as compared to BN systems. For the most severely degrading system, FT4060 (Figures 5-51 to 55-54), load reduction factors are perhaps 40% less than their BN system counterparts, whereas displacement modification factors are on the order of 60% higher. This difference is most severe in the period range from 0.5 sec to 1.0 sec. These systems, unlike their stiffness-degrading counterparts, are unable to permanently alter flexibility, and thus escape peaks in the spectral response. Also, they accumulate permanent offsets at a greater rate, and thus will accumulate displacements by ratcheting more readily than stiffness-degrading systems. Of the behaviors studied, FT exhibits the most limited post-yield behavior.

R Factors for FT4080 SDOF

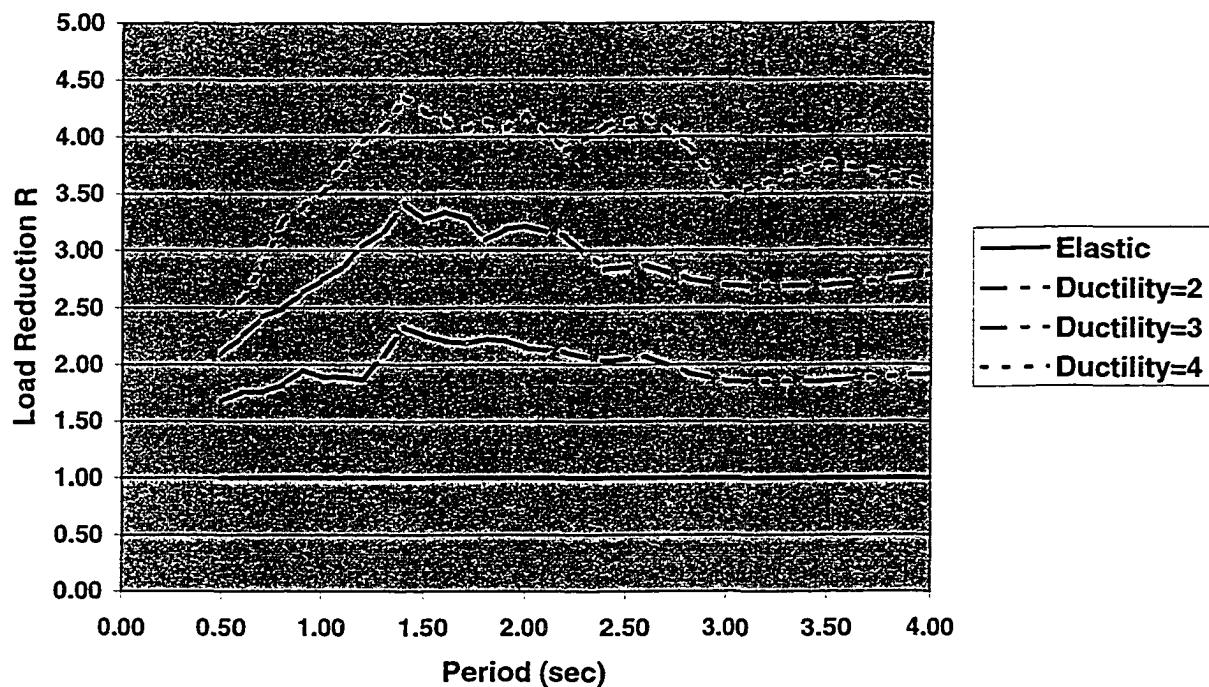


Figure 5-43: R Factor for FT

F-D Factors for FT4080 SDOF

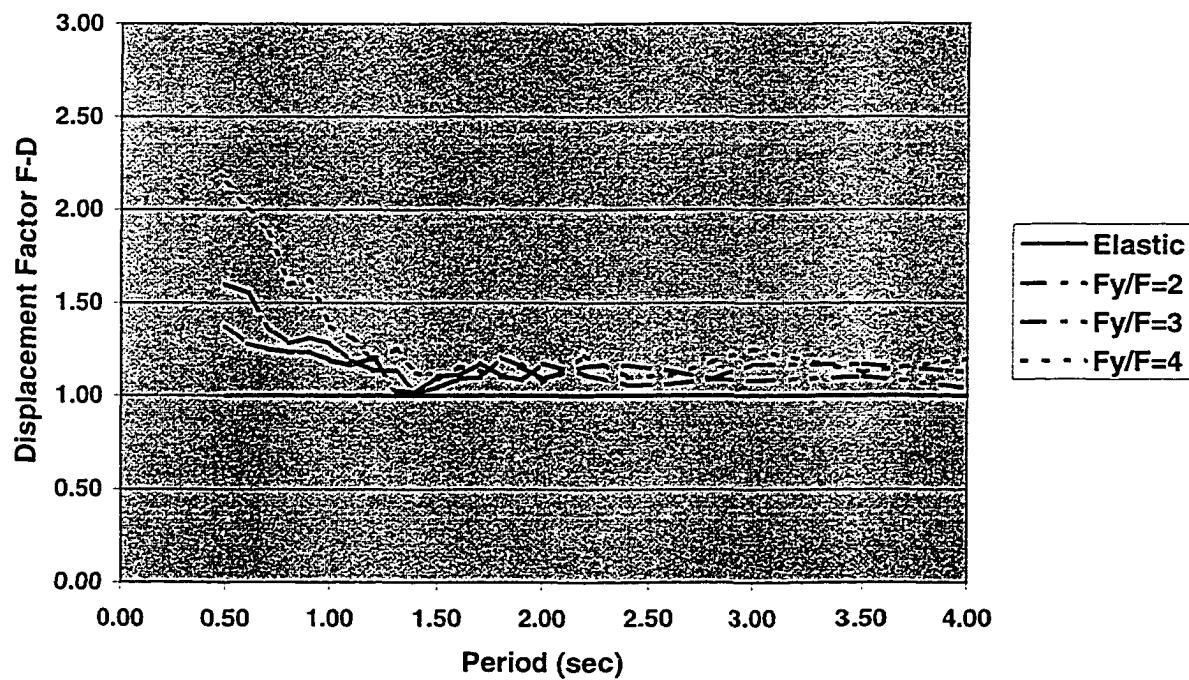


Figure 5-44: F_d Factor for FT

R Factor COV for FT4080 SDOF

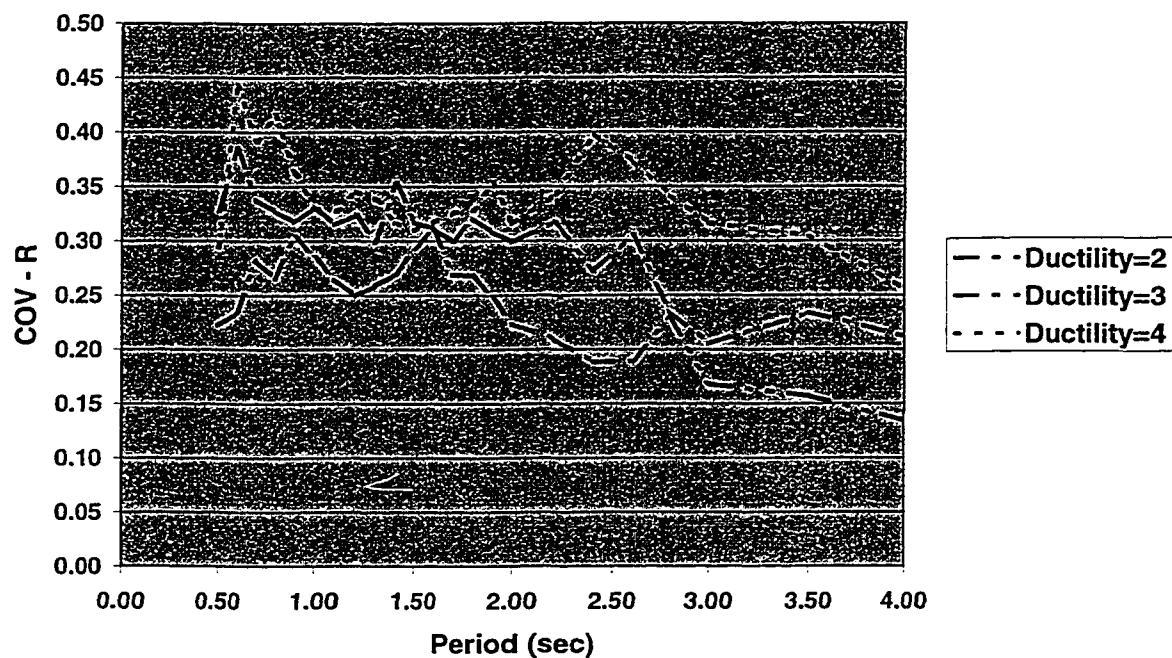


Figure 5-45: COV in R Factor for FT

F-D Factor COV for FT4080 SDOF

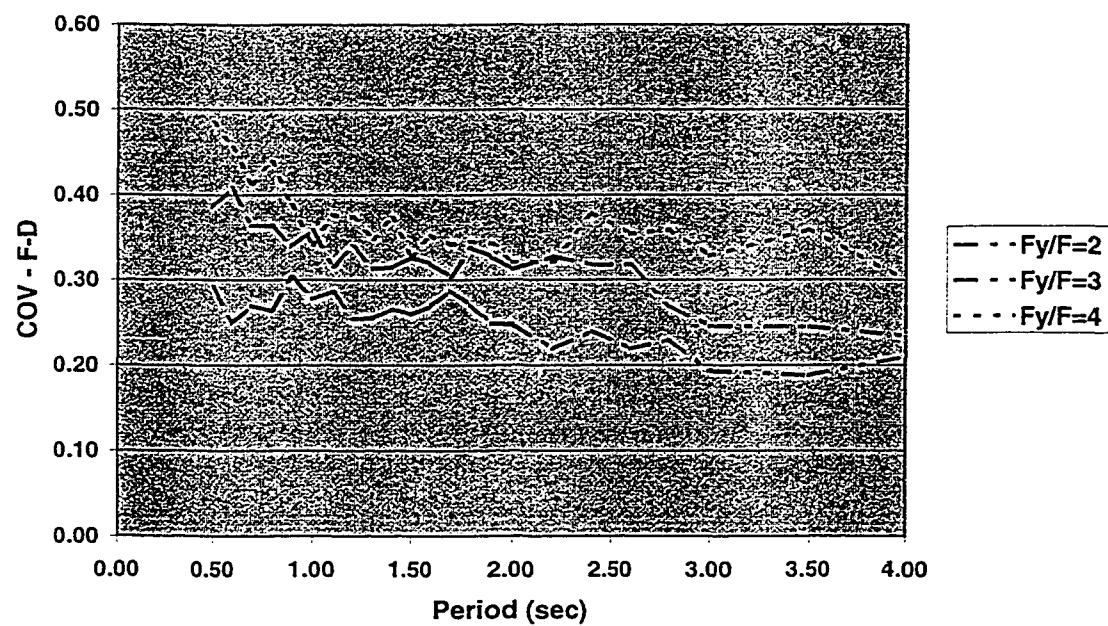


Figure 5-46: COV in F_d Factor for FT

R Factors for FT2080 SDOF

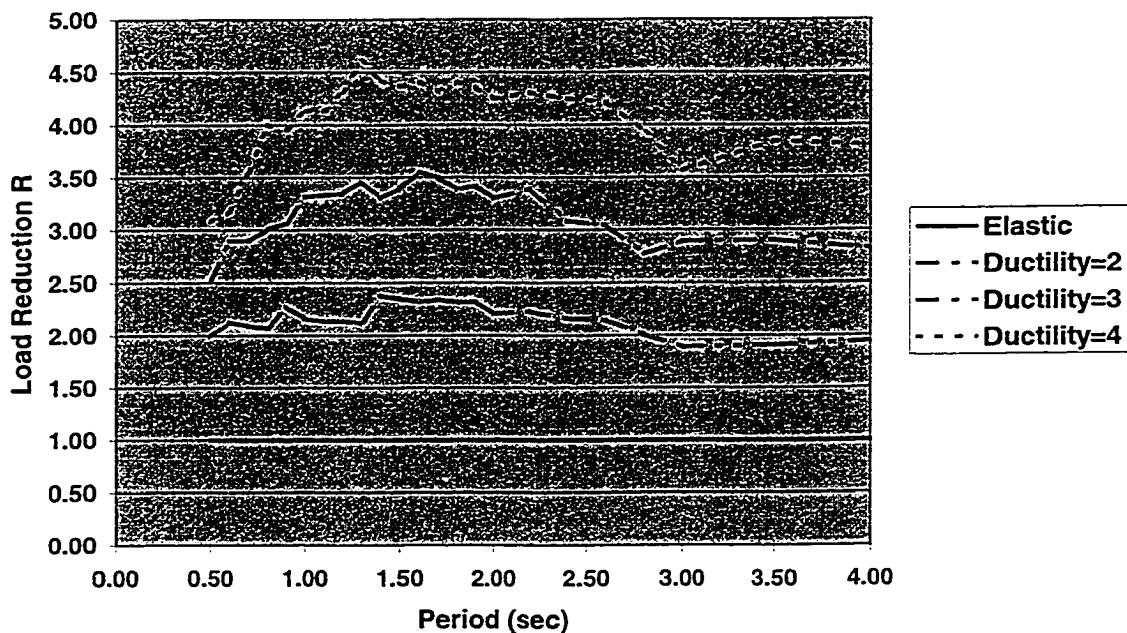


Figure 5-47: R Factor for FT

F-D Factors for FT2080 SDOF

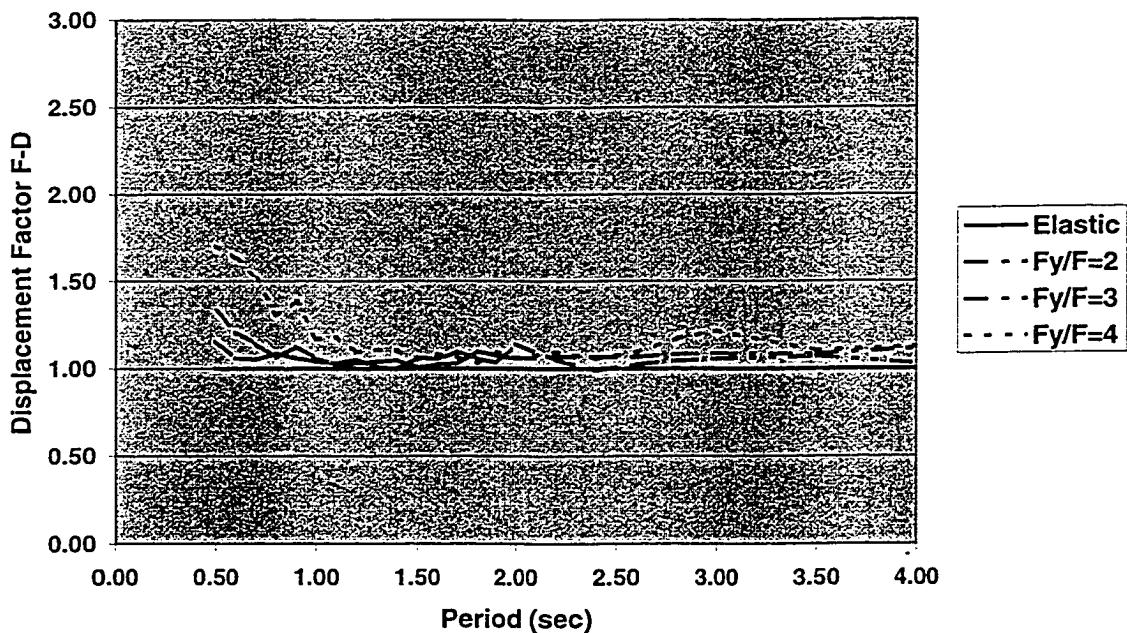


Figure 5-48: F_d Factor for FT

R Factor COV for FT2080 SDOF

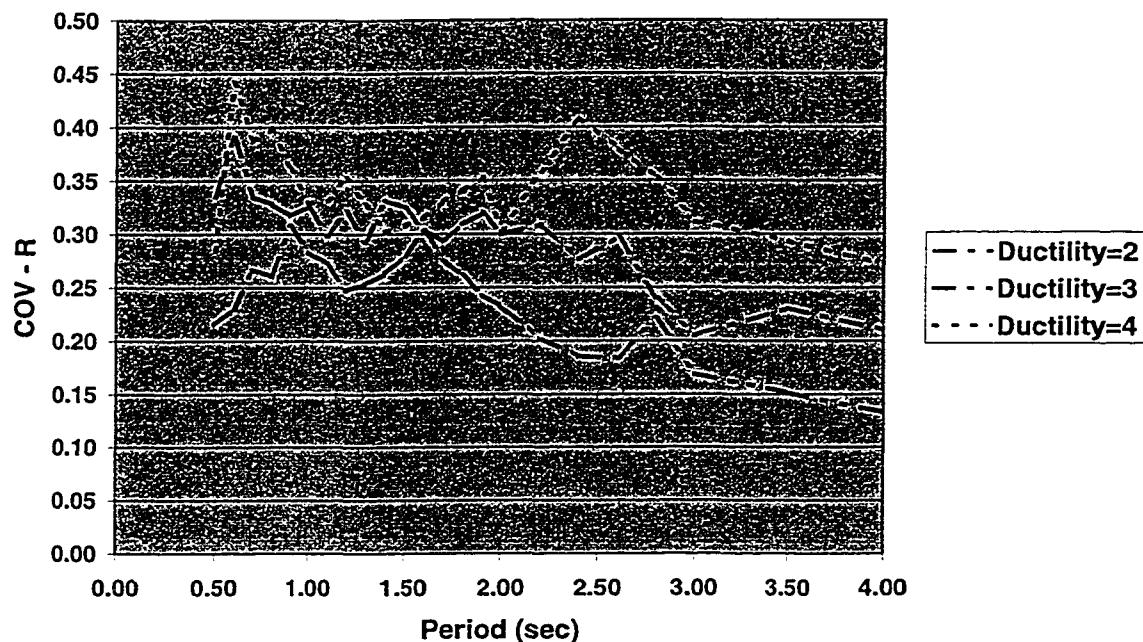


Figure 5-49: COV in R Factor for FT

F-D Factor COV for FT2080 SDOF

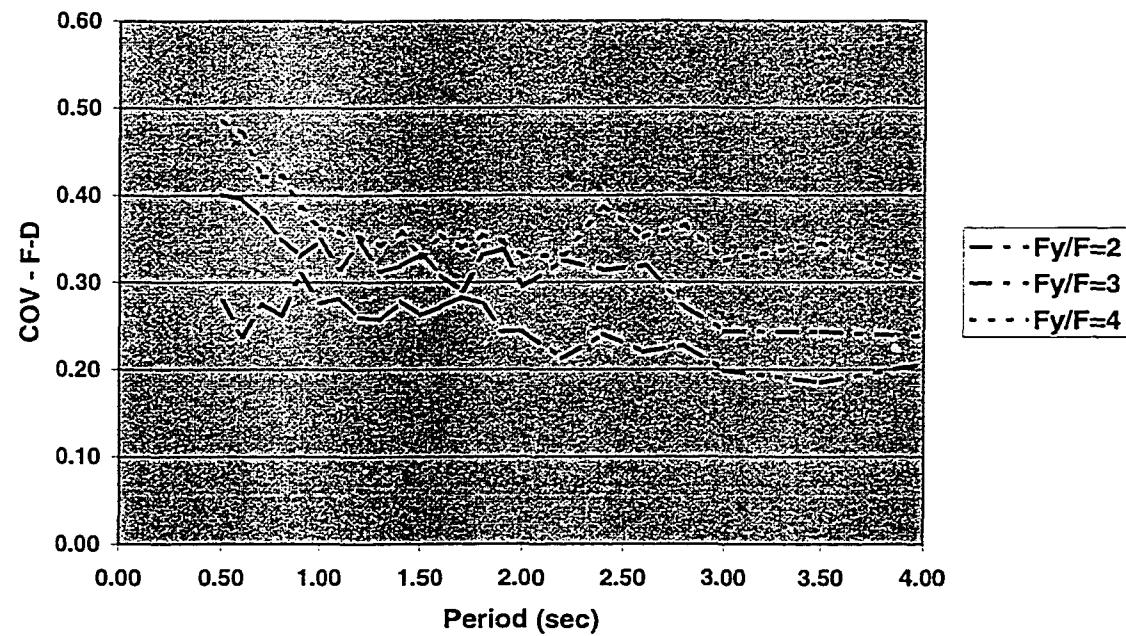


Figure 5-50: COV in F_d Factor for FT

R Factors for FT4060 SDOF

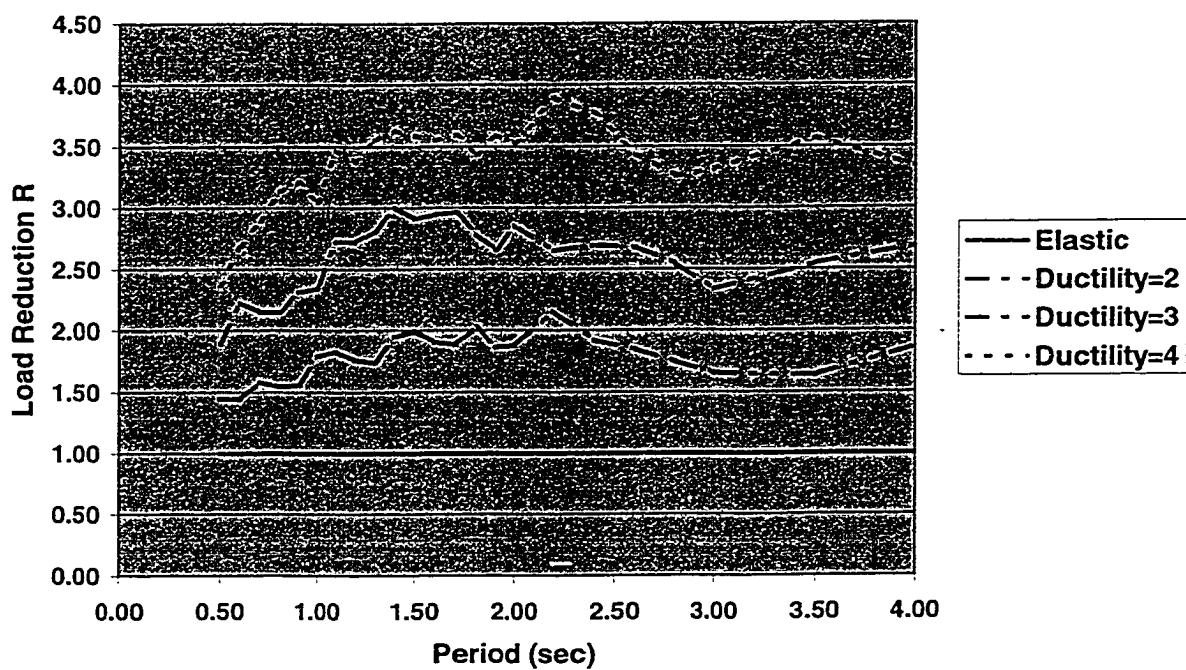


Figure 5-51: R Factor for FT

F-D Factors for FT4060 SDOF

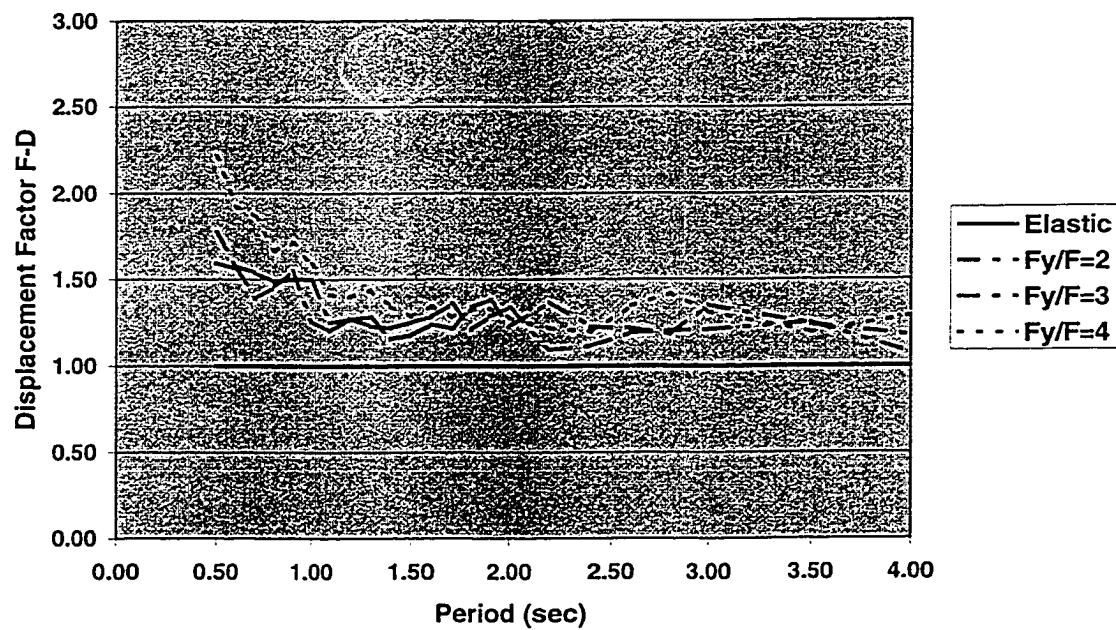


Figure 5-52: F_d Factor for FT

R Factor COV for FT4060 SDOF

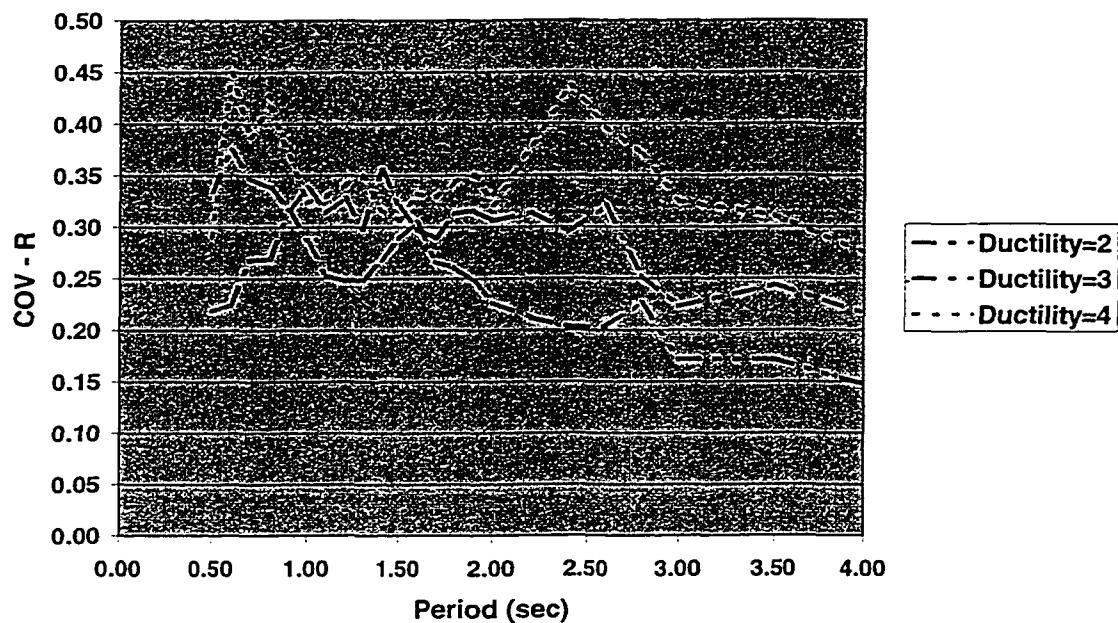


Figure 5-53: COV in R Factor for FT

F-D Factor COV for FT4060 SDOF

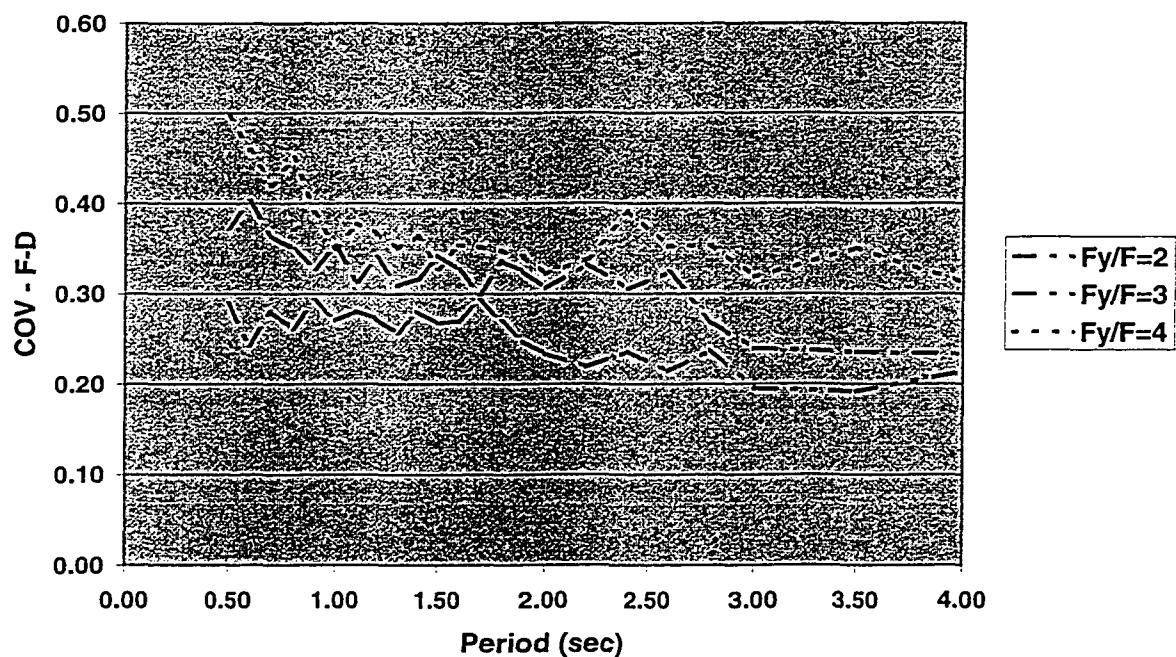


Figure 5-54: COV in F_d Factor for FT

R Factors for FT2060 SDOF

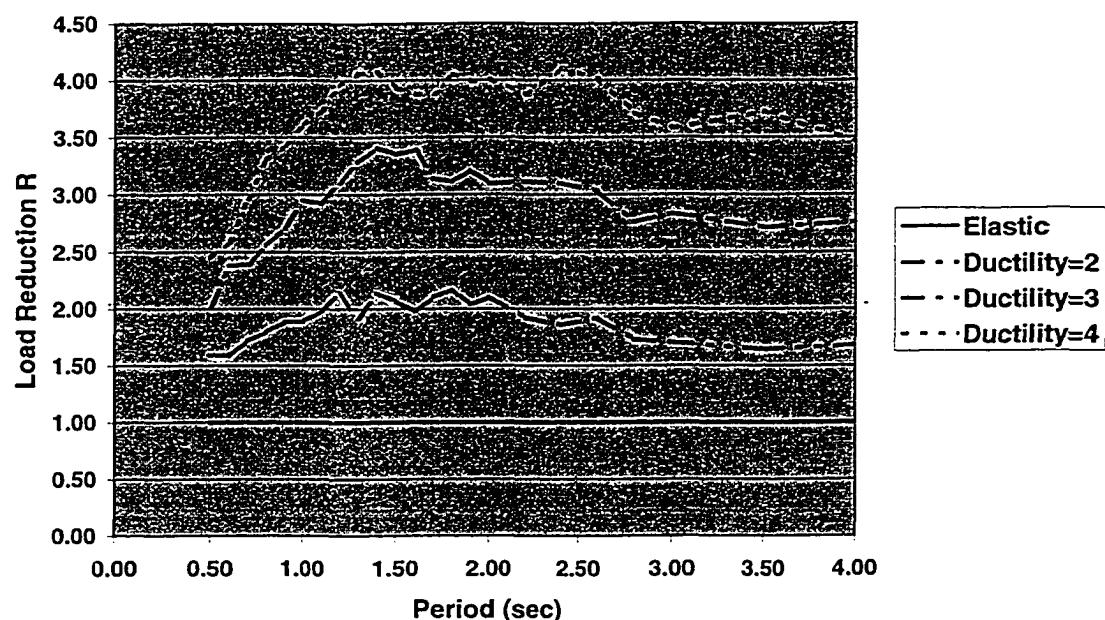


Figure 5-55: R Factor for FT

F-D Factors for FT2060 SDOF

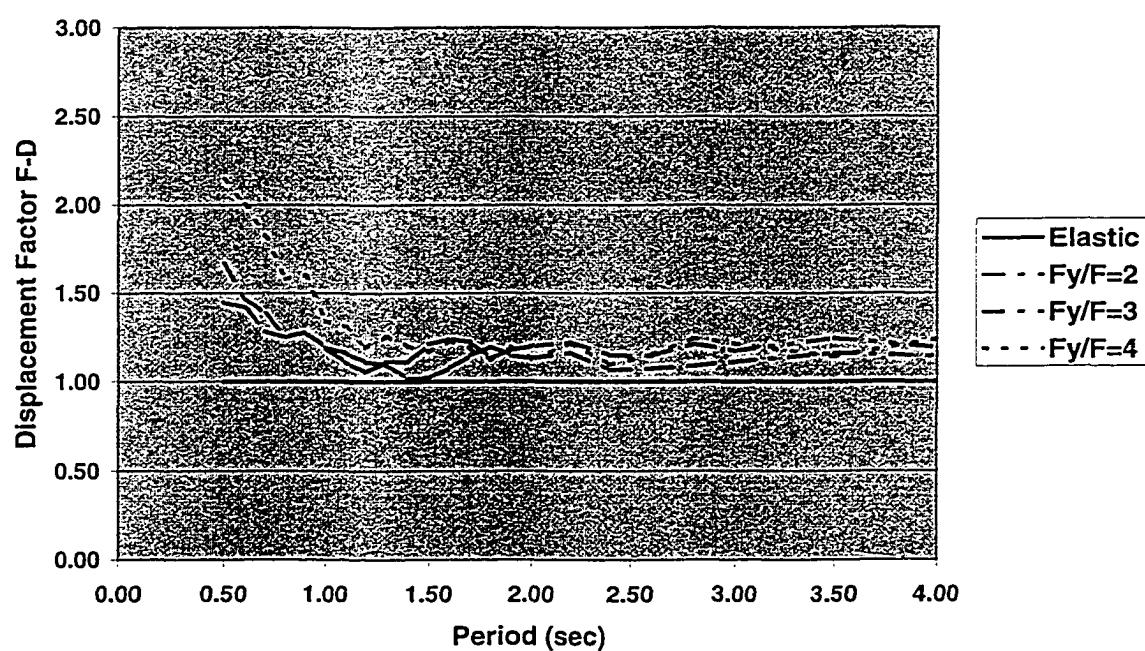


Figure 5-56: F_d Factor for FT

R Factor COV for FT2060 SDOF

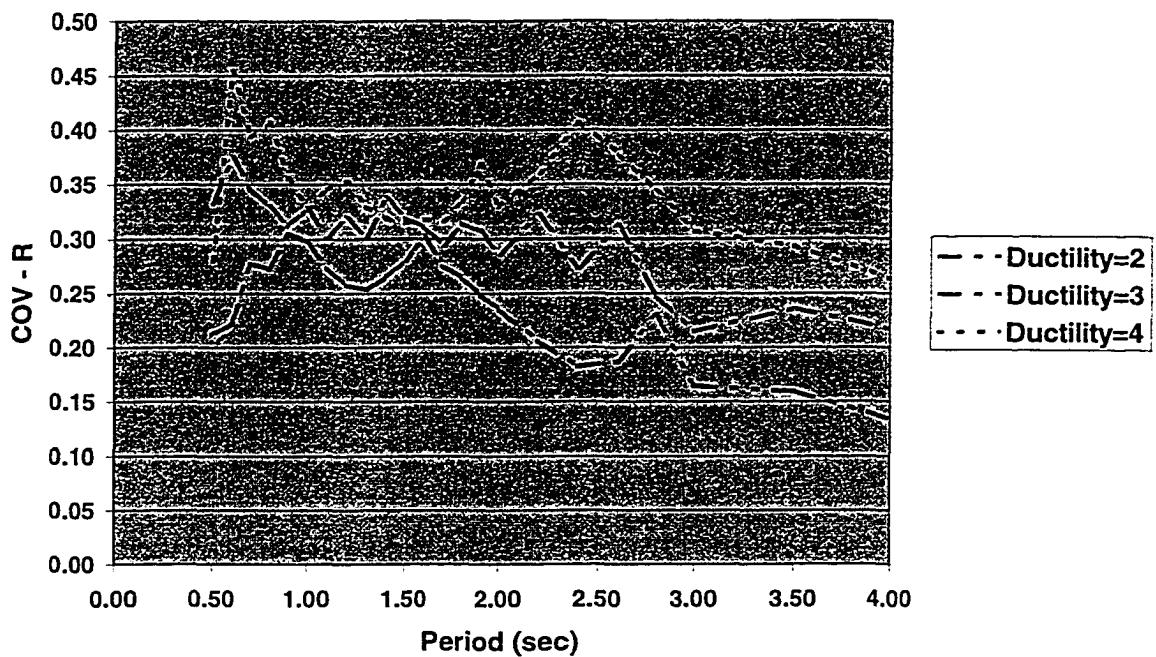


Figure 5-57: COV in R Factor for FT

F-D Factor COV for FT2060 SDOF

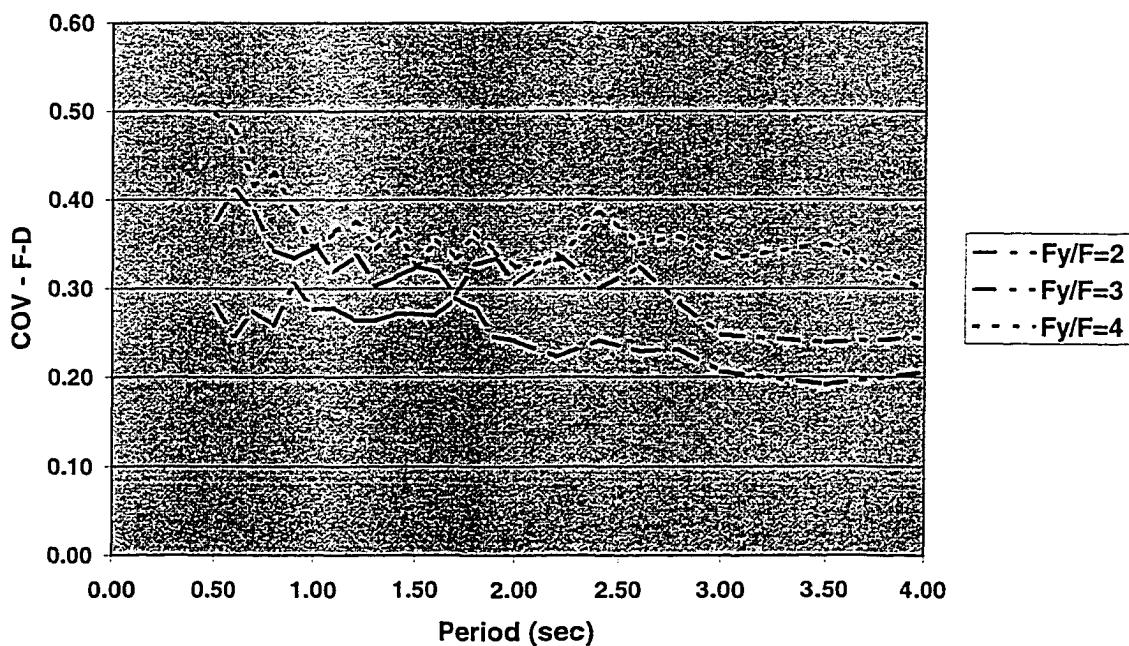


Figure 5-58: COV in F_d Factors for FT

5.3 ADDITIONAL PARAMETER STUDIES

In addition to determining load reduction factors for a variety of degrading systems, three additional parameter studies were conducted: (1) an evaluation of the significance of damping on factor values, (2) evaluation of the sensitivity of factors to local soil conditions, and (3) a comparison of the results of the load reduction factors study with current simple methods of estimating appropriate load reduction for degrading systems. Each of these studies is described in the following subsections.

5.3.1 Effects of Damping on Load Reduction Factors

The sensitivity of load reduction factors to viscous damping in a SDOF system has been previously studied by other researchers, and the effect has been found to be negligible for systems permitted to develop ductilities greater than two or three. However, many platform systems are not expected to possess the capability of developing global displacement ductility much larger than this, so the effect on load reduction factors for platform systems could be significant.

To evaluate the significance of damping, three systems were studied with increased viscous damping: BN, JT11060 and FT4060. BN was used as a base case, while the most severely degrading JT and FT systems were chosen. These systems were modified to allow for viscous damping of 10% critical, and then analyzed for the earthquakes listed in Table 5-3. The resulting mean load reduction factors are shown in Figures 5-59, 5-60 and 5-61.

Similar changes in load reduction factors are observed for all three systems. Systems capable of developing a displacement ductility of two see an increase in allowable load reduction of between 10% and 15% relative to load reduction factors calculated using the baseline 5% damping used in the studies. Systems capable of developing ductilities higher than this value, however, do not exhibit a significant change in load reduction. This is undoubtedly due to the fact that systems designed to yield significantly (i.e. with high displacement ductility capacities) dissipate the majority of energy through nonlinear hysteresis, as opposed to through viscous damping. Hence, these systems are much less sensitive to damping than systems designed for limited yielding.

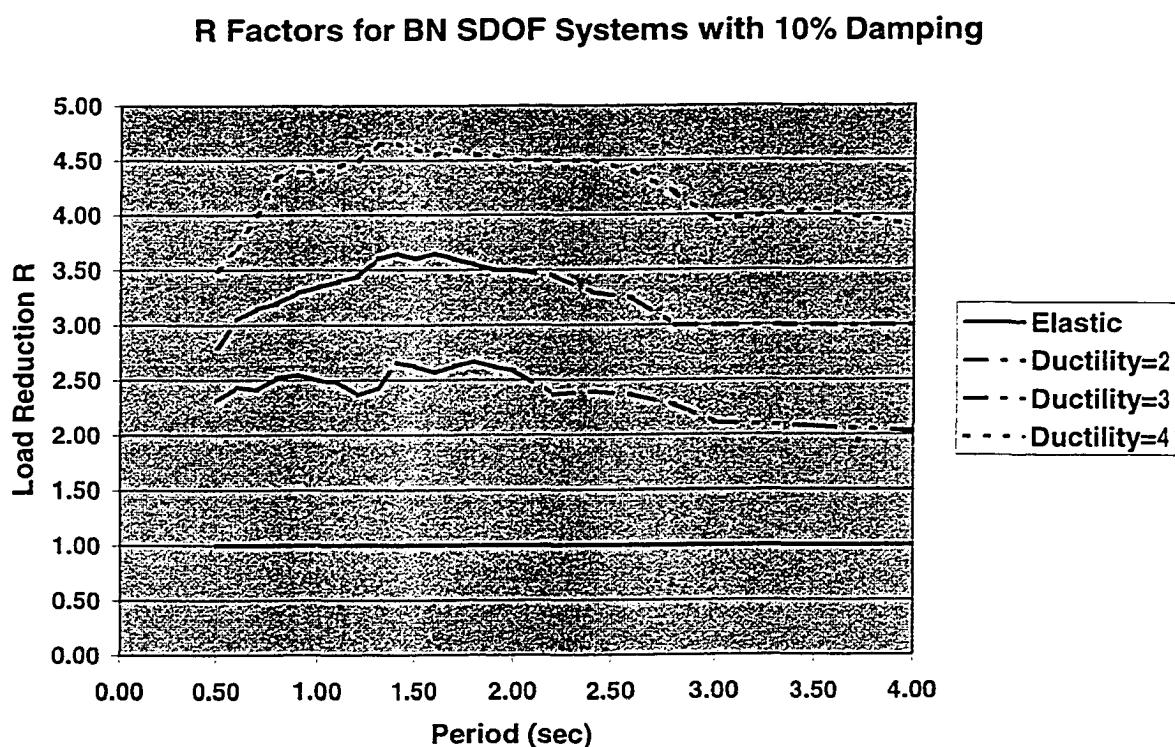


Figure 5-59: BN, 10% Damping

R Factors for JT11060 SDOF with 10% Damping

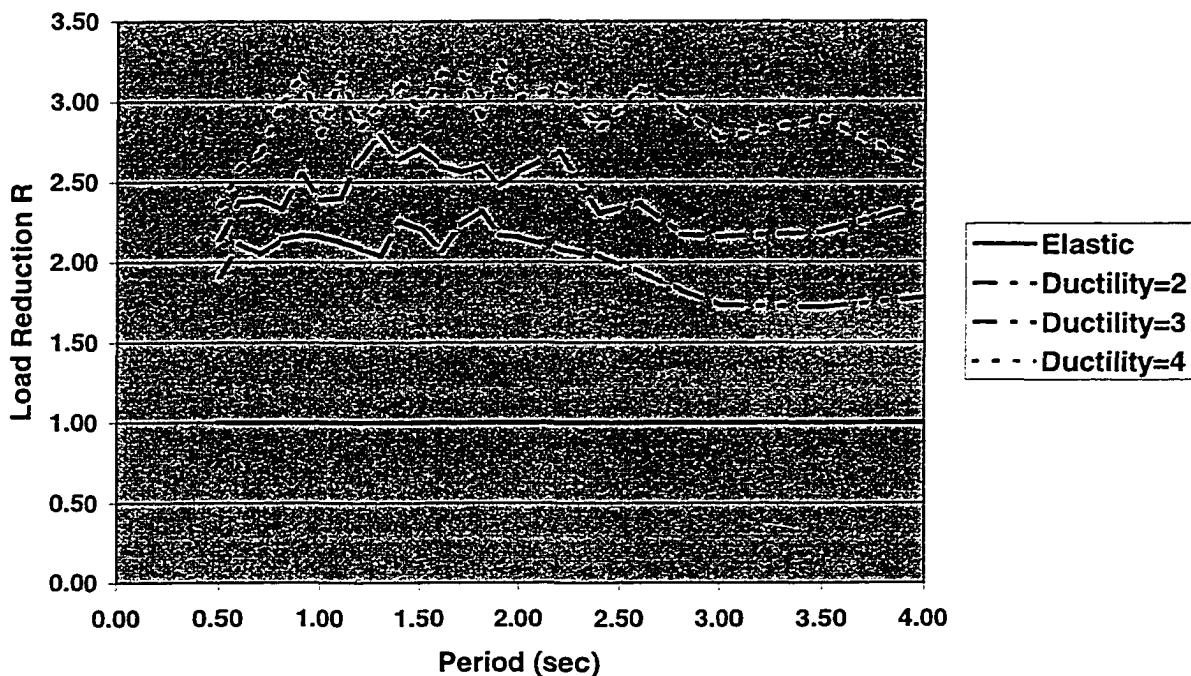


Figure 5-60: JT11060, 10% Damping

R Factors for FT4060 SDOF with 10% Damping

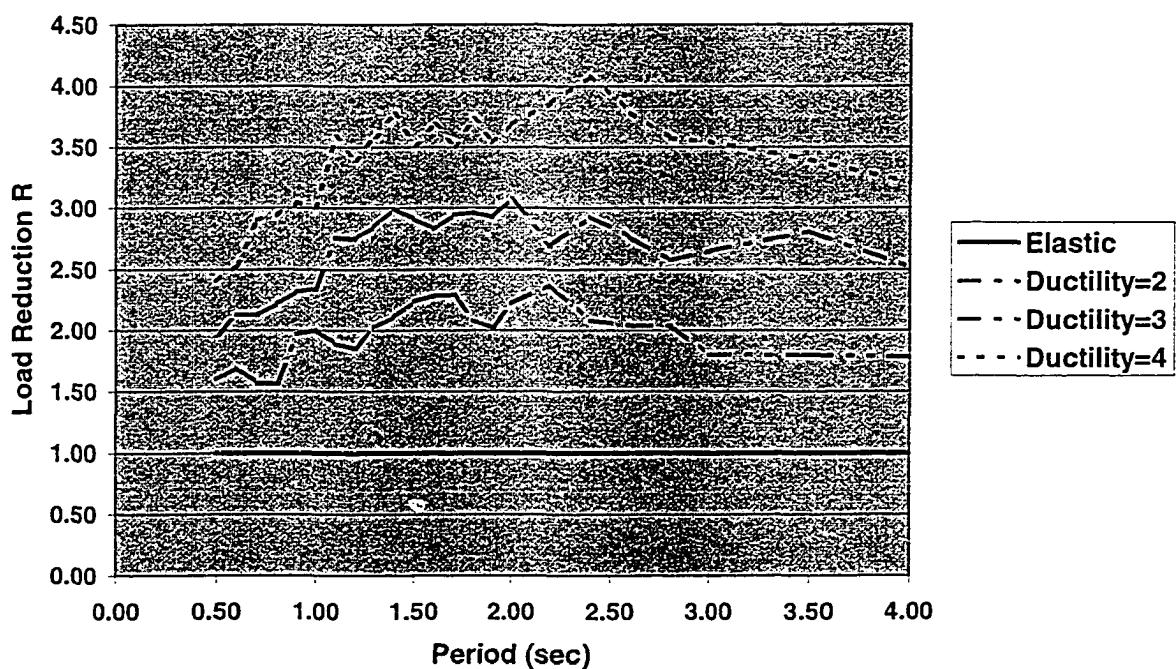


Figure 5-61: FT4060, 10% Damping

5.3.2 Effects of Medium Stiff and Soft Soils on Load Reduction Factors

Studies performed by Miranda (1991) have confirmed that load reduction factors are strongly dependent upon the ratio of site local period to structure fundamental period. Sites with foundation material consisting of rock or firm alluvium tend to have predominant periods much higher than most structures. However, sites with foundation material consisting of soft soils, such as those in the Mexico City and San Francisco Marine District areas can have very low periods which approach those of typical building structures. This site material, if affected by passing seismic waves of similar periodicity, can be excited into motion in resonant fashion, leading to very severe earthquake demands for structures with periods close to that of the site.

To study the effects of site local soil conditions on load reduction factors, the BN, JT11060 and FT4060 systems were analyzed subjected to two additional families of earthquake time histories: a set of 34 records made on firm alluvium, and a set of 22 records made on soft soil sites with local periods in the range of 1.0 sec to 2.0 sec. The resulting load reduction factors determined for these sites are shown below in Figures 5-62 to 5-67.

The alluvium records produce very similar load reduction factors as those determined using rock records. The soft soil records, however, confirm substantial dependence of the load reduction factor on the ratio between site and structure period. Allowable load reduction is greatest when the structure period is equal to or greater than that of the site. This is due to the fact that the yielding structure can escape the resonant period by yielding. Similarly,

allowable load reduction is smallest when the period of the structure is less than the site period, as yielding will now carry the structure towards the period of resonance.

R Factors for BN SDOF Systems on Alluvium

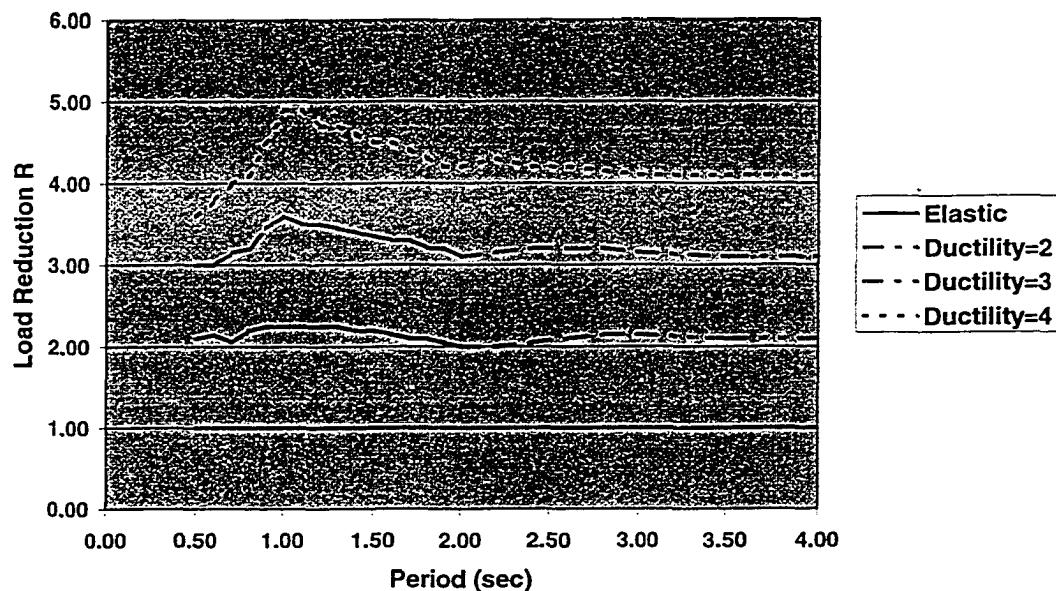


Figure 5-62: R for BN, Alluvium Records

R Factors for JT11060 SDOF on Alluvium

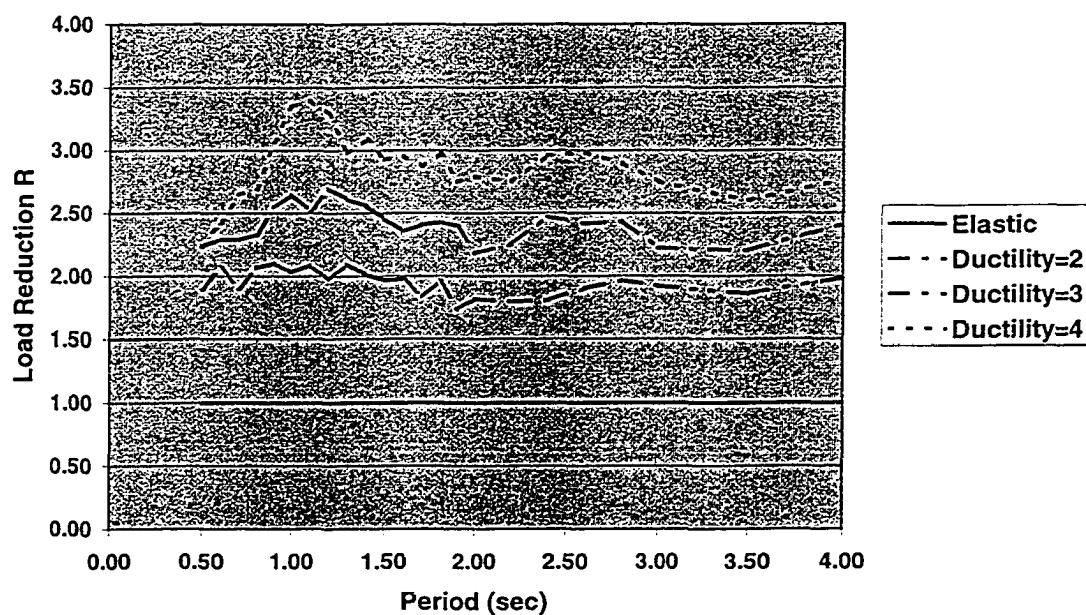


Figure 5-63: R for JT11060, Alluvium Records

R Factors for FT4060 SDOF on Alluvium

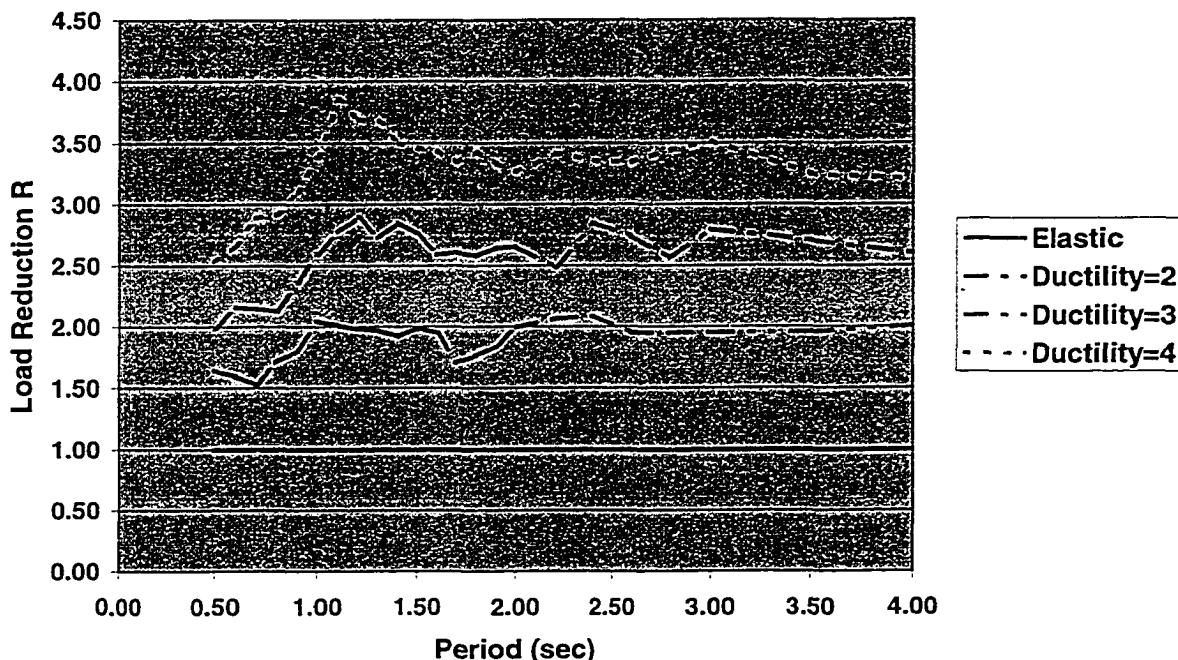


Figure 5-64: R for FT4060, Alluvium Records

R Factors for BN SDOF Systems on Soft Soil

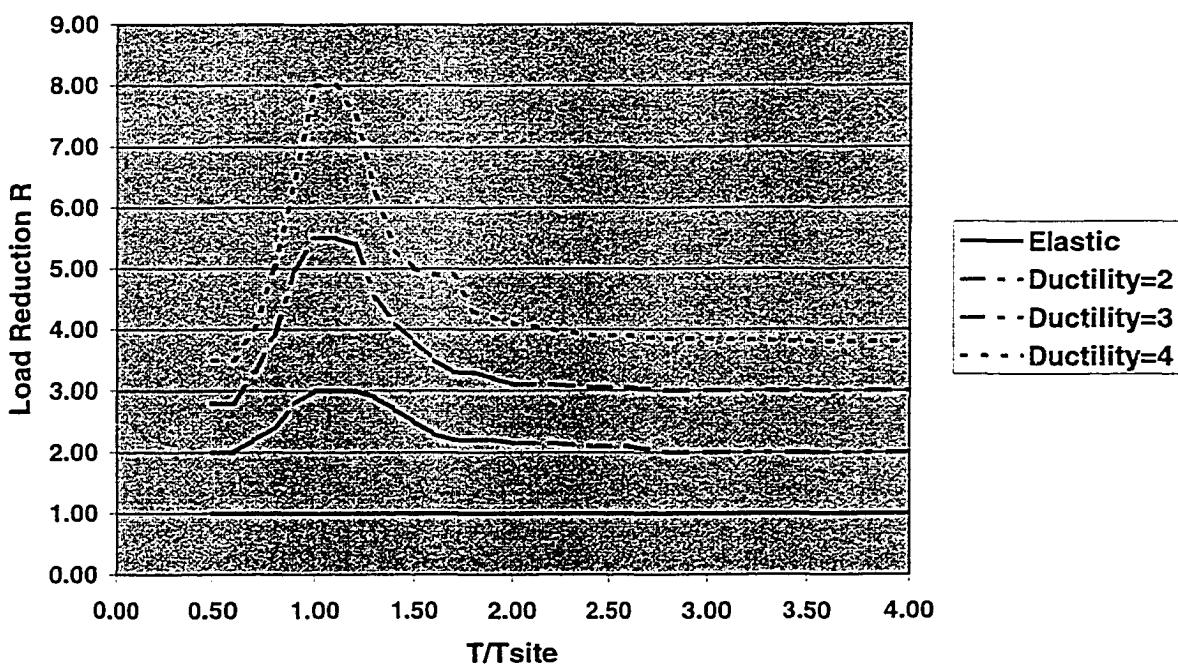


Figure 5-65: R for BN, Soft Soil Records

R Factors for JT11060 SDOF on Soft Soil

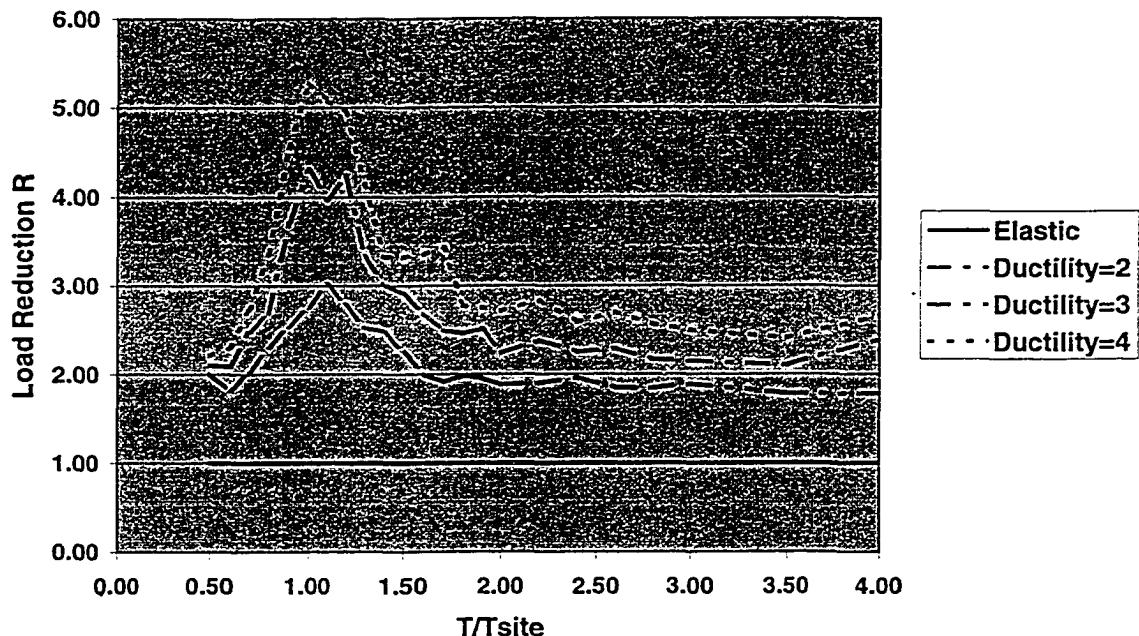


Figure 5-66: R for JT11060, Soft Soil Records

R Factors for FT4060 SDOF on Soft Soil

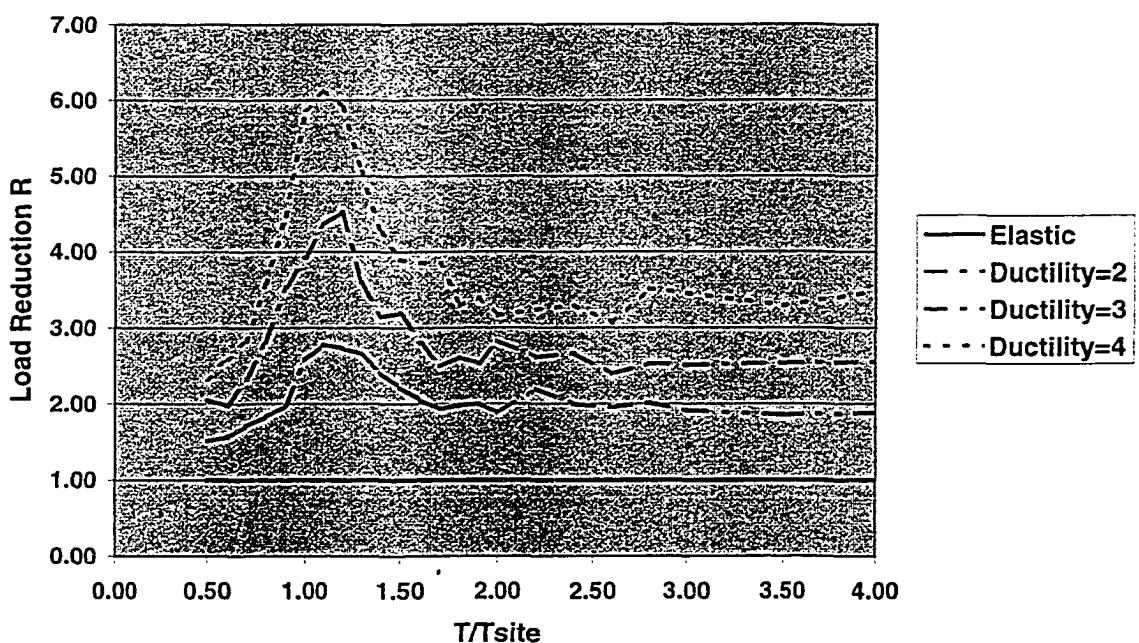


Figure 5-67: R for FT4060, Soft Soil Records

5.3.3 Results of Study Compared to Current Load Reduction Methods

Bea (1996) has suggested the use of a load reduction factor F_e of the following form for offshore platforms:

$$F_e = \alpha\mu$$

μ is the displacement ductility the system is capable of developing, and α is the ratio of the area of the hysteresis envelope of the actual system to that of an ideal elastic-plastic system. This factor is based on the results of a limited study on degrading systems performed using the program PC-ANSR in 1993 at U. C. Berkeley. If the system hysteresis is elastic-plastic, F_e converges to μ . This reflects the trend noticed by Veletsos and Newmark (1960) and others that load reduction is roughly proportional to the allowable displacement ductility for SDOF systems with periods greater than 1.0 sec subject to motions recorded on firm soils.

To validate this approach to estimating load reduction, the mean load reduction for the various types of degrading systems was listed in Table 5-6 for various periods and displacement ductilities (ground motions recorded on rock); the allowable load reduction was also estimated through application of the relationship for F_e . Figures 5-68 to 5-71 show graphically the effective load reduction for the Table 5-6 systems capable of a ductility of 4 through the period spectrum for different values of α . Comparing the results, it can be seen that the factor F_e provides a reasonably conservative approximation to the allowable load reduction for the strength and stiffness degrading (JT) systems for periods greater than 1.0 sec. For periods less than 1.0 sec, the estimated load reduction is unconservative for several of the degrading systems. For long periods (3.0 sec or greater), the simple approximation

estimates load reduction perhaps at most 10% beyond what was determined by the statistical study. For systems with just strength degradation (FT), however, the simple approximation appears excessively conservative for periods of 1.0 sec and higher, while becoming slightly unconservative at periods below 1.0 sec.

Table 5-6: Comparison of Response Factors, Rock

System	μ	R T=0.5	R T=1.0	R T=1.5	R T=2.0	R T=3.0	R T=4.0	F _e
-	-							-
BN	2	2.15	2.25	2.45	2.40	2.00	2.00	2
"	3	2.80	3.30	3.60	3.50	3.00	3.00	3
"	4	3.50	4.40	4.55	4.50	4.00	4.00	4
JT40080	2	2.10	2.20	2.40	2.30	1.95	2.00	1.85
"	3	2.60	3.30	3.40	3.30	2.80	2.80	2.78
"	4	3.30	4.20	4.25	4.20	3.60	3.60	3.70
JT30080	2	2.10	2.20	2.40	2.25	1.90	1.90	1.78
"	3	2.50	3.00	3.45	3.25	2.75	2.75	2.68
"	4	2.95	3.85	4.25	4.20	3.45	3.45	3.57
JT20080	2	2.00	2.10	2.35	2.25	1.85	1.85	1.71
"	3	2.45	3.05	3.40	3.20	2.75	2.75	2.56
"	4	3.00	3.75	3.90	3.75	3.50	3.25	3.42
JT11080	2	1.95	2.10	2.40	2.40	1.80	1.80	1.64
"	3	2.50	2.80	3.20	3.00	2.70	2.70	2.46
"	4	2.90	3.40	3.75	3.75	3.25	3.25	3.28
JT40060	2	1.95	2.15	2.35	2.25	1.80	1.90	1.67
"	3	2.50	2.85	3.25	3.20	2.70	2.60	2.50
"	4	2.95	3.65	3.75	3.75	3.25	3.25	3.33
JT30060	2	1.85	2.05	2.25	2.20	1.80	1.80	1.54
"	3	2.35	2.80	3.00	2.80	2.60	2.50	2.31
"	4	2.75	3.40	3.60	3.50	3.25	3.20	3.08
JT20060	2	1.80	2.00	2.25	2.25	1.75	1.80	1.43
"	3	2.35	2.65	2.75	2.75	2.25	2.35	2.14
"	4	2.50	3.00	3.60	3.30	2.90	3.00	2.86
JT11060	2	1.80	1.90	2.20	2.15	1.75	1.80	1.32
"	3	2.25	2.50	2.85	2.60	2.25	2.20	1.97
"	4	2.30	3.20	3.50	3.00	2.70	2.75	2.63
FT2080	2	2.00	2.20	2.35	2.25	1.85	2.00	1.60
"	3	2.50	3.40	3.40	3.30	2.90	2.70	2.40
"	4	3.15	4.20	4.40	4.30	3.60	3.70	3.20
FT4080	2	1.75	1.85	2.30	2.20	1.80	1.90	1.60
"	3	2.20	2.75	3.30	3.25	2.75	2.75	2.40
"	4	2.45	3.50	4.25	4.20	3.50	3.60	3.20
FT2060	2	1.60	1.90	2.00	2.10	1.70	1.70	1.20
"	3	2.00	2.75	3.40	3.20	2.80	2.75	1.80
"	4	2.40	3.50	4.10	4.00	3.60	3.50	2.40
FT4060	2	1.40	1.75	2.00	1.80	1.70	1.80	1.20
"	3	1.80	2.30	2.90	2.60	2.40	2.60	1.80
"	4	2.35	3.10	3.60	3.60	3.30	3.40	2.40
BD	2	2.30	2.60	2.80	2.50	2.30	2.25	2
	3	3.45	3.70	4.00	3.60	3.50	3.45	3
	4	3.90	5.00	5.30	4.50	4.45	4.50	4

R Factors for Alpha=1 (Fe vs. Statistical Study)

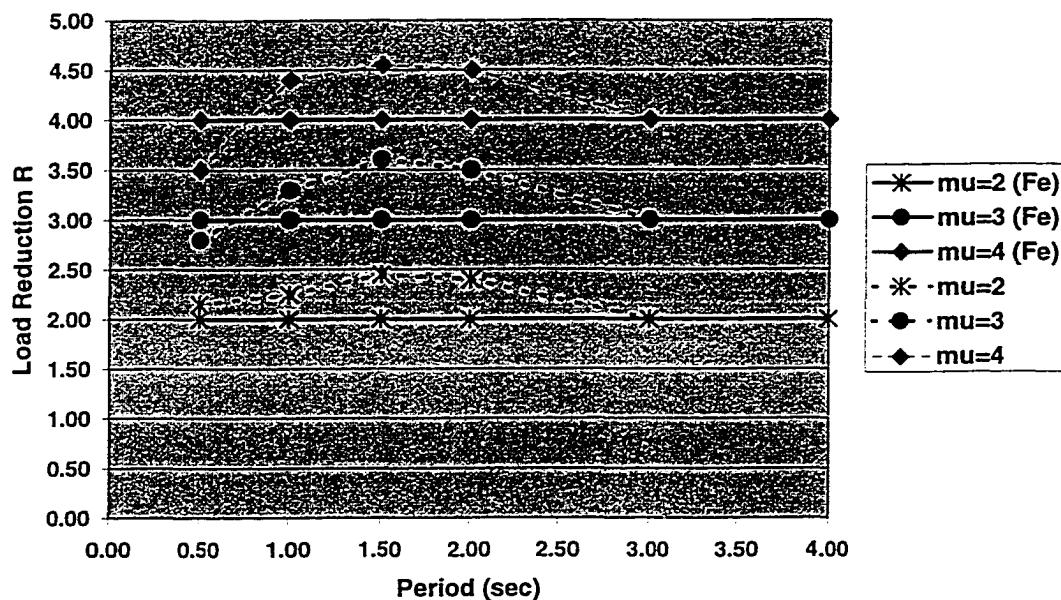


Figure 6-68: Effective Load Reduction (Non-degrading)

R Factors for Alpha=1 (Fe vs. Statistical Study)

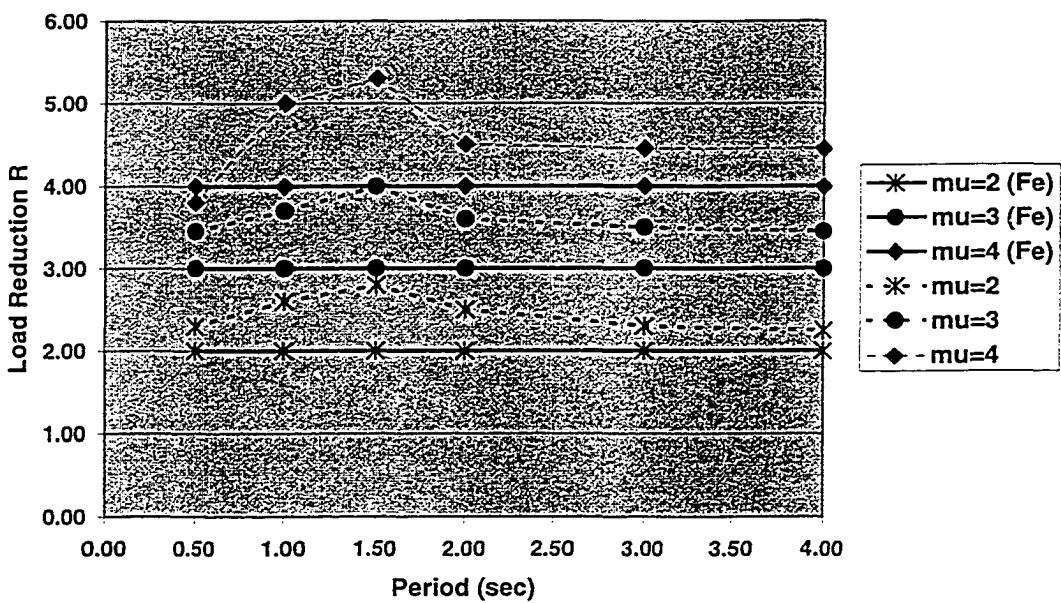


Figure 6-69: Effective Load Reduction (Stiffness Degrading)

R Factors for Alpha=0.66 (Fe vs. Statistical Study)

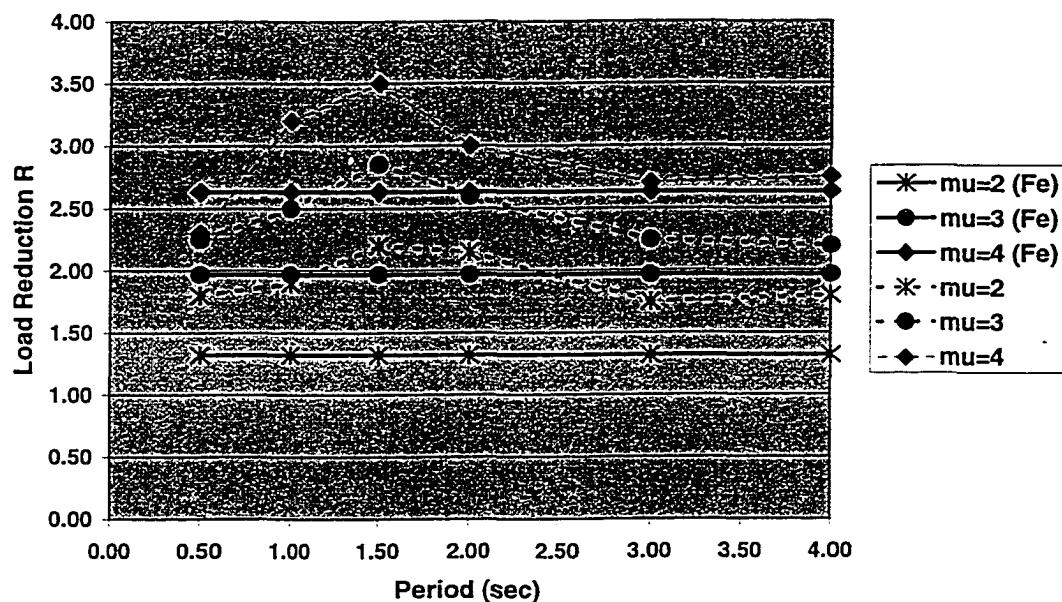


Figure 6-70: Effective Load Reduction (Strength and Stiffness Degrading)

R Factors for Alpha=0.60 (Fe vs. Statistical Study)

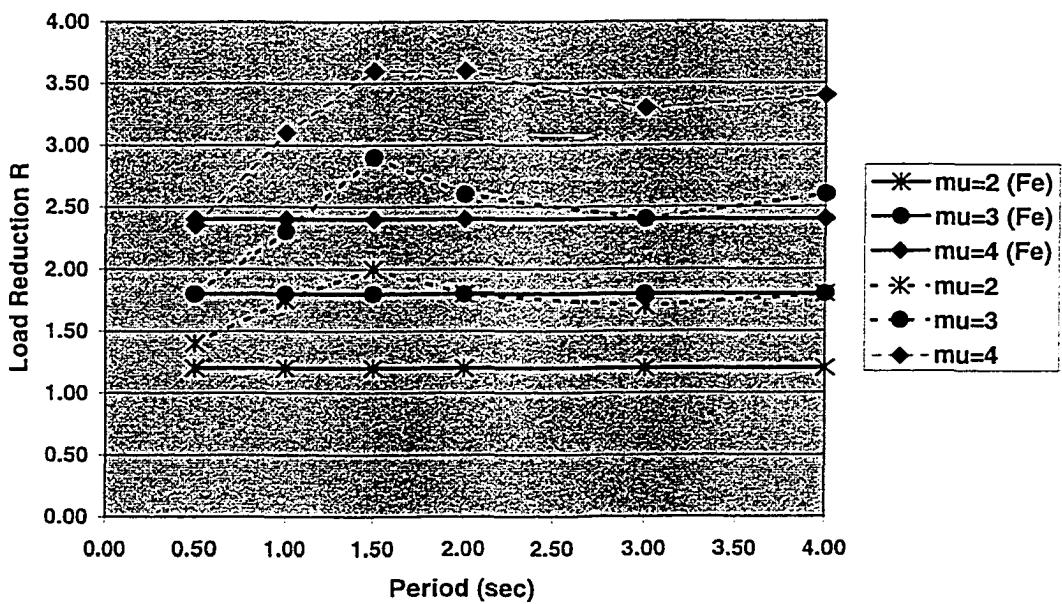


Figure 6-71: Effective Load Reduction (Strength Degrading)

Based on the data presented in Table 5-6, and taking into account the influence of local soil characteristics on effective load reduction, the following adjustments should be made to F_e :

- For strength- and stiffness-degrading systems in the period range between 0.5 sec and 1.0 sec, the allowable load reduction estimated by $\mu\alpha$ should vary from an unadjusted value at 1.0 sec to a 20% reduction at 0.5 sec. Beyond 1.0 sec, load reduction is bounded by $\mu\alpha$.
- For strength-degrading systems in the period range between 0.5 sec and 1.0 sec, the allowable load reduction estimated by $\mu\alpha$ should vary from an unadjusted value at 0.5 sec to a value increased by 20% at 1.0 sec. Beyond 1.0 sec, this increase should be maintained.
- In the range from T/T_{site} equal to 0.5 to 1.0, the load reduction should be scaled from two-thirds the normal (firm soil) value to twice the firm soil value. In the range from T/T_{site} equal to 1.0 to 1.5, the load reduction should be scaled back down from twice the normal value to the normal value.

It should be remembered that these calibrated values of empirical load reduction are based on mean value results from the statistical studies, with uncertainties in the range of 15% to 50%. For design purposes in which this uncertainty is not explicitly considered, it would be prudent to use the load reduction associated with the mean minus one standard deviation, or a similar correction. Given, however, that the mean can be estimated using the above relationship, and the uncertainty is a known range, by assuming either a normal or log-normal distribution, the

appropriate correction can easily be estimated. Statistical distributions for R factors are examined in Chapter Seven.

5.4 MDOF COMPARISONS

To evaluate the practicality of using equivalent SDOF systems to represent the behavior of MDOF systems with degrading behavior, two studies were performed using MDOF models containing elements exhibiting degrading behavior. These analyses were performed using the programs DRAIN-2DX and PC-ANSR. The first study focuses on strength degradation at the foundation level, while the second study concentrates on strength and stiffness degradation in the main portion of the simple structure. In the course of the studies, the number of DOF, the fundamental mode mass participation, and the yield strength of each level in the MDOF structures were varied, to provide a range of application over which the SDOF approximations could be judged.

Comparisons were carried out by first constructing and analyzing an equivalent SDOF of the simple MDOF structure in question. Each SDOF was analyzed for a family of six earthquake time histories (see Table 5-7); the mean value of the ratios between the scale factors on the time histories at system yield and the scale factors at an equivalent local (story) ductility demand of four were determined from these analyses. This value, here designated F_{μ} , is the allowable reduction associated with elastically-determined load the SDOF is entitled to due to ductile action. F_{μ} is the scale factor applied to the ground motion necessary to cause a given level of damage μ in a MDOF structure, once the ground motion has already been increased to the point of causing incipient yield in the structure. Bazzurro and Cornell (1994)

provide an excellent summary of the philosophy behind F_u and other generalized damage parameters.

The given MDOF structure was then also analyzed for the same family of time histories, and similar ratios were developed, using a local (story) displacement ductility of four as a target. The differences in the means of these ratios was then used to judge the effectiveness of the SDOF approximation to predicting the response of the MDOF system.

Table 5-7: Earthquake Time Histories Used

Event	Station	Direction
Imperial Valley May 18, 1940	El Centro Irrigation District	S90W
Kern County July 21, 1952	Taft Lincoln School Tunnel	S69E
San Fernando February 9, 1971	Hollywood Free Field	N90E
Miyagi-Ken-Oki June 12, 1978	Sendai City Kokutetsu Building	N90W
Imperial Valley October 15, 1978	James Road El Centro Array #5	S50W
Loma Prieta October 17, 1989	Hollister South and Pine	360

5.4.1 MDOF with Strength-Degrading Foundation

The first structural configuration considered was a two-bay frame (Figure 5-72). The program DRAIN-2DX was used to perform the analysis. The bottom column portions of the model were DRAIN-2DX “Type 15” elements, with end hinges which, upon yielding, would exhibit strength degradation. The story above the foundation level was made of “Type 02” elements with strength sufficient to keep them elastic. The structure was pin supported in the vertical at each mass in order to restrict response to lateral action only.

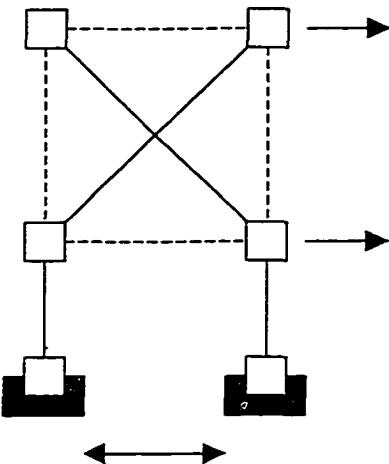


Figure 5-72: Two-Bay Frame

The 2-DOF model, with fundamental mode participating mass ranging from 60% to 90%, was studied by both the equivalent SDOF approach and MDOF analysis. Participating mass was altered by changing the ratio of the top mass to the total mass of the system and the stiffnesses of the top. In all cases, the fundamental period of each MDOF structure was kept at 1.5 sec.

Table 5-8 shows the mean values of the scale factors associated with the requisite displacement ductility demand from the time history analyses, along with mean values of the local story (foundation lateral) ductility demands. The comparisons between the equivalent SDOF and the 2-DOF system show that the SDOF approximation is quite reasonable for this system; mean results from the SDOF are within 15% of those found from MDOF analysis for this system. As the first mode dominance is relaxed, however, variability in the scale factor

needed to cause the requisite local ductility demand increases. Also, as first mode dominance is relaxed, the significance of degradation in the foundation level appears to be reduced.

Table 5-8: SDOF and MDOF Comparisons

System	$F\mu$ for Local $\mu = 4$	COV in $F\mu$
SDOF	2.18	0.26
MDOF 90% 1 st Mode Mass	2.15	0.22
MDOF 80% 1 st Mode Mass	2.25	0.28
MDOF 70% 1 st Mode Mass	2.10	0.39
MDOF 60% 1 st Mode Mass	2.54	0.58

5.4.2 MDOF with Strength- and Stiffness-Degrading Stories

The second structural configuration type studied was a series of braced frames with two, three and four stories (Figure 5-73).

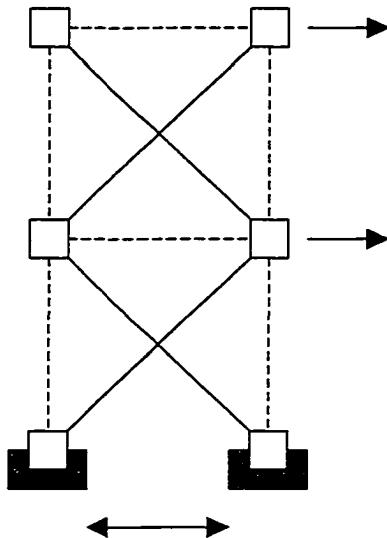


Figure 5-73: Braced Frame Model (Two Bay Shown)

The program PC-ANSR was used to perform these analyses. The braces are Marshall-Maison struts; post-buckling behavior was selected such that the post-yield behavior of the platform under monotonic loading approximated the JT20060 system studied above. Two

strength and stiffness configurations were chosen: one in which strength and stiffness were uniform, and one in which the bottom frame possessed one-half the strength and stiffness of the top frame or frames. The structure was pin supported in the vertical at each mass in order to restrict response to lateral action only.

The three models, with fundamental mode participating mass ranging from 60% to 90%, were studied by both the equivalent SDOF approach and MDOF analysis. Participating mass was altered by changing the ratio of the top mass to the total mass of the system. In all cases, the fundamental period of each MDOF structure was kept at 1.5 sec.

Tables 5-9 and 5-10 show the mean values of the scale factors associated with the requisite displacement ductility demand from the time history analyses, along with mean values of the local story (foundation lateral) ductility demands. For both systems, the scale factor needed to cause the requisite ductility demand is seen to decrease with increasing DOF; the scale factor appears to increase with decreasing fundamental mode mass participation. Variability in response appears to increase with decreasing fundamental mode mass participation.

Overall, the SDOF approximation appears to be insensitive to the presence of weak stories in the structure. This is likely due to the fact that the damage pattern is established by static pushover analysis, which will capture the presence of strength and stiffness discontinuities. This might also be due to the fact that the individual stories have poor post-yield behavior, leading to damage concentration following yielding. Nevertheless, the SDOF approximation works well at emulating the displacements the MDOF structure is likely to be subject to.

Table 5-9: SDOF and MDOF Comparisons, Uniform Strength and Stiffness

System	$F\mu$ for Local $\mu = 4$	COV in $F\mu$
SDOF of 2DOF	2.30	0.26
2DOF 90% 1 st Mode Mass	2.15	0.32
2DOF 80% 1 st Mode Mass	2.25	0.28
2DOF 70% 1 st Mode Mass	2.60	0.39
2DOF 60% 1 st Mode Mass	3.10	0.40
SDOF of 3DOF	2.18	0.22
3DOF 90% 1 st Mode Mass	2.20	0.30
3DOF 80% 1 st Mode Mass	2.40	0.39
3DOF 70% 1 st Mode Mass	2.02	0.67
3DOF 60% 1 st Mode Mass	2.70	0.50
SDOF of 4DOF	2.10	0.34
4DOF 90% 1 st Mode Mass	2.14	0.26
4DOF 80% 1 st Mode Mass	1.94	0.40
4DOF 70% 1 st Mode Mass	2.10	0.67
4DOF 60% 1 st Mode Mass	2.54	0.60

Figure 5-10: SDOF and MDOF Comparisons, Soft Story at Base

System	$F\mu$ for Local $\mu = 4$	COV in $F\mu$
SDOF of 2DOF	2.20	0.18
2DOF 90% 1 st Mode Mass	2.10	0.22
2DOF 80% 1 st Mode Mass	2.05	0.29
2DOF 70% 1 st Mode Mass	2.54	0.33
2DOF 60% 1 st Mode Mass	3.10	0.55
SDOF of 3DOF	2.12	0.19
3DOF 90% 1 st Mode Mass	2.02	0.35
3DOF 80% 1 st Mode Mass	2.32	0.32
3DOF 70% 1 st Mode Mass	2.25	0.54
3DOF 60% 1 st Mode Mass	2.29	0.62
SDOF of 4DOF	2.02	0.26
4DOF 90% 1 st Mode Mass	1.96	0.20
4DOF 80% 1 st Mode Mass	2.06	0.28
4DOF 70% 1 st Mode Mass	2.25	0.40
4DOF 60% 1 st Mode Mass	2.10	0.67

5.5 CONCLUSIONS

To develop a set of load reduction and displacement modification factors for platform systems, a statistical study was performed using SDOF systems with hysteretic behaviors characteristic of two typical platform yield mechanisms: (1) yielding in the jacket, and (2)

yielding in the foundation. Mean values of these factors, and their associated uncertainties, were determined for a range of hysteretic parameters. These factors will aid in both the preliminary design of new platforms for earthquakes, as well as the assessment of existing structures.

The statistical study also evaluated the effects of damping and of local soil conditions on the load reduction factors. Increases in damping were found to be of limited benefit for systems which develop displacement ductilities greater than two, and for periods greater than 1.0 sec. Ground motions recorded on firm alluvium resulted in load reduction factors similar to those generated using ground motions recorded on rock. Ground motions recorded on soft soils showed a strong dependence upon the ratio of the structure period to the natural period of the site.

A series of MDOF structures with degrading element behavior were analyzed both as MDOF systems and equivalent SDOF systems, with the intent of qualitatively assessing the utility of the equivalent SDOF approach with degrading systems. It was found that the equivalent SDOF approach provided estimates of damage to the MDOF structures which were very comparable to results obtained through the use of MDOF models, providing the structure is first-mode dominated. First mode dominance in this case was indicated by a fundamental mode participating mass of 70% to 80%. It should be noted, however, that this is an extremely limited study of MDOF systems; additional application of the SDOF approach to predicting MDOF structural behavior is explored in Chapter Six for more complex structures.

CHAPTER SIX:

CASE STUDIES INVOLVING APPLICATION OF SIMPLIFIED METHODS

6.0 INTRODUCTION

Elements of a simplified method for assessing a platform's ability to survive earthquakes have been documented in Chapters Three, Four and Five. Chapter Three has dealt with (1) approximate methods useful for estimating platform modal properties which, together with a response spectrum, can be used to determine earthquake loads on a platform, and (2) approximate methods for estimating the ductility demands imposed on platform components during a strong earthquake. Chapter Four has documented methods by which (1) the strength and displacement ductility of primary platform structural components (deck bay, jacket bays, foundation lateral and overturning) can be determined, and (2) how these component strengths and ductilities can be related to an effective platform global strength and ductility. Finally, Chapter Five has documented the determination of (1) a set of load reduction factors R used to scale down elastic response spectrum forces, and (2) a set of displacement modification factors F_d used to correlate elastic and inelastic peak displacements from earthquake excitation. Both factors are based on the hysteretic behavior and displacement ductility of the platform; the R factors can be used to assess the ultimate displacement ductility capacity of the platform in terms of forces (yield force and response spectrum load, both indexed on base shear), while the F_d factors can allow the ultimate displacement ductility capacity to be assessed in terms of displacements (yield displacement and response spectrum displacement, both indexed on deck displacement). Displacement ductility assessments made using these factors assume the platform is first-mode dominated.

The complete method is applied to the assessment of five jacket-type platforms in this chapter, with the objective of benchmarking the method's accuracy and limitations. To accomplish the benchmarking, the following comparisons are made:

- Modal properties from the simplified procedures of Chapter Three against modal properties from 3-D modal analysis using detailed (full frame) models.
- Strength-level demand-capacity analysis, using modal response spectrum forces from the simplified (Chapter Three) model and component strengths from Chapter Four, against using 3-D modal response spectrum analysis and element strengths based on state-of-the-art procedures.
- Global displacement ductility capacity, using the procedures of Chapter Four against conventional static pushover analysis with a 3-D full frame model.
- Ductility-level demand-capacity analysis, using (1) response factor-modified strength-level analysis results, with response factors selected on the basis of the global displacement ductility capacity analyses, and (2) nonlinear 2-D and 3-D time history analysis with a full frame model.

Comparison of the modal properties is straight-forward. The strength-level comparisons are expressed in terms of response spectrum ZPA, i.e. the scale factor which is applied to all response spectrum forces (and hence demands) in order to generate a load which exceeds an element or component strength. Global displacement ductility capacity is judged in terms of both the effective global strength (S_a associated with the fundamental lateral mode used to scale the load pattern to yield, or the base shear from first mode forces) and the global

displacement ductility, as determined from deck displacement, the platform exhibits prior to exceeding the ductile capacity of gravity supports or a pre-defined global residual strength limit. Ductility-level comparisons are performed in two ways: (1) by judging the effective load reduction R implied by the displacement ductility analyses against scale factors F_u determined from the MDOF time history analyses, and (2) by judging the displacement modification F_d implied by the displacement ductility analysis against the ratio of the deck displacement found from the MDOF time history analysis to the MDOF first mode elastic response spectrum displacement for the same time history. In addition, the mean value of S_a (associated with the dominant mode) which results in yielding is determined and compared to the value of S_a used to scale the force pattern to yield in the global ductility analysis; this provides a check on the significance of higher modes in reaching yield.

These case studies represent the first effort to evaluate the simplified ductility-level assessment procedures documented in Chapters Three and Four and the response factors in Chapter Five against what constitutes “state-of-the art” analysis of real platform structures. Previous work performed by Stear and Bea (1998) and Perez, et al. (1998) has resulted in the preliminary verification of the simplified modal response spectrum analysis procedures documented in Chapters Three and Four. The study conducted by Perez, et al. (1998) is significant in that it represents the first application of the simplified methods to screening a large group of platforms; in this study the simplified methods were applied to the ultimate-strength assessment of twenty platforms in the Gulf of Mexico – Campeche Bay area. A summary of this study with information supplied by PEMEX/IMP(1999) is contained in the last section of this chapter.

6.1 CASE STUDY #1: PLATFORM A

Platform A is a hypothetical design for a symmetric 4-leg production platform (see Figure 6-1). The structure is designed for 100 ft water depth. The deck is at +50 ft MWL and supports a load of 5,000 kips. The main diagonals in the first jacket bay are 24 inch-diameter (w.t. 0.5 inch), while those in the second bay are 30 inch-diameter (w.t. 0.625 inch); the diagonals in the deck bay are 36 inch-diameter (w.t. 0.75 inch). The joints into which the braces are framed are heavy-wall joint cans. The legs are 78 inch-diameter (w.t. 0.875 to 1.125 inches); the annulus between each leg and associated pile is grouted. The piles are 72 inch-diameter (w.t. 1 to 1.5 inches), and are designed for 150 ft penetration in medium to stiff clay. The shear strength of the clay is 2.5 kips/ft² at the surface, and increases by 0.01 kip/ft² per ft of depth. The pile ends are founded on a very stiff soil layer (rock) which has a shear strength of 184 kips/ft². All steel in the jacket is 36 ksi, while the pile steel is 50 ksi.

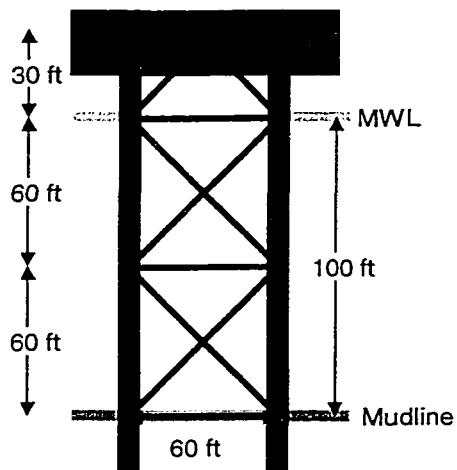


Figure 6-1: Platform A

This platform, commonly known as the Southern California Example Structure, was used as a case study in the development of early nonlinear time history analysis software for the offshore industry. Results of several such case studies have been documented in two papers (Gates, et al., 1977; Marshall, et al., 1977); results from these studies are used to assist in developing models for the benchmarking of the simplified screening methods.

6.1.1 Modal Analysis

Platform A was analyzed using the simplified modal procedure, and the results were compared to results from a 3-D frame modal analysis for the platform. Both analyses considered the effect of added mass on the platform. In the 3-D model, braces were modeled using strut elements, while the legs and piles were modeled using beam-column elements. The deck was assumed to act as a rigid diaphragm. A set of nonlinear springs was used to represent pile-head stiffnesses at the mudline in the 3-D model; these springs were developed from the analysis of a model of a single pile (beam-column elements supported by nonlinear spring elements). For the sake of consistency, the axial and lateral pile-head stiffnesses used in the 3-D model were also used in the simplified model. Table 6-1 lists the lateral and axial pile-head stiffnesses, as well as the approximate stiffnesses they correspond to.

Table 6-1: Pile-Head Axial and Lateral Stiffnesses

Pilehead Springs	Stiffness	Approximate k
Vertical	3150 kips / in	0.9EA/L
Horizontal	470 kips / in	$12EI/(0.25L)^3$

Figure 6-2 shows the lateral mode shapes and vibration periods of the platform as estimated by the simplified modal procedure, while Figure 6-3 shows these same quantities as derived from the 3-D model (torsional vibration has been neglected in the simplified model, and hence is not reported for the 3-D model). The differences between the results are very small; hence the simplified modal method is observed to provide excellent estimates of modal properties for Platform A relative to a 3-D frame model.

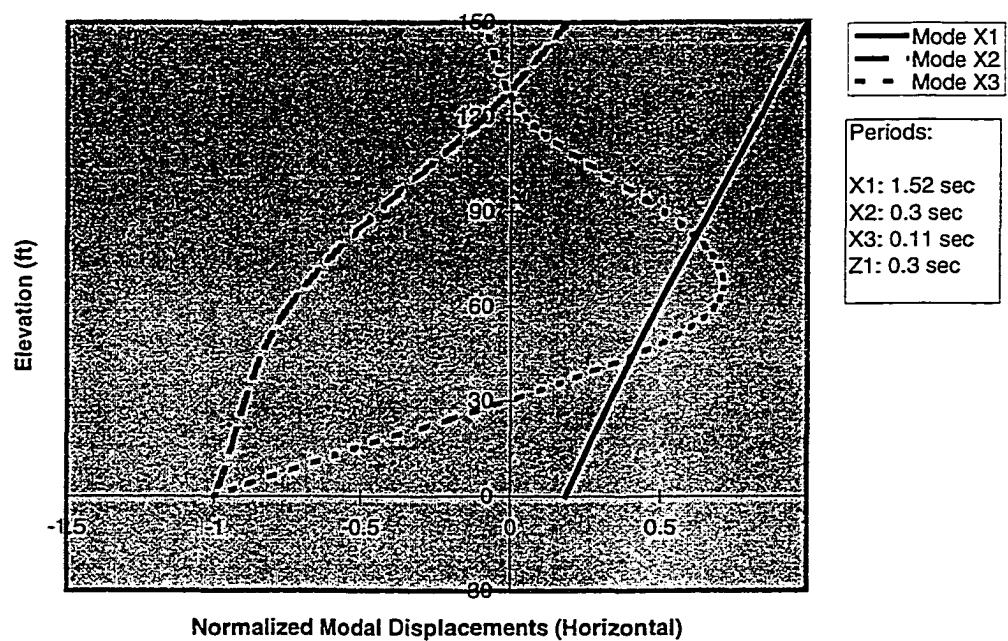


Figure 6-2: Platform Vibration Properties (Simplified Modal Approach)

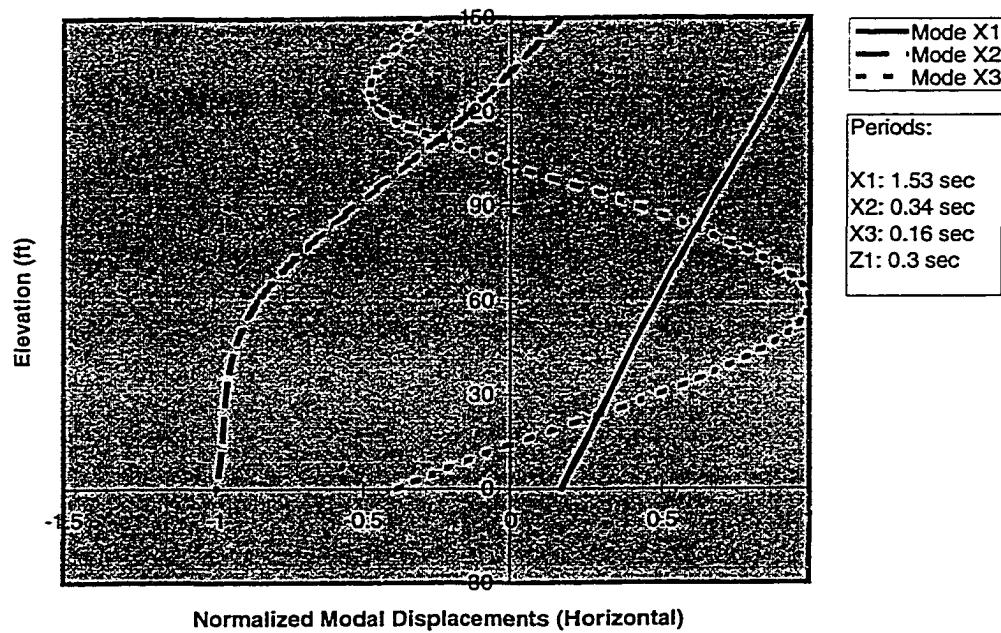


Figure 6-3: Platform Vibration Properties (3-D Model)

6.1.2 Strength-Level Demand-Capacity Analysis

Modal forces were estimated for both models using the API (1993) Soil B response spectrum together with the appropriate modal properties. For both models, forces were assumed to act on all three axis simultaneously, with a proportion of 1.0/0.66/0.5 used to scale the primary lateral (in principal direction of excitation), secondary lateral (perpendicular to principal direction of excitation), and vertical components of load. The SRSS combination rule was used in combining modal responses.

A comparison of the effective story shears and axial forces induced on the piles are shown in Table 6-2 and Figure 6-4 for a spectrum ZPA of 0.25 g. The shears shown in the figure are those associated with the primary lateral mode for all levels above the mudline; the mudline

shear is found from a SRSS combination of the two lateral components. The shears are shown in this fashion because the braced portions of the structure will typically only resist load in-plane with the braced frames, while the lateral load on the foundation will be resisted by all piles regardless of load direction. Given the similarity in modal properties, the estimated response spectrum shears and overturning forces are also quite close.

Table 6-2: Pile Loads, ZPA = 0.25 g

Pile Load	3-D (kips)	Simplified (kips)
Tension	359	362
Compression	3859	3862
Lateral	541	550

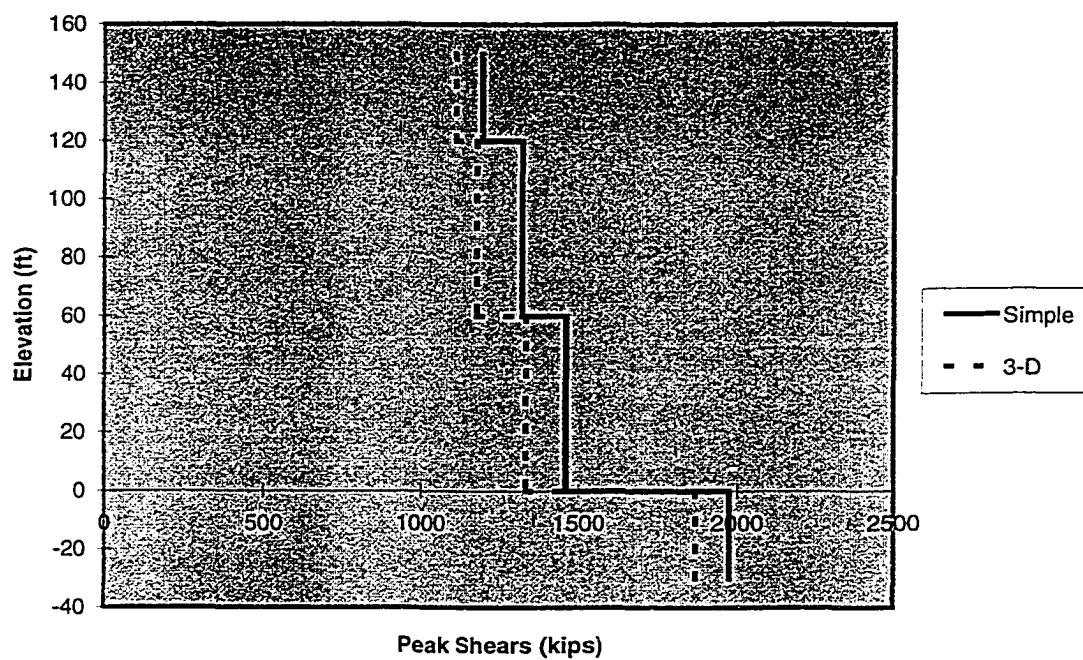


Figure 6-4: Platform Loads, ZPA = 0.25 g

When analyzing this platform, Marshall, et al. (1977) considered each X-brace strut to be capable of buckling over the full length of the X-brace, as opposed to the $\frac{1}{2}$ -length commonly

observed in tests. A 1.0g local load was used to envelope the local brace vibration load contribution. Brace buckling capacities used by Marshall, et al. (1977) are shown in Table 6-3, along with brace buckling capacities estimated through application of limit equilibrium principles assuming a buckling length equal to the full length of the X-brace, and a buckling length equal to $\frac{1}{2}$ the length of the brace. An effective length factor of $k = 0.5$ was used to derived the buckling capacity for both of the limit equilibrium estimates. It was assumed tubular joints would not govern the capacity of the braces; this assumption is based on the fact that the joints have heavy wall cans, and all joints (including the X-joints in the X-braces) are manufactured from higher grade material. Table 6-4 shows the ultimate strengths of the imbedded piles as found from analysis of the model of the single pile as well as estimates made using the limit equilibrium approach.

Table 6-3: Tubular Brace Buckling Capacities

Brace Diameter and Thickness	Axial Capacity (kips) – Marshall	Axial Capacity (kips) – ULSLEA (100% L)	Axial Capacity (kips) – ULSLEA (50% L)
24" ϕ 0.5"	920	940	1243
30" ϕ 0.625"	1590	1601	1983
36" ϕ 0.75"	2820	2887	NA – K braced

Table 6-4: Pile Capacities

Pile Strength	Capacity (kips) - Marshall	Capacity (kips) – ULSLEA
Tension	6000	6142
Compression	11200	10400
Lateral	1960	2176

The estimates made using the full unbraced length of the X-brace compare fairly well to those derived by Marshall, et al. (1977) during the earlier investigation of the platform, differing by at most 3%. As mentioned previously, however, testing of X-braces performed

by Zayas, et al. (1980) and others has indicated that these braces will tend to buckle across $\frac{1}{2}$ the overall length of the brace, as the center cross-point acts as a support; hence, the strengths estimated using $\frac{1}{2}$ the overall length are more likely to be representative of the true brace axial capacities. Relative to the strengths estimated by Marshall, et al. (1977), the X-braces could have capacities on the order of 35% higher.

The pile ultimate capacities compare very well, differing by at most 10%. The soil characteristics were deliberately chosen by Marshall, et al. (1977) to be very strong, so as to emphasize nonlinear behavior in the jacket of the platform.

Using the simplified loads and capacities, the earthquake "intensity" (expressed in terms of the response spectrum ZPA) resulting in the formation of a collapse mechanism is 0.55 g; the weak link is the first jacket bay braces. Gross shear demand for this level of load and the associated platform shear capacity profile are shown in Figure 6-5. Also shown on this graph is the demand-capacity profile of the platform without the approximate jacket-leg/pile bending contribution to bay strength; it is apparent that the legs, which are unusually massive for platforms of this type, develop noticeable resistance when the braces reached their buckling limits, as the intensity necessary to form a mechanism in this case is 0.43 g. The 3-D analysis indicates the earthquake intensity resulting in the formation of a collapse mechanism is 0.56 g; the elements which will fail first are the first jacket bay braces. The simplified method provides results that are in excellent agreement with those from the 3-D analysis.

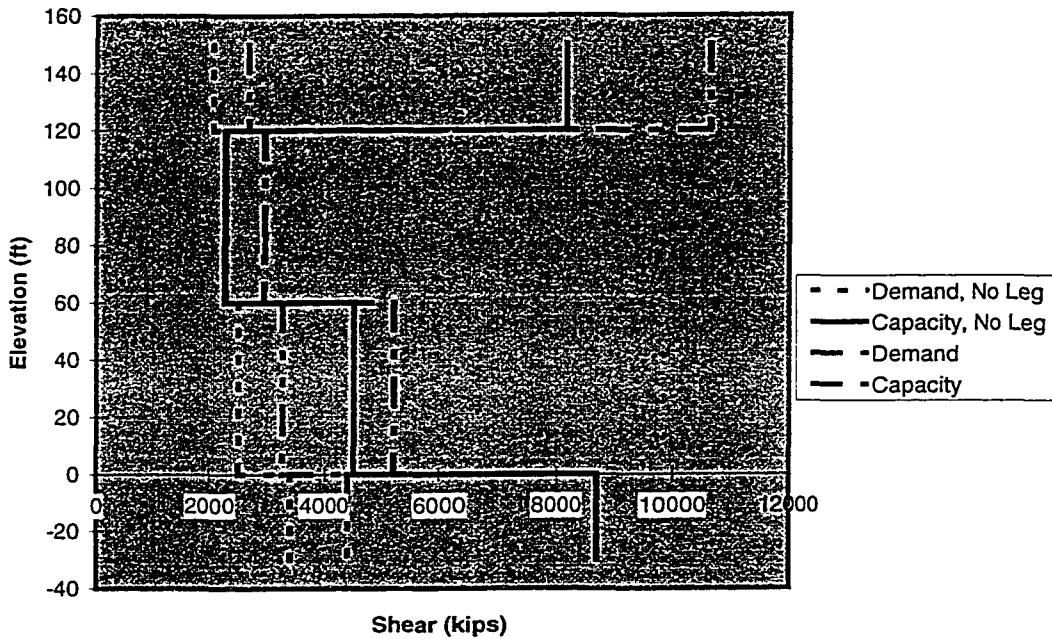


Figure 6-5: Gross Shear Demand - Capacity Profile from Simplified Method

Platform A was also used as a test case for benchmarking the equipment-structure interaction procedure described in Chapter Four used for determining the local load due to brace lateral acceleration. To qualitatively assess the significance of local acceleration load, the axial capacities of braces in Platform A were determined for three cases: (1) ignoring local lateral loads, (2) including local lateral loads calculated by the simplified method of Chapter Four, and (3) including local loads originally used in the platform design.

The characteristics of bracing members in the platform are shown below in Table 6-5. As this platform has heavy-wall joint cans, it was assumed that the end conditions of the braces could be considered fixed. The periods of the braces are very low compared to those of the structure, thus indicating that response will approach the limiting condition of very stiff

equipment. For the purpose of this comparison, X-braces were considered supported at the center of the X; thus brace vibration properties and axial capacities are determined using a length equal to 50% of the entire brace length.

Table 6-5: Tubular Brace Characteristics

Location	D (inches)	t (inches)	L (inches)	T (sec)
Deck Bay	36	0.75	509	0.03
1 st Jacket Bay	24	0.5	509	0.07
2 nd Jacket Bay	30	0.625	509	0.06

For the local load determined through application of the equipment-structure interaction method, acceleration contributions were determined based on excitation of both the two principal horizontal directions and the vertical direction, using the API (1993) Soil-B spectrum with a PGA of 0.5 g. The spectrum accelerations for the different directions were calculated assuming a ratio of 1.0 (horizontal in-plane with member):0.66 (horizontal perpendicular to member):0.5 (vertical) between the different spectrum scale factors. For the sake of simplicity, the local acceleration components were all assumed to be perpendicular to the axis of the brace irrespective of the structure mode associated with the acceleration component. Acceleration components appropriate to each mode, along with the modal participation factors, are shown in Table 6-6.

Table 6-6: Modal Acceleration Components for Platform A

	Mode 1 - X	Mode 2 - X	Mode 3 – X	Mode 1 – Z
T (sec)	1.53	0.30	0.11	0.30
Γ (part. factor)	1.10	0.65	0.02	1.07
\ddot{u}_D (g)	0.45	-0.14	0.01	0.67
\ddot{u}_1 (g)	0.38	0.12	0.01	0.62
\ddot{u}_2 (g)	0.21	0.71	-0.03	0.56
\ddot{u}_F (g)	0.08	0.82	0.01	0.48

Horizontal accelerations are dominated by the first two horizontal modes, while the vertical accelerations are quite large in the fundamental mode. Local acceleration components determined by the equipment-structure interaction method for the different braces are shown in Table 6-7, along with the axial capacities associated with the three conditions.

Table 6-7: Brace Axial Capacities

Location	D	T	Local \bar{u} (g)	P_u (kips) ₁	P_u (kips) ₂	P_u (kips) ₃
Deck Bay	36	0.75	0.88	2949	2898	2887
1 st Jacket	24	0.5	0.78	1289	1253	1243
2 nd Jacket	30	0.625	1.05	2036	1982	1983

The structure acceleration corresponding to the top of each bay was used to determine the response of braces within a bay. From the results in Table 6-7, the 1.0 g local acceleration originally used to envelope the brace accelerations at the design stage is slightly conservative for braces in the deck bay and first jacket bay, but matches the acceleration in the lower bay. However, it is apparent that the lateral load from local member response has a negligible effect on tubular brace capacity for this platform. Accounting for local acceleration changes the brace buckling capacities by at most 4%; the effect on overall platform capacity will be of similar (small) magnitude.

6.1.3 Global Ductility Analysis

The simplified methods of Chapter Four were used to assess the global displacement ductility of Platform A. As the structure is symmetric, and a previous analysis performed by Gates, et al. (1977) indicated the foundation did not control post-yield behavior, a 2-D analysis was performed. The global load-displacement behavior estimated by application of the simplified methods was compared to results from a static pushover analysis performed using PC-ANSR.

The PC-ANSR model was developed using member and soil characteristics specified by Gates, et al. (1977).

Platform A was analyzed using two different horizontal bracing schemes: weak braces (18 inch diameter, and 0.375 inch w.t.), and strong braces, with twice the wall thickness as the weak braces. Using both configurations allowed for an evaluation of both the concentrated damage and the distributed damage assumptions of the simplified ductility approach.

Using first mode forces as a load pattern, the simplified method indicates the platform has an effective lateral load yield strength of 3,900 kips; the strength is governed by buckling of the braces in the first jacket bay. This value of base shear corresponds to an API Soil B response spectrum ZPA of 0.60 g (S_a for the fundamental lateral mode equal to 0.47 g). The base shear including all lateral modes is 4,200 kips, indicating the potential error induced by indexing on base shear is small. Using PC-ANSR, the platform's lateral load yield strength is estimated to be 3,930 kips; this analysis confirms the first jacket bays braces are the first members to yield. The two strength estimates are in excellent agreement.

Figure 6-6 depicts the global load displacement behavior estimated by both the simplified method and PC-ANSR for the "weak" horizontal configuration. Using the simplified method, the horizontal braces are judged incapable of supporting the tension capacity of the braces in the bays around them; thus the jacket configuration is classed as "weak," and damage is assumed to concentrate in the first bay in which braces buckle. Strength drops quickly to the point at which braces in the first jacket bay reach their cyclic ductility limits,

and continues to degrade at a lesser rate beyond that point. The global load-displacement curve generated by PC-ANSR is similar in trend, but highlights the approximate nature of the simplified approach. The PC-ANSR analysis reveals that the braces in the first bay do buckle first; this is followed by the buckling of braces in the bottom bay, and then the buckling of the horizontals between these two bays. After the horizontals buckle, supportable lateral load begins to drop rapidly. A portal mechanism begins to form as displacement increases. While the simplified method captures the general trend in load-displacement behavior, the specifics of which members are buckling and yielding are not represented. The simplified method will not capture the propagation of damage into the second jacket bay due to the bending of the jacket legs.

Using the 70% residual strength criteria documented in Chapter Four, Platform A would possess very limited ductility. Using this criteria to establish global displacement limits, the simplified analysis indicates Platform A should be limited to a global displacement ductility of 1.3. Using the same criteria, the PC-ANSR analysis also indicates global displacement ductility should be limited to 1.3.

Figure 6-7 depicts the global load displacement behavior estimated by both the simplified method and PC-ANSR for the “strong” horizontal configuration. Using the simplified method, the horizontal braces are judged capable of supporting the tension capacity of the braces in the bays around them; thus the jacket configuration is classed as “strong,” and damage is assumed to concentrate in the jacket, but distributed between bays. Strength drops gradually to the point at which braces in the first jacket bay reach their cyclic ductility limits,

and then degrades more rapidly as damage is assumed to concentrate in the first jacket bay following the exceeding of the braces' local buckling limits.

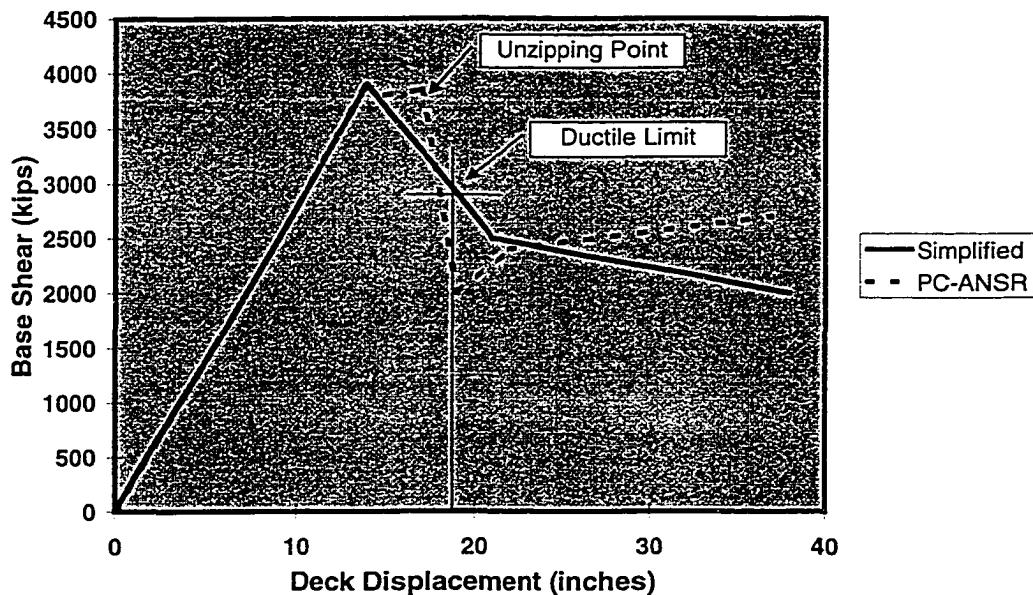


Figure 6-6: Global Load-Displacement Behavior of Platform A with Unzipping

The global load-displacement curve generated by PC-ANSR is very similar in trend. The PC-ANSR analysis indicates the braces in the first bay buckle first, followed by the buckling of braces in the bottom bay. Damage then begins to concentrate in these two bays. At a deck displacement of 38 inches, the horizontals between the first and second jacket bays buckle; supportable load begins to drop, and a portal mechanism begins to form in the legs. Again, while the simplified method captures the general trend in load-displacement behavior, the specifics of which members are buckling and yielding are not represented.

Using the 70% residual strength criteria, the simplified analysis indicates Platform A is capable of developing a global displacement ductility of 2.7. The PC-ANSR analysis indicates a global displacement ductility capacity of 2.9. It should be noted, however, that at these limits, severe damage will have occurred to the diagonal braces in both bays; PC-ANSR indicates braces in the first and second jacket bays will have been subjected to local ductility demands in excess of 12 at this level of deck displacement.

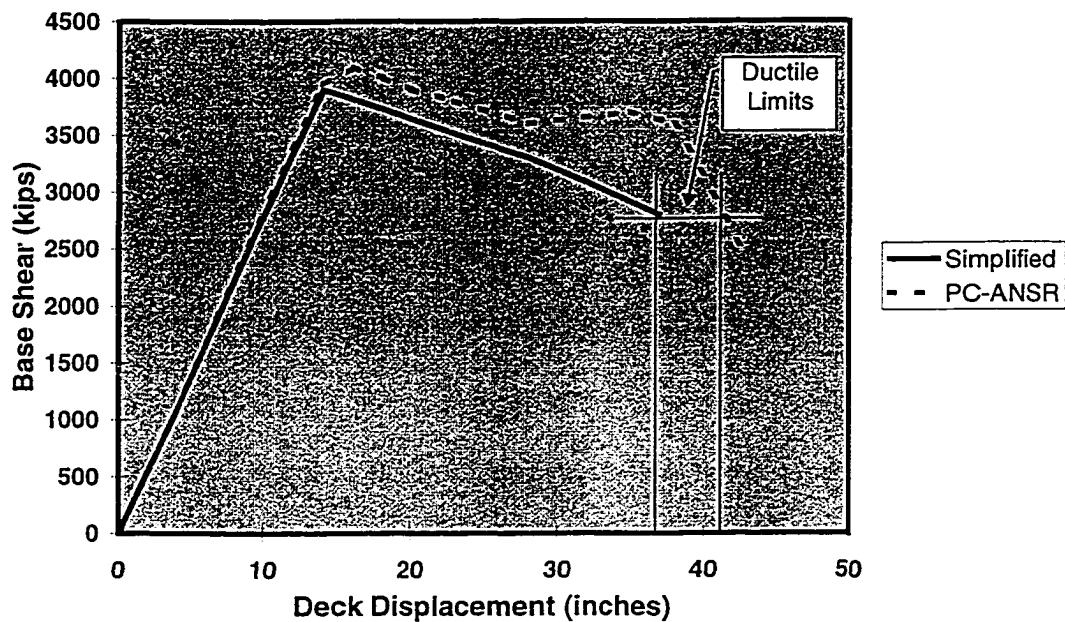


Figure 6-7: Global Load-Displacement Behavior of Platform A without Unzipping

6.1.4 Ductility-Level Demand-Capacity Analysis

Ductility-level comparisons were performed in two ways for Platform A: (1) by judging the effective load reduction R implied by the simplified displacement ductility analyses against scale factors F_u determined from MDOF nonlinear time history analyses, and (2) by judging the displacement modification F_d implied by the simplified displacement ductility analyses

against the ratio of the deck displacement found from the MDOF nonlinear time history analysis to the MDOF first mode component of displacement (assuming linear elastic behavior) for the same time history. Also, the mean fundamental lateral mode spectral acceleration S_a (assuming 5% damping) which represented the onset of nonlinear behavior in the platform was determined, to compare with the value determined in the global ductility analysis; this comparison checks the validity of indexing on first mode response to characterize platform strength capacity.

Load reduction and displacement modification factors were selected from Chapter Five. As noted earlier, factors are selected based on three parameters:

- The fundamental lateral period of the structure.
- The global displacement ductility capacity.
- The expected degradation mode associated with cycling to the global displacement ductility capacity limit.

For the weak configuration, use was made of Figures 5-35 and 5-37 for estimating R , and 5-36 and 5-38 for estimating F_d ; the data in these figures bounds the behavior exhibited by the platform in this structural configuration. At a period of 1.5 sec, and for small inelastic displacements, the load reduction is roughly proportional to the ductile capacity of the system. Hence, R is taken to be 1.3. Similarly, F_d will be very close to unity for overload ratios of 4.0 or less.

For the strong configuration, R was estimated using Figure 5-27, and Figure 5-28 was used for F_a . R will be close to 3.0, while F_a will be in the range of 1.0 to 1.2 providing the overload ratio is 4.0 or less.

The PC-ANSR models used in Section 6.1.3 were utilized to determine F_μ , the effective load reduction a nonlinear MDOF system is entitled to based on ductile action, and to evaluate the relationship between inelastic and equivalent elastic (first mode) deck displacements. Rayleigh damping was assumed, with mass and stiffness-proportional coefficients balanced such that 5% critical damping was achieved in the first two lateral modes. In lieu of rigorously calculating damping coefficients for structure and soil elements, stiffness-proportional damping was first assigned to steel elements in the platform, such that its fundamental lateral mode damping was increased to 1.5%. Mass-proportional and stiffness-proportional (soil only) damping was then balanced for the entire soil-structure system until 5% damping was achieved in the first two lateral modes. Each model was analyzed using a series of nine earthquakes (see Table 6-8); two damage measures, brace local ductility (using the cyclic limit as a target) and global displacement ductility (using the allowable as determined from the ductility analyses), were used as criteria for F_μ .

The mean values of F_μ for each damage measure, and the ratio of inelastic to elastic deck displacement, are shown in Table 6-9 for both structural configurations. The target global damage for the weak configuration was $\mu=1.3$, while for the strong configuration the target

was $\mu=2.7$. The target local damage was $\mu=5.0$ for any brace. The inelastic to elastic deck displacement ratio was averaged for overloads of two and three.

Table 6-8: Earthquake Time Histories Used

Event	Station	Direction
Imperial Valley May 18, 1940	El Centro Irrigation District	S90W + vertical
Kern County July 21, 1952	Taft Lincoln School Tunnel	S69E + vertical
San Fernando February 9, 1971	Hollywood Free Field	N90E + vertical
Miyagi-Ken-Oki June 12, 1978	Sendai City Kokutetsu Building	N90W + vertical
Imperial Valley October 15, 1979	James Road El Centro Array #5	S50W + vertical
Central Chile March 3, 1985	Vina Del Mar	S20W + vertical
Michoacan September 19, 1985	Zaculta	S00E + vertical
Whittier-Narrows October 1, 1987	Alhambra Freemont School	180 + vertical
Loma Prieta October 17, 1989	Hollister South and Pine	360 + vertical

Table 6-9: $S_{a\text{-yield}}$, F_μ and Deck Displacement Ratio

Platform A	$S_{a\text{-yield}}$ (g)	COV	F_μ Global	F_μ Global COV	F_μ Local	F_μ Local COV	$\Delta_{\text{inelastic}}/\Delta_{\text{elastic}}$	$\Delta_{\text{inelastic}}/\Delta_{\text{elastic}}$ COV
Weak	0.47	0.05	1.44	0.21	1.63	0.25	1.0	0.28
Strong	0.47	0.05	3.06	0.24	1.81	0.19	1.0	0.25

The mean value of $S_{a\text{-yield}}$, representing the level (as measured by first lateral mode spectral acceleration) to which excitation had to be scaled in order to initiate yielding in the platform, is in excellent agreement with the value estimated in the global ductility analysis. Higher mode effects do not greatly affect the onset of yielding in the platform. The R factors selected based on the results of the global ductility analyses compare very well with the F_μ factors derived using global displacement ductility capacities as targets. Using the static

pushover PC-ANSR results from Section 6.1.4, the weak configuration platform develops local ductility demands of five on tubular braces in the first jacket bay at a global displacement ductility of 1.5, while the strong configuration platform develops local ductility demands of five on tubular braces in the first jacket bay at a global displacement ductility of 1.6; assuming load reduction is directly proportional to global displacement ductility in this range, it is seen that these values match well with the F_μ values found using local ductility demand as a criteria. Similarly, for the levels of overload considered, the elastic and inelastic displacements are approximately equal.

6.1.5 Platform A: Summary of Results

Platform vibration properties estimated using the simplified method compare very well with those calculated by analyzing a full-frame model of the platform. Using the API Soil B response spectrum as a basis for loads, the simplified demand-capacity provides an excellent estimate of platform capacity, as expressed by response spectrum ZPA, as compared to results from use of the full-frame model. The simplified ductility analysis captures the approximate global displacement limit of the platform, and the general hysteretic envelope is similar to that estimated by static pushover analysis for two configurations of horizontal framing: weak and strong. However, it must be noted that the envelope curve estimated by the simplified method is very approximate, being a semi-empirical representation of the pushover behavior of the platform; member local demands will not be well-represented at large levels of global displacement.

MDOF response factors and elastic-to-inelastic deck displacement ratios derived from nonlinear time history analysis compare very well with factors and ratios selected based on the results of the global displacement ductility analyses. This indicates that the results of the static pushover analyses, modified by factors derived from the analysis of SDOF systems with hysteresis characteristics similar to those exhibited by the complete platform system, provide a good representation of the “effective” dynamic capacity of the platform. The factors link the static pushover analysis results to true dynamic behavior by implicitly accounting for the effects of time-varying structural yielding.

6.2 CASE STUDY #2: PLATFORM B

Platform B is an 8-leg drilling platform sited in 265 ft of water in San Pedro Bay off Southern California (see Figure 6-8). It was designed to support 80 24 inch-diameter conductors. The platform has two decks located at +45 ft MWL and +64 ft MWL respectively; the deck bay is braced. The jacket is battered 1:7 in the broadside direction, and 1:12 in the end-on direction. The main diagonals range from 20 inch-diameter (w.t. 0.75 inch) to 36 inch-diameter (w.t. 1.125 inches). The corner legs of the jacket are 71 inch-diameter (w.t. 1 to 2 inches), while the interior legs are 54 inch-diameter (w.t. 0.675 to 2 inches); the legs have heavy joint cans but are not grouted. The corner piles of the platform are 66 inch-diameter, and penetrate to 264 ft. The center piles are 48 inch-diameter, and penetrate to 232 ft. The soil at the site is predominantly clay (medium-stiff to stiff). The majority of the structural members are 36 ksi steel, while the piles are 50 ksi steel.

This platform was used as a case study in evaluating analysis methods used for the design of jacket-type platforms in earthquake-prone areas. Results of this case study were documented as part of an API-sponsored research project, API PRAC 26 (PMB, 1980 and 1981), and are used to assist in developing models for benchmarking the simplified approach.

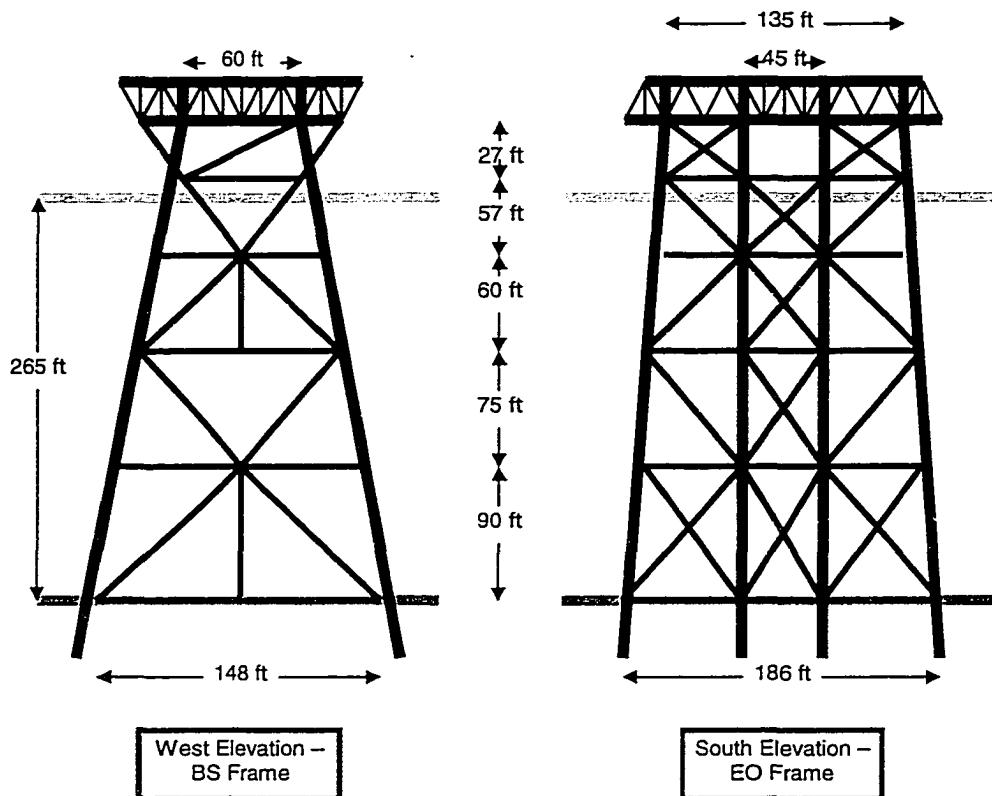


Figure 6-8: Platform B

6.2.1 Modal Analysis

Platform B was analyzed using the simplified modal procedure, and the results were compared to results from a 3-D frame analysis of the platform. In the 3-D model, braces were modeled using strut elements, while the legs and piles were modeled using beam-column elements. The lower deck were modeled simply with linear beams approximating the

major deck trusses; rigid stubs were extended to the elevation of the upper deck to allow for masses to be input at that level. Piles were modeled to a depth of 100 ft below the mudline, using beam-column elements supported by nonlinear springs. The axial behavior of the pile below 100 ft was approximated by use of a nonlinear truss element. Conductors were modeled by an equivalent single element at each jacket level, and modeled as a series of beam elements below the mudline supported by nonlinear springs. The conductors were left free to slip in the vertical direction.

Pile-head springs were derived for the simplified model by developing models of single piles based on P-Y and T-Z soil spring information contained in the PRAC report, and then analyzing these models using DRAIN-3DX for a series of unit loads. Linearized pile-head springs derived by this approach are shown below in Table 6-10, along with the approximate stiffness these springs correspond to.

Table 6-10: Pile-Head Axial and Lateral Stiffnesses

Pilehead Springs	Stiffness	Approximate k
Vertical – 66	4496 kips / in	1.6EA/L
Horizontal – 66	525 kips / in	$12EI/(0.15L)^3$
Vertical – 48	2825 kips/in	1.2EA/L
Horizontal - 48	315 kips / in	$12EI/(0.15L)^3$

Figures 6-9 and 6-11 show the lateral mode shapes and vibration periods of the platform as estimated by the simplified method, while Figures 6-10 and 6-12 show these same quantities as derived from the 3-D model (torsional vibration has been neglected in the simplified model, and hence is not reported for the 3-D model).

Comparing the results, it is seen that the simplified analysis underestimates the fundamental periods of vibration, with the differences on the order of 9% to 17%. The difference is due to the fact that the jacket is more prone to "warping" in shear due to ungrouted condition of the legs. The additional flexibility is not captured by the simplified method. For comparison purposes, both models were changed to reflect grouting; in this case the fundamental horizontal periods for end-on response were 2.24 sec (3-D) and 2.3 sec (simplified), while the fundamental periods for broadside response were 2.1 sec (3-D) and 2.2 sec (simplified). While the periods of higher modes are seen to drift apart as higher response modes are considered, and there are some slight differences in mode shape, the simplified analysis provides good estimates of vibration properties relative to those of the detailed analysis.

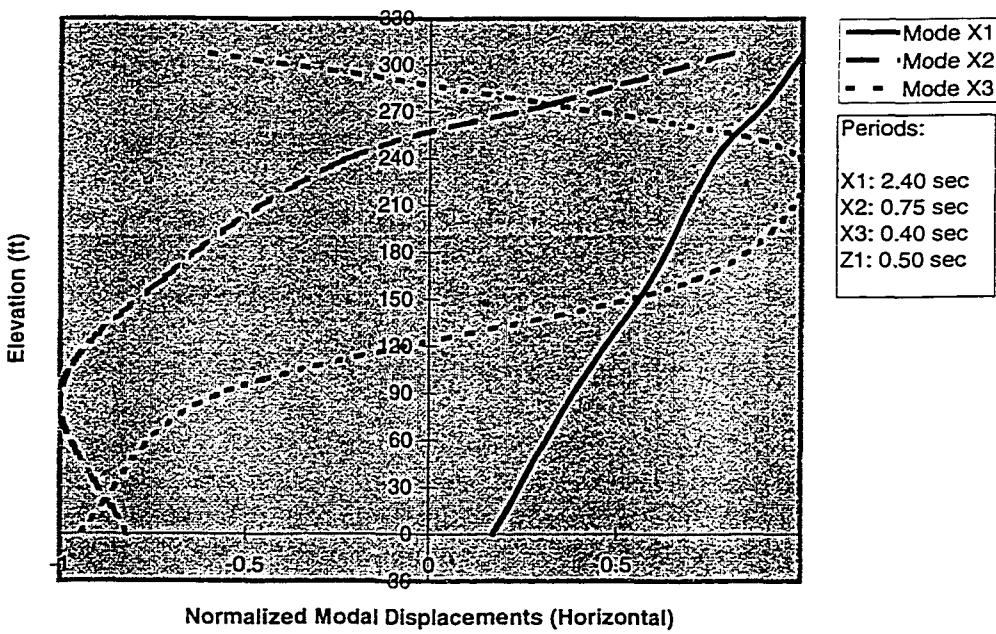


Figure 6-9: Platform B End-On Vibration Properties (Simplified Model)

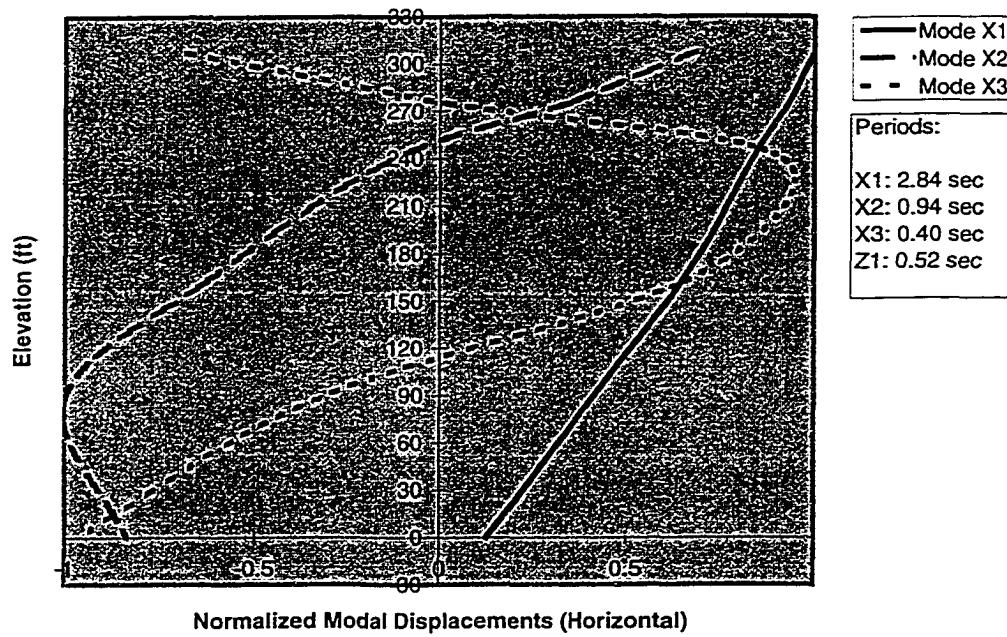


Figure 6-10: Platform B End-On Vibration Properties (3-D Model)

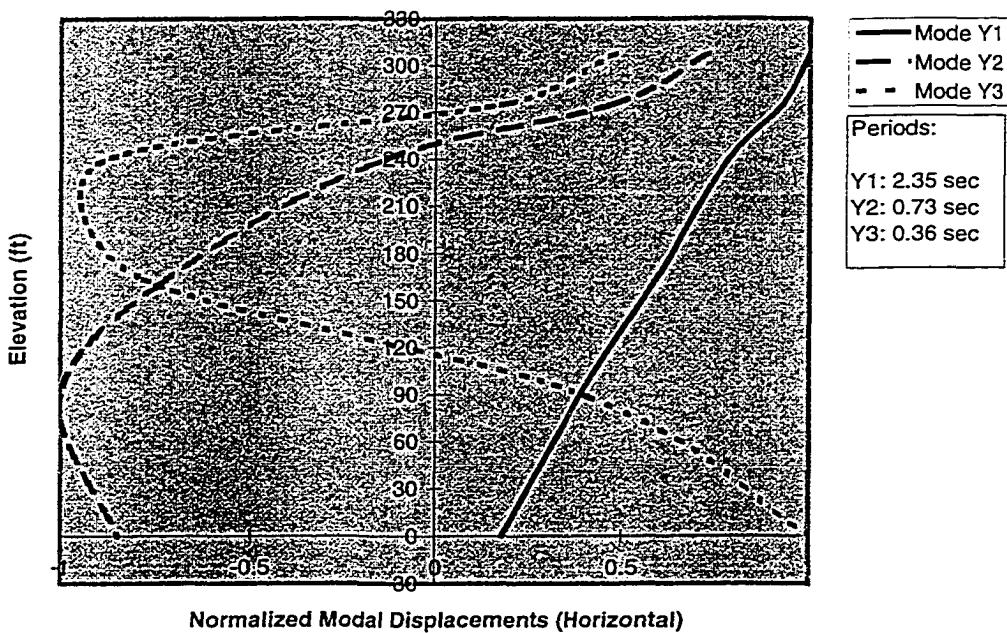


Figure 6-11: Platform B Broadside Vibration Properties (Simplified Model)

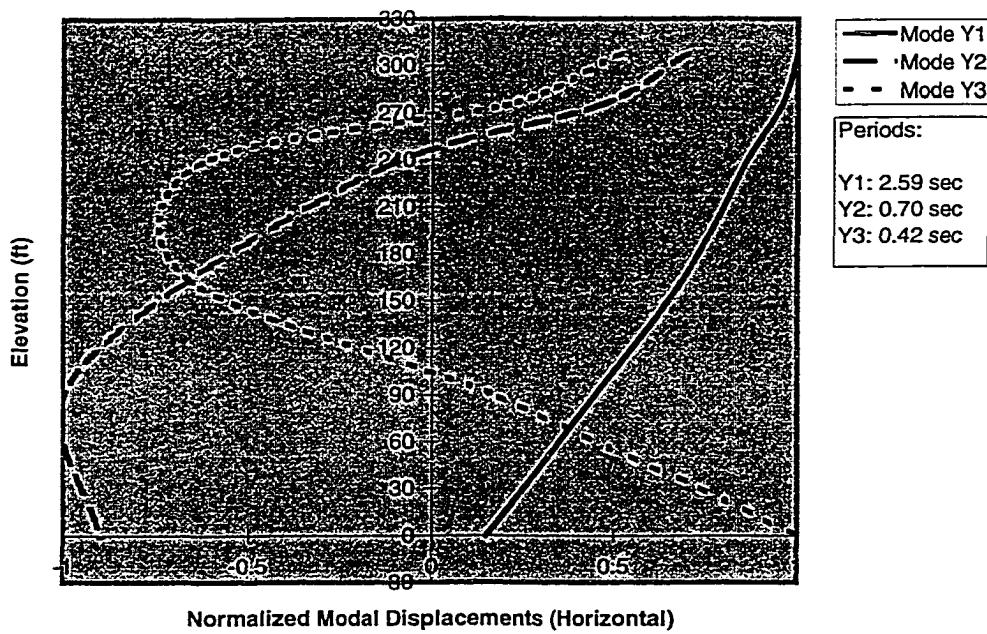


Figure 6-12: Platform B Broadside Vibration Properties (3-D Model)

6.2.2 Strength-Level Demand-Capacity Analysis

Modal forces were estimated for both models using the API (1993) Soil C response spectrum together with the appropriate modal properties. The SRSS combination rule was used in combining modal responses. Comparisons of the effective story shears and axial forces induced on the piles are shown in Table 6-11 and Figures 6-13 and 6-14 for a ZPA = 0.25 g. The shears shown in the figures are those associated with the directional response for all levels above the mudline; the mudline shear is found from a SRSS combination of the two lateral components, with the component perpendicular to the frame in question reduced by 33%. The estimated response spectrum shears are quite close, with those from the simplified model being slightly overestimated (by at most 15%) relative to those found from the 3-D analysis.

Table 6-11: Pile Loads on 66" ϕ

Pile Load (66" ϕ)	3D	Simple
Tension	4337	4571
Compression	7955	8036
Lateral	449	479

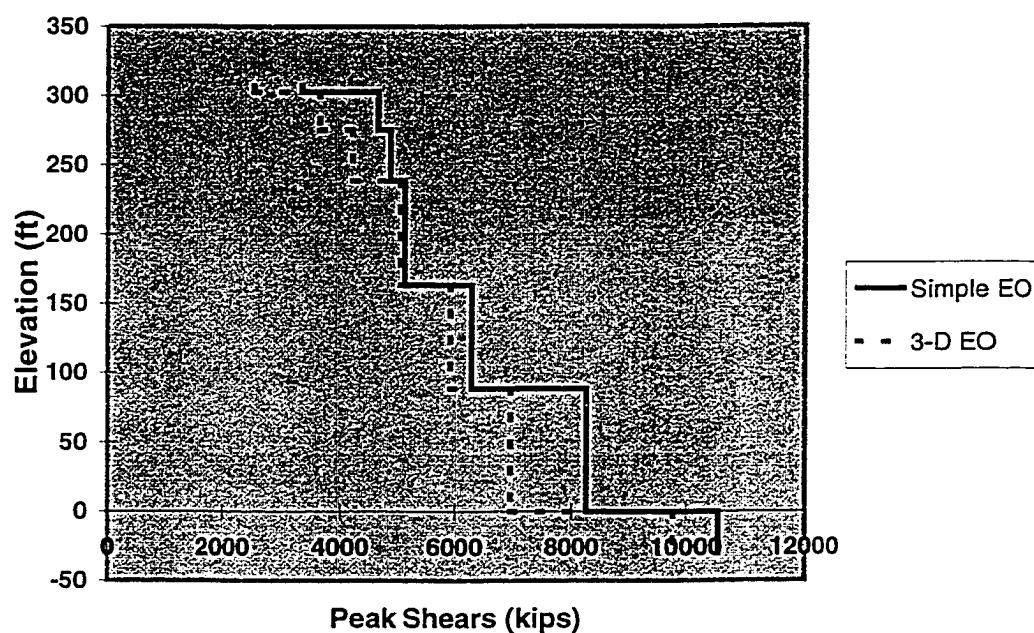


Figure 6-13: Comparison of Gross End-On Shears, ZPA = 0.25 g

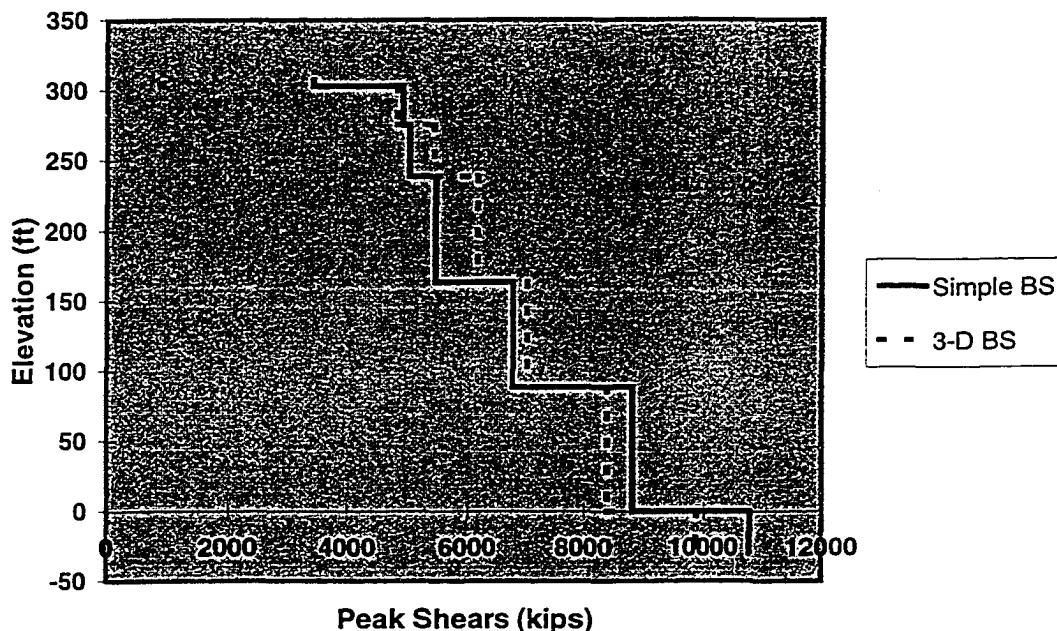


Figure 6-14: Comparison of Gross Broadside Shears, ZPA = 0.25 g

For demand-capacity assessment purposes, forces were assumed to act on all three axes simultaneously, with a proportion of 1.0/0.66/0.5 used to scale the primary lateral (in principal direction of excitation), secondary lateral (perpendicular to principal direction of excitation), and vertical components of load. Brace and pile capacities were estimated using the simplified procedures in Chapter Four; a local load associated with an acceleration of 0.625 g was used in determining brace axial capacities. Tubular joint capacities were not considered; the platform has heavy wall joint cans which are capable of supporting the full tension capacities of attached braces.

Using the simplified loads and capacities, the limiting load case was found to be that in which the major axis of excitation was end-on. For this load case, an earthquake intensity of

0.34 g results in the yielding of a corner pile in compression. To show the relative strengths of the different platform components at this level of load, end-on and broadside demand-capacity curves are shown in Figures 6-15 and 6-16. Examining the demand-capacity curves, it appears likely that the next elements to yield would be braces in the first or third jacket bays in the end-on frames.

Strengths for elements in the 3-D model were taken from PMB (1980, 1981) and from relationships documented by Marshall, et al. (1977). The 3-D analysis also indicates the load case in which the major axis of excitation is end-on governs capacity; a corner pile will be the first structural member to fail. Using the same loading strategy as for the simplified analysis, this damage occurs for loads corresponding to a spectrum ZPA of 0.38 g. The simplified analysis results are in very good agreement with the results from the 3-D frame analysis, with a difference in earthquake damage intensity of 10%.

The damage trends identified by the response spectrum analyses are in qualitative agreement with results from time history analyses documented by PMB (1981). These analyses indicated the platform would, for the case of principal excitation on the end-on axis, undergo yielding in the foundation, and suffer some minor damage to diagonal braces in the jacket.

Platform B was also used as a test case for benchmarking the equipment-structure interaction procedure described in Chapter Four used for determining the local load due to brace lateral acceleration. To qualitatively assess the significance of local acceleration load, the axial capacities of braces in Platform B were determined for three cases: (1) ignoring local lateral

loads, (2) including local lateral loads calculated by the simplified method of Chapter Four, and (3) including local loads originally used in the platform design.

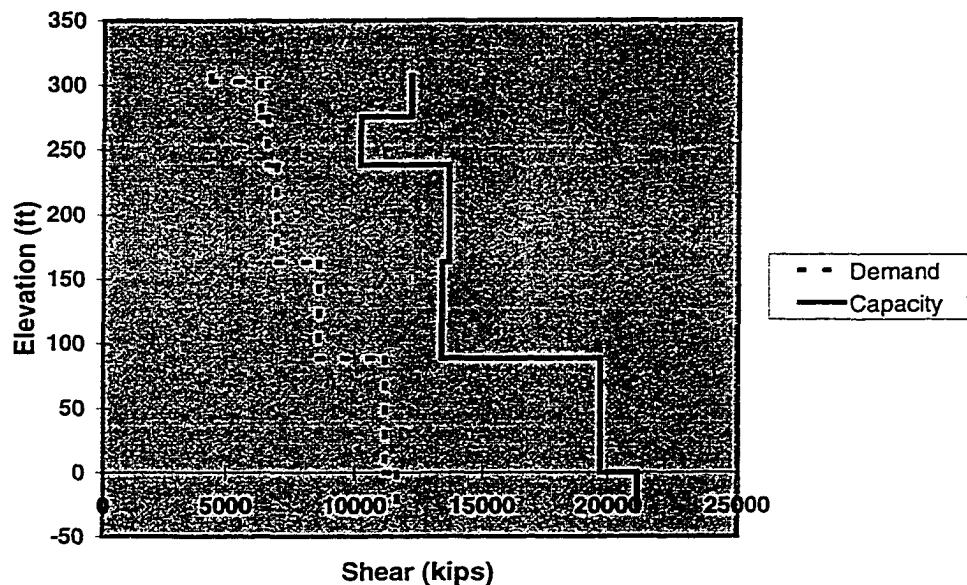


Figure 6-15: Platform B Gross Shear Demand – Capacity Profile from Simplified Method,
ZPA = 0.34 g, End-On Frames

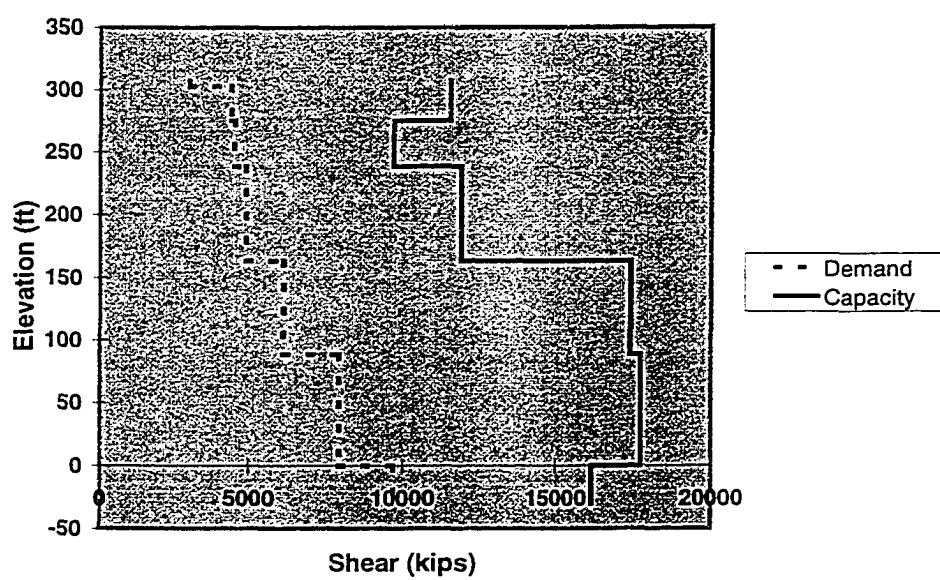


Figure 6-16: Platform B Gross Shear Demand – Capacity Profile from Simplified Method,
ZPA = 0.34 g, Broadside Frames

The characteristics of bracing members in the platform are shown below in Tables 6-12 and 6-13. As this platform has heavy-wall joint cans, end conditions of the braces were assumed to be fixed. The periods of the braces are for the most part very low compared to those of the structure, thus indicating that response will approach the limiting condition of very stiff equipment. However, several braces in the lower jacket bays (broadside frames) have periods close to the periods of several of the higher structure modes, which will result in some amplification.

Brace buckling capacities were determined for the bracing members in Tables 6-12 and 6-13 for three cases of local load: (1) zero local load, (2) local load determined using the equipment-structure interaction method, and (3) a local load associated with a 0.625 g acceleration perpendicular to the axis of the brace. The constant 0.625 g acceleration envelope was estimated by determining response spectra for the floor of each jacket bay associated with three earthquake time histories, and then taking the peak spectral acceleration value (out of all the spectra) associated with the period range covering brace lateral periods. In this case, the peak value was chosen for a brace period of 0.5 seconds, which was deemed a conservative assumption (this placed the brace vibration period close to several of the significant vibration periods of the platform).

For the local load determined through application of the equipment-structure interaction method, acceleration contributions were determined based on excitation of both the two principal horizontal directions and the vertical direction, using the API (1993) Soil-B spectrum with a PGA of 0.25 g. The spectrum accelerations for the different directions were

calculated assuming a ratio of 1.0 (horizontal in-plane with member):0.66 (horizontal perpendicular to member):0.5 (vertical) between the different spectrum scale factors. For the sake of simplicity, the local acceleration components were all assumed to be perpendicular to the axis of the brace irrespective of the structure mode associated with the acceleration component. Acceleration components appropriate to each mode, along with the modal participation factors, are shown in Table 6-14. Horizontal accelerations are dominated by the first two horizontal modes, while the vertical accelerations are quite large in the fundamental mode.

Table 6-12: Tubular Brace Characteristics, End-On Frames

Location	<i>D</i> (inches)	<i>t</i> (inches)	<i>L</i> (inches)	<i>T</i> (sec)
Deck Bay	24	0.5	315	0.02
1 st Jacket Bay	28	0.75	846	0.15
1 st Jacket Bay	20	0.75	395	0.04
2 nd Jacket Bay	36	0.75	958	0.16
2 nd Jacket Bay	24	0.75	434	0.04
3 rd Jacket Bay	36	1.0	1144	0.21
3 rd Jacket Bay	26	0.75	511	0.06
4 th Jacket Bay	36	1.0	701	0.08
4 th Jacket Bay	24	0.75	701	0.12
4 th Jacket Bay	26	1.0	608	0.08

Table 6-13: Tubular Brace Characteristics, Broadside Frames

Location	<i>D</i> (inches)	<i>t</i> (inches)	<i>L</i> (inches)	<i>T</i> (sec)
Deck Bay	24	0.75	898	0.13
1 st Jacket Bay	28	0.75	751	0.12
1 st Jacket Bay	24	0.625	376	0.04
2 nd Jacket Bay	30	0.75	944	0.18
3 rd Jacket Bay	34	1.0	1088	0.20
3 rd Jacket Bay	36	1.0	1088	0.19
4 th Jacket Bay	36	1.0	1426	0.33

Table 6-14: Modal Acceleration Components for Southern California Example Platform

	Mode 1 - EO	Mode 1- BS	Mode 2 - EO	Mode 2 - BS	Mode 3 - EO	Mode 3 - BS	Mode 1 – Z
T (sec)	2.84	2.59	0.94	0.70	0.40	0.42	0.52
Γ (part. factor)	1.26	1.24	0.57	0.52	0.24	0.30	1.11
\ddot{u}_D (g)	0.13	0.13	-0.16	-0.16	0.10	-0.08	0.27
\ddot{u}_1 (g)	0.12	0.13	-0.08	-0.11	0.00	-0.03	0.26
\ddot{u}_2 (g)	0.11	0.11	0.03	0.02	-0.14	0.09	0.24
\ddot{u}_3 (g)	0.09	0.09	0.15	0.15	-0.10	0.10	0.22
\ddot{u}_4 (g)	0.05	0.06	0.23	0.23	0.05	-0.03	0.20
\ddot{u}_F (g)	0.02	0.02	0.19	0.21	0.14	-0.15	0.18

Local acceleration components determined by the equipment-structure interaction method for the different braces are shown in Tables 6-15 and 6-16, along with the axial capacities associated with the three conditions. The structure acceleration corresponding to the top of each bay was used to determine the response of braces within a bay.

The 0.625 g local acceleration which was originally used to envelope the brace accelerations at the design stage is conservative relative to the specific values calculated explicitly considering brace-structure interaction for all braces in the platform. Local load based on the constant acceleration results in axial capacity reductions of up to 15%; using the local accelerations specific to each brace results in capacity reductions on the order of up to 7%. This difference is more significant than for Platform A; for structures with long, flexible braces, it will likely be advantageous from an assessment standpoint to expend the additional effort to better estimate the local load on the braces.

Table 6-15: Brace Axial Capacities, End-On Frames

Location	<i>D</i>	<i>t</i>	Local \ddot{u} (g)	P_u (kips) ₁	P_u (kips) ₂	P_u (kips) ₃
Deck Bay	24	0.5	0.38	1796	1791	1785
1 st Jacket	28	0.75	0.33	2678	2604	2475
1 st Jacket	20	0.75	0.33	2095	2085	2066
2 nd Jacket	36	0.75	0.37	3716	3584	3438
2 nd Jacket	24	0.75	0.37	2586	2574	2555
3 rd Jacket	36	1.0	0.44	4662	4348	4161
3 rd Jacket	26	0.75	0.44	2784	2758	2738
4 th Jacket	36	1.0	0.41	5171	5080	5025
4 th Jacket	24	0.75	0.41	2372	2280	2227
4 th Jacket	26	1.0	0.41	3587	3549	3514

Table 6-16: Brace Axial Capacities, Broadside Frames

Location	<i>D</i>	<i>T</i>	Local \ddot{u} (g)	P_u (kips) ₁	P_u (kips) ₂	P_u (kips) ₃
Deck Bay	24	0.75	0.38	2272	2217	2153
1 st Jacket	28	0.75	0.33	2828	2786	2703
1 st Jacket	24	0.625	0.33	2066	2045	2004
2 nd Jacket	30	0.75	0.35	3007	2936	2842
3 rd Jacket	34	1.0	0.44	4377	4194	4049
3 rd Jacket	36	1.0	0.44	4736	4558	4417
4 th Jacket	36	1.0	0.42	4380	4092	3791

6.2.3 Global Ductility Analysis

The simplified methods in Chapter Four for predicting ductility capacity were intended to be applied on the major axes of a platform; however, for instances in which off-axis response governs capacity (likely for weak foundations and unbraced deck bays), it is possible to approximate the post-yield response by considering the yielding component to behave as a rigid section whose displacements or rotations under the individual components of principal axis response are combined for the total displacement or rotation demand.

The ductility analyses considered excitation acting concurrently on all three axes of the platform, with vertical excitation acting downwards. Loads patterns for each direction were based on fundamental mode forces for each principal direction; the scaling between load patterns was 1.0 end-on/0.66 broadside/0.5 vertical. The global load-displacement behavior determined in the simplified analysis was compared to results from a static pushover analysis performed using DRAIN-3DX. While DRAIN-3DX does not have a Marshall-type strut element, indications from both the PMB (1980, 1981) reports and the modal analyses were that yielding in the foundation would govern capacity. Hence, the error of using bilinear strain-hardening struts for modeling tubular braces was accepted.

The simplified analysis indicated the first member in the platform to yield would be a corner pile (by failure in the supporting soil); this event occurred at a total resultant (from end-on and broadside directions) base shear of 12,100 kips. This base shear corresponds to the fundamental end-on and broadside load components being scaled with an API Soil C spectrum ZPA of 0.38 g (S_a for the fundamental end-on period is 0.29 g). This is 11% higher than the ZPA estimated including higher modes, indicating modes beyond the fundamental modes on each axis do not contribute significantly to initial yielding. Using DRAIN-3DX, the resultant base shear at yield was 13,250 kips; S_a for the fundamental end-on period in this case is 0.32 g.

Figures 6-17 and 6-18 depict the individual principal axis displacements and base shear components for Platform B for both the simplified analysis and the DRAIN-3D analysis. The simple model is slightly stiffer than the 3-D model, hence overall displacement magnitude is

less. Displacement beyond the yielding of the corner pile was estimated by assuming the foundation would continue to rotate as a rigid base, gradually forming a plastic mechanism. Loading continued until a second pile yielded completely; at this point, the resultant base shear had increased to 18,150 kips, and the platform had developed a global displacement ductility (as measured by resultant deck displacement at pile yield to resultant deck displacement at second pile yield) of 1.52. At this point, the load is high enough to cause buckling of end-on braces in the first jacket bay.

For the 3-D model, near-field soils begin yielding at a resultant base shear of 6,670 kips. Soil yielding continues until the corner pile forms a plastic mechanism, at which point gross nonlinearity becomes evident in the global hysteresis plots. If the point of corner pile yielding is taken as a reference, the 3-D model indicates Platform B is able to develop a global displacement ductility of 1.45 at the point of the yielding of a second pile, and the buckling of end-on braces in one frame in the first, second, and third jacket bays. As the model did not have Marshall-type struts, loading was halted after the braces developed local ductility demands of two.

While the general trend of yielding in the platform identified by the simple method for this load pattern is similar to that identified by the static pushover analysis, the estimated strength predicted by the simplified method at the point of second pile yielding is higher, and the change in stiffness following yielding is less pronounced. These differences are due to the assumption that the foundation rotates as a rigid section, as opposed to sections of it becoming more flexible as yielding occurs. More importantly, the global ductility analyses of

Platform B highlights some of the general difficulties in using static methods to assess potential earthquake damage in large, complicated structures which do not exhibit sudden yielding. The gradual yielding of soil, while not greatly affecting the hysteresis curve, indicates there will be increases in effective damping due to local soil plasticity. The magnitude of this effect cannot easily be judged from the static pushover results. Also, the indicated yield level and post-yield behavior are quite sensitive to the magnitude of the load components used in the analyses. If the end-on and broadside load components were considered to be similar in amplitude and phase, the yield capacity of the platform would be smaller. Similarly, if the end-on and broadside components are considered to be significantly out-of-phase, the yield capacity will be larger; damage to the steel portions of the structure will occur sooner for these single-axis loads. When performing an assessment of this type, care must be taken to choose a load pattern which will capture the most severe failure modes. While a given direction might be strong relative to others, it could have poorer post-yield characteristics.

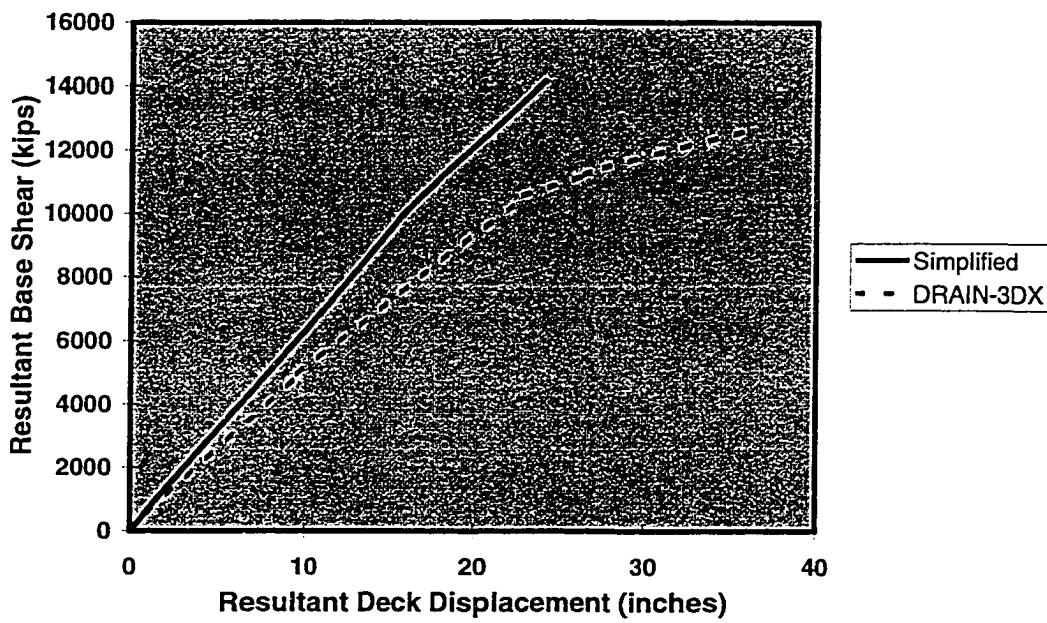


Figure 6-17: Global Load-Displacement Behavior of Platform B, End-On Components

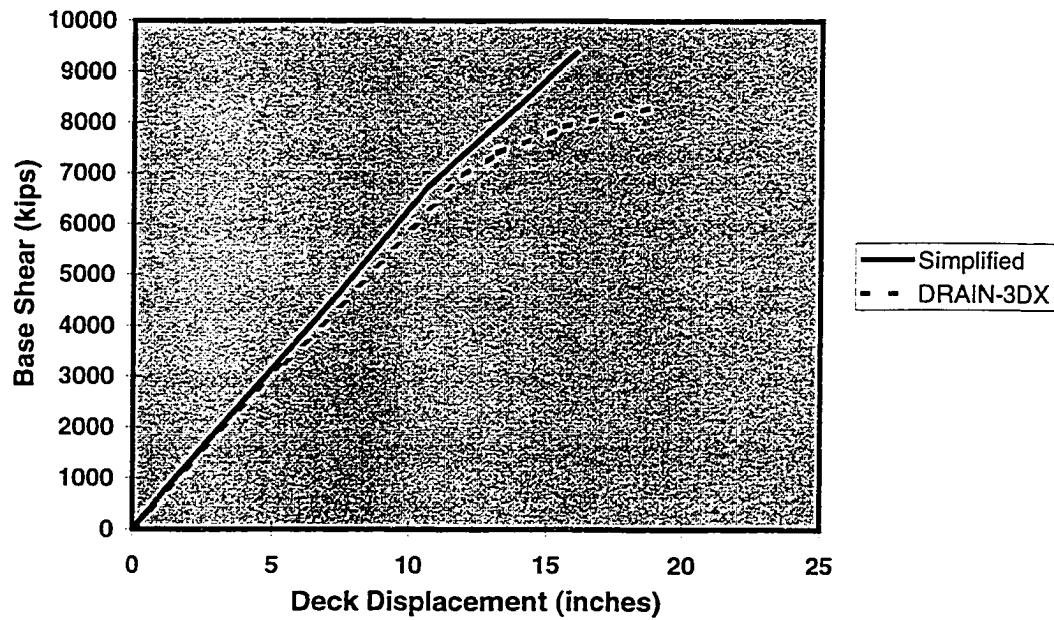


Figure 6-18: Global Load-Displacement Behavior of Platform B, Broadside Components

6.2.4 Ductility-Level Demand-Capacity Analysis

Ductility-level comparisons were performed in two ways for Platform B: (1) by judging the effective load reduction R implied by the simplified displacement ductility analyses against scale factors F_μ determined from MDOF nonlinear time history analyses, and (2) by judging the displacement modification F_A implied by the simplified displacement ductility analyses against the ratio of the deck displacement found from the MDOF nonlinear time history analysis to the MDOF first mode component of displacement (assuming linear elastic behavior) for the same time history. Also, the mean fundamental lateral mode spectral acceleration S_a (assuming 5% damping) which represented the onset of nonlinear behavior in the platform was determined from the time history analyses, to compare with the value determined in the global ductility analysis; this comparison checks the validity of indexing on first mode response to characterize platform strength capacity.

The DRAIN-3DX model used in Section 6.2.3 was utilized to determine F_μ , the effective load reduction a nonlinear MDOF system is entitled to based on ductile action, and to evaluate the relationship between inelastic and equivalent elastic (first mode) deck displacements. Rayleigh damping was assumed, with mass and stiffness-proportional coefficients balanced such that 5% critical damping was achieved in the first two fundamental lateral modes. DRAIN-3DX does not have spring elements capable of modeling strength degradation in near-field soils; therefore soil behavior was modeled as elastic-plastic. However, this platform is founded on fairly competent soils (stiff clays), where little degradation would be expected.

The model was analyzed using a series of nine earthquakes (see Table 6-8); the major component of motion was used on the end-on axis. Three damage measures, were used as criteria for F_μ : brace local ductility (using one half the cyclic ductility limit from Chapter Four as a target), global deck displacement (using the peak X displacement from the static pushover analysis as targets), and pile axial ductility (using a limit of two as a target). The ratio of inelastic to elastic displacement was averaged for an overload (using $S_{a-yield}$ from the static pushover analysis as a reference point) of two. The mean values of F_μ for each damage measure, and the ratio of inelastic to elastic deck displacement, are shown in Table 6-17.

Table 6-17: $S_{a-yield}$, F_μ and Deck Displacement Ratio for Platform B

Factor	Yield	Target	$S_{a-yield}$ (g)	COV	Mean	COV
F_μ Global	X=23"	X=33"	0.33	0.10	1.68	0.19
F_μ Local (brace)	buckling	$-\mu=2.5$	0.38	0.12	1.41	0.16
F_μ Local (pile)	full plast.	$\mu=2$	0.38	0.10	1.33	0.15
$\Delta_{inelastic}/\Delta_{elastic}$	-	-	-	-	0.85	0.20

While the reference yield end-on deck displacement used with the dynamic analyses was taken to be identical to the end-on deck displacement at the point of significant nonlinearity in the DRAIN-3DX static pushover analysis (which corresponded to the full yielding of soil supporting a corner pile), the dynamic analyses did not typically show full pile yielding at this point. Instead, pile yielding and brace buckling in the jacket were initiated at slightly higher levels of excitation. This difference is the result of two factors: the gradual yielding in the soils around the piles, which effectively increases damping in the platform, the fact that the Y-component of excitation is not always in phase with the X-component at a significant amplitude.

The brace buckling in the jacket was largely confined to the end-on frames, and was distributed between all four jacket bays. The buckling was predicted by the static pushover analyses to occur after the first complete yielding of a corner pile; however, the dynamic analyses indicated it was more likely to occur at the same level of excitation.

From the results of the global ductility analyses in Section 6.2.3, it would be reasonable to, at a minimum, classify the platform as bilinear non-degrading in that mode of deformation. Referring to Figures 5-3 and 5-59, SDOF non-degrading systems with 5% and 10% critical damping, it is reasonable to expect an effective load reduction on the order of 1.5. This value is in reasonable (conservative) agreement with that calculated from the dynamic analyses of Platform B using global end-on deck displacement as a measure. The local displacement ductility criteria for braces was achieved at a level of deck displacement close to 33 inches in nearly all cases; hence, it is not surprising that these two measures indicate consistent levels of equivalent elastic load. Using global deck displacement as a criteria, the platform will reach this displacement at a level of end-on fundamental mode spectral excitation corresponding to $1.68 \times 0.33 \text{ g} = 0.55 \text{ g}$. Using brace local displacement ductility as a criteria, this level is $1.42 \times 0.38 \text{ g} = 0.54 \text{ g}$. Using local axial ductility limit of two results in a smaller allowable level of excitation (0.51 g); however, it was been assumed the piles are capable of achieving higher local axial ductility than this for the purpose of the analysis. As noted in Chapter Four, pile axial ductility limits are very difficult to quantify, and will likely depend upon stability and the occurrence of local damage to elements forced into the foundation soil.

The ratio of inelastic to elastic displacements is seen to be less than one, whereas through referencing Figure 5-4, this ratio would be expected to be unity or slightly higher. The discrepancy is due to the gradual yielding of soil along the piles, which increases effective damping. As noted in Chapter Five and by others, damping is most helpful when displacement ductility demands are low, which is the situation here.

6.2.5 Platform B: Summary of Results

The simplified method used for estimating platform vibration properties compares reasonably well with those calculated by analyzing a full-frame model of the platform; period estimates were within 17% of those found using the frame model. Differences were attributed to the lack of accounting for the overall flexibility of a large, ungrouted jacket; the jacket is able to warp due to the lower leg stiffness.

Using the API Soil C response spectrum as a basis for loads, the simplified demand-capacity assessment provides a capacity estimate which is fairly close to that estimated from the 3-D analysis; a similar failure mode is identified using a similar load set.

The global displacement ductility analysis highlights the limitations of both applying a simplified method to a structure which has gradual yielding and multi-axis response, and to the application of equivalent static methods in general. While similar levels of global displacement ductility were predicted for various events along the hysteresis path, the

simplified method substantially overestimated the reserve strength of the platform. Foundations on large platforms will not likely remain plane after loading commences.

While it has been stated in previous chapters that the presumed ductile behavior is sensitive to the load pattern, this is quite evident in the results of sections 6.2.3 and 6.2.4. The initial failure mode was assumed to be pile yielding; however, the dynamic analyses indicated pile yielding and brace buckling would likely occur at similar load levels. Soil yielding, while not significantly changing the stiffness of the platform system, will result in noticeable energy dissipation. This effect is not represented in the SDOF systems studied earlier, which exhibit a sudden change in stiffness when yielding begins; this can be compensated for by using a response factor with higher initial damping. Differences due to gradual yielding are likely to be significant at low levels of global ductility, when the platform system is still developing some reserve strength.

6.3 CASE STUDY #3: PLATFORM C

Platform C is a 12-leg production platform sited in 257 ft of water in San Pedro Bay off Southern California (see Figure 6-19). The platform has two decks located at +45 ft MWL and +71 ft MWL respectively; the deck bay is braced. The jacket is battered 1:10 in the broadside direction, and 1:14 in the end-on direction. The main diagonals range from 24 inch-diameter (w.t. 0.625 inch) to 36 inch-diameter (w.t. 0.75 inches). The exterior legs of the jacket are 53 to 54 inch-diameter (w.t. 0.75 to 1 inch), while the two interior legs are 47 inch-diameter (w.t. 0.675 to 1 inch); the legs have heavy joint cans but are not grouted. The exterior piles of the platform are 48 inch-diameter; the corners penetrate to 252 ft, while the

remainder penetrate to 221 ft. The interior piles are 42 inch-diameter, and penetrate to 200 ft. The soil profile at the site is the same as for Platform B (Section 6.2). The majority of the structural members are 36 ksi steel, while the piles are 42 ksi steel.

6.3.1 Modal Analysis

Platform C was analyzed using the simplified modal procedure, and the results were compared to those obtained from a modal analysis conducted using the DRAIN-3D model. In the 3-D model, braces were modeled using simple strut elements, while the legs and columns were modeled using beam-column elements. The decks were modeled with beam elements approximating the stiffness of the deck trusses. Piles were modeled using a set of equivalent nonlinear springs representing pile-head behavior derived from models of single piles. P-Y and T-Z soil spring information contained in the PRAC report on Platform B (PMB, 1980) was used to develop appropriate springs for the pile analysis (Platform B and Platform C are located close to one another). Linear equivalents to these pile-head springs were used in the simplified analysis (Section 6.2, Table 6-10).

Figures 6-20 and 6-22 show the lateral mode shapes and vibrations periods of the platform derived from application of the simplified method, while Figures 6-21 and 6-23 show these same quantities as derived from the 3-D model; again, torsion has been neglected for the simplified model and hence is not reported for the 3-D model.

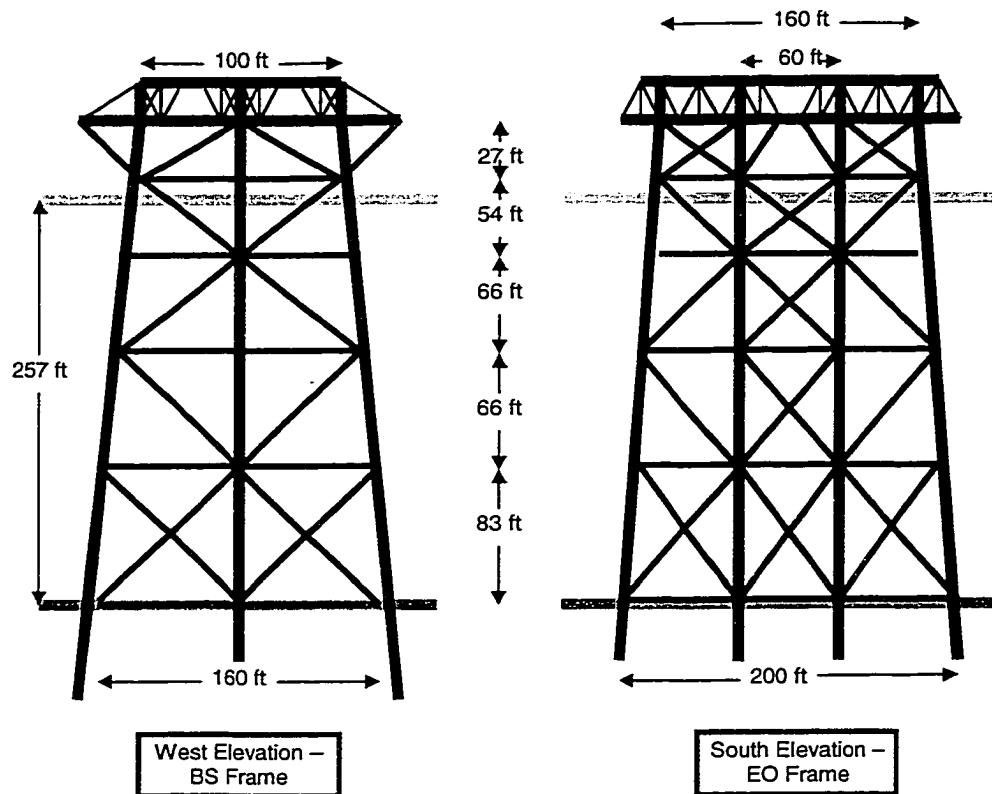


Figure 6-19: Platform C

The fundamental periods estimated by the simplified method are in good agreement with those from the 3-D model, the largest difference being 11% low. There is progressive deviation in period and mode shape for higher modes; however, the majority of response is in the fundamental modes. The variation, while slightly less pronounced than that for Platform B, is attributed to the size of the jacket and the lack of grout.

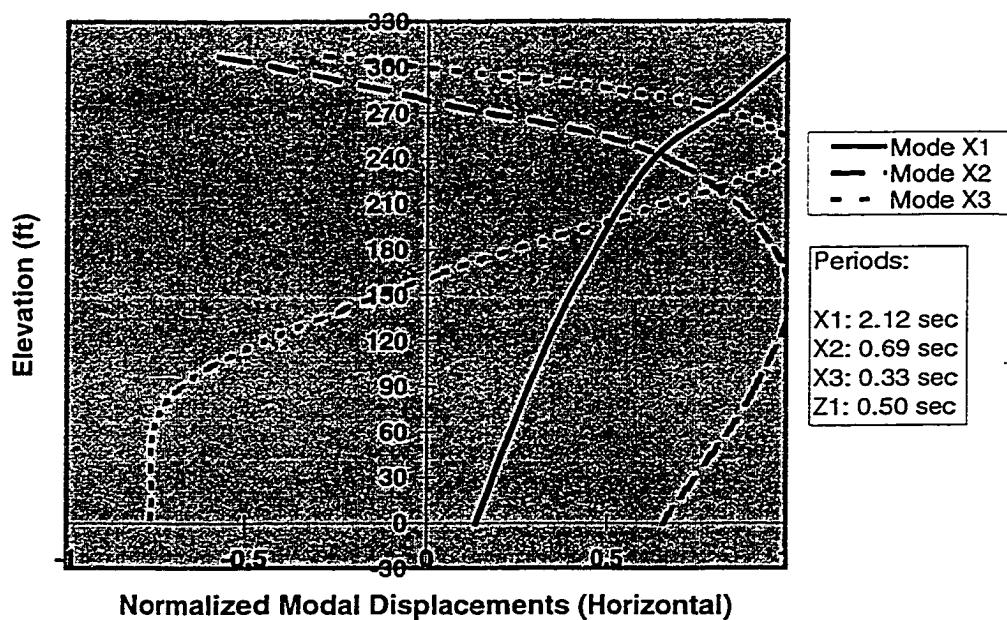


Figure 6-20: Platform C End-On Vibration Properties (Simplified Model)

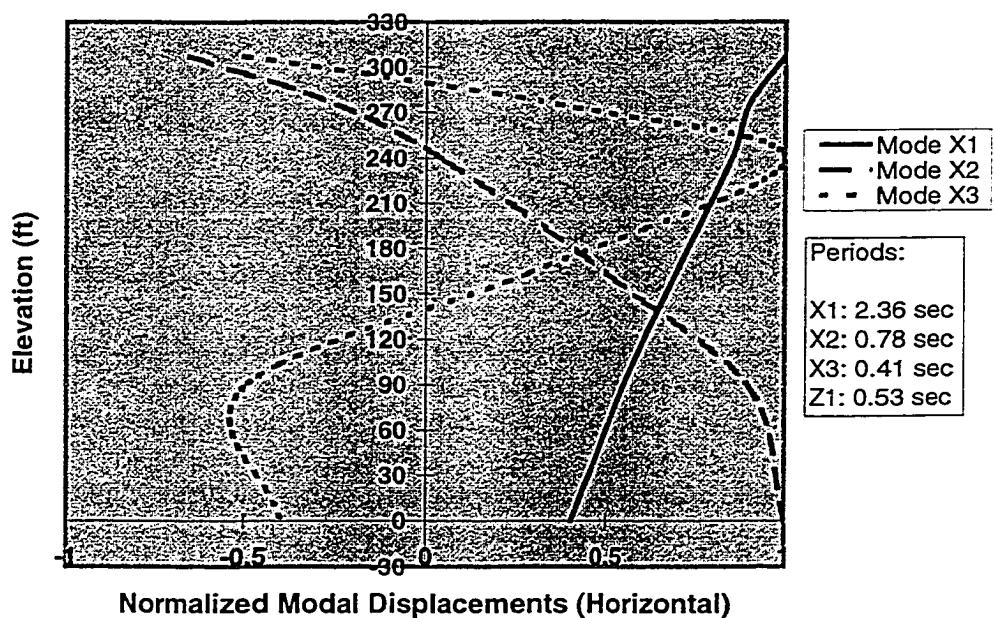


Figure 6-21: Platform C End-On Vibration Properties (3-D Model)

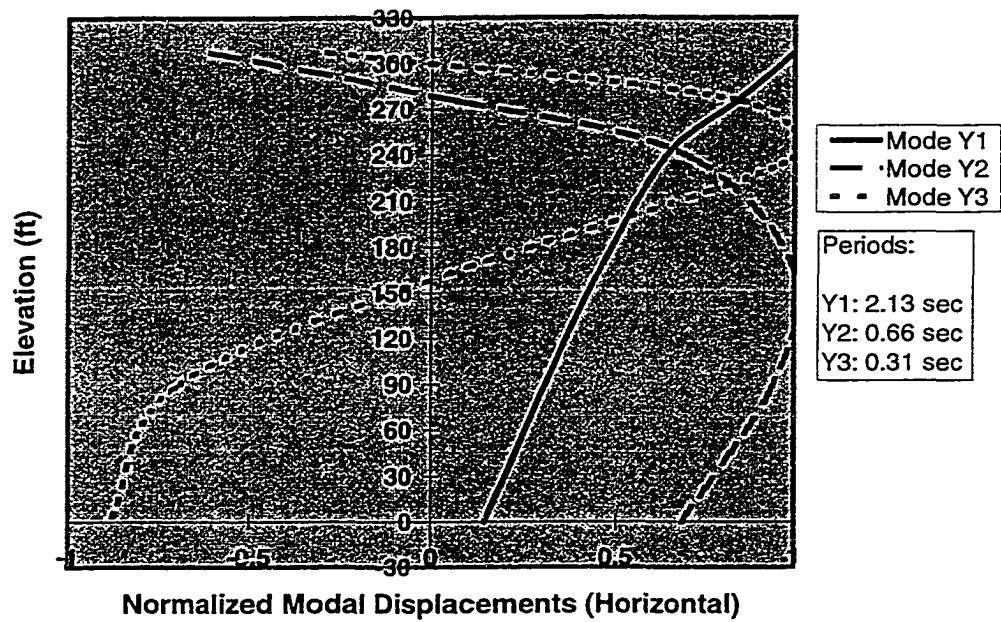


Figure 6-22: Platform C Broadside Vibration Properties (Simplified Model)

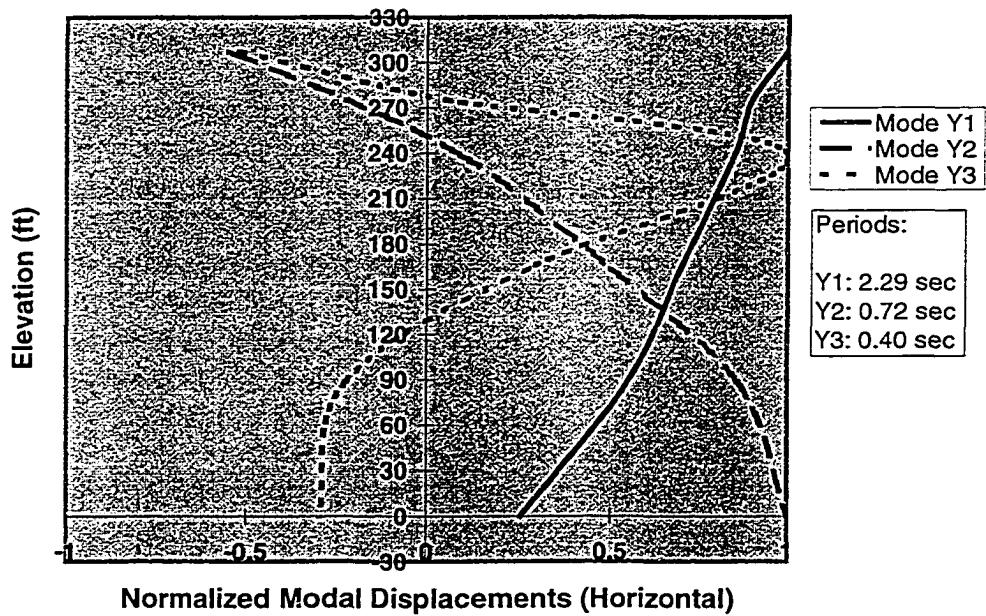


Figure 6-23: Platform C Broadside Vibration Properties (3-D Model)

6.3.2 Strength-Level Demand-Capacity Analysis

Modal forces were estimated for both models using the API (1993) Soil C response spectrum together with the appropriate modal properties. The SRSS modal combination rule was used in combining modal responses. A comparison of the effective story shears and axial forces induced in the piles are shown in Table 6-18 and Figures 6-24 and 6-25 for a response spectrum ZPA = 0.25 g. The shears shown in the figures are those associated with the primary lateral load for all levels above the mudline; the mudline shear is found from an SRSS combination of the two lateral components, with the component perpendicular to the frame in question reduced by 33%. The estimated response spectrum shears and pile loads are quite close, with those from the simplified model being slightly overestimated (by at most 9%) relative to those from the 3-D analysis.

Table 6-18: Pile Loads on 48" ϕ

Pile Load (48" ϕ)	3D	Simple
Tension	2940	3180
Compression	5860	5980
Lateral	780	850

Demand-capacity analysis was conducted using the simplified methods for both major horizontal axes of the platform. Forces were assumed to act on all three axes simultaneously, with a proportion of 1.0/0.66/0.5 used to scale the primary lateral, secondary lateral, and vertical components. Diagonal brace capacities were determined both including and excluding local acceleration loads of 0.625 g. As this platform has canned joints capable of developing the full tension capacities of attached braces, joint capacities are not shown.

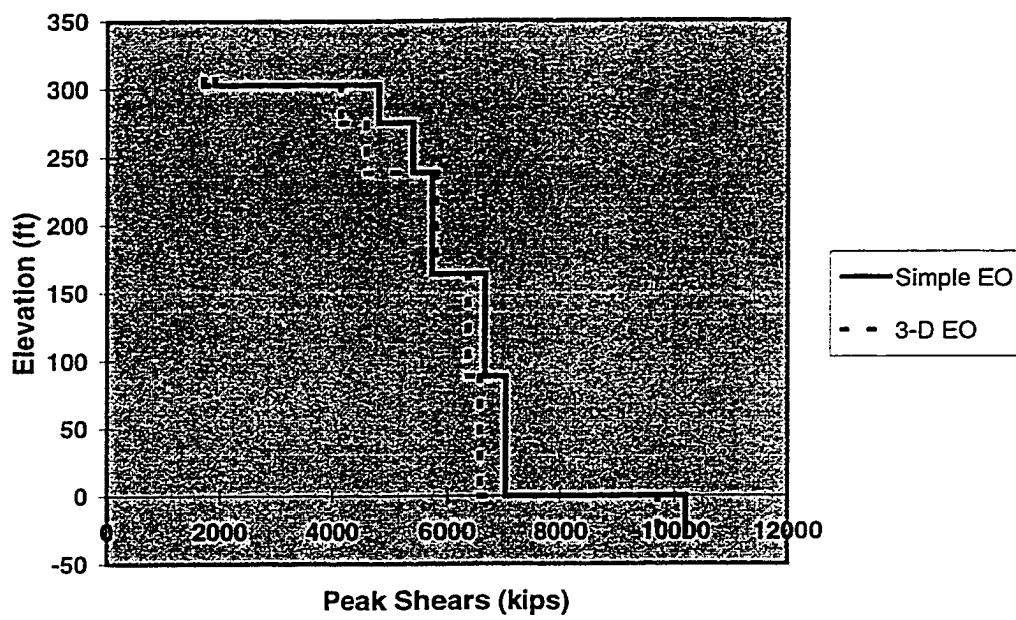


Figure 6-24: Comparison of Gross End-On Shears, ZPA = 0.25 g

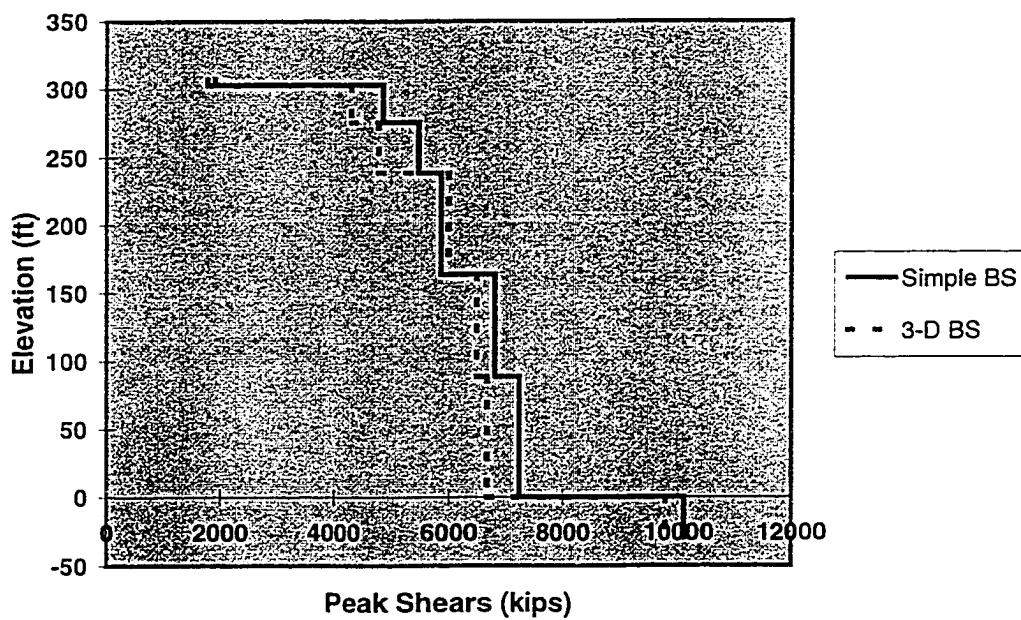


Figure 6-25: Comparison of Gross Broadside Shears, ZPA = 0.25 g

The simplified method identifies pile yielding/hinging as governing the strength of the platform, however, the axial capacity of the pile (based on the soils) is also close to being exceeded. As the simplified approach approximates the interaction between pile bending and axial stress components (axial load is assumed to be shed to the soil very quickly, and hence not affect the formation of the second hinge), the ductility each mechanism can develop should be evaluated. When the major axis of excitation is end-on, an earthquake intensity of 0.27 g provides the loads necessary to initiate the foundation lateral failure mechanism; a fully-plastic mechanism based on pile hinging will form at an intensity of 0.34 g. Behavior for major excitation on the broadside axis is very similar, due to similarities in load magnitude between the two directions. End-On and broadside demand-capacity curves are shown in Figures 6-26 and 6-27 for loads generated by a ZPA of 0.34 g. The gross deck and jacket bay shear capacities are seen to be moderately affected by the local acceleration load on braces; the presence of this load can change the strength of the most likely member to fail by as much as 20%, leading to similar changes in platform shear capacity. From these curves, the next elements to yield would likely be the braces in the second and third jacket bays of the end-on frames.

Strengths for elements in the 3-D model were determined using information from PMB (1980, 1981) and from relationships documented by Marshall, et al. (1977). The 3-D analysis also indicates the load case in which the major axis of excitation is end-on governs capacity; the failure mode in this analysis was lateral failure of a corner pile, although the pile axial capacity was also close to being exceeded (resultant loads are close to the gross pile axial and lateral capacities). Using the same loading strategy as the simplified method, this will occur

at an earthquake intensity of 0.30 g. The simplified analysis under-predicts the capacity of the platform by approximately 11%; this difference can be traced to two factors: the over-prediction of the base shear by the simplified modal analysis method, and a slightly conservative estimate of pile lateral strength from the simplified method as compared to the pile lateral strength estimated from the single pile analysis. Both analyses identify the foundation (either lateral or overturning) as the weak link in the platform system.

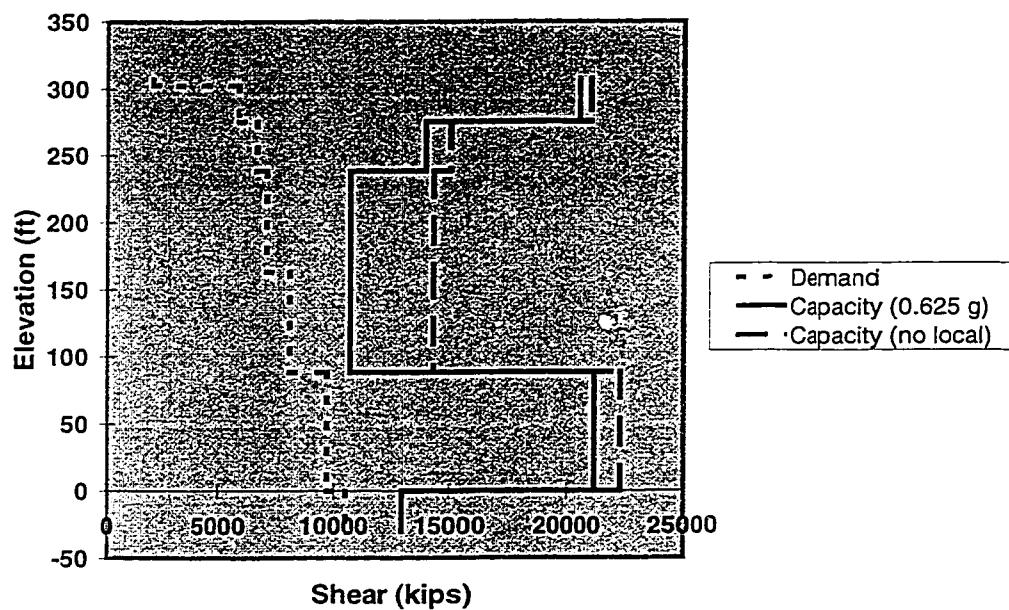


Figure 6-26: Platform C Gross Shear Demand – Capacity Profile from Simplified Method,
ZPA = 0.34 g, End-On Frames

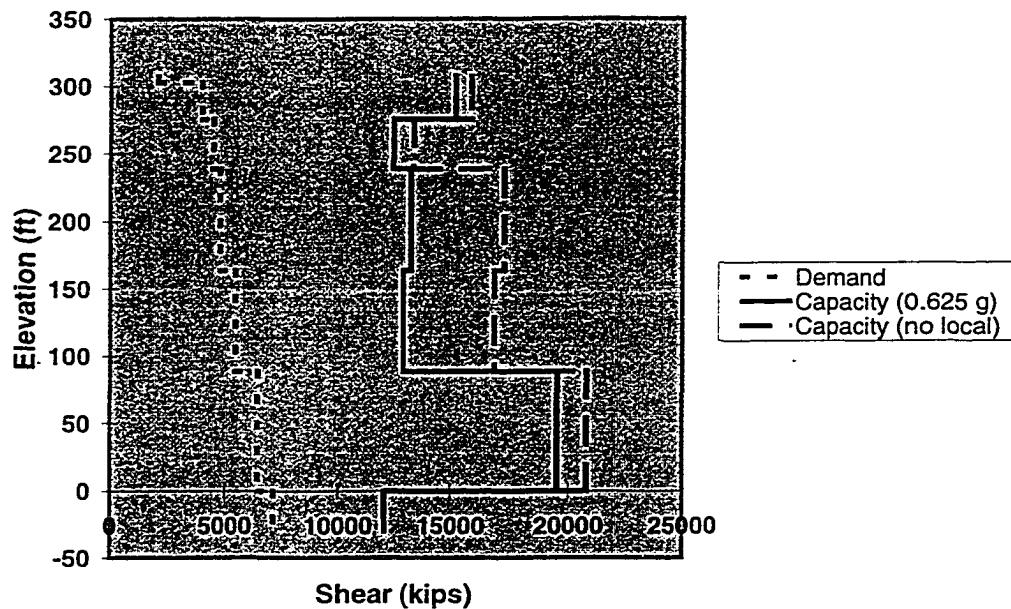


Figure 6-27: Platform C Gross Shear Demand – Capacity Profile from Simplified Method,
ZPA = 0.34 g, Broadside Frames

The similarity in behavior between Platform C and Platform B is not surprising; both platforms are of similar build and strength. Platform C has a weaker lateral foundation strength due to the absence of the conductors supported by Platform B.

6.3.3 Global Ductility Analysis

A simplified ductility analysis was performed for Platform C, and the results of this analysis were compared to results from a static pushover analysis performed using DRAIN-3DX. The limitations of DRAIN-3DX have been previously noted in Section 6.2.2; however, given the robust character of the foundation soils, and the fact that braces would not be the most critical mechanism, these limitations were accepted.

Load patterns for each direction in the analyses considered excitation acting concurrently on all three axes of the platform, with vertical excitation acting downwards. Load patterns for each direction were based on fundamental mode forces for each principal direction; the scaling used was 1.0 end-on/0.66 broadside/0.5 vertical.

Figures 6-28 and 6-29 show the principal axis deck displacements and associated base shears for Platform C for both the simplified analysis and the DRAIN-3DX analysis. The simplified analysis indicated yielding in the foundation piles (laterally) begins at a total resultant base shear of 12,300 kips. A fully-plastic mechanism will form at a total resultant base shear of 15,370 kips. This base shear corresponds to the end-on and broadside load components being scaled with an API Soil C spectrum ZPA of 0.30 g and 0.37 g respectively (S_a for the fundamental end-on period at these events is 0.25 g and 0.32 g). These values are 8% higher than the ZPA estimated including higher modes, and, as for Platform B, indicates modes beyond the fundamental modes on each axis do not contribute significantly to initial yielding. The hysteretic behavior of Platform B was estimated by assuming the pile will begin to yield at approximately 50% of its lateral strength capacity (as expressed by the load needed to form a two-hinge mechanism); at this point, its stiffness is assumed to reduce to 30% of its initial value. While all of the piles will not actually yield at the same point, the simplified method conservatively assumes all piles (of the same diameter and penetration) yield laterally as one group. While the plots in Figures 6-28 and 6-29 show a sudden change in stiffness, below the effective yield strength of the platform, in reality the behavior between these two points will be curvilinear, with slope decreasing as the load increases towards the mechanism strength. The formation of a complete double hinge mechanism in the piles is taken as the

limited point of global displacement ductility; the platform is able to develop a global displacement ductility of approximately 2.7, using the approximate point of pile yielding as a reference. Braces in the second and third jacket bays will likely buckle as this point is approached.

Using the 3-D model with DRAIN-3DX, near-field soils begin yielding at a resultant base shear of 6,200 kips. The global load-displacement behavior gradually becomes increasingly nonlinear, as more soil springs yield and the piles also begin to yield. Pile yielding occurs at a resultant base shear of 13,410 kips (S_a for the fundamental end-on period is 0.26 g); a fully-plastic mechanism has formed when the load reaches 17,430 kips (S_a for the fundamental end-on period is 0.34 g). Behavior becomes complicated at this point is approached; one pile begins to plunge, and braces in the second and third jacket bays of the end-on frames begin to buckle. Using pile hinge ductility as a measure, the platform is able to develop a global displacement ductility of 2.5 when complete double hinges have formed in the legs; at this point, brace local ductility demands are no greater than 2.5.

The results of the simple and detailed analyses are generally in good agreement. The post-yield reduction in pile stiffness used in the approximate plotting process appears to range from 50% to 25%, based on a cursory review of the load-displacement curves found when generating the equivalent linear stiffnesses used in the modal analyses of platforms A, B and C. While not exact, the approach provides an adequate method of estimating the load-displacement curves of piles in material with variable shear strength.

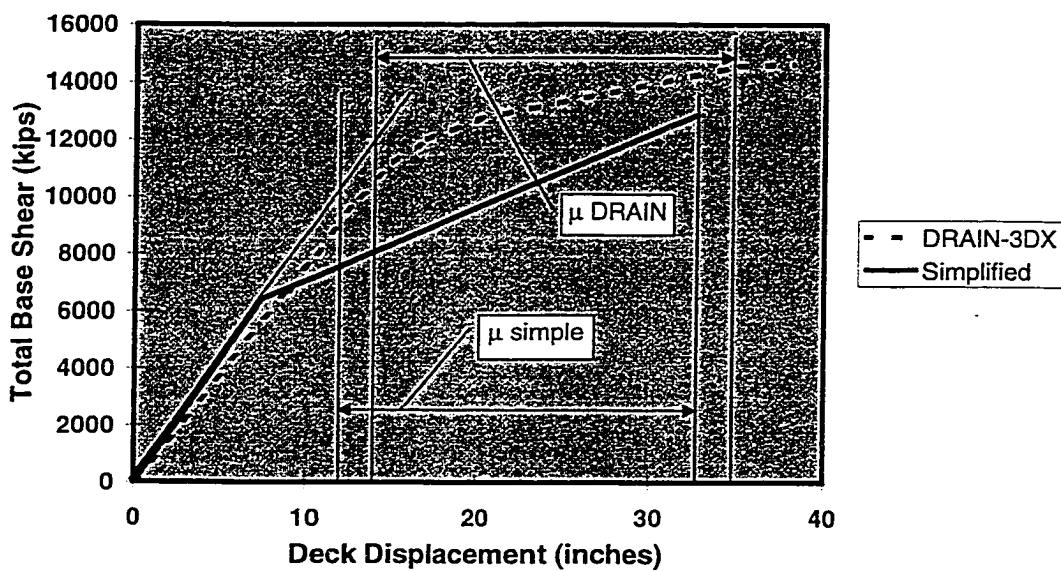


Figure 6-28: Global Load-Displacement Behavior of Platform C, End-On Components

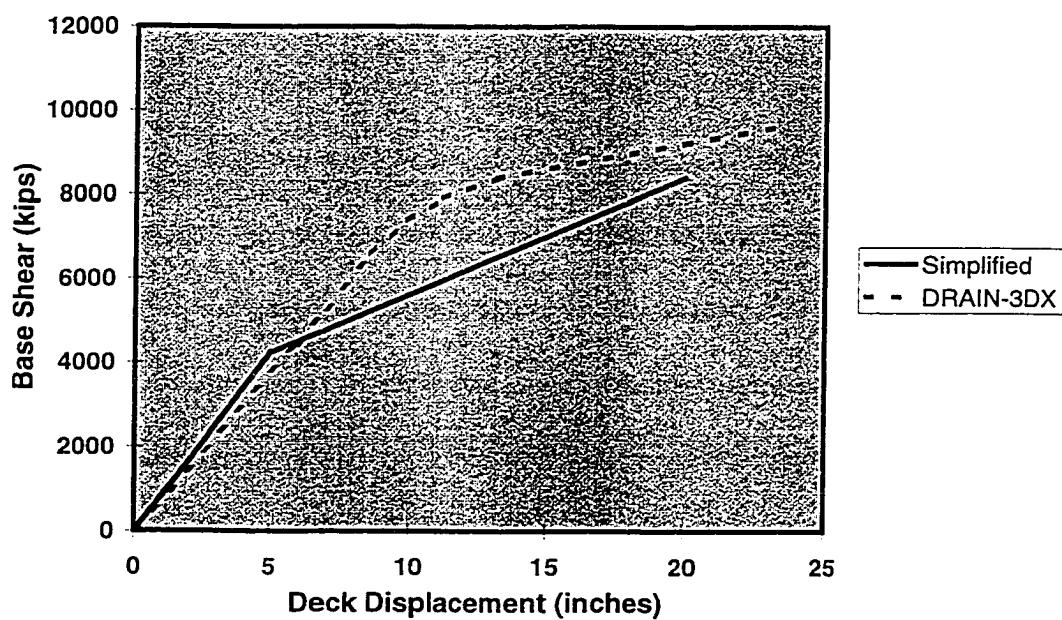


Figure 6-29: Global Load-Displacement Behavior of Platform C, Broadside Components

6.3.4 Ductility-Level Demand-Capacity Analysis

Ductility-level comparisons were performed in two ways for Platform C: (1) by judging the effective load reduction R implied by the simplified displacement ductility analyses against scale factors F_μ determined from MDOF nonlinear time history analyses, and (2) by judging the displacement modification F_d implied by the simplified displacement ductility analyses against the ratio of the deck displacement found from the MDOF nonlinear time history analysis to the MDOF first mode component of displacement (assuming linear elastic behavior) for the same time history. Also, the mean fundamental lateral mode spectral acceleration S_a (assuming 5% damping) which represented the onset of nonlinear behavior in the platform was determined from the time history analyses, to compare with the value determined in the global ductility analysis; this comparison checks the validity of indexing on first mode response to characterize platform strength capacity.

The DRAIN-3DX model used in Section 6.3.3 was utilized to determine F_μ , the effective load reduction a nonlinear MDOF system is entitled to based on ductile action, and to evaluate the relationship between inelastic and equivalent elastic (first mode) deck displacements. Rayleigh damping was assumed, with mass and stiffness-proportional coefficients balanced such that 5% critical damping was achieved in the first two fundamental lateral modes. As noted previously, DRAIN-3DX does not have spring elements capable of modeling strength degradation in near-field soils; therefore soil behavior was modeled as elastic-plastic. However, this platform is founded on fairly competent soils (stiff clays), where little degradation would be expected.

The model was analyzed using a series of nine earthquakes (see Table 6-8); the major component of motion was used on the end-on axis. Three damage measures, were used as criteria for F_μ : brace local ductility (using one half the cyclic ductility limit from Chapter Four as a target), global deck displacement (using the peak X displacement from the static pushover analysis as targets), and pile hinge ductility (using a limit of 2.5 as a target). The ratio of inelastic to elastic displacement was averaged for an overload (using $S_{a-yield}$ from the static pushover analysis as a reference point) of two. The mean values of F_μ for each damage measure, and the ratio of inelastic to elastic deck displacement, are shown in Table 6-19.

Table 6-19: $S_{a-yield}$, F_μ and Deck Displacement Ratio for Platform C

Factor	Yield	Target	$S_{a-yield}$ (g)	COV	Mean	COV
F_μ Global	X=14"	X=35"	0.30	0.11	3.10	0.29
F_μ Local (brace)	buckling	$\sim\mu=2.5$	0.60	0.18	1.40	0.16
F_μ Local (pile)	st. yield	$\mu=2.5$	0.36	0.14	1.60	0.22
$\Delta_{inelastic}/\Delta_{elastic}$	-	-	-	-	0.79	0.23

The results in Table 6-19 are very similar in trend to those obtained for Platform B, which is not unexpected. While the reference yield end-on deck displacement used with the dynamic analyses was taken to be identical to the end-on deck displacement at the point of significant nonlinearity in the DRAIN-3DX static pushover analysis (which corresponded to the full yielding of soil supporting a corner pile), the dynamic analyses did not induce pile yielding until excitation had been increased approximately 20%. The observed difference is the result of (1) the gradual yielding in the soils around the piles, which effectively increases damping in the platform, and (2) the Y-component of excitation not always being in phase with the X-component at a significant amplitude.

The brace buckling in the jacket was largely confined to the end-on frames, and was distributed between the first, second and third jacket bays. Buckling tended to occur after the point at which one or more plastic hinges had formed in the tops of piles; this is to be contrasted with the static pushover analyses, in which buckling did not occur until several piles had already formed double hinges.

The three damage measures used in the dynamic analyses are consistent with one another. The platform will reaches the prescribed global displacement limit at a level of end-on fundamental mode spectral excitation corresponding to $3.10 \times 0.30 \text{ g} = 0.93 \text{ g}$; diagonal braces, which tended to have buckled prior to this level of displacement, on average reached local ductility demands of 2.5 at an excitation of $1.40 \times 0.60 \text{ g} = 0.84 \text{ g}$. Similarly, the first instance of pile hinge formation tended to occur before braces buckled, at an excitation of $1.60 \times 0.36 \text{ g} = 0.58 \text{ g}$. Using the first occurrence of large plastic hinge rotations is the most restrictive limit in this example. While it is indeed likely that the platform could survive up to the formation of many plastic hinges in the piles, it is better from a safety standpoint to keep the ductility demands on gravity load-supporting members small.

From the results of the global ductility analyses in Section 6.3.3, it is reasonable to classify the platform as bilinear non-degrading in the mode of deformation studied. Referring to Figures 5-3 and 5-59, SDOF non-degrading systems with 5% and 10% critical damping, it is reasonable to expect an effective load reduction on the order of 2.75 to 3.0, associated with the formation of hinges in all of the piles. This effective load reduction is in good agreement

with that calculated from the dynamic analyses of Platform C using global end-on deck displacement as a measure. The local displacement ductility criteria for braces was achieved at a level of deck displacement close to 33 inches in nearly all cases; hence, it is not surprising that these two measures indicate consistent levels of equivalent elastic load. However, it would be prudent from a safety standpoint to select a load reduction factor associated with pile hinge ductility, in order to err on the side of conservatism.

The ratio of inelastic to elastic displacements is seen to be less than one, whereas through referencing Figure 5-4, this ratio would be expected to be unity or slightly higher. This situation was also noted in the analysis of Platform B. The discrepancy is due to the gradual yielding of soil along the piles, which increases effective damping. As noted in Chapter Five and by others, damping is most helpful when displacement ductility demands are low, which is the situation here for an overload ratio of two.

6.3.5 Platform C: Summary of Results

The simplified method used for estimating platform vibration properties compares very well with those calculated by analyzing a full-frame model of the platform; period estimates were within 11% of those found using the frame model. Using the API Soil C response spectrum as a basis for loads, the simplified demand-capacity assessment provides a capacity estimate which is very close to that estimated from the 3-D analysis; the correct principal failure mode is also identified.

The simplified ductility analysis compares well with results from a static pushover analysis; the global displacement ductility estimated for the point of pile hinging in the foundation varied at most by 6% between the two methods. The simplified method provided a generally conservative estimate of platform yield and reserve strength for the load pattern considered.

The dynamic analysis results of Platform C bring forth the same issues as the analysis of Platform B: sensitivity to load pattern, and the effects of minor yielding prior to gross nonlinearity in the structure. These can be addressed in the static case by using load reduction factors with higher initial damping, and by considering a variety of load patterns when performing the initial static pushover analyses.

6.4 CASE STUDY #4: PLATFORM D

Platform D is a 12-leg drilling and production platform sited in 58 ft of water off Huntington Beach in Southern California (Figure 6-30). The platform supports 42 20 inch-diameter conductors, 12 of which are guided at the mudline and can be expected to provide lateral resistance. The platform has two decks located at +34 ft and +58 ft respectively. There is minimal diagonal bracing between the decks and between the decks and the jacket. The main diagonals in the jacket range from 12 inch-diameter (w.t. 0.33 inch) to 14 inch-diameter (w.t. 0.375 inch). The jacket legs are 33 inch-diameter; the jacket legs possess 18 ft extensions which penetrate into the foundation soil. The annulus between each leg and associated pile is grouted. The piles are 30 inch-diameter (w.t. 0.875 to 1.5 inches), and penetrate between 60 to 80 ft through layers of silt, clay and sand. All steel is assumed to be 36 ksi, with 10%

increases taken for strain rate effects and correction from minimum specified strength to mean strength.

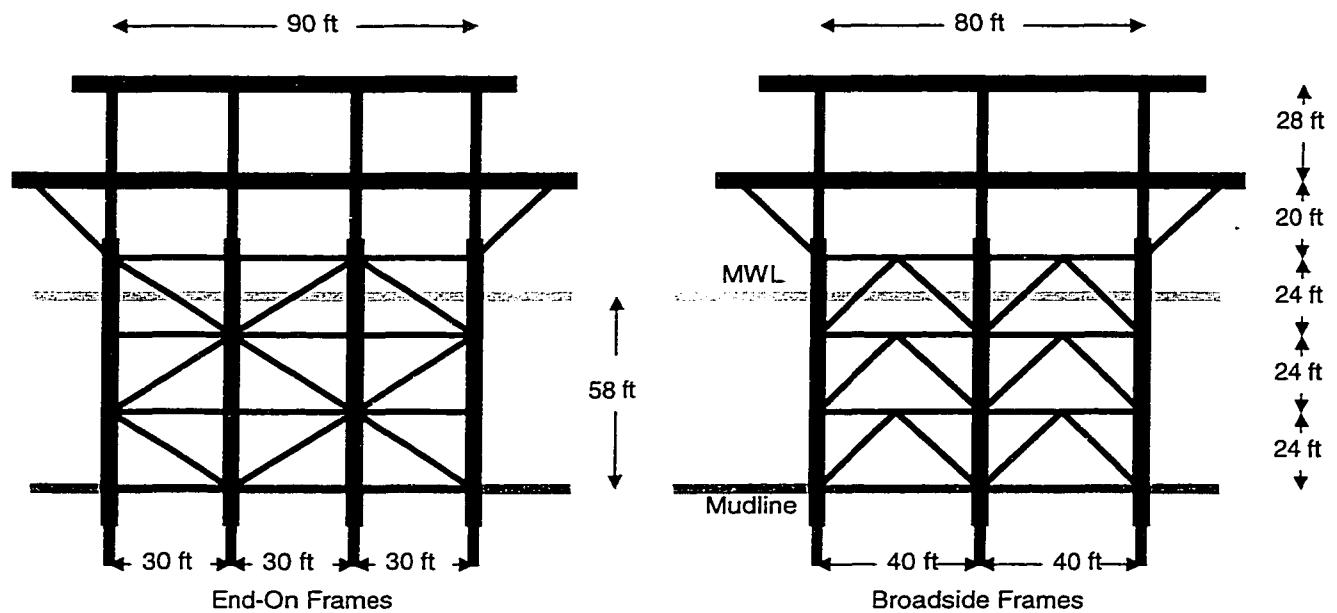


Figure 6-30: Platform D

This platform was the subject of an extensive requalification effort in the early 1990's. Based on the results of storm and earthquake assessments, the platform was upgraded to ensure its continued serviceability for an additional 20 years. The upgrades included grouting the leg-pile annulus, drilling out and grouting the piles below the mudline, adding saddles to strengthen the K-joints in the chevron braces in the broadside frames, and repair of minor cracks. In addition, marine growth and non-essential equipment was removed from the structure. The results of several of these analyses were made available by the California State Lands Commission (CSLC, 1998), and are used to assist in developing models for benchmarking the simplified approach.

6.4.1 Modal Analysis

Platform D was analyzed using the simplified modal procedure, and the results have been compared to those obtained using a 3-D frame model. In the 3-D model, diagonal braces and horizontal braces in the end-on frames were modeled using strut elements, while horizontal braces in the broadside frames, legs and piles were modeled using beam-column elements. Piles below the mudline were modeled by beam-column elements supported by nonlinear springs. The 12 conductors which are framed at the mudline were modeled as a single equivalent element. Masses on the 3-D model were moved onto the principal axes of the platform, to eliminate lateral-torsional coupling.

Pile-head springs were derived for the simplified model by analyzing the behavior of a single pile using DRAIN-3DX. Linearized pile-head springs derived by this approach are shown in Table 6-20.

Table 6-20: Pile-Head Axial and Lateral Stiffnesses

Pilehead Springs	Stiffness	Approximate k
Vertical – 30	6250 kips / in	1.9EA/L
Horizontal – 30	333 kips / in	$12EI/(0.3L)^3$

Figures 6-31 and 6-33 show the lateral mode shapes and vibration periods of the platform as estimated by the simplified method, while Figures 6-32 and 6-34 show these same quantities as derived from the 3-D model. Comparing the results, it is seen that the simplified analysis provides results which are in excellent agreement with those obtained from the full-frame model. Given the short, stocky configuration of this platform, this result is not unexpected.

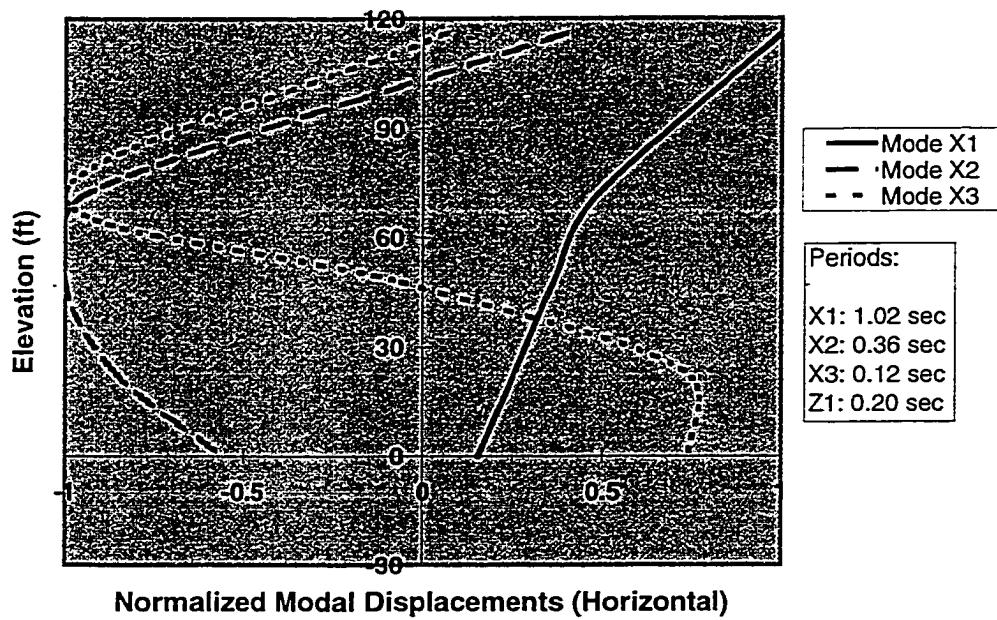


Figure 6-31: Platform D End-On Vibration Properties (Simplified Model)

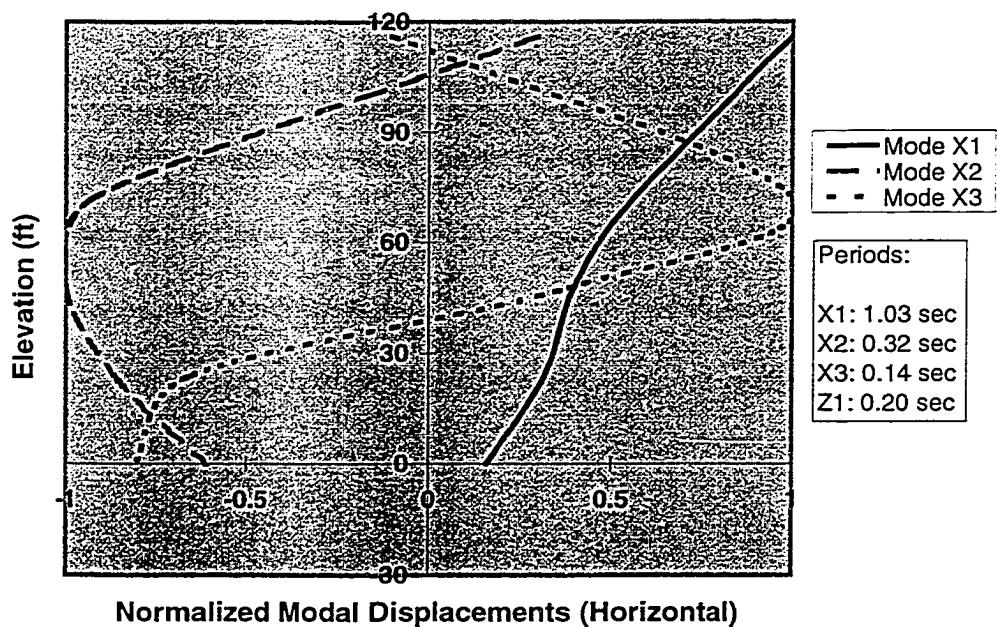


Figure 6-32: Platform D End-On Vibration Properties (3-D Model)

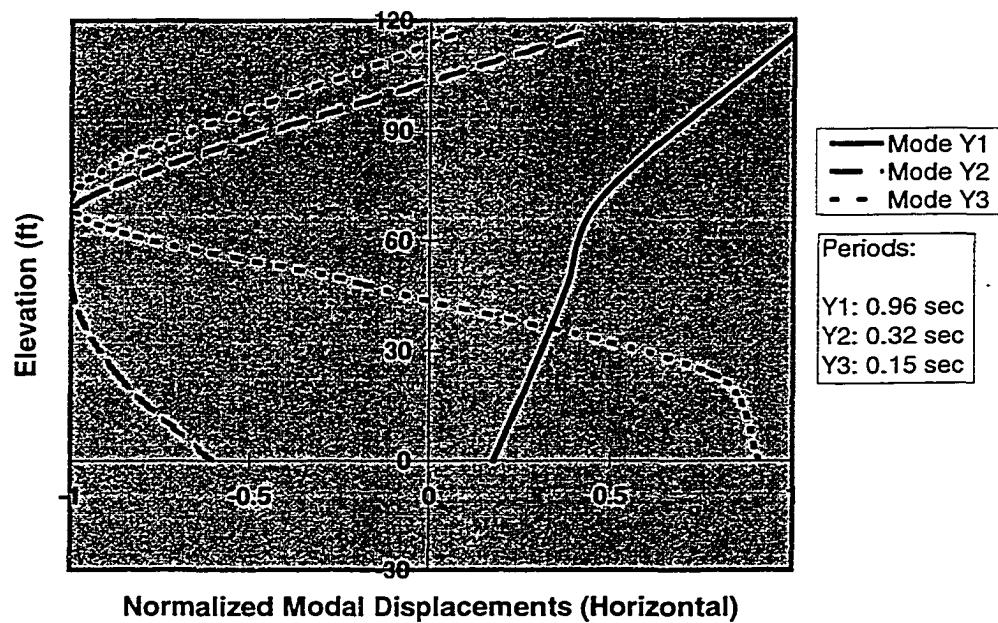


Figure 6-33: Platform D Broadside Vibration Properties (Simplified Model)

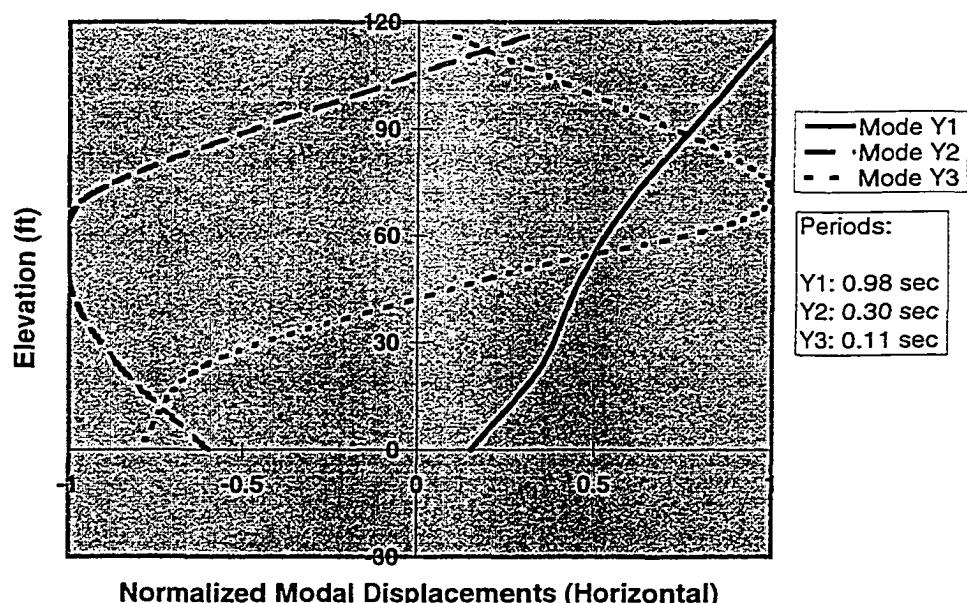


Figure 6-34: Platform D Broadside Vibration Properties (3-D Model)

6.4.2 Strength-Level Demand-Capacity Analysis

Modal forces were estimated for both models using the API (1993) Soil A response spectrum together with the appropriate modal properties. The SRSS combination rule was used in combining modal responses. Comparisons of the effective story shears and axial forces induced on the piles are shown in Table 6-21 and Figures 6-35 and 6-36 for a ZPA = 0.25 g. There is excellent agreement in shear demands between the two models; given the similarity in predicted response components, this is not an unexpected result. There is a 10% difference between peak pile loads; this is due to the approximate way in which pile loads are assumed to be shared (i.e. equally) by the simplified method. The piles were not placed in tension.

Table 6-21: Peak Pile Loads

Pile Load	3D	Simple
Tension	-	-
Compression	680	620
Lateral	220	200

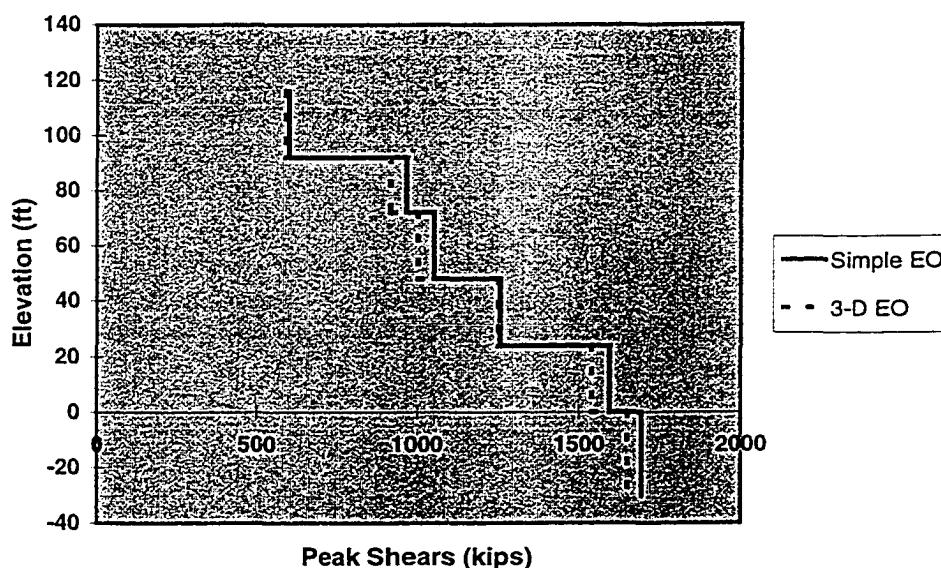


Figure 6-35: Comparison of Gross End-On Shears

For demand-capacity assessment purposes, forces were assumed to act on all three axes simultaneously, with both components of lateral load at 100% and the vertical component at 50%. Pile capacities and brace capacities for diagonals in the end-on frames were estimated using the simplified procedures of Chapter Four; a local load associated with an acceleration of 0.75 g was used in determining brace axial capacities. As this platform has grout in the leg-pile annulus, tubular joints at the legs were considered able to develop the full capacities of attached braces. However, it was decided to consider the joints at the apex of the chevron braces to be in an unmodified state; hence, the joint capacity, and not brace capacity, governed the strength of these composite elements. Joint capacities were derived from the API relationships listed in Chapter Four, and were used in lieu of the buckling and tension capacities of the broadside braces.

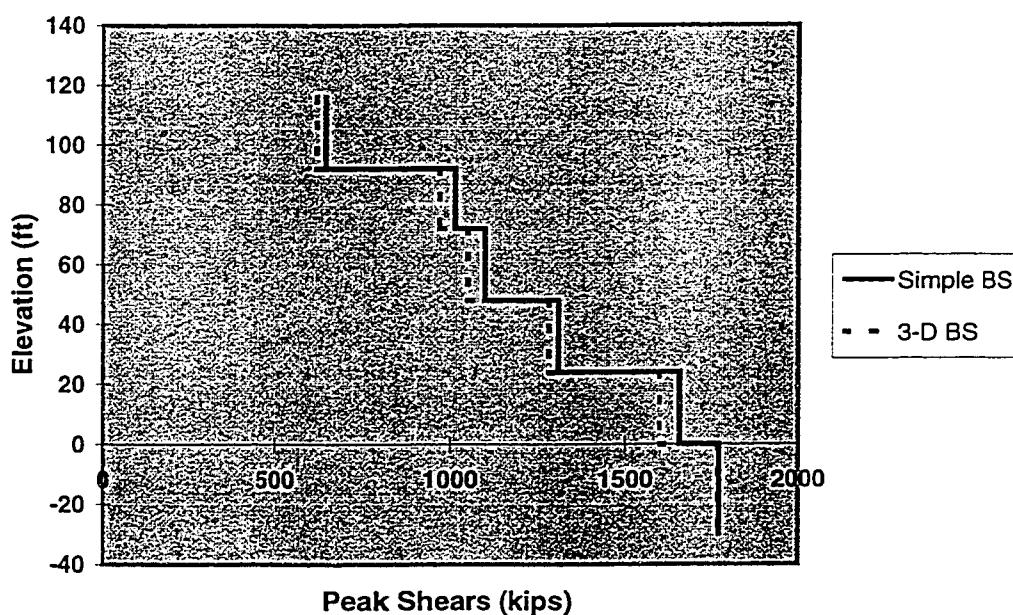


Figure 6-36: Comparison of Gross Broadside Shears

Using the simplified load and capacities, the broadside frames were found to govern platform strength for the load pattern considered. For this load case, an earthquake intensity of 0.38 g results in the yielding of joints in the chevron braces of the third jacket bay broadside frames. To show the relative strengths of members at this level of load, end-on and broadside demand-capacity curves are shown in Figures 6-37 and 6-38. Base shear in both cases in the SRSS combination of the individual base shear components from both principal axes. Examining the curves, it appears braces in the first and second jacket bays of the broadside frames and first jacket bay of the end-on frames are also weak links.

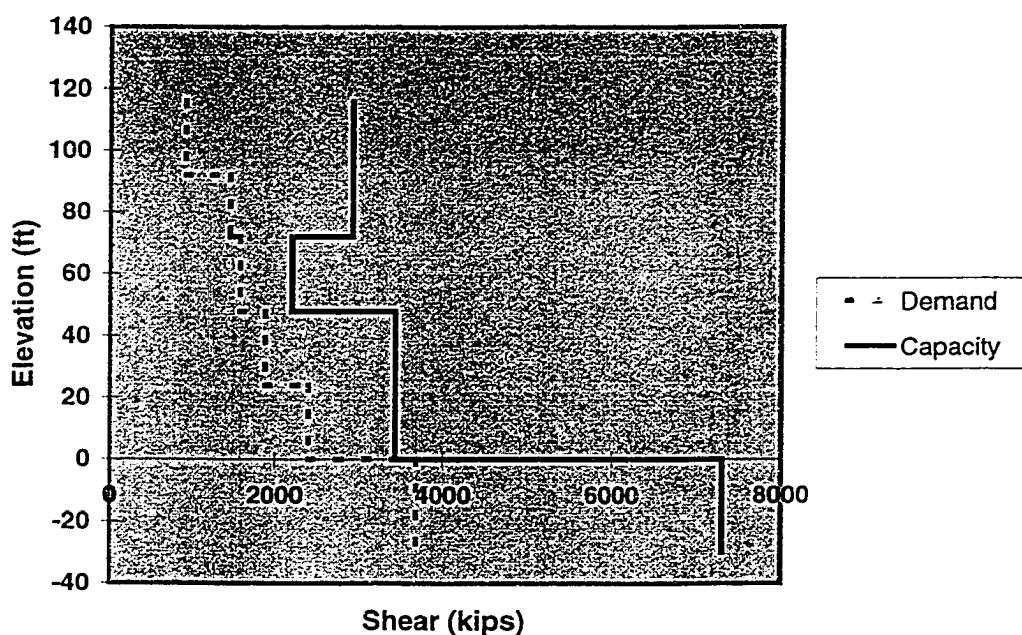


Figure 6-37: Platform D Gross Shear Demand – Capacity Profile from Simplified Method, ZPA = 0.38 g, End-On Frames

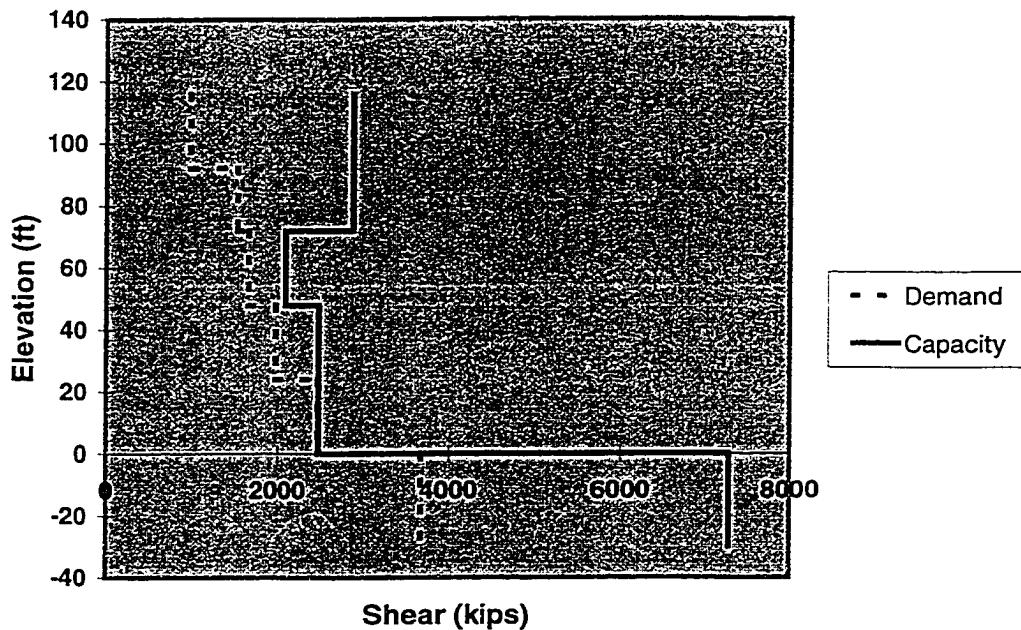


Figure 6-38: Platform D Gross Shear Demand – Capacity Profile from Simplified Method,
ZPA = 0.39 g, Broadside Frames

Strengths for the elements in the 3-D model were derived from single pile analysis and from relationships documented by Marshall, et al. (1977). API relationships were used to derive effective axial capacities for the braces in the chevron frames as with the simplified model. The 3-D analysis also indicates the broadside braces in the bottom jacket bay are the weak link. Using the same load strategy as for the simplified analysis, this damage will occur for loads corresponding to a spectrum ZPA of 0.39 g. This is practically identical to the value estimated by the simplified method. The damage trends identified by these response spectrum analyses are in qualitative agreement with results from analyses made available by CSLC (1998).

6.4.3 Global Ductility Analysis

A simplified ductility analysis was performed for Platform D, and the results of this analysis were compared to results from a static pushover analysis performed using PC-ANSR. The problem of joints being the weak link in the broadside frames posed a problem for PC-ANSR, which does not have a composite joint-type element. Instead, the same approach which was utilized in the original assessment analyses was applied here to emulate the behavior of the joint-brace system: if the joint capacity was less than 50% of the brace capacity, an elastic-plastic strut element with the joint axial capacity was used to model the brace; otherwise, a buckling-type strut was used, with the strength of the strut was matched to the joint capacity, and the post-buckling behavior scaled accordingly. The horizontal members in the chevron frames were modeled as beam-column elements, as PC-ANSR does not have a buckling-type beam-column element; as the horizontal braces are strong relative to the braces with reduced capacity, this is a reasonable assumption.

Load patterns for the two principal directions were based on first mode forces; vertical excitation forces were applied acting downwards. Figures 6-39, 6-40 and 6-41 show the principal axis displacements and base shears for Platform D for both the simplified analysis and the PC-ANSR analysis. Two analyses were performed for the end-on direction; as the framing in the platform is not symmetric, it is expected that the strength and post-yield behavior for each direction of load will be different.

These analyses indicate that the second mode on each principal horizontal axis contributes significantly to the base shear; and hence for the spectrum used will play a role in effective

platform capacity. Both analyses for the broadside frames indicate the bottom jacket bay chevron braces are the weak links; the base shear at the yield point approximately 2,800 kips. This base shear corresponds to a spectrum ZPA of 0.56 g (S_a for the fundamental broadside period is 0.46 g). However, the strength-level analyses indicated the broadside braces would likely reach capacity with all modes considered for a spectrum ZPA of 0.38 g, i.e. 33% lower in intensity. To account for this multi-mode effect in a conservative fashion, the effective fundamental mode spectral acceleration at yield should also be scaled back by 33%, or to 0.30 g. Note that this is an approximation, as the true phase between the modes is of course unknown. This has been manifested earlier in the analyses of platforms B and C, which had capacities governed by off-axis modal components.

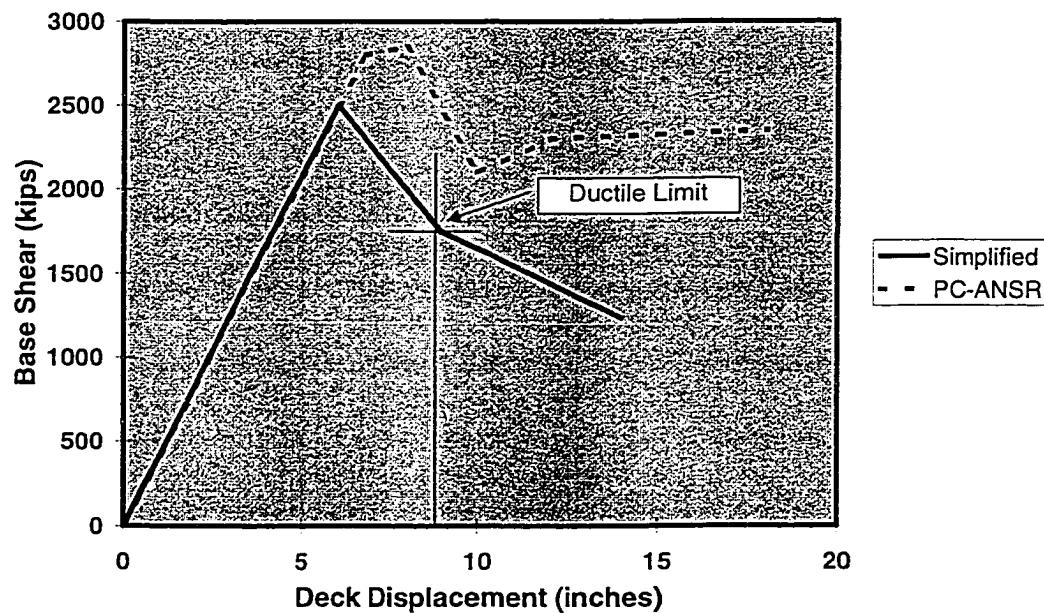


Figure 6-39: Global Load-Displacement Behavior for Platform D, End-On Direction (6 in Compression)

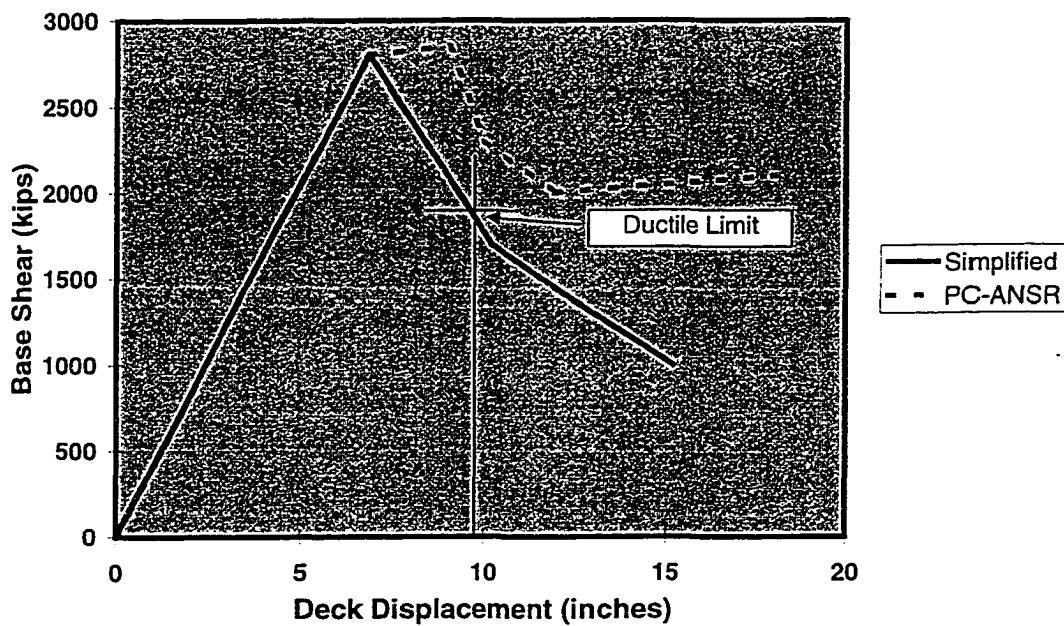


Figure 6-40: Global Load-Displacement Behavior for Platform D, Broadside Direction

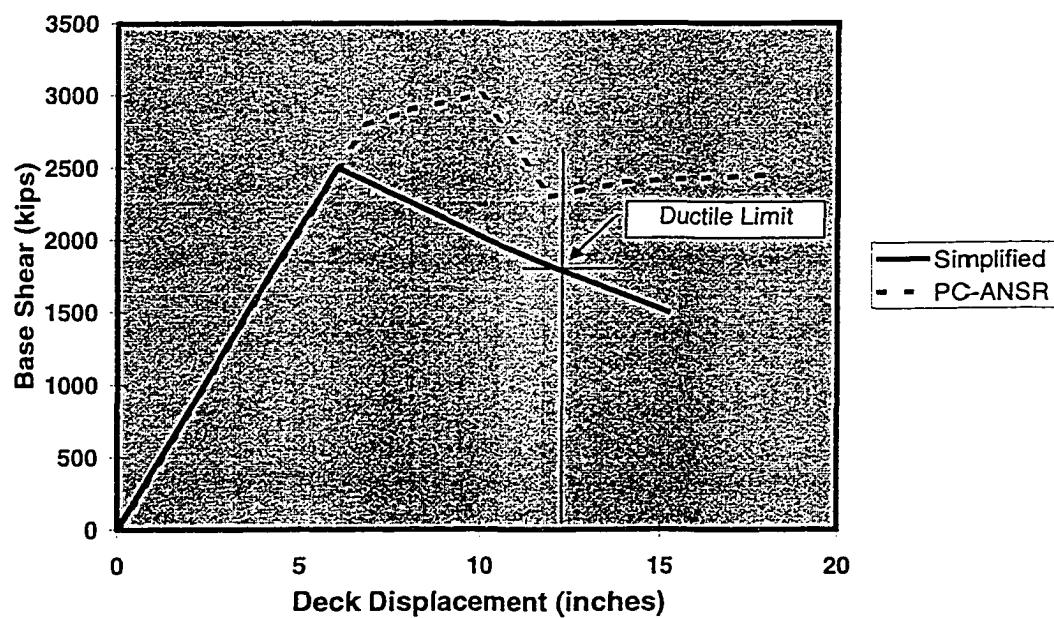


Figure 6-41: Global Load-Displacement Behavior for Platform D, End-On Direction
(3 in Compression)

The analyses for the end-on frames indicate the platform capacity is in the range of 2,500 kips (simplified) to 2,800 kips (PC-ANSR). This base shear corresponds to a spectrum ZPA of 0.53 g (S_a for the fundamental end-on period is 0.42 g). This is again higher than that needed to cause yielding in the chevron braces in the bottom of the broadside frames; hence, it appears the broadside frames will likely govern capacity of the platform.

For all directions of loading, the horizontal braces are capable of transferring the load of buckling main diagonals. Using the simplified method for the broadside direction, damage is assumed to concentrate in the jacket. Strength drops until the braces in the bottom jacket bay reach their cyclic ductility limits; at that point, displacement is assumed to concentrate in the bottom jacket bay. Using the 70% residual strength criteria as a cut-off, the platform is able to develop a global displacement ductility of 1.5. Using the simplified method for both end-on directions, damage is again assumed to concentrate in the jacket; strength drops until the braces in the first jacket bay reach their cyclic ductility limits, at which point displacement is assumed to concentrate in the top jacket bay. Using the 70% residual strength criteria as a cut-off, the platform is able to develop a global displacement ductility in the range of 1.5 to 2.0.

The global load-displacement curves generated by PC-ANSR contain a “plastic zone” of varying length, followed by a drop in strength. For the broadside frames, the braces in the bottom jacket bay buckle first, followed by braces in the second jacket bay. Strength begins to degrade, and hinges begin to form in the legs at a global displacement ductility of 1.9. For the end-on frames in the direction which places the most braces in compression, strength

plateaus briefly, and then begins to degrade. Hinges begin to form in the legs at a global displacement ductility of 1.7. Behavior is similar in the opposite direction, although the yield plateau is somewhat better; hinges form in the legs at a global displacement ductility of approximately 2.1.

The post-yield behavior estimated by the simplified method does not provide an indication of the “plastic zones” identified by the PC-ANSR analyses for either direction. However, the simplified method does provide a reasonable empirical estimate of global displacement ductility. The values estimated by the simplified method are on the order of 5% to 20% conservative relative to those derived from the PC-ANSR analyses. The amount of degradation predicted is fairly conservative; this will result in a selection of smaller response factors. It is once again emphasized that the simplified method cannot rigorously predict the true behavior of which members are yielding and buckling within the jacket following first member failure. The method is only intended to provide an estimate of the likely global behavior of the jacket, making assumptions about the redundancy and post-buckling performance of members in the structure.

6.4.4 Ductility-Level Demand-Capacity Analysis

Ductility-level comparisons were performed in two ways for Platform D: (1) by judging the effective load reduction R implied by the simplified displacement ductility analyses against scale factors F_u determined from MDOF nonlinear time history analyses, and (2) by judging the displacement modification F_d implied by the simplified displacement ductility analyses against the ratio of the deck displacement found from the MDOF nonlinear time history

analysis to the MDOF first mode component of displacement (assuming linear elastic behavior) for the same time history. Also, the mean fundamental lateral mode spectral acceleration S_a (assuming 5% damping) which represented the onset of nonlinear behavior in the platform was determined, to compare with the value determined in the global ductility analysis; this comparison checks the validity of indexing on first mode response to characterize platform strength capacity.

The PC-ANSR model used in Section 6.4.3 was utilized to determine F_μ , the effective load reduction a nonlinear MDOF system is entitled to based on ductile action, and to evaluate the relationship between inelastic and equivalent elastic (first mode) deck displacements. Rayleigh damping was assumed, with mass and stiffness-proportional coefficients balanced such that 5% critical damping was achieved in the first two fundamental lateral modes.

The model was analyzed using a series of nine earthquakes (see Table 6-8). By conducting a series of analyses, the major component of motion was alternately placed on the principal axes of the platform, to ensure both frames would be subject to the most severe component of motion. Three damage measures were used: brace local ductility (using the cyclic limit as a target) global displacement ductility (using the allowable as determined from the ductility analyses), and leg-pile hinge ductility (using a limit of two as a target) were used as criteria for F_μ . The ratio of inelastic to elastic displacement was averaged for an overload of two, using a spectral acceleration of 0.30 g as a reference. The mean values of F_μ for each damage measure, and the ratio of inelastic to elastic deck displacement, are shown in Tables 6-22 and 6-23.

Table 6-22: $S_{a\text{-yield}}$, F_μ and Deck Displacement Ratio (X major)

Factor	Yield	Target	$S_{a\text{-yield}}$ (g)	COV	Mean	COV
F_u Global	X=6"	Y=12"	0.42	0.14	2.02	0.18
F_u Local (brace)	buckling	$-\mu=5$	0.40	0.12	1.65	0.33
F_u Local (leg)	full plastic	$\mu=2$	0.58	0.10	1.36	0.22
$\Delta_{\text{inelastic}}/\Delta_{\text{elastic}}$	-	-	-	-	1.10	0.25

Table 6-23: $S_{a\text{-yield}}$, F_μ and Deck Displacement Ratio (Y major)

Factor	Yield	Target	$S_{a\text{-yield}}$ (g)	COV	Mean	COV
F_u Global	Y=6"	Y=12"	0.44	0.18	2.10	0.22
F_u Local (brace)	buckling	$-\mu=5$	0.38	0.12	1.57	0.28
F_u Local (leg)	full plastic	$\mu=2$	0.55	0.10	1.28	0.20
$\Delta_{\text{inelastic}}/\Delta_{\text{elastic}}$	-	-	-	-	1.12	0.30

The results obtained from the PC-ANSR analyses indicate there is a moderate contribution from higher modes to the response of the platform. In many cases, damage was recorded at lower levels of excitation that would have been assumed from the static analyses. In some instances, damage was initiated on braces in one set of frames, but then the damage target was reached by braces in the other. However, the mean initiating spectral acceleration value for damage to braces is still 25% higher than the “biased” value of S_a (0.3 g) proposed in Section 6.4.3.

From the results of the global ductility analyses in the previous section, it is reasonable to classify the platform, for both end-on and broadside frames, as moderately degrading. Referring to Figures 5-35 and 5-39, the effective load reduction, assuming the platform can develop a ductility of 1.7 to 2.0, would be in the range of 1.6 to 1.9. Given the target ductility for the MDOF analyses was effectively 2.0, and F_μ was found to be slightly higher than 2.0

for both directions, it can be seen that the values estimated from the static analyses are in good agreement with those from the MDOF dynamic analyses. Similarly, referring to Figures 5-37 and 5-39, the ratio of inelastic to elastic displacement is expected to be in the range of 1.0 to 1.2. These results are also in good agreement with those obtained from the MDOF analyses.

Overall, the factors generated using the MDOF analyses are in good agreement with those found from the static analyses; however, the issue of multi-mode effects indicates some caution is required when applying static methods. In this instance, the average impact of modal contributions beyond the fundamental modes was not as severe as anticipated; however, it did reduce the assumed platform yield strength by approximately 17% relative to the lowest value of S_a estimated from the static analyses. In addition, the variability (although sample size is small) is somewhat higher than that observed in previous analyses. The multi-mode effect on S_a will likely be dependent upon earthquake magnitude and distance; for a close earthquake, where frequency components are arriving at a site at the same time, there is a higher probability of different components being in phase. In lieu of considering this problem rigorously, one solution would be to analyze the platform statically using load patterns other than first mode forces, and then averaging the intensity levels indicating damage.

6.4.5 Platform D: Summary of Results

Platform vibration properties estimated using the simplified method compare very well with those calculated by analyzing a full-frame model of the platform. Using the API Soil A

response spectrum as a basis for loads, the simplified demand-capacity provides an excellent estimate of platform capacity, as expressed by response spectrum ZPA, as compared to results from use of the full-frame model.

The global ductility analyses indicated that higher mode effects could be significant for this platform; the difference in effective yield spectral intensities was on the order of 33% for considering and not considering higher modes. The simplified ductility analysis captures the approximate global displacement limit of the platform, and the general hysteretic envelope is similar to that estimated by static pushover analysis for two configurations of horizontal framing. However, it must be noted that the envelope curve estimated by the simplified method is very approximate, being a semi-empirical representation of the pushover behavior of the platform; member local demands are not well-represented at large levels of global displacement.

MDOF response factors and elastic-to-inelastic deck displacement ratios derived from nonlinear time history analysis compare very well with factors and ratios selected based on the results of the global displacement ductility analyses; however, the effective yield strength of the platform was in between the two values estimated during the global ductility analyses. This case points out the difficulties of applying the simplified approach when higher modes are an issue.

6.5 CASE STUDY #5: PLATFORM E

Platform E is a 12-leg drilling and production platform sited in 187 ft of water off Summerland, California (Figure 6-42). The platform supports 56 20 inch-diameter conductors; 36 are vertical while the remaining 20 are slanted. The platform has two decks located at +43 ft and +70 ft respectively.

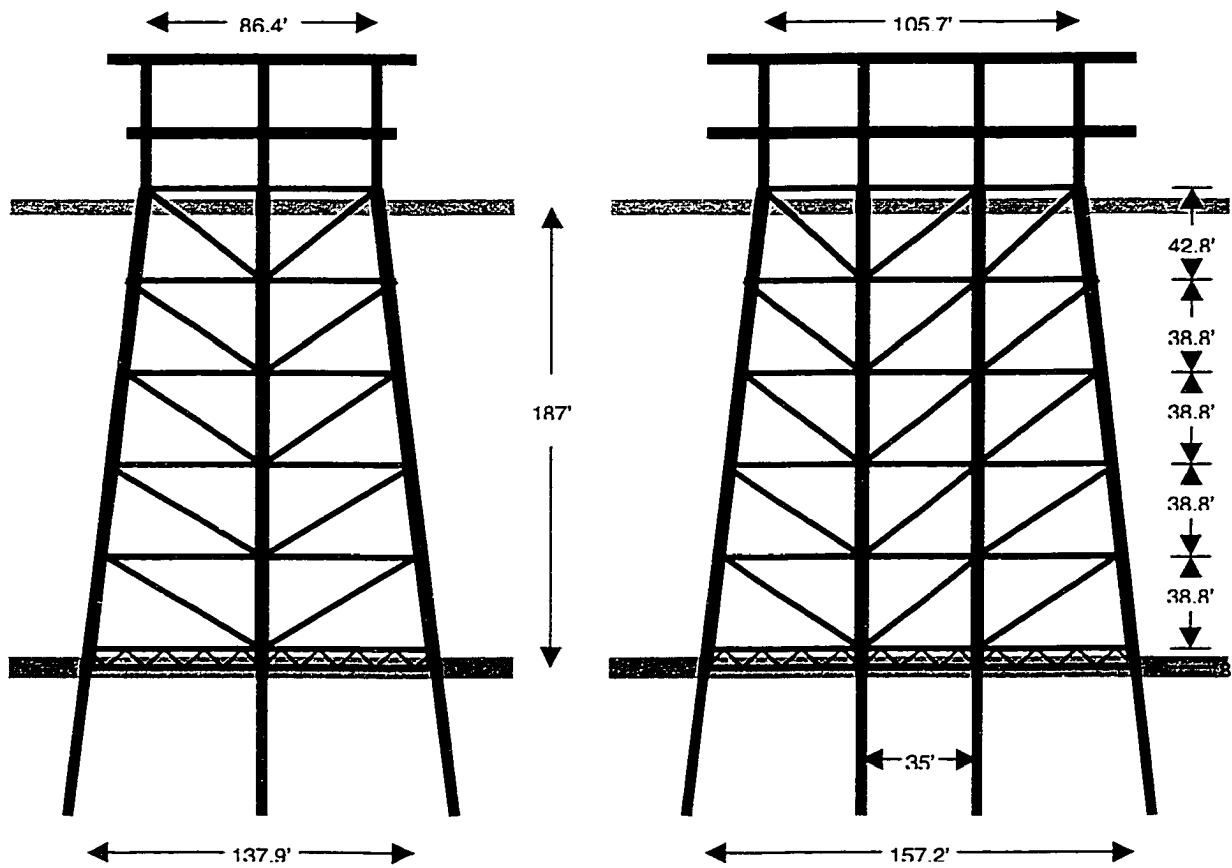


Figure 6-42: Platform E

There is minimal diagonal bracing between the decks and between the decks and the jacket. The main diagonals in the jacket range from 16 inch-diameter (w.t. 0.656 inch) to 24 inch-diameter (w.t. 0.562 inch). The annulus between each leg and associated pile is grouted. The

piles are 40 inch-diameter (w.t. 1.0 inch), and penetrate approximately 180 ft through a thin layer of silty sand into hard claystone. All steel is assumed to be 36 ksi, with a 10% increase taken to correct from minimum to average yield strength, and an additional 10% increase taken for strain rate effects.

This platform was also the subject of an extensive requalification effort in the early 1990's. Based on the results of storm and earthquake assessments, the platform was upgraded to ensure its continued serviceability for an additional 20 years. The upgrade effort focussed on strengthening the deck bays, which were found to possess insufficient lateral resistance for up-to-date loading conditions. The results of several of the analyses of the platform in the pre-upgraded condition were made available by Unocal (Unocal, 1991), and are used to benchmark the simplified approach.

6.5.1 Modal Analysis

Platform E was analyzed using the simplified modal procedure, and the results were compared to results from a 3-D frame analysis of the platform. In the 3-D model, braces were modeled using strut elements, while the legs and piles were modeled using beam-column elements. Piles below the mudline were modeled by beam-column elements supported by nonlinear springs. The 36 vertical conductors were modeled as a single equivalent element, while the slanted conductors were excluded from the structural model. The upper and lower deck frames were modeled as rigid. Masses on the 3-D model were moved onto the principal axes of the platform, in order to minimize lateral-torsional coupling.

Pile-head springs were derived for the simplified model by analyzing the behavior of a single pile using DRAIN-3DX. Linearized pile-head springs derived by this approach are shown in Table 6-24.

Table 6-24: Pile-Head Axial and Lateral Stiffnesses

Pilehead Springs	Stiffness	Approximate k
Vertical – 40	1840 kips / in	0.8EA/L
Horizontal – 40	350 kips / in	$12EI/(0.15L)^3$

Figures 6-43 and 6-45 show the lateral mode shapes and vibration periods of the platform as estimated by the simplified method, while Figures 6-44 and 6-45 show these same quantities as derived from the 3-D model. Comparing the results, it is seen that the simplified analysis provides results which are in good agreement with those obtained from the full-frame model. Modal periods differ by at most 6%; there are minor variations in the mode shapes but the overall trends are very similar.

6.5.2 Strength-Level Demand-Capacity Analysis

Modal forces were estimated for both models using the API (1993) Soil A response spectrum together with the appropriate modal properties. The SRSS combination rule was used in combining modal responses. Comparisons of the effective story shears and axial forces are shown in Table 6-25 and Figures 6-46 and 6-47 for a ZPA = 0.30 g. The estimated response spectrum shears and pile loads are close, with those from the simplified modal being overestimated by at most 10% relative to those from the 3-D analysis.

Table 6-25: Peak Pile Loads

Pile Load	3D	Simple
Tension	357	396
Compression	1504	1646
Lateral	130	155

Demand-Capacity Analysis was conducted using the simplified methods for both major horizontal axes of the platform. Forces were assumed to act on all three axes simultaneously, with a proportion of 1.0/1.0/0.5 used to scale the primary lateral, secondary lateral, and vertical components. Diagonal brace capacities were determined including a local acceleration load from 1.0 g. As this platform has grouted legs, the strength of tubular brace-leg connections were not considered in the analysis.

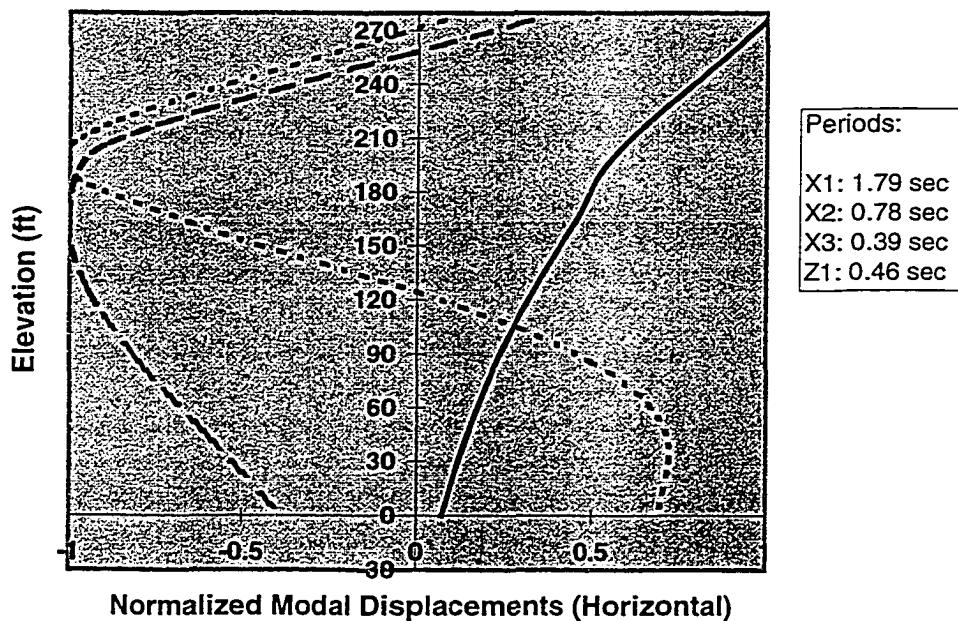


Figure 6-43: Platform E End-On Vibration Properties (Simplified Model)

The simplified method identifies hinging of the deck legs as the mechanism which governs the strength of the platform. An earthquake intensity of 0.31 g results in loads necessary to initiate a collapse mechanism in the deck bay; a fully-plastic mechanism will form at an intensity of 0.42 g. End-On and broadside demand-capacity curves are shown in Figures 6-49 and 6-50 for loads generated with a ZPA of 0.31 g; the deck section shear and base shear components shown are the resultants of the end-on and broadside shear components, while the shears at each jacket bay are the respective end-on and broadside components. From these curves, the next elements to yield would likely be the braces in the second broadside jacket bay, and the brace in the second and third end-on jacket bays.

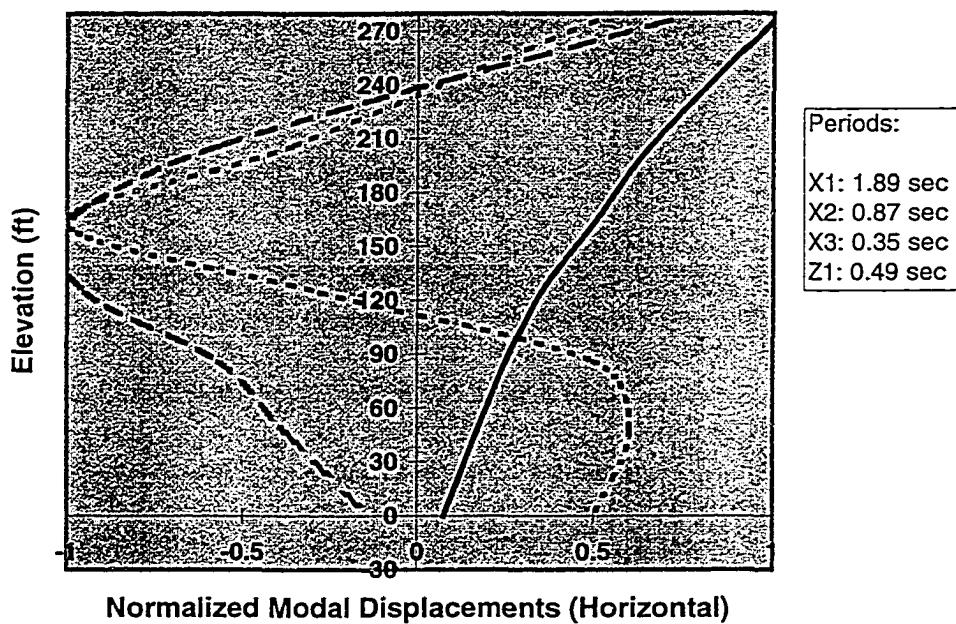


Figure 6-44: Platform E End-On Vibration Properties (3-D Model)

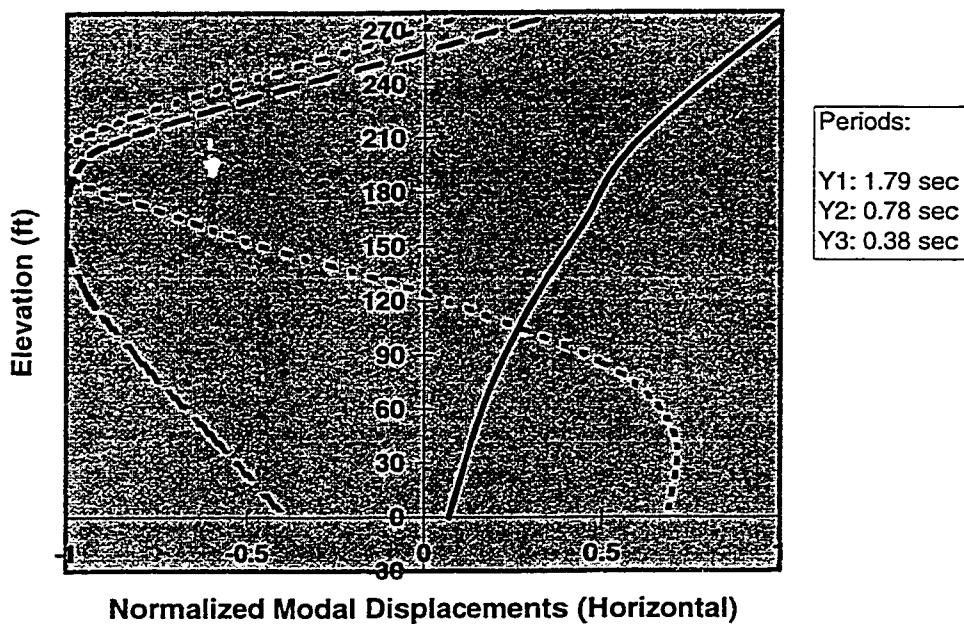


Figure 6-45: Platform E Broadside Vibration Properties (Simplified Model)

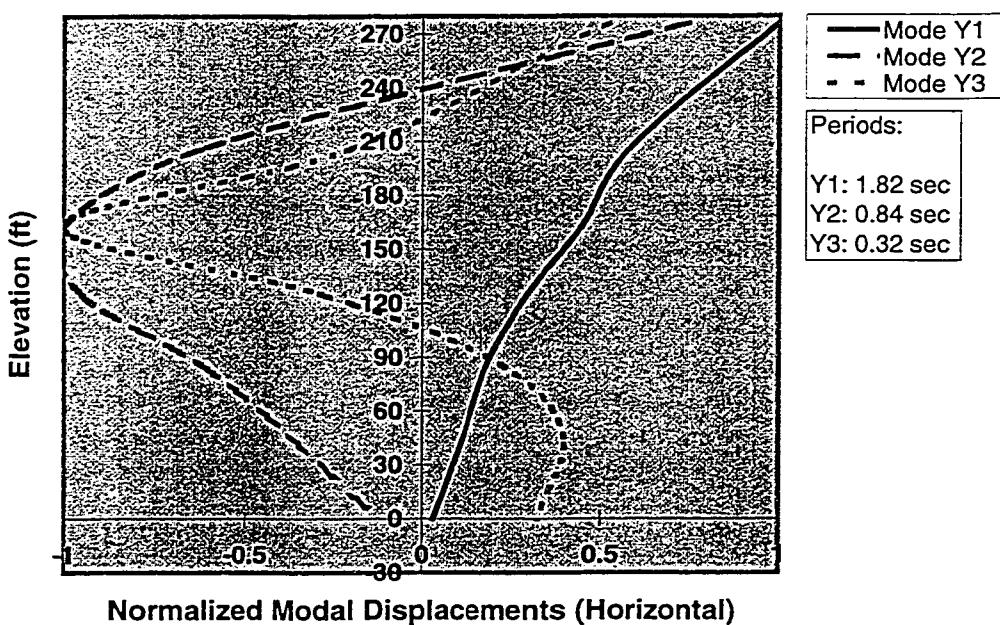


Figure 6-46: Platform E Broadside Vibration Properties (3-D Model)

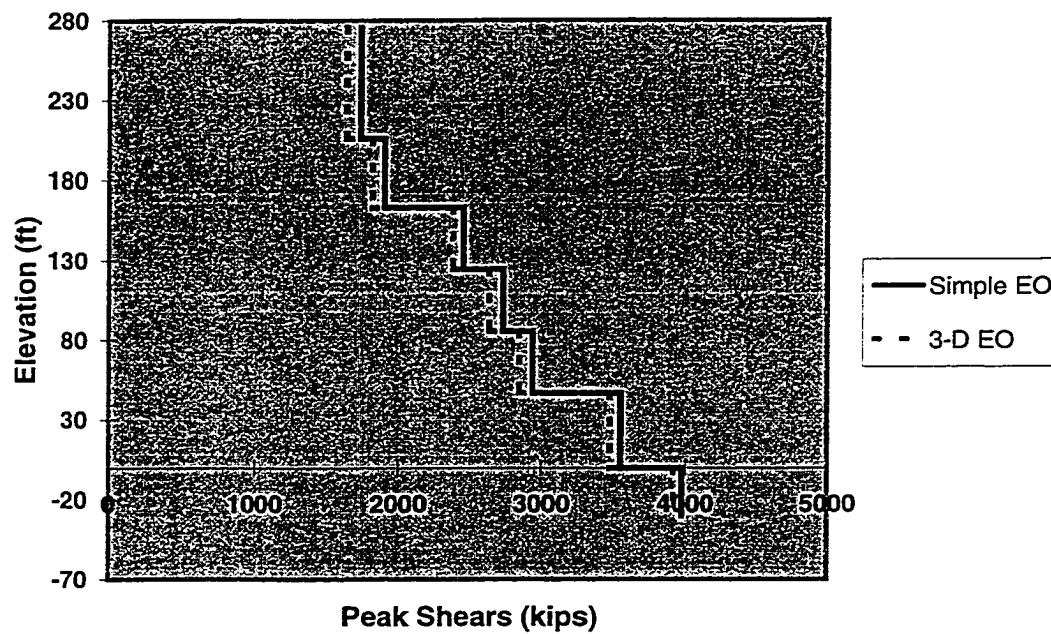


Figure 6-47: Comparison of Gross End-On Shears, ZPA = 0.30 g

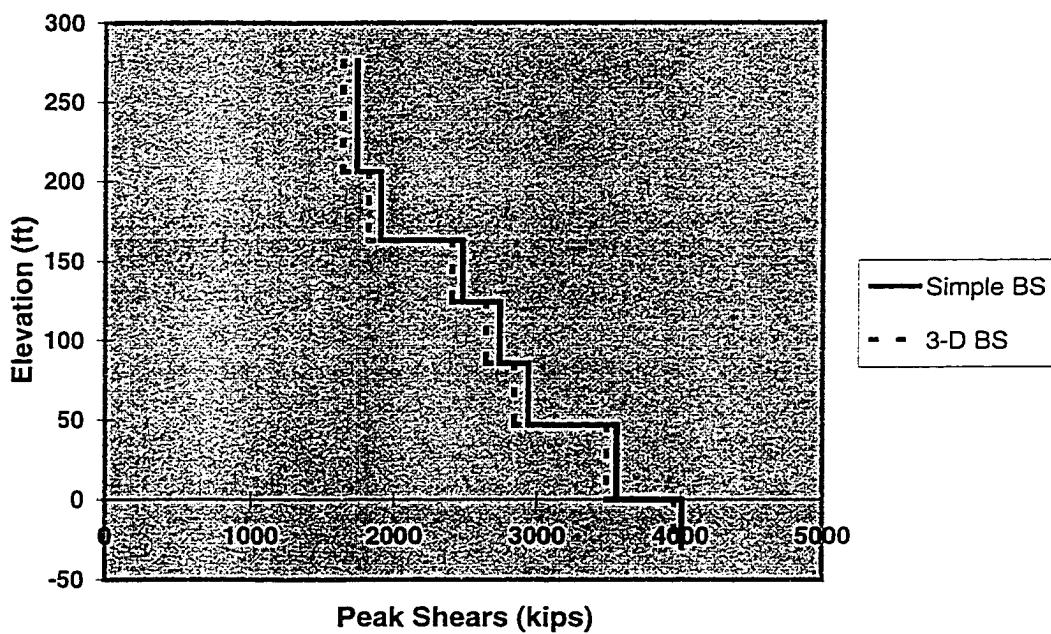


Figure 6-48: Comparison of Gross Broadside Shears, ZPA = 0.30 g

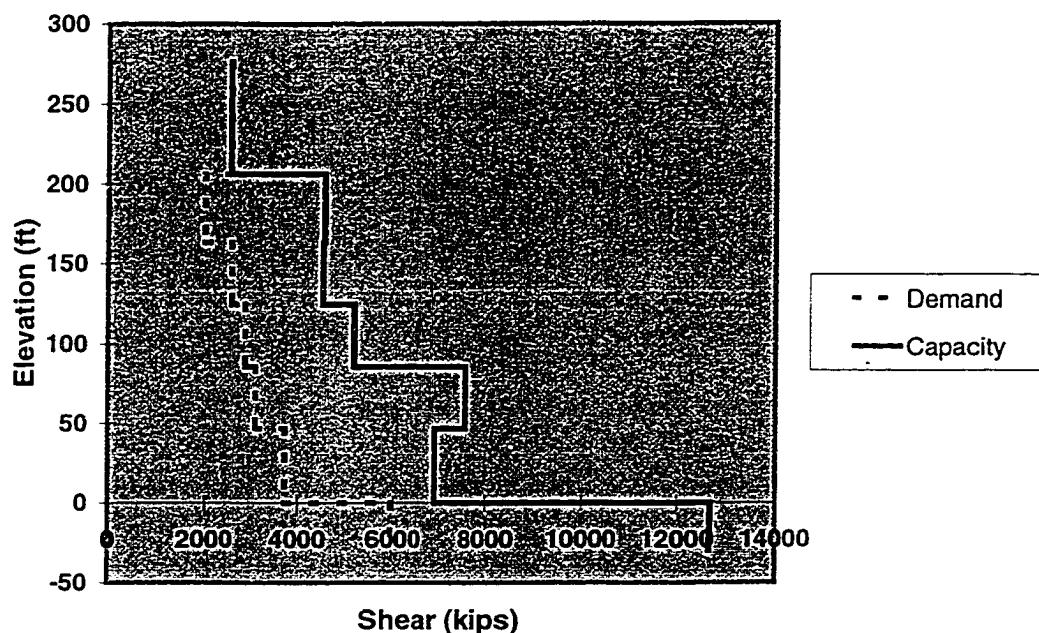


Figure 6-49: Platform E Gross Shear Demand-Capacity Profile from Simplified Method,
ZPA = 0.31 g, End-On Frames

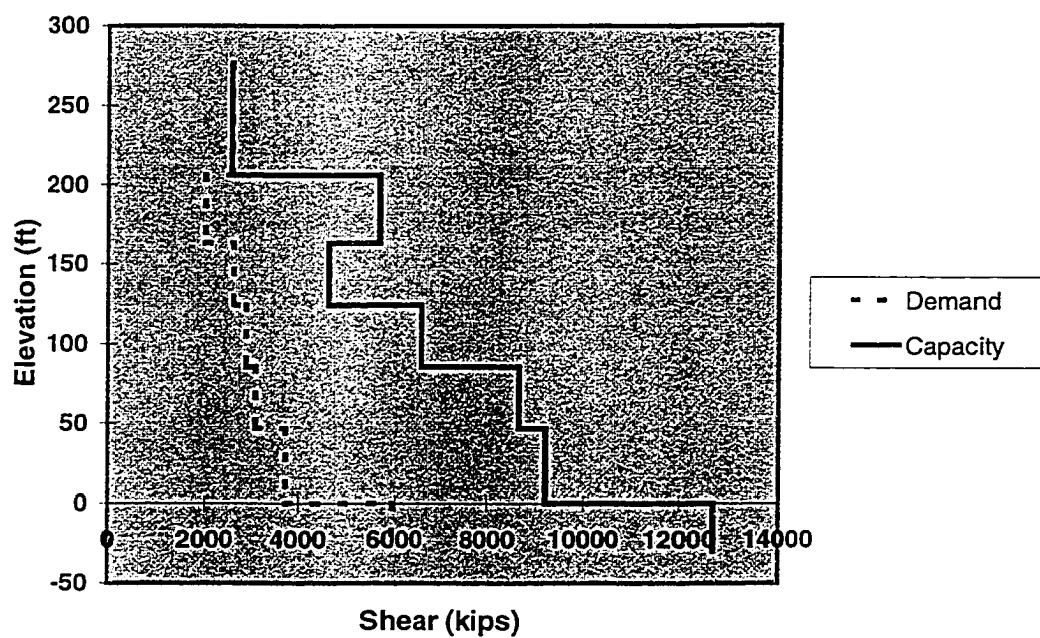


Figure 6-50: Platform E Gross Shear Demand-Capacity Profile from Simplified Method,
ZPA = 0.31 g, Broadside Frames

Strengths for elements in the 3-D model were determined using information provided by Unocal (1998) and from relationships documented by Marshall, et al. (1977). The 3-D analysis also indicates the deck structure is the weak component in the platform; using the same loading strategy as for the simplified method, yielding begins in the deck frames and legs at an earthquake intensity of 0.33 g. This is very close to the intensity estimated from the simplified method.

6.5.3 Global Ductility Analysis

A simplified ductility analysis was performed for Platform E, and the results of this analysis were compared to results from a static pushover analysis performed using PC-ANSR. Load patterns for the two principal directions were based on first mode forces; vertical excitation forces were applied acting downwards. Loads on the principal axes were scaled using relative ratios of 1.0 for end-on, 1.0 for broadside, and 0.5 for vertical.

Figure 6-51 shows the resultant displacements and base shears for Platform E for both the simplified analysis and the PC-ANSR analysis. The simplified analysis indicates the deck legs will yield at a total resultant base shear of 5,490 kips, and a fully-plastic mechanism will form in the upper deck section at a base shear of approximately 7,140 kips. These base shears correspond to principal axis components being scaled to an API Soil A spectrum ZPA of 0.42 g and 0.55 g respectively (S_a for the fundamental end-on period at these events is 0.19 g and 0.25 g). Noting that the strength-level demand-capacity analysis indicates a spectrum ZPA of 0.31 g will result in deck leg yielding, the effective fundamental mode spectral

acceleration at yield should be scaled back by 28% or to 0.14 g to account for higher mode effects. As noted in the analysis of Platform D, this reduction can be very conservative. Using leg hinge ductility as the controlling criteria, the simplified method indicates Platform E is able to develop a global displacement ductility of approximately 1.6.

The PC-ANSR analysis confirms the trend identified by the simplified assessment; yielding occurs in the upper deck section at a resultant base shear of 5,153 kips, while a fully-plastic mechanism forms at a resultant base shear of 7,597 kips. Yielding corresponds to a spectral acceleration of 0.13 g including the reduction for higher mode effects. Using leg hinge ductility as the controlling criteria, the platform is able to develop a global displacement ductility of approximately 2.1.

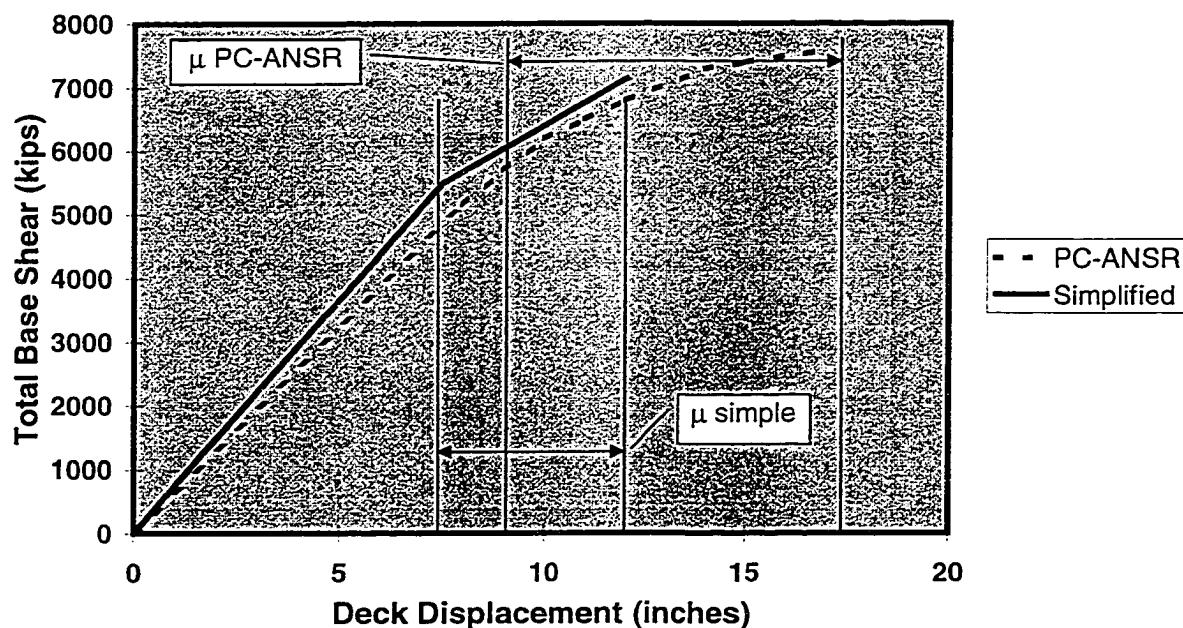


Figure 6-51: Global Load-Displacement Behavior of Platform E, Resultants

The simplified analysis and PC-ANSR results are in good general agreement; the predicted yield points are within 5% of one another, while the predicted ultimate strengths are within approximately 8% of one another. The global displacement ductility of the platform is underpredicted by the simplified method relative to application of PC-ANSR; this is due to the fact that yielding occurs gradually in the deck legs, as opposed to simultaneous yielding and hinging as is assumed by the simplified method.

6.5.4 Ductility-Level Demand-Capacity Analysis

Ductility-level comparisons were performed in two ways for Platform E: (1) by judging the effective load reduction R implied by the simplified displacement ductility analyses against scale factors F_μ determined from MDOF nonlinear time history analyses, and (2) by judging the displacement modification F_d implied by the simplified displacement ductility analyses against the ratio of the deck displacement found from the MDOF nonlinear time history analysis to the MDOF first mode component of displacement (assuming linear elastic behavior) for the same time history. Also, the mean fundamental lateral mode spectral acceleration S_a (assuming 5% damping) which represented the onset of nonlinear behavior in the platform was determined, to compare with the value determined in the global ductility analysis; this comparison checks the validity of indexing on first mode response to characterize platform strength capacity.

The PC-ANSR model used in Section 6.5.3 was utilized to determine F_μ , the effective load reduction a nonlinear MDOF system is entitled to based on ductile action, and to evaluate the

relationship between inelastic and equivalent elastic (first mode) deck displacements. Rayleigh damping was assumed, with mass and stiffness-proportional coefficients balanced such that 5% critical damping was achieved in the first two fundamental lateral modes.

The model was analyzed using a series of nine earthquakes (see Table 6-8). By conducting a series of analyses, the major component of motion was alternately placed on the principal axes of the platform, to ensure both frames would be subject to the most severe component of motion. Three damage measures were used: brace local ductility (using the cyclic limit as a target) global displacement ductility (using the allowable as determined from the ductility analyses), and leg-pile hinge ductility (using a limit of two as a target) were used as criteria for F_μ . The ratio of inelastic to elastic displacement was averaged for an overload of two, using a spectral acceleration of 0.13 g as a reference. The mean values of F_μ for each damage measure, and the ratio of inelastic to elastic deck displacement, are shown in Tables 6-26 and 6-27.

Table 6-26: $S_{a-yield}$, F_μ and Deck Displacement Ratio (X major)

Factor	Yield	Target	$S_{a-yield}$ (g)	COV	Mean	COV
F_μ Global	X=8"	Y=16"	0.19	0.23	2.20	0.24
F_μ Local (brace)	buckling	$\sim\mu=5$	0.38	0.18	1.67	0.33
F_μ Local (leg)	full plastic	$\mu=2$	0.16	0.21	1.40	0.21
$\Delta_{inelastic}/\Delta_{elastic}$	-	-	-	-	1.01	0.22

The results obtained from the PC-ANSR analyses indicate there is a moderate contribution from multiple modes to the response of the platform. In several of the analysis cases, damage was recorded at lower levels of excitation that would have been assumed from the static

analyses. However, the mean initiating spectral acceleration value for damage to the deck legs is still 20% higher than the “biased” value of S_a (0.13 g) proposed in Section 6.5.3.

Table 6-27: $S_{a-yield}$, F_μ and Deck Displacement Ratio (Y major)

Factor	Yield	Target	$S_{a-yield}$ (g)	COV	Mean	COV
F_u Global	Y=8"	Y=16"	0.18	0.20	2.16	0.26
F_u Local (brace)	buckling	$-\mu=5$	0.36	0.21	1.44	0.28
F_u Local (leg)	full plastic	$\mu=2$	0.17	0.20	1.38	0.23
$\Delta_{inelastic}/\Delta_{elastic}$	-	-	-	-	0.95	0.26

From the results of the global ductility analyses in the previous section, it is reasonable to classify the platform as bilinear non-degrading. Referring to Figure 5-3, the effective load reduction, assuming the platform can develop a ductility of 1.6 to 2.1, would be in the range of 1.8 to 2.2. Given the target ductility for the MDOF analyses was effectively 2.0, and F_μ was found to be slightly higher than 2.0 for both directions, it can be seen that the values estimated based on the results of the static analyses are in good agreement with those from the MDOF dynamic analyses. Similarly, referring to Figure 5-4, the ratio of inelastic to elastic displacement is expected to be close to unity. These results are also in good agreement with those obtained from the MDOF analyses.

Overall, the factors generated using the MDOF analyses are in good agreement with those found from the static analyses; however, as for Platform D, the issue of multi-mode effects indicates some caution is required when applying static methods. In this instance, multiple modal contributions tended to increase scatter in the results, as the weak links in the platform system (the deck bays) were sensitive to both multi-axis and higher-order modes.

6.5.5 Platform E: Summary of Results

Platform vibration properties estimated using the simplified method compare very well with those calculated by analyzing a full-frame model of the platform. Using the API Soil A response spectrum as a basis for loads, the simplified demand-capacity provides an excellent estimate of platform capacity, as expressed by response spectrum ZPA, as compared to results from use of the full-frame model.

The global ductility analyses indicated that multi and higher mode effects could be significant for this platform; the difference in effective yield spectral intensities was on the order of 30% for considering and not considering higher modes. The simplified ductility analysis captures the approximate global displacement limit of the platform, and the general hysteretic envelope is similar to that estimated by static pushover analysis for two configurations of horizontal framing. However, it must be noted that the envelope curve estimated by the simplified method is very approximate, being a semi-empirical representation of the pushover behavior of the platform; member local demands are not well-represented at large levels of global displacement.

MDOF response factors and elastic-to-inelastic deck displacement ratios derived from nonlinear time history analysis compare very well with factors and ratios selected based on the results of the global displacement ductility analyses; however, the effective yield strength of the platform was in between the two values estimated during the global ductility analyses. This case points out the difficulties of applying the simplified approach when multi-axis response and higher-ordered modes are an issue.

6.6 LARGE-SCALE APPLICATION OF SIMPLIFIED METHODS: BAY OF CAMPECHE PLATFORMS

In 1997 PEMEX/IMP undertook an effort to assess a number of aging platforms in the Bay of Campeche region, as documented by Perez, et al. (1998). Twenty platforms were analyzed by the program TOPCAT (Template Offshore Platform Capacity Assessment Tools), which performs the simplified analysis calculations; seventeen of these were also analyzed by the programs DAMS (Brown and Root, 1997) and SACS Collapse (EDI, 1997). DAMS is a modal analysis program which can generate force patterns for use with SACS Collapse. This effort by PEMEX/IMP (1999) presented an opportunity to perform further benchmarking of the simplified earthquake assessment approach on a large scale. Information on the TOPCAT program is documented in the User Manual by Stear and Bea (1999). Table 6-28 lists the platforms and selected analytical results.

Comparisons were made between the following: (1) fundamental vibration periods estimated by DAMS and TOPCAT, (2) resultant base shears corresponding to the 200-year return period earthquake estimated by DAMS and TOPCAT, and (3) reserve strength ratios (RSRs) defined by the scale factor needed to increase the load pattern established from the 200-year return period earthquake to the point at which collapse has occurred. Collapse was defined in this case as the point of ultimate lateral strength. No accounting for dynamics, i.e. R factor load reduction, was taken in the analyses, so the results should be viewed as conservative.

Ratios of the TOPCAT/DAMS-SACS results were determined and are show in Figure 6-52. Table 6-29 shows the means of the ratios and the associated coefficients of variation. The

TOPCAT program tends to overestimate the fundamental periods of the structures, and correspondingly underestimate the base shear from the response spectrum. This is due to the fact that base shear determined from the response spectrum decreases with increasing period. The mean ratio of the RSRs is, surprisingly, 1.00; however, there is some statistical variability which encourages caution on the part of the analyst when applying the simplified methods. The significance of this variability is highlighted in Figure 6-52.

Table 6-28: Results from Application of Simplified Screening to PEMEX/IMP Platforms

	Platform	# Legs	Water Depth (ft)	Fundamental Period (sec)		200-Year Earthquake Base Shear (kips)		RSR Against Collapse SACS TOPCAT
				DAMS	TOPCAT	DAMS	TOPCAT	
1	Abkatum-A Compression	8	120.3	2.1	2.2	2617	2857	4.02 4.03
2	Abkatum-A Production	8	120.6	1.7	1.9	1133	1161	5.40 4.79
3	Abkatum-A Gathering	8	121.6	1.7	1.8	1948	1348	3.81 4.36
4	Abkatum-A Drilling	8	119.7	2.0	2.6	1628	1266	3.15 3.39
5	Abakatum-D Production	12	125.0	2.1	2.2	3323	3210	4.60 4.24
6	Batab-1A Min. Platform	4	148.0	1.7	1.6	570	532	4.66 5.58
7	Pol-A Drilling	8	115.3	1.8	1.9	1876	1722	4.60 5.11
8	Pol-D Drilling	8	123.7	2.0	2.0	1806	1730	4.50 5.18
9	Caan-A Drilling	8	84.7	1.8	1.9	1918	1713	4.60 5.11
10	Pol-A Production	8	116.3	1.4	1.5	1400	1177	4.80 5.02
11	Pol-A Gathering	4	115.0	1.5	1.7	974	708	6.23 6.71
12	Pol-A Habitation	8	115.5	1.4	1.5	1609	1374	6.02 6.79
13	Pol-A Compression	8	114.9	2.2	2.5	2532	2079	4.28 4.33
14	Uech-A Drilling	8	158.8	2.2	2.4	1859	1664	4.20 5.73
15	Abkatum-A Production	12	120.7	2.0	2.4	3394	3220	4.20 3.05
16	Abkatum-A Bridge	4	122.3	1.5	1.7	848	672	6.05 6.45
17	Ixtoc-A Telecom.	8	160.7	1.8	3.0	1414	1534	3.60 2.45
18	Caan-C Drilling	8	84.6	1.8	2.0	1980	1508	4.40 4.26
19	Chuc-A Drilling	8	104.0	1.9	2.4	2202	1685	4.51 2.28
20	Abakatum-D Drilling	8	127.3	2.1	2.6	2121	1593	4.30 3.87

While there is a reasonably level trend in RSR for the first 12 platforms, the last 8 show wide variation. This is due in part to the limited nature by which structural configurations can be modeled in TOPCAT; the program requires special adaptation for certain structural configurations which was not done in for this test. The trend for the first 12 platforms also indicates TOPCAT is overpredicting the RSR relative to DAMS-SACS; however, this can likely be traced to underprediction of the initial load pattern.

TOPCAT/DAMS-SACS Comparisons

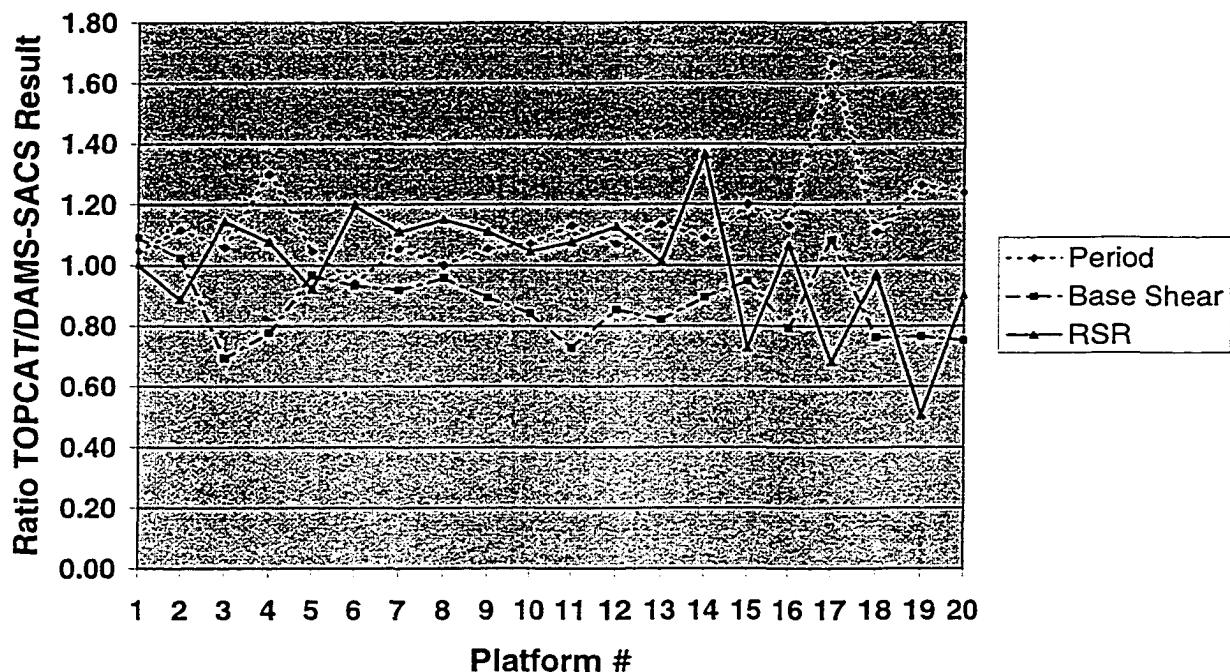


Figure 6-52: Trends in TOPCAT/DAMS-SACS Ratios

Table 6-29: Mean Ratios of Period, Base Shear and RSR (TOPCAT/DAMS-SACS)

	Mean	COV
Fundamental Period	1.14	0.13
Base Shear	0.87	0.13
RSR	1.00	0.19

Table 6-30 shows the platforms ranked in terms of RSR by each analysis method. While several of the platform RSR estimates are significantly apart in position, notably platforms 14 and 19, most others are within a few positions of one another.

Table 6-30: Ranking of Platforms by RSR

	Platforms by Number.....															Least Critical				
	Most Critical.....							Platforms by Number.....												
T	19	17	15	4	20	1	5	18	13	3	2	10	9	7	8	6	14	16	11	12
D	4	17	3	1	14	15	13	20	18	8	19	5	7	9	6	10	2	12	16	11

T=TOPCAT, D=DAMS-SACS

The simplified methods as implemented in the TOPCAT program provide a reasonably accurate and affordable means of assessing platforms for earthquake loads. Based on the comparisons performed in this section, a bias of 1.15 should be used to factor up earthquake loads determined by the TOPCAT program. In addition, caution is needed when platforms of special configuration are encountered.

6.7 OBSERVATIONS AND CONCLUSIONS

The simplified methods documented within this chapter provide an effective static means of evaluating the dynamic performance of jacket-type platforms. The following are points of note from the analyses:

- The vibration property-estimating approach is seen to work quite well for structures in less than 300 ft of water with grouted legs; for Platforms B and C, which did not have grout in the annulus, the simplified approach underpredicted the periods by approximately 15%. Modal force estimates using the simplified properties compared well to those found using a 3-D model.

- The capacities derived from the methods of Chapter Four compare well with capacities derived using more rigorous methods or empirical calibration. The simplified ductility analysis provides a fairly good qualitative assessment of global displacement ductility capacity; however, it is emphasized that this is a semi-empirical approach, and does not rigorously track member forces and load redistribution. The envelop curves derived from this method do not compare with those derived from a complete static pushover analysis; they are intended to qualitatively reflect the robustness of the platform based on component (deck bay, jacket bay, foundation) strength and post-yield behavior.
- For platforms which possess long braces, the local load associated with excitation of the brace's vibration modes can result in axial capacity reductions on the order of 10%. The most severe case would result from a platform with short (1 second or less) fundamental modes, and very flexible braces; however, this condition is unlikely to occur in practice. Nevertheless, it is important that these forces be accounted for when performing reassessments as well as preliminary design. Most braces will have periods much shorter than those associated with the vibration of the platform itself, and hence the braces may be treated as rigidly-mounted equipment with little or no additional amplification. In lieu of rigorously evaluating the brace-structure interaction, these preliminary results suggest that a local acceleration of twice the PGA of the API RP 2A (1993) spectrum used in the analysis is sufficient to envelope the associated excitation of braces in platforms with fundamental lateral periods in the range of 1.4 seconds to 2.9 seconds. However, additional case studies should be performed before this approximation is used in practice.

- The response factors derived in Chapter Five compared reasonably well with those estimated using MDOF models. Effective dynamic capacity for a platform can be estimated using the relationship:

$$F_{yield} > \frac{F_{elastic}}{R}$$

where $F_{elastic}$ is the base shear corresponding to the first mode forces determined from the elastic response spectrum for the level of earthquake excitation specified, and R is the load reduction factor associated with platform hysteresis. F_{yield} is the base shear from first mode forces which results in yielding in the platform determined from the static pushover analysis. It must be noted that this base shear is not the true base shear from the earthquake; it is used as a convenient reference to quantify the total lateral load needed to induce yielding. However, it must be recognized that higher mode effects can have a significant effect on the indicated yield strength and post-yield behavior of a platform (by changing which component is the component to yield). Simply using first mode forces to derive post-yield behavior works well if the platform is first mode dominated. If it is not, a more effective means of biasing the strength of the platform must be found. As a gross approximation, it is possible to consider all modal forces when deriving the yield strength of the platform; however, this is deemed very conservative.

Based on the results of both the case studies and the PEMEX/IMP(1999) experience, the simplified approach appears suitable to the task of assessing platforms for earthquake loads. Care must be taken, however, when applying static methods to a dynamic problem. The

following guidelines should be taken as “good practice” recommendations when using response factor-modified static analysis for earthquake assessment:

- Excitation should be considered on both principal axes (and both loading directions on each axis) as well as on the diagonal. For an 8-leg jacket with no symmetry in framing, this would correspond to performing eight analyses: four on the principal axes and four on the diagonals.
- More than one load pattern should be used; as a minimum, a pattern associated with first mode forces and a pattern which results in demands similar to those from multi-mode excitation should be considered.
- The response factor associated with the least combination of strength and ductility will govern the capacity of the platform. If several components are close to yield, the effective dynamic capacity should be determined based on the least ductile yield mechanism.
- Ductile capacities of elements should be observed when using static methods. Elements such as braces might not be able to develop local ductilities higher than four or five, which can effectively limit the global ductility to two or less depending on the structural configuration.

Following these guidelines should ensure that ductile behavior is incorporated into a platform’s design without the need of resorting to time history analysis. However, it should be emphasized that these methods have been developed with application to shallow-water locations. Platforms in deeper waters, and platforms with a high consequence of failure,

should always be checked using time history analysis to ensure yield mechanisms develop as expected when the structure is subjected to severe earthquake ground motions.

CHAPTER SEVEN:

A SIMPLIFIED SEISMIC RELIABILITY ANALYSIS

7.0 INTRODUCTION

Previous chapters of this dissertation have focussed on deterministic analysis of platforms subjected to earthquakes. However, there are many uncertainties in both the expected ground motions and the structural properties of a platform which require application of probabilistic methods in order to obtain a more meaningful indication of analytically-predicted performance beyond the simple pass-fail result of a deterministic analysis.

Structural reliability methods provide an orderly approach for accounting for load and strength uncertainties in an earthquake assessment. Readers desiring detailed information on structural reliability are referred to Thoft-Christiansen and Baker (1981); only essential details are summarized here. Structural reliability can be approximately defined as the probability that a structure will not fail when subjected to a given load or set of loads over a set time interval. Structural reliability theory has two fundamental assumptions:

- Structural components exist in discrete “states.” For practical purposes, two-state behavior (either failed or unfailed) is often assumed.
- The state of a component can be described by a collection of random variables.

Assuming the load and strength behavior of a simple structural system is completely described by a set of random variables $X(x_1, x_2, \dots, x_n)$, and these variables possess a joint probability density function $f_X(x)$, and further assuming the state of the system is described by

a limit-state function $g(x)$ such that $g(x) \leq 0$ indicates failure, the probability of failure p_f can be determined from the n-fold integral:

$$p_f = \int_{g(x) \leq 0} f_x(x) dx$$

The reliability of the system p_s is thus:

$$p_s = 1 - p_f = P[g(x) > 0]$$

Simple linear limit-state functions with random variables demand S and capacity R can often be used to characterize the performance of structural elements, components, and complete systems:

$$R - S = g(x) \geq 0$$

For seismic reliability analysis, a variety of demand and capacity measures can be used; for example, S can represent load, displacement, or hysteretic energy, and is hence compared with a corresponding R of yield strength, drift or ductility limit, or hysteretic energy absorption capacity. It is important to recognize, however, that S is determined from a combination of variables and analytical processes that relate general earthquake source parameters such as magnitude and distance to element, component and system demands for a specific structure. As noted in Chapters Two and Three, evaluation of S is a multi-staged process; magnitude and distance are related to time-varying ground displacements at a given site location, which are then translated into demands using the dynamic equations of motion of the structural system as a transfer function. For linear (non-yielding) systems, this translation of ground motions into demands is relatively straight-forward, as the demand on linear systems can be evaluated using either MDOF time history analysis or superposition of

modal responses. However, performing this translation for yielding systems poses special challenges in assessing reliability due to the interaction of demand and capacity; in this case the demand-capacity interaction must be linearized or evaluated explicitly through the use of time history analysis.

Chapters Three, Four and Five have described a deterministic analysis framework by which the “global” demand-capacity behavior of a jacket-type platform subjected to earthquake excitation can be assessed. Using global forces as a common measure, yield limit state performance of a platform is governed by:

$$F_{yield} \geq F_{elastic}$$

where F_{yield} is the minimum base shear determined from static pushover analysis which results in yielding of platform components, and $F_{elastic}$ is the force pattern used in the static pushover analysis scaled to an elastic response spectrum parameter (either S_A or ZPA).

Ductile or collapse limit state performance of a platform is governed by:

$$F_{yield} \geq \frac{F_{elastic}}{R} \text{ or } F_{yield} R \geq F_{elastic}$$

where R is the effective reduction in elastic response spectrum forces which can be taken in recognition of yielding and hysteretic energy dissipation in the platform.

In this Chapter, a simple approach to evaluating the “global” yield and collapse reliabilities of jacket-type platforms is developed, using the above limit state equations but recognizing the demand, capacity and demand-capacity interaction are random variables. The yield and collapse reliability of each platform component (deck bay, jacket bays, foundation) are formulated using mean-value first-order second-moment (MVFOSM) approximations. Yield

and collapse behaviors of platform components are assumed to be governed by simple linear limit-state functions. The demand and capacity variables which make up these functions are assumed to be log-normally distributed. A platform is assumed to behave as a series system of components, whereby achieving a component yield or ductile limit state results in yielding or ductile failure of the platform. Hence, the “global” reliability of the platform structural system is bounded by assuming at the lower-bound that all component failure states are perfectly correlated, and at the upper-bound that all component failure states are uncorrelated.

The yield and collapse reliabilities, as expressed by safety indices, of a small platform are determined using the simple approach. From these safety indices, the respective probabilities of yielding and collapsing are estimated. These failure probabilities are then compared to the yield and collapse probabilities determined from application of a more rigorous approach; in the rigorous approach, Monte Carlo simulation is used together with nonlinear time history analysis to evaluate the trend in platform behavior for 1000 random trials.

7.1 MVFOSM RELIABILITY ANALYSIS

The mean-value first-order second-moment (MVFOSM) reliability method has been developed to allow for solution of reliability problems when the actual joint probability density function governing system performance cannot be determined, and/or when the integration necessary to solve the probability of failure is too complex for practical solution. An excellent description of the method is contained in Mansour (1987); the essentials of the method are summarized here for completeness.

For a simple linear system with capacity R and demand S , a safety margin M can be defined as:

$$M = R - S$$

The mean μ_M and variance σ_M^2 of M are given by:

$$\mu_M \equiv \mu_R - \mu_S$$

$$\sigma_M^2 \equiv \sigma_R^2 + \sigma_S^2 - 2\rho_{RS}\sigma_R\sigma_S$$

where:

μ_R, σ_R = mean and standard deviation of capacity function

μ_S, σ_S = mean and standard deviation of demand function

ρ_{RS} = correlation between demand and capacity

Defining a standardized margin G , such that G has zero mean and unit standard deviation,

$$G = \left(\frac{M - \mu_M}{\sigma_M} \right)$$

the probability of failure p_f associated with the state $M \geq 0$ can be expressed by:

$$p_f = F_M(0) = F_G\left(\frac{-\mu_M}{\sigma_M}\right) = F_G(-\beta)$$

where F_M and F_G refer to the cumulative distribution functions. β is referred to as the safety index. If the distribution function F_G is known, then the exact probability of failure associated with β can be determined. For an unknown or unspecified distribution function, however, there will be a corresponding (though unspecified) probability of failure for each β . Therefore, β can be taken as a safety measure when applying the MVFOSM method.

Assuming both R and S are normally-distributed, the probability of failure can be found from:

$$p_f = \Phi(-\beta)$$

where Φ is the standard normal variate function.

The lognormal distribution is often found to provide a good fit to most variables in engineering applications (Ang, Tang, 1975). Assuming R and S to be lognormally-distributed, the limit state function M can be expressed by:

$$M = \ln(R) - \ln(S)$$

The probability of failure is again estimated from:

$$p_f = F_M(0) = F_G\left(\frac{-\mu_M}{\sigma_M}\right) = F_G(-\beta)$$

but in this case:

$$\mu_M = \ln\left(\frac{\mu_R}{\mu_S} \sqrt{\frac{1+V_S^2}{1+V_R^2}}\right)$$

$$\sigma_M^2 = \ln(1+V_R^2) + \ln(1+V_S^2) - 2 \ln(1+\rho_{RS} V_R V_S)$$

where:

μ_R, V_R = mean and coefficient of variation of capacity function

μ_S, V_S = mean and coefficient of variation of demand function

ρ_{RS} = correlation between demand and capacity

A more-general formulation for M is discussed in the following. Assuming M is a general function of random variables ($x_1, x_2, x_3, \dots, x_n$) with correlation coefficient matrix Σ , μ_M and σ_M^2 can be approximated by:

$$\mu_M \equiv M(\bar{X})$$

$$\sigma_M^2 \equiv \nabla M|_{\bar{X}} \sum \nabla M^T|_{\bar{X}}$$

where:

$$\begin{aligned} \bar{X} &= [\mu_{x_1} \quad \mu_{x_2} \quad \dots \quad \mu_{x_n}] \\ \Sigma &= \begin{bmatrix} \sigma_{x_1}^2 & \rho_{x_1 x_2} \sigma_{x_1} \sigma_{x_2} & \dots & \rho_{x_1 x_n} \sigma_{x_1} \sigma_{x_n} \\ \rho_{x_2 x_1} \sigma_{x_2} \sigma_{x_1} & \sigma_{x_2}^2 & \dots & \rho_{x_2 x_n} \sigma_{x_2} \sigma_{x_n} \\ \dots & \dots & \dots & \dots \\ \rho_{x_n x_1} \sigma_{x_n} \sigma_{x_1} & \rho_{x_n x_2} \sigma_{x_n} \sigma_{x_2} & \dots & \sigma_{x_n}^2 \end{bmatrix} \end{aligned}$$

and:

$$\nabla M = \left[\frac{\partial M}{\partial x_1} \quad \frac{\partial M}{\partial x_2} \quad \dots \quad \frac{\partial M}{\partial x_n} \right]$$

In the next two sections, approximate distributions for demand and capacity at the platform component level are formulated in accordance with the MVFOSM method.

7.2 PROBABILISTIC FORMULATION OF DEMAND

Earthquake demands for the simplified assessment approach are expressed as modal forces and moments from response spectrum analysis, as discussed in Chapter Three. Variability in the resulting component demands will depend upon the following, assuming linear structural response:

- Variability in the response spectrum ordinates, for a given period and damping ratio.

- Variability in structural periods, mode shapes and modal damping ratios.
- Variability in the phasing between modes.

Variability in response spectrum ordinates is primarily due to Type I uncertainties. The input to the response spectrum, ground motion from earthquakes, is essentially a random process; in addition, there are uncertainties affecting the relationship between earthquake source parameters and the scale factors on the ground motion. Variability in load due to uncertainties in the structural system (masses, stiffnesses and damping values) is primarily due to Type II uncertainties. These can stem from the lack of statistical data on structural parameters, but will also reflect approximations in the way response is evaluated. Variability in the phasing between modes is a combination of Type I and Type II uncertainties; the phase is random, and there are approximations in how it is accounted for in an analysis. Determining the composite load variability and bias is discussed in the next three subsections.

7.2.1 Variability in Response Spectrum Ordinates

The ordinates of an elastic response spectrum are random variables, with scatter resulting from the range in responses to the family of ground motions used to make up the spectrum for each specific period and damping combination. The variability in the ordinates is dependent to some degree on the scale parameter used to derive the spectrum; use of peak ground velocity (PGV) as a scale parameter typically provides less scatter in response spectrum ordinates than the use of peak ground acceleration (PGA) in the period range from 1 to 2 sec and above for firm soil spectra, as noted by Naeim and Anderson (1993). This is

illustrated in Figures 7-3 for the two response spectra (5% damping) in Figures 7-1 (PGV scaled) and 7-2 (PGA scaled) derived from the family of five time histories shown in Table 7-1. Examining Figure 7-3, it is observed that scaling by PGA provides less variability in the period range below 2 sec, while PGV provides less variability for periods higher than 2 sec.

Table 7-1: Time Histories Used for Spectra

Event	Station	Direction	Magnitude	Distance (km)
Imperial Valley May 18, 1940	El Centro Irrigation District	S90W	7.1 ML	8
Kern County July 21, 1952	Taft Lincoln School Tunnel	S69E	7.7 ML	56
San Fernando February 9, 1971	Los Angeles 445 Figueroa St.	N52W	6.5 ML	41
Imperial Valley October 15, 1979	El Centro James Road	S50W	6.6 ML	22
Loma Prieta October 17, 1989	Hollister Airport	255	7.1 ML	45

Much effort has been expended in studying appropriate distributions for elastic response spectrum ordinates; as noted by Miranda (1991) many studies have suggested the use of normal, log-normal, Rayleigh, exponential, Gumbel Type I, and gamma distributions. To evaluate the statistical properties of spectral ordinates, the ordinates associated with three periods (0.5 sec, 1.0 sec, 2.0 sec) from a mean elastic response spectrum developed from the spectra in Figure 7-2 were plotted in Figures 7-4, 7-5 and 7-6 for three distributions: log-normal, normal, and exponential. It is observed the normal and log-normal distributions provide a reasonable fit; a Kolmogorov-Smirnov test comparing the difference between the estimated and presumed probabilities showed the maximum differences were 0.27, 0.36 and 0.37, respectively, for the three distributions. While recognizing this is a small (5) set of samples, the log-normal distribution will be assumed for spectral ordinates.

Response Spectrum, PGV = 20 in/sec

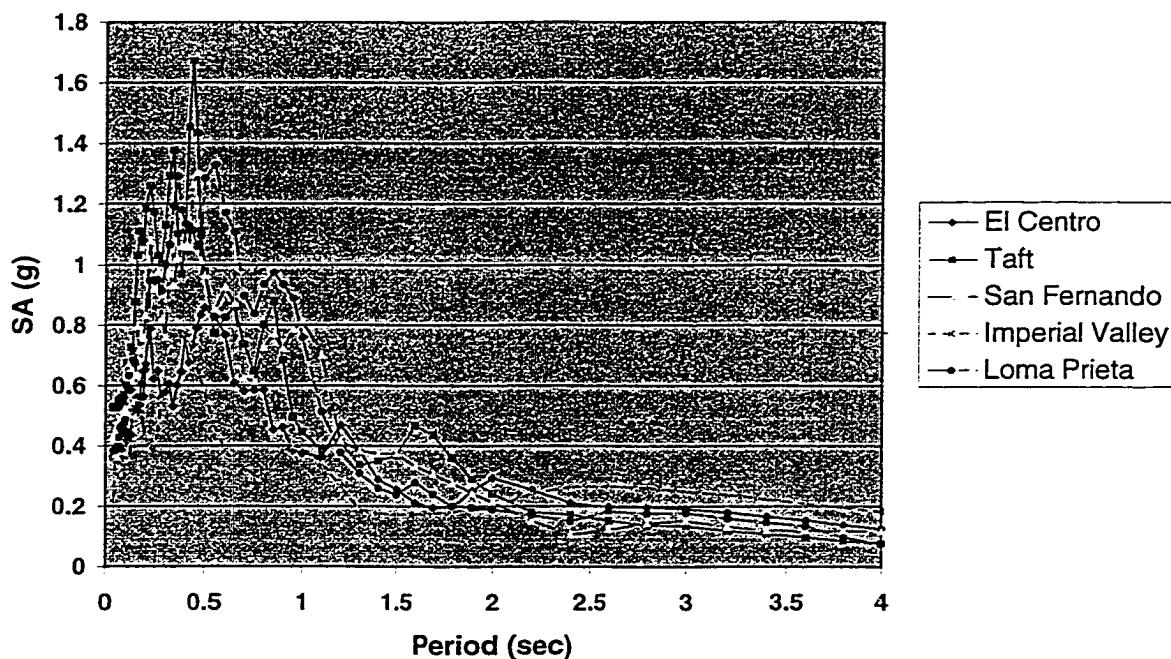


Figure 7-1: Response Spectrum, PGV Scaling

Response Spectrum, PGA = 0.3 g

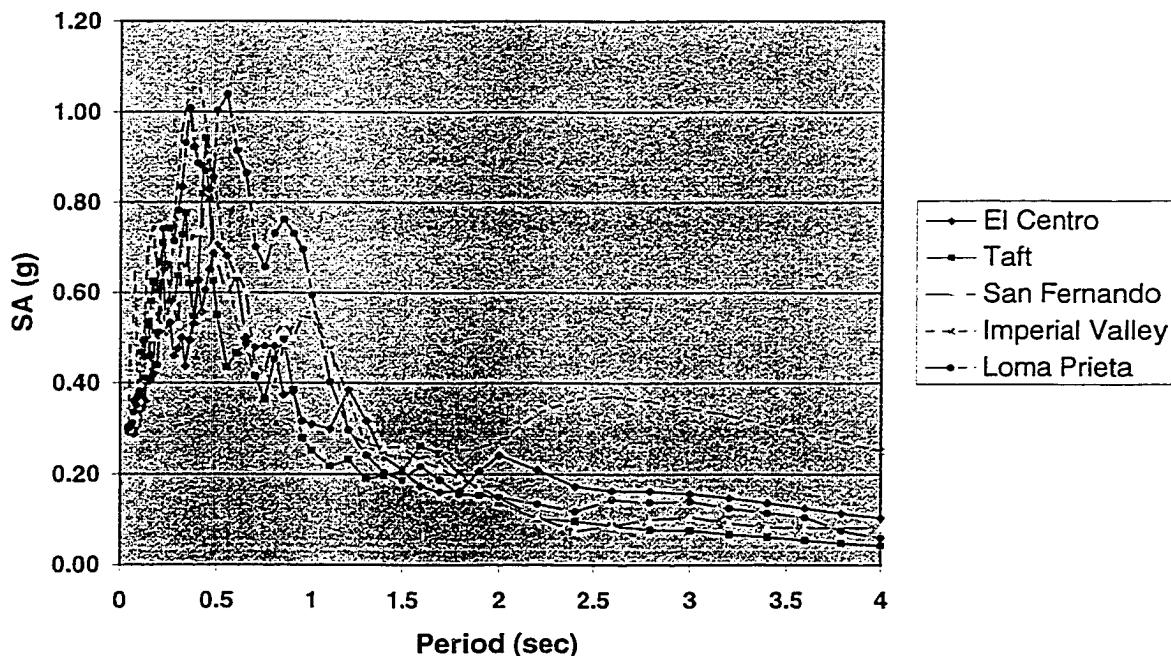


Figure 7-2: Response Spectrum, PGA Scaling

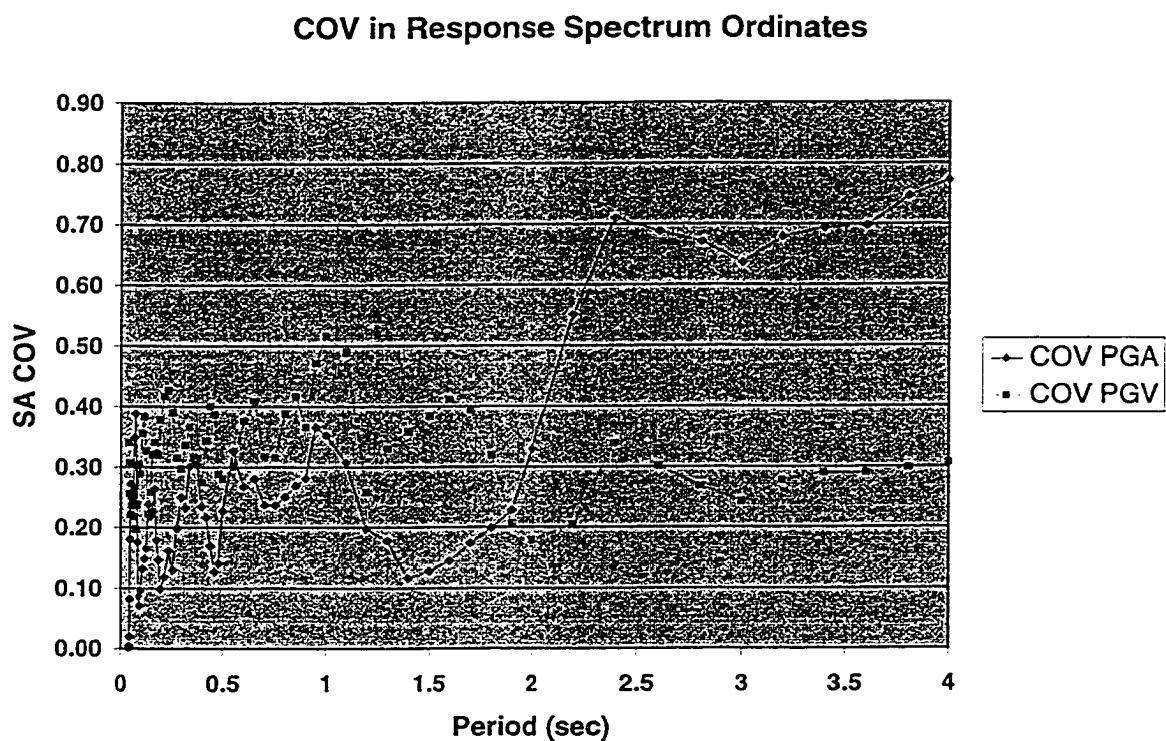


Figure 7-3: Uncertainty in Response Spectrum Ordinates

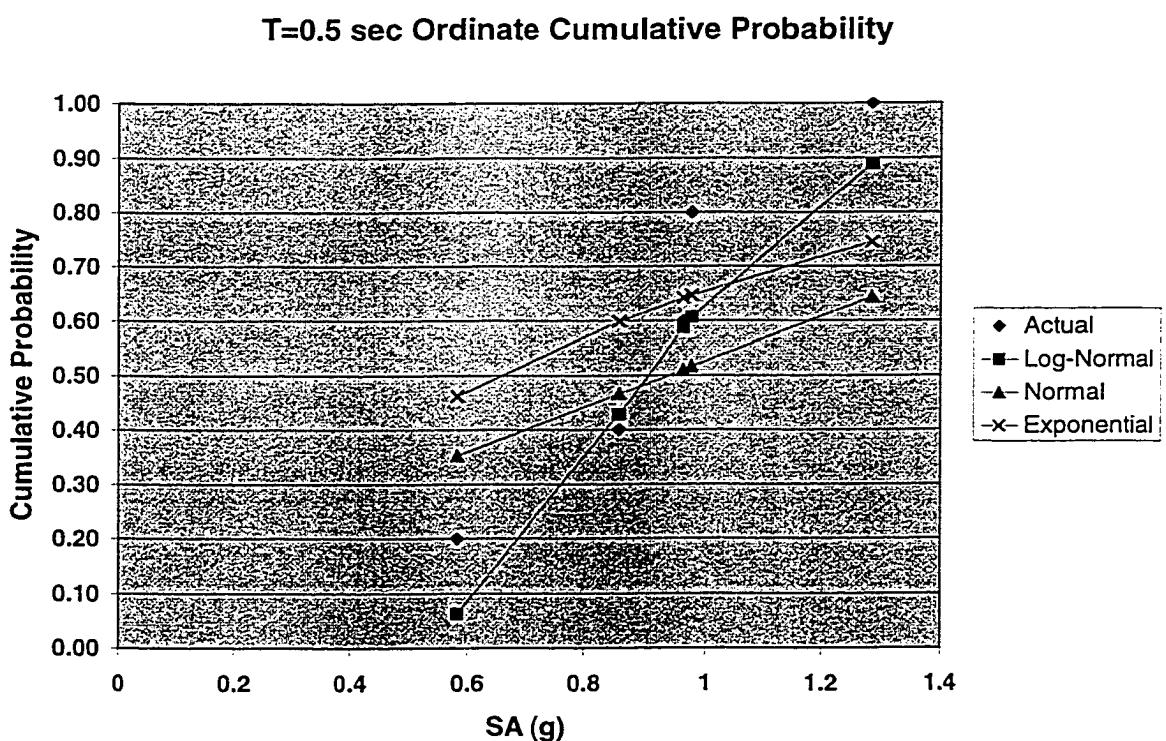


Figure 7-4: Spectral Ordinate Cumulative Probability, $T = 0.5$ sec

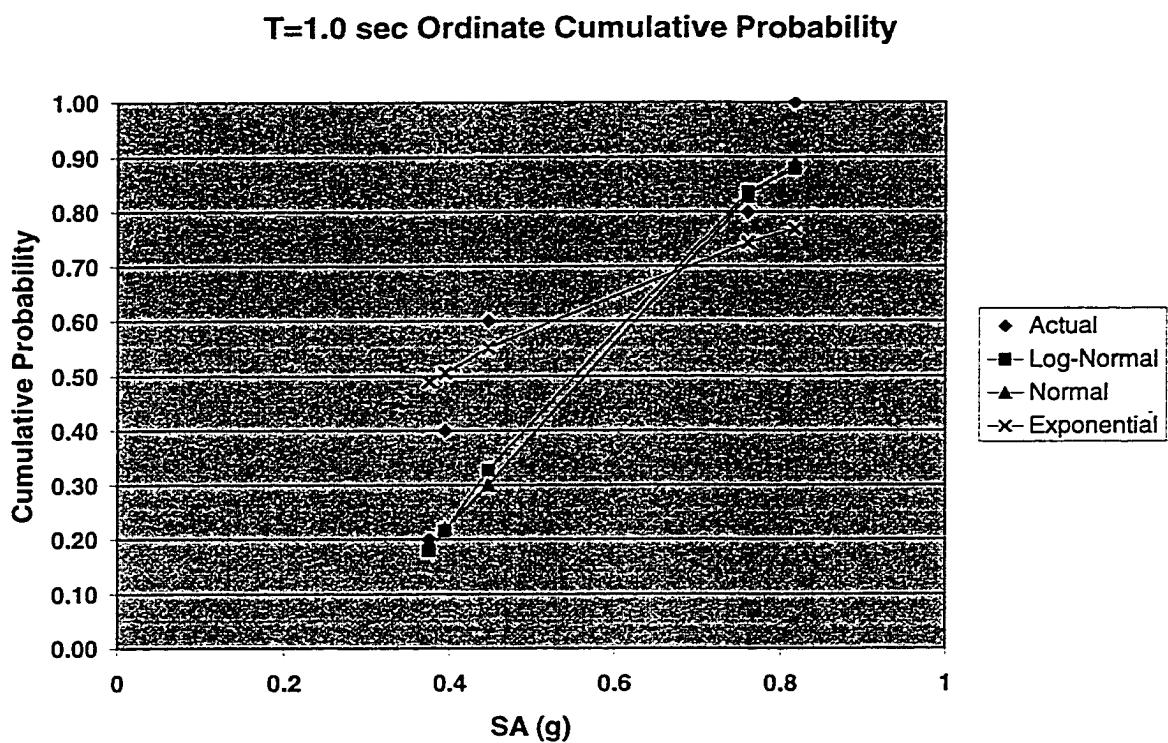


Figure 7-5: Spectral Ordinate Cumulative Probability, $T = 1.0$ sec

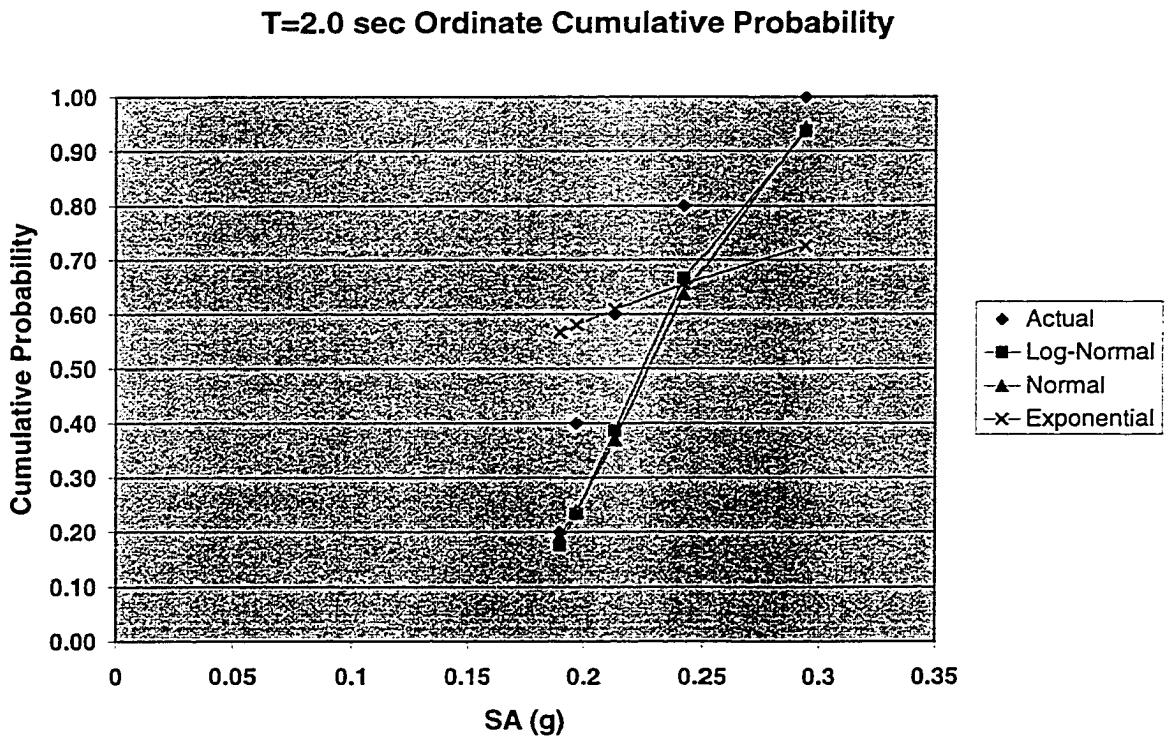


Figure 7-6: Spectral Ordinate Cumulative Probability, $T = 2.0$ sec

The variability in the ordinates will increase further when uncertainties in the earthquake source-PGA/PGV relationships and earthquake magnitude are considered; total variabilities (again expressed by COV) of 300% have been noted by Bea (1991) for spectrum ordinates derived from a family of time histories from southern California earthquakes in the surface magnitude range of 6.0 to 6.5, with recording distances in the range of 20 km to 30 km. For the purposes of assessment, spectral ordinates are assumed to be linearly related to the scaling parameter PGA or PGV. Hence, the total variability in the spectral ordinates will be given by:

$$\sigma_{S_A-Total}^2 = S_A^2 \sigma_{PGX}^2 + PGX^2 \sigma_{S_A}^2$$

7.2.2 Variability Due to Structural Parameters

Additional variability will be introduced into the selection of response spectrum ordinates associated with each mode due to variations in structural parameters such as mass and stiffness, which affect period; the ordinates will also be affected by the assumed level of modal damping. Response spectrum forces will also be affected by changes in mode shape. However, providing mass, stiffness and damping COV's are small, these additional sources of variability will have a minor effect when compared to the inherent variability in the spectral ordinates. To illustrate this point, a sensitivity study was performed using Platform A from Chapter Six (refer to Section 6.2). The parameters shown in Table 7-2 were varied according to the ranges shown, and the resulting range in fundamental period and response spectrum gross story shears (API Soil B response spectrum, ZPA = 0.25 g) were determined.

Table 7-2: Platform A Sensitivity of Response to Structural Properties

Variable	Range	T ₁ (sec)	Deck Bay Shear (kips)	1 st Jacket Bay Shear (kips)	2 nd Jacket Bay Shear (kips)	Foundation Shear (kips)
Deck Weight	+10% to -10%	1.60 to 1.47	1252 to 1147	1369 to 1281	1497 to 1421	1683 to 1613
Brace Added Mass, C _M	0.0 to 1.0	1.52 to 1.54	1185 to 1201	1300 to 1325	1423 to 1460	1590 to 1648
Brace Stiffness	+10% to -10%	1.52 to 1.56	1212 to 1187	1339 to 1309	1474 to 1443	1664 to 1630
Pile Axial Stiffness	+40% to -40%	1.42 to 1.78	1289 to 1054	1432 to 1149	1577 to 1269	1750 to 1495
Pile Lateral Stiffness	+40% to -40%	1.50 to 1.62	1226 to 1146	1345 to 1275	1495 to 1392	1678 to 1565
Damping, % Critical	2% to 20%	1.54	1568 to 645	1731 to 712	1906 to 784	2153 to 886

For this platform, structural parameters provide little additional variation in response, with the exception of modal damping ratios, which have a pronounced affect. As noted in Chapter Three, determination of the proper amount of modal damping to use is a challenge, as the damping is a representation of energy dissipation though localized material hysteresis and yielding of soil beneath the jacket. The damping will increase as the excitation increases; hence determination of this damping is an iterative process. In lieu of rigorously correlating damping and excitation, the following simplification is suggested:

- Damping is initially assumed at 5% critical for all platforms, and include jacket-bottom contact when determining foundation stiffness.
- If the induced loads exceed the strength of soil beneath the jacket (which is assumed to be the primary source of additional energy dissipation without grossly changing the platform's vibration properties), recalculate the periods and mode shapes of the platform without including jacket-bottom contact, and recalculate loads using 10% critical damping.

7.2.3 Variability Due to Modal Combination

The last source of uncertainty is the phase between the modal response components. Phasing is somewhat dependent upon distance from the earthquake source; close to the source, components are more likely to be in phase, but at distant locations, the seismic wave trains will likely become separated in time. Unfortunately, phasing information is not contained in the response spectrum, and hence it is accounted for approximately through the use of modal combination rules. As noted in Chapter Three, the SRSS modal combination rule is widely used. According to Chopra (1995), it will generally provide excellent estimates of peak combined responses if:

- Periods of the structure are well-separated (this can be overcome by use of the CQC rule), and damping is greater than 0.5%
- Earthquake excitations have a wide band of frequencies with long phases of strong shaking (i.e. several times longer than the fundamental period of the structure)

The SRSS rule will become less accurate for short-duration impulsive ground motions and ground motions with many cycles of harmonic motion.

To account for variability in the modal combination, a simple bounding approach is taken. An upper-bound response will be determined from using the SRSS modal combination rule, while the lower-bound response will be taken as the single highest modal response.

Variance in the lower-bound response is assumed to be equal to the uncertainty in the associated response spectrum ordinate. The variance of the combined upper-bound modal responses will be given by the following:

$$\sigma_{total}^2 = \sum_{i=1}^N \sigma_i^2 \left(\frac{\partial R_{total}}{\partial R_i} \right)^2$$

where R_{total} is the SRSS combination of all responses R_i . All responses are assumed uncorrelated.

7.3 PROBABILISTIC FORMULATIONS OF CAPACITIES

Strength and ductility capacities of platform elements and components have been formulated in Chapter Four. The strength of the platform system was described by either the base shear corresponding to yielding of a platform component, or the scale factor applied to the force pattern corresponding to yielding of a platform component. The effective ductile capacity of the platform was defined by the product of the strength of the platform and a response factor; this response factor was selected based on the post-yield load-displacement behavior the platform exhibited under a pattern of loads similar to first mode forces or an equivalent general load pattern. Response factors suitable for platform systems have been determined in Chapter Five.

Mean values of platform component strength and ductility, and hence platform system strength and ductile capacities, can be determined using the mean values of the associated element strengths and ductilities in the component capacity formulations. While component strength and ductility uncertainties are small compared to the uncertainties in the loads, these will be documented in this section for completeness.

7.3.1 Unbraced Bays

For the evaluation of mean and variance of unbraced deck bay strength and ductility, M_y , P_{crl} and μ_ϕ are treated as the controlling random variables. The relationships in Sections 4.1.1 and 4.2.1 are used to develop the means and variances. Thus approximate mean yield strength P_u will be found from evaluating the following relationships at the means of M_y and P_{crl} :

$$P_u = \left(\frac{2nM_y^*}{H_d} - V_{p\Delta} \right)$$

where:

$$M_y^* = M_y \cos\left(\frac{\pi}{2} \frac{Q}{P_{crl}}\right)$$

$$V_{p\Delta} = \frac{Q\Delta}{H_d}$$

and:

$$\Delta = M_y^* H_d \left(\frac{H_d}{6EI_d} + \frac{1}{k_{\phi-leg}} \right)$$

Assuming perfect correlation between M_y and P_{crl} , the variance of the strength will be:

$$\sigma_{P_u}^2 = \sigma_{M_y}^2 \left(\frac{\partial P_u}{\partial M_y} \right)^2 + \sigma_{P_{crl}}^2 \left(\frac{\partial P_u}{\partial P_{crl}} \right)^2 + 2\sigma_{M_y}\sigma_{P_{crl}} \left(\frac{\partial P_u}{\partial M_y} \right) \left(\frac{\partial P_u}{\partial P_{crl}} \right)$$

where all partial derivatives are evaluated at the means of M_y and P_{crl} .

The mean maximum displacement the unbraced bay can tolerate is given by:

$$\Delta_{max} = \mu_\phi \Delta_y$$

where:

$$\Delta_y = \frac{6M_y * H^2}{EI}$$

with all relationships evaluated at the means of M_y , P_{crl} and μ_ϕ . The variance of the maximum displacement is found from:

$$\sigma_{\Delta_{max}}^2 = \sigma_{M_y}^2 \left(\frac{\partial \Delta_{max}}{\partial M_y} \right)^2 + \sigma_{P_{crl}}^2 \left(\frac{\partial \Delta_{max}}{\partial P_{crl}} \right)^2 + \sigma_{\mu_\phi}^2 \left(\frac{\partial \Delta_{max}}{\partial \mu_\phi} \right)^2 + 2\sigma_{M_y}\sigma_{P_{crl}} \left(\frac{\partial \Delta_{max}}{\partial M_y} \right) \left(\frac{\partial \Delta_{max}}{\partial P_{crl}} \right)$$

$$\sigma_{\Delta_{max}}^2 = \nabla \Delta_{max} \Sigma \nabla \Delta_{max}^T$$

where:

$$\Sigma = \begin{bmatrix} \sigma_{M_y}^2 & \sigma_{M_y}\sigma_{P_{crl}} & \sigma_{M_y}\sigma_{\mu_\phi} \\ \sigma_{M_y}\sigma_{P_{crl}} & \sigma_{P_{crl}}^2 & \sigma_{P_{crl}}\sigma_{\mu_\phi} \\ \sigma_{M_y}\sigma_{\mu_\phi} & \sigma_{P_{crl}}\sigma_{\mu_\phi} & \sigma_{\mu_\phi}^2 \end{bmatrix}$$

$$\nabla \Delta_{max} = \begin{bmatrix} \frac{\partial \Delta_{max}}{\partial M_y} & \frac{\partial \Delta_{max}}{\partial P_{crl}} & \frac{\partial \Delta_{max}}{\partial \mu_\phi} \end{bmatrix}$$

assuming perfect correlation between all three variables.

7.3.2 Braced Bays

For the evaluation of braced bay strength and ductility, the axial capacities of the braces and tubular joints, the local and batter forces, and the local ductility of braces are treated as random variables. Relationships from Sections 4.1.2 and 4.2.2 are used to develop the means and variances. Mean yield strength of a bay will be given by:

$$P_{u bay} = \sum_{i=1}^N \Delta_{1st} K_i + F_{1L}$$

while variance of the bay strength will be given by:

$$\sigma_{P_{\text{bay}}}^2 = \left(\sum_{i=1}^N K_i \right)^2 \sigma_{\Delta_{1u}}^2 + \sigma_{F_{1u}}^2$$

where:

$$\Delta_{1st} = (P_{u-1st}/K_{1st}) \cos \theta_{1st}$$

P_{u-1st} will be given by the series joint-brace-joint system for each brace position. The mean and standard deviation of this system can be solved by first determining the cumulative distribution function for the combined system, and then applying numerical integration. Means and standard deviations for tubular joint strengths can be taken from test data. Mean brace compression capacity variance can be estimated by first re-arranging the equation governing brace performance:

$$P_u = \frac{M_u}{\left(\frac{1}{1 + 2 \frac{\sin 0.5\epsilon}{\sin \epsilon}} \right) \frac{1}{\epsilon^2} \left(\frac{1}{\cos 0.5\epsilon} - 1 \right) 8\Delta_0} - \frac{wl^2}{8\Delta_0}$$

Assuming the first term is equal to P_{cr} , and assuming the calibration Δ_0 is unity, the variance is given by:

$$\sigma_{P_u}^2 = \sigma_{P_{cr}}^2 + \left(\frac{l^2}{8} \right)^2 \sigma_w^2$$

For the sake of simplicity, the mean of the acceleration used to derive the local load per unit length w is assumed to be equal to the peak spectral acceleration, and the variance in local load is assumed to be equal to the variance in peak spectral acceleration.

The maximum displacement the bay can tolerate will be given by:

$$\Delta_{max} = \min(\mu_{ci}\Delta_{ci})$$

The variance associated with the maximum displacement is estimated from:

$$\sigma_{\Delta_{max}}^2 = \mu_{ci}^2 \sigma_{\Delta_{ci}}^2 + \Delta_{ci}^2 \sigma_{\mu_{ci}}^2$$

The latter two approximations assume all braces will have similar yield/buckling and cyclic ductility variances.

7.3.3 Foundation Lateral and Overturning

Relationships from Sections 4.1.3, 4.1.4 and 4.2.3 are used to estimate the mean strength and ductility of the foundation lateral and overturning mechanisms. However, as noted by Mortazavi and Bea (1997), the lack of data regarding modeling uncertainties precludes the ability to rigorously develop variances for the axial and lateral capacities of the piles. Instead, total capacity uncertainties, such as those documented by Tang and Gilbert (1990), will be used to establish the appropriate variances. For foundation lateral strength, these variances are combined with the variance in the batter forces to estimate the total variance.

7.3.4 Effective Component Ductility Capacities

Distributions of bay and foundation strength are assumed to be log-normally distributed, with means and variances established by the methods described in the previous subsections. Effective ductility capacities are also assumed to be log-normally distributed, but are estimated in the following manner. First, using either a load pattern associated with first-mode forces or a uniform load pattern, the deck displacement associated with the mean yielding of each component is estimated. From this “global” yield point, the “global” post-yield behavior of the platform is determined, using the procedures described in Section 4.3.

Based on the shape of the resulting load-displacement curve and the fundamental period of the platform, a load reduction factor R can be estimated using the modified relationship for F_e described in Section 5.3.3 or by studying the graphs for R as related to specific systems in Chapter Five. The variance in the selection of this factor is taken to be equal to the variance of the component ductility that can be developed in the respective collapse mechanism.

In addition to the variance associated with factor selection, there is also the inherent variance of the factor itself. Distributions for three of the response factors from Chapter Five have been plotted in Figures 7-7, 7-8, 7-9, 7-10, 7-11 and 7-12. All factors are have been derived from the analysis of the bilinear degrading system; results are presented at three periods for two levels of ductile capacity. It is observed that the log-normal distribution provides a reasonable fit to the statistical information collected; a Kolmogorov-Smirnov test comparing the difference between the estimated and presumed probabilities showed the maximum difference for the factors considered was 0.20. Hence, the total variance associated with the effective load reduction is the sum of the variance in factor selection and the variance inherent to the factor.

Once a response factor has been established, the ductile capacity of the component is taken as the product of the component yield or static strength and the response factor:

$$F_{dynamic} = F_{static} R$$

R Factor Distribution for BD T=0.5 sec, Mu=2

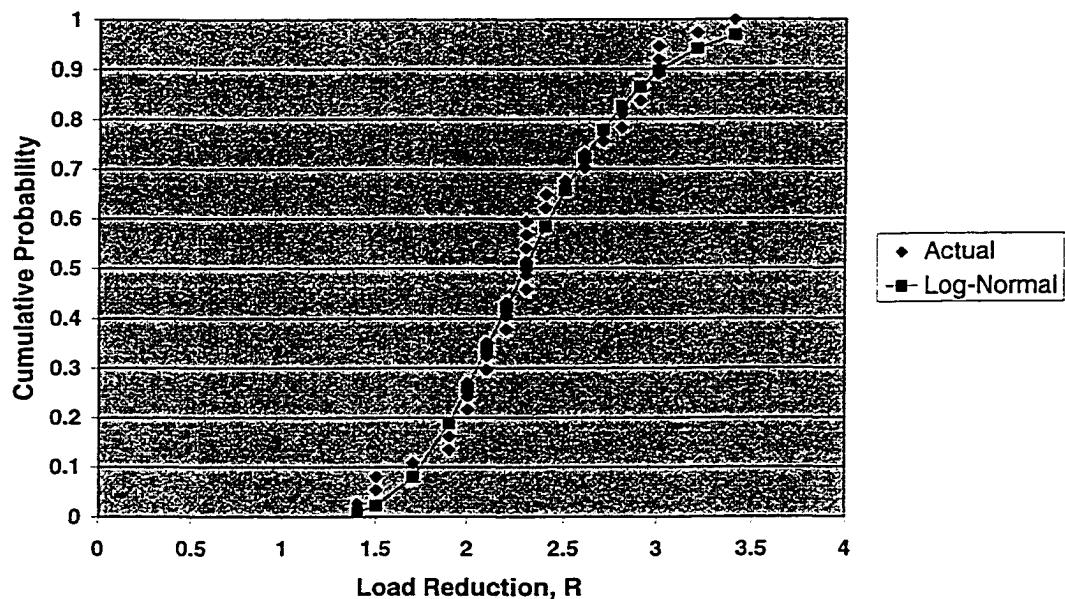


Figure 7-7: Statistics of R Factor: $T = 0.5$ sec, BD, $\mu = 2$

R Factor Distribution for BD T=1.0 sec, Mu≈2

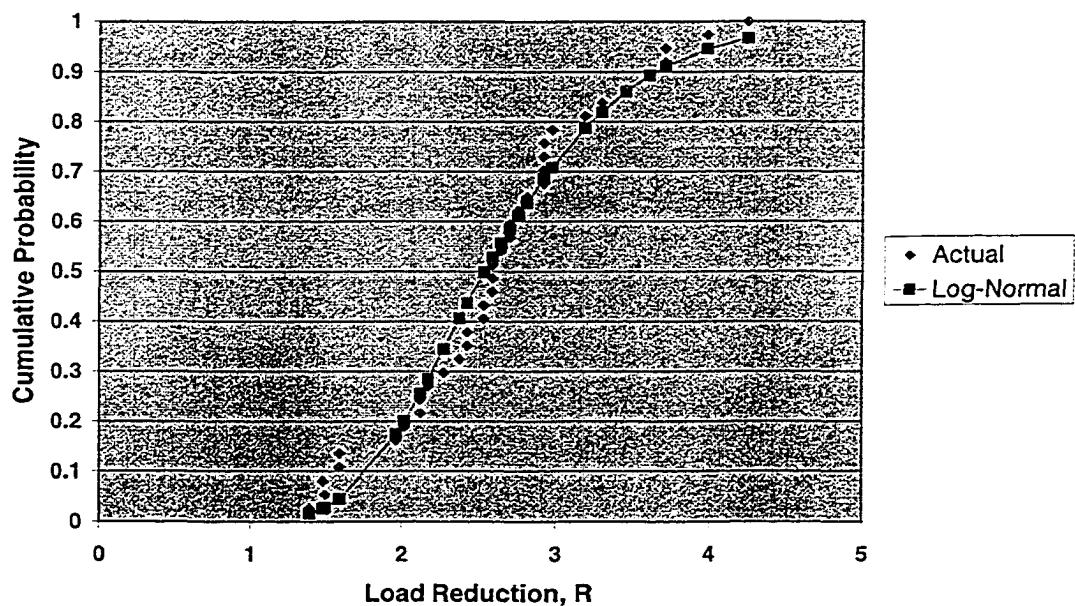


Figure 7-8: Statistics of R Factor: $T = 1.0$ sec, BD, $\mu = 2$

R Factor Distribution, BD T=2.0 sec, Mu=2

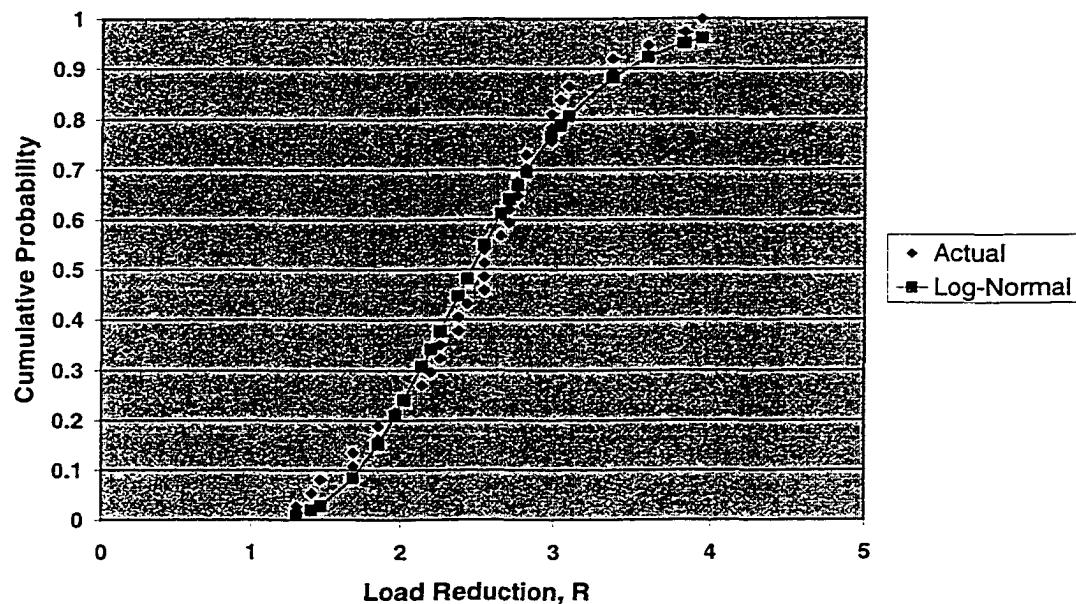


Figure 7-9: Statistics of R Factor: $T = 2.0$ sec, BD, $\mu = 2$

R Factor Distribution for BD T=0.5 sec, Mu=4

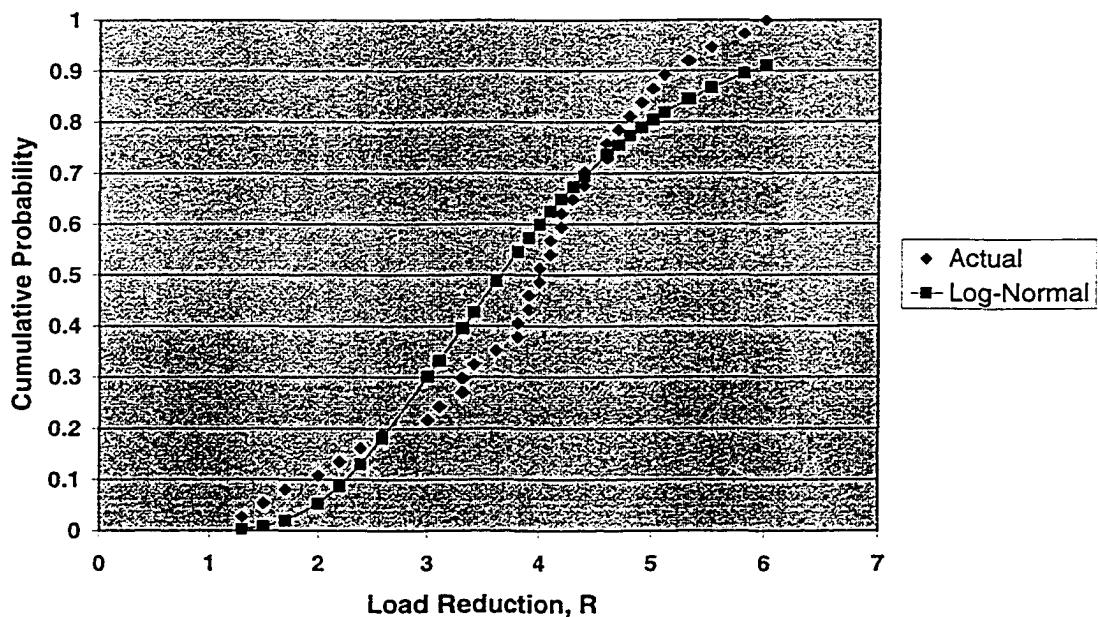


Figure 7-10: Statistics of R Factor: $T = 0.5$ sec, BD, $\mu = 4$

R Factor Distribution for BD T=1.0 sec, Mu=4

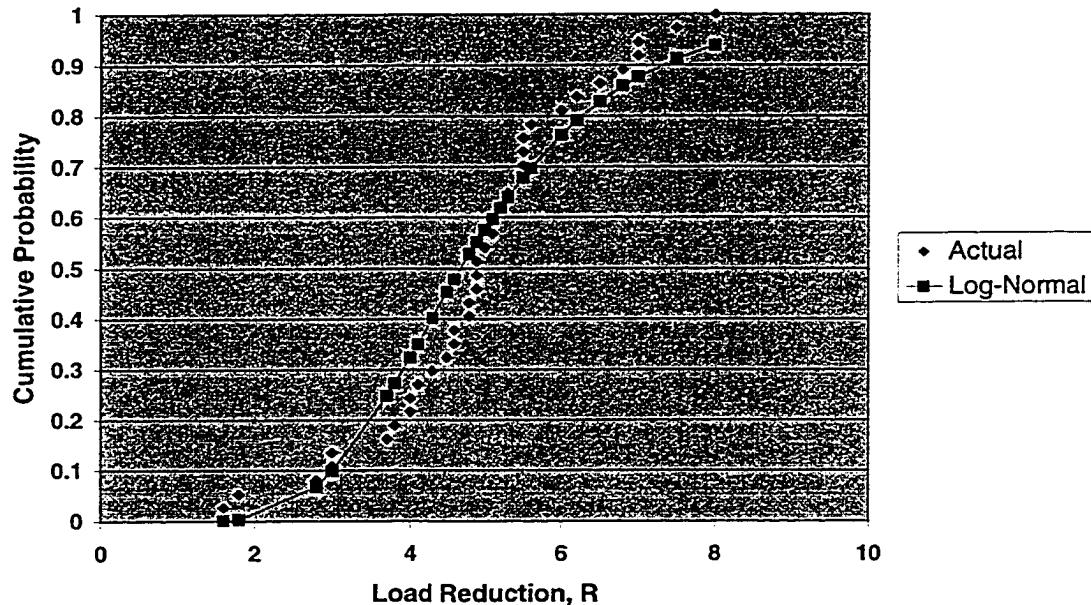


Figure 7-11: Statistics of R Factor: $T = 1.0$ sec, BD, $\mu = 4$

R Factor Distribution, BD T=2.0 sec, Mu=4

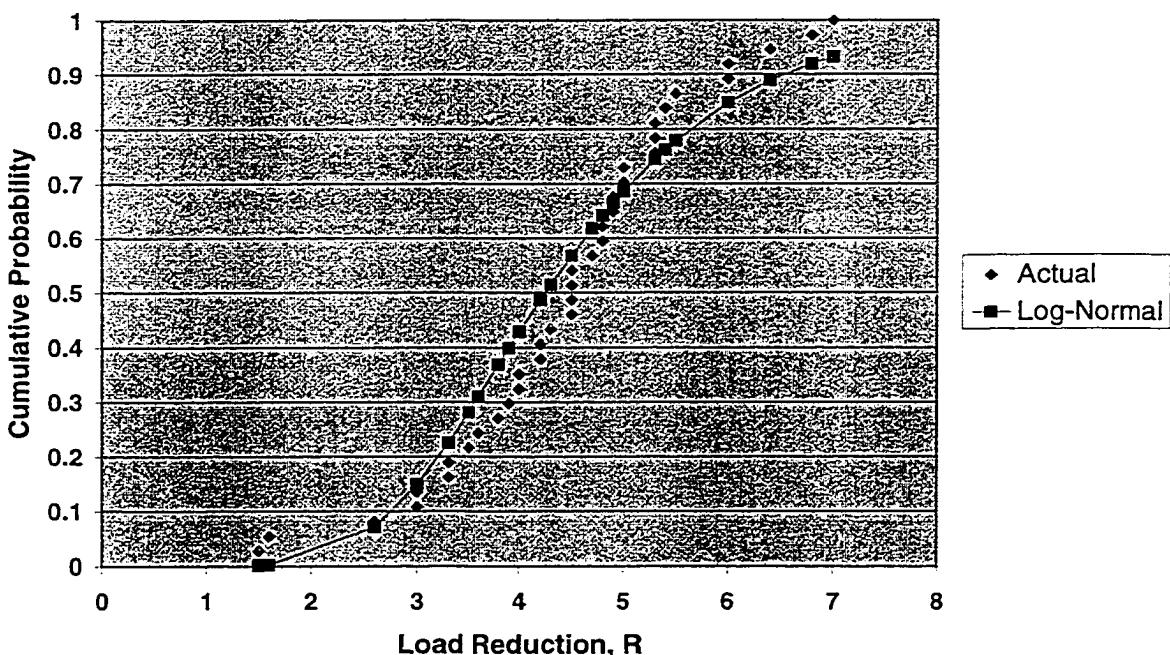


Figure 7-12: Statistics of R Factor: $T = 2.0$ sec, BD, $\mu = 4$

Hence, ductile behavior of platform components are represented by establishing an “effective” dynamic strength. The composite variance associated with the dynamic strength is given by:

$$\sigma_{F_{dynamic}}^2 = F_{static}^2 \sigma_R^2 + R^2 \sigma_{F_{static}}^2$$

It must be remembered that these dynamic strengths are determined by assuming damage concentrates in the component after it yields as described in Section 4.3.

7.4 PLATFORM YIELD AND COLLAPSE PROBABILITIES

Platform yield probability is established by first evaluating the yield reliability β of each platform component (deck bay, jacket bays, foundation lateral and overturning) for earthquake forces; the demands and capacities are assumed to be log-normally distributed. Probabilities of failure are then determined for each component using:

$$p_f = \Phi(-\beta)$$

Yield probability of the platform system is then bounded by considering the platform to behave as a series system. At the lower bound, all platform components are assumed perfectly correlated, and thus p_{f-y} of the platform is given by:

$$p_{f-y} = \sum_{i=1}^N p_{f_i}$$

At the upper bound, all platform components are assumed uncorrelated, and p_{f-y} is given by:

$$p_{f-y} = \max(p_{f_i})$$

Collapse probability of the platform is established by first evaluating the dynamic strength reliability of each platform component for earthquake forces. Again, demands and capacities are assumed to be log-normally distributed. Probabilities of failure are then determined from the safety index as with for yield probabilities of failure, and overall collapse probability is bounded in the same manner. The upper bound probability of failure should itself be bounded based on whether or not damage concentrates in the first component to yield; however, it is conservative to assume the platform collapse capacity is governed by the single component with the highest probability of failure, regardless of whether that component was also the most likely to yield. This distinction is diagrammed below in Figure 7-13.

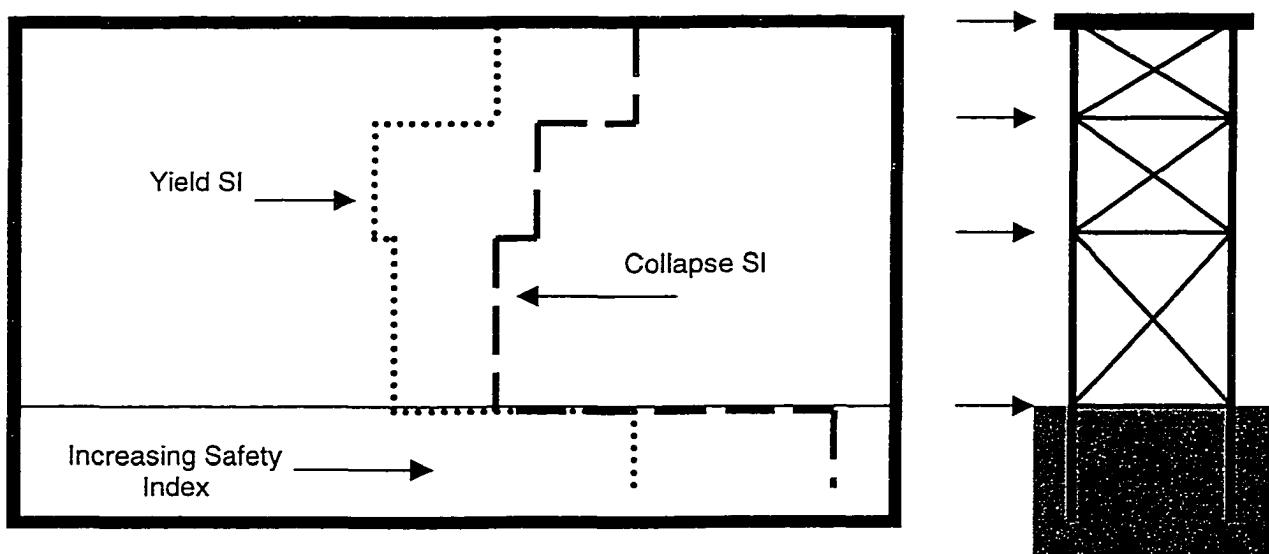


Figure 7-13: Determination of Governing Collapse β

7.5 SIMPLIFIED SEISMIC RELIABILITY ANALYSIS: EXAMPLE

To demonstrate the simplified seismic reliability analysis, the method has been used to determine the yield and collapse probabilities of a simple 2-D platform subject to loads

associated with an arbitrary level of “severe earthquake.” For comparison purposes, the yield and collapse probabilities of the simple platform have also been determined using Monte Carlo simulation together with time history analysis.

The platform analyzed for the exercise is Platform A. Particulars of the platform can be found Chapter Six (Section 6.2). For the purposes of the reliability assessment, stiffness, mass and modal damping ratios (Rayleigh damping was assumed to develop damping coefficients for the time history analysis; 5% critical was assumed) of the platform structure were assumed to be constant. Joint failure in the platform was neglected. The COV's assumed for different platform structural variables are shown in Table 7-3.

Table 7-3: Platform Structural Variables

Structural Variable	COV
P_{crl}	10%
M_v	10%
μ_{cyclic}	30%
Pile P_z	40%
Pile $P_{u,l}$	40%
Pilehead k_z	40%
Pilehead k_x	40%

It is assumed a single source governs ground motions at the site. The response spectrum in Figure 7-2 is presumed to govern the relationship between PGA and spectral acceleration; PGA for the severe earthquake is assumed to be log-normally distributed, with a mean of 0.3 g and a COV of 50%. The spectrum is shown for the period range of interest in Figure 7-14; a uniform spectral uncertainty of 30% is assumed for periods below 2.0 sec. For comparison

purposes, the API Soil B spectrum is also shown. Vertical excitation was ignored in both analyses.

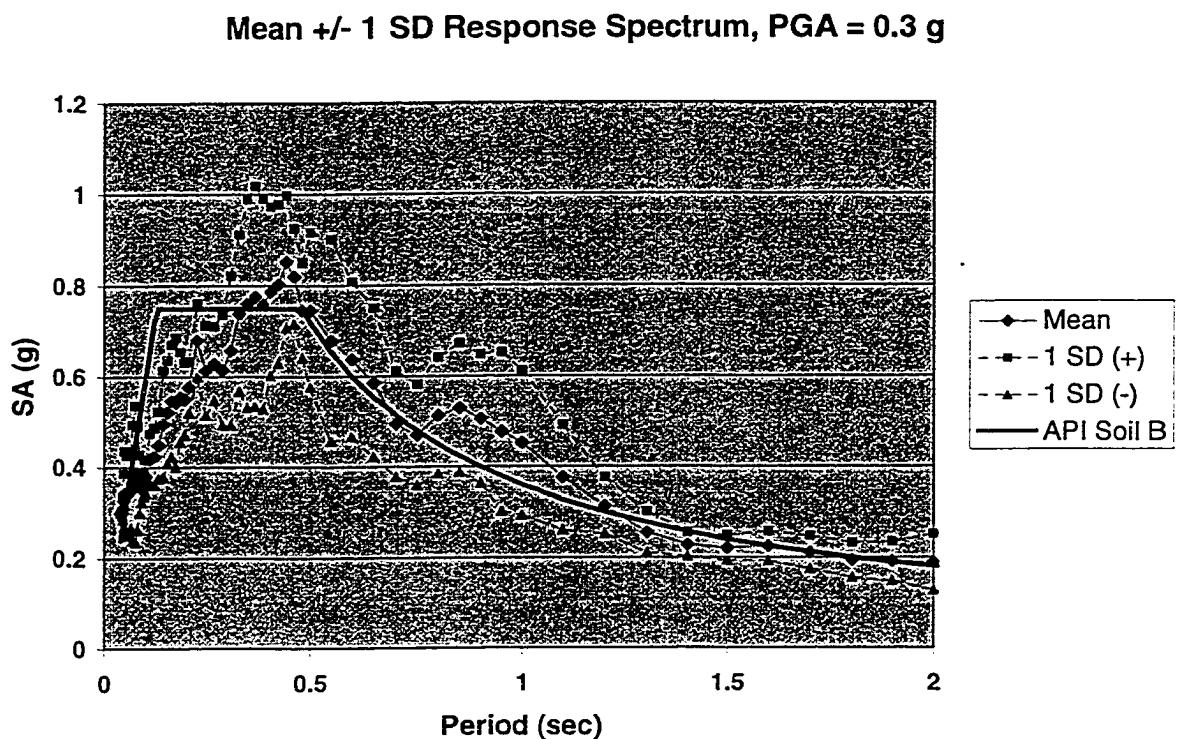


Figure 7-14: Site Response Spectrum

7.5.1 Simplified Reliability Method

Vibration properties for the platform were determined using the simplified modal method described in Chapter Three, and are listed in Section 6.1.1. To account for variability in the response spectrum ordinates due to foundation stiffness uncertainty, the foundation lateral and rotational stiffnesses were approximately related to first mode period by the following period lengthening relationship:

$$\tilde{T}_l = T_l \sqrt{1 + \frac{k_1^*}{K_x} \left[\frac{1}{1 - (T_o / \tilde{T}_l)^2} + \frac{K_x h_1^{*2}}{K_\theta} \right]}$$

where:

T_1 = fixed-base fundamental period

T_o = natural period of foundation mass

k_1 = effective horizontal stiffness of fixed-base fundamental

K_x = horizontal stiffness of foundation

K_θ = rotational stiffness of foundation

h_1^* = effective mass center above base, not including foundation mass

The effective horizontal stiffness may be approximated by:

$$k_1^* = \frac{4\pi^2(0.9M_1)}{T_1^2}$$

where:

M_1 = inertial mass of platform (it is assumed the first lateral mode has 90% mass participation)

The natural period of the foundation mass may be estimated from:

$$T_o = 2\pi\sqrt{\frac{W_o}{gK_x}}$$

where:

W_o = weight of foundation mass included in model

g = acceleration due to gravity

Hence, the variance in period is taken to be equal to:

$$\sigma_{T_1}^2 = \sigma_\theta^2 \left(\frac{\partial T_1}{\partial K_\theta} \right)^2 + \sigma_x^2 \left(\frac{\partial T_1}{\partial K_x} \right)^2 + 2\sigma_\theta\sigma_x \left(\frac{\partial T_1}{\partial K_\theta} \right) \left(\frac{\partial T_1}{\partial K_x} \right)$$

assuming perfect correlation between foundation axial and lateral stiffness. The variability in the fundamental period due to foundation flexibility is assumed to be representative of the

variability in all periods due to foundation flexibility. To carry this variability through to load uncertainty, the relationship between T and S_A is linearized at the mean value of T .

Effective load reduction was determined based on the likely collapse mechanisms to form: collapse of deck or jacket bays, foundation lateral subsidence, or foundation overturning. For each mechanism, the global ductility which could be tolerated was established, and then used to select an R factor to modify the associated yield capacity. The platform was assumed to possess “strong” horizontal framing for the purpose of determining jacket capacity. Hence, load reduction factors for the deck and jacket bay mechanisms were selected from Figure 5-27. The foundation mechanisms were assumed to exhibit minimal softening and strength reduction, hence Figure 5-3 was used to select load reduction factors for these mechanisms. The uncertainty associated with effective load reduction R was set at 30%. Reviewing the graphs in Chapter Five, it is seen 30% provides a reasonable bound on COV_R in the neighborhood of the fundamental period of this platform for different load reduction mechanisms.

Table 7-4 depicts the mean and COV for loads and platform component capacities and the associated component safety indices for yielding. Results for both lower-bound and upper-bound loading are shown. The mean and COV of the global ductility attainable in each mechanism and the associated effective load reduction R is shown in Table 7-5, along with safety indices for collapse.

Probabilities of yielding and collapse are shown in Table 7-6 based on individual component strengths and collapse mechanisms. Using the concept of upper and lower bounds on yield and collapse, it is observed that the lower bound on yielding probability is 7.5% (yielding of 1st jacket bay braces), while the upper bound is 17.4%. Similarly, the lower bound on collapse probability is 0.5% (hinging of piles, although 1st jacket bay braces are close), while the upper bound is 2.3%.

Table 7-4: Yield Reliability

Component	LB Load (kips)	COV	UB Load (kips)	COV	Capacity (kips)	COV	LB β	UB β
Deck Bay	1448	0.63	1483	0.71	8197	0.18	3.11	2.86
1 st Jacket	1680	0.63	1702	0.71	3539	0.22	1.44	1.35
2 nd Jacket	1835	0.63	1895	0.71	5634	0.22	2.05	1.88
Pile Lat.	520	0.63	534	0.71	2192	0.40	2.20	2.07
Pile Axial	2969	0.63	3058	0.71	10400	0.40	1.81	1.81

Table 7-5: Collapse Reliability

Component	Global Ductility	COV	R	COV	Capacity (kips)	COV	LB β	UB β
Deck Bay	3.2	0.36	3.5	0.30	28690	0.46	4.21	3.96
1 st Jacket	2.7	0.40	3.0	0.30	10617	0.50	2.54	2.42
2 nd Jacket	2.7	0.40	3.0	0.30	16902	0.50	3.05	2.87
Pile Lat.	1.6	0.50	1.8	0.30	3946	0.60	2.55	2.42
Pile Axial	2	0.50	2.4	0.30	24960	0.60	2.67	2.54

Table 7-6: Probabilities of Yield and Collapse

Component	Yielding		Collapse	
	LB	UB	LB	UB
Deck Bay	0.0009	0.0021	0.0000	0.0000
1 st Jacket	0.0751	0.0882	0.0055	0.0078
2 nd Jacket	0.0203	0.0299	0.0012	0.0020
Pile Lat.	0.0137	0.0194	0.0054	0.0077
Pile Axial	0.0263	0.0348	0.0037	0.0055

7.5.2 Monte Carlo Simulation with Time History Analysis

A Monte Carlo simulation was performed to benchmark the results of the simplified reliability method. The Monte Carlo simulation consisted of performing 1000 trials, with each trial consisting of a time history analysis of Platform A using the program ANSR. For

the Monte Carlo simulation, the variables listed in Table 7-3 were varied in accordance with the means and variances listed assuming log-normal distribution. The time history scale factor was varied according to the mean and variance listed above; the actual ground motion time history used with each run was selected randomly according to a uniform distribution.

1000 trials conducted in order to determine the associated probabilities of failure for the yielding and collapse condition. Yield was defined as the yielding of any element, while the collapse condition was established by exceeding the cyclic ductility of any element. Based on the results of the simulation, the probability of yielding during the severe earthquake was determined as 91/1000 or 9.1%. This compares very well with the lower bound estimated from the simplified method. The probability of collapse during the severe earthquake was determined as less than 1/1000 or < 0.1%; cyclic ductilities were not exceeded during any of the trials conducted. This estimate also compares favorably with the lower bound estimated from the simplified analysis.

7.5.3 Comparison of Results

The bounded probabilities of failure determined in the simplified reliability assessment compare favorably with those from the simulation exercise. The orders of magnitude are similar for both the yield and collapse probabilities; however, the simulation exercise did not contain enough trials to sufficiently resolve collapse probabilities. However, the simplified values should clearly be sufficient for the purposes of preliminary screening. In addition, the exercise confirms that the use of static methods to resolve the demand-capacity evaluation for this platform is sufficient in comparison with time history analysis.

It should be noted that this exercise has been framed in terms of reliability against an arbitrary level of severe earthquake. Hence, the probabilities determined are for satisfaction of the yield and collapse limit states for that severe event. This information can easily be used to construct annual or lifetime probabilities of yield or collapse, by combining the event-specific results with the probability of occurrence of severe earthquakes. Thus, annual probabilities of failure would be given by:

$$P_{f\text{-annual}} = \left(p_f \Big|_{severe} \right) P_{severe\text{-annual}}$$

7.6 CONCLUSIONS

A simplified seismic reliability analysis procedure using the mean-value first-order second-moment (MVFOSM) method has been presented. Reliability is resolved at the component level, assuming yield and collapse demands and capacities are log-normally distributed. Overall platform yield and collapse probabilities of failure are then determined by considering the platform to behave as a series system. Upper and lower bounds are determined by alternately considering the behavior of components to either be uncorrelated or perfectly correlated.

An example simplified reliability analysis has been conducted using a simple platform. Annual yield and collapse probabilities determined by application of the simplified method were compared to yield and collapse probabilities determined through application of Monte Carlo simulation and time history analysis. The probabilities of yield and collapse are found to bound the simulation results quite well.

CHAPTER EIGHT: CONCLUSIONS AND RECOMMENDATIONS

8.0 SUMMARY

Although the number of platforms in seismically-active regions remains small today, with new technology extending the life of old oil fields, these platforms are being called upon to serve past their original design lives. While there exist comprehensive structural analysis programs capable of determining the nonlinear response of large jacket-type platforms in the time domain, these programs require a high degree of expertise and computational resources to operate.

In this study, simplified procedures have been developed to assess the structural integrity of jacket-type platforms for earthquake loading. The following issues have been addressed:

- Determination of platform vibration properties; simple procedures for deriving the principal vibration properties of a platform were developed and tested.
- Estimate forces on platform components from earthquake excitation; using the modal properties from the vibration procedure together with a response spectrum, reasonable estimate of component loads were established.
- Estimate platform displacements and accelerations at different framing levels; this is accomplished using methodology associated with determining the response of mounted equipment.
- Determination of the strength and ductility of platform structural components; using virtual work, the strength of likely collapse mechanisms in the platform can be

determined, while through consideration of platform element cyclic ductilities and the presumption of damage concentration in a collapse mechanism, estimates of the global displacement ductility which can be tolerated in platform component mechanisms can be made.

- Determination of the effective increases in static lateral load capacity of platform systems by implicitly accounting for the nonlinear hysteretic action of a yielding platform system. 68,816 SDOF systems with four types of hysteresis were analyzed, and both effective reduction in elastic load R and displacements of nonlinear systems normalized by displacements of linear systems were evaluated. Adjustments to an earlier rule on deriving load reduction factors were suggested. Comparisons were also made between yielding MDOF and SDOF systems to evaluate the utility of using SDOF R factors to represent load reduction/effective capacity increase in MDOF systems.
- Developing a simplified reliability framework by which estimates of platform yield and collapse probabilities can be estimated. A MVFOSM approach was taken to formulating platform component yield and collapse reliabilities; from these reliabilities, bounds on the probabilities of yielding and collapse can be estimated.
- Verification of the simplified procedures; six case studies and seven examples were performed to evaluate the simplified methods.
- Development of software which performs the simplified procedures; a program called TOPCAT (Template Offshore Platform Capacity Assessment Tools) has been developed to perform the simplified demand and capacity analyses described herein. This program is documented in the User Manual by Stear and Bea (1999).

8.1 CONCLUSIONS

The effective reduction in elastic load R due to nonlinear hysteresis has been evaluated for 68,818 nonlinear SDOF systems with four general types of nonlinear behavior: bilinear non-degrading, bilinear stiffness-degrading, stiffness and strength degrading, and strength degrading. This study confirms the dependence of R on period and local soil conditions, and has resulted in proposed modifications to a simple rule used from estimating effective load reduction from static analysis. In addition, the displacements of nonlinear systems normalized by the displacements of equivalent linear systems (i.e. with the same period and damping) have been studied, and a displacement ratio factor F_d has been developed; results indicate the “equal displacements” rule is a good approximation for determining the displacement of a nonlinear SDOF system from the displacement of an equivalent linear system, but is also sensitive to period and local soil conditions. Use of SDOF systems to represent the response of MDOF systems appears to be a good approximation so long as the MDOF system is 1st mode dominated, i.e. participating mass in the first mode is 70% to 80%. The factors developed in this study should be of use in further enhancing simple preliminary design procedures for yielding structures.

The results of the deterministic case studies in Chapter Six indicate the simplified procedures developed in Chapters Three and Four provide estimates of platform demand-capacity behavior which are in good agreement with the results of more detailed analyses. Periods and mode shapes were estimated within 17% of those found using 3-D frame models; associated response spectrum loads were determined within a similar margin. Simplified procedures used to estimate global displacement ductility provided reasonable identification

of collapse mechanisms and the ductility which could be tolerated in those mechanisms; ductility tended to be estimated on the low side by was within ~20% of the ductility estimated from a static pushover analysis. Finally, the *R*-factor modified static capacities of the platforms were found to give good approximations to the dynamic performance of the platforms, and the equal displacement rule was again confirmed to be a reasonable approximation. A large-scale assessment exercise of twenty platforms has further confirmed the utility of the simplified methods in the screening of platform fleets.

The reliability exercise performed as part of Chapter Seven has highlighted the importance of including the effects of uncertainties on response; while earthquake loads tend to have large inherent (Type I) uncertainties, platform components such as piles can also have significant uncertainty (Type II), due to lack of data regarding soil properties and an inability to represent local nonlinear effects such as strain-rate strength dependence outside of a detailed context. These uncertainties will change the focus of likely failure modes, as seen in the example. The use of the simplified methods together with bounding approximations on platform loads result in probabilities of yielding and collapse which are in reasonable agreement with those found from simulation analysis.

It is clear the simplified procedures documented herein can provide a reasonable basis for assessing structural integrity. However, the procedures can also be used in preliminary design and the checking of more involved analyses. Given the recent progress in computer technology, it is not unlikely that within ten years, an analysts will have the capability to develop extremely detailed models of structures and analyze them for a variety of complex

dynamic loading. It should be remembered, however, that as systems become more capable of representing detail, they also become more prone to error via mistakes in data entry or a lack of physical understanding on the part of the user. Simplified procedures such as the one outlined herein provide very useful “sanity checks” against the results of detailed analysis programs, and emphasize physical understanding; hence, simplified procedures should always have a place in an analyst’s toolbox.

8.2 RECOMMENDATIONS

Further verification of the simplified procedures documented within this study should be performed. In particular, the platforms studied herein tended towards shallow depth with heavy decks; these structures are clearly first-mode dominated. Loads in the simplified assessment procedure are bounded, in order to envelope both multi-mode effects and yielding of platform systems; it would be interesting to apply the procedures to the evaluation of several of the very deep (600 ft +) structures currently located in seismically-active regions.

Additional data should be obtained to further develop the simplified ductility estimating procedures described in Chapter Four. Additional data needs to be collected on the cyclic ductility of braces and beam-columns. These limits, while simplified, provide a designer with an excellent starting point in the identification of what limits should be taken in both static and dynamic analyses of structures subjected to earthquake excitation. It must be recognized that many analysts still rely upon numerical instability as a limit in the analysis of structures, without rigorously addressing what could be low-cycle fatigue or other limits which are not explicitly addressed by computer analysis software.

A great weakness of using static methods is the inability to account for load duration. One means of approximating the duration is to use input energy spectra. While this assessment process suggests the use of cyclic ductility limits, which represent an upper-bound of the likely number of extreme-displacement cycles within which no serious degradation occurs, a more satisfactory approach would be to develop dual strength criteria: one limit based on a maximum excursion, and other based on energy which much be absorbed.

Foundations still provide a significant source of uncertainty. Behavior of the foundation system is bounded so as to capture its impact on platform vibration properties and hence induced earthquake loads. Development and verification of simplified procedures to account for soil sampling, testing, and cyclic-dynamic loading conditions is a significant research topic. It has been established from field tests that jacket-bottom contact is a significant source of stiffness, and that effective modal damping increases as excitation of these structures increases; simple methods for estimating the relationship between damping and excitation are needed.

The factors documented in this study should contribute significantly to the body of knowledge which has developed around this subject over the past thirty years. However, additional research is needed on response factors for nonlinear systems. In particular, the application of response factor techniques to large multi-story buildings should be considered. In addition, response factors for non-standard structures such as bridges and unique buildings

should also be considered. Another source of research would be response factors for piping and refinery and powerplant equipment.

REFERENCES

- Al-Sulaimani, G., and Roessett, J. M., "Design Spectra for Degrading Systems," Journal of Structural Engineering, Vol. 111, No. 12, ASCE, New York, NY, December 1985. J
- American Petroleum Institute, "Recommended Practice for Planning, Designing and Constructing Fixed Offshore Platforms – Load and Resistance Factor Design," RP 2A-LRFD, 1st Edition, Washington, D.C., July 1993. B
- American Petroleum Institute, "Recommended Practice for Planning, Designing and Constructing Fixed Offshore Platforms – Working Stress Design," RP 2A-WSD, 1st Edition, Washington, D.C., 1969. B
- American Petroleum Institute, "Recommended Practice for Planning, Designing and Constructing Fixed Offshore Platforms – Working Stress Design," RP 2A-WSD, 15th Edition, Washington, D.C., 1984. B
- American Petroleum Institute, "Recommended Practice for Planning, Designing and Constructing Fixed Offshore Platforms – Working Stress Design," RP 2A-WSD, 20th Edition, Washington, D.C., July 1993. B
- American Petroleum Institute, "Recommended Practice for Planning, Designing and Constructing Fixed Offshore Platforms – Working Stress Design," Supplement 1, RP 2A-WSD, 20th Edition, Washington, D.C., December 1996. B
- Anagnostopoulos, S. A., "Nonlinear Dynamic Response and Ductility Requirements of Building Structures Subjected to Earthquakes," R72-54, Department of Civil Engineering, MIT, Cambridge, MA, September 1972. T
- Ang, A. H-S. and Tang, W. H., Probability Concepts in Engineering Planning and Design, Wiley and Sons, New York, NY, 1975. B
- Astaneh-Asl, A., "Plastic Design of Steel Structures," CE248N Class Notes (based on Carquinas Bridge Report), Department of Civil and Environmental Engineering, University of California at Berkeley, Fall 1996. T
- Barkan, D. D., Dynamics of Bases and Foundations, McGraw-Hill, New York, NY, 1962. B
- Bazzurro, P., and Cornell, C. A., "Seismic Hazard Analysis of Nonlinear Structures. I: Methodology," Journal of Structural Engineering, ASCE, Vol. 120, No. 11, November 1994. J
- Bea, R. G., "Background for the Proposed International Standards Organization Reliability Based Seismic Design Guidelines for Offshore Platforms," Proceedings of the Earthquake Criteria Workshop: Recent Developments in Seismic Hazard and Risk Assessments for Port, Harbor, and Offshore Structures, Yokohoma, Japan, April 1997. C

Bea, R. G., "Dynamic Response of Piles in Offshore Platforms," Dynamic Response of Pile Foundations: Analytical Aspects, editors: M. W. O'Neill and R. Dobry, ASCE, New York, NY, 1980.

B

Bea, R. G., "Dynamic Response of Marine Foundations," Proceedings of the Ocean Structural Dynamics Symposium, Oregon State University, 1986.

C

Bea, R. G., "Dynamic Loading Effects on Pile Capacities," H. Bolton Seed Memorial Symposium Proceedings, Vol. 2, editors: J. Michael Duncan, Vancouver, B.C., May 1990.

B

Bea, R. G., "Probability Based Earthquake Load and Resistance Factor Design Criteria for Offshore Platforms," Proceedings of the 26th Annual Offshore Technology Conference, OTC 8106, Houston, TX, May 1996.

C

Bea, R. G., "Loading and Load Effects Uncertainties: Verification Program for the CSA Code for the Design, Construction, and Installation of Fixed Offshore Structures," Canadian Standards Association Project No. D-3, Department of Naval Architecture and Offshore Engineering and Department of Civil Engineering, University of California at Berkeley, October 1991.

? .

Bea, R. G., Audibert, J. M., and Akky, M. R., "Earthquake Response of Offshore Platforms," Journal of the Structural Division, ASCE, Vol. 105, No. ST2, February, 1979.

J

Bea, R. G., and DesRoches, R., "Development and Verification of a Simplified Procedure to Estimate the Capacity of Template-Type Platforms," Proceedings of the 5th International Symposium on the Integrity of Offshore Structures, 1993.

C

Bea, R. G., and Mortazavi, M. M., "Simplified Evaluation of the Capacities of Template-Type Offshore Platforms," Proceedings of the 5th International Offshore and Polar Engineering Conference, The Hague, The Netherlands, June 1995.

C

Bea, R. G., Mortazavi, M. M., and Loch, K. J., "Evaluation of Storm Loadings and Capacities of Offshore Platforms," Journal of Waterway, Port, Coastal and Ocean Engineering, Vol. 123, No. 2, ASCE, March/April 1997.

J

Bea, R. G., Mortazavi, M. M., Loch, K. J., and Young, P. L., "Verification of a Simplified Method to Evaluate the Capacities of Template-Type Platforms," Proceedings of the 27th Annual Offshore Technology Conference, OTC 7780, Houston, TX, May 1995.

C

Biggs, J. M., and Roessel, J. M., "Seismic Analysis of Equipment Mounted on a Massive Structure," Seismic Design of Nuclear Power Plants, editor: R. J. Hansen, MIT Press, 1970.

B

Billington, C. J., Bolt, H. M., and Ward, J. K., "Reserve, Residual and Ultimate Strength Analysis of Offshore Structures: State of the Art Review," Proceedings of the 3rd International Offshore and Polar Engineering Conference, Singapore, June 1993.

C

Blaney, G. W., Kausel, E., and Roessel, J. M., "Dynamic Stiffness of Piles," Proceedings of the 2nd International Conference on Numerical Methods in Geomechanics, ASCE, Blacksburg, VA, 1976.

Bolt, B. A., Earthquakes, W. H. Freeman and Co., New York, NY, 1993. B

Bolt, H. M., Billington, C. J., and Ward, J. K., "Results from Large-Scale Ultimate Load Tests on Tubular Jacket Frame Structures," OTC 7451, Proceedings of the Offshore Technology Conference, Houston, TX, May 1994. C

Boroschek, R. L., "PCNSPEC Manual," v0.99, 1991. ?.

Bowen, C. M., and Bea, R. G., "Simplified Earthquake Floor Response Spectra for Equipment on Offshore Platforms," Proceedings of the International Workshop on Wind and Earthquake Engineering for Coastal and Offshore Facilities, U. C. Berkeley, January 1995. C

Brebbia, C. A., and Walker, S., Dynamic Analysis of Offshore Structures, Newness-Butterworths, London, 1979. ?

Broms, B. B., "Lateral Resistance of Piles in Cohesionless Soils," Proceedings, ASCE, Vol. 90, No. SM3, May 1964. C

California State Lands Commission, Information on Requalification of Southern California Platforms, 1998. ?

Chopra, A. K., Dynamics of Structures - Theory and Applications to Earthquake Engineering, Prentice-Hall, Englewood Cliffs, NJ, 1995. B

Clough, R. W., "Effects of Earthquakes on Underwater Structures," Proceedings of the 2nd World Conference on Earthquake Engineering, Tokyo, 1960. C

Clough, R. W., and Benuska, K. L., "Nonlinear Earthquake Behavior of Tall Buildings," Journal of the Engineering Mechanics Division, June 1967. S

Clough, R. W., and Johnston, S. B., "Effect of Stiffness Degradation on Earthquake Ductility Requirements," Proceedings of the Japan Earthquake Engineering Symposium, Tokyo, 1967. C

Craig, M. J. K., "Overview and Interfaces: International Standards Organization Design Guidelines for Platforms to Resist Earthquakes," Proceedings of the 28th Annual Offshore Technology Conference, OTC 8104, Houston, TX, May 1996. C

Craig, M. J. K., and Digre, K. A., "Assessments of High-Consequence Platforms: Issues and Applications," Proceedings of the 26th Annual Offshore Technology Conference, OTC 7486, Houston, TX, May 1994. C

Craig, M. J. K., Dolan, D. K., and Hopper, D. M., "Rehabilitation of a 96-Slot Platform," Proceedings of the 25th Annual Offshore Technology Conference, OTC 7147, Houston, TX, May 1993.

Crouse, C. B., "Estimation of Ground Motion for Design or Reassessment of Offshore Platforms," Proceedings of the International Workshop on Seismic Design and Reassessment of Offshore Structures, Pasadena, CA, 1992.

Crouse, C. B., "Seismic Exposure and Site Response Characteristics for Offshore Platform Design," Proceedings of the 28th Annual Offshore Technology Conference, OTC 8105, Houston, TX, May 1996.

Dawson, T. A., Introduction to Offshore Engineering, 1982.

Dobry, R., Vicente, E., and O'Rourke, M., "Equivalent Spring and Damping Coefficients for Individual Piles Subjected to Horizontal Dynamic Loads," paper submitted for publication in the Journal of the Geotechnical Division, ASCE, 1980.

Elghadamsi, F. E., and Mohraz, B., "Inelastic Earthquake Spectra," Earthquake Engineering and Structural Dynamics, Vol. 15, 1987.

Focht, J. A., and Kraft, L. M., "Axial Performance and Capacity of Piles," Planning and Design of Fixed Offshore Platforms, editors: McClelland, B., and Reifel, M. D., 1986.

Gates, N. C., "The Earthquake Response of Deteriorating Systems," Report No. EERL 77-03, Earthquake Engineering Research Laboratory, California Institute of Technology, Pasadena, CA, March 1977.

Gates, W. E., Marshall, P. W., and Mahin, S. A., "Analytical Methods for Determining the Ultimate Earthquake Resistance of Fixed Offshore Structures," Proceedings of the 9th Annual Offshore Technology Conference, OTC 2751, Houston, TX, May 1977.

Goyal, A., and Chopra, A. K., "Earthquake Analysis and Response of Intake-Outlet Towers," Report No. UCB/EERC-89/04, Earthquake Engineering Research Center, University of California at Berkeley, CA, July 1989.

Haviland, R. W., Biggs, J. M., and Anagnostopoulos, S. A., "Inelastic Response Spectrum Design Procedures for Steel Frames," Publication No. R76-40, Department of Civil Engineering, Massachusetts Institute of Technology, Cambridge, MA, September 1976.

Hellan, O., Tandberg, T., and Hellevig, N. C., "Nonlinear Re-Assessment of Jacket Structures Under Extreme Storm Cyclic Loading, Part IV – Case Studies on Existing North-Sea Platforms," Proceedings of OMAE, Glasgow, 1993.

Hidalgo, P. A., and Arias, A., "New Chilean Code for Earthquake-Resistant Design of Buildings," Proceedings of the 4th U.S. National Conference on Earthquake Engineering, Palm Springs, CA, 1990.

Holmquist, D. V., and Matlock, H., "Resistance-Displacement Relationships for Axially-Loaded Piles in Soft Clay," Proceedings of the 8th Annual Offshore Technology Conference, OTC 2474, Houston, TX, May 1976.

Idriss, I. M., "Evaluating Seismic Risk in Engineering Practice," Proceedings of the 11th International Conference on Soil Mechanics and Foundation Engineering, San Francisco, CA, August 1985.

Jain, A. L., Goel, S. C., and Hansen, R. D., "Hysteretic Behavior of Bracing Members and Seismic Response of Braced Frames with Different Proportions," University of Michigan Report UMEE 78R3, July 1978.

Kallaby, J., Digre, K. A., Kim, H., and Eskijian, M. L., "Platform Emmy Strengthening and Requalification," Proceedings of the 25th Annual Offshore Technology Conference, OTC 7139, Houston, TX, May 1993.

Kallaby, J., and Millman, "Inelastic Analysis of Fixed Offshore Platforms for Earthquake Loadings," Proceedings of the 7th Annual Offshore Technology Conference, OTC 2357, Houston, TX, May 1975.

Khatib, I. F., Mahin, S. A., and Pister, K. S., "Seismic Behavior of Concentrically Braced Steel Frames," Report No. UCB/EERC-88/01, Earthquake Engineering Research Center, U. C. Berkeley, January 1988.

Lai, S.-P., and Biggs, J. M., "Inelastic Response Spectra for Aseismic Building Design," Journal of the Structural Division, ASCE, Vol. 106, No. ST6, 1980.

Lawson, R. S., Vance, V., and Krawinkler, H., "Nonlinear Static Pushover Analysis - Why, When and How?" Proceedings of the 5th U. S. Conference on Earthquake Engineering, Vol. 1, Chicago, 1994.

Lin, J. and Mahin, S. A., "Construction of Inelastic Response Spectra for Single Degree of Freedom Systems," Report No. UCB/EERC-83/17, Earthquake Engineering Research Center, U. C. Berkeley, June 1983.

Luyties, W. H., III, Anagnostopoulos, S. A., and Biggs, J. M., "Studies on the Inelastic Dynamic Analysis and Design of Multi-Story Frames," Publication No. R76-29, Department of Civil Engineering, Massachusetts Institute of Technology, Cambridge, MA, July 1976.

MacRae, G., and Kawashima, K., "Effects of Post-Elastic Stiffness on the Response of Single Degree of Freedom Systems," Proceedings of the Annual Meeting of the Japan Society of Civil Engineers, Tokyo, Japan, 1991.

- Mahin, S. A., "Effects of Duration and Aftershocks on Inelastic Design Earthquakes," Proceedings of the 6th World Conference on Earthquake Engineering, Rome, 1976. C
- Mahin, S. A., and Boroschek, R. L., "Influence of Geometric Nonlinearities on the Seismic Response and Design of Bridge Structures," Report to CalTrans Division of Structures, U. C. Berkeley, October 1991. 1.
- Mahin, S. A., and Lin, J., "Construction of Inelastic Response Spectra for Single-Degree-of-Freedom Systems: Computer Program and Applications," Report No. UCB/EERC-83/17, Earthquake Engineering Research Center, University of California at Berkeley, CA, June 1983. 2?
- Maison, B., PC-ANSR, Department of Civil Engineering, University of California at Berkeley, CA, 1990. 2?
- Mansour, A. E., "Theory of Ship Structures," NA240B Class Notes, Department of Naval Architecture and Offshore Engineering, University of California at Berkeley, December 1987. 2?
- Marshall, P. W., "An Overview of Recent Work on Cyclic Inelastic Behavior and System Reliability," Structural Stability Research Council, Annual Meeting and Technical Sessions, New Orleans, LA, 1982. 2?
- Marshall, P. W., Gates, W. E., and Anagnostopoulos, S., "Inelastic Dynamic Analysis of Tubular Offshore Steel Structures," Proceedings of the 9th Annual Offshore Technology Conference, Houston, TX, May 1977. C
- Mason, A. B., Beck, J. L., Chen, J., and Ullmann, R. R., "Modal Parameter Identification of an Offshore Platform from Earthquake Response Records," Proceedings of the ASCE Structures Congress, San Francisco, CA, May 1989. C
- Matlock, H., "Correlations for Design of Laterally Loaded Piles in Soft Clay," Proceedings of the Offshore Technology Conference, Houston, TX, May 1970. C
- Matlock, H., Foo, S. H. C., and Bryant, L. M., "Simulation of Lateral Pile Behavior Under Earthquake Motion," Proceedings of the ASCE Conference on Earthquake Engineering and Soil Dynamics, Pasadena, CA, 1978. C
- Miller, T. M., Dolan, D. K., Eskijian, M. L., and Craig, M. J. K., "Requalification of an Older California Platform: API and Risk-Based Approaches," Proceedings of the 22nd Annual Offshore Technology Conference, OTC 6648, Houston, TX, May 1990. C
- Miranda, E., "Seismic Evaluation and Upgrading of Existing Buildings," Ph.D. Dissertation, Department of Civil Engineering, University of California at Berkeley, CA, June 1991. Prelis

- Miranda, E., and Bertero, V. V., "Reductions in Seismic Strength Demands Due to Inelastic Behavior," Proceedings of the 5th U. S. National Conference on Earthquake Engineering, Vol. II, EERI, Oakland, CA, 1994. C
- Mortazavi, M. M., and Bea, R. G., "A Reliability Based Screening Procedure for Platform Assessments and Requalifications," Proceedings of the 15th International Conference on Offshore Mechanics and Arctic Engineering, Florence, Italy, June 1996. C
- Mortazavi, M. M., and Bea, R. G., "Experimental Validation of the Ultimate Limit State Limit Equilibrium Analysis (ULSLEA) with Results from Frame Tests," Proceedings of the 7th International Offshore and Polar Engineering Conference, Honolulu, HI, May 1996. C
- Naeim, F., and Anderson, J. C., "Classification and Evaluation of Earthquake Records for Design," NEHRP Fellowship Report, FEMA, Washington, D. C., 1993. ?
- Nassar, A., and Krawinkler, H., "Seismic Demands for SDOF and MDOF Systems," Report No. 95, John Blume Earthquake Engineering Center, Stanford University, Palo Alto, CA, 1990. ?
- Newmark, N. M., "A Method of Computation for Structural Dynamics," Journal of the Engineering Mechanics Division, ASCE, 85, 1959. 3
- Newmark, N. M., and Hall, W. J., "Seismic Design Criteria for Nuclear Reactor Facilities," Building Practices for Disaster Mitigation, Report No. 46, National Bureau of Standards, U. S. Department of Commerce, 1973. ?
- Newmark, N. M., and Hall, W. J., Earthquake Spectra and Design, Earthquake Engineering Research Institute, Oakland, CA, 1982. ?
- Newmark, N. M., and Rosenblueth, E., Fundamentals of Earthquake Engineering, Prentice-Hall, Englewood Cliffs, NJ, 1971. B
- Novak, M., "Dynamic Stiffness and Damping of Piles," Canadian Geotechnical Journal, Vol. 11, No. 4, 1974. 3
- Parlett, B., The Symmetric Eigenvalue Problem, Prentice-Hall, Englewood Cliffs, NJ, 1980. B
- PEMEX/IMP, Information on Assessment of Platforms in the Bay of Campeche, 1999. ?
- Peng, M.-H., Elghadamsi, F. E., and Mohraz, B., "A Stochastic Procedure for Nonlinear Response Spectra," Proceedings of the 9th World Conference on Earthquake Engineering, Vol. V, Tokyo-Kyoto, Japan, 1988. C
- Penzien, J., "Seismic Analysis of Platform Structure-Foundation Systems," Proceedings of the 7th Annual Offshore Technology Conference, OTC 2352, Houston, TX, May 1975. C

Perez, F., Vazquez, R., and Ortega, R., "Risk Assessment and Management (RAM) Based Requalification of Offshore Platforms in the Bay of Campeche, Offshore Mexico," Proceedings of the 8th International Conference on Offshore Mechanics and Arctic Engineering, Lisbon, Portugal, July 1998.

PMB Systems Engineering, Inc., "Earthquake Analysis Studies for Offshore Structures, Stage I: Baseline Analysis," San Francisco, CA, November 1980.

PMB Systems Engineering, Inc., "Earthquake Analysis Studies for Offshore Structures, Stage II: Time History Analysis," San Francisco, CA, October 1981.

Powell, DRAIN, Department of Civil Engineering, University of California at Berkeley, CA, December 1993.

Prakash, V., Powell, G. H., and Campbell, S., "DRAIN-2DX: Base Program Description and User Guide, Version 1.10," Report No. UCB/SEMM-93/17, Department of Civil Engineering, University of California at Berkeley, Berkeley, CA, November 1993.

Randolph, M. F., Houlsby, G. T., "The Limiting Pressure on a Circular Pile Loaded Laterally in Cohesive Soil," Geotechnique, London, England, 1984.

Reece, E. W., Ryerson, D. E., and McNeill, R. L., "Long-Term Measurements of Ground Motions Offshore," Proceedings of the International Conference on Recent Advances in Geotechnical Earthquake Engineering and Soil Dynamics, Rolla, MO, 1981.

Reese, L. C., Cox, W. R., and Koop, F. D., "Analysis of Laterally Loaded Piles in Sand," Proceedings of the 6th Annual Offshore Technology Conference, OTC 2080, Houston, TX, May 1974.

Reese, L. C., Cox, W. R., and Koop, F. D., "Field Testing and Analysis of Laterally Loaded Piles in Stiff Clay," Proceedings of the 6th Annual Offshore Technology Conference, OTC 2312, Houston, TX, May 1975.

Reinhorn, A., IDARC, SUNY, 1995.

Richart, F. E., Jr., Hall, J. R., Jr., and Woods, R. D., Vibration of Soils and Foundations, Prentice-Hall, Inc., Englewood Cliffs, NJ, 1970.

Riddell, R., Hidalgo, P., and Cruz, E., "Response Modification Factors for Earthquake Resistant Design of Short Period Structures," Earthquake Spectra, Vol. 5, No. 3, 1989.

Riddell, R., and Newmark, N. M., "Statistical Analysis of the Response of Nonlinear Systems Subjected to Earthquakes," Structural Research Series No. 468, Department of Civil Engineering, University of Illinois, Urbana, 1979.

Rosenblueth, E., "A Basis for Aseismic Design," Ph.D. Thesis, submitted to the Department of Civil Engineering, University of Illinois at Urbana-Champaign, Urbana, IL, 1951.

Ruhl, J., "Offshore Platforms: Observed Behavior and Comparisons with Theory," Proceedings of the 8th Annual Offshore Technology Conference, OTC 2553, Houston, TX, May 1976.

Saiidi, M., and Sozen, M. A., "Simple and Complex Models for Nonlinear Seismic Response of Reinforced Concrete Structures," Structural Research Series Report No. 465, Department of Civil Engineering, University of Illinois at Urbana-Champaign, Urbana, IL, August 1979.

Schiff, D., Dynamic Analysis and Failure Modes of Simple Structures, Wiley and Sons, New York, NY, 1990.

Sherman, D. R., "Experimental Study of Post Local Buckling Behavior in Tubular Portal Type Beam-Columns," Report to Shell Oil Company, Department of Civil Engineering, University of Wisconsin-Milwaukee, October 1979.

Sleefe, G. E., "The Long-Term Measurement of Strong-Motion Earthquakes Offshore Southern California," Proceedings of the 22nd Annual Offshore Technology Conference, OTC 6336, Houston, TX, May 1990.

Sherman, D. R., "Experimental Study of Post Local Buckling Behavior in Tubular Portal Type Beam-Columns," Report to Shell Oil Company, Department of Civil Engineering, University of Wisconsin-Milwaukee, October 1979.

Sherman, D. R., "Post Local Buckling Behavior of Tubular Strut Type Beam Columns: An Experimental Study," Report to Shell Oil Company, Department of Civil Engineering, University of Wisconsin-Milwaukee, June 1980.

Shibata, M., and Wakabayashi, M., "Hysteretic Behavior of K-Type Braced Frame," Proceedings of the 8th World Conference on Earthquake Engineering, Vol. 6, San Francisco, CA, June 1984.

Smith, C. E., "Dynamic Response of Offshore Steel-Jacket Platforms Subject to Measured Seafloor Seismic Ground Motions," Dr. Sc. Dissertation, Graduate School of Engineering and Applied Science, George Washington University, Washington, D.C., March 1994.

Stear, J. D., and Bea, R. G., "Ultimate Limit State Capacity Analyses of Two Gulf of Mexico Platforms," Proceedings of the 29th Annual Offshore Technology Conference, OTC 8418, Houston, TX, May 1997(A).

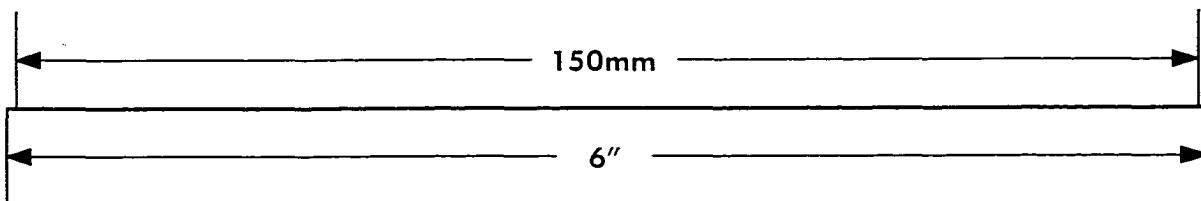
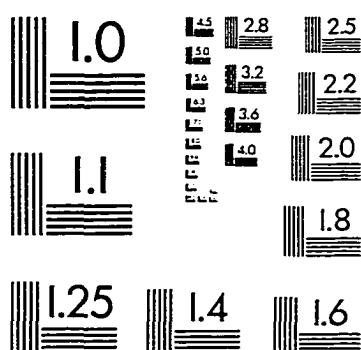
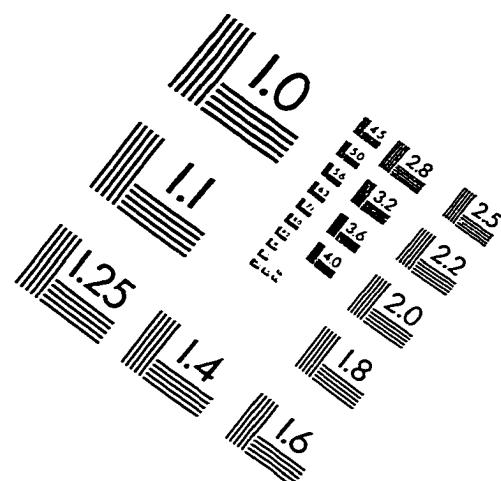
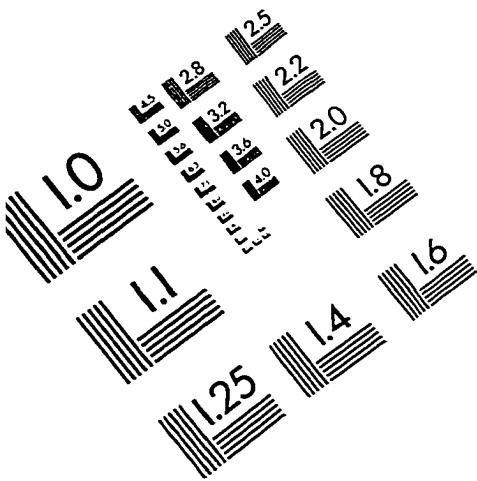
Stear, J. D., and Bea, R. G., "Evaluating Simplified Analysis Approaches for Estimating the Load Capacities of Gulf of Mexico Jacket-Type Platforms," Proceedings of the 16th International Conference on Offshore Mechanics and Arctic Engineering, Yokohama, Japan, April 1997(B).

- Stear, J. D., and Bea, R. G., "Simplified Strength-Level Earthquake Assessment of Jacket-Type Platforms," Proceedings of the 8th International Conference on Offshore and Polar Engineering, Montreal, Canada, May 1998. C
- Stear, J. D., and Bea, R. G., "TOPCAT User Manual," Report to JIP Sponsors and Office of Technology Licensing, Marine Technology and Management Group, Department of Civil and Environmental Engineering, University of California at Berkeley, CA, May 1999. T
- Tang, W. H. and Gilbert, R. B., "Offshore Lateral Pile Design Reliability," Research Report for Project PRAC 87-29, API, 1990. T
- Thoft-Christiansen, P. and Baker, J., Structural Reliability Theory and Its Applications, Springer-Verlag, 1981. J
- Timoshenko, S., Young, D. H., and Weaver, W., jr., Vibration Problems in Engineering, 4th Edition, John Wiley and Sons, New York, NY, 1974. B
- Unocal Corporation, Information on Requalification of Southern California Platforms, 1998. T
- Uniform Building Code, 1994. T
- US National Geophysical Data Center, "Earthquake Strong Motion 3-Volume CD-ROM Collection," National Oceanic and Atmospheric Administration, Boulder, CO, March 1996. T
- Veletsos, S. A., "Maximum Deformations of Certain Nonlinear Systems," Proceedings of the 4th World Conference on Earthquake Engineering, Vol. I, Santiago, Chile, 1969. C
- Veletsos, A. S., "Dynamics of Structure-Foundation Systems," Structural and Geotechnical Mechanics: A Volume Honoring Nathan M. Newmark, editor: W. J. Hall, Prentice-Hall, Englewood Cliffs, NJ, 1977. B
- Veletsos, A. S., and Boaz, I. B., "Effects of Soil-Structure Interaction on Seismic Response of a Steel Gravity Platform," OTC 3404, Proceedings of the 11th Annual Offshore Technology Conference, Houston, TX, May 1979. C
- Veletsos, A. S., and Meek, J. W., "Dynamic Behavior of Building-Foundation Systems," Earthquake Engineering and Structural Dynamics, Vol. 3, 1974. J
- Veletsos, A. S., and Newmark, N. M., "Effect of Inelastic Behavior on the Response of Simple Systems to Earthquake Ground Motions," Proceedings of the 2nd World Conference on Earthquake Engineering, Vol. 2, Tokyo, Japan, 1960. C
- Zayas, V. A., Mahin, S. A., and Popov, E. P., "Cyclic Inelastic Behavior of Steel Offshore Structures," Report No. UCB/EERC-80/16, Earthquake Engineering Research Center, University of California at Berkeley, CA, June 1980 (A). ?

Zayas, V. A., Popov, E. P., and Mahin, S. A., "Cyclic Inelastic Buckling of Tubular Steel Braces," Report No. UCB/EERC-80/27, Earthquake Engineering Research Center, University of California at Berkeley, CA, August 1980 (B). 7

Zayas, V. A., Shing, B. P. S., Mahin, S. A., and Popov, E. P., "Inelastic Structural Modeling of Braced Offshore Platforms for Seismic Loading," Report No. UCB/EERC-81/04, Earthquake Engineering Research Center, University of California at Berkeley, CA, June 1981. 9

IMAGE EVALUATION TEST TARGET (QA-3)



APPLIED IMAGE, Inc.
1653 East Main Street
Rochester, NY 14609 USA
Phone: 716/482-0300
Fax: 716/288-5989

© 1993, Applied Image, Inc., All Rights Reserved

